DESIGN OF AN AFFORDABLE ANTHROPOMORPHIC MECHANICAL PROSTHETIC HAND

SEVERIN TENIM

SUPERVISOR: DR GEORGE VICATOS

DISSERTATION SUBMITTED TO THE UNIVERSITY OF CAPE TOWN IN FULL FULFILMENT OF THE REQUIREMENTS FOR THE DEGREE OF MASTER OF SCIENCE IN MECHANICAL ENGINEERING

SEPTEMBER 2014

Abstract

This dissertation outlines the conceptualisation, design, manufacture, assembly and experimental testing of an affordable anthropomorphic mechanical hand prosthesis. In many countries, upper-limb amputees lack access to prosthetic hand devices. Furthermore, currently available mechanical devices require a large amount of effort to actuate; fatiguing and frustrating patients who have no other alternative but to use them. Consequently, a need has arisen to provide a mechanical device that is affordable enough to be accessible to low and middle-income patients, is functional enough to allow users to easily perform their Activities of Daily Living (ADLs), and is aesthetically appealing enough to ensure that patients feel comfortable and confident when wearing it.

Concept solutions of several mechanisms were identified and evaluated from which the final design was selected. Analytical force analysis was used to generate a mathematical model to analyse the response of each dynamic member in the hand. A linear relationship between the input-force and applied grasp-forces of the hand was identified. Finite Element Analysis (FEA) used to investigate the lateral and hyperextensive loading limits of the phalanges, generated results that corresponded well to the experimental outcomes. Amongst the utilised actuation mechanisms (levers, pulleys, tendon-wires, bearings and springs), the tendon-wires were of concern due to their repetitive tensile loading and relative movement with the phalanges. Tensile testing of various tendon-wires and endurance testing of the phalangeal tendon-channels, yielded a combination which surpassed the infinite life requirement of 1,200,000 loading cycles; with carbon-nylon contact wearing at the lowest rate as confirmed by gravimetric tests in accordance with ASTM F2025 (2000).

Manufacture of the hand used rapid prototyping in combination with traditional machining methods and standard components, enabling a fully-assembled cost of R 11,628.37; below the required R 18,000 limit. Various power and precision grasping configurations were achieved and the contact forces satisfactorily maintained, using the hand's built-in locking mechanism. Feedback gathered from the prosthetist and patients suggested making slight alterations to the hand's aesthetics and to address minor functional challenges, such as the control of the closing trajectory for precision grasps.

Acknowledgements

"In ordinary life we hardly realise that we receive a great deal more than we give, and that it is only with gratitude that life becomes rich" – *Dietrich Bonhöffer.*

After many sleepless nights, seemingly endless deadlines, and many ups and downs, this undertaking would not have been possible had it not been for remarkable people involved. I would hereby like to express my sincere gratitude and thank the following people:

Dr George Vicatos for his patience, enthusiasm, tutelage, guidance and his endless supply of innovative ideas. It has truly been a great experience to work with someone who is passionate about what he does, and able to effortlessly combine creativity, understanding and sound engineering principles into novel design. His positive attitude, approachability and willingness to help has been invaluable.

In the mechanical engineering workshop, a special thanks to Glen for his optimism and ability to 'machine anything'. Pierre for his great turning work, Dillion for the precision milling, as well as Tyrone, Hubert, Peter and Gavin for organising all the odds and ends.

Johan, Gerrie and Ludrick for their expertise, professionalism, quick turnaround time and high production standards of all their laser-sintered, additive manufactured components made at the Central University of Technology's (CUT) Centre for Rapid Prototyping and Machining (CRPM). With regard to their input and assistance with the intellectual property, Dr Andrew Bailey at UCT's RCIPS and Mike von Seidel at Von Seidels Intellectual Property Attorneys. Furthermore, to the prosthetists involved, Mr Eugene Rossouw and Ms Olwen Nel, for their vital insights, inputs relating patient needs and supervision during preliminary device testing.

UCT's Department of Mechanical Engineering and Centre for Materials Engineering, for use of their testing equipment and facilities. Penny and Liezl for their assistance with the laboratory equipment and Instron® tensile tester. Julian and Tracy for assisting with the electrical components used in the pneumatic fatigue testing setup. Trevor Cloete for his conceptual input and Andrew Mowat for his eagerness to assemble and critique anything cast in his direction. At Gellini Spring Manufacturing, a special thanks to Francois Brand for his assistance with the cold-winding of custom springs. Lastly, to the National Research Foundation (NRF) for their funding assistance through their SET Scarce Skills Scholarship.

To all of the above, and anyone else who has contributed.

Thank you.

Table of Contents

List of Tables

List of Figures

Definitions and Abbreviations

(It should be noted that some terms have been adapted to relate specifically to the hand or wrist and are not generalised)

Abduction	-	Motion that moves the structure *away* from the midline of the body.
Adduction	-	Motion that moves the structure *towards* from the midline of the body.
ADLs	-	Activities of Daily Living.
Anterior	-	The frontal side. Toward the front.
Anthropometrics	-	The comparative study of human body measurements, proportions and properties.
Anthropomorphic	-	Mimics human form.
ASTM	-	American Society for Testing and Materials.
Carpal	-	Of the wrist.
Digit	-	Finger.
DIP	-	Distal Interphalangeal (Joint).
Distal	-	The part of the limb furthest from the centre of the body. Opposite to proximal.
Dorsal	-	Toward the back, posterior. Opposite to palmar. The back of the hand.
DSM	-	Decision Support Matrix
Electrogoniometric	-	The use of an electrical device to measure flexibility or angles.
Epidemiology	-	The science that studies the patterns, causes and effects of health and disease conditions in defined population groups.
Ergonomics	-	The science of making a safer, more comfortable human working environment
Etiology	-	The study of causation or origination.
Extension	-	Motion that increases the angle between to parts. (i.e. when standing up, the knees are extended). Opposite to flexion.
FEA	-	Finite Element Analysis.
Flexion	-	Motion that decreases the angle between to parts. (i.e. clenching hand into a fist)
Inferior	-	Below or bottom. Opposite to superior.
ISO	-	International Organisation for Standardisation.
Lateral	-	Outward side, away from the midline. Opposite to medial.
Medial	-	Inward side. The side of the knee closest to the other knee.
MCP	-	Metacarpophalangeal (Joint).
OPUS	-	Orthotics and Prosthetics User Survey.
Palmar	-	Of the palm. Anterior side.
PEQ	-	Patient Evaluation Questionnaire.

PHEQ	-	Prosthetic Hand Evaluation Questionnaire.
PIP	-	Proximal Interphalangeal (Joint).
Posterior	-	The rear side. Toward the back.
Prosthesis	-	Externally applied device used to replace wholly, or in part, an absent or deficient limb segment.
Prosthetics	-	Science and art involved in treating patients by the use of prostheses (ISO 8549, 1989).
Prosthetist	-	Person who, having completed an approved course of education and training, is authorised by an appropriate national authority to design, measure and fit prostheses.
Proximal	-	The portion of the limb closest to the centre of the body or rotation centre. Opposite to distal. (i.e. the elbow is proximal to the wrist).
PTFE	-	Polytetrafluoroethylene (Teflon).
RoMs	-	Ranges of Motion.
SF	-	Factor of safety / Design factor.
Superior	-	Above or top.
UEFS	-	Upper Extremity Functional Status.
UHMWPE	-	Ultra High Molecular Weight Polyethylene.
Underactuation	-	There are more degrees of freedom (Dof) than there are actuators.
UTS	-	Ultimate Tensile Strength.
VAT	-	Value Added Tax.
VC	-	Voluntary Closing.
VO	-	Voluntary Opening.

Nomenclature

(In order of apperance)

- F_{IN} = primary input force from shoulder harness
- F_{RES} = resultant pulley force
- F_{RC} = routing cable force
- F_{DIG} = digit cable force
- M_{XY} = resultant moment in XY-plane
- M_{XZ} = resultant moment in XZ-plane
- M_{YZ} = resultant moment in YZ-plane
- θ_{RES} = inclination angle of resultant pulley force
- θ_{RC} = inclination angle of routing cable force
- $L_{X\,RES}$ = length to resultant force in x-direction
- $L_{Z\,RES}$ = length to resultant force in z-direction
- $L_{X\,IN}$ = length to input force in x-direction
- $L_{Z\,IN}$ = length to input force in z-direction
- F_{RC1} = routing cable force from pulley carriage
- F_{RC2} = central routing cable force
- F_{RC3} = routing cable force to thumb transfer lever
- F_{RES1} = left bearing reaction (normal) force
- F_{RES2} = right bearing reaction (normal) force
- θ_{RC1} = inclination angle of routing cable force
- θ_{RC2} = inclination angle of routing cable force
- μ_b = coefficient of bearing friction
- P = normal contact load
- d_b = bearing bore diameter
- F_{TH2} = thumb cable force to thumb bearing
- L_{T1} = length to thumb cable
- L_{T2} = length to routing cable
- θ_{T1i} = inclination angle of thumb cable force
- θ_{T2i} = inclination angle of routing cable force
- β_T = angular motion of transfer lever
- $F_{TH\,RES}$ = thumb bearing reaction (normal) force
- F_{TH1} = thumb cable force to proximal phalanx
- θ_{TH} = inclination angle of thumb cable
- F_{23} = force to 1st secondary seesaw
- F_{45} = force to 2nd secondary seesaw
- θ_{S1} = lever arm inclination angle
- β_{S1} = angular deviation of the lever
- θ_{23} = angulation of 23 lever arm
- θ_{45} = angulation of 45 lever arm
- L_{23} = length of the 23 lever arm
- L_{45} = length of the 45 lever arm
- F_2 = force to 2nd digit (index finger)
- F_3 = force to 3rd digit (middle finger)
- θ_{S2} = lever arm inclination angle
- β_{S2} = angular deviation of the lever
- θ_2 = angulation of F_2 lever arm
- θ_3 = angulation of F_3 lever arm
- L_2 = length of the F_2 lever arm
- L_3 = length of the F_3 lever arm
- F_4 = force to 4th digit (ring finger)
- F_5 = force to 5th digit (little finger)
- θ_{S3} = lever arm inclination angle
- β_{S3} = angular deviation of the lever
- θ_4 = angulation of F_4 lever arm
- θ_5 = angulation of F_5 lever arm
- L_4 = length of the F_4 lever arm
- L_5 = length of the F_5 lever arm
- $_{\wedge}{}^{i}$ = identifier for fingers/digits (i.e. 1-5, thumb to little finger resp.)
- $_{v\,1,2,3}$ = identifier for respective phalanges (i.e. proximal, middle, distal resp.)
- L_G = distance from pivot to centre of gravity
- F_G = applied grasp force
- T = cable (tendon) tension
- $R_{X/Y}$ = hinge reaction forces in x and y directions
- M_O = hinge reaction moment
- m = mass of phalanx
- g = gravitational acceleration
- r = radial channel distance from pivot
- β = angle of interphalangeal phalanx face
- L_F = distance from pivot to applied grip force and/or normal force
- θ = flexion angle of each phalange
- d = spring wire diameter
- E = Young's Modulus
- D = mean coil diameter
- Na = number of active turns of spring
- μ_r = estimated coefficient of hinge friction (static)
- r_p = hinge pin radius
- L = length of phalanx
- N = normal reaction force of cable/tendon on the phalanx
- h = distance of tendon friction force from hinge/pivot
- μ_C = coefficient of channel friction (static)
- α = angle of deviation of actuating wire
- τ_{all} = allowable shear stress
- F_S = maximum shear force
- A = shear area
- δ = deflection

1

CHAPTER 1: INTRODUCTION

1.1. Background

In third world countries, many upper-limb amputees lack access to modern prosthetic hand devices. In South Africa, currently available prosthetic devices include a passive/cosmetic hand, a cable-driven metal hook and a voluntary-opening cable-driven hand. The passive hand while aesthetically appealing is non-functional, the hook has increased functionality but is aesthetically unappealing, and the voluntary-opening hand is aesthetically appealing with limited functionality. Furthermore, these purely mechanical devices are undesirable, as the cable mechanism which initiates their motion, requires a large amount of effort to actuate. This fatigues and frustrates the users of these devices.

The focus of modern commercial upper limb prosthetic development has generally shifted from purely mechanical devices to electromechanical/myoelectric devices that employ electrical motors, sensors, circuitry, computer processors and battery power. These myoelectric prosthetic devices offer improved functionality and usability, as actuation is achieved through an electric motor, reducing the workload for the user. Sadly, most of the third world amputees are unable to afford such prosthetic hand devices, even with the assistance of government subsidies or medical aid contributions.

1.2. Objectives of this Dissertation

This dissertation aims to develop an affordable, anthropomorphic, highly functional and aesthetically appealing mechanical prosthetic hand. Furthermore, the device needs the commercial viability to be incorporated into a state-run prosthetics centre, be affordable enough to be covered by the Workmen's Compensation Fund and be adaptable to fit both transradial (below elbow) and transhumeral (above elbow) amputees. According to a Western Cape prosthetist, Eugene Rossouw, the cost-price of the hand will be viable up to a value of approximately R18,000 (Rossouw, 2013) and the unit should be maintenance-free for a period exceeding two years. Furthermore, the efficiency of the device should be

optimised to minimise actuation energy, such that future versions may incorporate the use of an external myoelectric system.

1.3. Scope and Limitations

The scope of this dissertation includes the design, development, prototyping, manufacture, assembly, and testing of an affordable mechanical prosthetic hand.

It does not deal with the development of an external actuating system, or fitment of the device to a patient, as this will be done by a qualified prosthetist.

1.4. Plan of Development

This report looks at existing prosthetic hand technologies and designs, as well as various types of underactuated mechanisms through a literature review. It moves on to a concept formation of different mechanical hand designs and actuating mechanisms from which a desired solution is chosen. Next, an analysis is performed on all critical sections of the design, including a quasi-static analytical force model, calculations for linear and torsion springs, as well as a finite element analysis to determine the lateral and hyperextensive loading limits of the phalanges. Thereafter, the final mechanical designs are made, followed by a brief solution specification and assembly of the prototype. A risk assessment is performed for each harmful activity or procedure, ethical considerations are made and the impact of this technology on society is assessed, after which experimental procedures and tests are carried out, and their results discussed. Finally, conclusions are drawn based on the findings of experimental outcomes and research, and recommendations are made based on these conclusions.

2

CHAPTER 2: LITERATURE REVIEW

This section of the report looks at existing technologies and standards applicable to this dissertation. It highlights key aspects to be taken into consideration in the formulation of the final solution.

2.1. Anatomy of the Hand and Wrist

"The hand is an extension of the human brain" – Immanuel Kant (German philosopher)

It is one of the most complex osseo-muscular systems in our body, containing a network of bones, muscles, ligaments, tendons, connective tissue, blood vessels and nerves, which work together to produce a highly functional and versatile tool, used thousands of times each day. The fingertips contain some of the densest concentrations of nerve endings in the human body (Gilroy, et al., 2008); hence touch is often associated with the hands and not the feet. Furthermore, a highly complex network of muscles and tendons, initiate the movement of the hand through contractions known as flexion or extension (Strandring, 2008). Muscles are divided into the flexor (palmar-side) and extensor compartment (dorsal-side). Detailed views of these sections are shown in Figure 1.

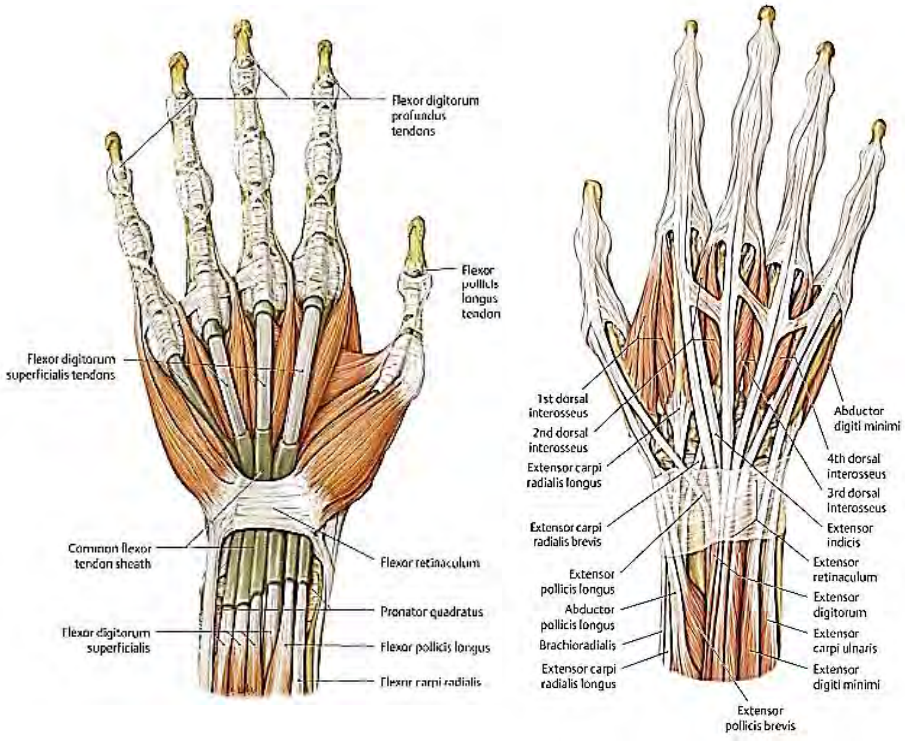

Figure 1 - Anterior (palmar) view of flexor compartment and posterior (dorsal) view of extensor compartment of the hand (left and right respectively) (Gilroy, et al., 2008, pp. 307, 310).

The hand contains a total of 27 bones, which are divided into 3 major compartments; namely the finger, the palmar and the wrist (carpal) compartments. The finger compartment is made up of 14 phalanges (distal, middle and proximal) whereas the palmar compartment is made up of only 5 metacarpal bones, joining to the fingers and the wrist at the metacarpo-phalangeal and the carpo-metacarpal joints respectively. The wrist is made up of 8 carpal bones, as seen in Figure 2, divided by the midcarpal joint and joins to the forearm at the radio-carpal joint. Figure 2 below, shows a transverse section of the hand highlighting the various bones and joints.

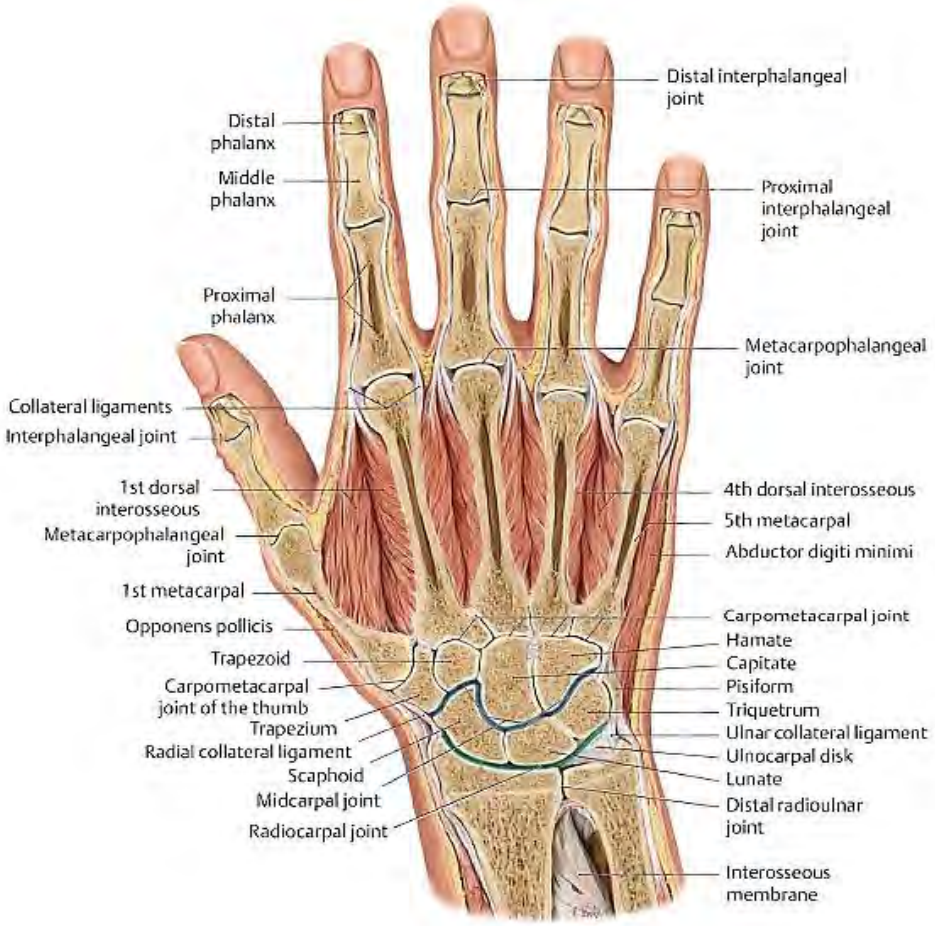

Figure 2 - Anatomy of the hand and wrist (dorsal view) (Gilroy, et al., 2008, p. 301).

A comprehensive understanding of the joints in the hand is essential to enable mimicking of its functionality through the use of a prosthesis. There are four major types of joints in the hand and wrist. Namely, hinge, condyloid, gliding and saddle joints (Strandring, 2008). The joints of the fingers (interphalangeal joints) are hinge joints which allow extension and flexion. The knuckle joints (metacarpophalangeal joints) are condyloid joints which allow flexion and extension but also slight lateral deviation. Gliding joints are found between the carpal bones (metacarpal-carpal & midcarpal joints), they allow bones in the wrist to slide relative to one another. Lastly, saddle joints are ones which include opposing surfaces that are reciprocally convex and concave, such as the carpo-metacarpal joint of the thumb. This joint can be thought of as a universal type joint, allowing

articulation in all directions. In order to assist in the understanding of certain medical terminology it is essential to establish a reference frame in relation to the hand. Figure 3 outlines important reference directions and motions relating to the hand that will be referred to in subsequent sections.

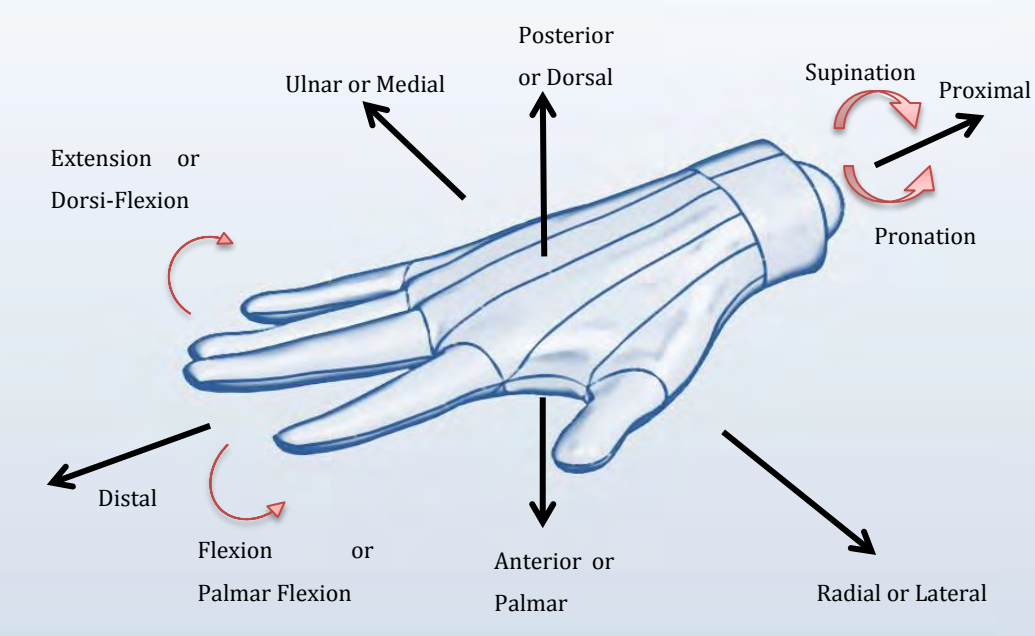

Figure 3 - Orientation and reference frame of the hand.

2.2. Anthropometrics of the Hand

The anthropometry of the hand has been extensively studied throughout the literature. Studies conducted by numerous academics including Kember, et al. (1981), Gooderson, et al. (1982) and Peebles & Norris (1998), were reviewed to determine the ideal data for anthropometric and ergonomic design of an artificial hand. The most comprehensive study was one conducted by Pheasant and Haslegrave (2006), which used a host of existing studies as well as their own investigation to compile the data given in Table 1.

Table 1 – Anthropometric estimates for the hand (in mm) by Pheasant & Haslegrave (2006, p. 144).

	Dimension	Men				Women			
		5th %ile	50th %ile	95th %ile	SD	5th %ile	50th %ile	95th %ile	SD
1	Hand length	173	189	205	10	159	174	189	9
2	Palm length	98	107	116	6	89	97	105	5
3	Thumb length	44	51	58	4	40	47	53	4
4	Index finger length	64	72	79	5	60	67	74	4
5	Middle finger length	76	83	90	5	69	77	84	5
6	Ring finger length	65	72	80	4	59	66	73	4
7	Little finger length	48	55	63	4	43	50	57	4
8	Thumb breadth (IPJ) [1]	20	23	26	2	17	19	21	2

9	Thumb thickness (IPJ)	19	22	24	2	15	18	20	2
10	Index finger breadth (PIPJ) [2]	19	21	23	1	16	18	20	1
11	Index finger thickness (PIPJ)	17	19	21	1	14	16	18	1
12	Hand breadth (metacarpal)	78	87	95	5	69	76	83	4
13	Hand breadth (across thumb)	97	105	114	5	84	92	99	5
14	Hand breadth (minimum) [3]	71	81	91	6	63	71	79	5
15	Hand thickness (metacarpal)	27	33	38	3	24	28	33	3
16	Hand thickness (max incl. thumb)	44	51	58	4	40	45	50	3
17	Maximum grip diameter [4]	45	52	59	4	43	48	53	3
18	Maximum spread	178	206	234	17	165	190	215	15
19	Maximum functional spread [5]	122	142	162	12	10	127	145	11
20	Minimum square access [6]	57	67	77	6	51	59	66	5

[1] IPJ is the interphalangeal joint, i.e. the articulation between the two segments of the thumb.

[2] PIPJ is the proximal interphalangeal joint, i.e. the finger articulation nearest to the hand.

[3] As for dimension 12, except that the palm is contracted to make it as narrow as possible.

[4] Measured by sliding the hand down a graduated cone until the thumb and the middle finger only touch.

[5] Measured by gripping a flat wooden wedge with the tip end segments of the thumb and the ring fingers.

[6] The side of the smallest equal-sided aperture through which the hand will pass.

Note: All dimensions are in millimetres (mm). Visual descriptions are shown in Figure 4.

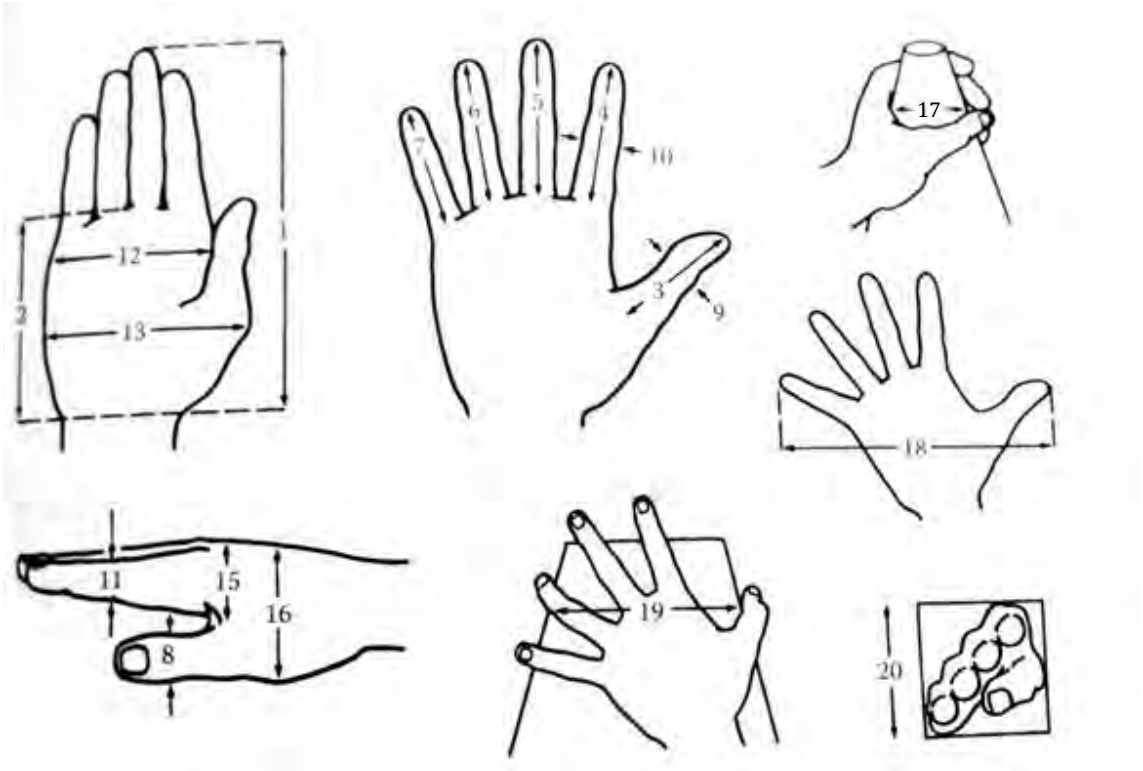

Figure 4 - Anthropometry of the hand, as given in Table 1 by Pheasant & Haslegrave (2006).

Referring to Table 1 & Figure 4, the anthropometric data for the hands of male and female patients is shown. Furthermore, natural human variation is accounted for by the 5th, 50th and 95th percentile of each gender. To further assess the validity of the data, it was compared to that of a study by Chandra,

et al. (2011), which yielded similar results. However, their study also included anthropometric data for the phalanges of the 3rd and 5th digits as shown in Table 2 below, and was more extensive in that it covered a broader range of dimensions of the hand.

Table 2 - Anthropometric data of the hand adapted from Chandra, et al. (2011).

Dimension		5th %ile	50th %ile	95th %ile	Mean	Min	Max	SD
Hand length		175	187	201	**185.77**	170	202	1.68
Palm length		97	106	115	**105.59**	94	118	4.57
Hand breadth (knuckles)		80	85	92	**84.85**	78	92	2.82
Hand breadth (max incl. thumb)		95	102	110	**101.83**	95	110	3.38
Hand thickness (metacarpal)		25	28	31	**28.04**	24	32	1.68
Hand thickness (max at thumb)		40	45	51	**44.62**	35	54	3.41
3rd Digit	Overall length	71.44	79.18	88.41	**79.05**	69.79	90.80	4.31
	DIPJ to root	45.13	52.51	59.36	**52.06**	43.76	60.51	3.54
	PIPJ to root	21.21	25.72	30.52	**25.53**	19.46	32.41	2.71
5th Digit	Overall length	52.97	59.95	66.89	**59.13**	49.79	68.1	3.39
	DIPJ to root	28.16	34.37	39.33	**34.23**	27.31	41.58	2.76
	PIPJ to root	14.12	17.45	21.53	**17.52**	12.93	22.55	1.96
Note: All dimensions in millimetres (mm). Sample size: N = 878 people.								

Referring to Table 1 and Table 2, it can be seen that the values for hand length, breadth and thickness, as well as those for palm length correspond relatively well. In Table 2, the dimensions for the 3rd and 5th digit (i.e. the middle and little finger respectively) are shown as well as their percentile distribution; the dimension of primary interest being the mean value.

Another method of calculating the hand length, mass and centre of mass is done in terms of segment length/mass as a function of body height/mass. The research by Dempster (1955) and Drillis & Contini (1966) found the hand length to be *0.108 x Body Height* as published by Richards (2008, p. 20). Moreover, the hand mass is approximated as *0.006 x Body Mass* and the centre of mass is located *0.506 x Segment length* from the proximal end of the hand (i.e. from the wrist). In Belter, et al. (2013), the average weight of the human hand was 400 grams, or 0.6% total body weight for men and 0.5% for women.

This anthropometric data will be incorporated into design calculations and force optimisation studies in Chapter 4, adapting them to the final design of the prosthetic device in Chapter 5. As a result, this combination will ensure that the final dimensions are optimised to transmit the best anatomical force balance for stability and grip, as well as obtain the most anthropomorphic proportions. The following section will look at the background of prosthetic hands and the patients who use them.

2.3. Background of Prosthetic Hands and Patients

2.3.1. History of Prosthetic Hands

Ancient literature and poems contain references to prosthetic limbs, but the earliest historical references originated in the Greek, Roman and Egyptian times. The first prosthetic hands were made up of wood and leather, and were purely for aesthetic appeal. It was not until famous Roman general, Marcus Sergius, lost his hand in the Punic War (218 to 210 BC), that the first iron hand was made (Kulley, 2003). However, this device served only to enable him to hold his shield. Later, during the Dark Ages (500-1500 AD), the first hook prosthesis was made which had very limited functionality and would assist its wearer with only the simplest of tasks. Sadly, at this time there was an 80% mortality rate for amputees, due to poor wound-care practices, thus further scientific research to develop the technology was deemed unnecessary.

It was not until 1504, when Götz von Berlichingen, a German Imperial Knight, lost his hand in battle that a functional, spring-laden mechanical iron hand was developed (Figure 5). From here on out, the development of the prosthetic hand gradually evolved due to the rising number of amputees who lost their hands in battle. The American Civil War and World Wars I and II were major catalysts into the research of more functional devices due to the rising numbers of amputees. Moreover, advances in modern medicine reduced the amputee mortality rate, further increasing the demand for more hands. Other causes of limb loss are more prevalent in modern times, these will be discussed below.

Figure 5 - First mechanically operated hand prosthesis used by Götz von Berlichingen (Angerburg, 2010).

2.3.2. Causes of Upper Limb-Loss

The loss of a limb is one of the most psychologically, physically and financially devastating events that can happen to a person (Gitter & Bosker, 2005). Despite advances in medicine and surgery, amputation continues to be a major problem worldwide, predominantly for older adults, reducing mobility and decreasing the quality of life (Kurichi, et al., 2010). It is difficult to distinguish the leading cause of limb loss worldwide, as the main causes vary for different regions of the world. However, limb loss can be the result of trauma, malignancy, disease or congenital anomaly (Kurichi, et al., 2010). Both developed (first world) and developing (third world) countries will be considered to highlight characteristics that are more prominent in each of these areas, making a more distinguished comparison between their specific needs.

Two studies conducted by the National Limb Loss Information Centre (2008) and the UK Limb Loss Information Centre (2013), considered the leading causes of amputations in the United States and the United Kingdom respectively. Another study by Davies et al. (1970) considered the processes leading up to upper limb amputation, but in the United States only. The findings of these reports are summarised in Figure 6 below, their epidemiology representative of developed nations.

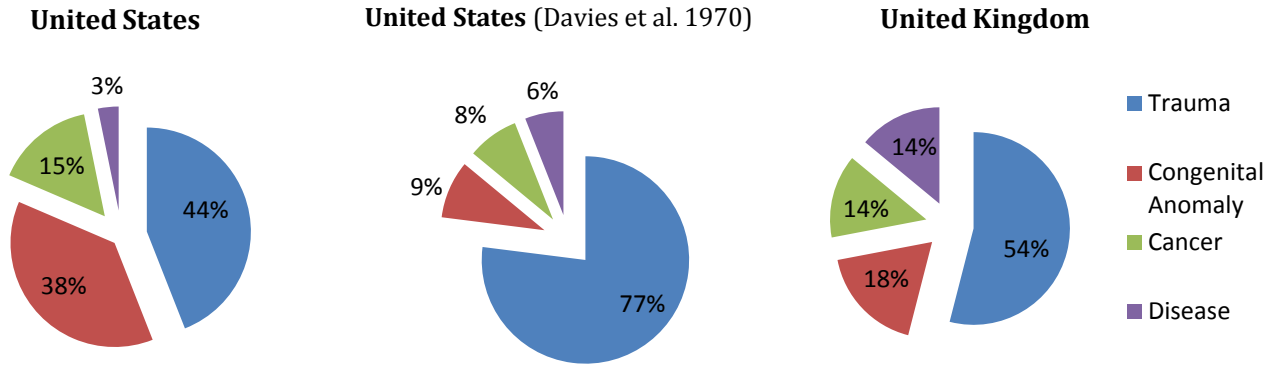

Figure 6 - Upper limb loss by etiology in developed countries by USNLLIC (2008), Davies et al. (1970) and UKLLIC (2013) from left to right respectively.

It can be seen from Figure 6 that the leading cause of upper extremity loss is trauma, which includes mainly mechanical trauma but also electrical, thermal and chemical trauma. Congenital anomalies are the next major cause followed by cancer and disease respectively.

According to Engstrom & Van de Van (1999), issues to consider in developing countries are not only those which affect the developed nations but also additional factors affecting people in these parts of the world. These include warfare, inadequate shelter (e.g. freezing conditions leading to frostbite), poor sanitation (infection), poor accessibility to healthcare and lack of access to modern medicines. Their study conducted on upper extremity limb loss covered both the developed and the developing world, with their comparative results shown in Figure 7.

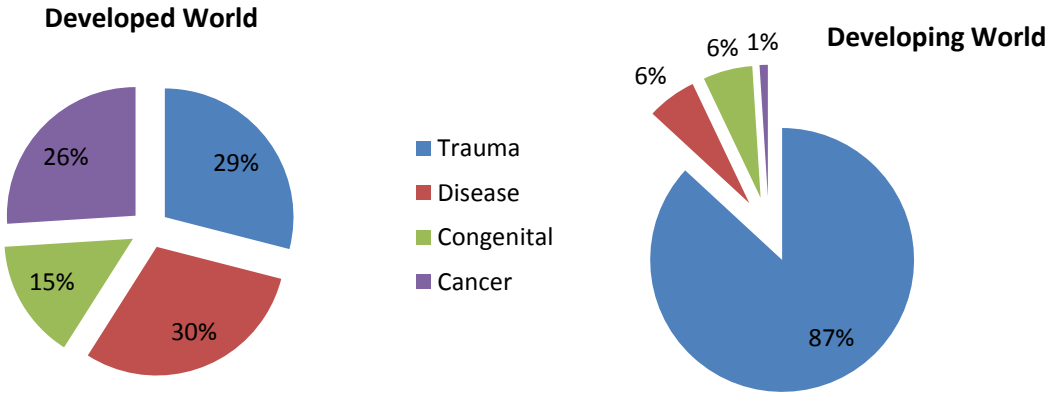

Figure 7 - Upper extremity limb loss by etiology in developed (left) and developing (right) countries by Engstrom & Van de Ven (1999).

Referring to Figure 7, it can be seen that primary cause in the developing world is trauma (87%). This differs substantially from the 29% trauma rate in developed countries, and is primarily a result of

mechanical trauma due to the prevalence of warfare, harsh environmental elements and industrial accidents (Engstrom & Van de Ven, 1999). It can also be noted that the results obtained in Figure 7 for the developed world differ somewhat from those obtained in Figure 6, this can be attributed to the inclusion of other developed countries (other than the US and UK) in which the cause of upper extremity amputation are predominantly diseases such as dysvascularity, infection and neurological disorder; not trauma.

The applicability of this data to this report is that differing causes of limb loss have differing residual limbs/stumps which affect the type of prosthesis design and interface. For example, patients born with a congenital birth defect predominantly have a functioning wrist and hence partial prostheses are made for them. Patients who lose their hand through mechanical trauma have varied amputation locations depending on the incident, whereas diseased or cancer ridden limbs are mostly amputated in a controlled environment enabling surgeons to decide, to a certain extent, where it is best to amputate. Due to the prevalence of mechanical trauma, the largest target market and applicable countries will be discussed.

2.3.3. Target Market Patients and Countries

The targeted patients for the prosthetic hand device are major upper limb amputees, both unilateral and bilateral. More specifically, it will be designed to accommodate the following patients:

- BE - below-elbow (transradial)
- Disarticulation (either through-elbow or through-shoulder)
- AE - above-elbow (transhumeral)

Furthermore, it should be noted that through-hand amputees (minor amputation) will not be included due to the limited space requirements and the unique nature of these types of amputations. Also, the device interface with the socket will be a universal design, whereas the sockets designed by prosthetists are unique to each patient.

The prosthetic device is expected to be used predominantly in the developing world. However, since there is a large gap in the market between low-cost mechanical devices and expensive myoelectric devices, even in developed countries, the application of this device would be widespread (McNaught, 2009). Amongst others, developed countries such as the United States, United Kingdom and Israel are possible target markets. In 2005, the United States alone had an estimated 41,000 major upper limb amputees. Moreover, this number continues to increase due to aging population, diabetes mellitus and dysvascular disease, and is expected to double by 2050 (Ziegler-Graham, et al., 2008). It should also be noted that if a person becomes limb deficient while they are adults, they will typically go through

about 15-20 limbs during their lifetime (Strait, 2006). This increases the market potential for the devices as patients may elect to own multiple devices.

Statistics for amputees in developing countries are more challenging to obtain as they are scarce and in most cases, do not exist. In South Africa, various organisations including Statistics South Africa, Department of Labour, Department of Health, Medical Research Council, and SA Institute for Medical Research (now the NHLS) were contacted regarding amputee data, yet no amputee-specific information was disclosed. Further investigation yielded a report titled "Prevalence of disability in South Africa" (Statistics South Africa, 2001), yet it only referred to disabled persons in South Africa as a whole. This report indicated that 2,255,982 people were suffering from a disability; constituting 5% of the total population. Of this 5%, it stated that 668,082 people (29.6%) had a physical disability. In a more recent survey (Statistics SA, 2010), indications were that number of disabled citizens had increased to 6.3% of the total population. Although these figures are indicative of an increase in the disabled population, they do not specify the type of disability, nor does the prior data suggest what proportion of the physically-disabled population are upper-limb amputees.

Market research conducted by McNaught (2009), involved contacting 27 hospitals, rehabilitation centres and prosthetists to obtain estimates to the prevalence of upper-limb amputees in South Africa. The results yielded a very poor response in terms of completion of data sets, yet of the six responses he obtained from various prosthetists and a hospital, indications were that approximately 50 new upper-limb amputees are seen by them each year. Furthermore, an interview with prosthetist Eugene Rossouw (2013) indicated that he alone receives in excess of 30 new upper limb patients each year. To estimate a total national value would be speculative thus further investigation into the total amputee population would be necessary.

Worldwide, the Landmine Monitor (working in conjunction with 9 European Governments and UNICEF) reported that in 2011 there were a total of 4 286 landmine victims of which 2 907 survived (ICBL, 2012). Furthermore, there were 11-12 reported casualties per day for both 2009 and 2010, whereas a decade ago there were 32 casualties per day. While these do not specify what sort of injury the victims sustained, it very likely resulted in major trauma to the body such as limb loss. The countries affected most by landmines were Afghanistan, Pakistan and Colombia, followed by Burma, Cambodia, Libya, Somalia and Iraq. Furthermore, estimates indicate that the number of amputees in India alone increases by 17,000 each year (Meanley, 1995).

In conclusion, it is clear that a concise number of worldwide amputees cannot be inferred through the statistical resources currently available. However, indications do illustrate that the number of amputees are increasing throughout the developed and developing world. These amputees require access to prosthetic devices to aid them in their Activities of Daily Living (ADLs). As a result, locally

available hand prostheses that are accessible to low to medium income patients in South Africa will be looked at, followed by a discussion of the numerous types of hand prostheses worldwide.

2.4. Standard Government-issued hands in South Africa

In South Africa, low to middle income patients generally have a choice between two categories of prosthetic devices. These are either cosmetic/passive prostheses or cable-controlled prostheses as seen in Figure 8. The latter can be divided into anthropomorphic devices (Figure 8, right), which visually mimic the human hand, and non-anthropomorphic devices such as a hook (Figure 8, middle).

Figure 8 - Cosmetic/passive prosthesis (left), hook type prosthesis (middle) and cable-controlled anthropomorphic prosthesis (right) (Otto Bock®, 2013).

There are two main factors influencing the selection of such prosthetic devices; affordability and patient preference (Rossouw, 2013). The first of these factors is primarily determined by government funding through organisations such as the Workmen's Compensation Fund. However, the limited amount of funding available to patients impairs their access to more functional and aesthetically appealing medical devices which could greatly improve their quality of life (Nel, 2013). Funding is also available through private channels such as medical aid schemes, but since 88.4 % of South Africa's population does not have health insurance (Harris, et al., 2011), the majority of the population is at the mercy of state funding. When considering the cost of these terminal devices, the cosmetic prosthesis costs ± R 6,000, the cable-driven hook ± R 10,000 and the cable driven hand ± R 9 000 (Rossouw, 2013) and does not include the socket, shoulder-harness, consultation or fitment of the device.

Patient preference is primarily determined by the activities that users are inclined to do on a daily basis. If they work with their hands, such as carpentry, they generally opt to use a hook type prosthesis as it is more functional and enables them to perform a host of different activities. Alternatively, if they consult customers on a daily basis and are more concerned with outward appearances, they generally select a cosmetic prosthesis (Rossouw, 2013). In order to better understand the workings of these

devices and compare them to other available devices worldwide, the ensuing section will look at existing types of hand prostheses.

2.5. Existing Types of Hand Prostheses Worldwide

This section details various types of prosthetic hands, the primary emphasis being on the low to medium cost prostheses upon which this dissertation is focussed. In general, the hand designs are either anthropomorphic or non-anthropomorphic in nature.

2.5.1. Cosmetic and Passive Hand Prostheses

Cosmetic or passive hands are hands which are designed for patients who place great emphasis on the natural (anthropomorphic) appearance of the hand. They prefer to substitute active functionality, for a natural look, easy handling, high comfort and a light-weight design. These hands are generally in a lower cost bracket than functioning hands. Two predominantly used cosmetic hands are shown in Figure 9 below.

Figure 9 - Otto Bock cosmetic hand (left) (Otto Bock®, 2013) and RealLifeSkin™ prosthetic hand (right) (RealLifeSkin , 2012).

The Otto Bock® cosmetic hand dominates the world market in terms of units sold and comes in a broad range of models and colours (Rossouw, 2013). The less commercialised RealLifeSkin™ cosmetic hand uses flexible/malleable knuckle joints that allow users to position the fingers into different positions (RealLifeSkin , 2012). Numerous other manufacturers and passive hand designs exist, yet their purpose and function remains the same. Patients inclined to prefer functionality usually select cable-controlled prostheses, which lack aesthetic appeal in comparison to their passive counterparts. These cable-controlled or body-driven prostheses are discussed in the ensuing section.

2.5.2. Cable-Controlled (Body-driven) Prostheses

Cable-controlled prostheses are the original concepts for the functioning mechanical prosthetic hand. The name "cable-controlled" is self-explanatory as these devices combine the use of cables with a guidance system, coupled to a shoulder harness (Figure 10) to actuate the hand. This system enables users to provide an actuating force by simply flexing their shoulders forward, increasing their span and generating linear displacement of the actuating cable. Furthermore, these devices are generally underactuated through the use of various mechanisms such as pulleys, linkages or gears, which allow more degrees of freedom than there are inputs.

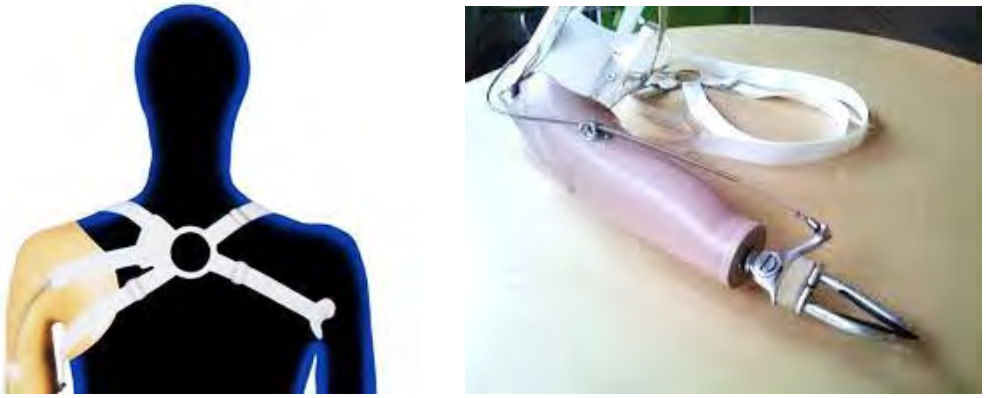

Figure 10 - Body harnesses used to actuate cable-controlled prostheses by Otto Bock® (2013).

This dissertation focuses on incorporating such a mechanical device and coupling it to an actuating system such as a harness (or an electrical actuating system at a later stage), thus it is important to identify and discuss key characteristics of these devices, as well as their advantages and limitations.

The most commonly used cable-controlled prosthesis for finer motor functions is the split-hook type; with two leading commercial producers of these types being Hosmer and Otto Bock® (Rossouw, 2013). Numerous configurations of these devices have been invented (Figure 11), including voluntary opening, voluntary closing and adjustable grip force devices.

Figure 11 – Voluntary-opening spring hook (Otto Bock®, 2013), voluntary-opening elastic hook (Hosmer, 2012), voluntary-closing hook (Hosmer, 2012) and adjustable grasp force hook (Veatch, 2011); from left to right respectively.

Referring to Figure 11, the voluntary-opening split hooks (elastic and spring) are most commonly selected. These voluntary opening devices are made of a host of different materials including aluminium, stainless steel or titanium (Hosmer, 2012), are easy to clean and can grip objects as small as nails. Unfortunately, since gripping an object with a voluntary opening prehensor is passive, users have no control of the force exerted on the object they are gripping (Veatch, 2011), unless the spring or elastic is changed. This factor led to the development of the voluntary opening hand, such as the one by Hosmer (2012), which allowed the user to grasp the object with more force control. Moreover, this device included a locking mechanism that enabled the user to release the tension in the actuating cable while still gripping the object, minimising the effort required to keep hold of the object. Next, a voluntary opening device was developed by Veatch (2011). This device would allow the grasping force to be altered by repositioning a lever which would adjust the tension of the spring member.

While split hook prostheses are favourable in functionality, they lack the aesthetic appeal that the cable-controlled hands have. These types of devices generally make use of an internal mechanical structure (chassis) that is covered by a shaped inner hand and a cosmetic glove. Figure 12 below displays four anthropomorphic hand devices, each from different manufacturers. They are all unique in their own way, yet all provide the similar outputs in terms of motions and grips.

Figure 12 - Anthropomorphic cable-controlled hands by Becker (2013), RSL Steeper (2012), Hosmer (2012), and Otto Bock® (2013), from left to right respectively.

To evaluate their relative performance, the efficiencies of various voluntary-opening cable-controlled devices were compared by Smit, et al. (2012). Nine specimens (five hands and four hooks) from leading manufacturers (including those above) were quantitatively evaluated; measuring actuating forces, pinch forces, mass, cable displacements, opening span, work done and hysteresis. It was found that hooks required the lowest activation force and delivered the highest pinch force, whereas all the hand's pinch forces were lower than required. Furthermore, all the data collected was compared to a similar study conducted by Corin, et al. (1987) and it was found that there was no improvement in device performance, for either the hands or the hooks, bearing in mind that 24 years of research and

development had transpired. A study on commercial voluntary-closing cable-controlled devices by Smit & Plettenburg (2010) was also made, but will be discussed in Section 2.9.3.2, p. 36.

Overall, the primary concern patients have with cable-driven prosthetic devices is the discomfort that the body harness causes; especially in the axilla (armpit) region, due to the large actuating force required to open the hands/hooks (Kargov, et al., 2008). Consequently, alternative actuation systems have been investigated to mitigate the effects caused by body harnesses. These are brought about in the form of hybrid and myoelectric prosthetic systems.

2.5.3. Hybrid Prostheses

Hybrid prosthetic hand systems are ones that incorporate a mechanical hand, with an actuating system that does not draw power exclusively from the body. There are a wide range of designs incorporating drive systems both new and old. A host of actuating methods have been developed including hydraulic, pneumatic and electro-mechanical systems.

Hydraulic systems, such as the one developed by Kargov, et al. (2008) in Figure 13, make use of compliant joints in the fingers with expandable flexible membranes that create a moment about the hinge point when pressurised. The system makes use of a miniaturised hydraulic pump in conjunction with a multiple-valve system, battery pack and control algorithms that trigger individual valves to open or close, moving the interphalangeal joints of the digits.

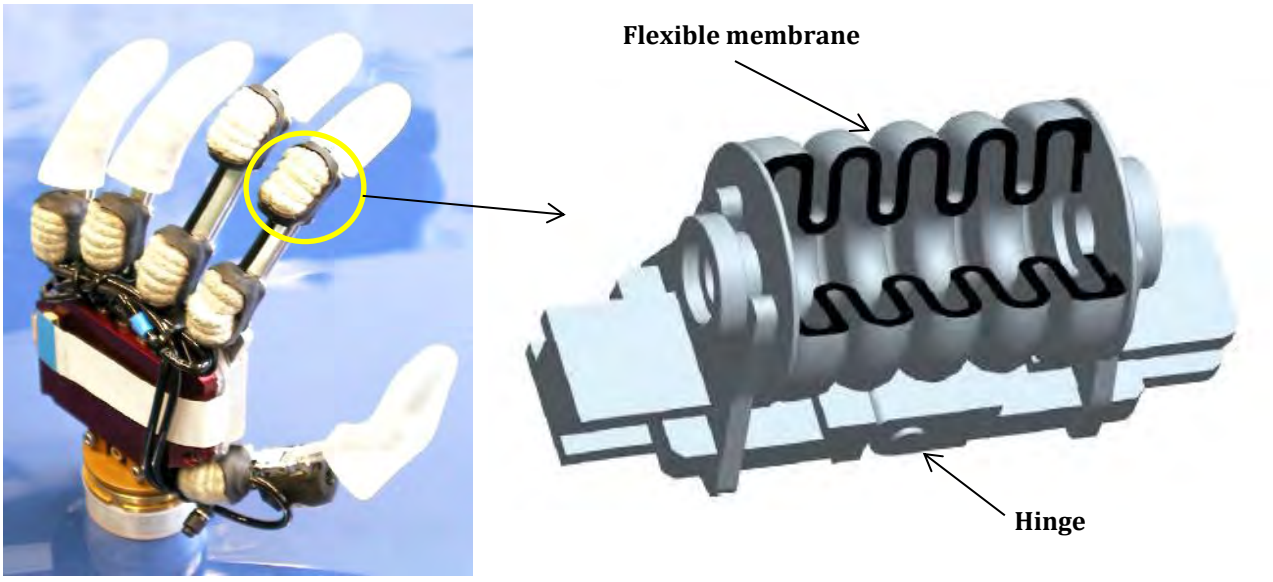

Figure 13 - Hydraulically actuated hand with compliant joints by Kargov, et al. (2008).

These devices are capable of providing a variety of grasps and substantial grasp force, as outlined by Pylatiuk, et al. (2004), while being compact, relatively lightweight and simple. On the other hand, electro-mechanical devices are generally more complex. Pinson (1981) designed a device of this nature (Figure 14) using a host of stepper motors, microprocessors and a control system available at the time.

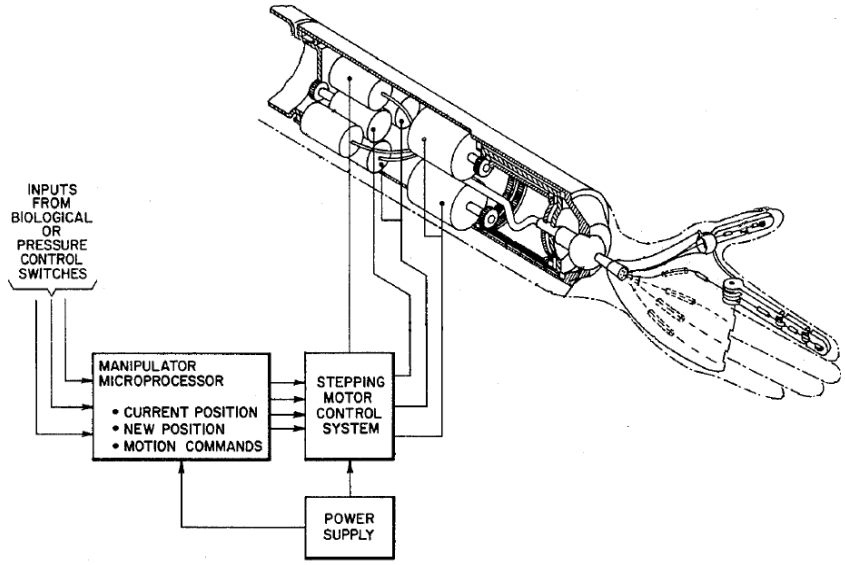

Figure 14 - Electromechanical artificial hand with control system (Pinson, 1981).

However, this system was bulky, contained a lot of components and would not be feasible or comfortable for a patient to wear. Hence, with the advancement of technology and rapid prototyping techniques, Dalley et al. (2009) of Vanderbilt University developed a more compact yet complex extrinsically-actuated servomotor hand (Figure 15). This hand would be powered by servomotors and weigh a total of 580 g. Furthermore, it is able to actuate each finger individually, as well as rotate the thumb to create opposition or a lateral pinch grip. Nevertheless, the size of both of the aforementioned devices makes it challenging to adapt to all below-elbow (transradial) patients because the actuation unit is located in the forearm compartment.

Pneumatically operated devices such as the RAPHaEL Hand (RoMeLa, 2010) shown in Figure 15, use compressed air to actuate compliant joints. These joints work according to the same physical principles as the aforementioned hydraulic hand, with corrugated flexible tubing and a hinge. Moreover, this hand combines the use of flex sensors and force sensitive resistors for position and force measurements respectively. Overall, their cost, size and complexity has led these hands to remain in the research domain, while the more compact myoelectric hands, discussed in the following section, experience the greatest commercial exposure.

Figure 15 – Hybrid servomotor extrinsically-actuated hand (Dalley, et al., 2009) and the pneumatic RAPHaEL hand (RoMeLa, 2010).

2.5.4. Myoelectric Prosthetics

These are the prostheses into which most research and development is being invested, as well as the most public interest. These devices are actuated through a series of electric motors, driven by a battery pack and are triggered through the use of muscle-signals collected on the skin of a patient by using EMG (electromyographic) surface electrodes. Moreover, these signals are filtered and undergo signal processing before reaching the motors and other components. There are multiple companies developing these devices on a commercial platform; examples of some of their designs are shown in Figure 16 below.

Figure 16 - Myoelectric hands: Bebionic 3 by RSL Steeper (2013), iLimb™ by Touch Bionics (2013), Michelangelo Hand by Otto Bock® (2013) & EPFL sensory hand (Paik, et al., 2012). (Top left & right, bottom left & right respectively).

Referring to Figure 16, it can be seen that the design and aesthetics of these devices are similar. The EPFL Sensory Hand has touchpads on the fingers of the device which provide sensory feedback to a vibrating motor inserted onto the patients forearm, telling them when contact has be made and how much grip force is being exerted. The remaining hands each use between 5 & 7 motors to actuate individual fingers to allow a host of various grip types.

In general, these devices offer advantages in appearance, increased pinch strength, lack of harness and ease of operation (Biddiss & Chau, 2007). Furthermore, their compactness and simplicity of recharging the energy source makes electrically powered devices superior to other externally actuated hands such as the aforementioned hybrid hands (Kargov, et al., 2008). However, disadvantages include increased maintenance such as battery and glove replacement, higher weight, slower actuation speed and high cost (between R60,000 and R500,000 (Rossouw, 2013)). Most significantly, these devices cannot operate without their stored battery power, as a manual crossover to body-power is not possible. In light of this, it would be beneficial to design an efficient mechanically-actuated hand in combination with a myoelectric system, such that a manual crossover mechanism would be possible should difficulties with the electrical system be encountered.

The four primary classes of hand prostheses have been discussed, and their benefits and drawbacks considered. Even with current technology, the split-hook type devices still remain the most frequently used prosthetic device. The reasons for this include their "*practicality and ease of use for accomplishing typical tasks, high durability, light weight, and low cost*." (Belter, et al., 2013). If their specifications and features alone were compared to those of other devices, they would never be considered the "best" device, but through its practicality the split hook remains the most common choice. Focus should therefore be attuned to not only develop a hand which functions and performs well, but also caters to the needs and concerns that patients currently have.

2.6. Patient Preferences, User Needs and Concerns

Even though relevant features and specifications of prosthetic hands can be compared, the end goal is to create a device which is practical to users. It is important to take these practical factors into consideration as users may abandon the devices if they experience discomfort and unnecessary frustration. Consequently, it is essential to identify the key preferences, needs and concerns that patients have previously experienced, in order to address them appropriately.

A study conducted by Biddiss & Chau (2007) looked at numerous investigations on the use and abandonment of upper limb prosthetics over a twenty-five year period. The scope included studies on adults as well as paediatric cases with focus on cosmetic, body-driven and electrical/myoelectric prostheses. Although body-driven systems (hooks and hands) are the prosthetics of choice, they found that these had a rejection rate between 16% and 66 %. Moreover, the rejection rate of body-powered hands was as high as 80% to 87% in some cases, with major complaints being slowness in movement, difficulty in cleaning and maintenance, awkward use, excessive weight, insufficient grip strength and high energy expenditure needed to operate them. Other consumer complaints included harness

discomfort and/or breakage, abrasion of clothing, wire failure, unattractive appearance and excessive wear temperatures.

Short term goals to improve these devices included developing more durable cables, improving glove material and creating more comfortable harnesses. Long-term goals were aimed at increasing wrist movement, improving control mechanisms and enabling coordination of multiple joints. To alleviate attachment problems, researchers are focussing on customised socket design and osseo-integration of attachment stems, but a key contributor to interface discomforts and user fatigue is weight (Belter, et al., 2013). In an internet survey of myoelectric prosthetic users 79% considered their devices too heavy (Pylatiuk, et al., 2007), and similarly when questioned on design priorities users rated weight at 70 on a scale of 0 (not important) to 100 (important) (Biddiss & Chau, 2007). The hand design is therefore aimed at being as lightweight possible, to minimise user discomfort.

A concern raised in an interview conducted by the author with a bilateral amputee using two hook prostheses (Lapsley, 2013), is that gripping a spherical object such as a doorknob is almost impossible for him. He went on to say that he would be willing to test a new prosthetic device yet needed to be convinced that it would improve his quality of life; before spending unnecessary time adapting to a device that would not provide this benefit . This is a critical factor to consider in the adoption of a new device, as it will not be viable if prosthetists and patients do not trust the device. Kyberd, et al. (2007), compared the satisfaction of patients using cosmetic devices to that of patients using electric devices and found no significant statistical difference in the results between the two. However, of the numerous factors mentioned, donning and doffing the device more easily as well as providing easier maintenance were two major concerns (Figure 17). Furthermore, the numerous areas of improvement identified by users can be seen in Figure 18. It should be noted that the sum of percentages are greater than 100% as users were allowed to name as many as three improvements.

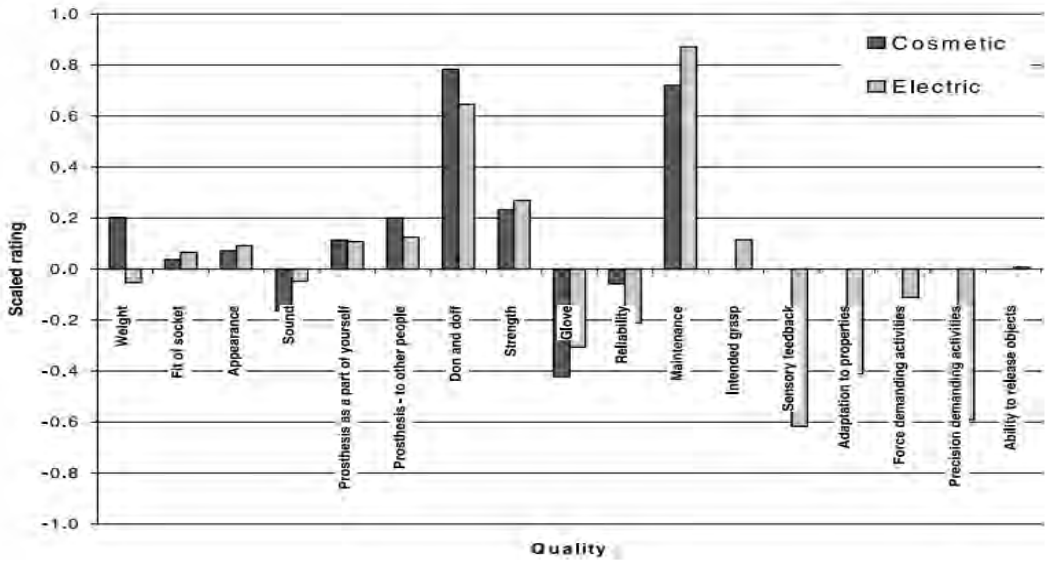

Figure 17- The areas of improvement identified by the respondents analysed as a percentage of the number of respondents for electric and cosmetic prostheses by Kyberd, et al. (2007).

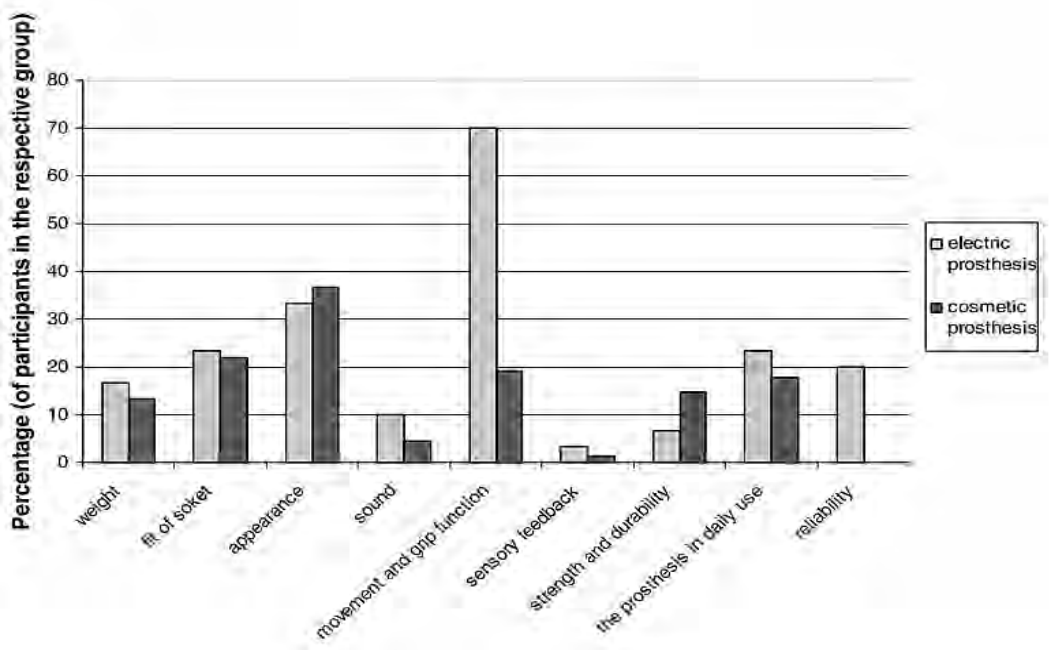

Figure 18 - Areas identified for improvement by users of electric and cosmetic prostheses. Values are expressed as percentages of the number of respondents in each group, electric (30) and cosmetic (68).

Referring to Figure 18, appearance, fit of socket, and movement & grip function rated the highest amongst the identified areas of improvement. This conforms to the three C's, namely "Cosmetics, comfort, and control", mentioned by a Delft University researcher when asked on what one should focus during the design of hand prostheses. The qualitative factors mentioned in this section will be used to aid in the weighting of performance measures utilised in the Decision Support Matrices in Chapter 3; assisting in the quantitative selection of concept solutions.

2.7. Underactuated Finger Systems

In the design of the fingers, actuation can be achieved through numerous mechanisms. Furthermore, to increase the simplicity of the design and reduce the cost, these mechanisms/systems are predominantly underactuated. Underactuated mechanical mechanisms ensure that these designs have a cost advantage over similar electronic solutions which use one motor per output, and electronics to synchronise them (Rothenhofer, 2009). Designs of this nature include tendon-pulley systems, linkage systems and gear driven systems.

2.7.1. Tendon-actuated Finger Systems

Tendon-actuated systems most closely mimic the anatomical mechanisms of the fingers. Anatomically, the flexors of the fingers are continuous, each travelling through a guide known as a sheath or retinaculum (A1-A5, Figure 19), and insert at the inferior distal end of the distal phalanges. This mechanism has been perfected by the evolution of the body, and is also at its most efficient physiological state (Vicatos, 2013).

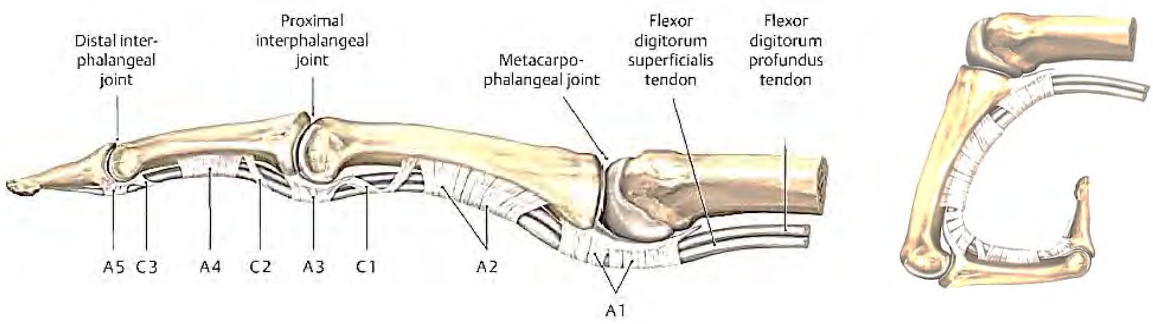

Figure 19 - Tendons of the finger used for flexion (Gilroy, et al., 2008, p. 304).

The flexure the tendons initiates the closing of the hand. Prosthetic hand designs incorporating the use of tendon mechanisms, require only a single actuating force (F_a in Figure 20) at the proximal member to flex the entire finger. In order to guide the tendon cable to its insertion point on the distal

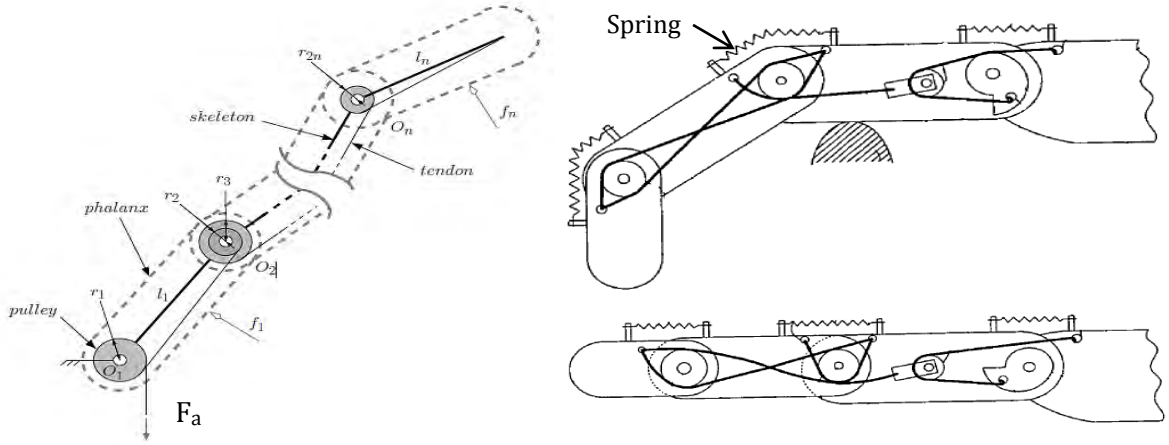

Figure 20 - Tendon-pulley systems using three phalanges by Birglen, et al. (2008) and Higuchi & Harada (2005); left and right respectively.

phalanx, two primary types of routing schemes are used, namely tendon-pulley or tendon-channel routing. Tendon-pulley routing, as in Birglen, et al. (2008) and Higuchi & Harada (2005) uses a pulley system which enables the fingers to close according to a predetermined trajectory as seen in Figure 20. To return the finger to the open/extended position Higuchi & Harada (2005) use linear springs located superiorly to the interphalangeal joints. Advantages include low-friction due to the pulleys and control of closing trajectory, whereas disadvantages include reduced grip conformability and dislocation of actuating wires from pulleys when actuating tension is lost.

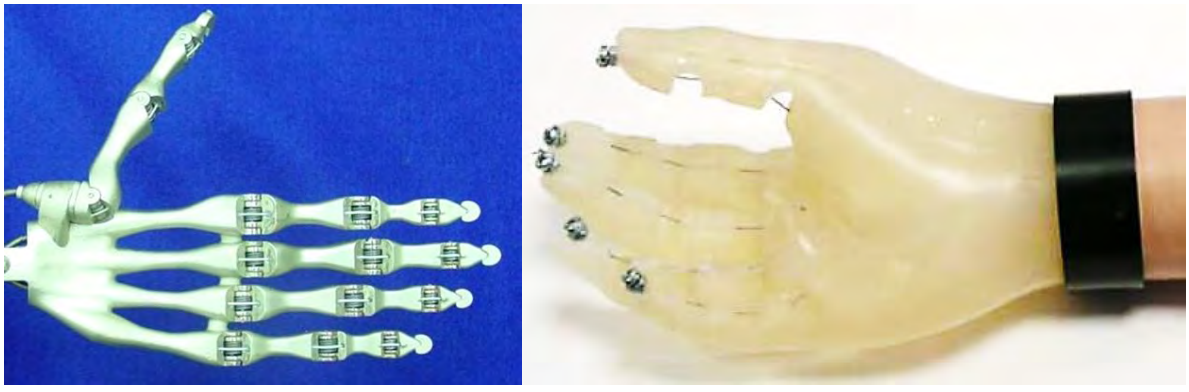

Figure 21 - Tendon-actuated myoelectric hand (left) and silicon hand (right) by Dalley, et al. (2009) & Carrozza, et al. (2005) respectively.

Tendon-channel routing, as in Dalley, et al. (2009) and Carrozza, et al. (2005), use tendons running directly on the channel material as seen in Figure 21. Advantages of these designs include simplicity, compactness, ease of manufacture and low cost, whereas drawbacks involve abrasive and thermal wear of phalangeal channel due to cable contact forces and friction heat generated during relative translative motion. The following section will look at the workings of underactuated linkage systems.

2.7.2. Linkage-driven Finger Systems

Mechanical linkages are used in numerous applications due to their ability to precisely follow a fixed trajectory as well as transmit & amplify an input force through mechanical advantage. The main benefit of this finger mechanism is that shape-adaption to a grasped object is easily attained; ensuring repeatability and grasp stability during each cycle (Birglen, 2006). Furthermore, they have a cost advantage over similar electronic solutions that use one motor per output instead, of an underactuated mechanism. Figure 22 shows two types of mechanisms by Dechev, et al. (2001) and Jang, et al. (2013), which incorporate multiple rigid members to create an underactuated finger mechanism.

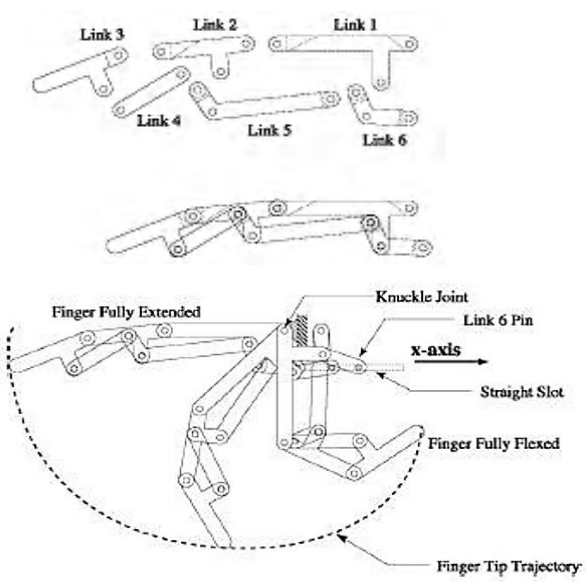

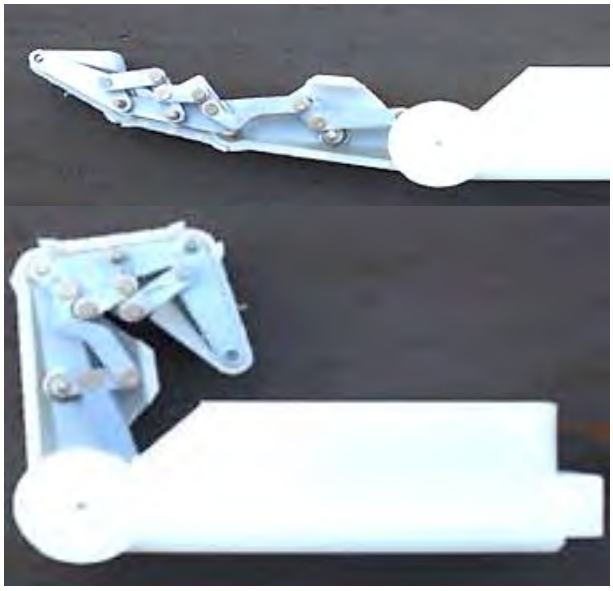

Figure 22 - Finger linkage system (left) with exploded view (top), assembled (middle) and trajectory (bottom) (Dechev, et al., 2001) as well as a Multiple Linkage Mechanism by Jang, et al. (2013) (right).

The trajectory of the mechanism by Dechev, et al. (2001) can be seen on the bottom left of Figure 22, requiring only a single input force along the x-axis to initiate the motion. However, both of these mechanisms require an input force to flex and to extend the finger, whereas the spring mechanism shown in Figure 20 ensures that strain energy will return the finger to its neutral position. A finger mechanism by Bacon & McNaught (2011) uses a similar mechanism to Dechev, et al. (2001) but incorporates a linear spring in series with the straight slot seen in Figure 22 to perform the same function.

Disadvantages of linkage designs include large numbers of components and links, making them more susceptible to fail/loosen if not joined correctly. Moreover, assembly of this mechanism is lengthy and if over-tightened, the friction between adjoining members create a need for a large actuating force.

2.7.3. Geared Finger Systems

Geared systems, much like linkage systems, require many components to function. They generally make use of linkage structures for the phalanges, gears to transmit the driving force and motors to initiate movement of the mechanism. Furthermore, alignment and lubrication of the gears is critical to ensure smooth meshing and reduced noise. An example of this mechanism is shown in Figure 23 below.

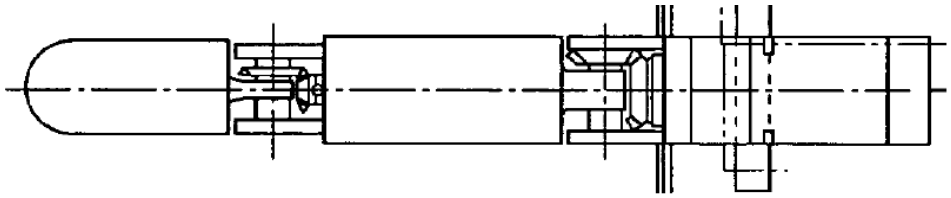

Figure 23 - Bevel gear finger actuation mechanism by (Kameda, et al., 2006).

The detailed design of this bevel gear system is outlined in US Patent 7059645-B2 by Kameda, et al. (2006) and makes use of a single motor in the base of the finger which rotates the bevel gear, which in turn rotates the proximal joint. Similarly, the distal bevel gear combination is driven by a second motor located inside the middle compartment, closing the distal joint. Another design incorporating gears and linkages is shown in Figure 24. It makes use of a planetary gear system to drive the mechanism and has rigid linkages attached to the planet gears, which allow medial and lateral deviation of the finger. However, this system is bulky, complex and likely to be too costly for the scope of this dissertation.

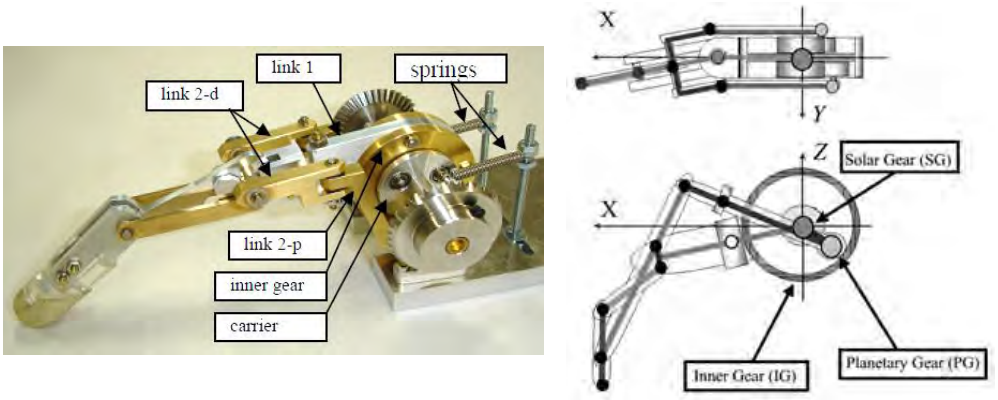

Figure 24 - Planetary gear driven system by (Koganezawa & Ishizuka, 2008).

Lastly, a geared finger design by Zhang, et al. (2009) makes use of a bevel gear, rack & pinion combination as seen in Figure 25. Moreover, it incorporates a torsion spring to keep the distal end of the finger extended until the middle phalanx is blocked by the grasped object. Once blocked, an active

pinion on the proximal shaft engages the rack, which in turn engages a passive pinion on the distal shaft, rotating it and causing the distal joint to flex.

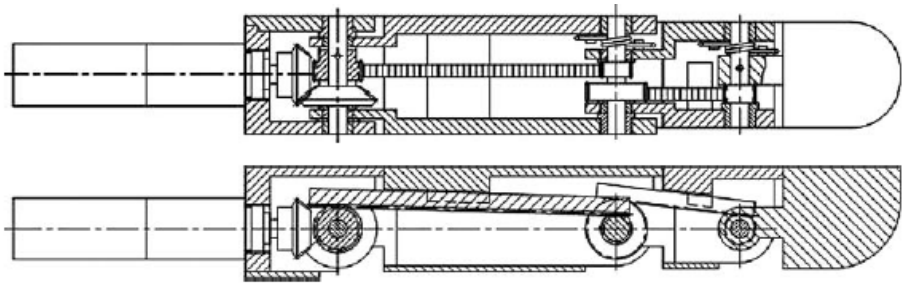

Figure 25 - Bevel gear, rack & pinion underactuated finger by Zhang, et al. (2009).

While this system is novel in its design, it is overly complex and requires many moving parts. Moreover, the mechanism requires actuation by means of a rotary input such as a motor (likely a brushed DC motor) or a purely mechanical linear-to-rotary motion mechanism.

The concept evaluation and selection of the underactuated finger system that is best suited to fulfil the requirements of this dissertation can be found in Section 3.1. (p. 50) in the ensuing chapter.

2.8. Underactuated Differential Systems for the Hand

Now that underactuated finger mechanisms have been discussed, there is a need to couple the digits by further underactuating the hand. Since each finger/digit requires a single input force to operate, a differential mechanism is needed to link the fingers, carrying forward the underactuation principle to the hand. Consequently, the entire hand can be actuated by a single input force through one of the differential systems discussed below. Namely, the moveable pulley system, the seesaw (differential lever) mechanism, the fluidic T-pipe system and the planetary/bevel gear differential systems.

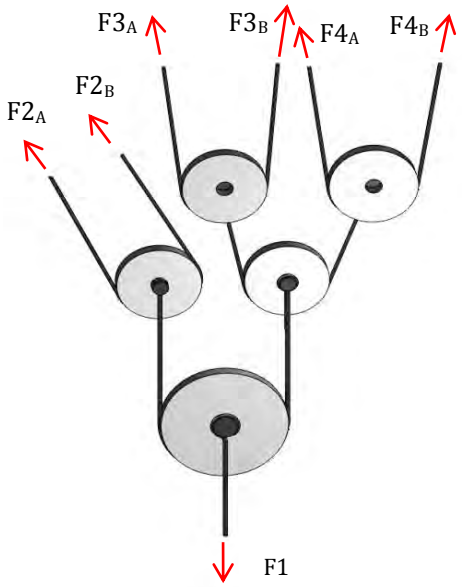

Figure 26 - Moveable pulley system for underactuated hand/palm mechanism.

2.8.1. Moveable Pulley System

Moveable pulleys are used in numerous applications and are beneficial in that they create multiple outputs for a single input, generate mechanical advantage and are force isotropic (i.e. the two output forces are equal). Furthermore, the use of tendons/cables as driving elements generates a low friction platform for efficient force transmission. On the contrary, poor tendon routing may predispose the system to increased friction and poor force distribution (Birglen, et al., 2008). Referring to Figure 26, it can be seen that there are a total of 6 outputs ($F2_A$ to $F4_B$) and only a single input force (F1). Moreover, each pulley has two degrees of freedom, namely

rotation about its central axis and translation perpendicular to that axis. A practical example of this mechanism is shown in Figure 27 whereby underactuated fingers are driven through a moveable pulley mechanism.

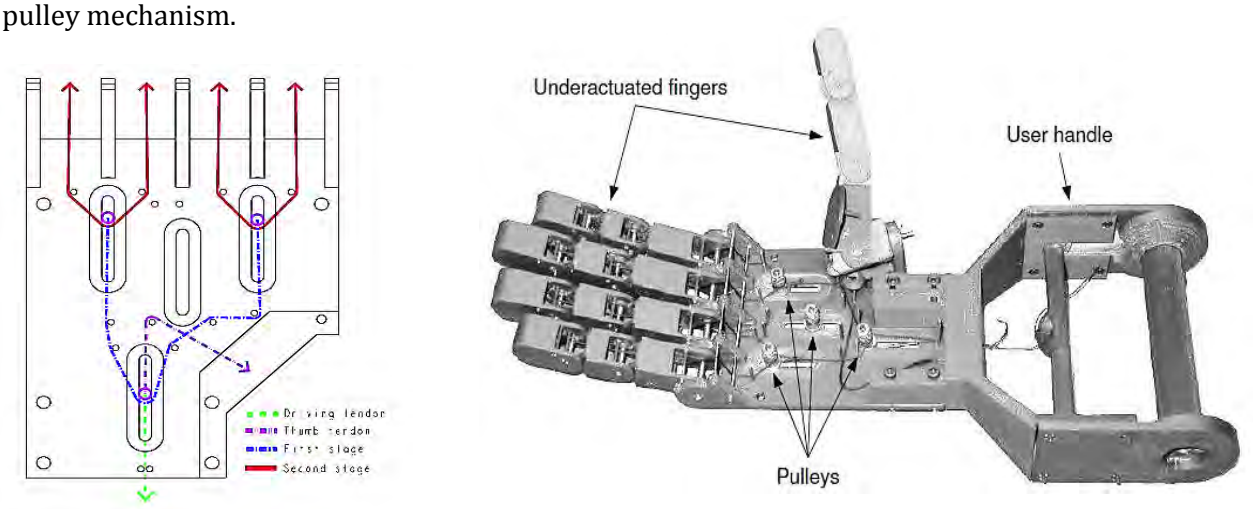

Figure 27 - Moveable pulley system with tendon routing for an underactuated hand by Gosselin, et al. (2008) and Birglen, et al. (2008, p. 165) left and right respectively.

2.8.2. Seesaw (Differential Lever) Mechanism

The seesaw mechanism, or differential lever, works in a similar fashion to that of the movable pulley system. Each time a seesaw is linked in series to an adjoining member, the degree of underactuation is increased. Furthermore, each individual seesaw has a single input and two outputs, classifying it as a differential mechanism according to the IFToMM (1991), which defines a differential mechanism as a "*mechanism for which the degree of freedom is two and which may accept two inputs to produce one output or, may resolve a single input into two outputs."* A representation of the seesaw mechanism by Birglen, et al. (2008) as well as a differential lever hand is shown in Figure 28 below.

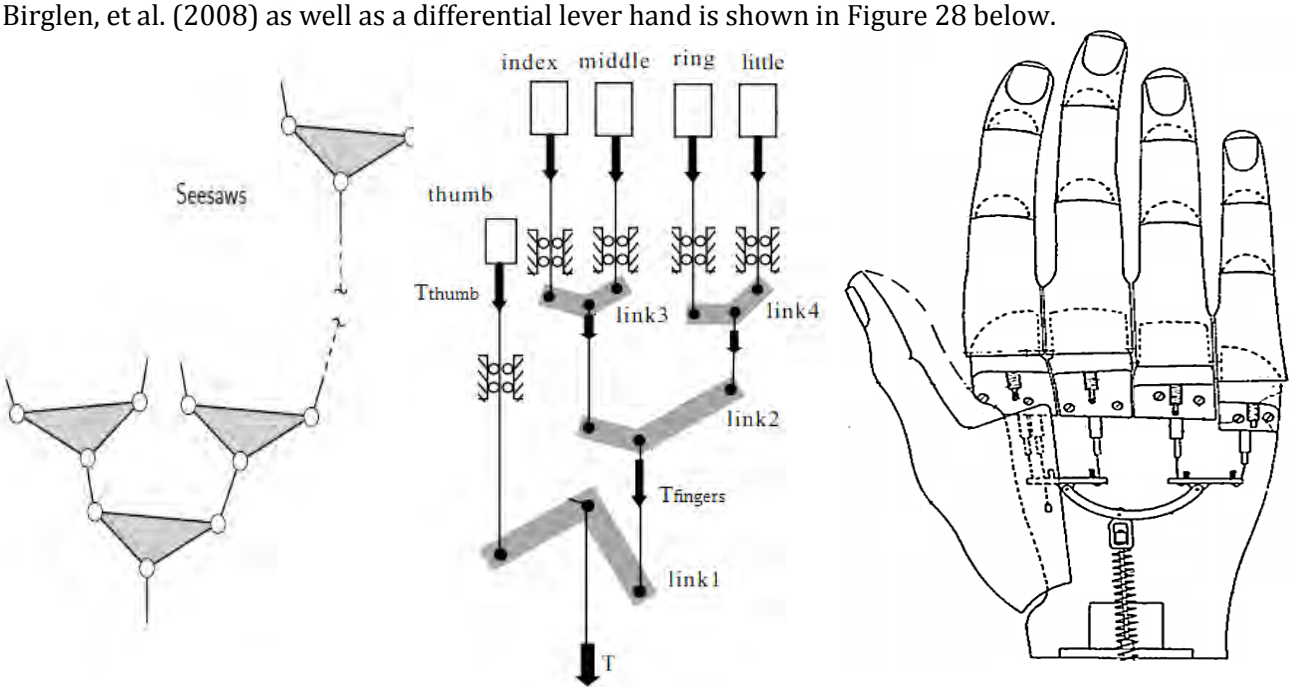

Figure 28 - Seesaw mechanism (left) by Birglen, et al. (2008, p. 16), differential lever hand configuration (centre) by Kamikawa & Maeno (2008) and underactuated hand design (right) by Monestier (1987).

The benefit of the seesaw mechanism over the moveable pulley system is that the tendons are fixed to each seesaw; ensuring that the tendons remain connected if tension is lost. Also, the geometry of the seesaws can be altered to modify the lever length of the outputs, which enables uneven distribution of force. This distribution mechanism is effectively used by Kamikawa & Maeno (2008), who focussed primarily on mimicking the human hand's force distribution. The differential lever hand in Figure 28 above is another example of a seesaw mechanism, using a hinge point on the medial aspect of the hand and an input force on the lateral aspect. Moreover, the tendons to the fingers are attached between these points allowing the lateral digits to flex prior to the medial digits, similarly to the anatomical grasp. Similarly, Monestier (1987) disclosed a design using a differential lever mechanism in combination with a linearly-actuating spring as shown in US Patent 4685929.

2.8.3. Fluidic T-Pipe System

The simplest method to distribute one input into two outputs may be using a T-pipe scheme. It takes advantage of the deformability of fluids to flow/separate into two or more distinct streams, which enable these systems to be less complex than equivalent pulley and seesaw transmissions (Birglen, et al., 2008). Furthermore, the output forces of this system are constant and independent from the output position. Moreover, force isotropy is easily achieved by making the areas of the output sections equal; using the conservation of pressure in a fluid, directly relating the pressure of the system to the output force. Other advantages of these systems are their low space requirements, design simplicity, and efficiency of force transmission. Figure 29 shows a basic representation of how T-pipes may be connected in series to provide multiple inputs.

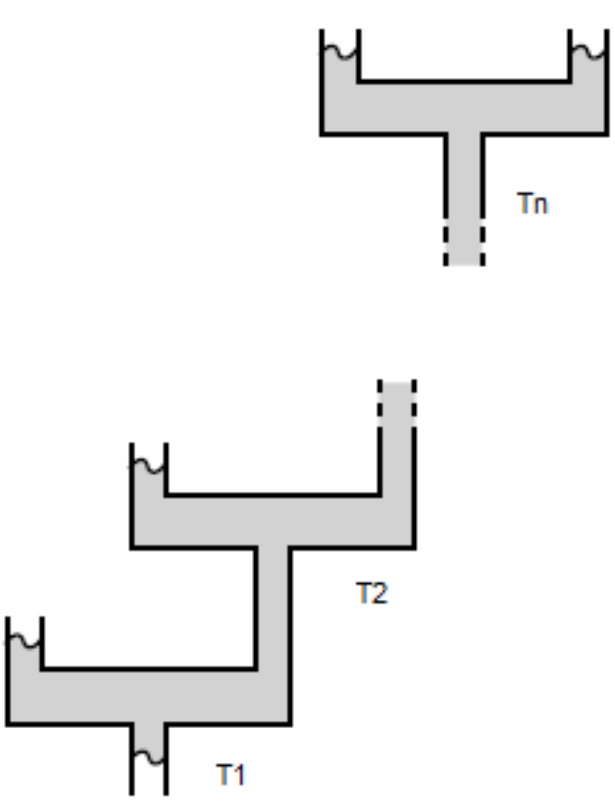

Figure 29 - Basic representation of a fluidic T-pipe system in series (Birglen, et al., 2008, p. 16).

Challenges related to these systems are increased weight due to the transmission fluid, the need for a fluid reservoir, risk of leakage and the need for a pressurising/pumping mechanism to mobilise the fluid. Adjustment of forces either requires new piping and flow nozzles, or it requires a more complex throttling system that may or may not fit within the confines of the prosthesis.

2.8.4. Planetary and Bevel Gear Differentials

These differential mechanisms are predominantly, if not exclusively, used in applications using electronically actuated hand systems. The planetary gearing system is used in the Michelangelo hand by Otto Bock (2013) and by Luo, et al. (2004). These mechanisms, as seen in Figure 30, allow a constant torque output which is independent of its output position; much like the fluidic T-pipe system allows a constant force. Furthermore, they are able to mechanise multiple geared outputs simultaneously as incorporated by the SARAH hand Figure 30 (Laliberté & Gosselin, 2003).

Advantages of these devices are their reliable mechanical transmission and constant torque output. However, disadvantages include complexity in design, size, high cost, increased mass and requirement of rotary actuation energy.

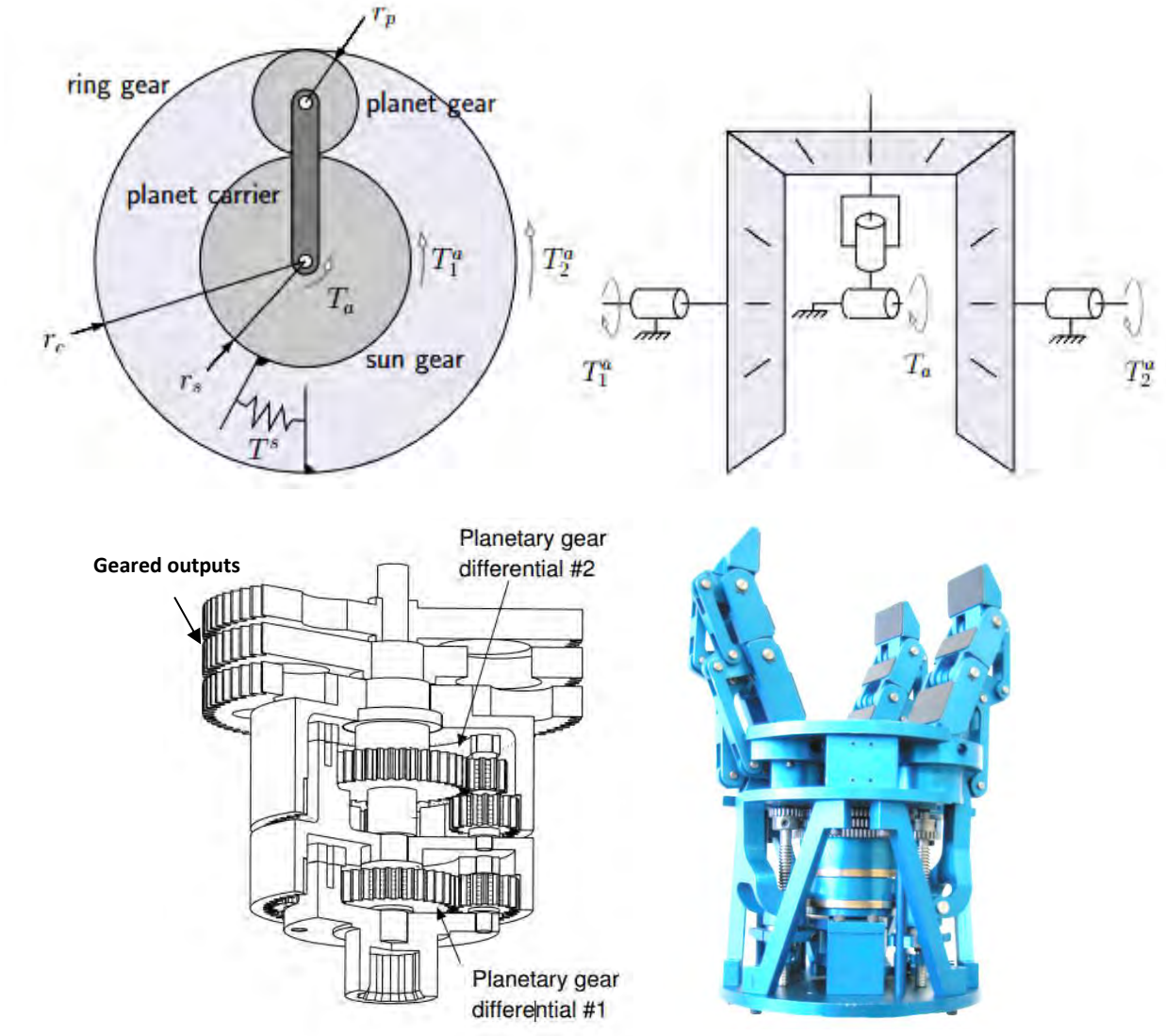

Figure 30 - Planetary (top left) and bevel gear (top right) differential systems for use in underactuation of hands by (Birglen, et al., 2008, p. 147) with SARAH hand planetary gearbox (bottom left) and assembly (bottom right) (Martin, et al., 2001).

2.9. Ranges of Motion, Grasp Types and Grasp Forces

In order to understand the mechanisation needs of the hand; its motion and force transmission needs to be evaluated. Consequently, this section will deal with the types of grasps, ranges of motion and typical loading conditions & forces experienced by the hand.

2.9.1. Types of Grasps

The movements of the anatomical hand can be divided into two main groups; namely, prehensile movements and non-prehensile movements. Prehensile movements are of interest as they involve the hand gripping an object within the compass of the hand, whereas non-prehensile movements are those involving the hand pushing or lifting an object, without grasping it. Moreover, a fundamental requirement for a prehensile grip is grasp stability, i.e. that the object being grasped is stable, regardless of whether it is fixed or freely moveable (Napier, 1956).

Prehensile grips are then further divided into two primary categories; namely, power grips and precision grips. Power grips are ones in which the object being held is clamped between the fingers and the palm; with the thumb lying more or less in the plane of the palm. On the other hand, precision grips are ones in which the object is held between the partly flexed fingers and the opposing thumb (Napier, 1956). Both of these grip types can be further subdivided into specific grasp types, as identified by Cutkosky (1989). The taxonomy of these grasps is identified in Figure 31 below.

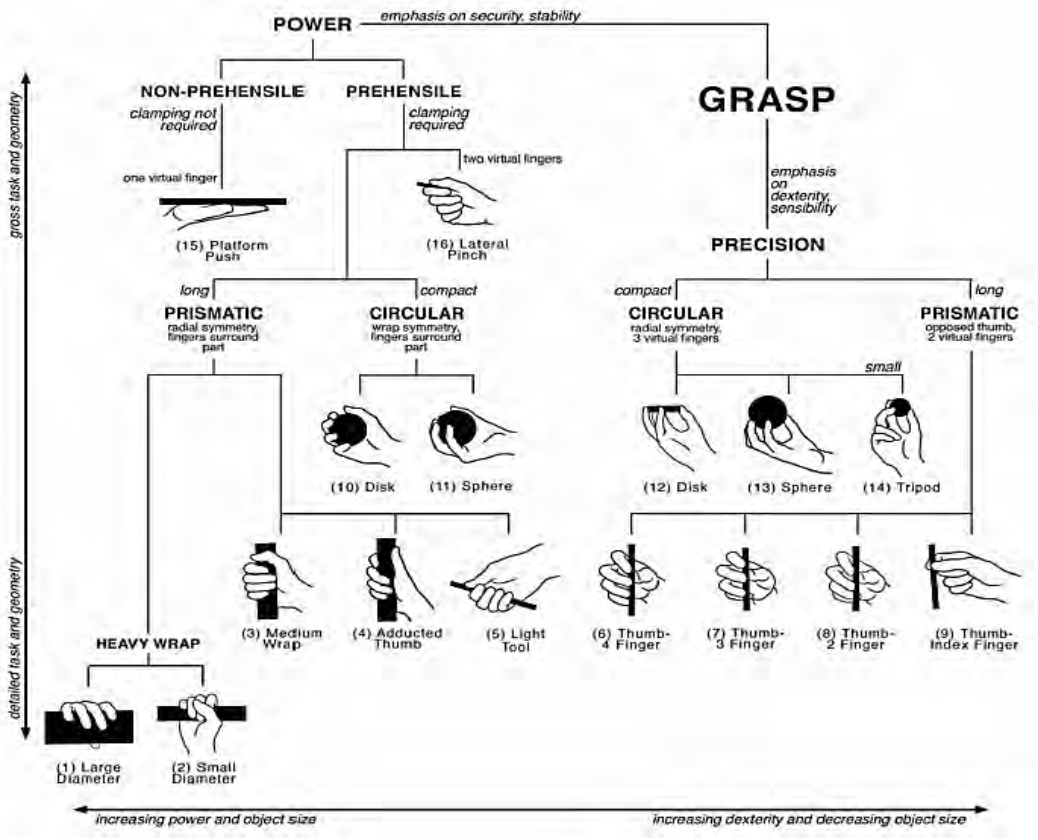

Figure 31 – Cutkosky grasp taxonomy adapted from Cutkosky (1989) by Zheng, et al. (2011, p. 4170). Re-printed with permission.

Although it would be ideal to mimic all functions of the anatomical hand, cost and time restraints make it necessary to identify the grips most commonly used. Consequently, a study by Zheng, et al. (2011) was considered to interpret which grasps were best suited to cover the broadest range of activities. Moreover, this study extended that of Cutkosky (1989) and included both machinists & housemaids; identifying the prominent types of grasps used by each group in their Activities of Daily Living (ADLs). The top six grasps of each group is shown in Figure 32 below.

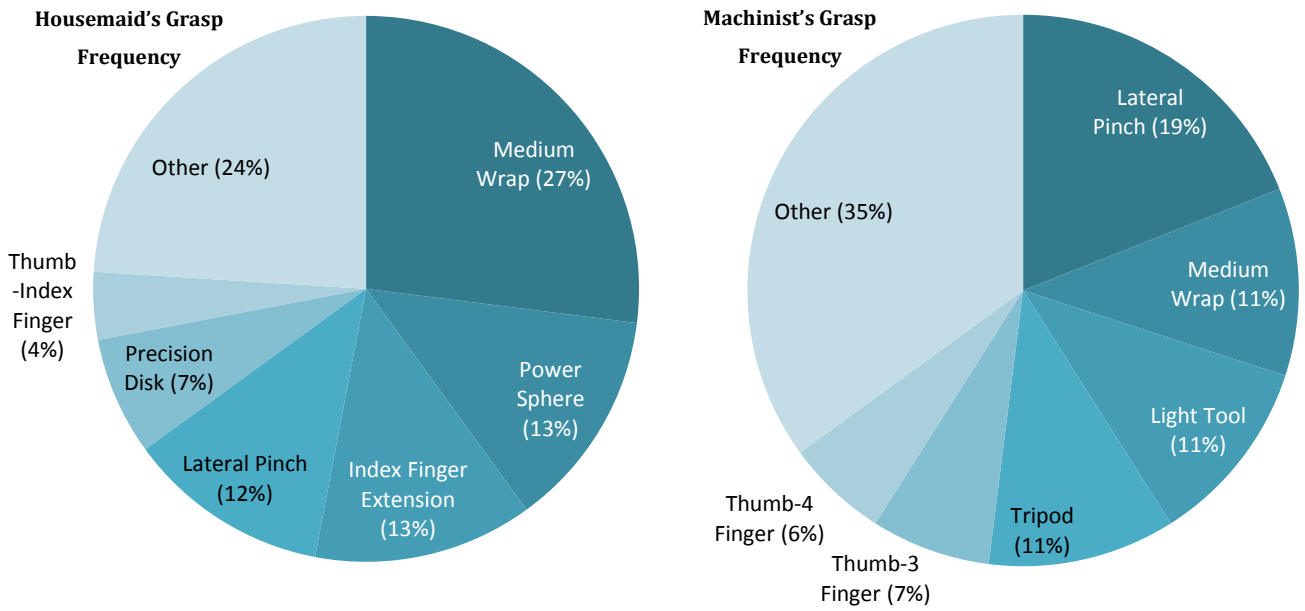

Figure 32 - Grasp taxonomy of a machinist (left) and housemaid (right) by Zheng, et al. (2011) indicating frequencies of use.

The data obtained by Zheng, et al. (2011) correlates well with data obtained by Light, et al. (2002), in which a standardised method of evaluation for pathologic and prosthetic hand functionality was established. This method, known as the Southampton Hand Assessment Procedure (SHAP), reduces eight types of grasp patterns in the Sollerman method, identified by Sollerman & Ejeskar (1995), to six main types of grasps used in ADLs. Their estimated frequencies of use are shown in Table 3 as follows:

Table 3 - Grasp taxonomy for the SHAP protocol identified by Light, et al. (2002).

Grasp	Estimated Frequency of Use
Power Grip (Medium wrap)	25%
Lateral Grip (Lateral Pinch)	20%
Tip Grip (Thumb and Fingers)	20%
Spherical Grip (Power Sphere)	10%
Tripod Grip	10%
Extension Grip (Index finger Ext.)	10%
Other	5%

Referring to Table 3, it can be seen that power grips are most prominent, followed closely by lateral and tip grips. The power grip defined here is similar to the medium wrap and power sphere defined by Zheng, et al. (2011). Furthermore, they had similar frequency of use for both the housemaid and the machinist. In fact, the same could be said for the lateral grip, which had only a 1% deviation from the machinist's result and 8% deviation from the housemaids'. In an interview with a bilateral amputee (Lapsley, 2013) at the Pinelands Prosthetic Centre, the amputee told the author that it was challenging to open spherical doorknob; hence, a spherical precision grip shall be included into the final grasp taxonomy too.

Consequently, the minimum grasp requirements for the prosthetic hand will include, but are not limited to, the following six grasp types shown in Table 4:

Table 4 - Final grasp selection for the prosthetic hand (minimum requirements).

Grasp Classification	Grasp Type		Application
Power	Medium Wrap	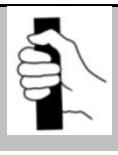	Holding a cylindrical jar.
	Power Sphere		Pouring water from a carton or using a cloth.
	Lateral Pinch	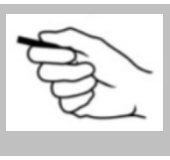	Pouring water from a jug or using a key.
Precision	Index Finger Extension		Simple page turning or typing.
	Tripod grasp		Grasping food while chopping. Eating crisps.
	Thumb - 3 Finger (tip grasp)		Picking up a pencil.
	Precision Sphere	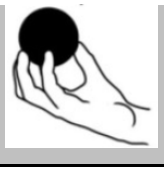	Turning a doorknob.

* All images reprinted with permission from (Zheng, et al., 2011)

2.9.2. Ranges of Motion and Kinematics of the Hand

Now that the grasp types have been selected, the ranges of motion (RoMs) for each joint of the hand need to be identified. These include the motion of the three finger joints; namely, the metacarpo-phalangeal (MCP), the proximal interphalangeal (PIP) and the distal interphalangeal (DIP) joint. Moreover, they include movements of the thumb at the basal joint, metacarpo-phalangeal and interphalangeal joints, as well as the degree of extension/flexion and radial/ulnar deviation of the wrist.

Ranges of motion can be divided into either active RoMs or functional RoMs. Active RoMs are ones in which the motion is achieved using only the muscles, without external assistance; whereas functional RoMs specify the range in which ADLs are performed (Bain, et al., 1997). In order to mimic the anatomical hand as far as possible, studies containing anatomical hand motions (not robotic hands) were considered, both active and functional. While individuals have varying RoMs due to age, body habitus and genetic background, the selected studies included a broad range of test subjects; hence the results may be considered representative of healthy, asymptomatic adults. Active ranges of motion obtained from five independent studies are shown in Table 5 below.

Table 5 – Active ranges of motion of the joints of the anatomical hand.

	Joint(s)	Motion	Angular Range			
			[1]	[2]	[3]	[4]
Finger(s)	Metacarpophalangeal (MCP)	Hyper Ext. / Flex.	45H/90°	0/100°	0/109°	30H/90°
	Proximal Interphalangeal (PIP)	Extension/Flexion	0/100°	0/105°	0/108°	0/100°
	Distal Interphalangeal (DIP)	Extension/Flexion	0/80°	0/85°	0/90°	0/90°
Thumb	Basal	Palmar Add. / Abd.	Contact/45°	×	×	0/35°
		Radial Add. / Abd.	Contact/60°	×	×	0/70°
	Metacarpophalangeal (MCP)	Hyper-Ext. / Flex.	10H/55°	0/56°†	×	0/35°
	Interphalangeal (IP)	Hyper-Ext. / Flex.	15H/80°	5H/73°	×	0/80°
Wrist	Carpometacarpal, midcarpal & radio-ulnar	Extension/Flexion	70/75°	×	74/76°[5]	70/80°
		Radial / Ulnar Dev.	20/35°	×	22/36°[5]	20/30°

[1] - Data from the American Society for Surgery of the Hand **(ASSH, 2013)**
[2] - Data adapted from Hume, et al. **(1990)**
[3] - Data adapted from Bain, et al. **(1997)**
[4] - Data adapted from Lowe **(2006)**
[5] - Data adapted from Boone & Azen **(1979)**
† - valid for 85% of the population, 0/27° for the remaining 15%.
× - Data unavailable

Referring to the data in Table 5, relatively similar results for active ranges of motion are reflected for all five studies. These values will be accounted for in the design of the active ranges of motion of the

hand which will determine the boundaries of the grasp trajectory. It should be noted that the data from the American Society for Surgery of the Hand (ASSH, 2013) and Lowe (2006) specify values for typical active RoMs, but do not specify which type of population distribution they are applicable to. An assumption is therefore made that the patients were healthy, asymptomatic adults. On the contrary, the results for wrist ranges of motion by Boone, et al. (1979) specified the use of 109 male test subjects between the ages of 18 months and 54 years.

Hume, et al. (1990) measured both active and functional RoMs of the joints of the hand for 11 activities of daily living. Furthermore, they incorporated electrogoniometric and standard test methods for all measurements on their 35 male test subjects aged between 26 and 28 years. To broaden the scope of the aforementioned study, Bain, et al. (1997) included 5 male and 5 female subjects between 18 and 53 years of age, also measuring active and functional ranges of motion; this time for the 8 ADLs specified in the Sollerman method (Sollerman & Ejeskar, 1995). The functional ranges of motion for both studies are listed in Table 6 below.

Table 6 - Functional ranges of motion of the joints of the fingers and thumb of the anatomical hand.

	Joint(s)	**Motion**	**Angular Range** [1]	**Angular Range** [2]
Finger(s)	Metacarpophalangeal (MCP)	Hyper Ext./Flex.	33-73°	19-71°
	Proximal Interphalangeal (PIP)	Extension/Flexion	36-86°	23-87°
	Distal Interphalangeal (DIP)	Extension/Flexion	20-61°	10-64°
Thumb	Metacarpophalangeal (MCP)	Hyper-Ext./Flex.	10-32°	×
	Interphalangeal (IP)	Hyper-Ext./Flex.	2-43°	×

[1] - Original data from Hume, et al. **(1990)**
[2] - Original data from Bain, et al. **(1997)**
× - Data unavailable

Referring to both data sets in Table 6, it can be seen that the values for functional RoMs correlate relatively well with one another. The largest discrepancies between the studies are the values for extension and hyperextension of the three fingers joints; consequently, the widest range will be considered in any subsequent force analysis study.

While Table 5 and Table 6 consider the anatomical ranges of motion of the human hand, a comprehensive survey by Belter, et al. (2013) investigated, among other things, the ranges of motion of seven commercial prosthetic hands as well as those of twelve research hands. In fact, the ranges of motion of the commercial hands corresponded well with the active ranges of motion of the anatomical hand, for both the MCP and the PIP joints. However, the DIP joints were found to be fixed at 20° in most

cases. The characteristics of a selection of these devices are summarised in Table 7; for the full range of results obtained in the study, refer to Belter, et al. (2013).

Table 7 - Ranges of motion for commercial & research prostheses adapted from Belter, et al. (2013).

	Joint(s)	Motion	Angular Range			
			Commercial Hands		Research Hands	
			[1]	[2]	[3]	[4]
Finger(s)	Metacarpophalangeal (MCP)	Extension/Flexion	0/90°	0/90°	0/45°	0/90°
	Proximal Interphalangeal (PIP)	Extension/Flexion	0/90°	0/90°	0/55°	0/80°
	Distal Interphalangeal (DIP)	Extension/Flexion	Fixed at 20°	Fixed at 20°	0/70°	Fixed at 35°
Thumb	MCP and IP	Extension/Flexion	0/60°	×	×	×
	Circumduction Axis 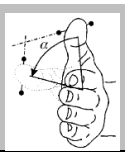	Add./Abd	0/95°	0 or 68°	10/85°	0/90°
		Orientation	0°	0°	+ 45° †	-10°‡

[1] - Data for the Commercial iLimb range adapted from Belter, et al. **(2013)**
[2] - Data for the Commercial Bebionic range by RSL Steeper adapted from Belter, et al. **(2013)**
[3] - Data for the Research MANUS hand adapted from Belter, et al. **(2013)**
[4] - Data for the Research FluidHand III adapted from Belter, et al. **(2013)**
† - i.e. 45° towards thumb from wrist axis
‡ - i.e. 10° towards little finger from wrist axis
× - Data unavailable

Referring to Table 7, it can be seen that the RoMs of the MCP and PIP joints of commercial and research hands correspond well with the anatomical ranges shown in Table 5, except for that of the MANUS Hand[3]. The DIP joints of the majority of designs are fixed at either 20° or 35°; the exception once again being the MANUS Hand[3], which in this instance better approximates anatomical behaviour by being freely moveable between 0° and 70°. By fixing the DIP joint, the complexity of the system is reduced as well as the number of components, with the trade-off being a reduced degree of freedom.

Interestingly, when considering the kinematics of the thumb, the motions of the prosthetic thumbs are simple flexion/extension about a circumduction axis, as opposed to the more complex anatomical motion about the saddle joint of the thumb, as mentioned in Section 2.1, p. 3. The rotation of the thumb about the circumduction axis allows the user to alternate between lateral grasps and power/precision grasps. Furthermore, the circumduction axis in commercial hands is generally orientated parallel (0°) to the rotation axis of the wrist, but may also be oriented away from this axis, as seen for the MANUS Hand[3] (45°) and FluidHand III[4] (-10°). By angling the axis away, thumb flexion and circumduction can be approximated by a single DOF. Consequently, desired trajectories are easily achieved for grasp patterns and system complexity is greatly reduced (Belter, et al., 2013). Further interpretations of this angled mechanism can be found in Vinet, et al. (1995) and Coert, et al. (2003).

A summary of the selected design criteria for the prosthetic hand design is shown in Table 8 below. These angular ranges of the joints will be used in the final design.

Table 8 - Summary of selected ranges of motions of the joints of the hand.

	Joint(s)	Motion	Angular Range
Finger(s)	Metacarpophalangeal (MCP)	Extension/Flexion	0/90°
	Proximal Interphalangeal (PIP)	Extension/Flexion	0/90°
	Distal Interphalangeal (DIP)	Extension/Flexion	0/60°
Thumb	Metacarpophalangeal (MCP)	Extension/Flexion	0/60°
	Interphalangeal (IP)	Extension/Flexion	0/80°
	Circumduction Axis 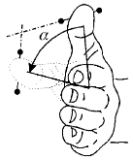	Add./Abd	0/80°
		Orientation	0°

2.9.3. Typical Hand Loading Conditions and Forces

Typical loading of the hand is a major factor to consider in the mechanics of the design. The success of usable grips, the practicality, functionality and ease of use of the hand, is directly related to the types of loading it experiences and the magnitude of these loads. Factors of dependence when considering types of loading are posture, object geometry, friction, contact points, transmission method and mass properties (Belter, et al., 2013).

The loading conditions and forces will be investigated in the following sequence:

- 2.9.3.1. Anatomical hand capabilities.
- 2.9.3.2. Actuation and grasp forces of existing VC devices.
- 2.9.3.3. Grasp forces of existing myoelectric devices.
- 2.9.3.4. Typical number of loading cycles
- 2.9.3.5. Typical force distributions

2.9.3.1. Anatomical hand capabilities

Numerous studies have been performed to determine the capabilities of the human hand and its grasping ability, especially with respect to ergonomic design of tool handles. These studies have covered an extensive range of ages for both male and female subjects; analysing their dominant and non-dominant hand. To cover all entries would be excessive, hence key results from four independent studies are summarised in Table 9 below.

Table 9 - Anatomical hand power grasp forces (N). †

		Lee, et al. **(2009)** *1		Bao, et al. **(2000)** *2		Lafayette **(1986)** *3		Edgren, et al. **(2004)** *4	
		Male	Female	Male	Female	Male	Female	Male	Female
Power Grasp	**Max**	495.6	×	×	×	394.7	215.7	331.9	192.8
	Mean	417.0	×	471.5	293.6	364.8	192.6	311.1	165.9
	Min	354.6	×	×	×	323.6	161.8	161.1	62.7

[1] - Study by Lee, et al. **(2009)** included 46 male subjects between the ages of 20 and 39.
[2] - Study by Bao, et al. **(2000)** included 120 subjects, both male and female (Data originally in lbs.)
[3] - Study by Lafayette **(1986)** included 2000 subjects, both male and female.
[4] - Study by Edgren, et al. **(2004)** included 61 subjects, both male and female between the ages of 20 and 59.
× - Data unavailable
† - All of the above data is related to the dominant hand and obtained using dynamometers.

As seen in Table 9, there is relatively good correlation between the respective studies. The anatomical hand in males was found to exert between 161.1 N and 495.6 N, averaging 391.1 N with a SD of 59.6 N. Females on the other hand, exerted between 62.7 N and 215.7 N, averaging 217.4 N with SD of 55.0 N. These correlate relatively well to Weir (2004), who mentioned the human hand could reach forces of up to 400 N in power grasps and average about 95.6 N in precision grasps. A minimum grip force, for practical use of prosthetic hands, of 45 N is suggested by Vinet, et al. (1995), whereas an estimated grip force of only 68 N is required to complete ADLs (Heckathorne, 1992). Moreover, grip forces between 2 lbs (8.9 N) and 14 lbs (62.3 N) were required to open numerous containers in the study by Rice, et al. (1998) and are representative of grasp forces needed in finer motor functions for ADLs.

2.9.3.2. Actuation and grasp forces of existing VC devices

Five voluntary closing body-powered hand prostheses were mechanically tested by Smit & Plettenburg (2010) and can be seen in Figure 33 below. Three of these terminal devices are VC hands

Figure 33 - VC prostheses used in the study by Smit & Plettenburg (2010), p. 414.

and the other two are VC hooks. Amongst others, properties such as mass, cable excursion, cable and pinch forces, activation energy, cycle hysteresis and work during closing were measured. Relevant entries are shown in Table 10 below.

Table 10 - Properties of existing body-powered VC prostheses by Smit & Plettenburg (2010).

Prosthesis	Mass (g)	Maximum Cable Excursion (mm)	Required Cable Force for a 15 N pinch (N)	Pinch Force at a cable force of 100N (N)	Pinch force drop at a 15 N pinch (N)
Hosmer APRL hand, 52541 (L)	347	37 ± 0.1	61 ± 0.6	41	7.3 ± 0.4
Hosmer APRL hook, 52601 (R)	248	38 ± 0.1	62 ± 0.0	30	10 ± 1.5
Hosmer soft hand, 61794 (R)	366	38 ± 0.3	131 ± 0.7	5	14 ± 1.7
Otto Bock, 8K24 (L), frame	220	60 ± 0.5	78 ± 0.3	28	6.7 ± 0.5
Otto Bock, 8K24 (L), frame + inner	350	41 ± 0.2	90 ± 0.9	19	5.9 ± 0.4
Otto Bock, 8K24 (L), frame + inner+ glove	423	38 ± 0.5	98 ± 0.5	14	6.5 ± 0.3
TRS hook, Grip 2S	318	49 ± 0.1	33 ± 0.2	58	-

Referring to Table 10, the mass of the prostheses ranged between 248 g and 423 g [1]. Furthermore, the maximum cable excursion of the actuating wire varied from 37 mm to 60 mm; similar to the measured limits of anatomical shoulder control (53 ± 10 mm) by Taylor (1954). Also, exerting a 15 N pinch force on a 10 mm thick sensor required a cable force of 131 ± 0.7 N for the Hosmer soft hand and only 33 ± 0.2 N for the TRS hook. While a shoulder harness can generate a maximum force of 280 ± 24 N (Smit & Plettenburg, 2010), factors relating to muscle fatigue (≅18% of max muscle load) need to be taken into consideration (Monod, 1985). Pinch forces between 5 N and 58 N were achieved under a 100 N cable force. Furthermore, these pinch forces dropped by up to 14 N when the respective locking mechanisms were engaged at a 15 N pinch.

2.9.3.3. Grasp forces of existing myoelectric devices

In addition to the VC devices, grasping forces of several commercially available myoelectric hand prostheses were investigated by Belter, et al. (2013). The manufacturer's published grip

[1] It should be noted that the 220 g Otto Bock 8K24 (L) entry is only the mass of the frame and will not be used by the patient in this configuration.

characteristics for precision, power and lateral grasps of six commercial prosthetic hand devices are shown in Table 11. In addition to these, the measured grasp holding forces can be seen in Table 12.

Table 11 - Published grasp characteristics of commercial prosthetic hands **

	Grip Force		
	Lateral Pinch (N)	**Precision Grasp (N)**	**Power Grasp (N)**
Sensor Hand	N/A	N/A	100
iLimb	17 to 19.6	10.8	-
iLimb Pulse	-	-	136
Bebionic	15	34 (tripod)	75
Bebionic v2	15	34 (tripod)	75
Michelangelo	60	70	N/A

** Results adapted from Belter, et al. **(2013)** p. 601 N/A = Not applicable

Table 12 - Measured overall grasp holding force during grasp postures **

	Lateral Pinch			**Palmar (Precision) Grasp**			**Power Grasp**		
	Total Force (N)	Number of Trials	Std. Dev.	**Total Force (N)**	Number of Trials	Std. Dev.	**Total Force (N)**	Number of Trials	Std. Dev.
iLimb	17.04	3	2.8	10.82	2	0.5	LG, 65.25	LG, 1	LG, –
iLimb Pulse*	32.10	3	2.0	17.11	2	0.3	LG, 71.44 SG, 50.81	LG, 2 SG, 1	LG, 4.0 SG, -
Bebionic	17.61	1	-	29.47	1	-	77.37	1	-
Bebionic v2	16.40	4	3.2	22.53	4	1.5	62.4	6	10.3
Michelangelo	50.84	4	3.1	78.14	8	4.4	GTU	GTU	GTU

** Results adapted from Belter, et al. **(2013)** p. 605 LG = Large Grip Std. Dev. = Standard Deviation
*Holding force after pulse mode SG = Small Grip GTU = Grasp Type Unachievable

Referring to Table 11 & Table 12, there are minor discrepancies in the published and measured forces, but nothing of major significance. Overall, the lateral pinch force varied between 16.4 N and 50.84 N, the precision grasp between 10.82 N and 78.14 N, and the power grasp between 50.81 N and 77.37 N.

Delving into further detail, the maximum holding force of various fingers were also measured; the results are shown in Table 13. These values varied between 3 N and 16.11 N for the individual fingers, averaging at 7.98 N (SD = 4.42 N) and 9.29 N (SD = 3.77 N) between fingers when excluding and including the pulse mode respectively.

Table 13 - Measured individual finger holding force at tip **

	Full Hand Actuated Individual Finger Holding Force		
Hand, respective finger(s)	**Force (N)**	**Number of Trials**	**Standard Deviation (N)**
Vincent, Large (Ring, Middle and Index)	4.82 or 8.44*	14 or 8*	0.8 or 1.3*
Vincent Small (Little)	3.00	2	0.1
iLimb Large (middle)	7.66	2	0.2
iLimb Medium (Index/Ring)	5.39	4	0.1
iLimb Small (little)	5.17	2	0.1
iLimb Pulse Medium (Index)	4.15 or 6.54*	1	-
iLimb Pulse Large (Middle)	3.09 or 6.24*	2 or 2*	0.7 or 0.4*
iLimb Pulse Medium (Ring)	6.43 or 11.18*	2 or 2*	0 or 0.3*
iLimb Pulse Small (little)	4.09 or 8.56*	2 or 2*	0.1 or 0*
Bebionic (Index)	12.47	1	-
Bebionic (Middle)	12.25	2	1.0
Bebionic (Ring)	12.53	2	1.1
Bebionic Small (Little)	16.11	2	0.2
Bebionic v2 Large (Ring, Middle, and Index)	14.5	2	1.2

** Results adapted from Belter, et al. **(2013)** p. 605 *Holding force after pulse mode

2.9.3.4. Typical number of loading cycles

During an 8 hour period in a working day, the unaffected dominant hand may perform between 2 500 and 3 000 grasping motions (Zheng, et al., 2011), whereas a prosthetic device will typically undergo 120 grasping motions every day (Van Lunteren & Van Lunteren-Gerritsen, 1997). The reduction in control and fine motor function of the amputated hand, leads the user to use the dominant hand when performing most ADLs.

According to Vinet, et al. (1995), electro-mechanical hands should be designed to perform a minimum of 300,000 grasping cycles and maintain all of its original functionality. Moreover, in Belter, et al. (2013), it is suggested that current devices last in excess of 500,000 grasp cycles between routine servicing. If correlating this suggested lifespan with the daily grasping frequency mentioned above, the prosthesis should last in excess of 6 years.

Fatigue-loading analysis on the mechanisms of the hand will therefore need to exceed 1,200,000 loading cycles without undergoing detrimental structural wear or degradation.

2.9.3.5. Typical force distributions

Force distributions govern the allocation of forces to certain parts of the hand. Evenly divided forces, such as those by Gosselin et al. (2008), divide the input force evenly between the fingers and the thumb (i.e. 50% - 50%), and again between the fingers and their phalanges as shown by Distribution A in Table 14. Distribution B is identical to Distribution A, except that the distribuion between fingers allocates 60% of the force to the 2nd and 3rd digits and the remaining 40% to the 4th and 5th digits. Distrubution C is a proposed distribution by Kamikawa & Maeno (2008) whose distribution biases most of the input force to the fingers (2nd to 5th digits) and splitting the distribution unevenly between phalanges. Their study dealt with optimisation of force distributions on 20 mm, 50 mm and 80 mm diameter cylinders.

Table 14 - Grasp force distributions between the digits and phalanges.*

	Digit distribution				Phalangeal distribution		
Digit	A	B	C	Phalange	A	B	C
1st	0.5	0.5	0.14	Proximal	0.25	0.25	0.07
				Distal	0.25	0.25	0.07
2nd	0.125	0.150	0.300	Proximal	0.0417	0.050	0.12
				Middle	0.0417	0.050	0.06
				Distal	0.0417	0.050	0.12
3rd	0.125	0.150	0.280	Proximal	0.0417	0.050	0.084
				Middle	0.0417	0.050	0.084
				Distal	0.0417	0.050	0.084
4th	0.125	0.100	0.190	Proximal	0.0417	0.033	0.038
				Middle	0.0417	0.033	0.038
				Distal	0.0417	0.033	0.114
5th	0.125	0.100	0.090	Proximal	0.0417	0.033	0.036
				Middle	0.0417	0.033	0.018
				Distal	0.0417	0.033	0.036

* Expressed as a fraction of the total input force

2.9.4. Frictional properties of the hand and various materials

Skin friction refers to the friction between in vivo human skin and an arbitrary contact material[2]. It is dependent on the properties of the skin, the properties of the contact material, the parameters of the material interface between the skin and the object (such as dust, lubrication etc.), and the environment surrounding the materials (e.g. temperature & moisture) (Veijgen, 2013). Consequently, this section

[2] It should be noted that skin friction is not a property of the human skin, as it involves the interaction of the skin and its contact material.

will be divided into two parts. The first looks at the coefficients of friction between in vivo human skin and various materials, whereas the second will use these attributes to select a suitable glove-covering of the prosthetic hand and the materials to mimic these coefficients.

2.9.4.1. Skin friction coefficients

The dynamic and static coefficients of friction of the anatomical skin and various contact materials is presented in Table 15.

Table 15 – Skin friction coefficients of the anatomical hand and various contact materials.

Anatomical Location	Contact Material	μ_{static}	$\mu_{dynamic}$	Reference sources
Finger	Rubber	1.938	-	1
		2.5	-	2
	Latex Glove	1.2	-	2
Distal Palm	Rubber	3.454	-	1
Proximal Palm		2.47	-	1
Index Finger		1.53	-	1
Thumb		1.272	-	1
Finger		-	2.4	3
	Steel	-	1.8	3
	Glass	-	1.2	3
	Paper	-	0.6	3

Reference sources:

1– Data from Uygur, et al. **(2010)**

2 – Data from Tomlinson, et al. **(2007)**

3 – Data from Gee, et al. **(2005)**

Referring to Table 15, the static coefficients of friction for the anatomical hand range between 1.2 and 3.454, whereas the dynamic coefficients of friction range between 0.6 and 2.4 depending on the contact surface. Distal palm contact with rubber had the highest overall friction coefficient; likely attributed to the combination of the cushioning/padding of that region of the hand, and the gripability & compressibility of rubber. The lowest coefficient of friction was the finger contacting paper, which has very low compressibility. The prosthesis should be able to grasp steel and glass objects securely with a natural 'feel', hence a material of dynamic coefficient of friction greater than the anatomical 1.8 should ideally be selected.

2.9.4.2. Frictional properties of prosthesis glove-coverings and various materials

These materials need to mimic the coefficients of friction of the natural hand. While exceeding the coefficients is favourable in maintaining a secure grasp, it has been shown by Klaassen (2007) that too high a coefficient of friction (especially relating to rubbers) leads to issues of increased dust collection,

cleanability and stickiness. Table 16 shows the coefficients of friction of possible glove-covering materials.

Table 16 – Estimated friction coefficients of glove and various contact materials.

Glove Material	Contact Material	μ_{static}	Reference source
Silicon Rubber	Rubber	>0.75	1
Rubber	Rubber	1.16	2
Rubber	Cardboard	0.5 - 0.8	2
Rubber	Smooth solid	1.0 - 4.0	3
Rubber	Metal	1.0	4
Silicon	Silicon compound	0.2 - 0.7	5
Silicon dioxide	Silicon dioxide (wet)	0.31 - 1.1	5
Silicon dioxide	Silicon (wet)	0.51 - 1.8	5
Rubber	PVC	0.45 – 0.82	6
Rubber	Epoxy	0.42 – 0.6	6
Rubber	Ceramic	0.45 – 0.54	6

Reference sources:

1 – Data from **(Albright Technologies Inc., 2014)**
2 – Data from **(Engineering Toolbox, 2014)**
3 – Data from **(Engineer's Handbook, 2006)**
4 – Data from (Tribology, 2014)
5 – Data from (Deng & Ko, 1992)
6 – Data form (El-Sherbiny, et al., 2012)

Comparing the results of Table 15 and Table 16, the static and dynamic coefficients of friction for the anatomical hand is generally higher than that of the rubber, silicon, silicon dioxide and silicon rubber, contacting various materials. Since lower hardness also leads to an increased coefficient of friction in polymers (PolyOne, 2014) and elastomers (Kalácska, 2013), a rubber or silicon should be selected with a low Shore hardness to account for the deficit in frictional coefficient. This will increase the conformity, grip and compressibility (and thereby contact area) of the grasp. Shore A hardness of 20-30 is specified for the outer cover of a hand prosthesis by Gill (2011), and between 10-40 Shore A hardness for the flesh of a prosthetic foot by Gajdos (1967). Consequently, a material with Shore A hardness of approximately 25 should be selected for the covering or grip surfaces of the prosthesis; its frictional coefficient being as high as possible, ideally greater than 1.8 for static and dynamic cases, mimicking the natural grasping of steel, and exceeding that of glass and paper as seen in Table 15.

2.10. Types of Ratchet and Locking Mechanisms

In order to accommodate the design of voluntary closing hands, a locking mechanism is required to keep the hand fixed at certain positions. This locking mechanism allows the user to rest while performing tasks, only requiring them to provide the initial tensioning force to the actuating cable. Consequently, user fatigue and harness discomfort can be greatly reduced when compared to designs

that rely on the user to maintain the locking force. A commonly used locking mechanism is a ratchet and pawl, as shown in Figure 34, and can be either linear or circular (rotational).

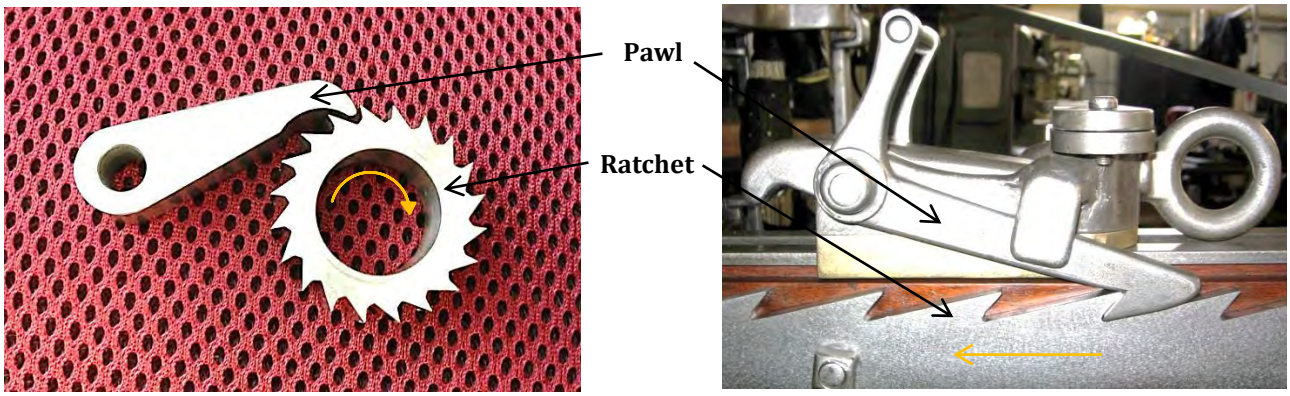

Figure 34 – Circular and linear ratchet and pawl mechanisms (left & right respectively) (Berg, 2013) & (Alexis, 2012).

Ratchet mechanisms are simplistic in nature and are generally made up of two main components; namely, a ratchet and a pawl. The ratchet is a rotating wheel or linear rack with jagged edges (teeth) whereas the pawl is a lever mechanism that allows the ratchet to rotate or translate in one direction and locks it in place when the motion is reversed. The inherent nature of this mechanism only allows for incremental locking, giving rise to a phenomenon known as backlash.

Backlash is the backward travel that the mechanism undergoes before securely locking in place; its maximum value is equivalent to the distance between two adjacent teeth. One method of reducing the degree of backlash is to increase the number of teeth, hence decreasing the incremental step size.

Another method to reduce backlash is to incorporate a toothless ratchet system with a high-friction material, such as rubber, and a smooth pawl to lock the mechanism in place. This mechanism is continuous instead of incremental, where the backward travel is a function governed by the compressibility of the high friction material and not the tooth-spacing.

However, while this mechanism appears appealing, it is challenging to quantitatively assess the workings of it, as frictional calculations, coupled with material properties of the mechanism may become highly non-linear. Furthermore, this mechanism does not have the security and mechanical advantage possessed by the aforementioned toothed-ratchet. To minimise the effects of backlash of the toothed mechanism, the author suggests increasing the compressibility of the glove material, allowing it to absorb any slack in the system while allowing to the hand to maintain contact force with the gripped object. Moreover, an additional spring mechanism can be included in the palmar design to absorb further slack as well as store extra energy to ensure contact forces with the gripped object are maintained once the tension in the actuating cable is released.

2.11. Mechanical Properties and Characteristics of Materials

Hand prostheses make use of a combination of various materials. Selection of materials is of paramount importance in implant design as they need not only sufficient mechanical strength, but also good durability characteristics, high corrosion resistance and biocompatibility. Suitability of various types of polymeric and metallic materials as well as their individual benefits and drawbacks is the primary focus of this section.

2.11.1. Polymeric Materials for Additive Manufacturing

Some commonly used polymeric materials used in bioengineering are listed in Table 17 below. Specific attention is paid to those suitable to additive manufacturing techniques such as Selective Laser Sintering (SLS) or Fused Deposition Modelling (FDM).

Table 17 - Mechanical properties of common medical polymers for additive manufacturing.*

Material	Tensile Modulus, (MPa)	Tensile Strength, (MPa)	Strain at Break, (%)	Flexural Modulus, (MPa)	Flexural Strength, (MPa)	Charpy, Notched Impact	Density (kg/m^3)	Bio-compatibility (Y/N)
EOS PA2200 Nylon**	1650	48	18	1500	-	$4.8kJ/m^2$	930	Y
EOS Alumide**	3800	48	4	3600	72	$4.8kJ/m^2$	1360	N
ABS-M30i*	2400	36	4	2300	61	139 J/m	1040	Y
EOS ** PEEK HP3	4250	90	2.8	-	-	-	1310	Y

* Material data obtained from Stratasys **(2013)**. Charpy notched impact test according to ASTM D256 @ 23°C.
** Material data for each of these obtained directly from CRPM CUT or EOS **(2014)**. Charpy test using ISO 180 @ 23°C.
Materials above are listed in ascending order of cost, from top to bottom. (i.e. PA2200 is cheaper than Alumide)

Of the materials listed above, it can be seen that all the materials are biocompatible except for the Alumide. While the PEEK HP3 has the greatest stiffness and tensile strength, it has the second highest density and the lowest ductility. The EOS Alumide has good flexural properties and the second highest tensile strength of the four selected options, but is limited by its ductility (4% strain at break), which matches that of the ABS-M30i, and by its density. The cost of the ABS-M30i is exceeded only by the EOS PEEK HP3 making it a costly option for a material with low ductility and low tensile and flexural strengths.

The EOS PA2200 Nylon offers the most favourable balance of mechanical properties for the required application. It has low relative cost and lower density when compared to the other materials, making it cheaper and lighter. Furthermore, its lower stiffness allows it to have a superior ductility (18% strain

at break) which is beneficial when grasping objects, and makes it more forgiving when loaded beyond its elastic limit as brittle fracture behaviour is less likely to occur. It has good chemical resistance and detailed resolution, with a tensile strength matching that of the Alumide. Moreover, its biocompatible properties conform to ISO10993-1 and have been tested for cytotoxicity, sensitisation for both polar and non-polar extracts, as well as intracutaneous reactivity. Low-friction characteristics of this material allow it to be resilient to wear; the extent of this resilience is outlined in the extract of the manufacturer's material datasheet (EOS, 2004) shown in Appendix G.

2.11.2. Metallic Materials

Some commonly used metallic materials used in bioengineering are listed in Table 18 below. Their properties will not be discussed here, but relevant excerpts will be used in subsequent sections.

Table 18 - Properties of metallic materials commonly used in medical devices.

Material	Elastic Modulus, E (GPa)	Ultimate Tensile Strength, UTS (MPa)	0.2% Yield Strength, (MPa)	Elongation at Break (%)	Ultimate Shear Strength (MPa)	Hardness (DIN ISO 6508-1) (Brinell)	Bio-compatible (Y/N)
TiV4Al6*	114	1000	910	18	576	290	Y
NiTi 1 †	-	1240	> 483	> 10	-	359	Y**
Nitinol SE ††	41.75	> 1100	> 380	> 10	-	319	Y**
Stainless Steel 316L*	193	515	205	60	425	149	Y
Stainless Steel 304*	193	505	215	70	505	146	N

* The following material properties obtained from Matweb **(2014)**.
** With biocompatible coating.
† Mechanical properties from manufacturer's material datasheets converted to SI units **(Fort Wayne Metals, 2014)**.
†† Data for mechanical properties from manufacturer's datasheets **(Euroflex GmbH, 2014)**.

2.12. Applicable Standards and Testing Methods

2.12.1. Standards Relating to Upper Limb Prosthetic Devices

The following standards will be briefly discussed in their order of relevance relating to the stages of the design and development process of upper limb prostheses. Key considerations made in each of these will be highlighted and adhered to in subsequent development and testing stages.

Vocabulary relating to the field of external limb prosthetics in this dissertation will adhere to the standards outlined in ISO 8549:1989. It defines the general terms used to describe these prostheses, the anatomical parts commonly interfacing with these devices, and the personnel and procedures

involved in the practice of prosthetics (ISO 8549, 1989). It will be incorporated into subsequent sections to ensure uniformity and prevent, where possible, ambiguity. It should be noted that the fourth part of this standard ISO/DIS 8459-4, defining terms relating to limb amputation, is currently under development and that the pre-amended terms, trans-radial (below-elbow) and trans-humeral (above-elbow), shall be used.

Limb deficiencies relating to prosthetics and orthotics are defined in ISO 8548. The first two parts of this standard, ISO 8548-1 (1989) and ISO 8548-2 (1993), will not be considered as they relate to the method of describing limb deficiencies present at birth and the method of describing lower limb amputation stumps respectively. The third part, ISO 8548-3 (1993), defines the methods for describing upper limb amputation stumps and uses the vocabulary formulated in ISO 8549 (1989). Sections 5.4 to 5.6 of this standard are of particular interest, as they relate to trans-humeral, elbow-disarticulation and trans-radial amputations respectively; applicable to the focus of this dissertation. ISO 8548-4 (1998) describes the causal conditions leading to amputation; including mechanical trauma, as well as clinical, pathological and specific disease conditions. Clear classification and epidemiology of these conditions and their prevalence are crucial to identify the extent of possible target markets and their projected rate of growth. ISO 8548-5 (2003) focuses more on the clinical condition of the patient, including their physical, mental, musculoskeletal and emotional states; assessing their motivation and perceived needs. Its contents generate a critical link to how patients respond to terminal devices.

The classifications of prosthetic components are outlined in ISO 13405-1 (1996). They are broken down into general (i.e. upper limb, lower limb, etc.), interface components, functional components, alignment components, structural components and cosmetic components. Adherence to the relevant classification allows for simple identification of various components and their classes, without confusing them with their innumerable trade names given to them by different manufacturers. ISO 13405-2 (1996) relates to lower limbs and will be ignored. ISO 13405-3 (1996) describes the numerous upper limb prosthetic components under the classification classes outlined in ISO 13405-1 (1996). While many technological advances have been made since the publication of this standard in 1996, it will be consulted until the updated version of ISO 13405, which is currently under development (ISO, 2014), is published.

Design and testing of the hand will be performed in accordance to ISO 22523 (2006), paying special attention to requirements outlined in the standard. While not part of the scope of this dissertation, it is recommended that future quality management systems for the production of this device incorporate the use of ISO 9001:2008.

2.12.2. Standards for Compressive & Tensile Testing of Polymeric & Metallic Structures

To determine the strength of the components of the hand, testing standards relating to the tensile and compressive loading of structures, as well as flexural loads, are required to ensure usable experimental results are attained.

More particularly, the hyper-extensive and lateral loading of the digits will adhere to strain-rates outlined in ISO 178 (2010) and ASTM D790 (2003), which are applicable to both thermoplastics and thermosets. Both methods make use of three-point bending of the structure, with input parameters being support span, speed of loading and maximum deflection. ISO 178 (2010) and ASTM D790 (2003) have two test methods, Method A and Method B. For ISO 178 (2010), Method A uses a strain rate of 1% gauge length/min throughout the test whereas Method B uses 1 %/min to determine flexural modulus and 5 %/min or 50 %/min for the remainder of the test to determine the remainder of the flexural stress-strain curve (ISO 178, 2010). ASTM D790 (2003) makes use of 0.01 mm/mm/min and 0.1 mm/mm/min strain rates for Methods A and B respectively. For ASTM D790 (2003), the test is stopped when the specimen reaches 5% deflection or the specimen breaks before 5%, whereas ISO 178 only ends when the specimen has broken or the test has continued as far as possible and the stress is reported at 3.5% conventional deflection. Due to the unique geometry of the digits, ISO 178's (2010) end condition will be adhered to with the 1% gauge length/min strain rate of Method A, which is the same for both standards. It should also be noted that ASTM D638 (2003) should be referred to when testing the tensile properties of plastics.

The tensile testing of the actuating wires and the strength determination of the knots will adhere to ASTM D6320 (2002) in which a crosshead speed of 25 mm/min with a specified specimen gauge length of 250 mm ±0.5%. Breaking force, yield strength and elongation are determined by tensioning the specimen to failure. Initial pre-tension on the wire may not exceed 1 N and fracture may not occur within 5 mm from the gripping points, else the results must be discarded. According to the standard, knot strength will be performed at a crosshead speed of 10 mm/min with an overhand knot. With reference to Section 6.2.9 (p. 133) and Section 7.3 (p. 153), a Figure-8 stopper knot will be employed bilaterally on the wire to determine its breaking point.

2.12.3. Standards Relating to Accelerated-life Testing of Medical Polymers

There are numerous accelerated-life or fatigue testing standards applicable to the testing of medical polymers. For total hip-joint and total knee-joint prostheses, ISO 14242 (2012) and ISO 14243 (2009) are commonly referred to. These standards clearly define two different techniques known as the load-control and displacement-control method for accelerated-life tests. While the load-control method

ensures a constant load is exerted onto the test specimen throughout the test, regardless of the wear, it is more beneficial to knee-joint and hip-joint prostheses as their loading patterns are directly related to the person's bodyweight, gait and level of activity. It is more challenging to accurately model general loading conditions for the hand as the complex nature and variety of grasps are dependent on the weight and geometry of the grasped object; and independent of the patients mass. As a result, the displacement-control method will be used as it will allow the hand to repeatedly flex through its entire range in a controlled environment. This ensures the actuating tendons slide over the greatest amount of surface area, with loads increasing as a function of flexion, generating the greatest amount of wear.

Assessment of the extent of wear can be done through various methods. Wear testing methods of total joint prostheses are described in ASTM F732 (2000) whereas wear assessment of materials using a tribometer is disclosed in ASTM G99 (2004) and DIN 50324 (2007). In implantable prostheses, it is often important to retrieve and inspect the wear particles themselves, as their composition, shape and size adversely influence the soft-tissue within the human body (ISO 17853, 2011). For external prostheses however, it is more important to assess the damage to the prosthetic device itself rather than the worn particles. This can be done qualitatively, through a visual inspection, or quantitatively, through gravimetric test methods such as those disclosed in ASTM F2025 (2000). Both approaches will be used in the accelerated-life testing of the prosthetic hand together with guidelines extracted from the displacement-control method outlined in ISO 14243 (2009).

2.12.4. Patient Surveys and Questionnaires

In order to completely evaluate a patient's experience when using a prosthesis, numerous factors both qualitative and quantitative need to be considered. Qualitative assessment is necessary to evaluate factors involving emotional and social responses, whereas quantitative assessment is needed to gauge the functional performance and ability of the device. Many different methods have been used in the literature to assess these criteria, but it is seldom that a survey or questionnaire includes all of these factors. In the development of such a patient questionnaire, excerpts from two studies have been used; namely the Patient Evaluation Questionnaire (PEQ) by Legro, et al. (1998) and the modified Upper Extremity Functional Status (UEFS) module of the Orthotics and Prosthetics User Survey (OPUS) by Burger, et al. (2008).

The PEQ was developed to fill the need for a comprehensive self-report instrument for individuals with lower limb loss (Legro, et al., 1998). According to Prosthetics Research Study (2006), "*Psychometric analysis supported the reliability and validity of the PEQ for evaluating the function of the prosthesis and the major health related quality of life domains. The PEQ has been widely used in rehabilitation health service research settings. In recent years, other instruments have been developed that assess prosthetic use, factors facilitating prosthetic use, or the patients' ability to perform various*

skills. However, the PEQ remains a unique instrument with comprehensive multidimensional scales for evaluating both prosthesis function and prosthesis related quality of life." While comprising the required components for a comprehensive analysis, PEQ is focussed on evaluating patients with lower limb loss; consequently, it will be modified to relate to patients with upper limb loss.

In addition to the PEQ, the UEFS module of OPUS was made using an advisory committee that included orthotists, prosthetists, clients, occupational therapists, physical therapists and psychiatrists. Their study included 23 self-care and instrumental activity of daily living items, which patients would assess according to 5-point rating scale on their ease to perform. Burger, et al. (2008) used Rasch analysis to improve on the UEFS, by reducing the amount of response categories from 5 to 4, and ADLs from 23 to 19. This enabled them to generate higher confidence in the consistency for both person-ability and item-difficulty estimates. Consequently, the 19 revised OPUS criteria by Burger, et al. (2008) combined with the reduced response categories will be used to further assess functional categories and the degree of manual function patients have with the device.

The Prosthetic Hand Evaluation Questionnaire (PHEQ) compiled for patient use in the assessment of their experience with the prosthesis can be referred to in Appendix F, p. F-2.

The following chapter will look at numerous concept designs to aid in the selection of a final design solution. Merits and drawbacks of each of the mechanisms will be critically analysed and discussed, after which the final concept solutions are chosen.

3

CHAPTER 3: CONCEPT FORMATION

Various concept solutions are formulated in this section. They aim to satisfy the product requirements while considering key findings and fundamental concepts obtained from the literature. Conceptualisation of the design solution is built-up as follows:

3.1. Underactuated Finger Mechanism Concept
3.2. Differential Palmar Mechanism to Link the Fingers
3.3. Differential Mechanism to Link the Fingers and the Thumb
3.4. Finger Locking Mechanism Concepts
3.5. Thumb Swivel Transmission Concepts
3.6. Thumb Swivel Locking Mechanism Concepts
3.7. Palmar Cushion Concepts
3.8. Morphological Chart of Chosen Concept Solutions

A brief description of each concept solution is given, followed by a list of advantages and disadvantages of each. Thereafter, a weighted Decision Support Matrix (DSM)[3] quantitatively assesses system properties, through which a final design solution is selected and described. Lastly, a morphological chart is inserted to combine chosen concept solutions, on which the final design and calculations are based.

3.1. Underactuated Finger Mechanism Concept

Three concept solutions are selected for the underactuated finger mechanism; namely, linkage-driven fingers, tendon-actuated fingers and gear-driven fingers, as discussed in Section 2.7, p. 21. Advantages and disadvantages of each of these mechanisms are listed in Table 19, and a DSM for these concepts is shown in Table 20.

[3] DSM according to UCT MEC4055Z course notes (Kuppuswamy & Redelinghuys, 2012) and Ertas & Jones (1993, p. 74).

Table 19 - Advantages and Disadvantages of Underactuated Finger Mechanism Conceptual Designs.

	Concept 1: Linkage-driven actuation	**Concept 2:** Tendon actuation	**Concept 3:** Geared actuation
			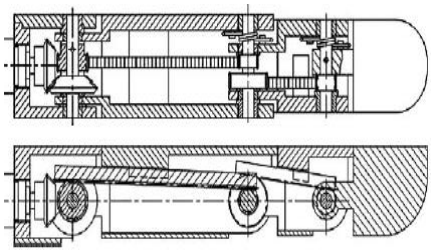
Advantages	▪ Mechanically sound ▪ Accurate control of closing trajectory ▪ Reliable ▪ Relatively inexpensive ▪ Able to amplify input force through mechanical advantage	▪ Lightweight ▪ Inexpensive ▪ Fewer moving parts ▪ Easily conforms to varying geometries ▪ Mimics anatomical tendon mechanism ▪ Ease of assembly and production ▪ Simple and compact	▪ Constant torque throughout closing range ▪ Rapid closing speeds ▪ Precise control of individual digits possible ▪ Adjustable closing trajectories using control system
Disadvantages	▪ Many moving parts ▪ Limited conformability to varying geometries ▪ Challenging assembly	▪ Wear due to actuating tendon ▪ Dislocation of actuating wire from routing pulleys ▪ Individual control of digits challenging	▪ Requires rotary actuation (i.e. motor) and control system ▪ Difficulty machining due to small components ▪ Complex assembly ▪ Heavy and noisy ▪ Expensive

Table 20 - Decision Support Matrix for Conceptual Design of the Underactuated Finger Mechanism.

Evaluation Criteria	**Weighting (%)**	**Concept 1**		**Concept 2**		**Concept 3**	
		Rating*	Weighted Total**	Rating*	Weighted Total**	Rating*	Weighted Total**
Low Cost	***15***	3	45	5	75	1	15
Reliability	***10***	5	50	3	30	3	30
Low Weight	***5***	3	30	5	50	1	10
Simplicity of design	***15***	3	45	5	75	1	15
Grasp conformability	***20***	3	60	5	100	5	100
Controllability of closing trajectory	***10***	5	25	1	5	5	25
Ease of manufacture	***10***	3	30	3	30	1	10
Ease of assembly	***10***	1	10	5	50	3	30
Ease of maintenance	***5***	3	15	3	15	1	5
Total	*100*		**310**		**430**		**240**

*Rating Scale: 1 = Bad 3 = Moderate 5 = Good ** Weighted total = Rating *x* Weighting

DSM according to UCT MEC4055Z course notes **(Kuppuswamy & Redelinghuys, 2012)** and Ertas & Jones **(1993)**

Final Concept Selection: Tendon actuation

Advantages and disadvantages of the three types of underactuated finger systems have been identified and discussed. The DSM scored the tendon actuation mechanism as its top ranking concept, followed by the linkage-driven and geared actuation mechanism respectively.

While geared systems can transmit uniform forces at higher speeds than conventional methods of actuation, they are still cumbersome and noisy, requiring many moving parts. Furthermore, they utilise motors to actuate them and a control system, hence need electrical energy. Also, the design tolerance which these mechanisms require makes them expensive and difficult to manufacture.

The linkage driven fingers have a set trajectory, allowing the grasp to be controlled, and grasp forces to be easily analysed and optimised. However, the reduced conformity of the fingers due to this trajectory presents challenges when manipulating objects of varying geometry. Furthermore, the linkages make use of numerous components which may lead to difficulties in assembly and maintenance.

The tendon finger systems are appealing in that they are simple, reliable, compact, closely mimic the anatomical tendon-sheath mechanism, and require minimal components. Their disadvantages relate mostly to degradatory wear of the tendon and its guide-channel, and to dislocation of the tendon from its pulley in certain designs. To reduce wear, a modification to this mechanism is made by using channel linings (much like anatomical sheaths) to wear sacrificially. The channels are curved to increase leverage, amplifying the grip force. Reductions in cost will be made by removing the moving parts (pulleys), further simplifying the mechanism. Torsion springs will be used in the hinge-joints to extend the fingers once flexed.

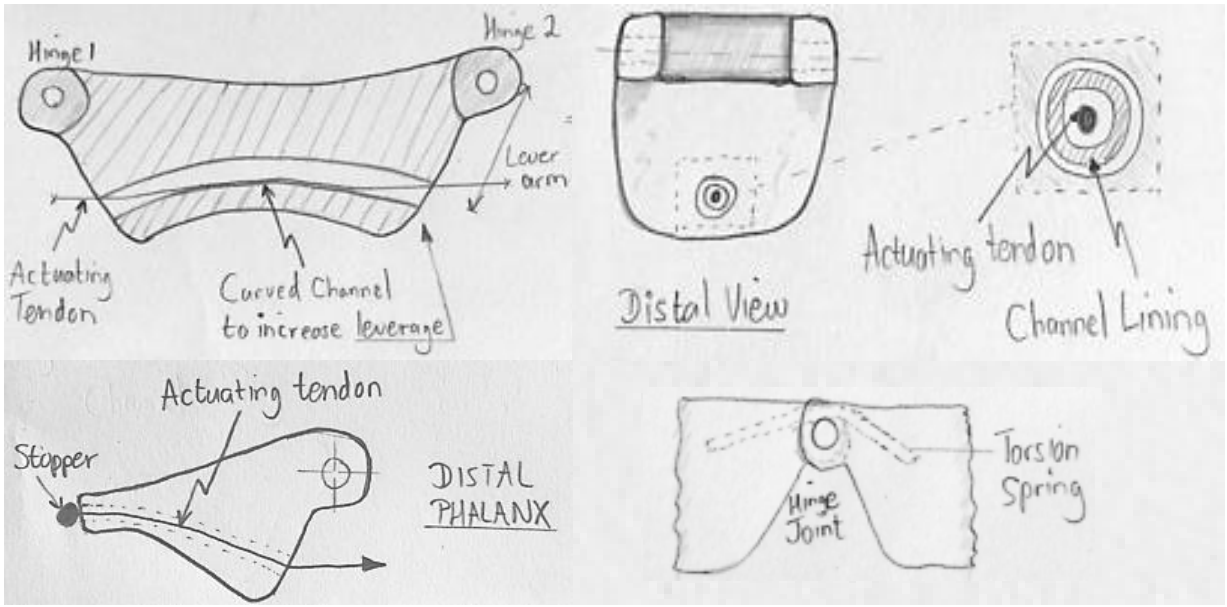

Figure 35 - Concept solution for the underactuated tendon-actuation of the fingers.

3.2. Differential Palmar Mechanism to Link the Fingers

Four selected concept solutions for the differential palmar mechanism of the hand are compared; namely, differential levers (seesaws), moveable pulleys, fluidic t-pipes and planetary gear differentials, as previously mentioned in Section 2.8, p. 25. Advantages and disadvantages of each of these mechanisms are listed in Table 21, and a DSM for these concepts is presented in Table 22.

Table 21 - Advantages and Disadvantages of Differential Palmar Mechanism Conceptual Designs.

	Concept 1: Differential Levers (Seesaws)	**Concept 2:** Moveable Pulleys	**Concept 3:** Fluidic T-pipes	**Concept 4:** Planetary Gearing
	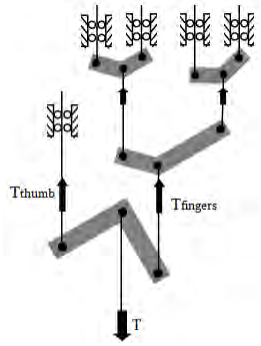	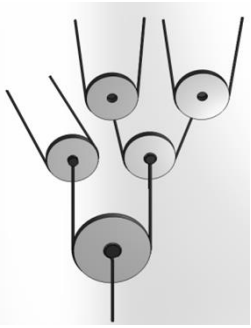	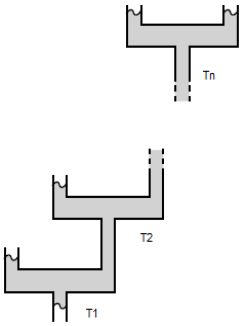	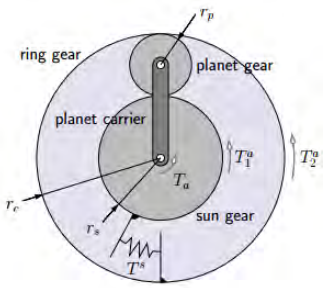
Advantages	▪ Easily adjusted lever arm length, enabling uneven force distribution between fingers ▪ Pivoting levers allow relative motion between fingers ▪ Ease of manufacture ▪ Design simplicity	▪ Low resistance and friction ▪ Simple design ▪ Easy system analysis ▪ Relative motion allowed between fingers	▪ Uneven force distribution between fingers possible ▪ Low space requirements ▪ Design simplicity ▪ Efficient force transmission when using incompressible fluid	▪ Constant force transmission independent of position ▪ Mechanically reliable ▪ Large transmission ratios
Disadvantages	▪ Large operating space requirement ▪ Risk of dislocation of the actuating wires ▪ Low efficiency when in guided-slots	▪ Derailment of actuating wires when tension released ▪ Uneven adjustment of lever arm not possible ▪ Low efficiency when in guided-slots	▪ Requires a fluid reservoir ▪ Increased weight due to fluid ▪ Pumping/pressurising mechanism required ▪ Risk of leakage ▪ Adjustment of forces requires new piping/flow-nozzles	▪ Expensive ▪ Difficulty in manufacture and assembly ▪ Complex design ▪ Noisy transmission ▪ Fixed gear-ratios ▪ Needs rotary force input

Table 22 - Decision Support Matrix for Conceptual Design of the Differential Palmar Mechanisms.

Evaluation Criteria	**Weighting (%)**	**Concept 1**		**Concept 2**		**Concept 3**		**Concept 4**	
		Rating*	Weighted Total**	Rating	Weighted Total	Rating	Weighted Total	Rating	Weighted Total
Low Cost	***15***	5	75	3	45	3	45	1	15
Reliability	***10***	3	30	1	10	1	10	3	30
Lightweight design	***10***	3	30	3	30	1	10	1	10

Compactness	***15***	1	15	3	45	5	75	3	45
Simplicity of design	***5***	5	25	5	25	5	25	1	5
Ability to distribute forces unevenly	***10***	5	50	1	10	5	50	5	50
Controllability of force distribution	***15***	5	75	3	45	3	50	3	45
Ease of manufacture	***5***	5	25	3	15	5	25	1	5
Ease of assembly	***10***	3	30	1	10	3	30	1	10
Ease of maintenance	***5***	3	15	3	15	3	15	1	5
Total	*100*		**370**		**250**		**335**		**220**

*Rating Scale: 1 = Bad 3 = Moderate 5 = Good ** Weighted total = Rating *x* Weighting

DSM according to UCT MEC4055Z course notes **(Kuppuswamy & Redelinghuys, 2012)** and Ertas & Jones **(1993)**

Final Concept Solution: Modified Differential Levers (Seesaws)

According to the DSM for the differential palmar mechanisms, the differential lever mechanisms ranked the highest with a score of 370, followed closely by the fluidic T-pipes with 335 and then the moveable-pulleys and planetary gearing, scoring 250 & 220 respectively. Consequently, the differential levers will be selected as the final concept with modifications to the original concept.

Their disadvantages will be addressed as follows. The large operating space requirements for the levers will be reduced by stacking/staggering the seesaws above one another. Furthermore, the dislocation of the actuating wires will be prevented by drilling holes through the seesaw, looping the actuating cable through and securely fastening it, either through crimping a ferrule onto it or tying a stopper-knot. Guided slots are necessitated to increase the accuracy of force distribution as well as to control the range of travel of the internal mechanisms due to limited internal space. Lastly, the efficiency of the linear translation of the levers will be increased through the use of a single linear roller bearing instead of guided slots. The final concept design can be seen in Figure 36 below.

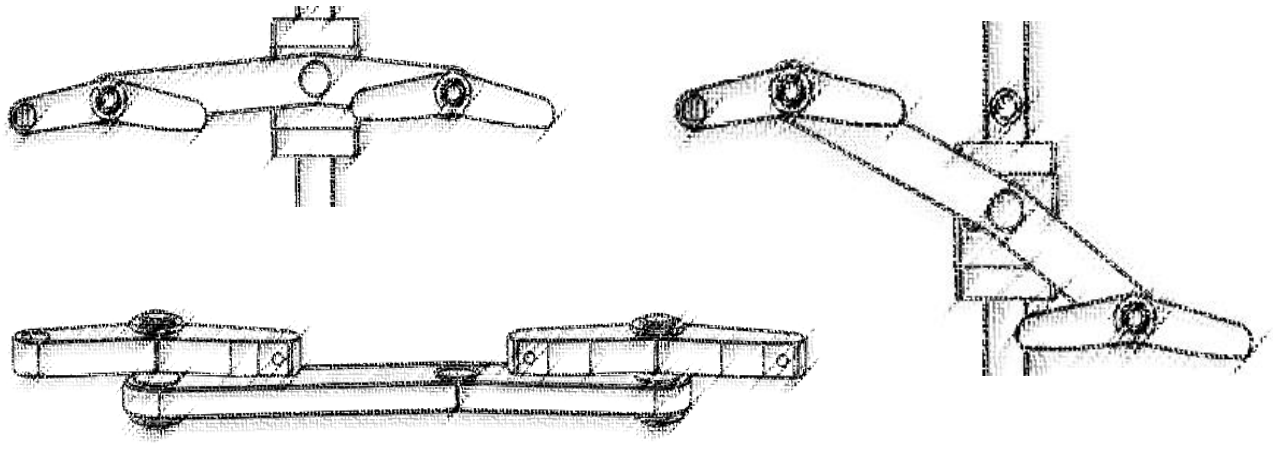

Figure 36 - Final concept solution for the differential mechanism between fingers, with the neutral position (left top), proximal view (left bottom) and position for flexed 2nd and 3rd digits (right).

3.3. Differential Mechanism to Link the Fingers and the Thumb

Concept 1: Fixed Pulleys (Bacon & McNaught, 2011)

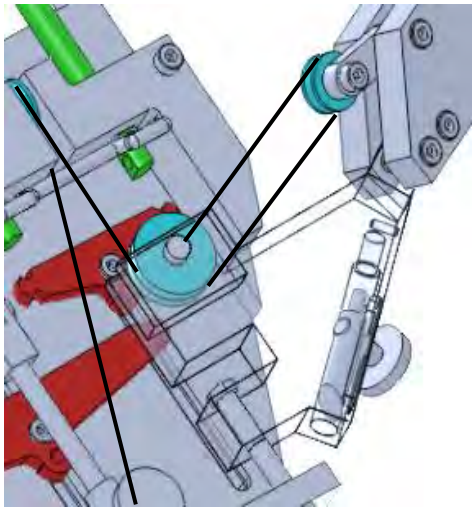

The fixed pulley routing scheme by Bacon & McNaught (2011) makes use of three rigidly attached pulleys. One is attached to the thumb swivel, one to the proximal phalanx and one to the distal palmar structure. This particular configuration doubles the input thumb actuation force and halves the displacement of the cable. Alignment of the pulleys is not consistent throughout the motions of the thumb, and is likely to lead to dislocation/derailment of the cable. The motion of the thumb is independent to that of the fingers.

Concept 2: Guided Sliders with Bearings (Gosselin, et al., 2008)

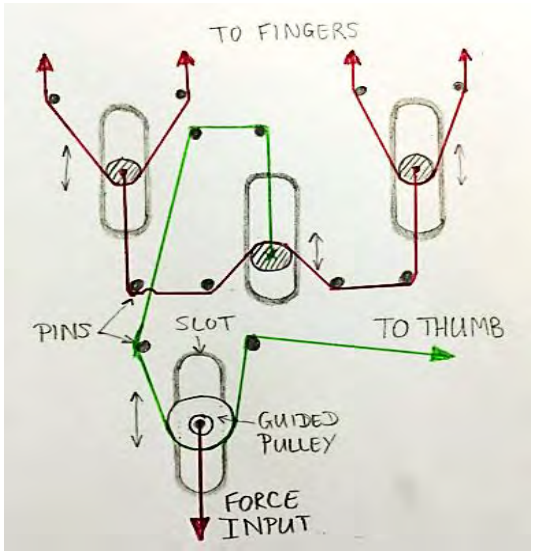

In this configuration the thumb is directly coupled to the fingers, with its actuating cable (green) routed around a guided pulley running in a linear slot. Moreover, it passes around four fixed routing pins and inserts onto the central slider of the underactuated finger differential. 15 DOFs are achieved with this configuration and a theoretical 50-50 force distribution in a frictionless system. However, poor routing schemes lead to large losses, distributing a larger force to the thumb than the fingers.

Concept 3: Differential Lever (Seesaws) (Kamikawa & Maeno, 2008)

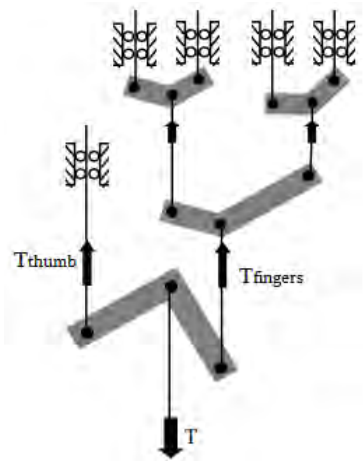

The final concept makes use of a differential lever (seesaw) to distribute the force between the fingers and the thumb, either evenly or unevenly. Similarly to the slider concept, it enables relative motion to the fingers. The lever pivots about its central axis where the input force (T) attaches, translating linearly during flexion and extension. Table 23 lists the advantages and disadvantages of the three concepts, and Table 24 evaluates their features according to a weighted measure.

Table 23 - Advantages and Disadvantages of Finger to Thumb Linking Mechanism Conceptual Designs.

	Concept 1: Fixed Pulleys	**Concept 2:** Guided Sliders with Bearings	**Concept 3:** Differential Levers (Seesaws)
Advantages	▪ Pulleys allow low friction ▪ Independent motion to fingers ▪ Easily manufactured ▪ Simplicity	▪ Simple design ▪ Uses standard components ▪ Independent motion to fingers ▪ Controllable linear displacement	▪ Easily adjustable force distribution ▪ Ease of manufacture ▪ Simplicity ▪ Distributed force can vary according to grasp type ▪ 15 DOFs possible for entire hand
Disadvantages	▪ Derailment of actuating wire when tension is lost ▪ Inefficiency due to poor routing ▪ Challenging assembly	▪ Inefficient routing leads to excessive friction, especially large changes in angles. ▪ Sliders are inefficient	▪ Attachments may loosen ▪ Large space requirements ▪ Distributed force not constant

Table 24 - Decision Support Matrix for Conceptual Design of the Finger to Thumb Linking Mechanism.

Evaluation Criteria	**Weighting (%)**	**Concept 1**		**Concept 2**		**Concept 3**	
		Rating*	Weighted Total**	Rating	Weighted Total	Rating	Weighted Total
Low Cost	***10***	5	50	5	50	5	50
Reliability	***15***	1	15	5	75	3	45
Low space requirement	***5***	5	25	5	25	1	5
Low Weight	***5***	5	25	5	25	5	25
Efficiency of routing	***10***	1	10	1	10	3	30
Simplicity of design	***5***	5	25	5	25	5	25
Grasp conformability	***15***	1	15	5	75	5	75
Independent motion to fingers	***10***	5	50	5	50	1	10
Degrees of Freedom	***15***	3	45	3	45	5	75
Controllability of grasp force	***10***	1	10	3	30	5	50
Ease of manufacture	***5***	5	25	5	25	5	25
Ease of assembly	***5***	3	15	3	15	3	15
Total	100		**260**		**400**		**380**

*Rating Scale: 1 = Bad 3 = Moderate 5 = Good ** Weighted total = Rating *x* Weighting

DSM according to UCT MEC4055Z course notes **(Kuppuswamy & Redelinghuys, 2012)** and Ertas & Jones **(1993)**

Final Concept Solution: Moveable pulley on Linear Bearing

According to the DSM, Concept 2 ranks as the leading concept design, yet only marginally. Consequently, a combination of distinguishing characteristics of each of the concepts will be used to generate the link between the finger and thumb. The low-friction pulleys from Concept 1 will be modified to prevent dislocation of the actuating cable, as shown in Figure 37. This pulley will be used

in combination with linear slots, similar to Concept 2, except that the slots will be substituted with linear roller bearings to reduce running friction. Furthermore, each angular change of the actuating cable in the routing network will be routed around roller bearings to increase efficiency. To maintain overall underactuation of 15DOFs as in Concept 3, the actuating cable will be directly linked to the finger differential mechanism shown in Figure 36. Moreover, the mechanism will allow a 50-50 force distribution between the fingers and the thumb.

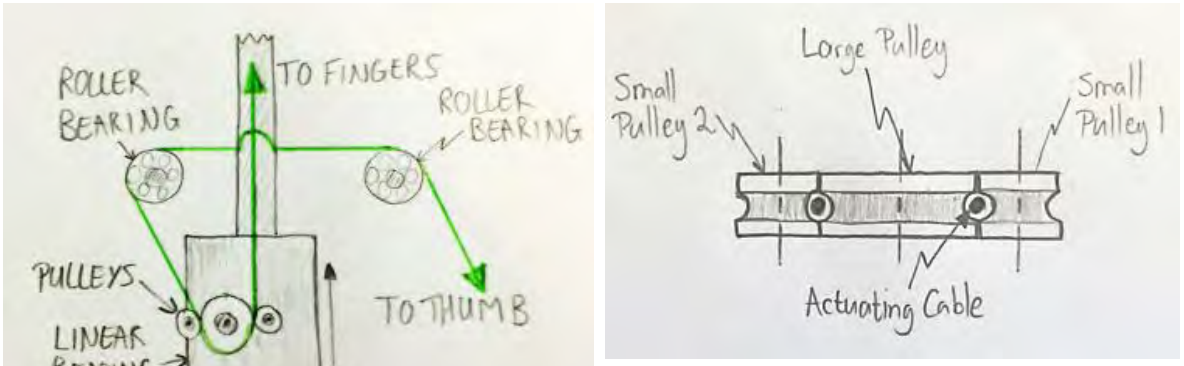

Figure 37 - Final concept solution for the differential mechanism between the thumb and fingers (left) with tri-pulley configuration (right) to prevent dislocation of the actuating wire when tension is lost.

3.4. Finger Locking Mechanism Concepts

In order to lock the hand in a set grasping position, enabling the user to release tension in their shoulder harness, it is essential to incorporate a locking mechanism that will not only provide sufficient retarding force, but also be easily released.

Concept 1: Rotating Ratchet & Pawl with drum

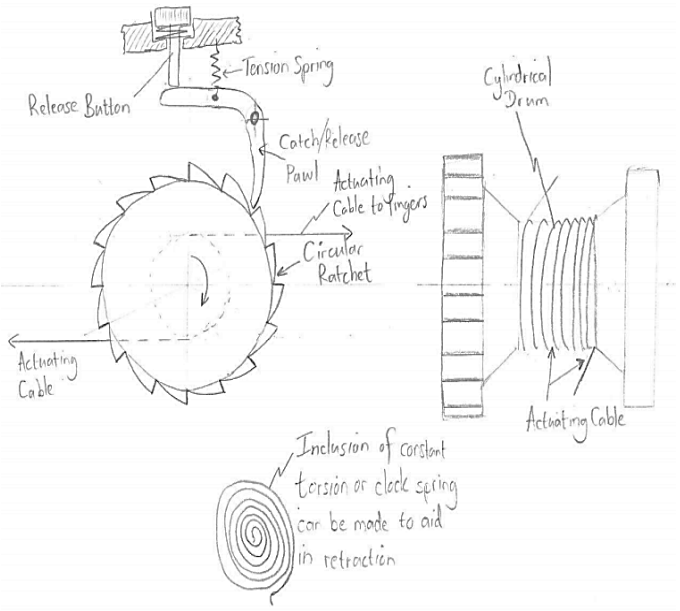

This concept utilises a unidirectional toothed ratchet wheel and a pawl to enable incremental locking actuation as described in Section 2.10, p. 42. The primary actuation cable of the hand wraps around a high-friction drum which may be designed in combination with a constant torque spring to aid in retraction of the device. Furthermore, a release button is included for easy-disengagement, bypassing the locking mechanism.

Concept 2: Linear Ratchet & Pawl

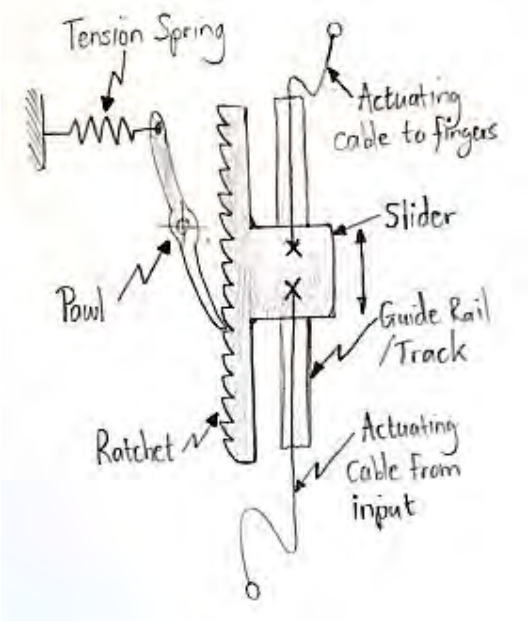

The operation of this concept is relatively simple. It relies on a spring-loaded pawl, similar to Concept 1, and makes use of a linear ratchet rack allowing the slider to move freely along the guide rail when moving downwards through tensioning of the input actuating cable. Upon upward retraction, it is locked in place and requires the tension in the spring to be released to disengage the pawl.

Concept 3: Friction Roller in Slot (Window Blind Lock)

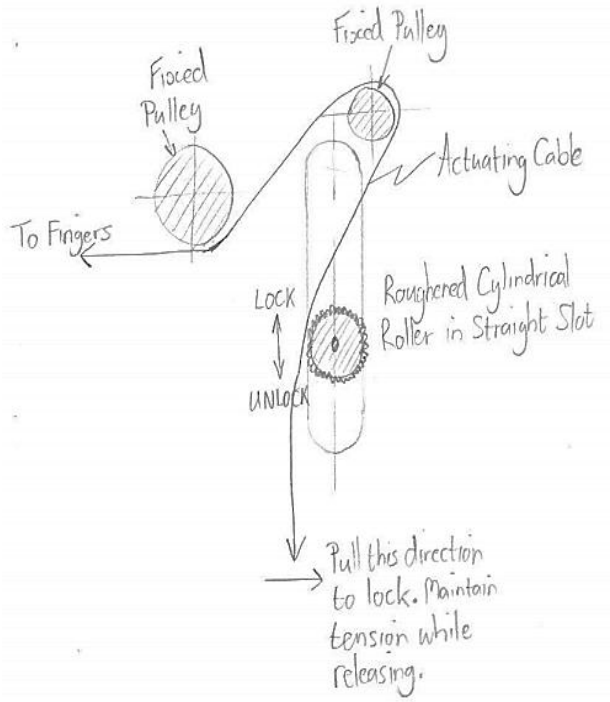

Concept 3 relies heavily on friction to enable locking of the actuating cable. When the actuating cable is tensioned, moved rightwards and released, the roughened cylindrical roller slides upwards in its guide-slot and "pinches" the cable in place. To release the mechanism, the cable is simply tensioned once more while holding it parallel or angled leftward of the axis of the slot. This mechanism is predominantly incorporated into window blind systems. Table 25 presents the advantages and disadvantages of each of the concepts, and Table 26 a DSM evaluating their system properties.

Table 25 - Advantages and Disadvantages of Hand Locking Mechanism Conceptual Designs.

	Concept 1: Rotating Ratchet & Pawl	**Concept 2:** Linear Ratchet & Pawl	**Concept 3:** Friction Roller in Slot (Window Blind Lock)
Advantages	▪ Secure mechanical lock ▪ Compact ▪ Easily released using pawl release button ▪ Can incorporate a constant torque (clock) spring to aid in retraction	▪ Secure mechanical lock ▪ Lower space requirement than rotating ratchet ▪ Independent to motion of actuating cable ▪ Easily released using pawl	▪ Self-tightening, once locked ▪ Easily released by user

Disadvantages	▪ Actuating cable may get tangled on drum and will not coil onto it unless tensioned ▪ Incremental locking (backlash) ▪ Complex to manufacture ▪ Inefficient mechanism due to friction between drum and cable.	▪ Incremental locking (backlash) ▪ Cost of machining may be high due to smaller tolerances to reduce backlash by increasing density of ratchet teeth.	▪ Dependent of friction for locking making it unreliable ▪ There is a large delay in locking as the roller translates towards the pulley ▪ Requires a change in angle of the actuating cable to initiate locking ▪ Requires multiple components and therefore space.

Table 26 - Decision Support Matrix for Conceptual Design of the Hand Locking Mechanism.

Evaluation Criteria	Weighting (%)	Concept 1		Concept 2		Concept 3	
		Rating*	Weighted Total**	Rating	Weighted Total	Rating	Weighted Total
Reliability of Lock	***25***	5	125	5	125	1	25
Compactness	***15***	3	45	5	75	1	15
Low Weight	***5***	1	5	3	15	5	25
Efficiency of mechanism	***10***	1	10	5	50	5	50
Simplicity of design	***5***	3	15	5	25	3	15
Reduced number of components	***5***	3	15	3	15	1	5
Low actuation energy needed from user	***15***	1	15	5	75	5	75
Cognitive ease to use	***10***	5	50	5	50	1	10
Ease of manufacture	***5***	1	5	3	15	5	25
Ease of assembly	***5***	3	15	5	25	3	15
Total	100		**175**		**345**		**235**

*Rating Scale: 1 = Bad 3 = Moderate 5 = Good ** Weighted total = Rating *x* Weighting

DSM according to UCT MEC4055Z course notes **(Kuppuswamy & Redelinghuys, 2012)** and Ertas & Jones **(1993)**

Final Concept Solution: Linear Ratchet & Pawl

According to the information in Table 25 and Table 26, the chosen concept solution was the linear ratchet and pawl due to its compactness, locking reliability, and relative ease of manufacture. It scored a total of 345, exceeding Concept 3 and Concept 1 by 110 and 170 points respectively. A release button similar to that of Concept 1 will be incorporated to rotate the pawl and unlock the ratchet. To reduce friction, the ratchet will be attached to a linear roller bearing, similarly to that of the finger and thumb differentials. Additionally, attachment of the mechanism to the existing linear bearing on which the tri-pulley configuration is located will enable a reduction in space and a reduced number of components. The final concept solution will not be re-sketched due to its similarity to Concept 2.

3.5. Thumb Swivel Transmission Concepts

The objective of the thumb swivel transmission mechanism is to route the actuating cable through the thumb, whilst reducing energy losses and degradative friction wear.

Concept 1: Grooved guide-pins

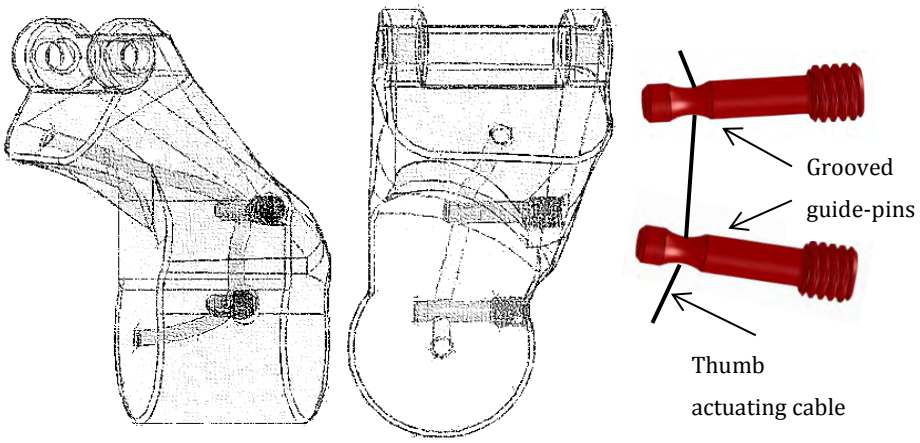

Concept 1 uses two grooved guide-pins over which the thumb actuating cable translates. These pins are threaded on one end for fastening into the thumb swivel material and the groove at their other end intersects with an internal channel in the swivel through which the cable runs. Their axes are not collinear to account for the change in angle between the phalanges and the channel exit in the palm.

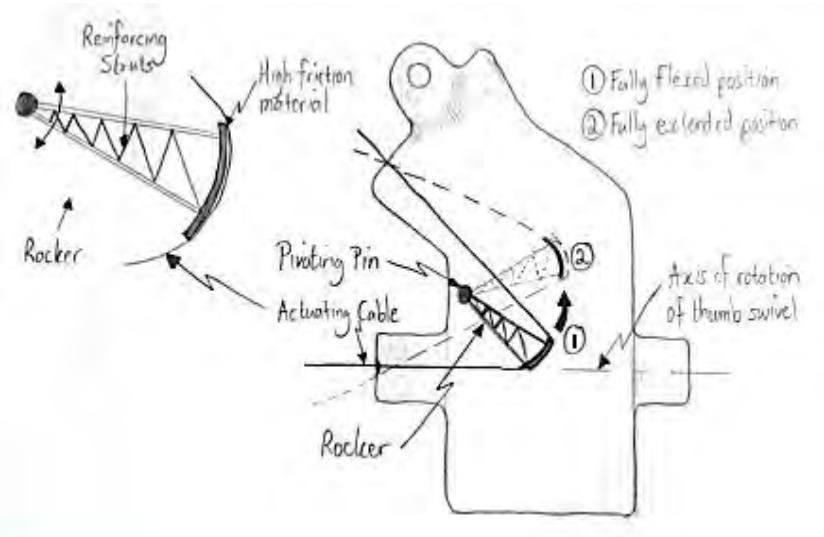

Concept 2: Pivoting Rocker

The pivoting rocker rotates about its pivoting pin from position ① to ② during extension of the thumb. A truss-like structure is selected to reinforce it, while a high friction pad at its end ensures the actuating cable does not slide relative to it; reducing routing losses and wear.

Concept 3: Roller Bearing with Lateral Washers

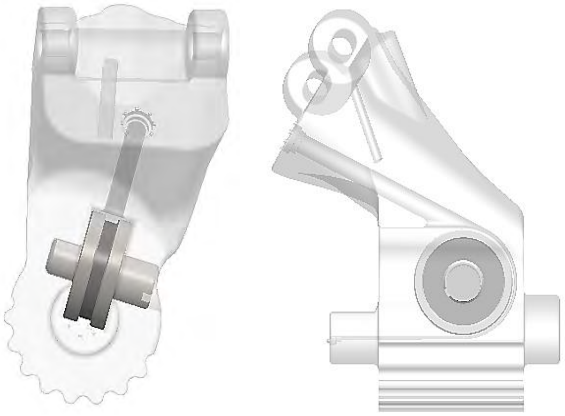

The roller bearing concept uses a deep-groove ball bearing in combination with a locating pin and two lateral washers on its outer-race preventing dislocation of the cable. This mechanism copes extremely well with force transmission, is efficient, and allows constant entry & exit angles, regardless of the adductive or abductive position of the thumb swivel. Referring to

Table 27 below, the advantages and disadvantages of the three concepts are tabularised and a DSM weighting their system properties is shown in Table 28.

Table 27 - Advantages and Disadvantages of Thumb Swivel Transmission Conceptual Designs.

	Concept 1: Grooved guide-pins	**Concept 2:** Pivoting Rocker	**Concept 3:** Roller Bearing with washers
Advantages	▪ Simple ▪ Low cost ▪ Grooved pins guide the cable ▪ Actuating cable in line with axis of rotation	▪ No relative motion between cable and rocker ∴no wear ▪ Large radius of curvature ▪ Could be printed/grown in assembly using rapid prototyping	▪ Low friction transmission ▪ Uses standard bearing ▪ Constant angular transmission ▪ Actuating cable in line with axis of rotation ▪ 3-point alignment of bearing ensures actuating cable self-aligns ▪ Function is independent of cable translation, unlike the rocker
Disadvantages	▪ Friction due to pins generates wear ▪ Large change in angle increases normal reaction forces ▪ Inefficient routing ▪ Non-standard components	▪ Complexity of assembly & manufacture ▪ Large stroke is required ±15mm ▪ Large space requirement leading to weakening of structure due to cavity ▪ Exit angles of the cable are not constant	▪ Needs washers on either side to prevent wire dislocation/ derailment ▪ Size of bearing cavity weakens structure

Table 28 - Decision Support Matrix for Conceptual Design of the Thumb Swivel Transmission.

Evaluation Criteria	**Weighting (%)**	**Concept 1**		**Concept 2**		**Concept 3**	
		Rating*	Weighted Total**	Rating	Weighted Total	Rating	Weighted Total
Low Wear	***15***	*1*	15	3	45	5	75
Mechanism Reliability	***20***	*3*	60	3	60	5	100
Compactness	***10***	*5*	50	1	10	3	30
Efficiency of routing transmission	***15***	*1*	15	3	45	5	75
Simplicity of design	***5***	*5*	25	1	5	3	15
Ease of manufacture	***5***	*5*	25	1	5	5	25
Ease of assembly	***10***	*5*	50	1	10	3	30
Gradual change in transmission angles	***10***	*1*	10	3	30	5	50
Use of standard parts	***10***	*1*	10	1	10	3	30
Total	100		**245**		**175**		**355**

*Rating Scale: 1 = Bad 3 = Moderate 5 = Good ** Weighted total = Rating *x* Weighting

DSM according to UCT MEC4055Z course notes **(Kuppuswamy & Redelinghuys, 2012)** and Ertas & Jones **(1993)**

Final Concept Solution: Roller Bearing

The ability to simply and reliably route the actuating cable with minimal friction losses, gradual change in transmission angles and efficient routing through the use of a standard bearing component enables this concept solution to be the favoured choice. The DSM in Table 28 ranks the properties of this mechanism above those of the grooved guide-pins and pivoting rocker respectively. To ensure structural strength of the thumb swivel is maintained, the size of the bearing cavity will be minimised and an insert will be used to seal the bearing inside after assembly.

3.6. Thumb Swivel Locking Mechanism Concepts

Concept 1: Waved mating surfaces with Spring-loaded plate

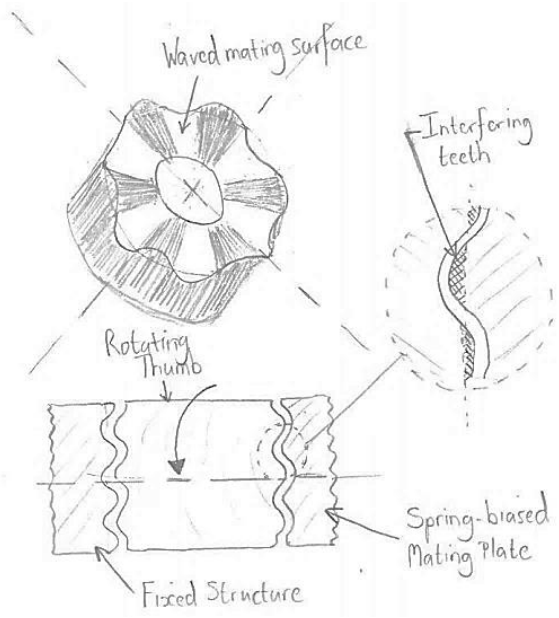

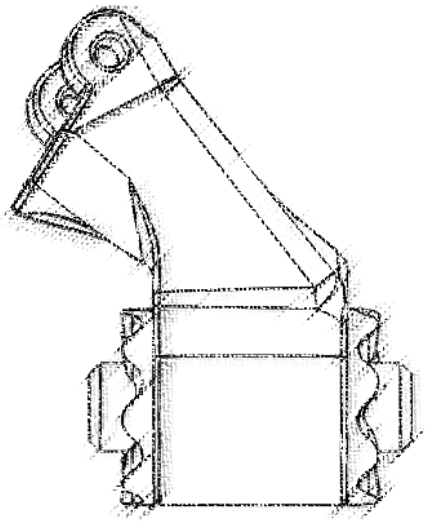

This concept makes use of spring-loaded waved mating plates to lock the thumb swivel in place. Upon rotation, the spring is compressed, moving the mating plate linearly away, allowing the swivel to rotate about its central axis of rotation, adducting or abducting the thumb.

Concept 2: Spring-loaded Ball-and-Cup

The orientation of the locking mechanism is on the lateral borders of the thumb swivel, similar to that of the previous concept. Locking is enabled through spring-loaded balls inserting into recesses in the opposing palmar structure. Once enough rotational force is applied to compress the springs sufficiently, the thumb swivel will be free to rotate until aligning with the adjacent recess; locking once more.

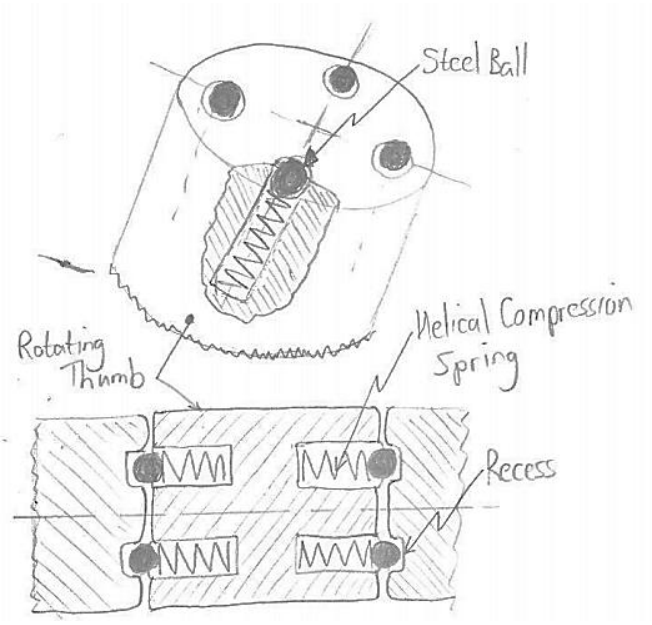

Concept 3: Linearly-actuated locking plate with Sinusoidal or Cylindrical mating profile

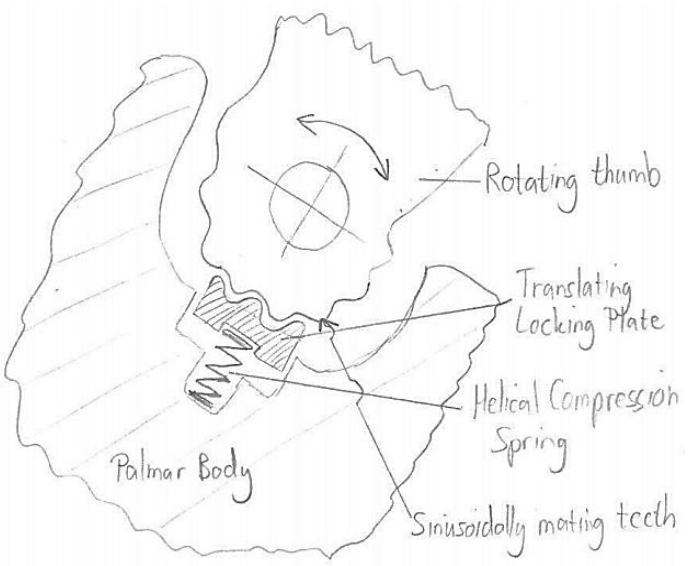

In order for locking not to interfere with the routing of the actuating cable and location of the thumb swivel (which both coincide with the central axis of rotation), this concept utilises sinusoidal or cylindrical mating teeth. A linearly spring-actuated locking plate secures the thumb swivel externally, increasing the lever arm, thereby the resisting moment, and also increasing the available internal space for a thumb swivel transmission mechanism, as discussed in the previous section. Rotation of the swivel depresses the locking plate, compressing the spring(s), unlocking the mechanism and allowing rotation. Incremental locking is achieved through interference of consecutive teeth; the number of locking positions being proportional to their frequency.

Referring to Table 29 below, the advantages and disadvantages of the three thumb swivel locking mechanism concepts are tabularised.

Table 29 - Advantages and Disadvantages of Thumb Swivel Locking Mechanism Conceptual Designs.

	Concept 1: Waved Surface	**Concept 2:** Ball-and-Cup	**Concept 3:** Linearly-actuated Plate
Advantages	▪ Multiple points of contact ▪ Multiple locking orientations possible	▪ Multiple points of contact ▪ Failsafe design through multiple independent ball-and-cup mechanisms	▪ Minimal moving parts ▪ Mechanism is built into the palmar structure, increasing space for the thumb swivel transmission mechanism ▪ Easily assembled ▪ Easily located and doesn't inhibit the routing of actuating cable
Disadvantages	▪ Difficulty in routing actuating cable past plate ▪ Locating the swivel is challenging ▪ Complex surface geometry	▪ Complexity in restraining balls ▪ Many moving parts ▪ Internal design reduces space within thumb swivel ▪ Tight tolerances required ▪ Weakened structure due to large amount of recesses	▪ Moment generated when swivel rotates, tends to tilt the locking plate ▪ Complex surface geometry ▪ Only has three lines of contact

A DSM weighting the systems' properties is shown in Table 30.

Table 30 - Decision Support Matrix for Conceptual Design of the Thumb Swivel Locking Mechanism.

Evaluation Criteria	Weighting (%)	Concept 1		Concept 2		Concept 3	
		Rating*	Weighted Total**	Rating	Weighted Total	Rating	Weighted Total
Compactness of mechanism	***15***	*3*	45	3	45	3	45
Reliability of lock	***20***	*3*	60	3	60	3	60
Low internal space needs	***15***	*3*	45	1	15	5	75
Simplicity of design	***5***	*3*	15	3	15	3	15
Number of incremental locking positions achievable	***10***	*3*	30	1	10	5	50
Reduced component numbers	***10***	*5*	50	1	10	5	50
Ease of assembly	***5***	*3*	15	1	5	5	25
Controllably of locking force	***15***	*3*	45	3	45	3	45
Ease of manufacture	***5***	*3*	15	1	5	3	15
Total	100		**275**		**165**		**335**

*Rating Scale: 1 = Bad 3 = Moderate 5 = Good ** Weighted total = Rating *x* Weighting

DSM according to UCT MEC4055Z course notes **(Kuppuswamy & Redelinghuys, 2012)** and Ertas & Jones **(1993)**

Final Concept Solution: Linearly-actuated locking plate

The chosen thumb swivel locking concept is Concept 3, scoring above the other two concepts according to the criteria shown in Table 30. Its distinguishing feature is its external setting to the thumb swivel, allowing there to be more space for internal mechanisms of the thumb transmission. In addition to this, the external mounting does not weaken the structural integrity of the swivel as is the case with Concept 2. Incremental locking positions are increased by increasing the number of teeth which run along the entire length of the swivel to increase contact area. To overcome the tilting moment generated on the plate during transverse loading, the edges of the plate will be extended and the clearances between them and the palmar structure reduced as shown in Figure 38 below.

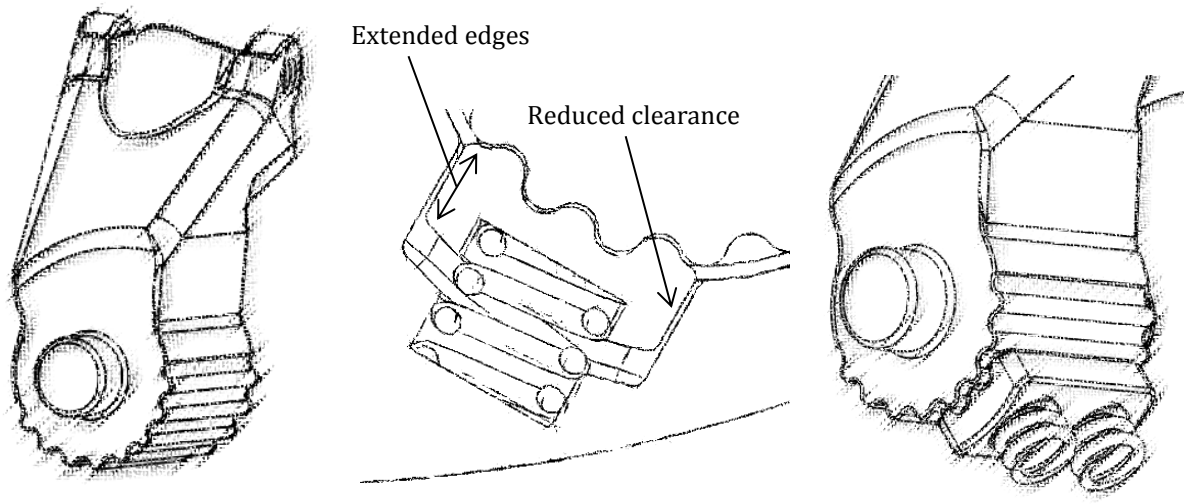

Figure 38 - Final concept solution for the thumb swivel locking mechanism with transverse section view (centre) and infero-lateral perspective view (right).

3.7. Palmar Cushion Concepts

The inclusion of a palmar cushion is envisioned to provide a grasp platform similar to the hypothenar region of the anatomical hand, and enable storage of spring energy when gripping an object. This spring energy will be utilised to compensate for the backlash caused by the incremental locking of the ratchet mechanism described in Section 2.10, p. 42, with the aim being to maintain grasp forces between the hand and the grasped object.

Concept 1: Swivelling Hypothenar region

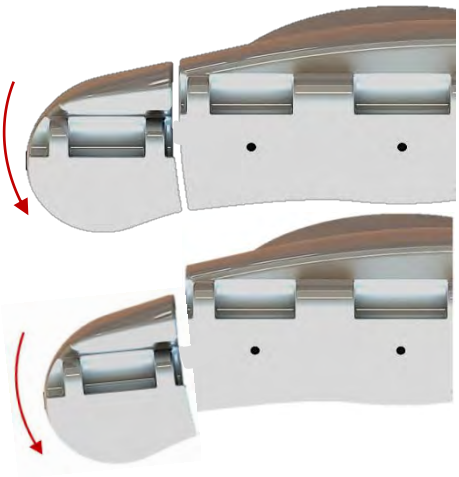

The swivelling hypothenar region of the palmar cushion rotates the lateral portion of the palm (metacarpal region) on an axis parallel to that of the forearm. Furthermore, the 5th digit (small finger) is attached to this swivel and rotates inwards, generating a medial force component, toward the centre of the hand, much like the anatomical grasps. Spring-loaded cantilevers within the palm will provide the translational motion and store energy.

Concept 2: Palmar cushion with meshing teeth

The second concept solution utilises a palmar cushion located at the lateral edge of the palmar surface which uses torsion springs to keep the cushion in the open position. Once loaded, the springs are twisted and the spring energy stored in them forces the cushion to maintain contact force with the grasped object. Mating teeth on lateral protrusions at either end of the cushion prevent it from over-extending. These teeth mate with opposing teeth built into the palmar structure as shown by the sketch on the right.

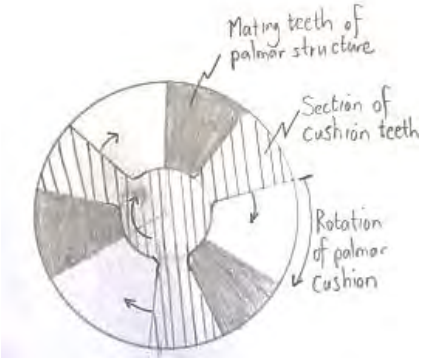

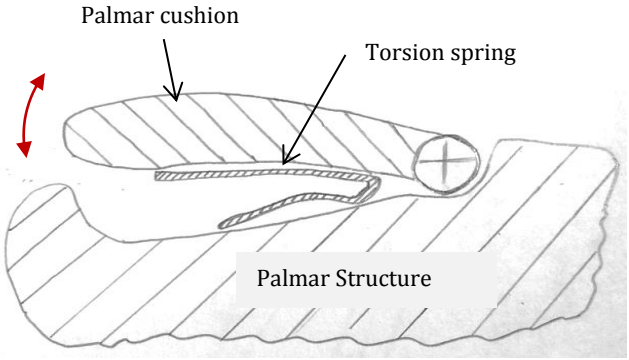

Concept 3: Palmar cushion with Medial Protrusions

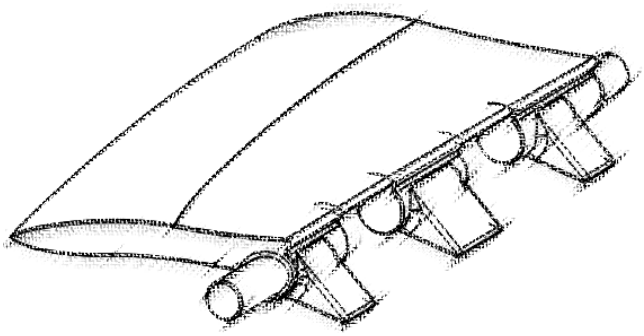

The location of this palmar cushion coincides with that of Concept 2. The differences in the two designs are the hyperextensive mechanism and the spring-type used. To prevent hyperextension, medial protrusions provide resistance to rotation when the cushion is in its fully extended position. Linear compression springs are located behind the cushion, maintaining it in the open position. Pins on the proximal and distal ends locate into slots in the palm, whose centrelines coincide with the axis of rotation.

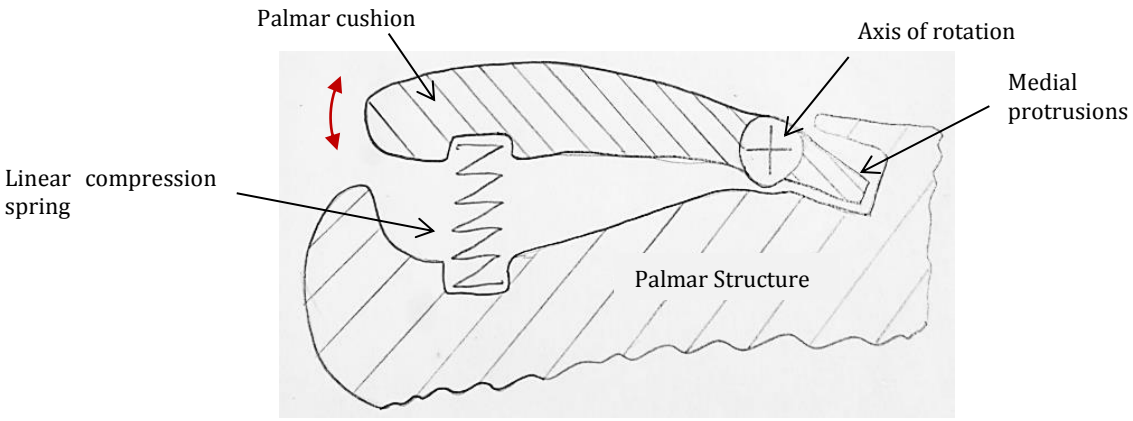

Table 31 and Table 32 describe the advantages and disadvantages of each of the palmar cushion concepts and compare their relative weighted system properties respectively.

Table 31 - Advantages and Disadvantages of Palmar Cushion Conceptual Designs.

	Concept 1: Swivelling Hypothenar region	**Concept 2:** Palmar Cushion with Meshing teeth	**Concept 3:** Palmar Cushion with Medial Protrusions
Advantages	▪ Able to store large amounts of strain energy ▪ Enables inward rotation of the 5th digit, generating a medial grip force component	▪ Set rotation stroke (limits) ▪ Internally stored energy from torsion springs ▪ Springs easily interchangeable ▪ Coincides with hypothenar muscle group ▪ More space allowed for internal differential mechanisms	▪ Set rotation stroke (limits) ▪ Internally stored energy from linear compression springs ▪ Springs easily interchangeable ▪ Coincides with hypothenar muscle group ▪ Medial protrusions are able to resist higher hyperextensive loads than Concept 2 ▪ Looser tolerancing reduces the cost of production ▪ More space for internal mechanisms

Disadvantages	▪ Complex internal mechanism to cope with structural rotation ▪ Reduces space for internal components due to relative translation of the palmar structures ▪ Difficulty in sealing unit ▪ Cannot be used with glove	▪ Weak resistance to hyperextensive loading due to small lever arm of mating teeth. ▪ Tight tolerances increase the cost of manufacture ▪ Must be printed in assembly; requires drainage for excess powder residue	▪ The component of spring force changes as the angle of the cushion changes due to a change in the relative angle between the springs mating surfaces. ▪ Linear springs may buckle as a result or dislodge. ▪ Must be printed in assembly; requires drainage for excess powder residue

Table 32 - Decision Support Matrix for Conceptual Design of the Palmar Cushion.

Evaluation Criteria	**Weighting (%)**	**Concept 1**		**Concept 2**		**Concept 3**	
		Rating*	Weighted Total**	Rating	Weighted Total	Rating	Weighted Total
Hyperextensive Strength	***15***	*5*	75	1	15	3	45
Reliability	***20***	*3*	60	3	60	3	60
Low space requirement	***20***	*1*	20	5	100	5	100
Ability to store energy	***15***	*5*	75	3	45	3	45
Ease of manufacture	***5***	*1*	5	3	15	5	25
Simplicity of design	***5***	*1*	5	3	15	5	25
Grasp conformability	***10***	*3*	30	3	30	3	30
Ease of access to springs	***5***	*1*	5	5	25	5	25
Total	100		**205**		**305**		**325**

*Rating Scale: 1 = Bad 3 = Moderate 5 = Good ** Weighted total = Rating *x* Weighting

DSM according to UCT MEC4055Z course notes **(Kuppuswamy & Redelinghuys, 2012)** and Ertas & Jones **(1993)**

Final Concept Solution: Palmar cushion with Medial Protrusions

Referring to Table 32, Concept 3 ranked the highest, followed closely by Concept 2. The hyperextensive strength, ease of manufacture and simplicity of the design set it apart from the second concept. Hyperextensive strength due to its medial protrusions, simplicity due to it having tabs instead of teeth, and ease of manufacture as looser tolerances are required when compared to the resolution needed to manufacture the mating teeth of Concept 2. The effective spring force of the linear springs decreases as the angle of the cushion increases, and they may be susceptible to buckling. As a result, Concept 3 will be selected as the concept solution for the palmar cushion with the inclusion of torsional springs.

A summary of the selected concept solutions is presented in the Morphological Chart (Table 33) in Section 3.8; with the forerunners highlighted in red. Modifications to made to these concept designs were discussed in their respective sections. Following this chart, Chapter 4 deals with relevant design calculations and a Finite Element Analysis.

3.8. Morphological Chart of Chosen Concept Solutions

Table 33 - Morphological Chart of selected Concept Solutions.

Underactuated Finger Mechanism Concept			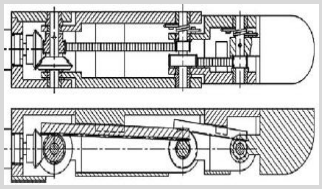	
Differential Palmar Mechanism to Link the Fingers	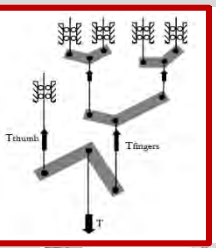	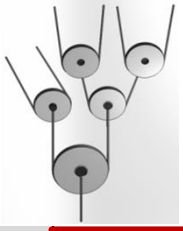	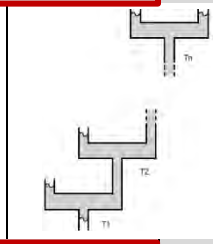	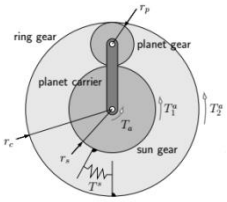
Differential Mechanism to Link the Finger and the Thumb	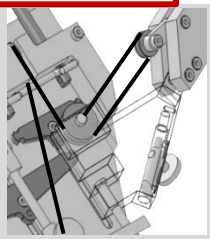	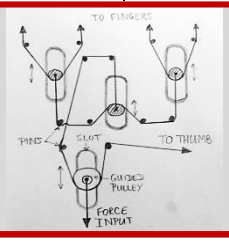	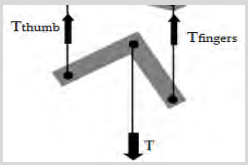	
Hand Locking Mechanism Concepts	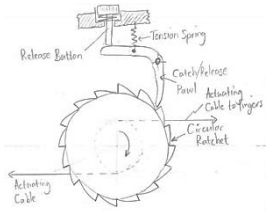	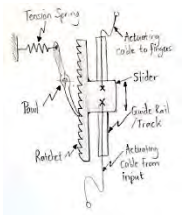	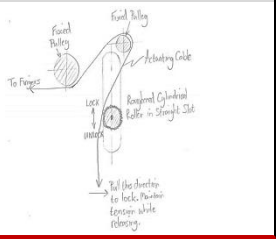	
Thumb Swivel Transmission Concepts	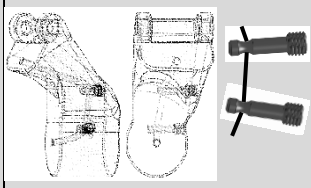	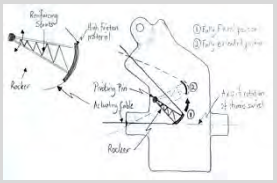	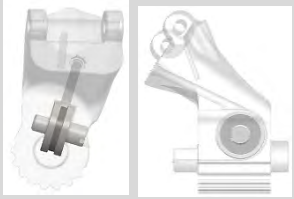	
Thumb Swivel Locking Mechanism Concepts	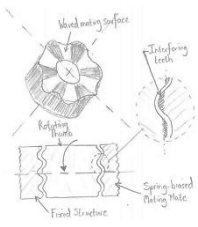	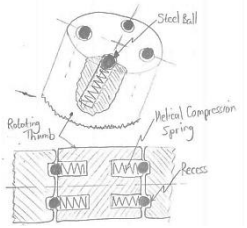	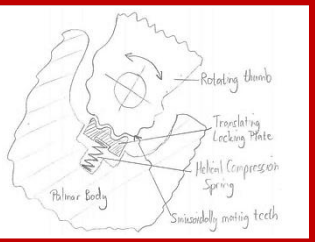	
Palmar Cushion Conceptualisation	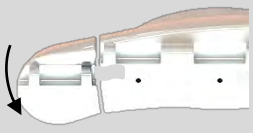	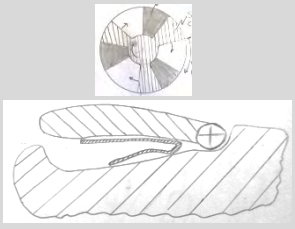	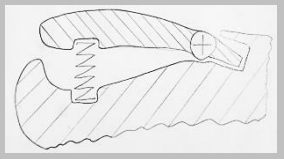	

4

CHAPTER 4: DESIGN CALCULATIONS AND ANALYSIS

4.1. Analytical Force Model (Quasi-static)

An analytical model was initially generated in MATLAB® and later compiled in Excel® to analyse the forces experienced by different members of the hand. It also investigated the interaction of these forces and the behaviour of each member in the system as a function of the input/ cable-actuation force. This model assisted in the design and optimisation of components, ensuring a functional system was generated. The analytical model is iteratively built up in the following order:

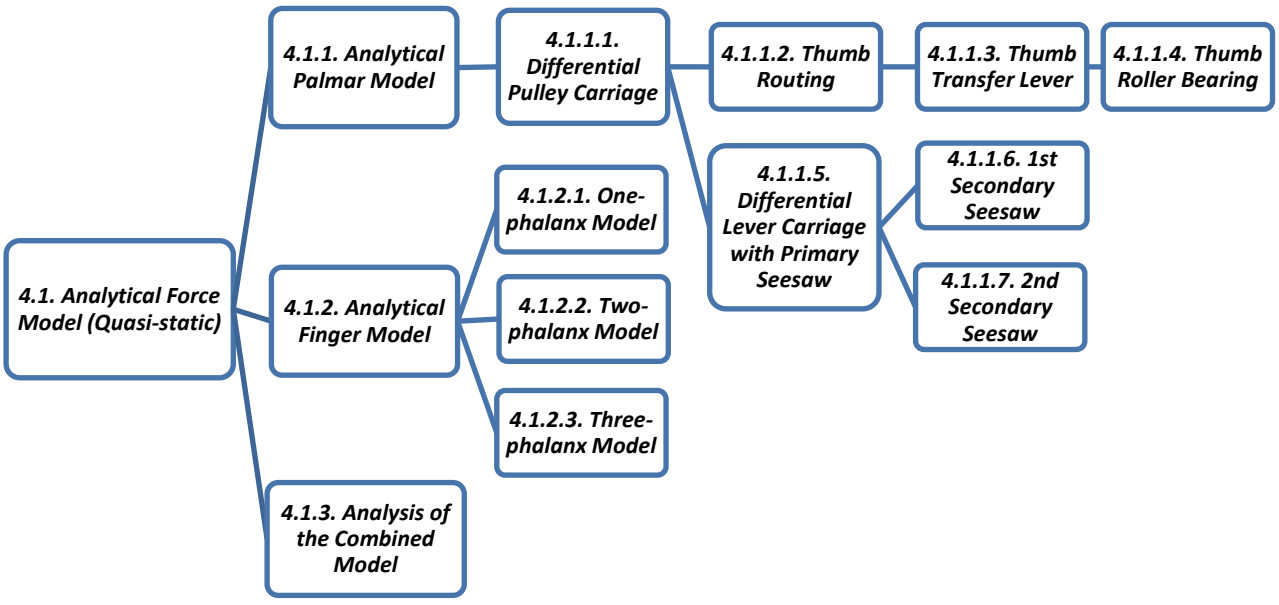

Figure 39 - Structural Diagram of the Analytical Force Model for the Hand Prosthesis.

4.1.1. Analytical Palmar Model

The analytical palmar model is built-up as shown in Figure 39. After analysing the differential pulley carriage, the upper echelon (thumb) will be resolved first, after which the lower tier will be evaluated. Figure 40 below shows the differential lever carriage with its pulleys.

4.1.1.1. Differential Pulley Carriage

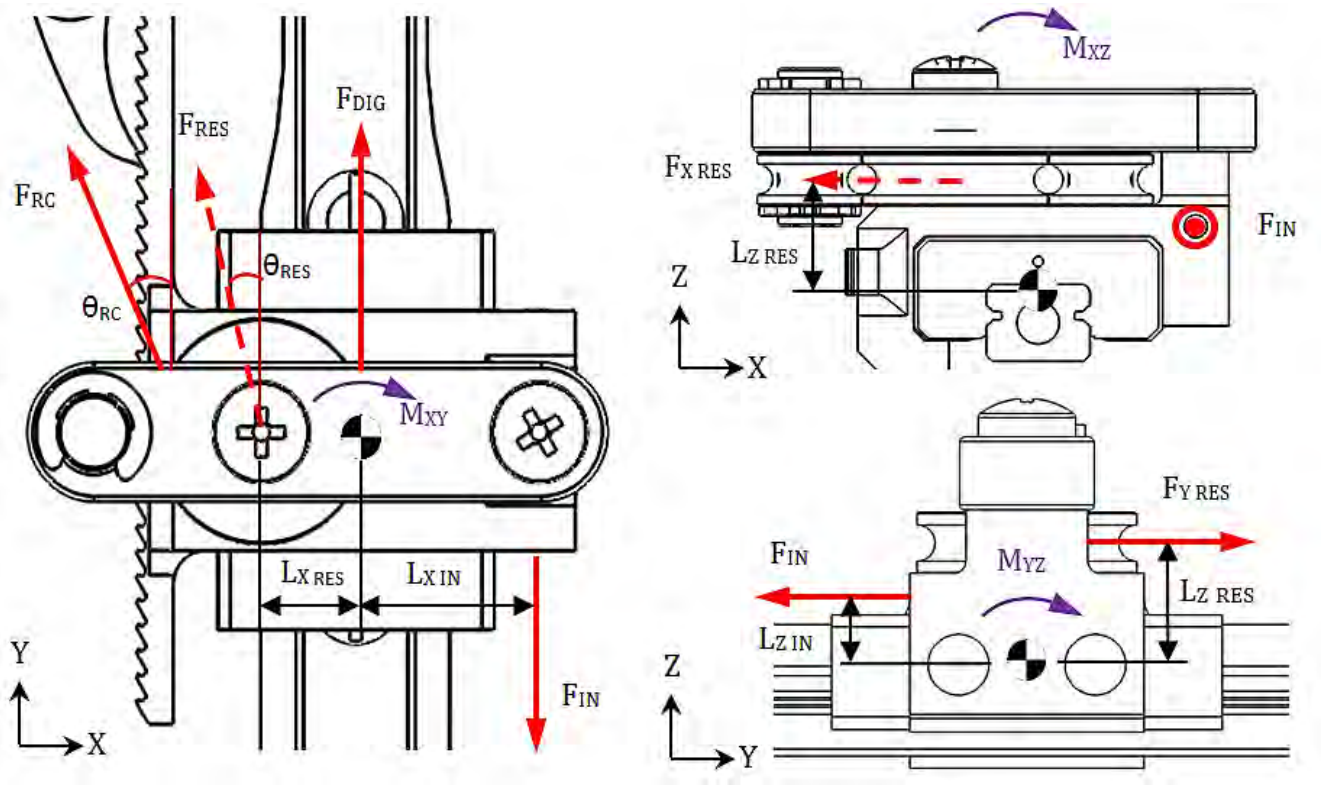

Figure 40 - Force diagram of the differential pulley carriage

where:

- F_{IN} = Primary input force from shoulder harness
- F_{RES} = Resultant pulley force
- F_{RC} = Routing cable force
- F_{DIG} = Digit cable force
- M_{XY} = Resultant moment in XY-plane
- M_{XZ} = Resultant moment in XZ-plane
- M_{YZ} = Resultant moment in YZ-plane
- θ_{RES} = Inclination angle of resultant pulley force
- θ_{RC} = Inclination angle of routing cable force
- $L_{X\,RES}$ = Length to resultant force in x-direction
- $L_{Z\,RES}$ = Length to resultant force in z-direction
- $L_{X\,IN}$ = Length to input force in x-direction
- $L_{Z\,IN}$ = Length to input force in z-direction

Resolving Forces in Y-direction (XY-plane):

$F_{DIG} + F_{RC}\cos(\theta_{RC}) = F_{IN}$ (Assume frictionless pulley $\therefore F_{RC} = F_{DIG}$)

$$\therefore F_{DIG} = F_{RC} = \left(\frac{1}{1+\cos(\theta_{RC})}\right) F_{IN} \qquad [4.1]$$

Also, $F_{RES} = \sqrt{(F_{DIG} + F_{RC}\cos(\theta_{RC}))^2 + (F_{RC}\sin(\theta_{RC}))^2}$

$$\therefore F_{RES} = \left(\frac{\sqrt{2+2\cos(\theta_{RC})}}{1+\cos(\theta_{RC})}\right) F_{IN} \quad [4.2]$$

Next determine the moments on the carriage to determine safe working limits of bearing.

CW Moments about CG (XY-plane):

$$M_{XY} = F_{IN}(L_{X\,IN}) + F_{RES}(L_{X\,RES}\cos(\theta_{RES}))$$

$$\therefore M_{XY} = \left(L_{X\,IN} + \left(\frac{\sqrt{2+2\cos(\theta_{RC})}}{1+\cos(\theta_{RC})}\right)(L_{X\,RES}\cos(\theta_{RES}))\right) F_{IN} \quad [4.3]$$

CCW Moments about CG (XZ-plane):

$$M_{XZ} = F_{RES}\sin(\theta_{RES})(L_{Z\,RES})$$

$$\therefore M_{XZ} = \left(\left(\frac{\sqrt{2+2\cos(\theta_{RC})}}{1+\cos(\theta_{RC})}\right)\sin(\theta_{RES})(L_{Z\,RES})\right) F_{IN} \quad [4.4]$$

CCW Moments about CG (YZ-plane):

$$M_{YZ} = F_{IN}(L_{Z\,IN}) - F_{RES}\cos(\theta_{RES})(L_{Z\,RES})$$

$$\therefore M_{YZ} = \left(L_{Z\,IN} - \left(\frac{\sqrt{2+2\cos(\theta_{RC})}}{1+\cos(\theta_{RC})}\right)(L_{Z\,RES}\cos(\theta_{RES}))\right) F_{IN} \quad [4.5]$$

4.1.1.2. Thumb Routing

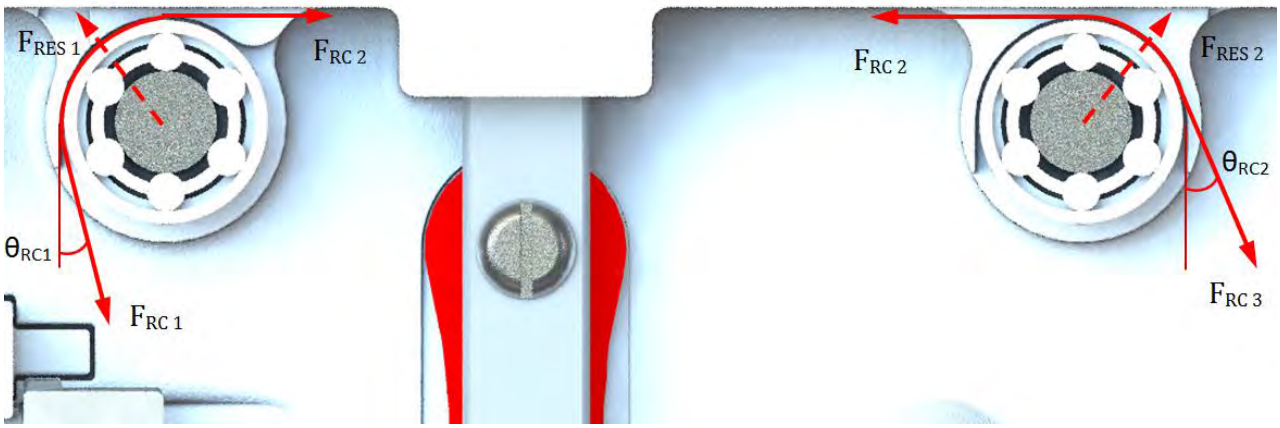

Figure 41 - Force diagram of the routing cable around needle roller bearings

where:

- F_{RC1} = Routing cable force from pulley carriage
- F_{RC2} = Central routing cable force
- F_{RC3} = Routing cable force to thumb transfer lever
- F_{RES1} = Left bearing reaction (normal) force
- F_{RES2} = Right bearing reaction (normal) force
- θ_{RC1} = Inclination angle of routing cable force
- θ_{RC2} = Inclination angle of routing cable force

Determine friction losses due to needle roller bearings using:

Bearing Friction Moment [4] : $M_{bf} = \mu_b P \frac{d_b}{2}$ where:

- μ_b= Coefficient of bearing friction
- P = Normal contact load
- d_b = Bearing bore diameter

But the routing cable is at Ø8mm, and bearing bore is Ø4mm therefore:

Bearing Friction Force : $F_{bf} = \mu_b P \frac{d}{2}\frac{2}{D} = \frac{1}{2}\mu_b P$ [4.6]

From Eqn. 4.1: $F_{RC} = F_{RC1} = \left(\frac{1}{1+\cos(\theta_{RC})}\right) F_{IN}$ [4.7]

Assume frictionless bearing to determine worst case for $F_{RES\,1}$:

$$\therefore F_{RC1} = F_{RC2} \quad [4.8]$$

Hence: $F_{RES1} = \sqrt{(F_{RC2} + F_{RC1}\sin(\theta_{RC1}))^2 + (F_{RC1}\cos(\theta_{RC1}))^2}$

$$\therefore F_{RES1} = F_{RC1}\sqrt{2 + 2\sin(\theta_{RC1})} \quad [4.9]$$

Next include losses due to pulley friction using Eqn. 4.6:

$$F_{RC2} = F_{RC1} - \frac{1}{2}\mu_b F_{RES1} \quad [4.10]$$

Similarly for the right bearing, assume frictionless to determine worst case for $F_{RES\,2}$:

$$\therefore F_{RC2} = F_{RC3} \quad [4.11]$$

$$F_{RES2} = \sqrt{(F_{RC3} - F_{RC2}\sin(\theta_{RC2}))^2 + (F_{RC3}\cos(\theta_{RC2}))^2}$$

$$\therefore F_{RES2} = F_{RC2}\sqrt{2 - 2\sin(\theta_{RC2})} \quad [4.12]$$

Determining losses:

$$F_{RC3} = F_{RC2} - \frac{1}{2}\mu_b F_{RES2} \quad [4.13]$$

Substituting Eqns. 4.7, 4.9, 4.10 & 4.12 into Eqn. 4.13:

$$F_{RC3} = \left(\left(\frac{1}{1+\cos(\theta_{RC})}\right)\left(1 - \frac{1}{2}\mu_b\sqrt{2 + 2\sin(\theta_{RC1})}\right)\left(1 - \frac{1}{2}\mu_b\sqrt{2 - 2\sin(\theta_{RC2})}\right)\right) F_{IN} \quad [4.14]$$

[4] Equation 37 from IKO Bearing Catalogue (IKO, 2009) p. A56

4.1.1.3. Thumb Transfer Lever

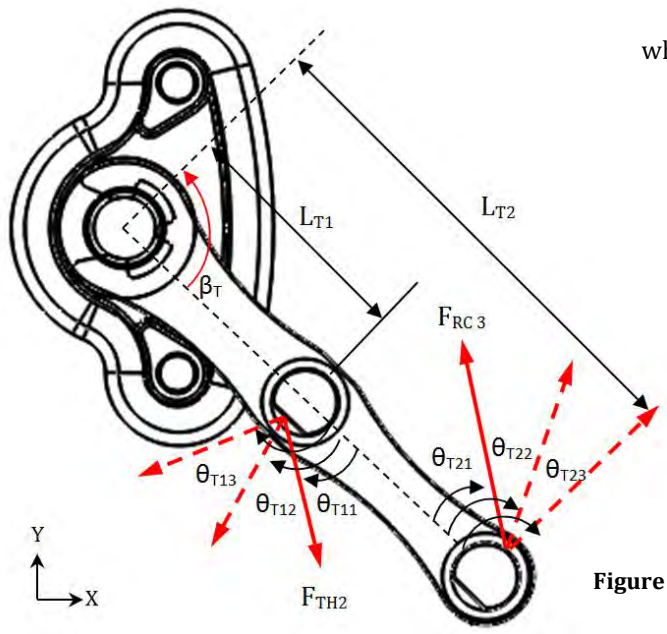

where:

- F_{RC3} = Routing cable force from roller bearing
- F_{TH2} = Thumb cable force to thumb bearing
- L_{T1} = Length to thumb cable
- L_{T2} = Length to routing cable
- θ_{T1i} = Inclination angle of thumb cable force
- θ_{T2i} = Inclination angle of routing cable force
- β_T = Angular motion of transfer lever

Figure 42 - Force diagram of the thumb transfer-lever.

Taking CCW Moments about the pivot of the thumb transfer-lever:

$$F_{RC3}\sin(\theta_{T2i})(L_{T2}) = F_{TH2}\sin(\theta_{T1i})(L_{T1}) \qquad [4.15]$$

$$\therefore F_{TH2} = \frac{\sin(\theta_{T2i})(L_{T2})}{\sin(\theta_{T1i})(L_{T1})} F_{RC3}$$

$$\therefore F_{TH2} = \left(\left(\frac{\sin(\theta_{T2i})(L_{T2})}{\sin(\theta_{T1i})(L_{T1})}\right)\left(\frac{1}{1+\cos(\theta_{RC})}\right)\left(1-\mu_b\sqrt{2+2\sin(\theta_{RC1})}\right)\left(1-\mu_b\sqrt{2-2\sin(\theta_{RC2})}\right)\right) F_{IN} \qquad [4.16]$$

4.1.1.4. Thumb Roller Bearing

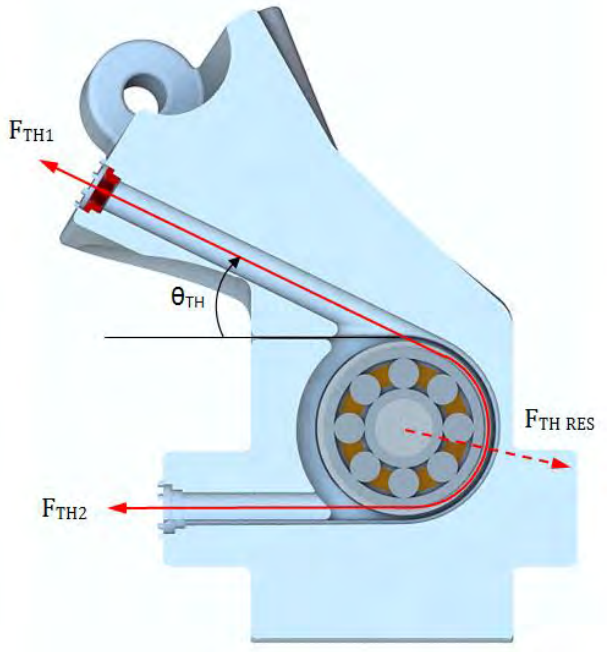

where:

- F_{TH2} = Thumb cable force from transfer lever
- $F_{TH\,RES}$ = Thumb bearing reaction (normal) force
- F_{TH1} = Thumb cable force to proximal phalanx
- θ_{TH} = Inclination angle of thumb cable

Figure 43 - Force diagram of the thumb roller bearing arrangement.

Assume frictionless bearing to determine worst case for $F_{TH\,RES}$:

$$\therefore F_{TH2} = F_{TH1} \quad [4.17]$$

Hence: $$F_{TH\,RES} = \sqrt{(F_{TH2} + F_{TH1}\cos(\theta_{TH}))^2 + (F_{TH1}\sin(\theta_{TH}))^2}$$

$$\therefore F_{TH\,RES} = F_{TH2}\sqrt{2 + 2\cos(\theta_{TH})} \quad [4.18]$$

Next include losses due to pulley friction using Eqn. 4.6:

$$F_{TH1} = F_{TH2} - \frac{1}{2}\mu_b F_{TH\,RES} \quad [4.19]$$

Substitute Eqns. 4.16 & 4.18 into 4.19:

$$F_{TH1} = \left(\left(\left(\frac{\sin(\theta_{T2i})(L_{T2})}{\sin(\theta_{T1i})(L_{T1})}\right)\left(\frac{1}{1+\cos(\theta_{RC})}\right)\left(1 - \mu_b\sqrt{2 + 2\sin(\theta_{RC1})}\right)\left(1 - \mu_b\sqrt{2 - 2\sin(\theta_{RC2})}\right)\right)\left(1 - \frac{1}{2}\mu_b\sqrt{2 + 2\cos(\theta_{TH})}\right)\right)F_{IN} \quad [4.20]$$

4.1.1.5. Differential Lever Carriage with Primary Seesaw

The primary seesaw is free to rotate about its central axis (coinciding with the screw) and is restrained from translation in the x and y directions relative to the slider carriage.

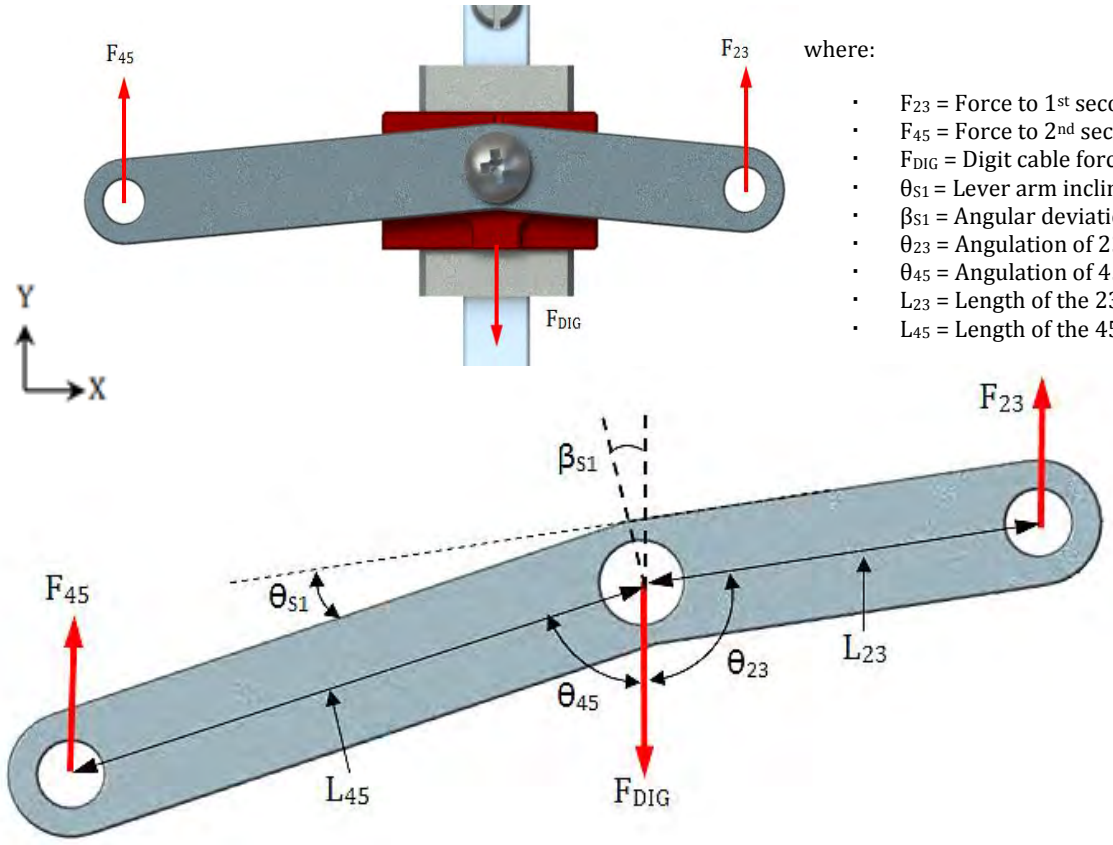

where:

- F_{23} = Force to 1st secondary seesaw
- F_{45} = Force to 2nd secondary seesaw
- F_{DIG} = Digit cable force
- θ_{S1} = Lever arm inclination angle
- β_{S1} = Angular deviation of the lever
- θ_{23} = Angulation of 23 lever arm
- θ_{45} = Angulation of 45 lever arm
- L_{23} = Length of the 23 lever arm
- L_{45} = Length of the 45 lever arm

Figure 44 - Force diagram of the differential lever carriage and primary digital seesaw

Resolve Forces in Y-direction:

$$F_{45} + F_{23} = F_{DIG} \quad [4.21]$$

Taking CCW Moments about the pivot:

$$F_{23}(L_{23}\sin(\theta_{23})) = F_{45}(L_{45}\sin(\theta_{45}))$$

$$\therefore F_{23} = \frac{L_{45}\sin(\theta_{45})}{L_{23}\sin(\theta_{23})} F_{45} \quad [4.22]$$

Substituting Eqn. 4.1 & 4.22 into 4.21:

$$F_{45} = \left(\left(\frac{1}{1+\cos(\theta_{RC})} \right) \Big/ 1 + \left(\frac{L_{45}\sin(\theta_{45})}{L_{23}\sin(\theta_{23})} \right) \right) F_{IN} \quad [4.23]$$

$$F_{23} = \left(\left(\frac{1}{1+\cos(\theta_{RC})} \right) \Big/ 1 + \left(\frac{L_{23}\sin(\theta_{23})}{L_{45}\sin(\theta_{45})} \right) \right) F_{IN} \quad [4.24]$$

The angles vary as a function of rotation of the seesaw (β_{S1}) as follows:

$$\theta_{45} + \theta_{23} = 180° - \theta_{S1} \quad [4.25]$$

$$\theta_{45} = \frac{1}{2}(180° - \theta_{S1}) - \beta_{S1} \quad [4.26]$$

$$\theta_{23} = \frac{1}{2}(180° - \theta_{S1}) + \beta_{S1} \quad [4.27]$$

4.1.1.6. 1st Secondary Seesaw

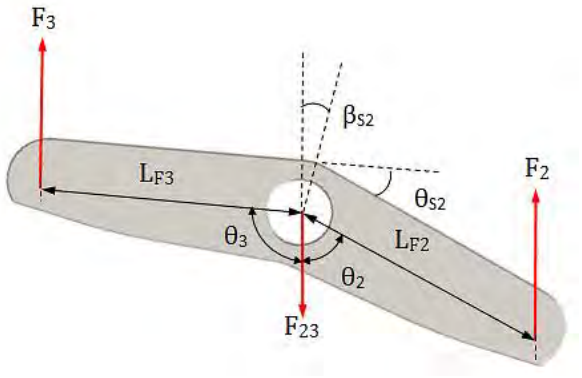

4.1.1.7. 2nd Secondary Seesaw

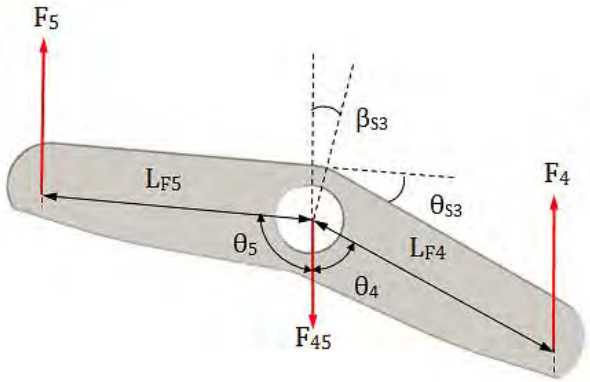

Figure 45 - Force diagrams of the 1st secondary seesaw (left) and the 2nd secondary seesaw (right)

Resolve Forces Vertically:

$$F_2 + F_3 = F_{23} \quad [4.28]$$

CCW Moments about pivot:

$$F_2(L_{F2}\sin(\theta_2)) = F_3(L_{F3}\sin(\theta_3)) \quad [4.29]$$

$$\therefore F_2 = \frac{L_{F3}\sin(\theta_3)}{L_{F2}\sin(\theta_2)} F_3$$

$$\therefore F_3 = \frac{L_{F2}\sin(\theta_2)}{L_{F3}\sin(\theta_3)} F_2$$

$$\theta_2 + \theta_3 = 180° - \theta_{S2} \quad [4.30]$$

$$\theta_2 = \frac{1}{2}(180° - \theta_{S2}) - \beta_{S2} \quad [4.31]$$

$$\theta_3 = \frac{1}{2}(180° - \theta_{S2}) + \beta_{S2} \quad [4.32]$$

Resolve Forces Vertically:

$$F_4 + F_5 = F_{45} \quad [4.33]$$

CCW Moments about pivot:

$$F_4(L_{F4}\sin(\theta_4)) = F_5(L_{F5}\sin(\theta_5)) \quad [4.34]$$

$$\therefore F_4 = \frac{L_{F5}\sin(\theta_5)}{L_{F4}\sin(\theta_4)} F_5$$

$$\therefore F_5 = \frac{L_{F4}\sin(\theta_4)}{L_{F5}\sin(\theta_5)} F_4$$

$$\theta_4 + \theta_5 = 180° - \theta_{S3} \quad [4.35]$$

$$\theta_4 = \frac{1}{2}(180° - \theta_{S3}) - \beta_{S3} \quad [4.36]$$

$$\theta_5 = \frac{1}{2}(180° - \theta_{S3}) + \beta_{S3} \quad [4.37]$$

where:

- F_2 = Force to 2nd Digit (Index finger)
- F_3 = Force to 3rd Digit (Middle finger)
- F_{23} = Force from 1st secondary seesaw
- θ_{S2} = Lever arm inclination angle
- β_{S2} = Angular deviation of the lever
- θ_2 = Angulation of F_2 lever arm
- θ_3 = Angulation of F_3 lever arm
- L_2 = Length of the F_2 lever arm
- L_3 = Length of the F_3 lever arm
- F_4 = Force to 4th Digit (Ring finger)
- F_5 = Force to 5th Digit (Little finger)
- F_{45} = Force from 2nd secondary seesaw
- θ_{S3} = Lever arm inclination angle
- β_{S3} = Angular deviation of the lever
- θ_4 = Angulation of F_4 lever arm
- θ_5 = Angulation of F_5 lever arm
- L_4 = Length of the F_4 lever arm
- L_5 = Length of the F_5 lever arm

Combining Eqns. 4.24, 4.28 & 4.29:

$$F_2 = \left(\frac{1}{1+\frac{L_{F2}\sin(\theta_2)}{L_{F3}\sin(\theta_3)}}\right)\left(\left(\frac{1}{1+\cos(\theta_{RC})}\right)\Big/\left(1+\left(\frac{L_{23}\sin(\theta_{23})}{L_{45}\sin(\theta_{45})}\right)\right)\right)F_{IN} \quad [4.38]$$

$$F_3 = \left(\frac{1}{1+\frac{L_{F3}\sin(\theta_3)}{L_{F2}\sin(\theta_2)}}\right)\left(\left(\frac{1}{1+\cos(\theta_{RC})}\right)\Big/\left(1+\left(\frac{L_{23}\sin(\theta_{23})}{L_{45}\sin(\theta_{45})}\right)\right)\right)F_{IN} \quad [4.39]$$

Combining Eqns. 4.23, 4.33 & 4.34:

$$F_4 = \left(\frac{1}{1+\frac{L_{F4}\sin(\theta_4)}{L_{F5}\sin(\theta_5)}}\right)\left(\left(\frac{1}{1+\cos(\theta_{RC})}\right)\Big/\left(1+\left(\frac{L_{45}\sin(\theta_{45})}{L_{23}\sin(\theta_{23})}\right)\right)\right)F_{IN} \quad [4.40]$$

$$F_5 = \left(\frac{1}{1+\frac{L_{F5}\sin(\theta_5)}{L_{F4}\sin(\theta_4)}}\right)\left(\left(\frac{1}{1+\cos(\theta_{RC})}\right)\Big/\left(1+\left(\frac{L_{45}\sin(\theta_{45})}{L_{23}\sin(\theta_{23})}\right)\right)\right)F_{IN} \quad [4.41]$$

4.1.2. Analytical Finger Model

Assumptions:

- The deflection of the phalanges are negligible (i.e. rigid)
- Grasp force remains normal to its respective phalanx throughout the motion
- Grasp force acts at the centre of the contact surface of each phalanx

4.1.2.1. One-phalanx analytical model (Distal phalanx)

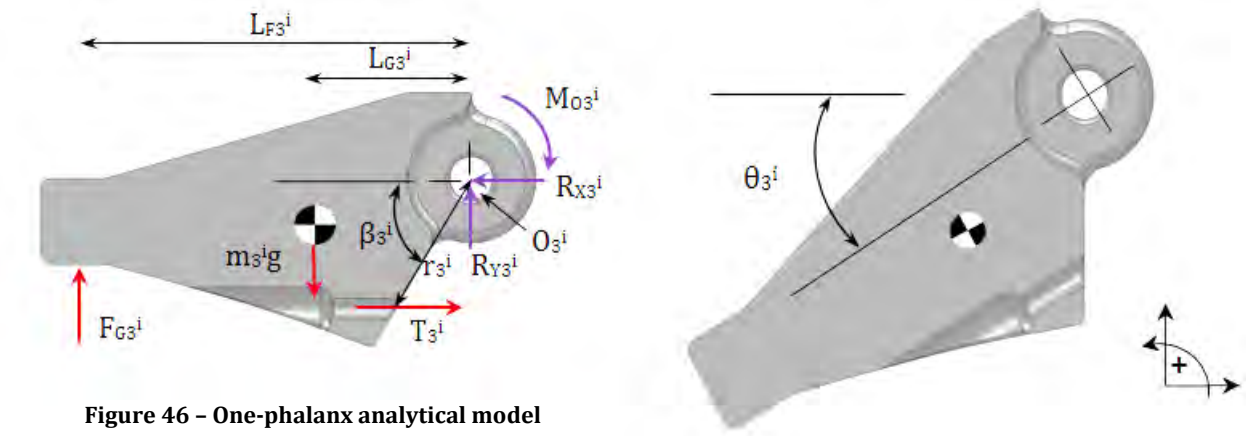

Figure 46 – One-phalanx analytical model

CCW Moments about O_3^i:

- Mass Moment : $$\sum M^i_{Mass\,3} = m^i_3 g\left(L^i_{G3}\cos\left(\theta^i_3\right)\right) \quad [4.42]$$
- Torsion Spring Moment: $$\sum \mathrm{M}^{\mathrm{i}}_{\mathrm{Spring}\,3} = -\frac{\theta^{\mathrm{i}}_3 \mathrm{d}^4 \mathrm{E}}{64\mathrm{DNa}} \quad [4.43]$$
- Tension Moment : $$\sum M^i_{Tension\,3} = T^i_3\left(r^i_3\sin\left(\beta^i_3+\theta^i_3\right)\right) \quad [4.44]$$
- Hinge Friction Moment : $$\sum M^i_{Hinge\,3} = -\mu_r r^i_p\sqrt{\left(m^i_3 g - F^i_{G3}\right)^2+\left(T^i_3\right)^2} \quad [4.45]$$
- Grasp Force Moment : $$\sum M^i_{Grasp\,3} = -F^i_{G3}\left(L^i_{F3}\right) \quad [4.46]$$

Total Moments$_3{}^i$: $$\sum MO^i_3 = \sum\left(M^i_{Mass\,3} + M^i_{Spring\,3} + M^i_{Tension\,3} + M^i_{Hinge\,3} + M^i_{Grasp\,3}\right) = 0 \quad [4.47]$$

where:

- L_G = distance from pivot to centre of gravity
- F_G = applied grasp force
- T = cable (tendon) tension
- $R_{X/Y}$ = hinge reaction forces in x and y directions
- M_O = hinge reaction moment
- m = mass of phalanx
- g = gravitational acceleration
- r = radial channel distance from pivot
- β = angle of interphalangeal phalanx face
- $_{\wedge}{}^{i}$ = identifier for fingers/digits (i.e. 1-5, thumb to little finger resp.)
- 1,2,3 = identifier for respective phalanges (i.e. proximal, middle, distal resp.)
- L_F = distance from pivot to applied grip force and/or normal force
- θ = flexion angle of each phalange
- d = spring wire diameter
- E = Young's Modulus of spring material
- D = mean coil diameter
- Na = number of active turns of spring
- μ_r = estimated coefficient of hinge friction (static)
- r_p = hinge pin radius

4.1.2.2. Two-phalanx analytical model (Middle & distal phalanx)[5]

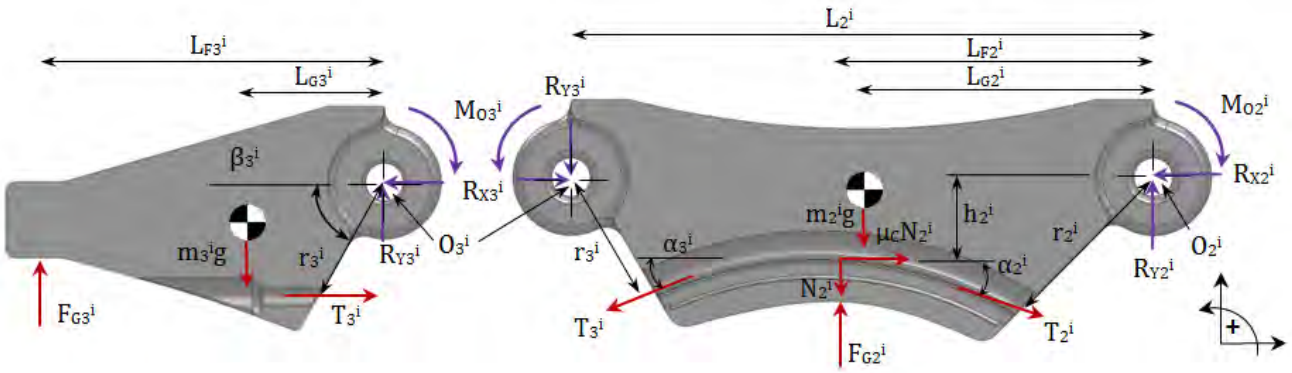

Figure 47 – Two-phalanx analytical model

where:

- L = length of phalanx
- N = normal reaction force of cable/tendon on the phalanx
- h = distance of tendon friction force from hinge/pivot
- μ_C = coefficient of channel friction (static)
- α = angle of deviation of actuating wire

CCW Moments about O_2^i:

- Mass Moment :

$$\sum M_{Mass\,2}^i = m_2^i g\left(L_{G2}^i \cos\left(\theta_2^i\right)\right) + m_3^i g\left(L_2^i \cos\left(\theta_2^i\right) + L_{G3}^i \cos\left(\theta_2^i + \theta_3^i\right)\right) \quad [4.48]$$

- Torsion Spring Moment:

$$\sum M_{Spring\,2}^i = -\frac{\theta_2^i d^4 E}{64DNa} \quad [4.49]$$

- Tension Moment :

$$\sum M_{Tension\,2}^i = T_3^i\left(r_3^i \sin\left(\beta_3^i + \theta_3^i\right)\right) + N_2^i\left(L_{F2}^i + \mu_C h_2^i\right) \quad [4.50]$$

- Hinge Friction Moment :

$$\sum M_{Hinge\,2}^i = -\mu_r r_p^i \sqrt{\left((m_2^i + m_3^i)g - (F_{G2}^i + F_{G3}^i) + N_2^i\right)^2 + \left(T_3^i + \mu_C N_2^i\right)^2} \quad [4.51]$$

- Grasp Force Moment :

$$\sum M_{Grasp\,2}^i = -F_{G2}^i\left(L_{F2}^i\right) - F_{G3}^i\left(L_2^i + L_{F3}^i cos\left(\theta_3^i\right)\right) \quad [4.52]$$

Total Moments$_2^i$: $\sum MO_2^i = \sum(M_{Mass\,2}^i + M_{Spring\,2}^i + M_{Tension\,2}^i + M_{Hinge\,2}^i + M_{Grasp\,2}^i) = 0$ [4.53]

[5] For the analysis of the thumb, a two-phalanx analytical model is selected due to its anatomical makeup.

4.1.2.3. Three-phalanx analytical model (Proximal, middle & distal phalanx)[6]

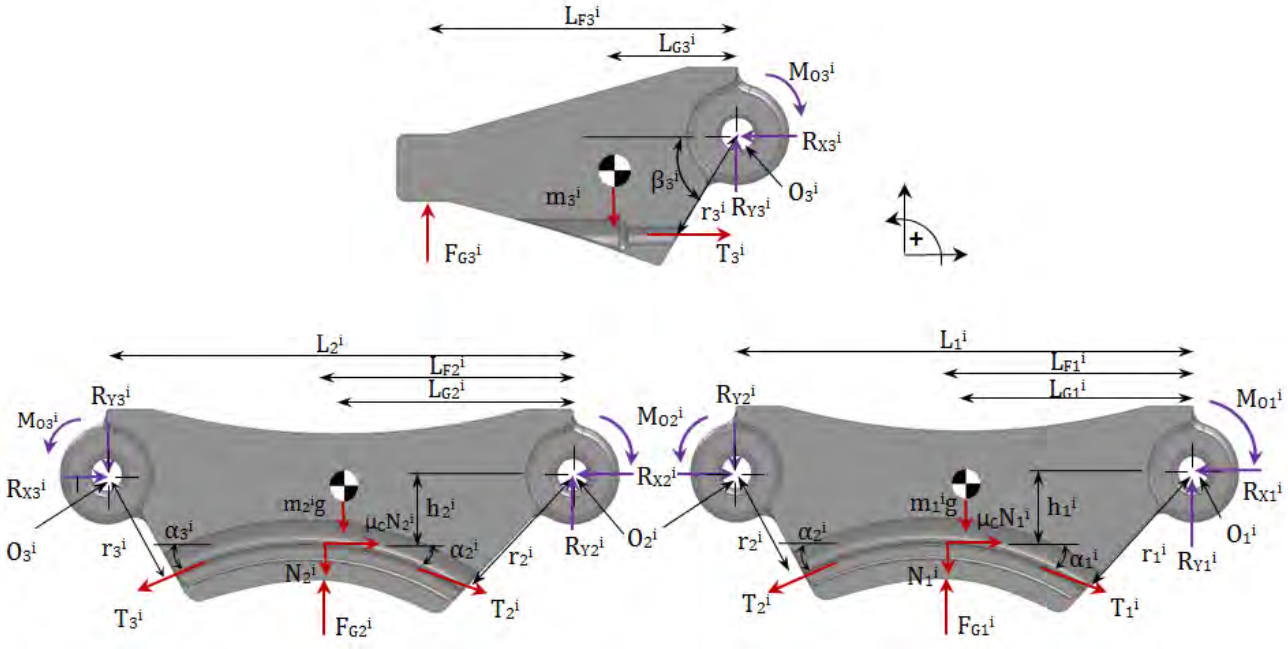

Figure 48 – Three-phalanx analytical model

CCW Moments about O_1^i:

- *Mass Moment* :

$$\sum M^i_{Mass\,1} = m^i_1 g\left(L^i_{G1}\cos(\theta^i_1)\right) + m^i_2 g\left(L^i_1\cos(\theta^i_1) + L^i_{G2}\cos(\theta^i_1+\theta^i_2)\right) + m^i_3 g\left(L^i_1\cos(\theta^i_1) + L^i_2\cos(\theta^i_1+\theta^i_2) + L^i_{G3}\cos(\theta^i_1+\theta^i_2+\theta^i_3)\right) \quad [4.54]$$

- *Torsion Spring Moment*:

$$\sum M^i_{Spring\,1} = -\frac{\theta^i_1 d^4 E}{64DNa} \quad [4.55]$$

- *Tension Moment* :

$$\sum M^i_{Tension\,1} = T^i_3\left(r^i_3\sin(\beta^i_3+\theta^i_3)\right) + N^i_2\left(\left(L^i_1+L^i_{F2}\right)+\mu_C h^i_2\right) + N^i_1\left(L^i_{F1}+\mu_C h^i_1\right) \quad [4.56]$$

- *Hinge Friction Moment* :

$$\sum M^i_{Hinge\,1} = -\mu_r r^i_P\sqrt{\left((m^i_1+m^i_2+m^i_3)g - \left(F^i_{G1}+F^i_{G2}+F^i_{G3}\right)+N^i_1+N^i_2\right)^2 + \left(T^i_3+\mu_C N^i_1+\mu_C N^i_2\right)^2} \quad [4.57]$$

- *Grasp Force Moment* :

$$\sum M^i_{Grasp\,1} = -F^i_{G1}\left(L^i_{F1}\right) - F^i_{G2}\left(L^i_1+L^i_{F2}\cos(\theta^i_2)\right) - F^i_{G3}\left(L^i_1+L^i_2+L^i_{F3}\cos(\theta^i_3)\right) \quad [4.58]$$

[6] For the analysis of the fingers, three phalanx models will be selected due to their anatomy.

$$Total\ Moments_1{}^i : \sum MO_1^i = \sum(M_{Mass\,1}^i + M_{Spring\,1}^i + M_{Tension\,1}^i + M_{Hinge\,1}^i + M_{Grasp\,1}^i) = 0 \quad [4.59]$$

The cable tension and normal forces used in the above calculations were simplified into the following forms:

$$N_1^i = T_1^i \sin(\alpha_1^i) + T_2^i \sin(\alpha_2^i) \quad [4.60]$$

$$N_2^i = T_2^i \sin(\alpha_2^i) + T_3^i \sin(\alpha_3^i) \quad [4.61]$$

where:

$$T_1^i = F_i \quad [4.62]$$

$$T_2^i = \left(1 - \mu_c \sin(\alpha_1^i) \Big/ 1 + \mu_c \sin(\alpha_2^i)\right) F_i \quad [4.63]$$

$$T_3^i = \left(1 - \mu_c \sin(\alpha_1^i)\right)\left(1 - \frac{\mu_c\,(2\sin(\alpha_2^i))}{1+\mu_c \sin(\alpha_2^i)} \Big/ 1 + \mu_c \sin(\alpha_3^i)\right) F_i \quad [4.64]$$

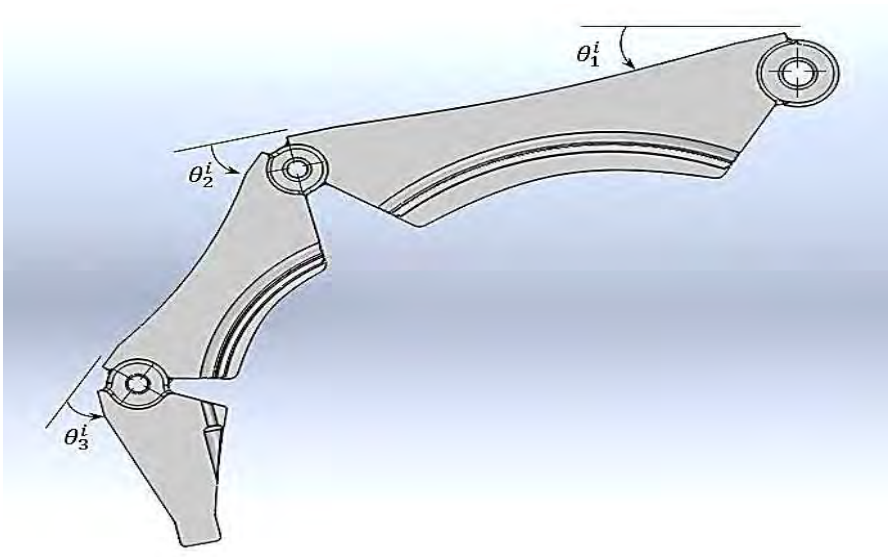

Figure 49 - Theta angles for respective digits

4.1.3. Analysis of the Combined Model

Using Equations 4.1 to 4.64 in combination with system properties, the total analytical model was built-up. The following order of approach was taken:

Palmar Model approach:

- Input all system lengths and angles as specified in Section 4.1.1., as well as the coefficients of rolling friction of the roller bearings from manufacturer's catalogues.
- Using equations 4.1 to 4.41, calculate all forces as a function of the primary cable actuation input force F_{IN} and export F_{TH1}, F_2, F_3, F_4 & F_5 into the Finger Model to calculate the respective tensions, normal reaction forces, hinge-friction moments and tension moments.

Finger Model approach:

- Input system dimensions and properties including m, L, Lg, r_p, r, β, h, g, μ_r, μ_c as specified in Section 4.1.2.
- Call Finger input forces from Palmar Model.
- Generate θ vectors in 1° increments for each interphalangeal joint, and the respective α-angle vectors as a function of θ's. (Selected θ ranges for the joints are shown in Table 8, p. 35).
- Calculate Mass Moments and Spring Moments as a function of θ's.
- Using the finger input forces from the Analytical Palmar Model, calculate T_i and N_i for the respective phalanges and determine Tension Moments as a function of θ's.
- Calculate Hinge Friction Moments and Grip Force Moments, as a function of θ's, the selected grasping forces and their distributions (see Table 14, p. 40).
- Calculate Resultant Moments as a function of θ's, both including and excluding Grip Forces.

4.1.3.1. Determine whether initial spring moments exceed initial mass moments at 0° flexion.

(To see if digits will remain open/extended when the palm is facing down)

$$\sum M^i_{Spring} - \sum M^i_{Mass} > 0$$

Table 34 - Difference in initial spring and mass moments (N.mm)

Digit	DIP	PIP (IP Thumb)	MCP
1st	-	*+16.1*	*+22.8*
2nd	*+1.71*	*+4.1*	*+4.0*
3rd	*+5.1*	*+5.2*	*+3.2*
4th	*+2.9*	*+4.1*	*+2.5*
5th	*+5.1*	*+2.3*	*+5.1*
Positive = Pass	Negative = Fail		

Referring to Table 34, it can be seen that all the springs have enough initial torque to maintain extend the fingers against their own weight. (*Refer to Section 4.2.2 for detailed spring calculations.*)

4.1.3.2. Check whether initial spring moments exceed estimated hinge-friction moments and initial mass moments at 0° flexion.

(To see if hand will open/extend from flexed position)

$$\sum M^{i}_{Spring} - \sum M^{i}_{Hinge} - \sum M^{i}_{Mass} > 0$$

Table 35 - Difference in initial spring, hinge-friction and mass moments (N.mm)

Digit	DIP	PIP (IP Thumb)	MCP
1st	-	+8.2	+9.6
2nd	+0.45	+1.6	-5.1
3rd	+3.8	+2.6	-6.6
4th	+1.9	+1.6	-7.0
5th	+4.2	+0.6	-0.8
Positive = Pass	Negative = Fail		

Referring to Table 35, the MCP joints of the 2nd to 5th digits have negative moments indicating insufficient restoring torque. To overcome this, either replace these MCP springs with stiffer ones, or increase initial deflections of the exiting springs and re-evaluate. To minimise the stresses associated with over-flexion of the springs that reduce fatigue life, it was decided to replace the MCP springs instead of increasing deflections. Table 36 presents the 2nd iteration of the resultant moments.

Table 36 - Second iteration of difference in initial spring, hinge-friction and mass moments (N.mm)

Digit	DIP	PIP (IP Thumb)	MCP
1st	-	+8.2	+9.6
2nd	+0.45	+1.6	+1.7
3rd	+3.8	+2.6	+0.2
4th	+1.9	+1.6	+1.3
5th	+4.2	+0.6	+0.7
Positive = Pass	Negative = Fail		

Table 37 - Initial and adjusted torsion spring distribution for the interphalangeal joints.[7]

	Initial spring distribution (Wire diameter x turns)			*Adjusted spring distribution (Wire diameter x turns)*		
Digit	*DIP*	*PIP (IP Thumb)*	*MCP*	*DIP*	*PIP (IP Thumb)*	*MCP*
1st	-	0.8mm x N5	0.9mm x N5	-	0.8mm x N5	0.9mm x N5
2nd	0.5mm x N7	0.6mm x N5	0.7mm x N5	0.5mm x N7	0.6mm x N5	**0.8mm x N5**
3rd	0.6mm x N5	0.6mm x N4	0.7mm x N5	0.6mm x N5	0.6mm x N4	**0.8mm x N5**
4th	0.5mm x N4	0.6mm x N5	0.6mm x N3	0.5mm x N4	0.6mm x N5	**0.8mm x N5**
5th	0.6mm x N5	0.5mm x N4	0.6mm x N3	0.6mm x N5	0.5mm x N4	**0.7mm x N5**

[7] The springs have a mean coil diameter of 5mm in the DIP & PIP joints and 7mm in the MCP joints, straight-wound lever-arms 12mm in length and are made of ASTM A228 Music wire, with initial deflection of 20° from their neutral position. Refer to Section 4.2.2, p. 106 and Appendix B2, p. B-6 for detailed calculations.

Referring to Table 36, the resultant moments of the joints are now positive indicating extensive-torques. It should be noted that while positive, these torques should be minimised to reduce the force input by the user. The initial and adjusted spring distributions are shown in Table 37.

4.1.3.3. Check input cable actuation force required to overcome initial internal moments. *(i.e. mass moments, spring moments & hinge-friction moments).*

$$\sum M^i_{Tension} - \sum M^i_{Mass} - \sum M^i_{Spring} - \sum M^i_{Hinge} > 0$$

The resultant moments at each of these joints was viewed as the input force was increased in 5 N increments. Positive resultant moments at joints were considered a pass; this means that the joints will begin to flex, overcoming their initial residual torque. The findings are tabularised in Table 38.

Table 38 – Input cable actuation force for flexion of unloaded joints (N)

Digit	DIP	PIP (IP Thumb)	MCP
1st	-	5	5
2nd	5	10	15
3rd	10	10	15
4th	10	15	20
5th	15	10	20

As shown in Table 38, the internal moments are overcome at input forces between 5 N and 20 N. As a result, flexion of all joints the hand can be expected at input loads exceeding 20 N.

4.1.3.4. Determine cable actuation force required to close the unloaded hand.

(i.e. fully-flexed).

The joints are considered to close when the tension moments exceed the internal moments. Looking at

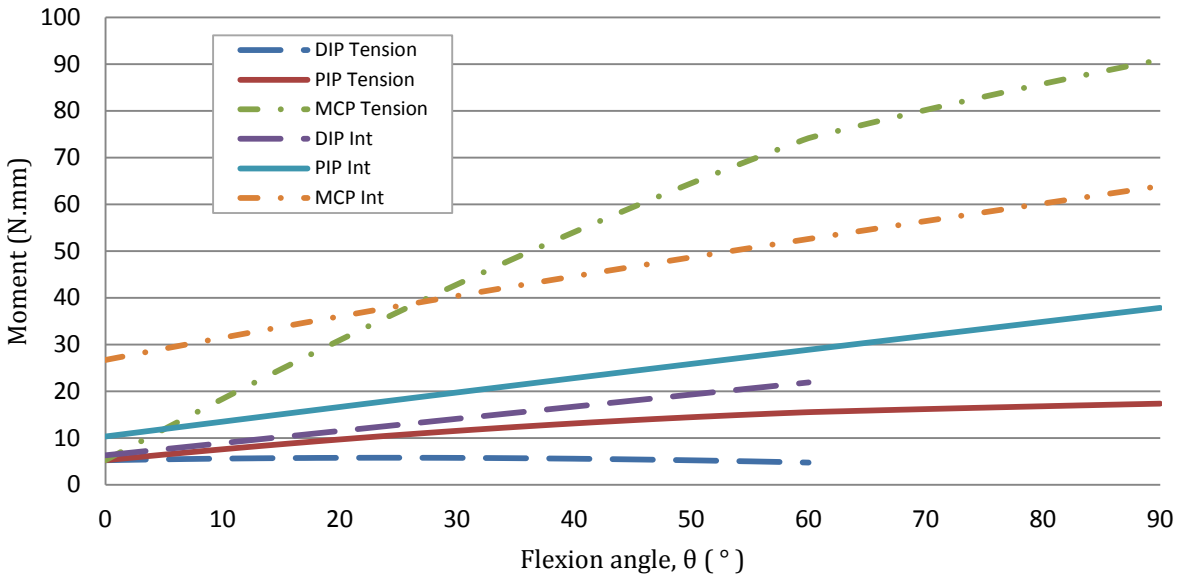

Figure 50 - 3rd digit tension moments vs. internal moments as a function of flexion angle at 5N input force.

Figure 50, the tension moments due to a 5 N input force do not exceed the internal moments, except after 27° flexion of the MCP joint. Increasing the input force to 20 N, as shown in Figure 51, allows the tension moments to exceed the internal moments, throughout the flexural range of the joints; indicative that closing of the finger is achievable for this force input.

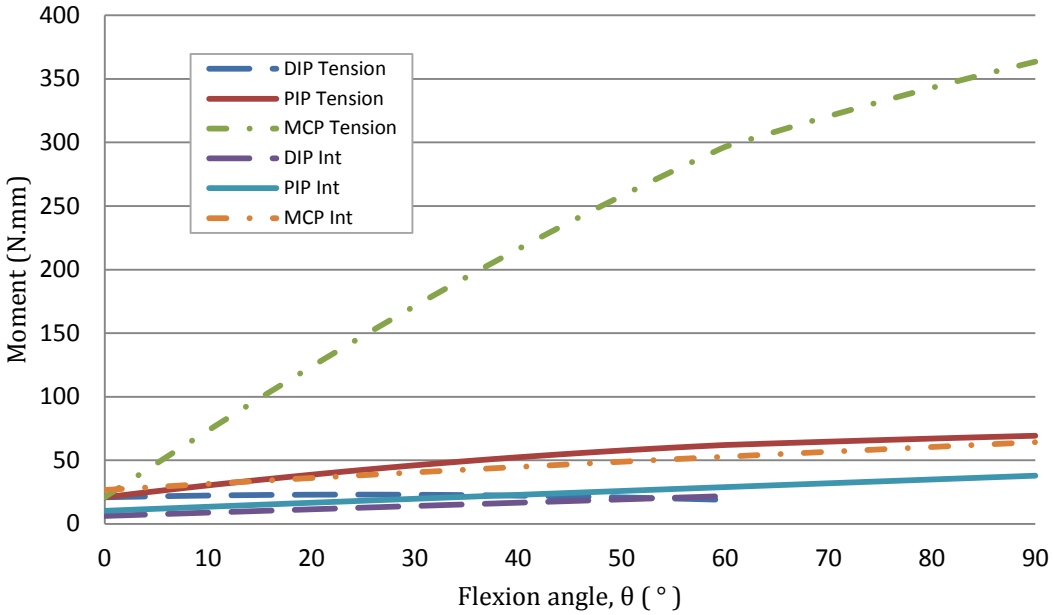

Figure 51 - 3rd digit tension moments vs. internal moments as a function of flexion angle at 20N input force.

The same procedure was followed for the remaining four digits, the 5th digit requiring the highest input force at 25 N in order to fully flex due to its DIP joint. Consequently, it is estimated that the unloaded hand will close if given an initial input force of **25 N.**

4.1.3.5. Determine input cable force to close hand at grasping forces between 20 N & 175 N.[8]

Table 39 - Input cable force to close hand for respective grasp force.

Total Grasp Force (N)	Input Cable Force (N)	Total Grasp Force (N)	Input Cable Force (N)
20	40	**90**	145
30	55	**100**	160
40	70	**115**	180
50	85	**130**	205
60	100	**145**	225
70	115	**160**	245
80	130	**175**	270

[8] It is assumed the grasping force is only applied after 20° of flexion for the MCP and PIP joints of the fingers, and 10° flexion for the DIP and MCP joints of the fingers and thumb respectively. The IP joint of the thumb will be considered from 0° flexion. These values coincide with the functional ranges of the digits selected in Table 6, p. 33. Consequently, the unloaded hand model will be used at angles below these values, as the hand is considered not to have made contact with the grasped object.

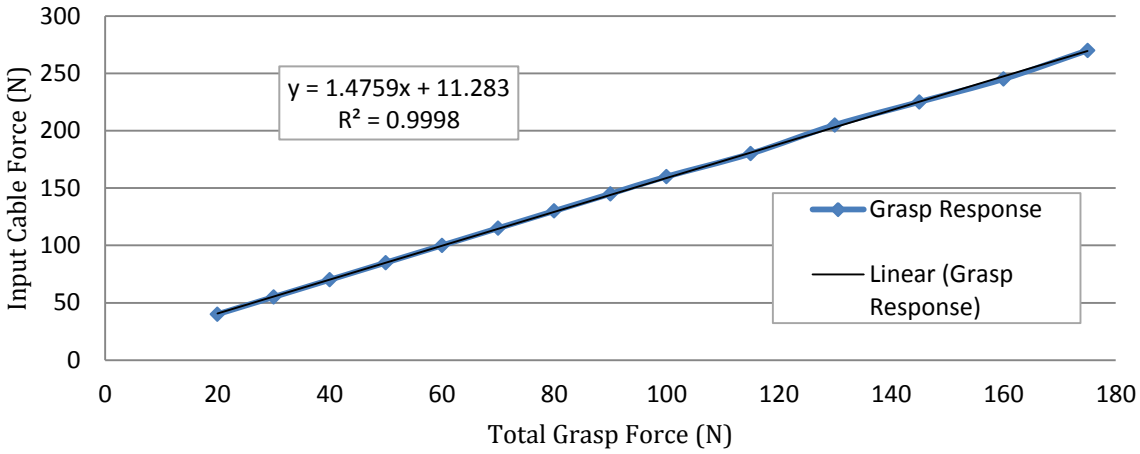

Figure 52 - Input cable force vs. total grasping force on object using analytical model.

The required input cable forces to exert the respective grasping force are shown in Table 39. The response of the curve can be linearly approximated by **y = 1.4759x + 11.283,** with a coefficient of determination of 0.9998 using regression analysis as seen in Figure 52.

In other words: $$\textbf{Input Force} = 1.4759(\textbf{Grasp force}) + 11.283 \quad [4.65]$$

This means the hand requires 33.4 N to exert 15 N of grasping force and is expected to exert 60.1 N of grasp force for a 100 N input force. When compared to the performance of other VC hands in Table 10 (p. 37), they closely matched that of the TRS hook; the most efficient hand in the study. Considering that most ADLs can be performed below approximately **68 N** of grasping force (as mentioned in Section 2.9.3.1, p. 36), the corresponding input force required from the user's shoulder harness is expected to be lower than **112 N** (39% of their maximum anatomical ability of 280 N[9]).

4.1.3.6. Check resultant moments on the linear bearing and determine its static loading limits.

Using Equations 4.3 – 4.5 the resultant moments on the proximal linear bearing carriage were calculated. The static loading limits were taken from the manufacturer's datasheet and compared to the loading response on the bearing in the xy-, xz- and yz-planes. The maximum input force for the given loading limits is shown in Table 40. Pass condition is considered if the bearing is below its static loading limit at loads greater than the maximum harness input force of 280 N[9].

Table 40 – Proximal linear roller bearing loading limits.

Plane	Bearing Limit (Nm)	Input force at Limit (N)	Pass (Y/N)
XY	1.2	105	**N** (< 280N)
XZ	2.3	391	**Y** (> 280N)
YZ	1.4	235	**N** (< 280N)

[9] Anatomical ability of the shoulder harness as mentioned in Section 2.9.3.2, p.36. according to Smit & Plettenburg(2010).

In order to reduce the moment on the bearing, the eccentricity of the input cable should be minimised (i.e. $L_{X\ IN}$ in Figure 40, p.70). By attaching the input cable centrally, the bearing is able to withstand the loading conditions tabularised in Table 41.

Table 41 – Adjusted proximal linear roller bearing loading limits with $L_{X\ IN} = 0$.

Plane	Bearing Limit (Nm)	Input force at Limit (N)	Pass (Y/N)
XY	1.2	289	**Y** (> 280N)
XZ	2.3	$5x10^3$	**Y** (> 280N)
YZ	1.4	622	**Y** (> 280N)

Referring to Table 41, the bearing passes in all three loading planes, remaining below its static loading limits.

4.1.3.7. Determine input forces to fingers, for varied seesaw angles, as a function of input-cable actuation force.

Five combinations of seesaw orientations are chosen. The resultant input forces into each finger as a function of the rotation of the seesaws is shown in Table 42 below. It should be noted that these forces are expressed as a percentage of the total input-cable actuation force. The angles βS1, βS2 and βS3 are shown in Figure 44 and Figure 45.

Table 42 – Variation of finger input forces for seesaw rotations.

Orientation	Rotation angle of Seesaws (°)			Percentage of total input-cable force (%)				Refer to:
	βS1	βS2	βS3	F2 Eqn. 4.38	F3 Eqn. 4.39	F4 Eqn. 4.40	F5 Eqn. 4.41	
1	+40	+40	+40	13.2	15.3	10.2	11.8	Figure 53
2	+40	0	0	14.2	14.2	11	11	Figure 54
3	0	0	0	15.1	15.1	10.1	10.1	Figure 55
4	-40	0	0	16	16	9.2	9.2	Figure 56
5	-40	-40	-40	17.2	14.8	9.9	8.5	Figure 57

Referring to Table 42, the finger input forces varied between 8.5% and 17.2% of the total input-cable force. Changing the angle of the primary lever varied F2 & F3 between 14.2% and 16%, and F4 & F5 between 9.2% and 11%; both varying a total of 1.8%. Rotating the secondary levers to their clockwise limits generates a 1% fluctuation between F2 & F3, and 0.8% between F4 & F5. When rotating the secondary levers to their anticlockwise limits, a 1.2% fluctuation is generated between F2 & F3, and 0.7% between F4 & F5. In total the input forces to F2 & F3 vary by 4% (13.2% to 17.2%), and F4 & F5 by 3.3% (8.5% to 11.8%) of the total cable input force. Considering the maximum cable input is 280 N, this translates to fluctuations of 11.4 N & 9.4 N respectively. If considering the fluctuation from their

neutral position (Orientation 3), the seesaws allow F2 & F3 to vary by ±13.25%, and F4 & F5 by ±16.34% of the individual finger input force. Figure 53 to Figure 57 show the behaviour of the finger inputs as a function of input cable actuation force for Orientations 1 to 5 respectively.

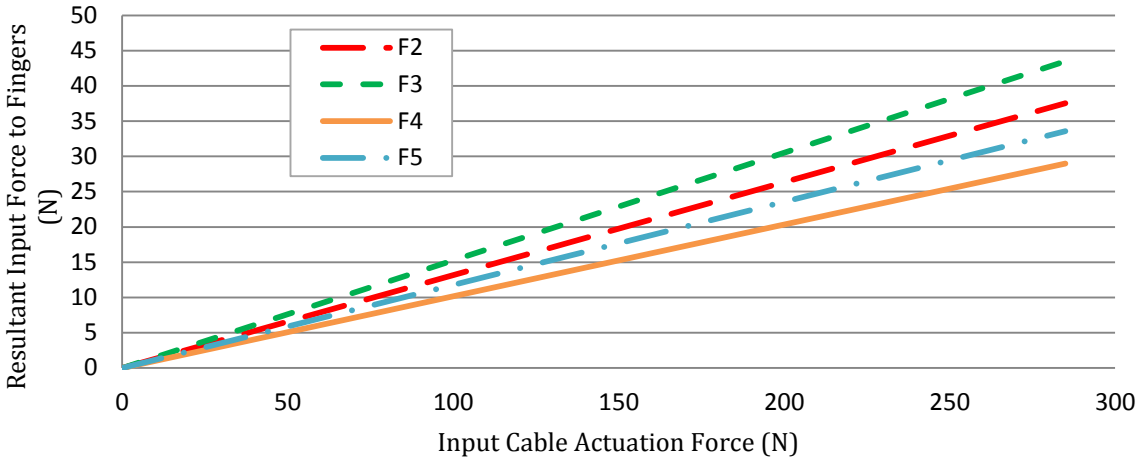

Figure 53 - Finger input forces as a function of input-cable actuation force for Orientation 1.

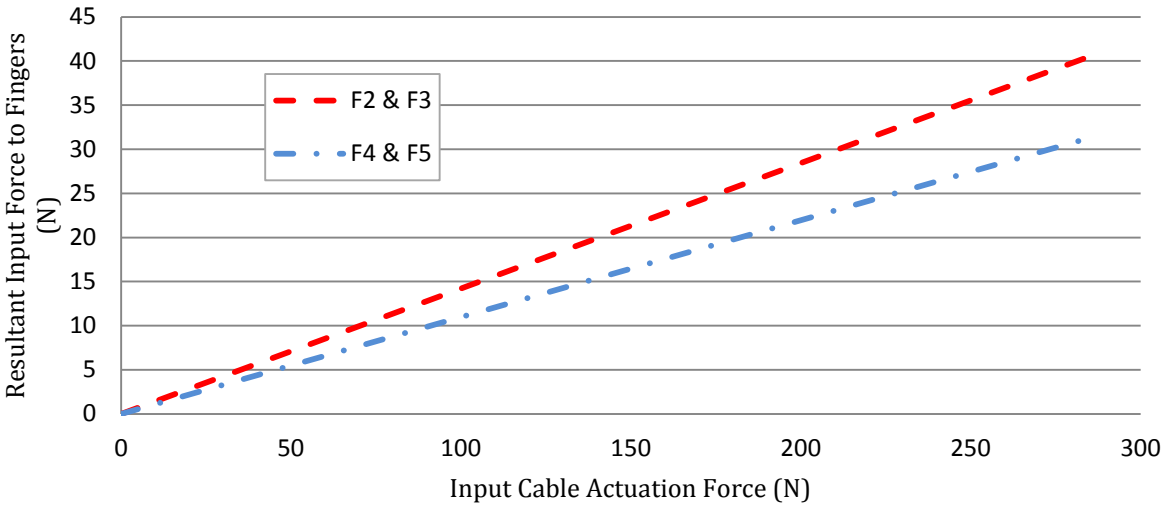

Figure 54 - Finger input forces as a function of input-cable actuation force for Orientation 2.

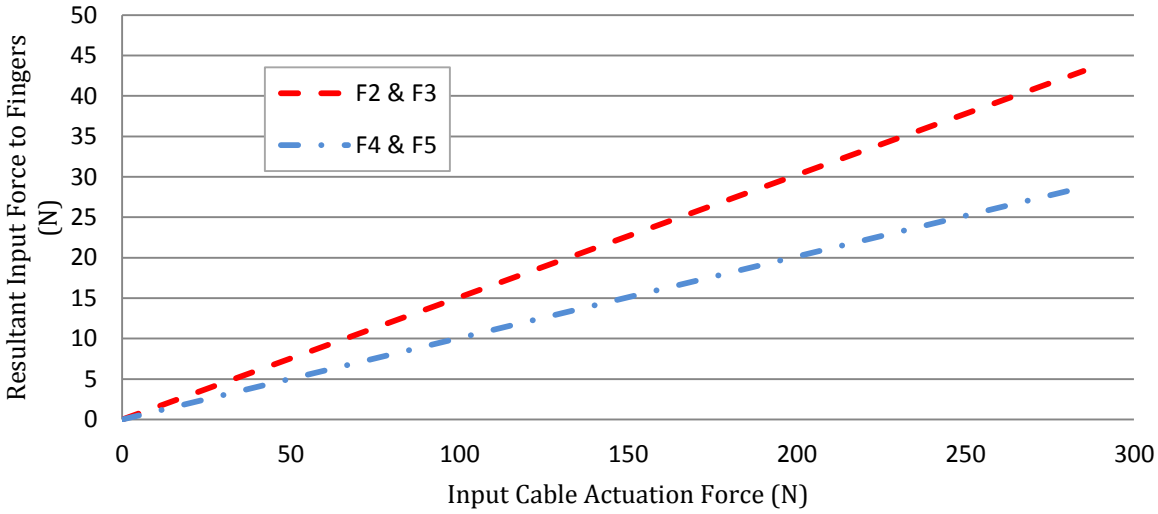

Figure 55 - Finger input forces as a function of input-cable actuation force for Orientation 3.

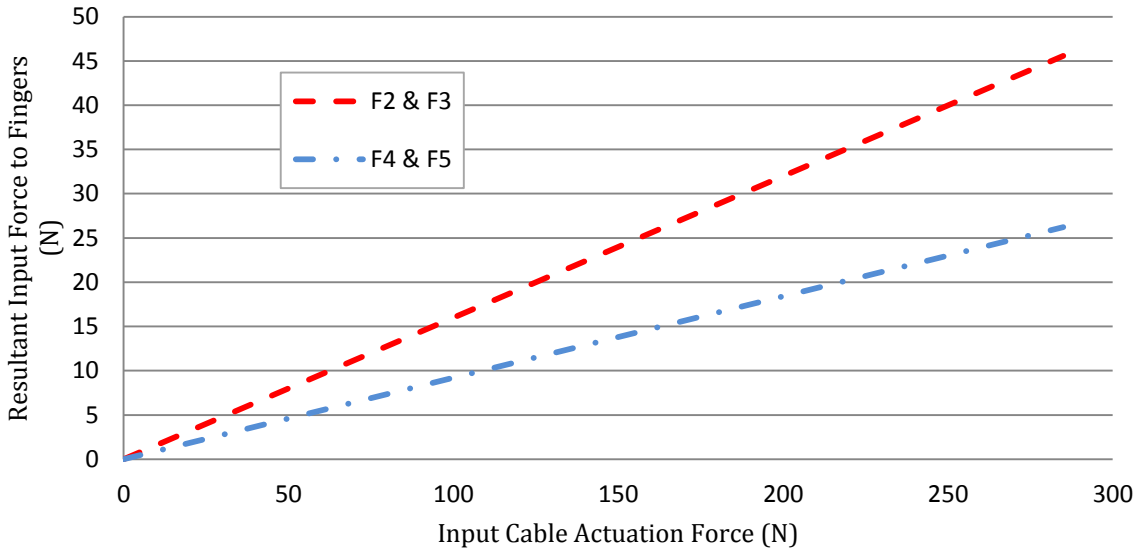

Figure 56 - Finger input forces as a function of input-cable actuation force for Orientation 4.

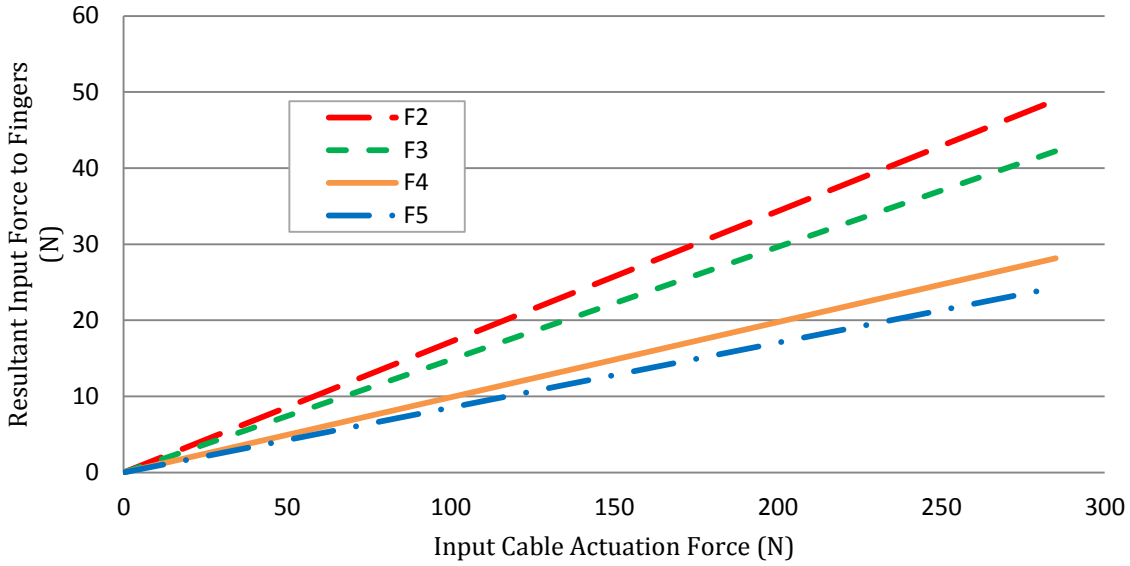

Figure 57 - Finger input forces as a function of input-cable actuation force for Orientation 5.

Referring to Figure 53 to Figure 57, a linear relationship between the input cable actuation force (F_{IN})and the finger input forces (F2-F5) is shown. Comparing Orientation 2 (Figure 54) and Orientation 4 (Figure 56) to Orientation 3 (Figure 55), F2 & F3 remain greater than F4 & F5 in all cases due to their 60%-40% split, however F4 & F5 encroach on F2 & F3 with $\beta_{S1} = +40°$ and veer away with $\beta_{S1} = -40°$. When comparing Orientation 1 (Figure 53) to Orientation 2 (Figure 54), and Orientation 5 (Figure 57) to Orientation 4 (Figure 56), F2 and F3 each deviate from the F2 & F3 line depending on the orientation of β_{S2}. Similar behaviour is shown for F4 and F5 in relation to β_{S3}. The degree of these deviations are a function of the magnitude of rotation of the secondary seesaws (i.e. β_{S2} and β_{S3}).

4.1.3.8. Response of system moments as a function of θ flexion angles.

The response of each of the system moments will be plotted as a function of theta. These moments include: Mass moments, Spring Moments, Hinge-friction Moments, Tension Moments, Grasp-force Moments as well as the Resultant Moments for both the Loaded and Unloaded cases. To plot all cases would be senseless; therefore the 3rd Digit is selected as a representative case, with the system having a total grasp force of 68 N [10] (except the unloaded case) and an input-cable force of 140 N. The aforementioned moments are represented by Figure 58 to Figure 66 respectively.

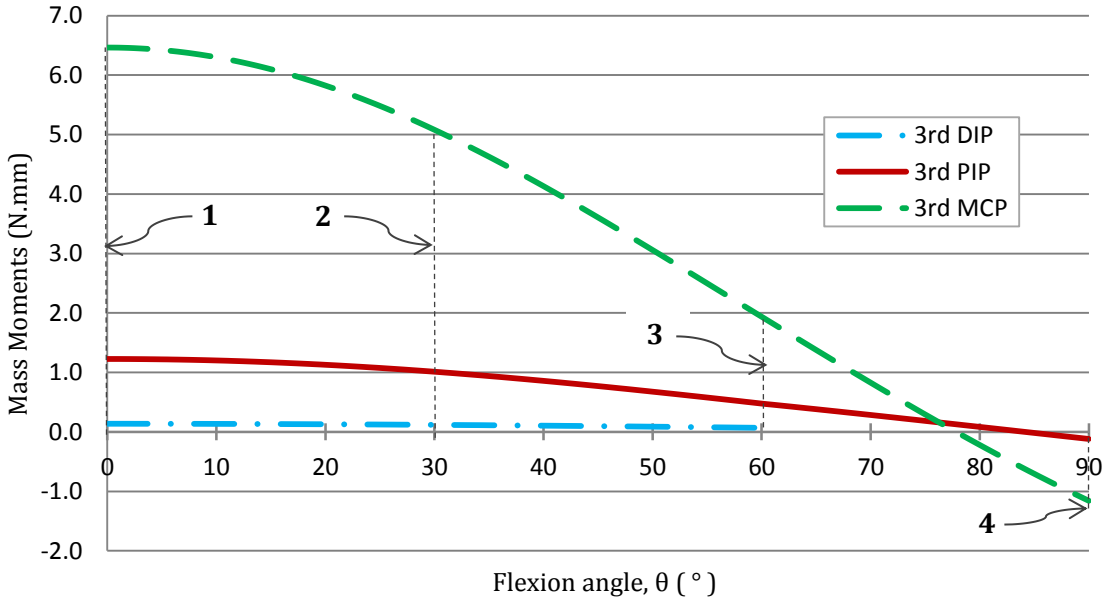

Figure 58 - Mass moments vs. flexion angle for the joints of 3rd digit.

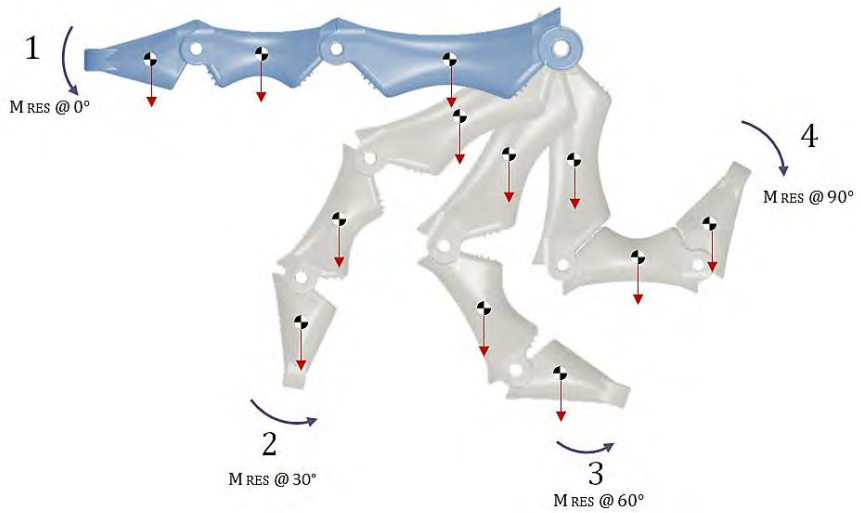

Figure 59 - Force diagram indicating resultant mass moments as a function of flexion.

Referring to Figure 58, the MCP joint has the highest initial **mass moment** followed by the PIP and DIP joints respectively, due to the most of the mass being located furthest from this joint. Also of

[10] Grasp force below which most ADLs can be performed; see Section 2.9.3.1, p. 36.

significance is that the moments for the MCP and PIP joints become negative at 77° and 85° respectively; this phenomenon is due to their dependence on the mass of the phalanges distal to them. When nearing their fully-flexed position the centre of mass of the other phalanges passes beyond the 90° midline of the hinges, consequently inducing a moment in the opposite direction, as shown by position **4** in Figure 59. It should also be noted that the overall behaviour of the mass moments is non-linear, and from distal to proximal they are represented by equations 4.42, 4.48 & 4.54.

Figure 60 shows a typical linear response of the torsion **spring moments** in the joints of the fingers. The stiffness of the springs is directly proportional to the gradient of their slopes, whose moments are determined by Equation 4.55. In this case, the selected MCP spring also happens to be the stiffest.

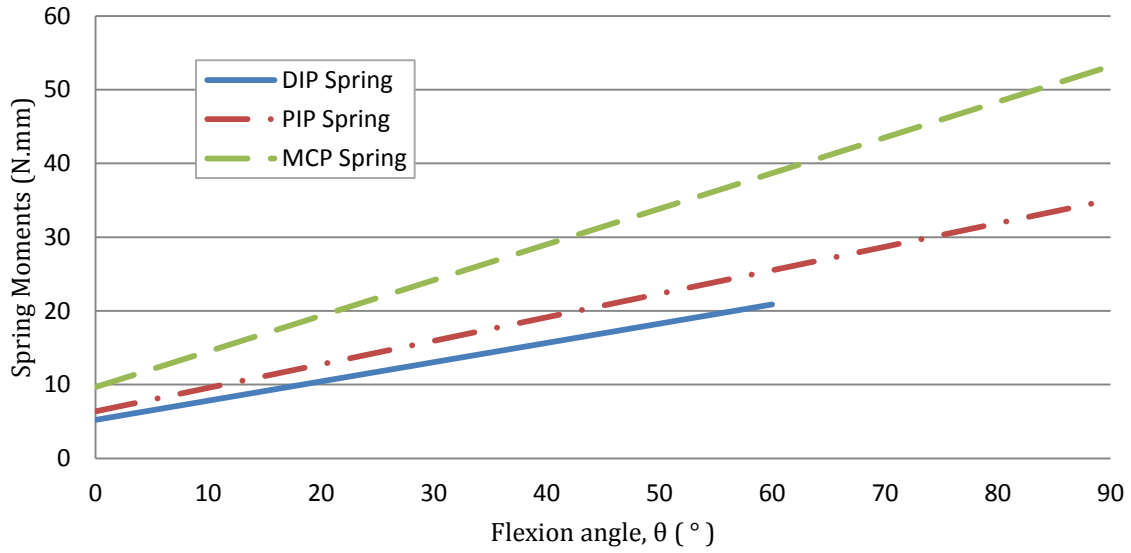

Figure 60 - Spring moments vs. flexion angle for the joints of 3rd digit.

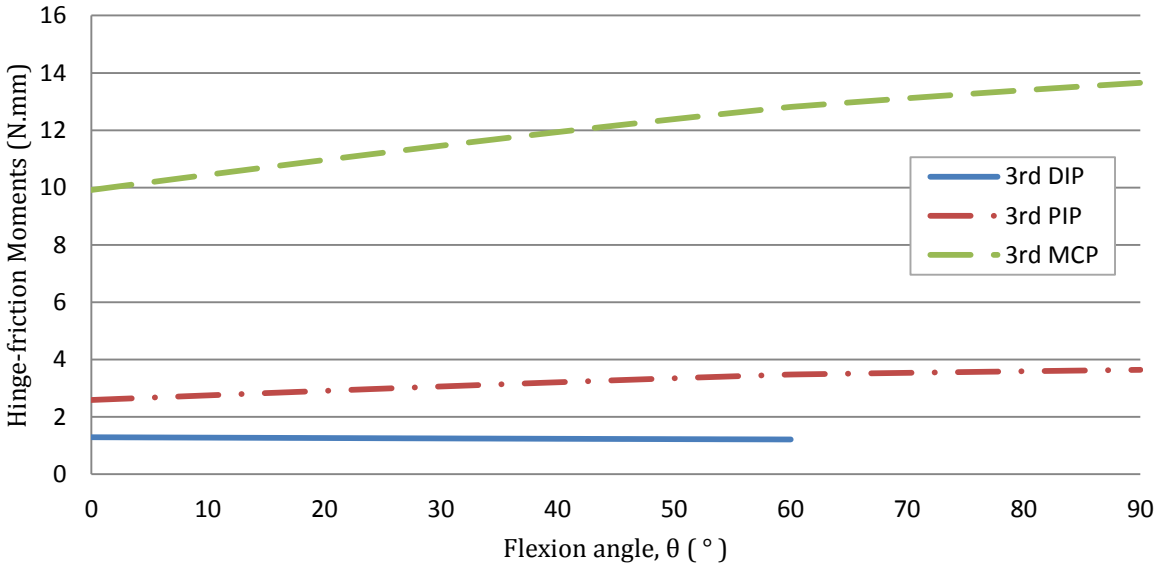

Figure 61 – Hinge-friction moments vs. flexion angle for the joints of 3rd digit.

On the other hand, a non-linear response is experienced when referring to the **hinge-friction moments** shown in Figure 61, which is governed by the resultant forces on the phalanges, varying according to loading conditions, system properties and angular position. Equations 4.45, 4.51 & 4.57 govern the response of these moments. Similarly to the mass moments, the magnitude of the moments are highest at the MCP joint, and lower for the PIP and DIP joints respectively. In this case however, it is due to the magnitude of the resultant forces being greatest at this hinge. Before moving on to tension moments, the tensile behaviour of the actuating cable and its normal reaction forces shown in Figure 62 need to be discussed.

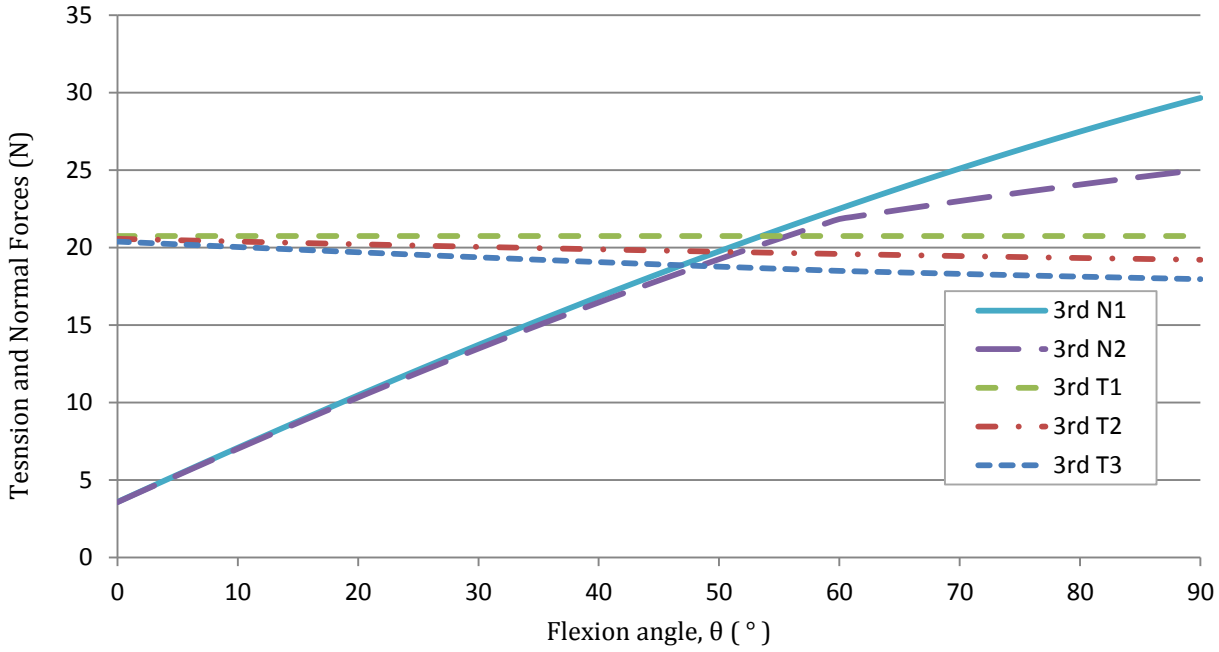

Figure 62 – Tension and normal forces vs. flexion angle for the phalanges of the 3rd digit.

Referring to Figure 62, the **normal contact forces** of the proximal and middle phalanges increase as a function of theta with decreasing slope; their behaviour characterised by equations 4.60 & 4.61. The kink in the curve of N2 at 60° is due to the distal phalanx having reached its fully-flexed position and N2 begin a function of the flexion of the PIP joint only. The **tension forces** of the finger tendons are represented by equations 4.62, 4.63 & 4.64 from proximal to distal respectively. These tension forces (except T1) decrease as a function of flexion angle due to the increased friction losses generated by the α-angles (see Figure 48), which in turn generate larger normal contact forces between the tendon and the channel surface. These alpha angles represent the angle between the phalange and the actuating wire/tendon.

Tension moments are those exerted on the phalanges as a result of the tension in the actuating cable, the normal reaction forces due to this cable, and the frictional force between the actuating cable and

its guide channel. The moments increase non-linearly as a function of flexion angle, much like the behaviour of the anatomical hand, with a decreasing slope as shown in Figure 63. This decrease in slope is associated with the increase in losses due to friction of the channels.

Importantly, the curvature of the tendon channels determines the variation in the aforementioned **α-angles**. An increase in curvature, increases the initial α-angles, increasing the normal reaction forces, which in turn increase tension moments and hence the grasping ability. However, the increase also brings about a decrease in cable tension caused by higher sliding friction losses in the channels, and generates more wear; the degree of which will be analysed in Chapter 7.4, p. 159. It should be noted that the α-angles increase as a function of flexion, and that the normal reaction component outweighs the frictional component throughout the flexion range of the phalanges.

An initial α-angle of 5° is applied to each of the channels to assist with the tension moments, especially at lower flexion angles. Upon flexion of the joints, the actuating cable's α-angles increase further, reaching a maximum of 50° for the MCP & PIP joints and 35° for the DIP joints of the fingers. Furthermore, the thumb's IP and MCP joints have angles reaching 45° and 35° respectively.

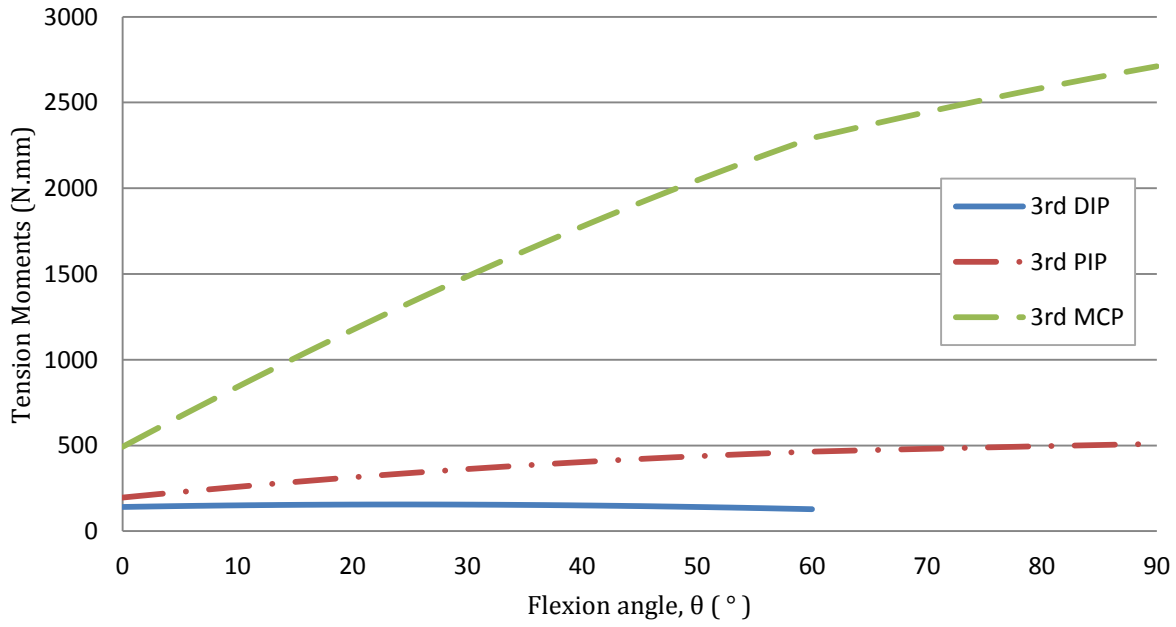

Figure 63 – Tension moments vs. flexion angle for the joints of 3rd digit.

Grasp-force moments are dependent on the geometry of the phalanges, the magnitude of the grasping force, and the distribution of this force between the phalanges. The three distributions considered in Table 14 (p. 40), were input into the analytical model. After comparing the effect that each of these had on the resultant moments of the digits, the distribution best suited to balance the forces of hand was distribution **B**. The grasp-force moments using this distribution are shown in Figure 64.

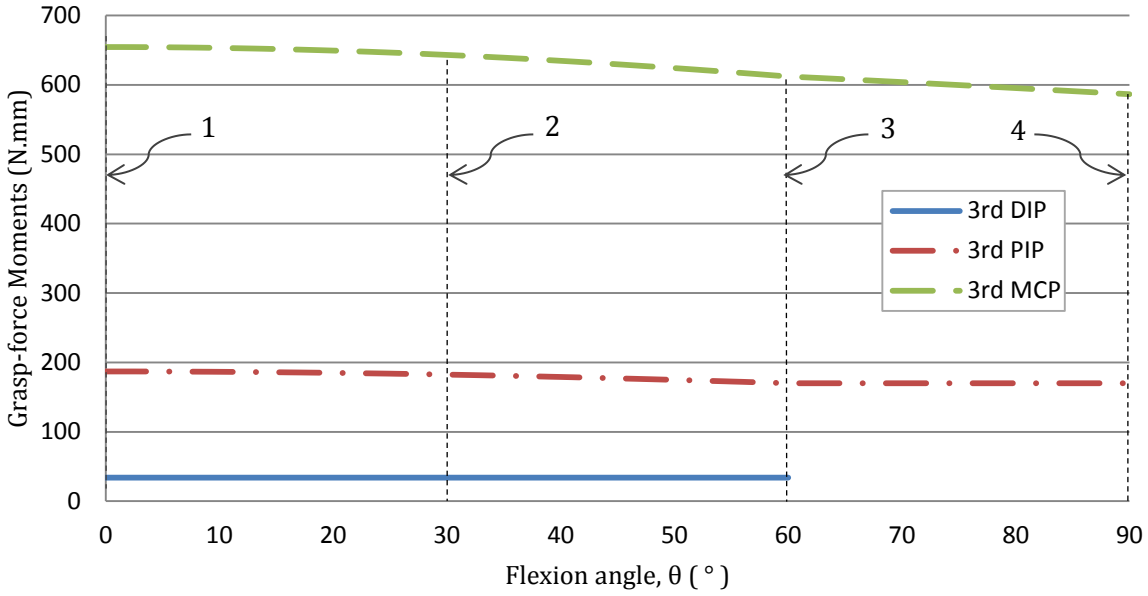

Figure 64 – Grasp-force moments vs. flexion angle for the joints of 3rd digit.

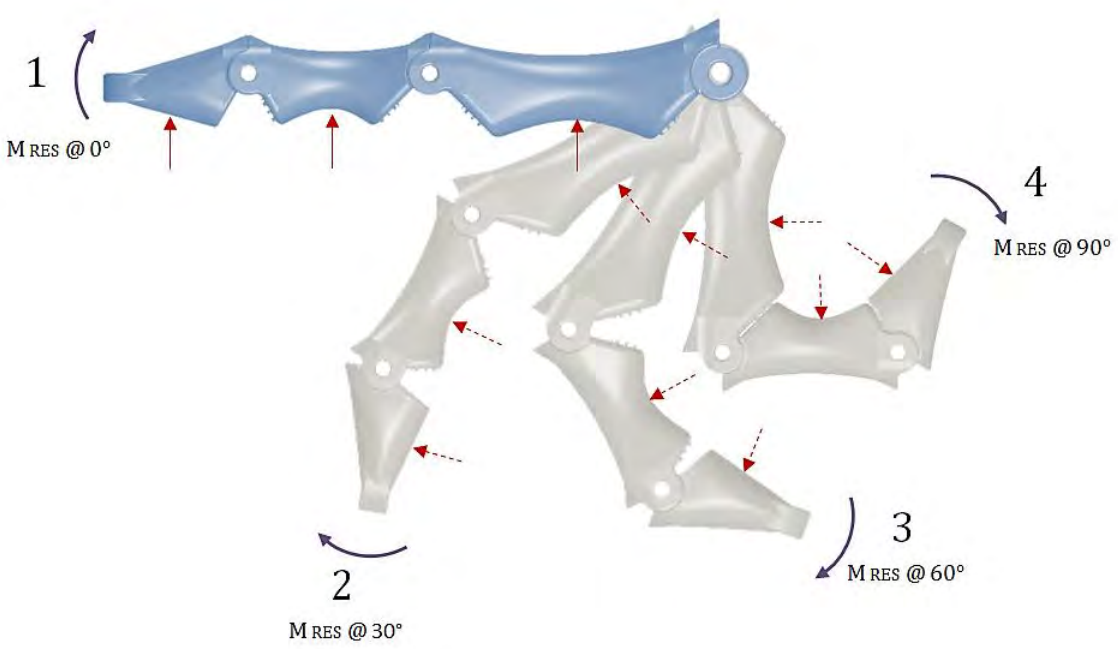

Figure 65 - Force diagram indicating resultant grasp-force moments as a function of flexion.

Referring to Figure 64, the moments generated by the grasp forces taper off non-linearly as the flexion angle increases. For the MCP joint this decrease can be attributed to a reduction in the perpendicular lever-arm distance between distal & middle phalanx grasp forces and the axis of the MCP joint. Similarly for the PIP joint, the distance between the distal grasp force and the axis of the PIP joint. These forces and their directions are shown in Figure 65. The grasp-force moment for the DIP joint remains constant as it is independent of the other phalanges. While the magnitude of these moments is represented as being positive in Figure 64, it should be noted that they are extensive moments, which act in opposition to the tension moments.

Consequently, the **resultant moments** of the digits for the **unloaded** case are calculated as follows:

$$\sum M^i_{Res\ Unloaded} = \sum M^i_{Tension} - \sum M^i_{Mass} - \sum M^i_{Spring} - \sum M^i_{Hinge}$$

The **resultant moments** of the digits for the **loaded** case are calculated as follows:

$$\sum M^i_{Res\ Loaded} = \sum M^i_{Tension} - \sum M^i_{Grasp} - \sum M^i_{Mass} - \sum M^i_{Spring} - \sum M^i_{Hinge}$$

Or alternatively: $$\sum M^i_{Res\ Loaded} = \sum M^i_{Res\ Unloaded} - \sum M^i_{Grasp}$$

Considering the unloaded case first, the resultant moments on the joints of third digit increase as a function of flexion angle as shown in Figure 66. Furthermore, the moments are positive throughout the flexural range indicative that the digit will close under the current loading conditions.

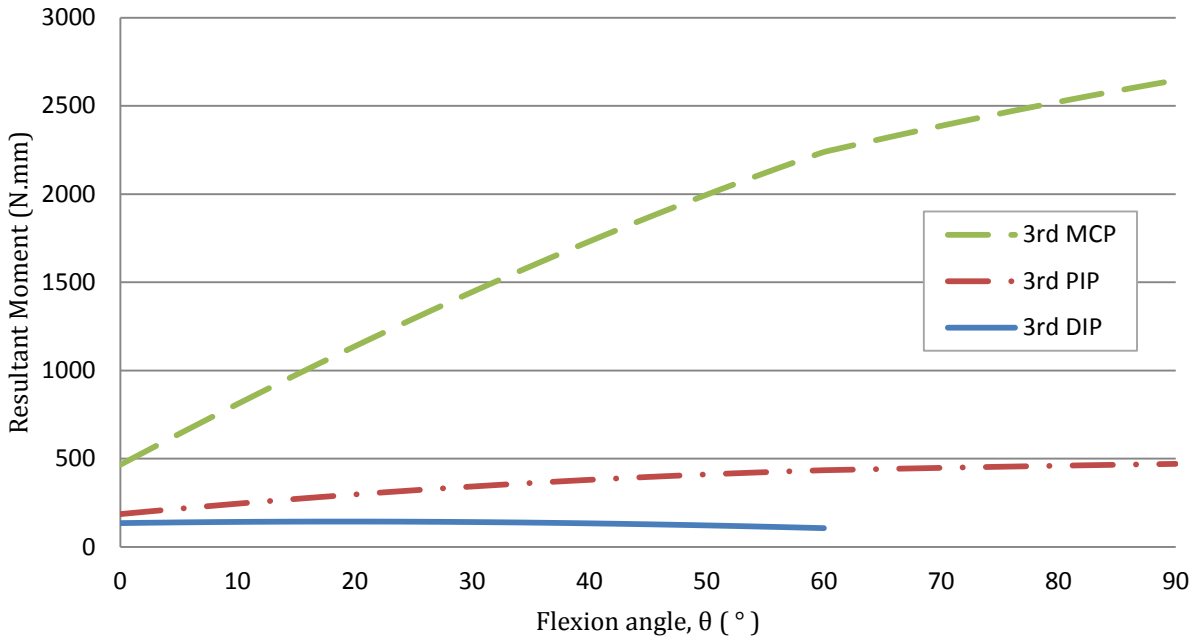

Figure 66 – Resultant moments vs. flexion angle for the joints of 3rd digit (unloaded).

The loaded case, represented by Figure 67, exhibits similar behaviour to that of the unloaded case, except that the moments between 0° and 5° flexion of the MCP joint are negative. However, the functional range of the 3rd MCP joint is between 20° and 70° as shown in Table 6, p. 33, and object contact is not yet expected to have been made; hence the moments pertaining to the unloaded hand will be considered between 0° and 20°. Consequently, the digit is expected to close under the given loading conditions. Anatomically, our grasps behave in a similar manner, as objects are seldomly grasped from the fully-extended hand position due to it being physiologically challenging.

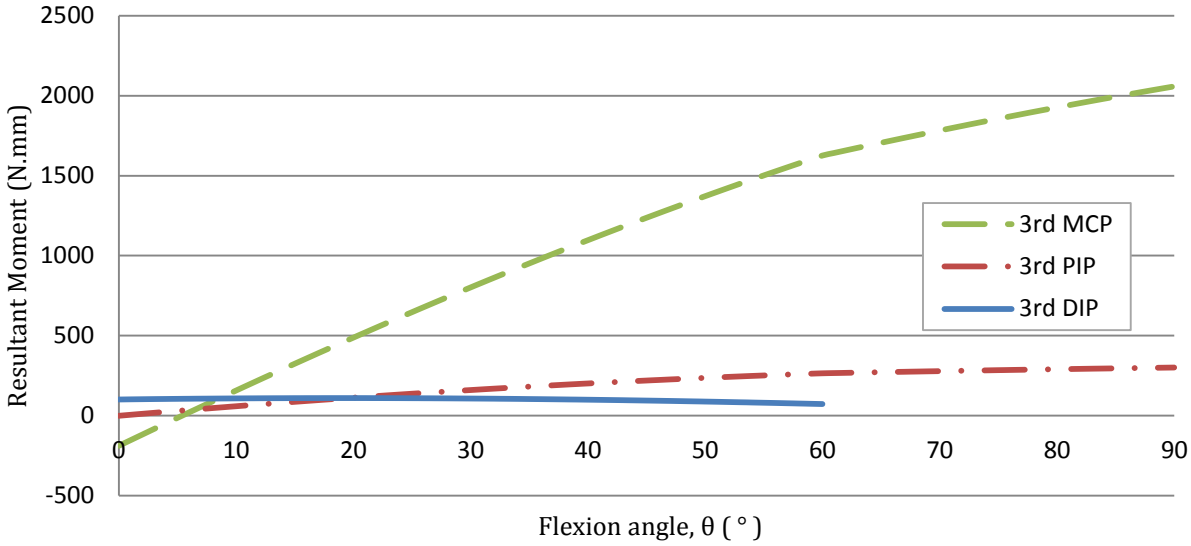

Figure 67 – Resultant moments vs. flexion angle for the joints of 3rd digit (loaded)

Using this approach, the combined response of the system moments were analysed for the entire hand. Applying input forces according to those outlined in Section 4.1.3.5 (p. 85) and Equation 4.65, the digits of the hand were found to achieve positive grasping forces on grasped objects that were within the functional range of the phalanges.

4.2. Spring Design

The design incorporates the use of springs to store energy and provide actuating forces in various locations. The dynamic use of linear compression springs as well as torsional springs requires that both static and fatigue analysis of these elements be made. Linear compression springs are used in the thumb locking mechanism and also the pawl pin mechanism, whereas the torsional spring elements are used in the interphalangeal and metacarpophalangeal joints of the hand.

Overall system assumptions are as follows:

- Hysteresis caused by friction between successive coils is neglected.
- Spring material is linear-elastic and isotropic.
- Thermal effects can be neglected

4.2.1. Linear Compression Spring Calculations

Linear springs are used in the thumb-locking-mechanism as well as in the pawl pin mechanism. While the analysis of linear compression springs is not as mathematically intensive as that of the torsion springs, it is essential to quantify their behaviour to ensure the locking mechanisms function in the manner intended.

4.2.1.1. Thumb-swivel locking mechanism spring specification and shear limit of thumb locking plate

The springs are required to provide sufficient contact force between the thumb swivel and thumb locking plate, to offer resistance to rotation during flexion of the thumb, using a factor of safety of no less than 2. Standard 302 stainless steel helical compression springs are selected.

Table 43 - Properties of selected 302 stainless steel compression springs.

Property	Dimension	Unit
Wire Ø, d	0.5	mm
Mean Ø, D	5	mm
Spring Constant, C	10	-
Shear Stress Correction Factor, K_S*	1.05	-
Pitch (p)	2	mm
Shear Modulus, G**	69.0	GPa
Spring Constant, A**	1867	MPa.mm^m
Spring Constant, m**	0.146	-
Number of active Turns, N_a	4.5	-

* Calculated using Eqn. 10-4 in Shigleys 8th Edition **(Budynas & Nisbett, 2008, p. 503)**

** From Table 10-4 & Table 10-5, **(Budynas & Nisbett, 2008)**

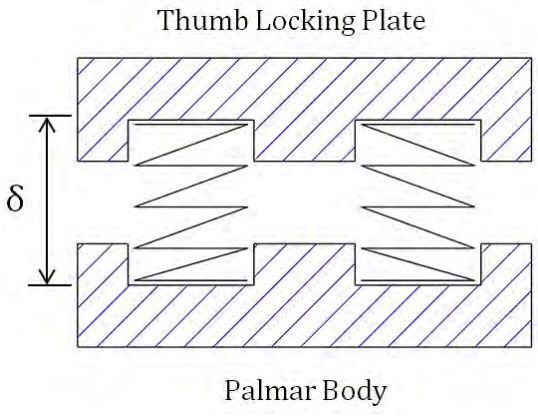

$$S_{UT} = \frac{A}{d^m} = \frac{1867}{(0.5)^{0.146}} = 2065.8 \text{ MPa}$$ [Eqn 10-14] [11]

$$S_{Sy} = 0.45 S_{UT} = 929.6 \text{ MPa}$$ [Using von Mises [11]]

$$\tau_{all} = \frac{S_{Sy}}{SF} = 464.81 \text{ MPa}$$

$$F_{all} = \frac{\pi d^3 \tau_{all}}{8 k_s D} = 4.34 \text{ N}$$ [Eqn 10-3] [11]

When at full-engaged position: $\delta = 5.65$ mm

When in release position: $\delta = 4.60$ mm

Determine spring constant: $$k = \frac{d^4 G}{8 D^3 N_a} = 0.958 \frac{N}{mm}$$ [Eqn 10-9] [11]

[11] (Budynas & Nisbett, 2008)

Unstretched length of spring: $l = pN_a = 2(4.5) = 9$ mm

Spring force at engaged position: F = kδ = 0.958(9 - 5.65) = 3.21 N

Spring force at release position: F = kδ = 0.958(9 - 4.60) = 4.22 N < $\mathbf{F_{all}}$

Total Spring Force at release due to both springs: F_{TOTAL} = 2 x 3.21 = **8.44 N**

Actual factory of safety on spring design: $SF = \frac{2 \times F_{all}}{F_{release}}$ = **2.06**

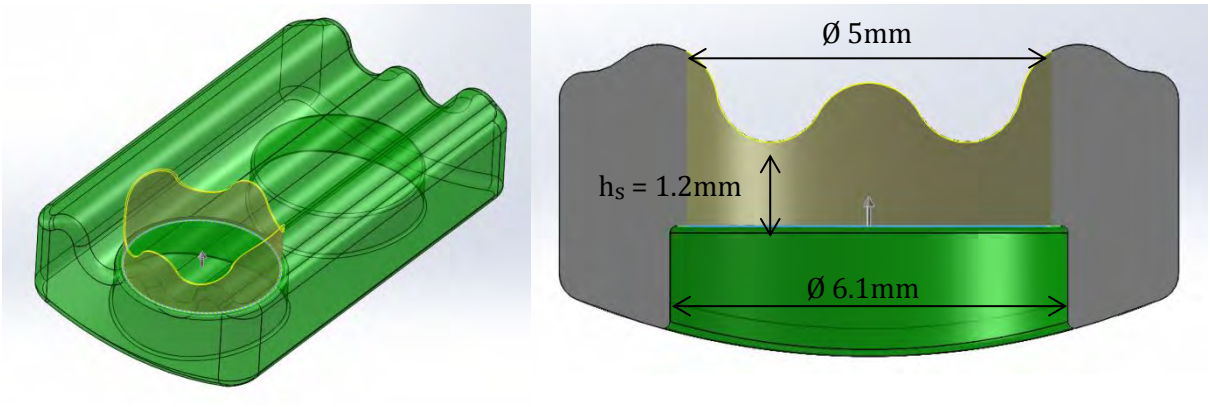

Figure 68 - Shear area (yellow) of thumb locking plate (left) with cross-sectional dimensioned view (right)

Determine maximum allowable shear force for the nylon PA2200 thumb locking plate using S_{UT} from Table 17, p. 44:

$$\tau_{all} = \frac{F_s}{A} = \frac{F_s}{\pi dh}$$

where:

- τ_{all} = allowable shear stress
- F_s = maximum shear force
- A = shear area

Assume worst case ∴ for minimum shear area: h = 1.2mm. Using MSS Theory $\tau = 0.45\ S_{UT}$

$$F_s = \pi dh\tau = \pi(6.1)(1.2)\left(\frac{9(48)}{20}\right) = 496.72 \text{ N} >> \mathbf{4.22\ N} \quad \therefore \text{Pass}$$

4.2.1.2. Linear spring calculations for the pawl-engagement mechanism

The objective of this spring is to store sufficient energy to keep the pawl engaged with the ratchet mechanism and also to provide sufficient retarding force to prevent involuntary unlocking of the mechanism through depression of the push button. It is desirable for the user to exert between 10 N and 20 N to release the mechanism.

Table 44 - Properties of selected 302 Stainless Steel Compression Spring.

Property	Dimension	Unit
Wire Ø, d	0.6	mm
Mean Ø, D	5	mm
Spring Constant, C	10	-
Shear Stress Correction Factor, K_S*	1.05	-
Pitch (p)	2	mm
Shear Modulus, G**	69.0	GPa
Spring Constant, A**	1867	MPa.mm^m
Spring Constant, m**	0.146	-
Desired Release Force, F_{PUSH}	10 - 20	N

* Calculated using Eqn. 10-4 in Shigleys 8th Edition **(Budynas & Nisbett, 2008, p. 503)**
** From Table 10-4 & Table 10-5, **(Budynas & Nisbett, 2008)**

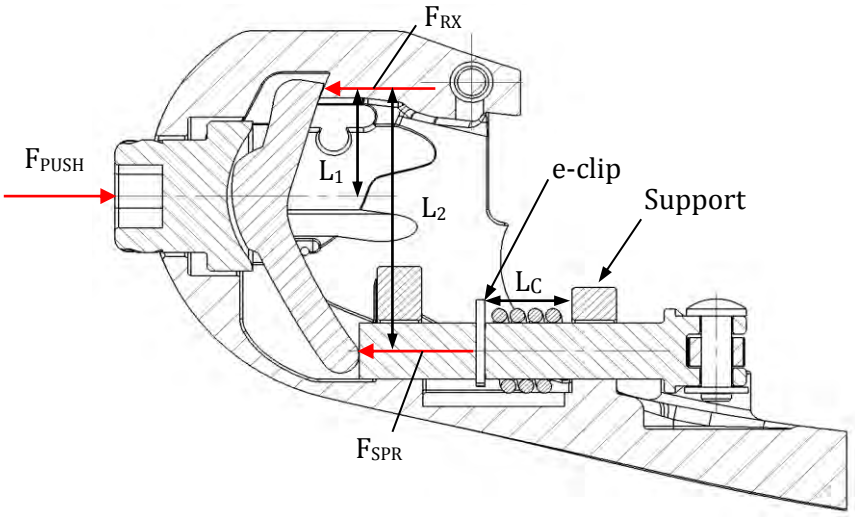

- L1 = 7 mm
- L2 = 18.6 mm

CCW Moments about Pivot:

$F_{PUSH} \times L_1 = F_{SPR} \times L_2$

At the engaged position:

$F_{SPR\,min} = \left(\frac{L1}{L2}\right) F_{PUSH} =$ **3.76 N**

$F_{SPR\,max} = \left(\frac{L1}{L2}\right) F_{PUSH} =$ **7.52 N**

Figure 69 - Free body force diagram of ratchet and pawl locking mechanism.

Adjusting the distance L_C between the support and e-clip: $L_{C\,MAX}$ = 11mm & $L_{C\,MIN}$ = 8 mm,

Hence $\boldsymbol{\delta_{MAX} = 3mm}$ ∴ desired spring constant is $\mathbf{k} = \frac{\Delta F_{SPR}}{\delta_{C\,MAX}} =$ **1.25 N/mm**

But $k = \frac{d^4 G}{8D^3 N_a}$ therefore: **Na** = 7.13 ≅ **7 turns**

Consequently uncompressed spring length = p x Na = **14 mm**

Calculate actual spring force and hence user force: $14 - L_{C\,MAX} < \boldsymbol{\delta} < 14 - L_{C\,MIN}$

∴ Using $F_{SPR} = k.\delta_0$ $3.75\ N < F_{SPR} < 7.5\ N$

Hence: $9.96\ N < F_{PUSH} < 19.93\ N$

Therefore the user exerts between 10 N and 20 N to release the ratchet and pawl locking mechanism using this spring configuration. The next section covers calculations for the torsional spring elements in the interphalangeal joints.

4.2.2. Torsion Spring Calculations

In order for the underactuated hand to extend, torsion springs placed within the interphalangeal joints need to store enough strain energy to overcome system friction, as well as the moments caused by the mass of the fingers. Although increasing the spring stiffness beyond the required amount still guarantees a functioning hand, care must be taken to minimise stiffness as any additional energy input will need to originate from the patient; leading to unnecessary fatigue. Referring to Figure 70, a typical representation of a torsion spring and its dimensions are shown. β is the free end location angle, α is the back angle and θ the rotational coordinate which is proportional to force (F) x length (*l*).

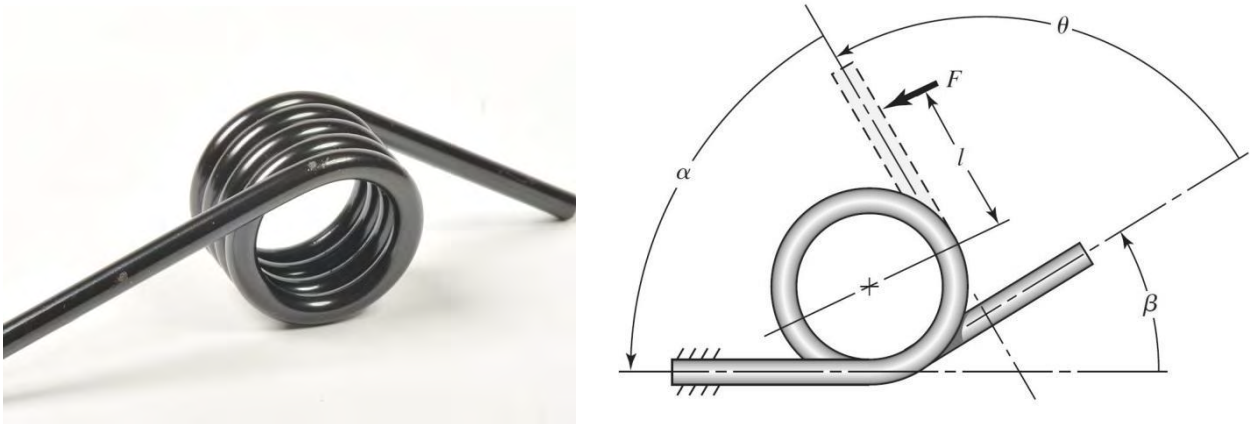

Figure 70 - Torsion spring (AW Direct, 2013)(left) with dimensions (right) (Budynas & Nisbett, 2008, p. 534).

For the design of the springs, the mean coil diameters were chosen as 5 mm, to fit within the DIP and PIP joints, and 7 mm for the MCP joints. Furthermore, a 12 mm lever arm length *l* was selected for the all the springs as it would provide sufficient seating within the phalanges. The properties of the selected spring material were chosen so as to maximise fatigue life and resilience to failure. Consequently, ASTM A228 music wire was selected above other grades of wire, including hard-drawn wire and stainless steel, due to its ability to endure.

With reference to Appendix B2, p. B-6, the selected torsion springs specified in the adjusted spring distribution in Table 37 (p. 83) all surpass their infinite life criteria and are expected not to fail whilst operating within their design limits.

4.3. Finite Element Analysis (FEA)

A finite element investigation was performed on the 3rd and 5th digits of the hand to determine their displacement behaviour and structural stress state under hyperextensive and lateral loading conditions. A summary of the key findings will be presented here, with reference to the report contents. Detailed results as well as the method and assumptions are made with reference to Appendix C, p. C-1.

Referring to Figure C1 (p. C-2) in Appendix C, the assembly of the test setup and the direction of the applied loads can be seen. Mesh refinement is shown in Appendix C4, p. C-3, with mesh details summarised in Table C1, p. C-4. The loading conditions applied to each of the digits vary between 20 N and 100 N as specified in Appendix C8, p. C-7. Ideally, the performance of the EOS PA2200 Nylon material should remain within the elastic region (i.e. below the yield and tensile limits of 40 MPa and 45 MPa respectively). Minor localised plastic deformation of the structure was deemed acceptable, provided it did not inhibit the operation/functionality of the digit.

On completion of the FEA, the regions of highest stress concentration are highlighted in Appendix C10, p. C-8, in Figures C12 & C13 for hyperextensive loading and Figures C14 & C15 for lateral loading. In the hyperextensive loading cases these were situated at the radii of the hinges, and at the lateral edges of the posterior protrusions and pinholes. The 3rd and 5th digits had their peak stresses located at the lateral edges of the inner pin-holes at the PIP joint of the middle phalanx, and at the lateral edges of the posterior protrusion at the MCP joint of the proximal phalanx respectively. While these stresses exceeded the yield point of the material under their maximum loading conditions of 82 N and 55.8 N respectively, they remained localised with the surrounding structures not surpassing the yield stress. The surface of the radii at the hinges of the MCP and PIP joints exceeded the yield at loads greater than 40 N for the 3rd digit and 30 N for the 5th digit.

Under lateral loading, the areas of highest stress concentration were located at the lateral borders of the hinges and at the lateral edges of the pin holes. The peak stresses of the 3rd and 5th digits were both located at the PIP joint; at the supero-lateral edge of the hinge and the lateral edge of the superior pin hole respectively. While they both exceeded yield the lateral pin-holes of the 5th digit had localised yielding that had no major impact on structural strength. On the contrary, while the stresses are initially localised at loads below ±60 N (Figure C34, p. C-23), the confluence of the pinhole stresses and supero-lateral hinge stresses of the 3rd digit at approximately 80 N present concerns regarding the structure's resistance to fracture at loads exceeding this value.

The load-displacement behaviour of the structures is summarised in Table C2, p. C-22. The findings of this investigation will be compared to experimental procedures outlined in Chapter 7 for validation.

5

CHAPTER 5: MECHANICAL DESIGN

"Design can be art. Design can be aesthetics. Design is so simple, that's why it is so complicated."- Paul Rand

5.1. Phalangeal Design

Each of the phalanges of the five digits of the hand, are designed according to anthropometric proportions outlined in Chapter 2.2 (p. 5) and are anatomically proportional to the 50th percentile of the population. The first digit (thumb) consists of two phalanges, proximal (1) and distal (2), whereas the second to fifth digits have three phalanges each; namely, proximal (3), middle (4) and distal (5). The fingers consist of three hinged-joints described from proximal to distal as metacarpophalangeal (6), proximal interphalangeal (7) and distal interphalangeal (8) joints respectively, as seen in Figure 71. The ranges of motion used for each of the joints is summarised in Table 8, p. 35.

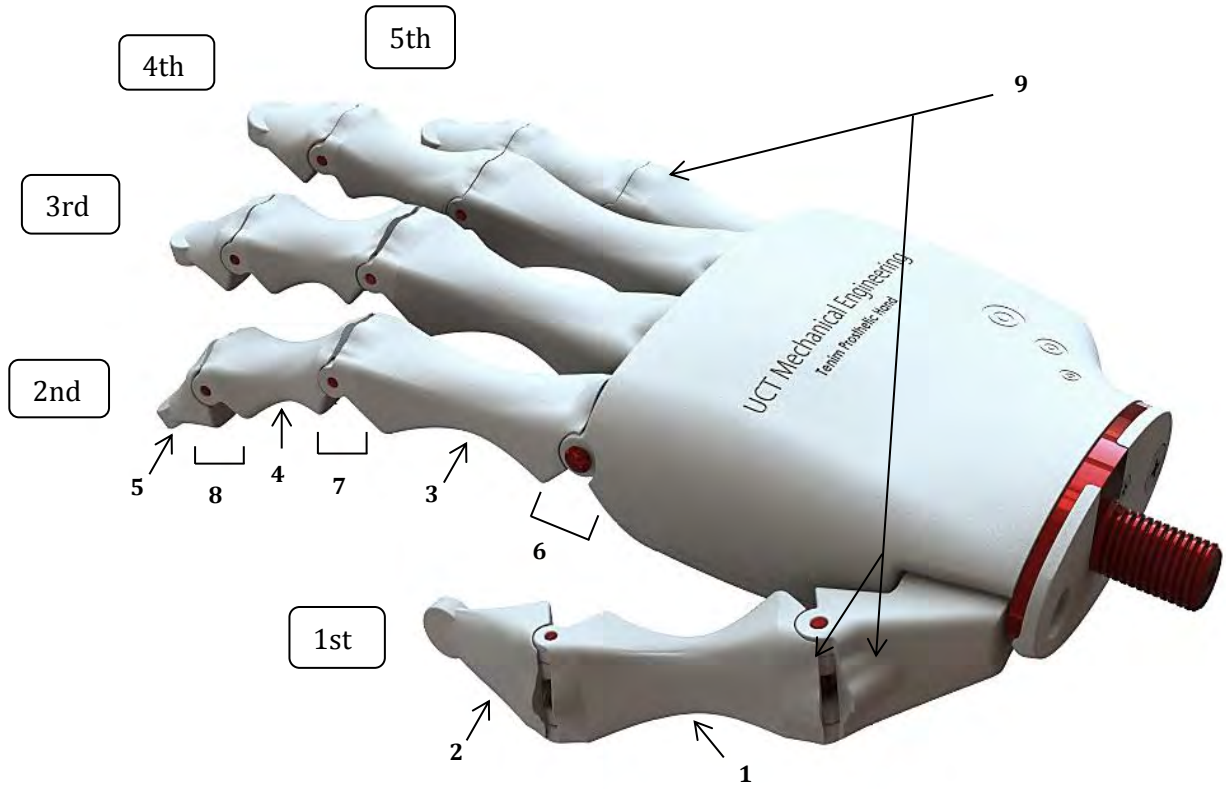

Figure 71 - Dorsal perspective view of the prosthetic hand with reference to the phalanges.

Referring to Figure 72, the joints pivot about a locking pin (10) that is secured from axial dislocation by two e-clips (11). Torsion springs (12), located around polymeric mandrels (13), are used in each joint to return the hand to the fully extended position after being flexed. Their arms locate into angled slots (14), whose 10° angular deviation from the horizontal ensures that the straight wound torsion springs have an initial residual tension. This residual tension not only fully extends the joint but also has enough combined energy with the other springs to restore the internal mechanisms of the hand back to their initial positions (i.e. when the hand is fully extended). Anatomically, this role is completed by the extensor muscle groups in the posterior compartment of the forearm.

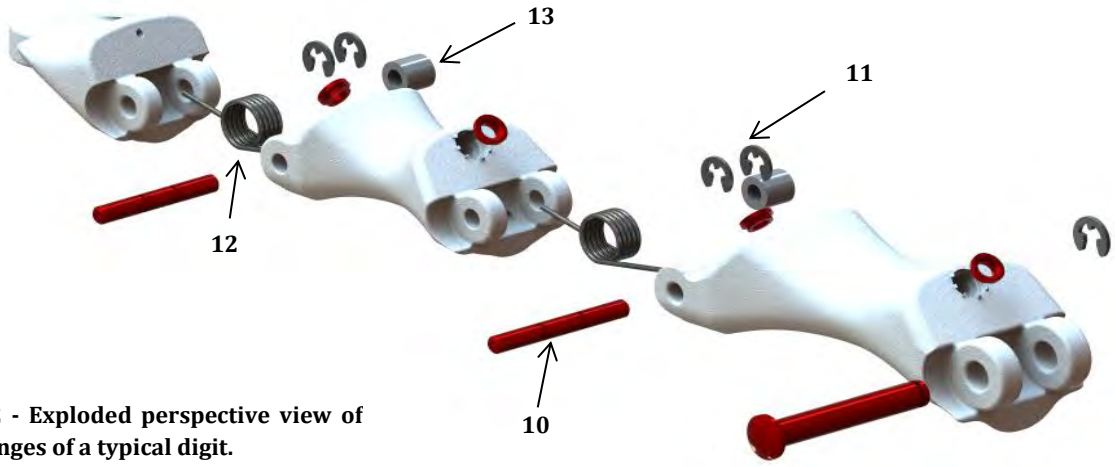

Figure 72 - Exploded perspective view of the phalanges of a typical digit.

The actuation of each finger is inspired by the natural tendon-sheath mechanism of the human hand. The nickel-titanium actuation wire (15), as seen in Figure 73, is inserted through tendon channels (16) within each of the phalanges and secured at the end through means of a welded bead, crimped ferrule or a knot (17). These channels (16) have a cross-sectional profile (18) similar to the Greek "Omega Ω" symbol and are arched to increase the leverage of the wire about the pivot (i.e. locking pin (10)) of each joint. This benefits the patient greatly as the activation energy needed to rotate the joint is lower, hence reducing the physical exertion needed to close the hand. This also reduces the required wire tension, which reduces the wire contact forces (in the normal direction) and ultimately decreases the wear of the mechanism.

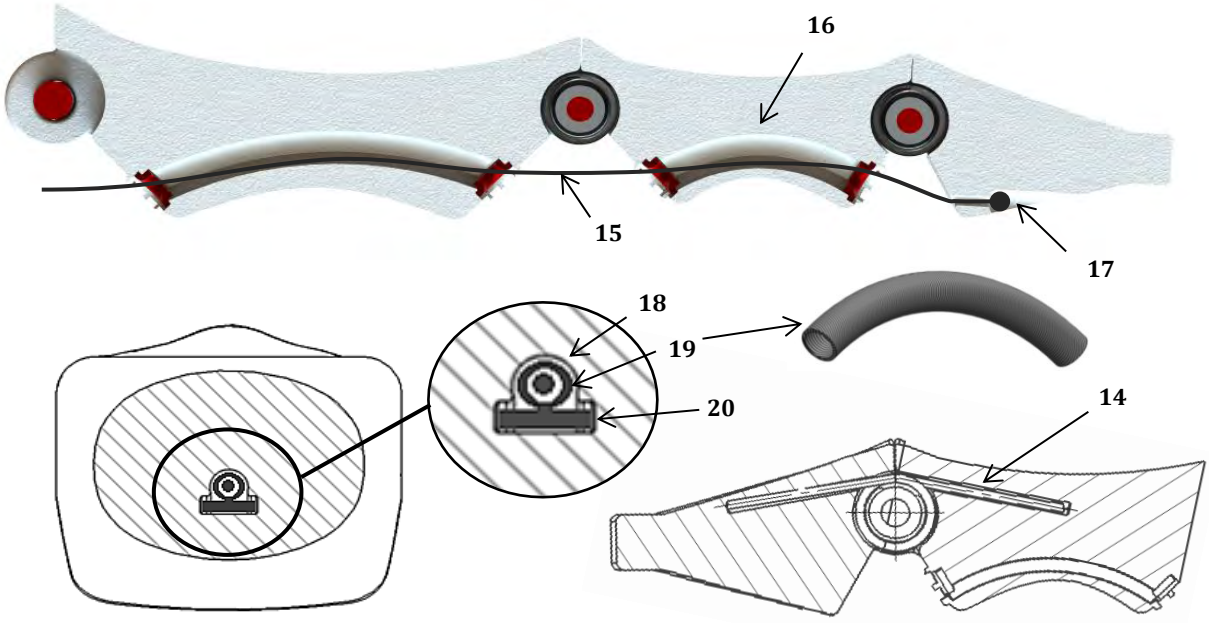

Figure 73 - Lateral and transverse section views of the internal channels of the phalanges with helical-hollow-strand tubing and spring-slots shown.

Due to a polymeric phalangeal parent material and the presence of cyclic loads, wear/fatigue of the wire/tendon contact surfaces are of concern. Consequently, more wear-resistant contact surfaces are required. The "Omega Ω" cross-section (18) allows for the insertion of two types of reinforcing

structures/linings, either cylindrical and/or plate material. Helical-hollow-strand (HHS) tubing (19) and/or a flat metallic plate (20) are selected. The tubing (19) and/or plate (20) are securely located within the channel structure (16) by punched channel rings (21) on either end, preventing axial movement (Figure 74). These channel rings (21) are glued into position, and then the channel ring retainers (22) (part of the parent material) are heated and bent over the channel ring (21); securing it.

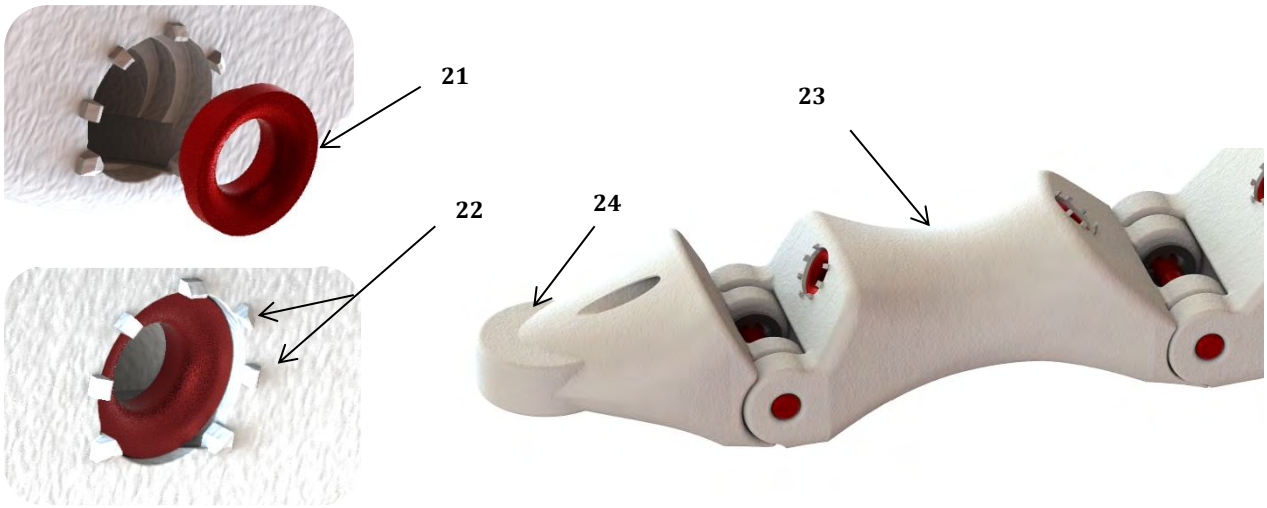

Figure 74 - Perspective views of the channel ring and the channel ring retainer, exploded (left top) and inserted (left bottom), with lateral perspective view of the curved surface and distal phalanx tip (right).

Externally, the curved palmar surface of the phalanges (23) allows for the insertion of rubber cushions/spray to increase the gripping capabilities of the hand. The tip of the distal phalanx (24) is pointed to allow finer motor functions to be performed as well as to enable picking up objects of smaller geometry. Inferior and lateral views of an assembled digit are shown in Figure 75 below.

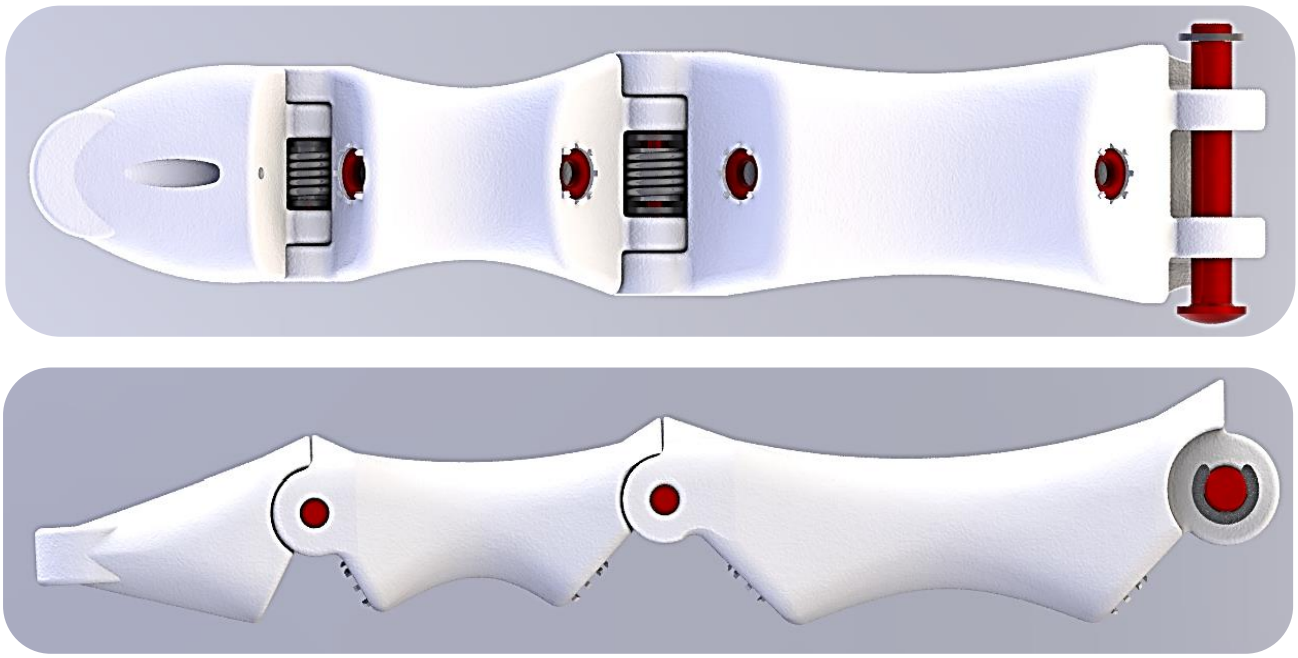

Figure 75 - Inferior and lateral views of an assembled digit; top and bottom respectively.

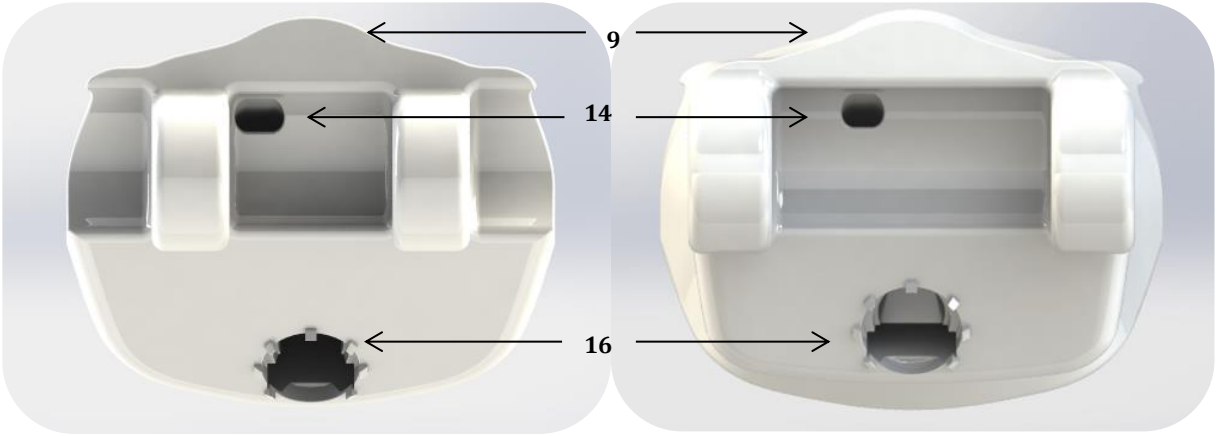

Figure 76 - Proximal and distal views of a typical phalanx, left and right respectively; showing the posterior protrusions, spring-slots & tendon channels.

Figure 76 shows the proximal and lateral views of a typical phalanx, with posterior protrusions (9), spring-slots (14) and tendon channels (16). What is more, the initial and final revisions of these protrusions and channels are shown in Figure 77 below.

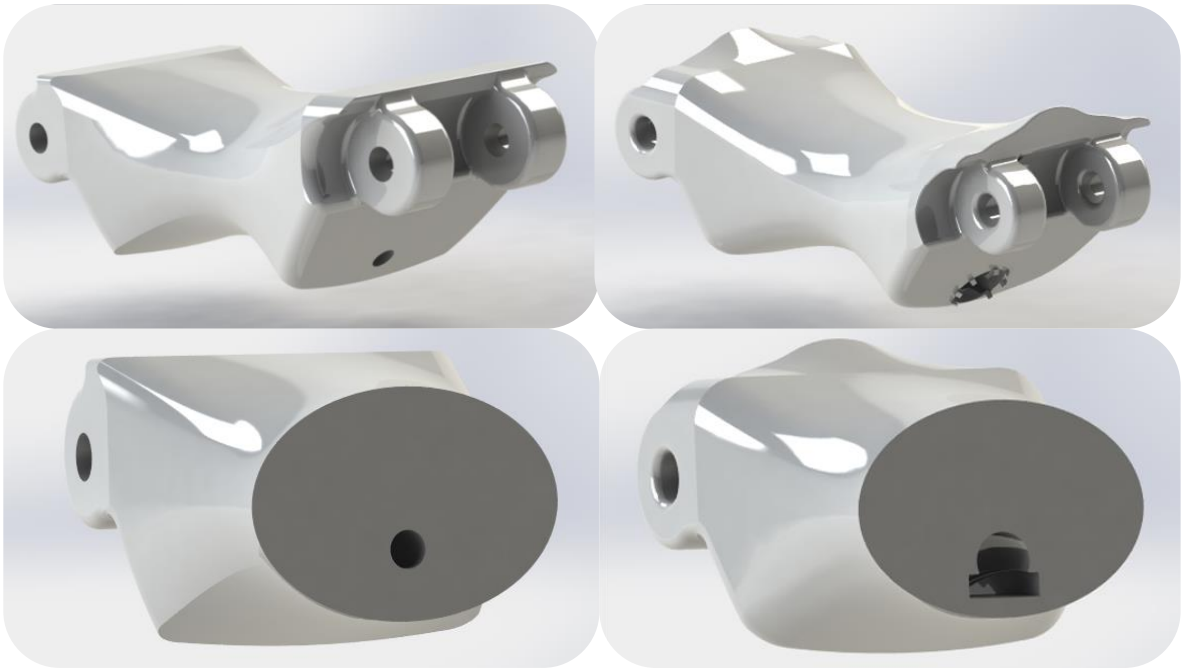

Figure 77 - Perspective views of Revision 0 (left) and Revision 1 (right) of the posterior protrusions (top) and the tendon channels (bottom) respectively.

5.2. Thumb Design

The two-phalanx thumb design (Figure 78) functions similarly to the aforementioned phalangeal design. However a rotating thumb-swivel (25), similar to the first metacarpal bone of the anatomical hand, allows the thumb to not only flex and extend, but also to adduct and abduct. This motion allows the user to manually switch between lateral and power grasps, or a combination of the two, enabling a broader range of grasps.

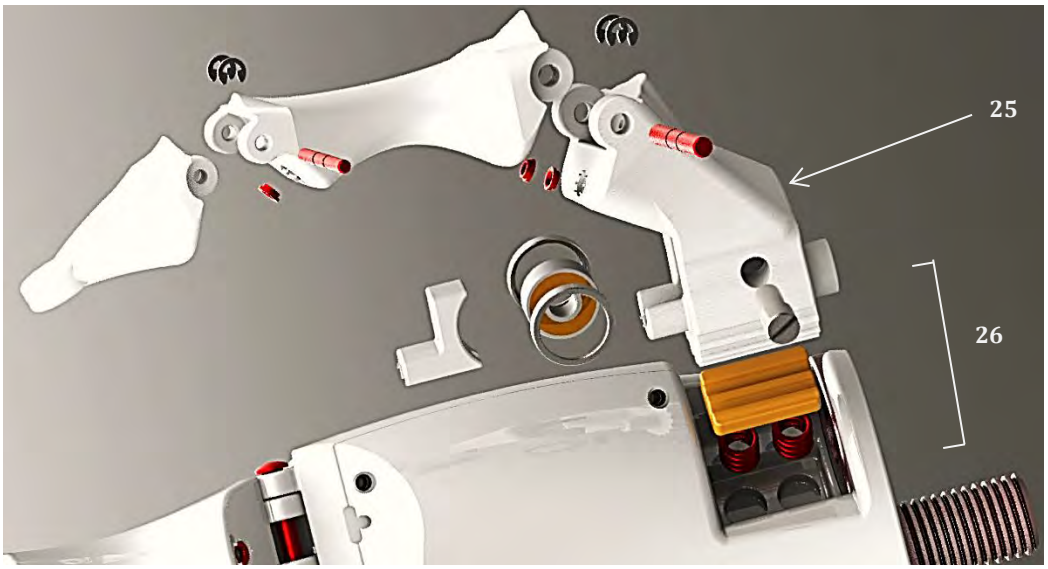

Figure 78 - Exploded perspective view of the thumb and its mechanisms

Furthermore, an incremental locking mechanism (26) allows the user to fix the thumb at five different orientations, each 20° apart. This locking mechanism (26) can be seen in Figure 79 and uses mating semi-cylindrically waved teeth (27), with a linearly spring-actuated locking plate (28) to retain the thumb-swivel (25) at a selected angular position. Two linear compression springs (29) are used to provide actuating force, and are secured by cylindrical recesses (30) in both the body of the palm (31) and in the locking plate (28) to prevent misalignment.

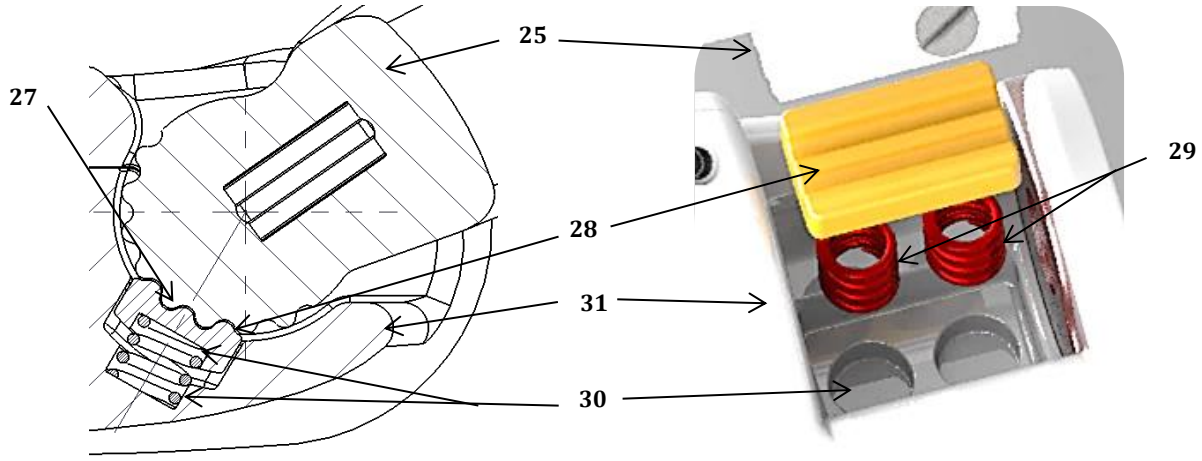

Figure 79 - Transverse section view and exploded perspective view of the incremental locking mechanism of the thumb

Due to a large angular change in the travel of the thumb actuating-wire (32), a roller ball bearing (33) is inserted into the bearing cut-out (34) in the thumb-swivel (25) and located securely by the locking pin (35) in Figure 80. To maintain alignment of the wire (32) and prevent it from sliding off the edges of the bearing (33), two cylindrical end-rings (36) are slid onto the bearing, between which the actuating wire (32) will travel. After the bearing arrangement is secured within the thumb-swivel (25), an end cap (37) is inserted to protect the unit, complete the cylindrical pivot for rotational stability and maintain geometrical uniformity; this assembly can be seen in Figure 81.

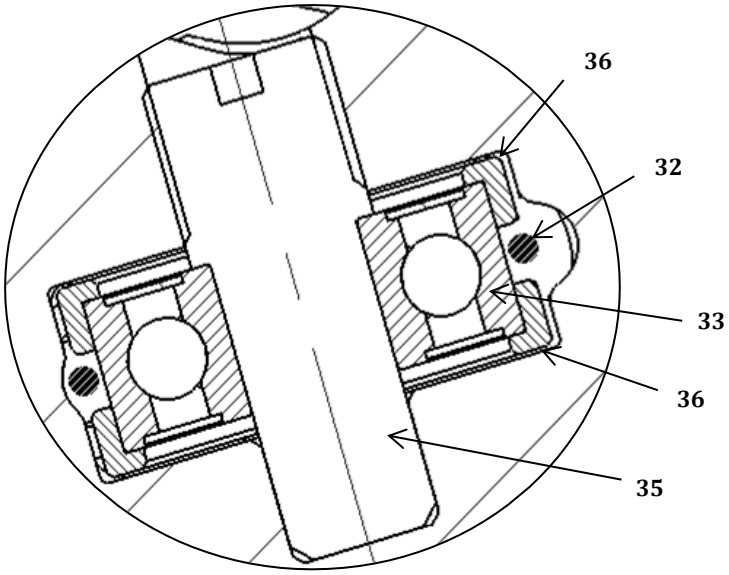

Figure 80 - Transverse section view of the thumb bearing unit.

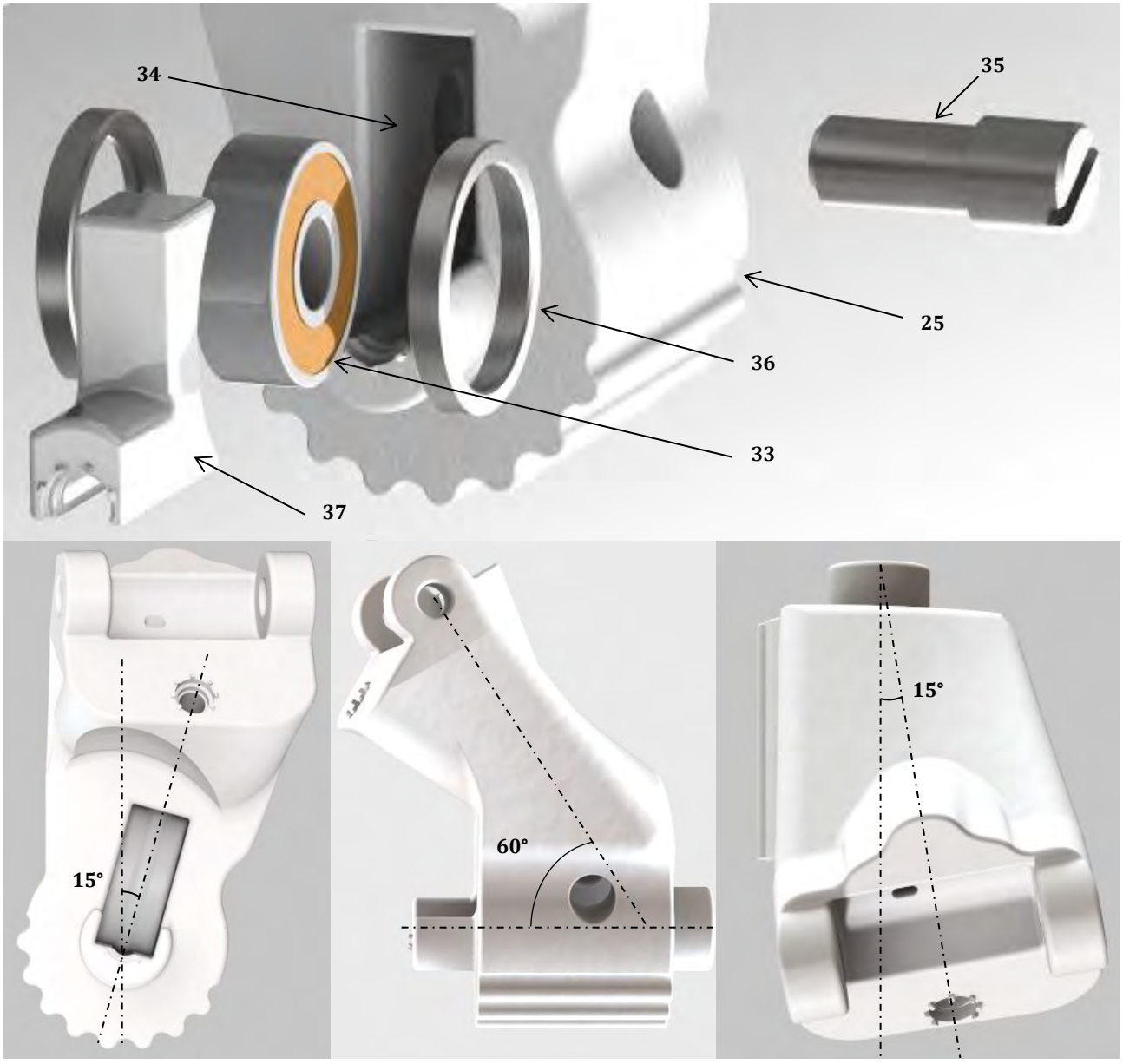

Figure 81 - Exploded view of the thumb bearing assembly (top) with anterior, lateral and superior views of the thumb (bottom left to right respectively).

5.3. Thumb Transfer-Lever Design

In order to enable a functional opposable grip, a few mechanical mechanisms are needed to create a link between the fingers and the thumb. The thumb, having only two phalanges, requires less linear translation than its three-phalanx finger counterparts hence a thumb transfer-lever (38) is employed (Figure 82) to adjust for the difference in linear displacement necessary to close the fingers and the thumb.

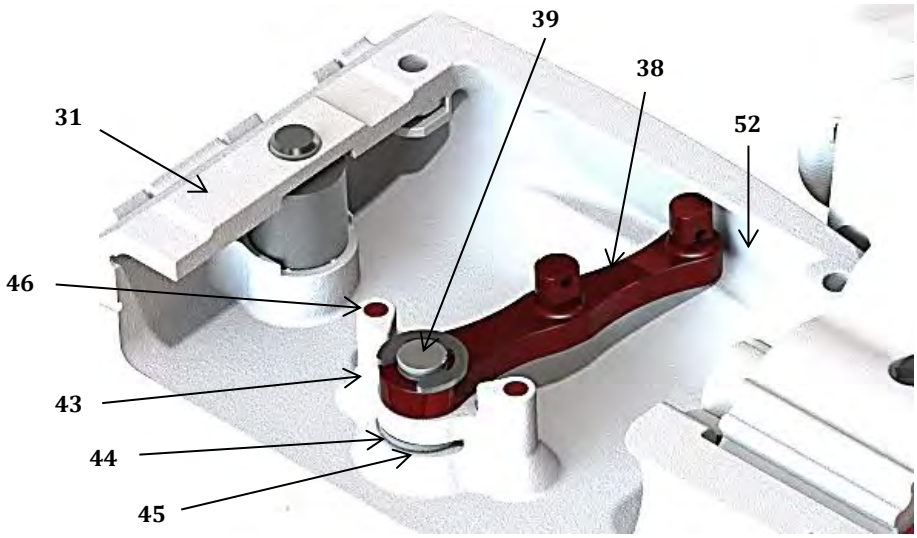

Figure 82 - Perspective view of the thumb transfer-lever unit

This lever (38) pivots about a locating pin (39) at its medial end. The pin (39) is inserted into a cylindrical cut-out (42) in a raised support platform (43) of the palmar structure (31) and located by an e-type circlip (44), which is inserted through a slot (45) from the medial side. Two metallic support pins (46) are inserted into the raised support platform (43) from the palmar side to reinforce the structure when contacting the lever at its fully-open (40) and fully-engaged (41) positions (Figure 84).

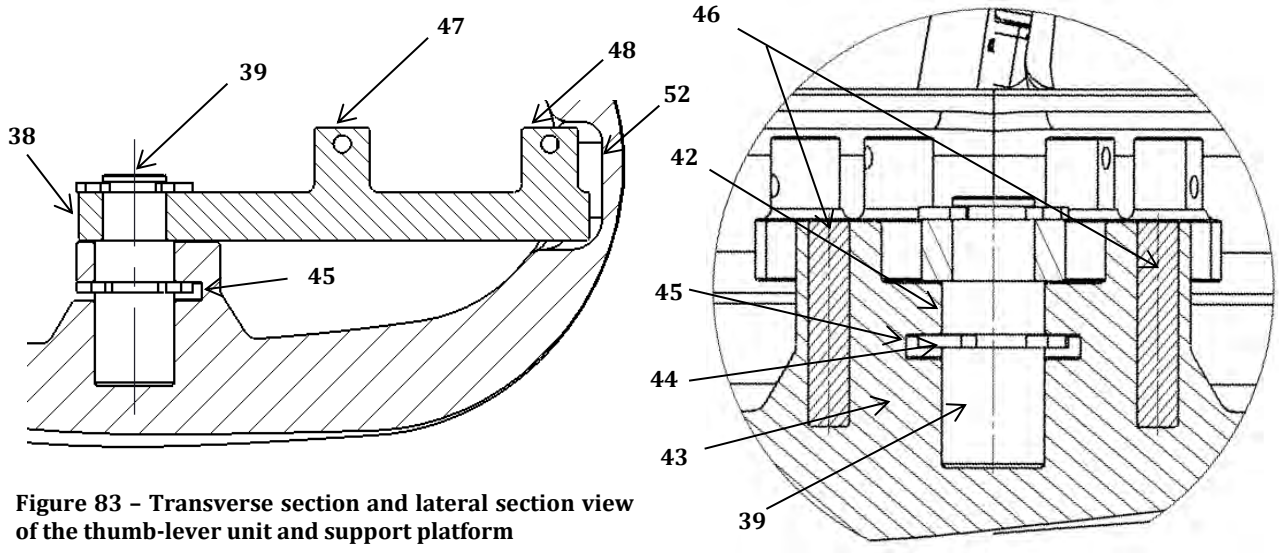

Figure 83 – Transverse section and lateral section view of the thumb-lever unit and support platform

The actuating wire of the thumb (32) inserts from the proximal side through the hole in the medial pin (47) of the lever. Conversely, the connecting wire on the distal end of the lever inserts through the hole on the lateral pin (48). Both the medial (47) and lateral pins (48) are raised to align with the plane linking the lower-end of the thumb bearing (33) and the flanged-guide-pulley (49) on the proximal linear-bearing slider (50) of the palmar differential mechanism (51). A lever cut-out (52) in the palmar structure (31) can be seen lateral to the thumb-lever (38) in order to provide clearance for its path of travel between 0° and 90° from its fully-open (40) to its fully-engaged (41) positions respectively.

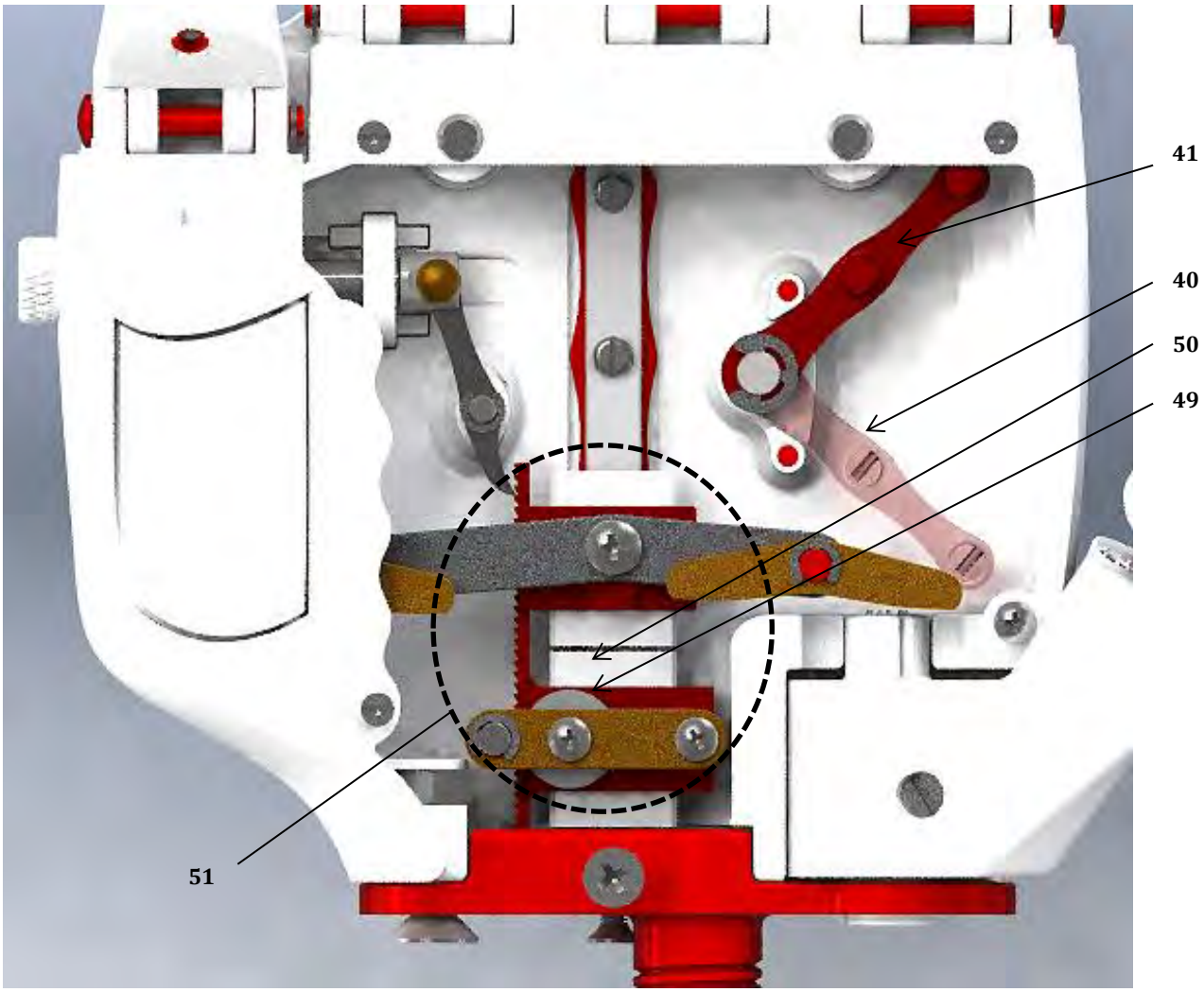

Figure 84 - Palmar view of the thumb transfer-lever in open and engaged positions

5.4. Palmar Cushion Design

The palmar cushion (53) uses potential-spring-energy stored in the cushion's springs (54) to assist in the whole or partial absorption of any slack in the cable-driven actuating system, as seen in Figure 85. The main objective being to maintain normal contact forces between the hand and the grasped object, when the tension in the primary actuating cable is released by the user.

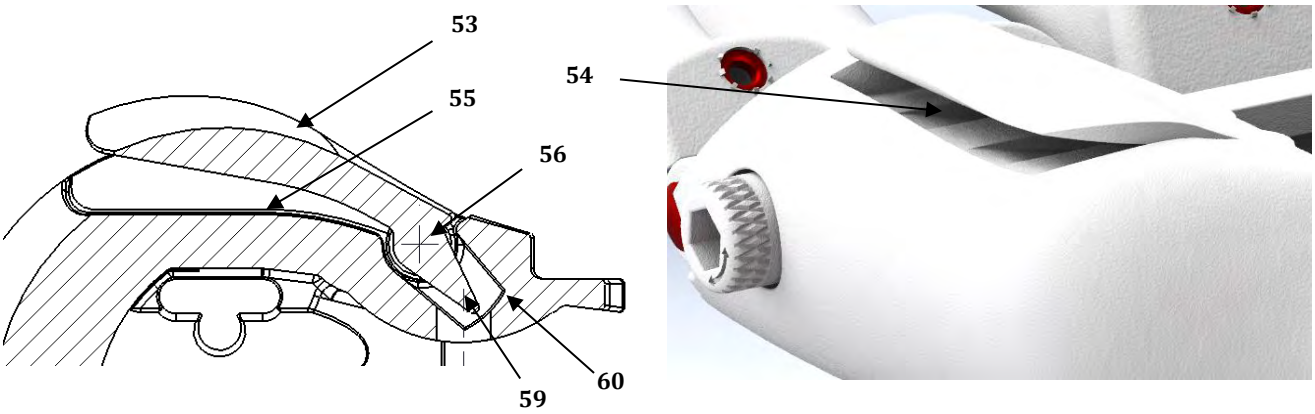

Figure 85 - Transverse section view and postero-lateral perspective view of the palmar cushion

The cushion (53) opens and closes through an angle of 15° with the two torsional spring elements (54) between the cushion (53) and the backing surface (55), maintaining the rest position as fully-opened. The cushion (53) pivots about the central axis (56) of the distal (57) and proximal (58) pins. Three protrusions/stems (59) are positioned on the medial side of the cushion (53), and locate within slots (60) to limit the angle to which the cushion (53) may open (i.e. 15°). Additionally, they also serve to prevent hyperextension of the cushion, should the mechanism encounter any unforeseen hyper-extensive loading. The holes (61) in the base of these slots (60) and on the dorsal surface inferior to the pins (57 & 58), serve as 'drainage' holes through which residual unmelted powder from the manufacturing process can be extracted.

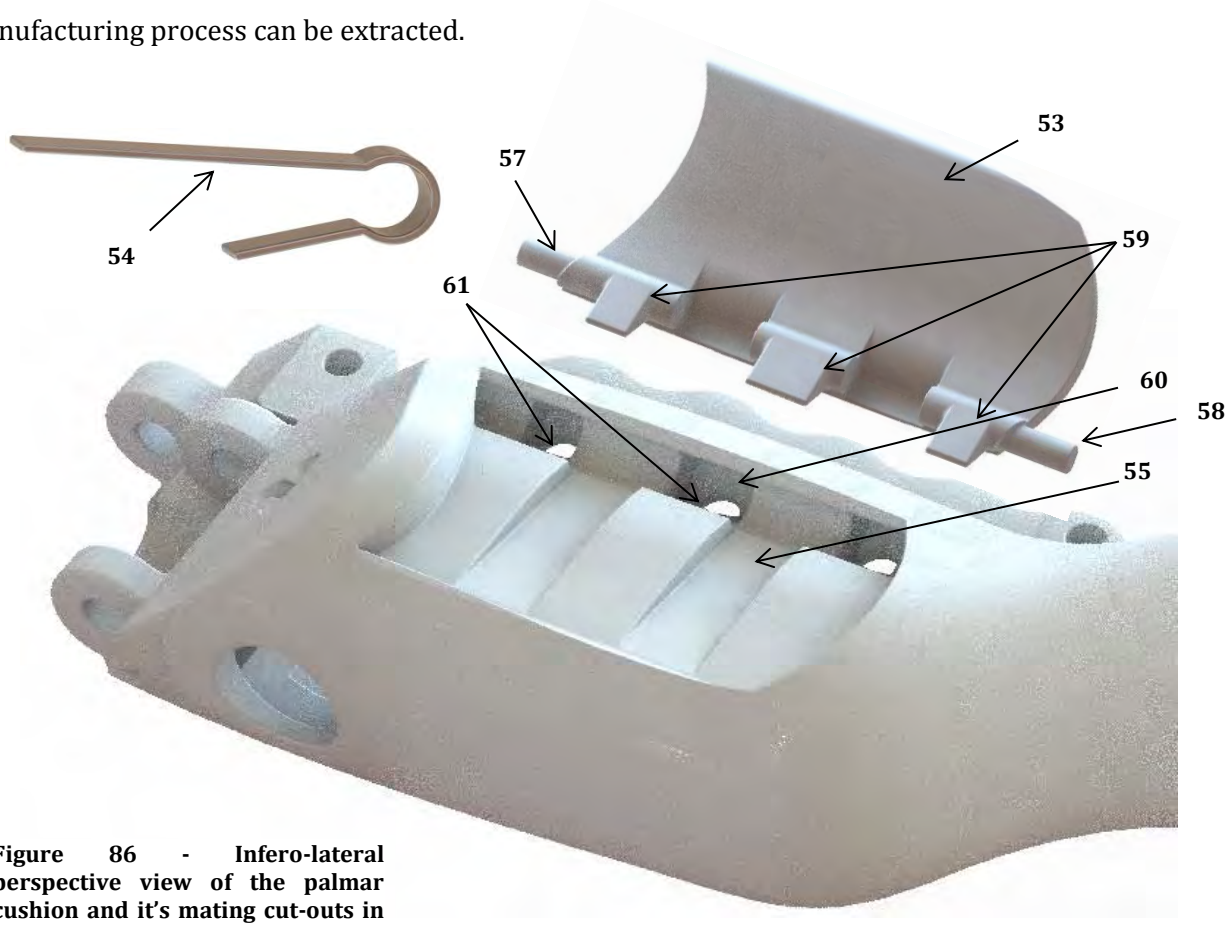

Figure 86 - Infero-lateral perspective view of the palmar cushion and it's mating cut-outs in the palmar superstructure

5.5. Differential Seesaw Mechanism

The differential seesaw/lever mechanism (62) is situated on the distal linear-bearing slider (63) of the hand, as shown in Figure 87 & Figure 88. Its function is to provide differential motion between the fingers of the hand; allowing it to close around objects of both uniform and non-uniform geometries. Furthermore, the distribution of actuating force between fingers can be controlled by changing the lengths of each respective lever.

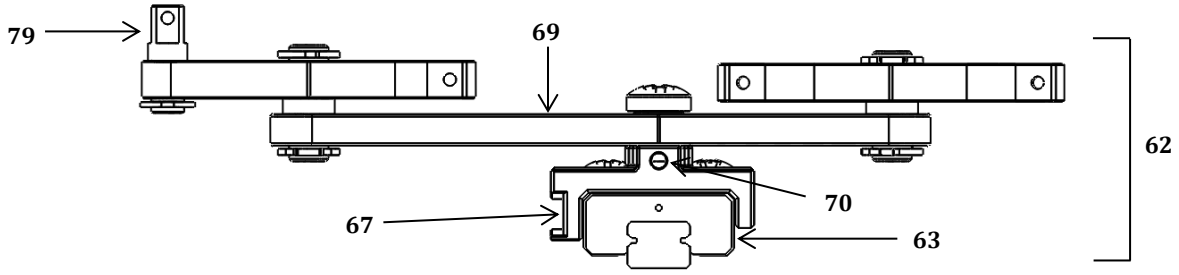

Figure 87 - Posterior view of the assembled differential seesaw mechanism

The invention has a lever-carriage (64) which is fastened to the distal linear-bearing slider (63) by two pan-head screws (65), whose heads locate into two recessed grooves (66) so as not to interfere with the moving mechanisms above. The lever-carriage (64) has a ratchet guide-way (67) on its lateral surface for location of the ratchet-rack (96) of the ratchet-carriage (83). Additionally, there is a centrally tapped, pin protrusion (68) on its superior surface which interfaces with the primary seesaw (69). The palmar actuating cable (121), linking the differential seesaw mechanism (62) to the thumb-lever (38), passes through the clamping hole (70) on the proximal surface. This hole (70) penetrates horizontally through to the distal end of the lever-carriage (64) and is intersected from above by the tapped hole (71) in the protrusion (68). The locking screw (72) from above secures the primary seesaw (69) as well as locks the palmar actuating cable (121) in place.

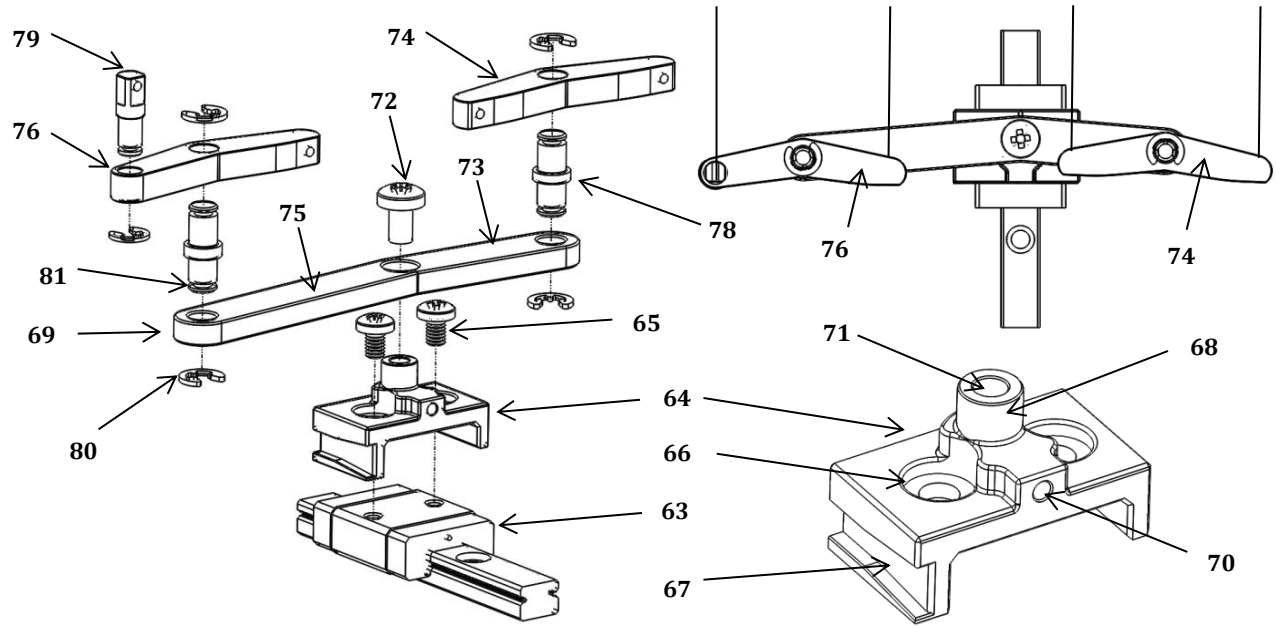

Figure 88 - Exploded perspective and superior views of the differential seesaw mechanism with supero-lateral perspective view of the slider carriage unit.

The primary seesaw (69) pivots about the protrusion (68) of the carriage. Its lever-arms are angled slightly backwards to increase the effective lever-arm when rotating towards the end which is loaded the most; allocating slightly higher actuating force. The lengths of the lever-arms are varied to allow uneven force distribution. The shorter lever-arm (73) distributes the greater force to the 1st secondary seesaw (74) which connects to the 2nd and 3rd digits. The longer lever-arm (75) connects to the 2nd secondary seesaw (76) which links the 4th and 5th digits. A 60-40 distribution of forces is given in favour of the 2nd and 3rd digits, according to the calculations of the analytical model in Chapter 4. Both secondary seesaws (74 & 76) are connected to the primary seesaw (69) by swivel-pins (78) and are free to rotate about them. These swivel-pins (78) locate inferiorly and superiorly through clearance holes to the primary seesaw (69) and secondary seesaws (74 & 76) respectively. An elevating pin (79) is inserted into the 2nd secondary seesaw (76) to account for the height difference between the 4th and 5th digit. The aforementioned pins (78 & 79) are axially located by e-type circlips (80) which insert onto undercuts (81) on the pins' extremities.

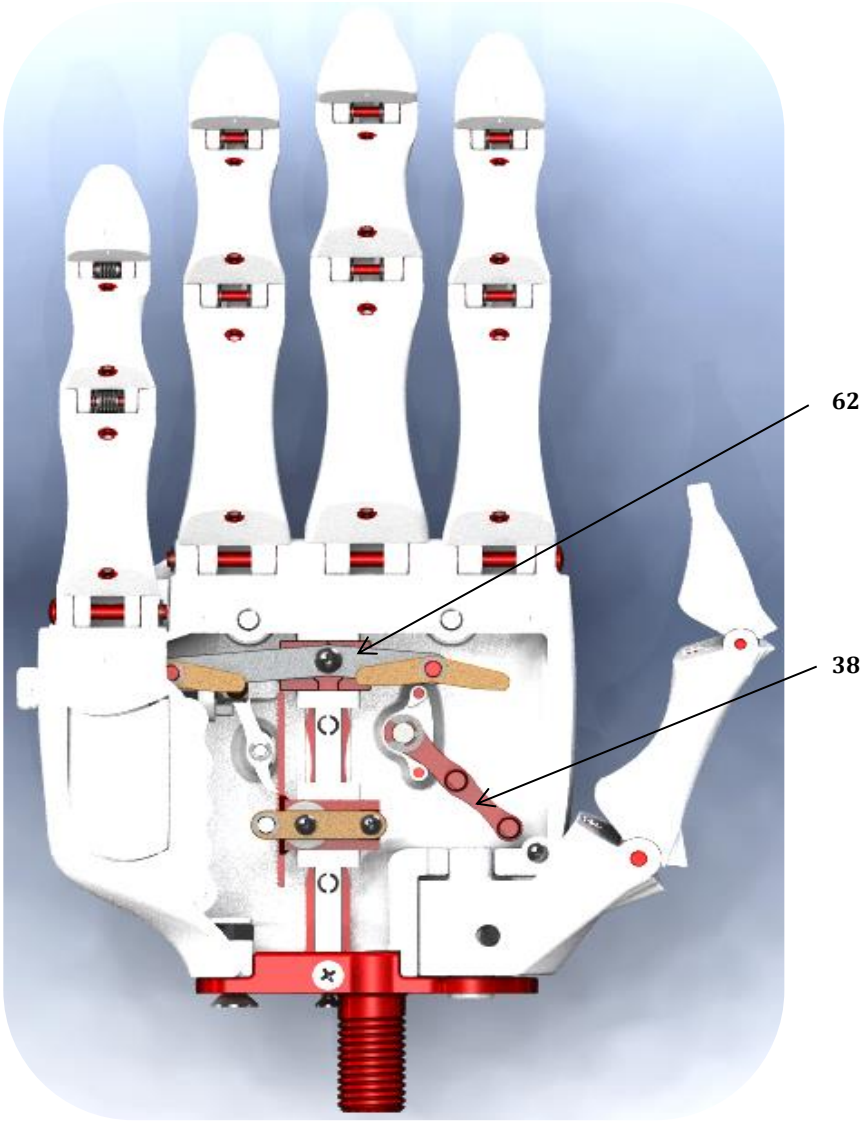

Figure 89 - Open palmar view of the assembled prosthetic hand with its internal mechanisms

5.6. Pulley-Ratchet Slider Mechanism

The pulley-ratchet slider mechanism (82), shown in Figure 90 & Figure 91, has two primary purposes; namely to guide the palmar actuating wire (121) coming from the thumb-lever (38), and to provide an incremental linear locking action. A ratchet-carriage (83) slides onto the proximal linear-bearing slider (50) from either the proximal or the distal side, and is held in place by overhanging lip (84) and two cone-point grub screws (85) which locate laterally against the surface of the proximal linear-bearing slider (50). A locating screw (86) inserts superiorly to locate the ratchet-carriage (83) as well as to secure the pulley clamping-plate (87) from above. Three flanged guide-pulleys, one large and two small, lie superior to the ratchet-carriage (83). The large (88) and a small (89) flanged guide-pulleys slide onto the two cylindrical pins (90) on the ratchet-carriage (83) whereas the second small flanged guide-pulley (91) locates centrally around an overhanging pin (92), fastened to the pulley-clamping-plate (87) by two e-type circlips (93). A fourth screw (94) secures the pulley clamping-plate (87) on its lateral end as well as clamps the hand's primary actuating cable (124), whose end inserts through the clamping hole (95) on the anterior surface of the ratchet-carriage (83) and origin interfaces externally with the shoulder harness and/or external motorised actuating system. On the left lateral side of the ratchet-carriage (83), a toothed linear ratchet-rack (96) extends distally and proximally. Its toothed-mating-surface (97) engages with the proximal end of the pawl (108 in Figure 95) throughout the linear-range of the pulley-ratchet slider mechanism (82).

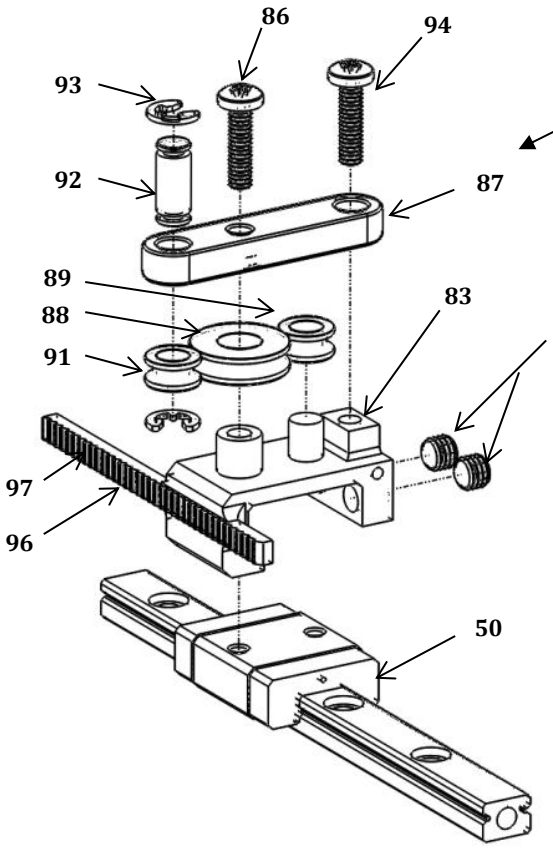

Figure 90 - Exploded perspective view of the assembled differential pulley and ratchet slider

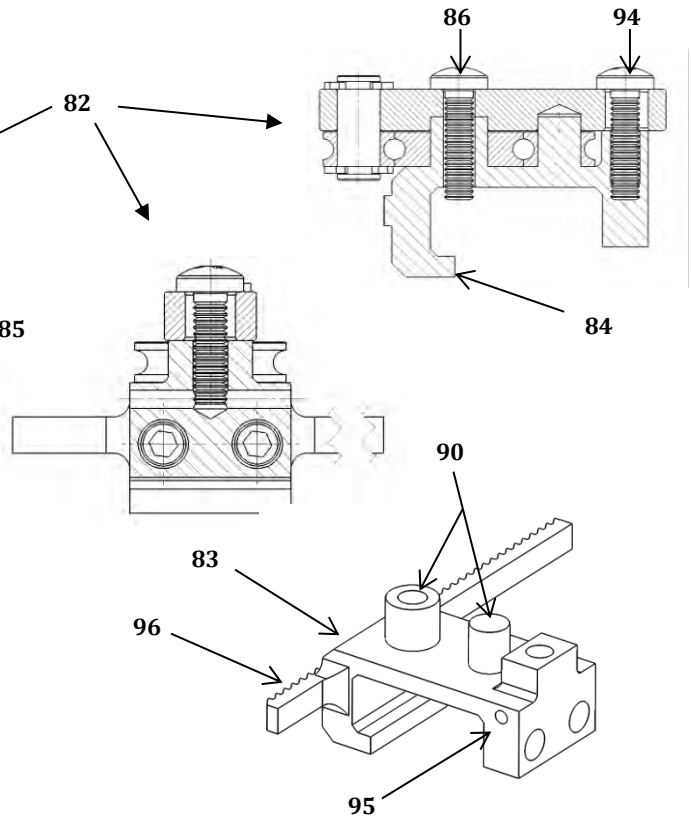

Figure 91 - Posterior and transverse section views of the differential pulley and ratchet mechanism assembly, with postero-lateral view of the ratchet carriage

5.7. Pawl-engagement Mechanism

Excluding the palmar superstructure, the pawl-engagement mechanism (98) is comprised of nine major components. Namely, the bayonet locking-button (99), pivoting-lever (100), posterior (101) and anterior (102) arch-inserts, spring-loaded pawl-shaft (103), compression spring (104), pawl locking-pin (105), pawl swivel-pin (106), e-clip (107) and the pawl (108) which can be seen in Figure 92 below. The pawl-engagement mechanism (98) is used to provide incremental locking for the hand during operation. It makes use of the spring-loaded pawl-shaft (103) to keep the pawl (108) engaged with the ratchet-rack (96) during flexion of the hand. Once the primary actuating cable's (124) tension is released, the hand's natural extension is prohibited by the locking of the toothed ratchet-rack (96) and pawl (108) mechanism, locking the hand in position. To release the hand, the locking-button (99) must be suppressed to disengage the pawl (108), allowing both linear-bearing sliders (50 & 63) to return to their distal most position, i.e. when the hand is fully extended.

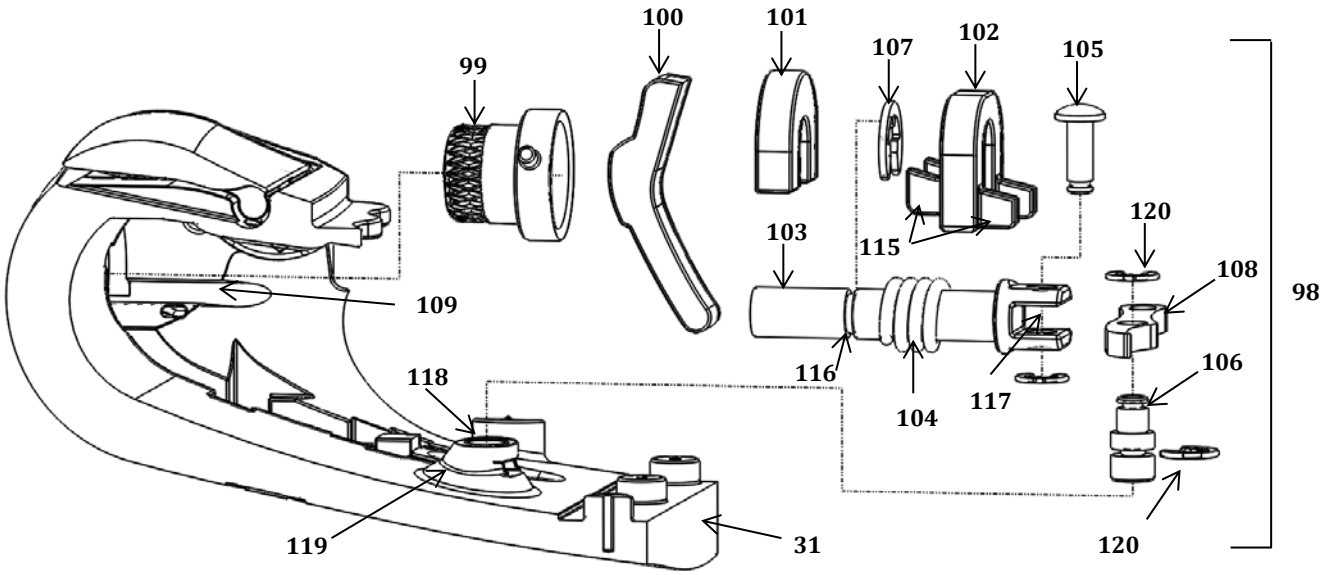

Figure 92 - Postero-lateral exploded section view of the pawl engagement mechanism

The bayonet locking-button (99) (Figure 93) inserts medially on the interior of the palm (31), into a cylindrical recess (108). Two opposing grooves (109) maintain the orientation of the button (99) during insertion and during locking. The button has a hexagonal recess (110) as well as a knurled outer-surface (111) for easy manipulation by the user when rotating it for locking. Directional arrows (112) are engraved on the outer surface for reference.

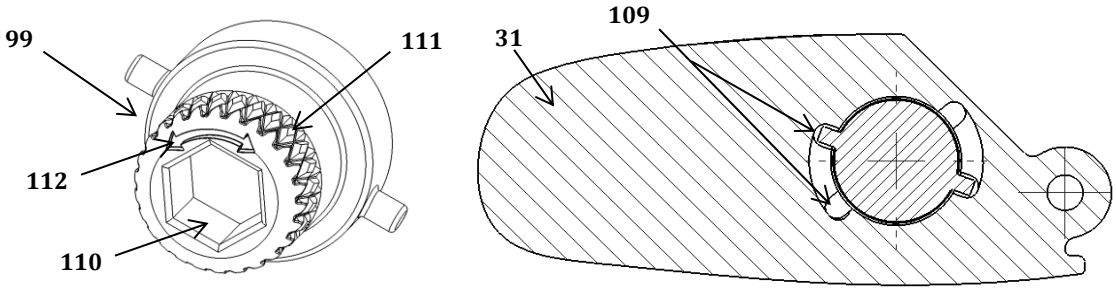

Figure 93 - Perspective and transverse section view of the bayonet locking button.

Referring to Figure 94, the pivoting-lever (100) pivots superiorly against a lip (113) in the structure of the palm (31) and is actuated centrally and inferiorly by the locking-button (99) and pawl-shaft (103) respectively. Its primary function is force transmission and linear motion amplification. The anterior (102) and posterior (101) arch-inserts locate into cut-outs (114) in the palmar structure (31) and are glued into position after assembly of the locking-button (99) and pivoting-lever (100) and radially locate the pawl-shaft (103). The anterior arch (102) provides a rigid surface against which the compression spring (104) can seat and has four ribs (115) to increase torsional stability and maintain alignment. The pawl-shaft (103) has an undercut (116) into which the e-clip (107) locates, creating a contact surface for the compression spring (104), allowing it to linearly actuate the pawl-shaft (103), keeping the pawl (108) engaged. On its medial end, the recess (117) houses the distal end of the pawl (108), with the pawl locking-pin (105) slotting in from above, creating a mechanical link.

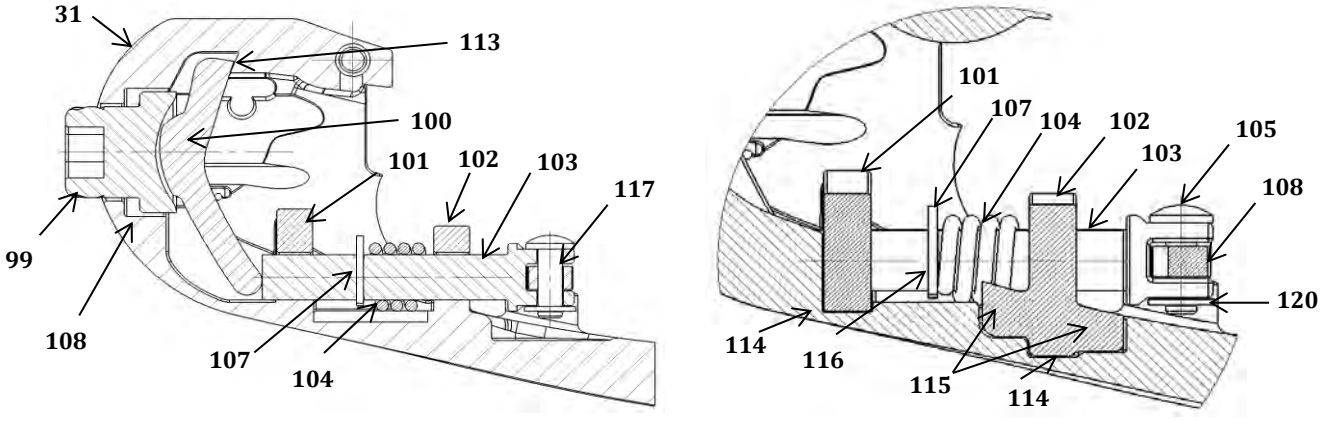

Figure 94 - Transverse section views of the pawl engagement mechanism and the arch inserts of the mechanism, viewed posteriorly.

The pawl (108) pivots near its centre about the pawl swivel-pin (106). The swivel-pin (106) fits into a cylindrical recess (118) in the elevated support structure (119) within the palm (31) and is held in place by an e-clip (120) which inserts from the medial side. The proximal end of the pawl (108) engages with the teeth of the ratchet-rack (96) in its rest position, deviating to the open position (dotted line) as seen in Figure 95 below.

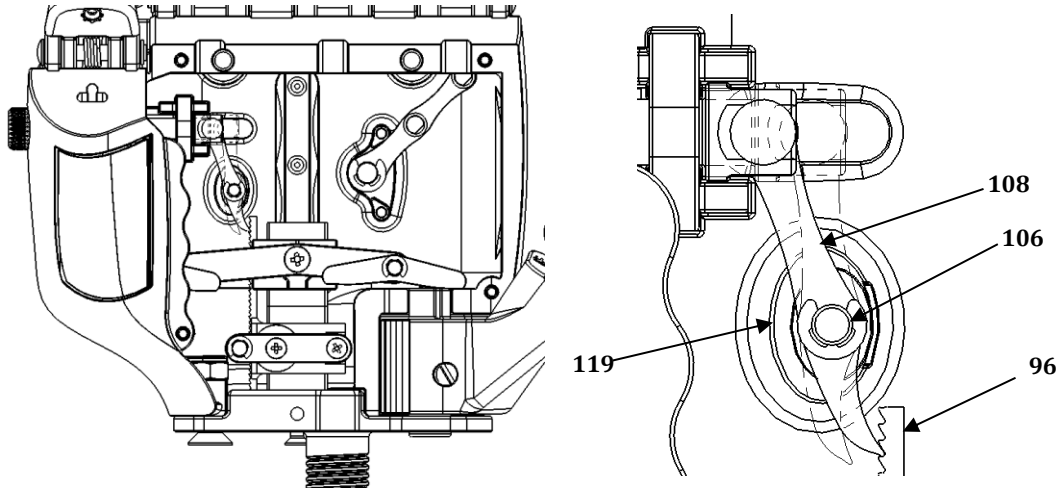

Figure 95 - Palmar and close-up view of the pawl mechanism with engaged and disengaged positions shown.

5.8. Actuating-cable Routing

Actuation of the mechanical hand is done through the use of actuating cables and wires, both mono- and multi-filament. However, in order to access each portion of the hand and to function in the manner intended, it is critical that the routing be such that friction is minimised and the utility of the space is optimised. The phalangeal and thumb routing has been described in the aforementioned sections and will therefore not be repeated. The routing within the palm (31) and the mechanisms used to guide the actuating wires are shown in Figure 96 below.

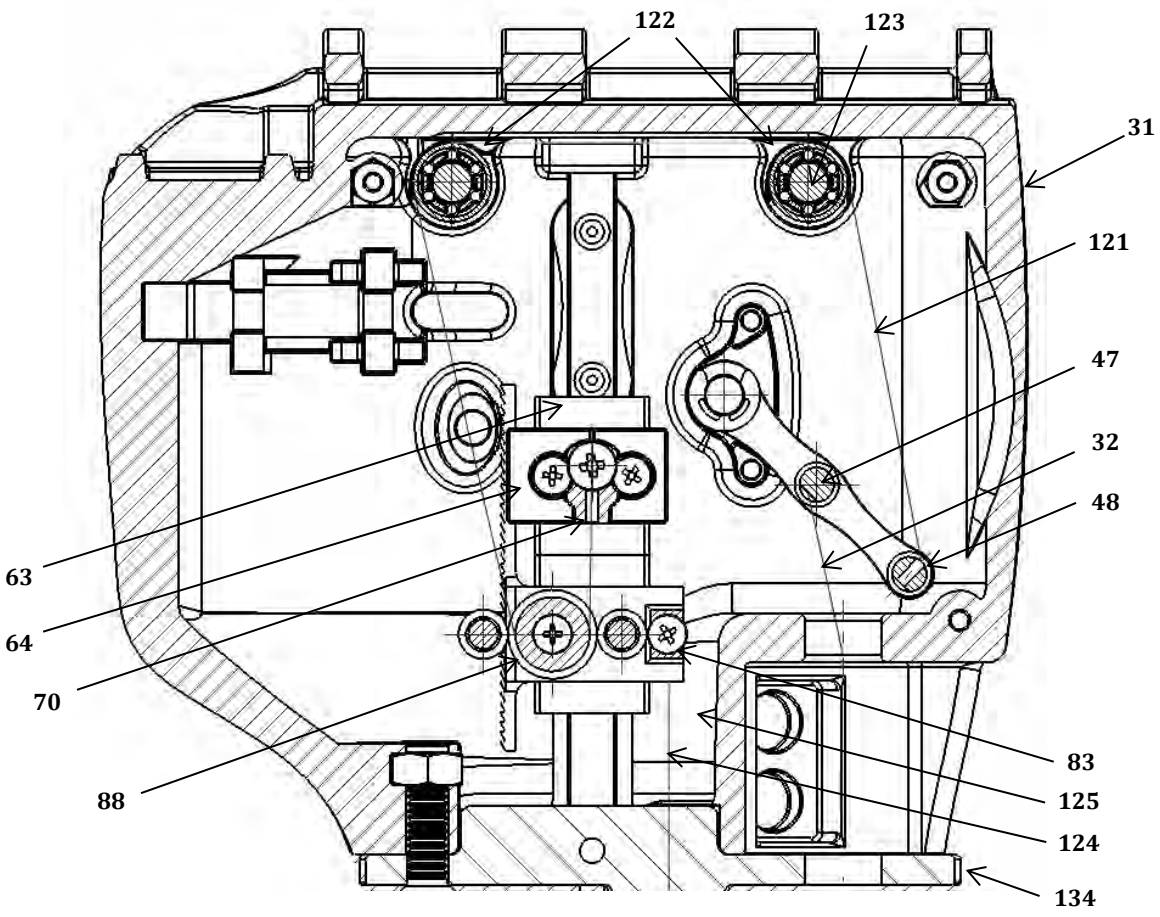

Figure 96 - Palmar section view indicating the routing of the primary, palmar and thumb actuating cables of the hand.

The thumb actuating-wire (32) travels from the thumb and inserts onto the medial thumb-lever pin (47). The palmar actuating cable (121) runs from the lateral thumb-lever pin (48) and travels around two needle-roller routing-bearings (122), located distally within the palm (31) by two bearing pins (123). Thereafter it travels around the large flanged guide-pulley (88) and through the clamping hole (70) in the lever-carriage (64) on the distal linear-bearing (63) to which it is attached. Fastened within the ratchet-carriage (83) (proximal linear-bearing slider (50)), the primary actuating cable (124) travels through the posterior cavity of the hand (125) and out of the exit hole (153) (Figure 99) in the threaded-interface (154) of the wrist stem (134).

The routing-bearing-supports (126) have an elevated cylindrical structure (127) with a central hole (128) into which the bearing pins (123) locate. Six semi-cylindrical ridges (129) protrude on the upper surface of the supports (126) and on their opposing surface (130) superior to it (i.e. the roof). The outer-race (131) of the needle bearings rest on these ridges (129), reducing the contact area to six line-loads, allowing the bearings (122) to rotate more-freely. Furthermore, the raised borders (132) of the supports (126) are in close proximity to the bearings' outer-race (131) and prevent the palmar actuating cable (121) from slipping beneath the bearings (122). Similarly, on the superior border of the bearing (122), the palmar structure (31) does the same. A grooved cut-out (133) on the interior, anterior face of the palm (31), spanning between the routing bearings (122), allows the actuating cable (121) to travel freely, without contacting the palmar structure (31). The bearing pins (123) are held in place axially by the palmar cover (160) from above, and radially by the palmar structure (31).

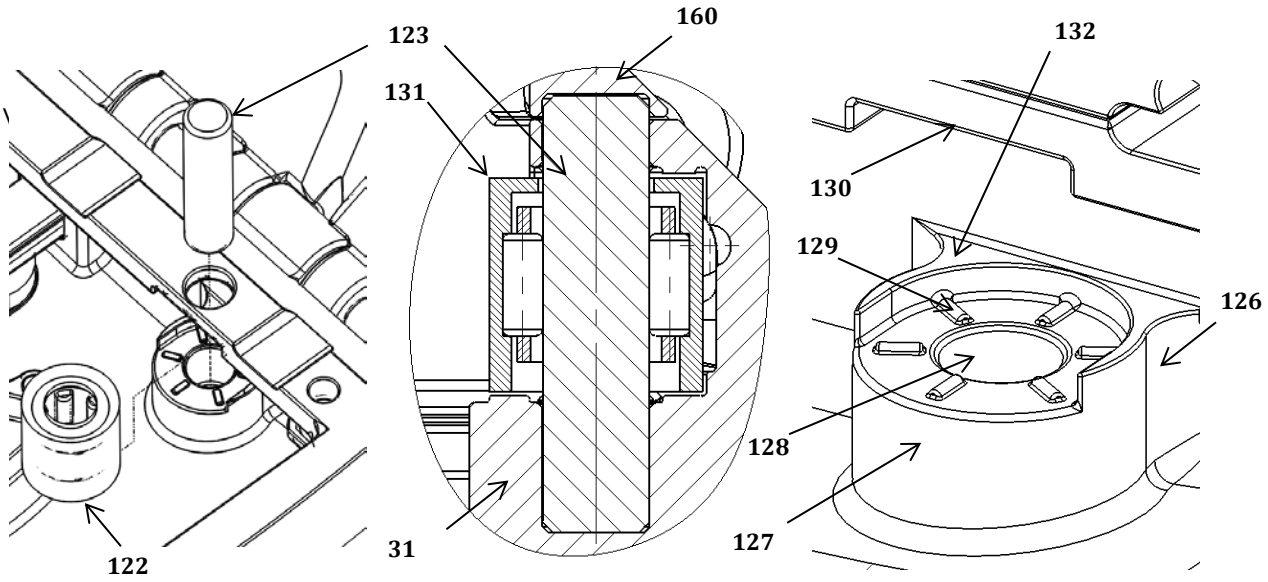

Figure 97 - Perspective and section view of the routing bearing assembly as well as a perspective view of the routing bearing support.

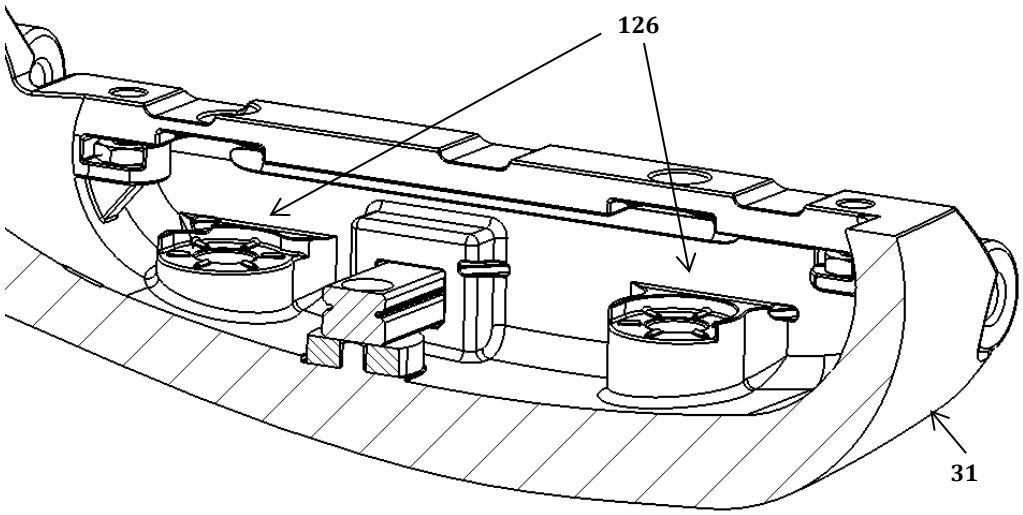

Figure 98 - Perspective section view of the routing-bearing and linear-bearing supports.

5.9. Wrist Stem and Linear-Bearing Fixation

The wrist stem (134) provides the hand with a rigid attachment interface to the prosthetic sleeve which fits onto the patient's stump, as well as provides connectivity to a wrist/carpal mechanism which allows pronation and supination of the hand.

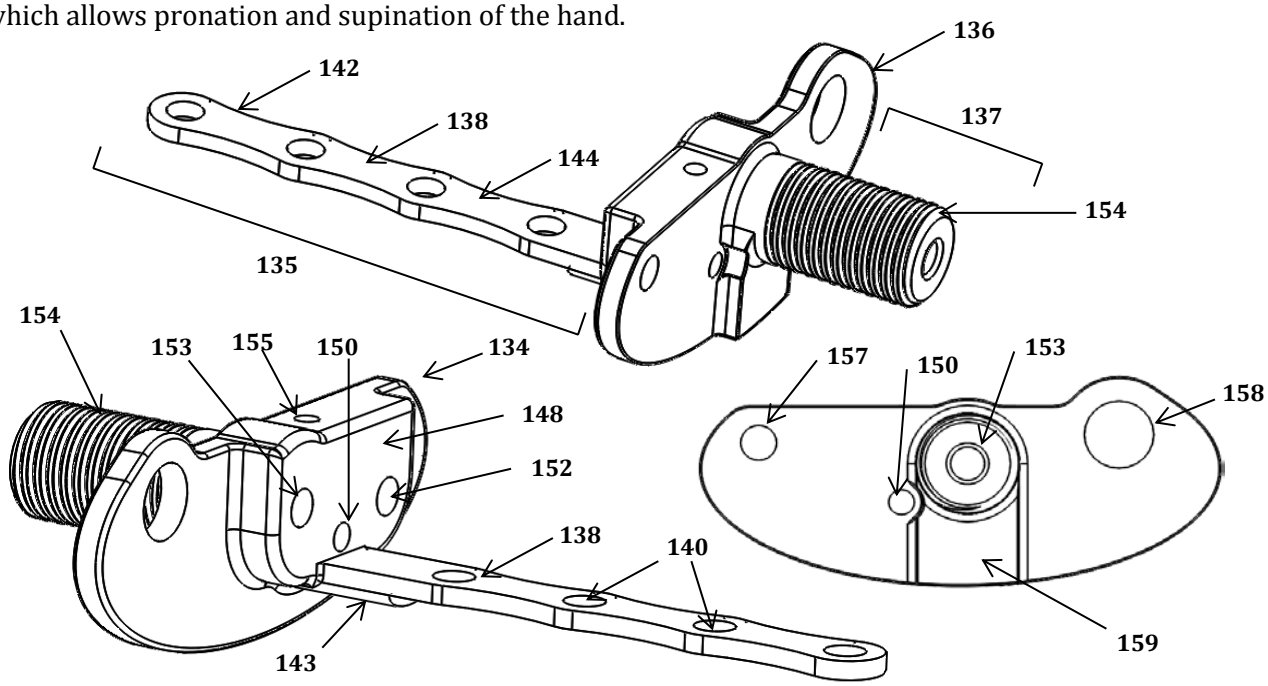

Figure 99 - Postero- and antero-lateral perspective and posterior view of the wrist stem

The wrist stem (134) is divided into an anterior portion (135), which is located distally from its central-flange (136), and a posterior portion (137), which is proximal to the flange (136). Anteriorly, the wrist stem (134) has a protruding spine (138) which inserts onto the inner dorsal surface (139) of the palm (31). The spine (138) has four equispaced holes (140), which locate around cylindrical protrusions (141) on the body of the palmar structure (31) to generate stability in the transverse plane. Additionally, radial cut-outs (142) on its lateral borders offer a reduction in weight. Furthermore, the spine (138) is met on its inferior proximal end by a semi-ellipsoidal projection (143) which increases its flexural-rigidity of the structure under loading. The superior surface (144) of the spine provides a foundation on which the linear-bearing rail (145) locates. Four self-tapping screws (146) fix the linear-bearing rail (145) and the spine (138) to the inner dorsal surface (139) of the palmar body (31).

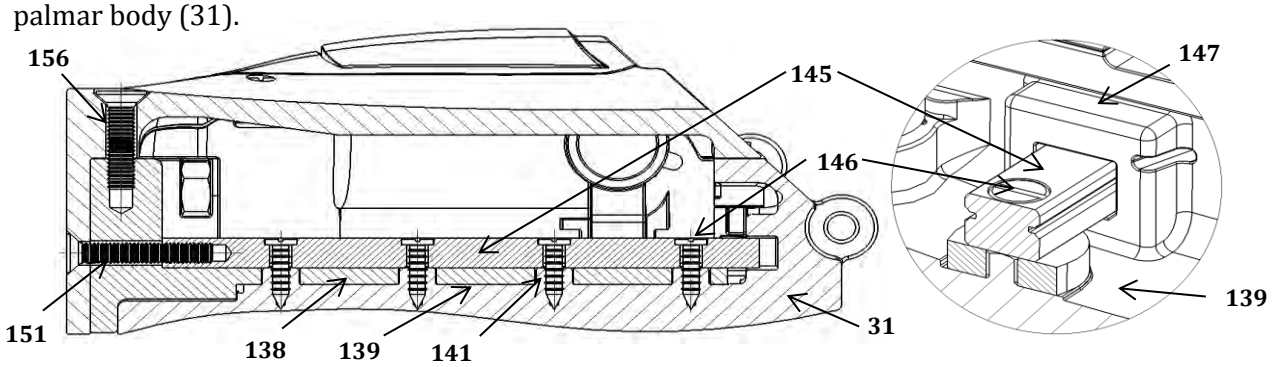

Figure 100 - Lateral section and postero-lateral perspective view of the wrist's and linear-bearing rail's fixation to the palmar structure

Anteriorly, the linear-bearing rail (145) is located by an outcrop (147) in the palmar structure (31) as seen in Figure 100. The outcrop (147) also serves as a bumper, against which the distal linear-bearing slider (63) stops. The anterior interface-protrusion (148), superior to the spine (138), mates with the inner border (149) of the palmar structure (31); providing torsional rigidity. When viewed anteriorly, the protrusion (148) has three holes. The central inferior clearance hole (150) guides the linear-bearing rail locking-screw (151), the right superior hole (152) provides linear clearance for the ratchet-rack (96) and the left superior exit-hole (153) travels straight through the threaded interface (154) of the wrist stem (134), guiding the primary actuating cable (124). On the superior border of the central-flange (136), a tapped hole (155) locates the large palmar cover clamping-screw (156).

Posteriorly, the wrist stem (134) has a clearance-hole (157) on its left lateral superior border, a thumb swivel locational hole (158) on its right lateral superior border and a central inferior protrusion (159) which mates with the border of the palmar cover (160). An exploded assembly view of the wrist stem, linear bearing rail and palmar cover is shown in Figure 101.

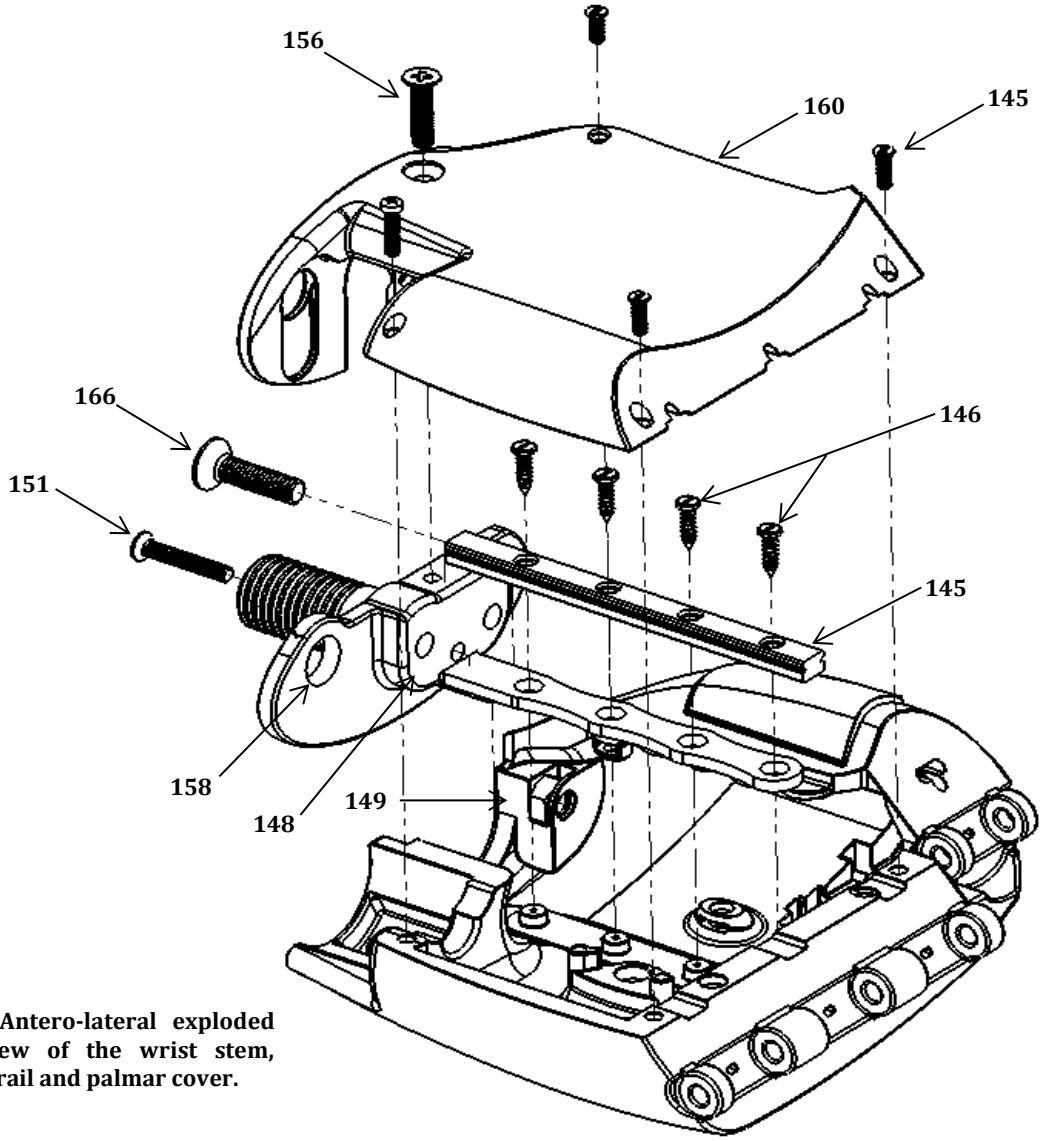

Figure 101 - Antero-lateral exploded perspective view of the wrist stem, linear-bearing rail and palmar cover.

5.10. Palmar Structure and Cover

Superiorly, the palmar cover (160) is held in place by five clamping-screws. The large palmar cover clamping-screw (156), as previously mentioned, and four smaller clamping-screws (161), which are affixed in the manner shown in Figure 102. To minimise costs, standard metric screws and hexagonal nuts (162) are used to fasten the palmar cover (160) to the palmar structure (31). Four recessed hexagonal grooves (163) are built into opposing corners of the palmar body (31), into which the hexagonal nuts (162) are inserted and aligned. The flat surfaces (164) at the rear of the grooved-cutouts (163) are toleranced such that they engage the faces of each nut (162) so as not to rotate during the fastening of the clamping-screw (161) from above. This allows the screw (161) to rotate relative to the nut (162), causing the nut (162) to move linearly upwards, towards the head of the screw (161) when tightened; eventually reaching the upper surface of the groove (165) and clamping the palmar cover (160) in place.

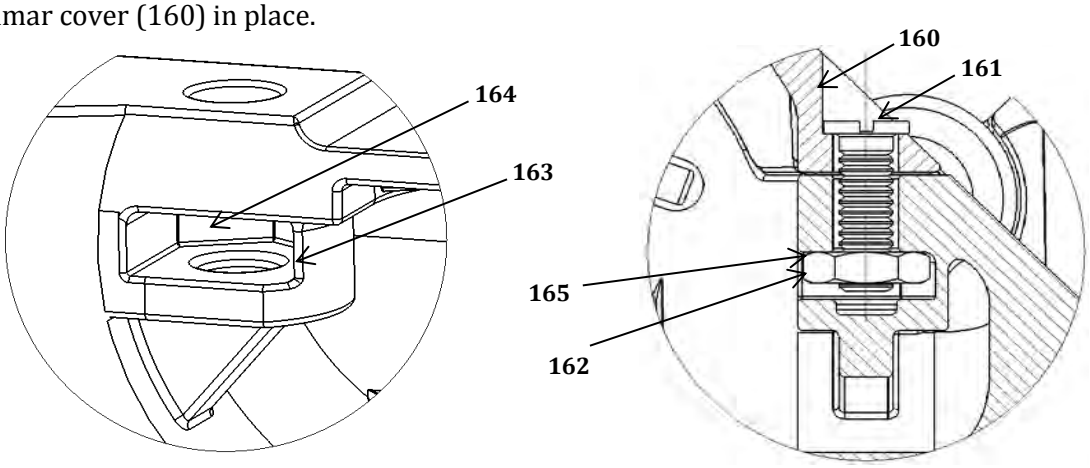

Figure 102 - Postero-lateral perspective and lateral section view of a palmar cover fixture

Two additional countersunk clamping-screws fasten the palmar cover (160) and stem (134) from the rear. The larger locking screw (166) travels through the clearance-hole (157) in the wrist stem (134) and palmar structure (31). It screws into the posterior hexagonal nut (167) which rests in the posterior grooved cut-out (168) of the palm (31). The smaller screw is the aforementioned linear-bearing rail locking-screw (151).

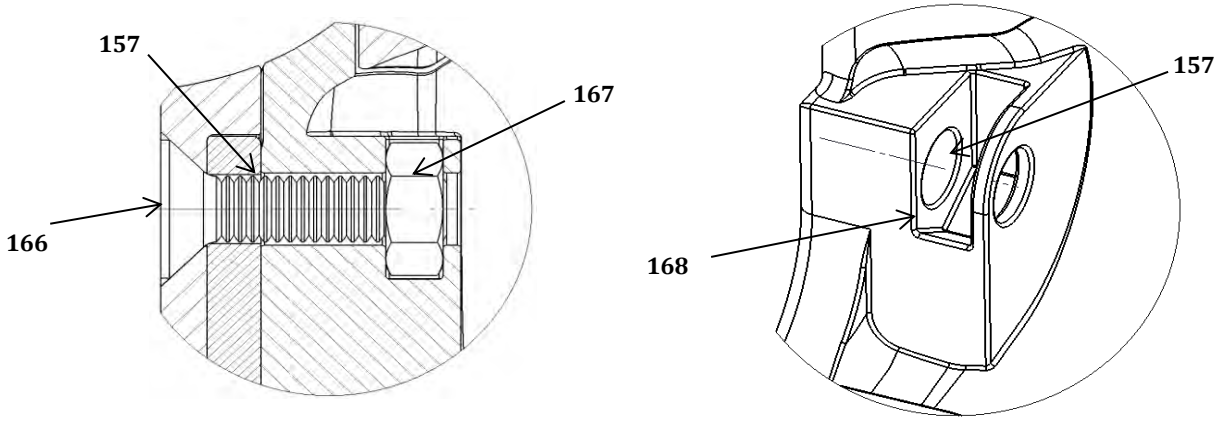

Figure 103 - Lateral section and antero-lateral perspective view of the posterior palmar cover and wrist stem fixture.

The palmar cover (160), Figure 104, has two rectangular indentations (169) on its inner surface to provide clearance for the linear movement of the differential seesaw mechanism (62). It has a waved recess (170) on its lateral border which interfaces with its mirrored counterpart (171) protruding from the palmar body (31). The interface (Figure 105) generates a stable support platform which assists the structural stability, rigidity, alignment and load-bearing capacity of the palmar surface. Five clearance holes (172) guide the palmar cover clamping-screws (156 & 161) with a further two locational recesses (173) on the anterior border which prevent the bearing pins (123) from translating axially. The postero-lateral (174) and medial radial grooves (175) on the internal surface of the palmar cover (160) securely locate the thumb-swivel (25) and the wrist-stem (134) respectively.

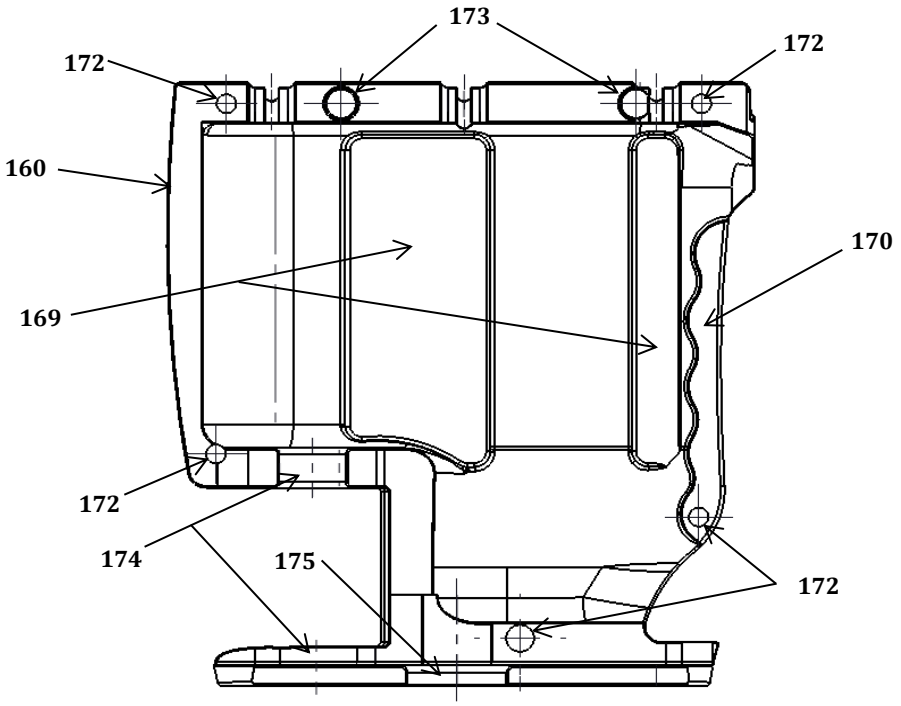

Figure 104 – Medial-dorsal view of the palmar cover.

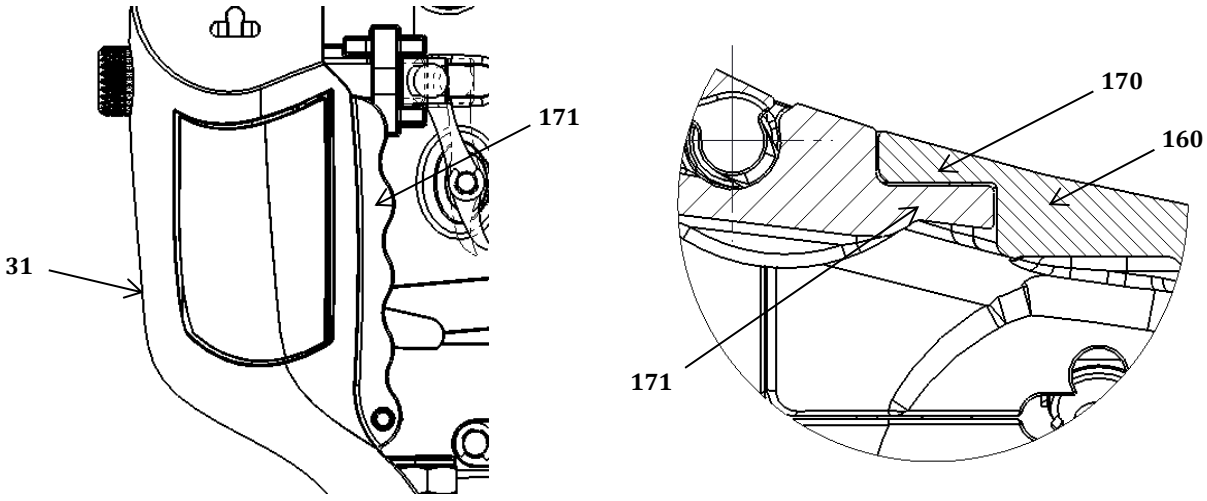

Figure 105 - Palmar and proximal section view of the waved protrusion and recess of the palm and palmar cover interface respectively.

6

CHAPTER 6: DESIGN SPECIFICATIONS & ASSEMBLY OF PROTOTYPE

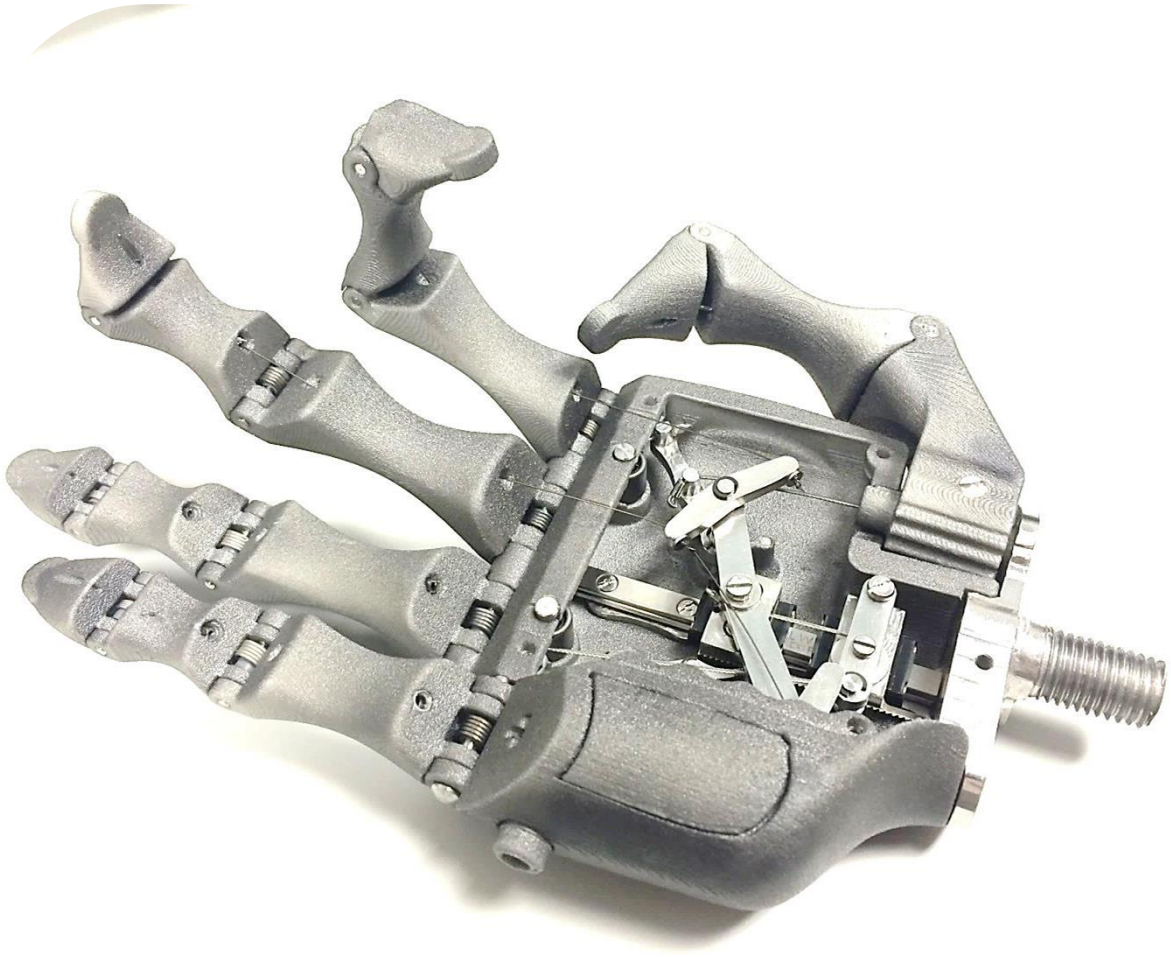

"*Manufacturing is more than just putting parts together. It's coming up with ideas, testing principles and perfecting the engineering, as well as final assembly.*" – *James Dyson*

6.1. Design Specifications of Hand Prosthesis

Table 45 –Specifications of final hand prosthesis

Total mass:	237g
Degrees of freedom:	15
Stem Attachment Type:	M12 x 1.5 (Standard Prosthetic Interface)
Actuation type:	Mechanical Shoulder-Harness
Stroke of Actuation Cable:	32mm
Input force to overcome initial-pretension	20N
Actuation Force to close Unloaded hand:	25N
Input force (IF) versus Grasp Force (GF):	*IF = 1.48(GF) + 11.28*
Force distribution between digits and thumb:	50-50

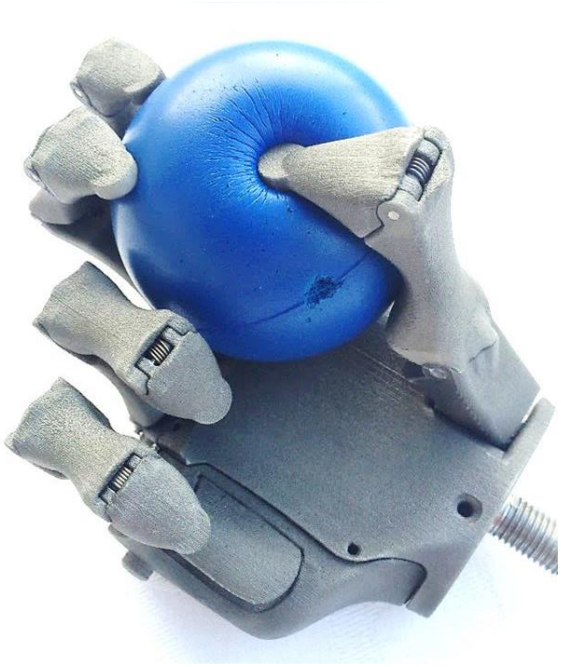

Manufacturing processes of prototype:

- Rapid prototyping of palmar structure, phalanges, thumb swivel, locking button, arch-inserts and palmar cushion.
- Milling and turning of differential slider carriages, internal mechanisms, pins and wrist stem.
- Wire cutting of ratchet and pawl.
- Laser-cutting and pressing of channel rings.
- Cold winding of torsion springs

Other characteristics:

- Design is anthropometrically proportional and physiologically mimetic.
- Able to switch incrementally between lateral grasp, index finger pinch, tripod pinch (index, middle finger and thumb), and power grasp.
- Incremental locking mechanism, with bypass option.
- Low friction transmission through linear, needle-roller and deep-groove ball bearings.
- Customisable sizes, engraved or embossed designs, proportional to the individual patient for left and right hands.
- Utilises palmar cushion to assist in maintaining normal contact forces with grasped object.
- Future versions will allow expansion to myoelectric actuation.

6.2. Assembly of Hand Prosthesis

This section shows the assembly stages of the manufactured prototype of the hand prosthesis.

6.2.1. Phalangeal assembly

For individual part descriptions, refer to Figure 72, Figure 73 & Figure 74 in Section 5.1, p. 104.

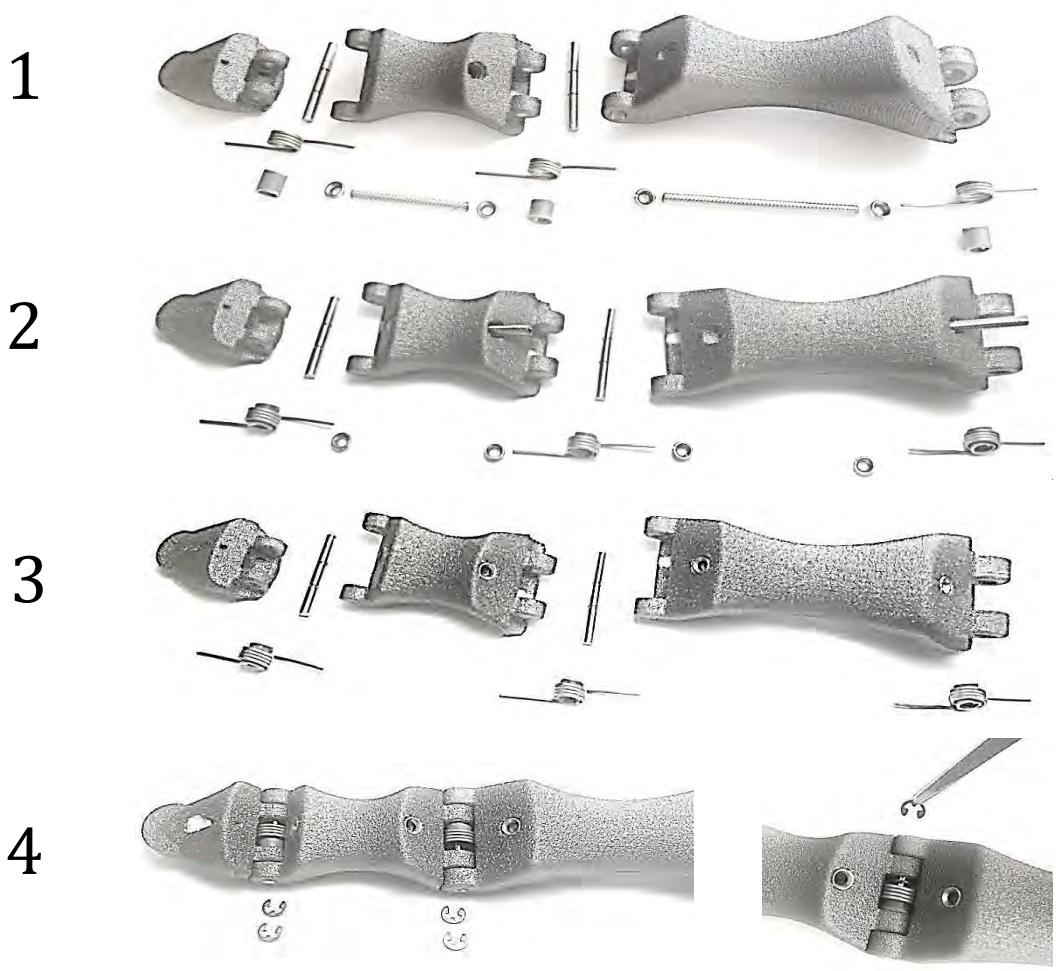

Figure 106 - Stages of phalangeal assembly for 1st to 5th digits.

Figure 107 - Final assembled view of digits.

Assembly stages of digits with reference to Figure 106:

1 – *Initial unassembled component view*

2 – *Insertion of channel lining and polymeric spring-mandrels*

3 – *Insertion and glueing of channel rings, after insertion of channel lining*

4 – *Assembly of remaining components, and insertion of E-clips to axially locate hinge-pins.*

6.2.2. Thumb-swivel assembly

For part descriptions refer to Figure 78, Figure 79, Figure 80 & Figure 81 in Section 5.2, p. 107.

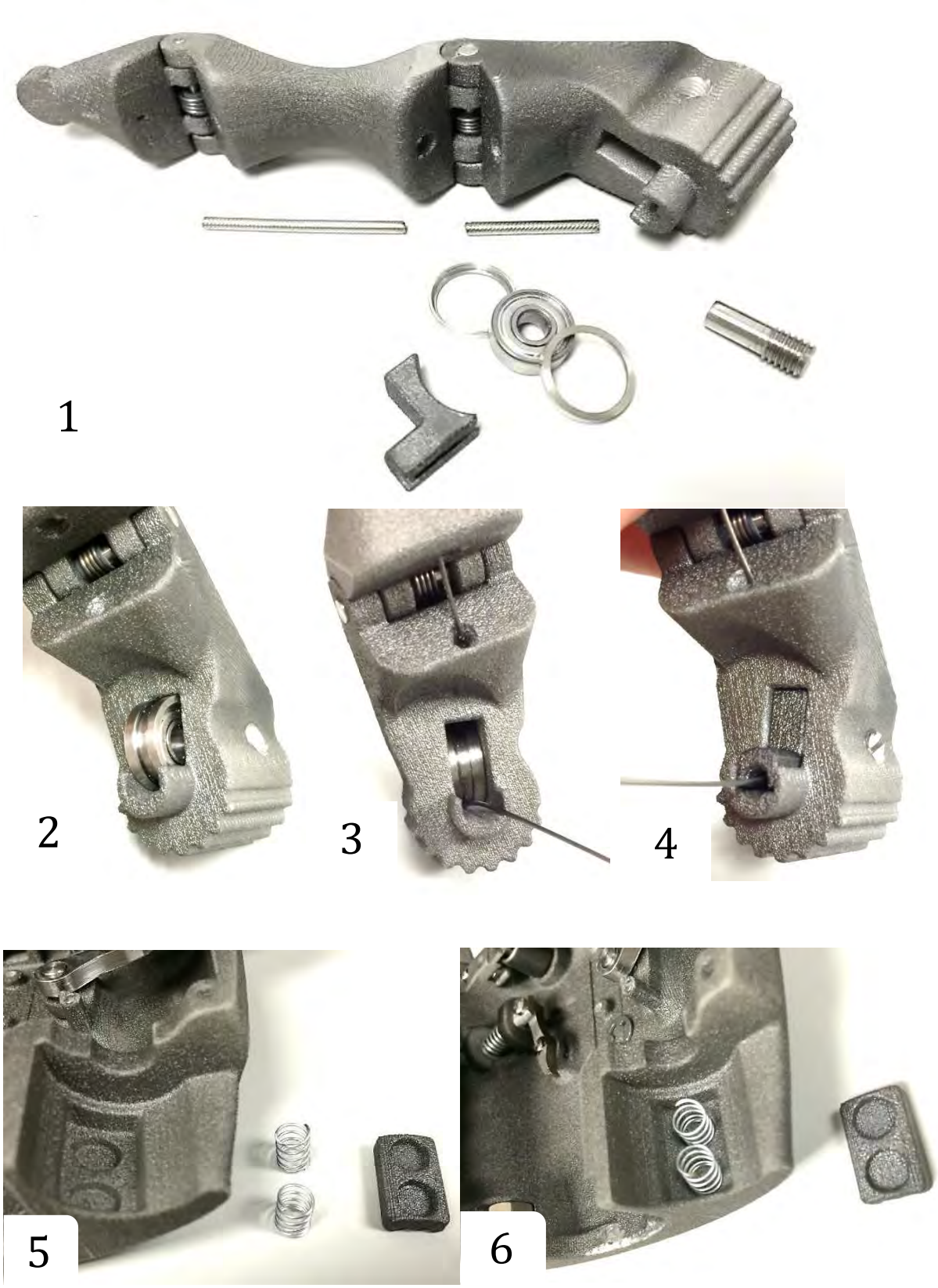

Figure 108 - Stages of thumb-swivel assembly (Part 1)

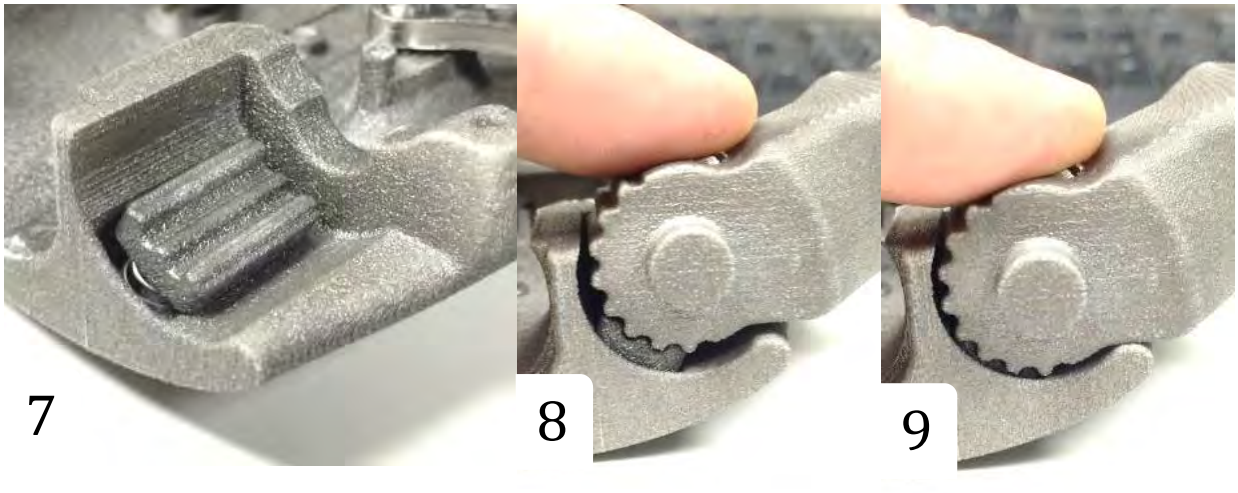

Figure 109 - Stages of thumb-swivel assembly (Part 2)

Assembly stages of thumb-swivel with reference to Figure 108 and Figure 109:

1 *– Unassembled thumb-swivel view.*

2 *– Insertion of deep-groove ball bearing with end-rings.*

3 *– Insertion of thumb actuating-wire.*

4 *– Insertion of end cap.*

5 *– Unassembled thumb locking mechanism.*

6 *–Insertion of linear compression springs.*

7 *– Insertion of spring-actuated locking plate.*

8 *– Vertical insertion of thumb swivel.*

9 *– Depression of thumb swivel to show final seating position.*

6.2.3. Thumb transfer-lever assembly

For individual part descriptions, refer to Figure 82 & Figure 83 in Section 5.3, p. 109.

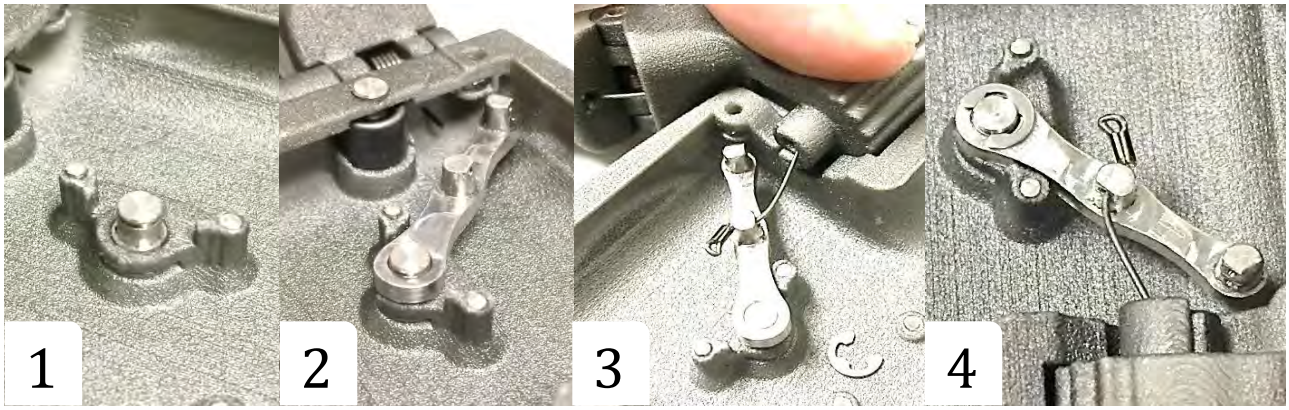

Figure 110 - Assembly stages of thumb transfer-lever.

Assembly stages of thumb transfer-lever with reference to Figure 110:

1 *– Insertion of support pins, locating pin and e-clip.*

2 *– Mounting of thumb transfer-lever.*

3 *–Attachment of thumb actuating-wire to medial pin.*

4 *– Insertion of e-clip to lock transfer-lever in place superiorly.*

6.2.4. Ratchet locking mechanism and pawl assembly

For individual part descriptions, refer to Figure 92, Figure 93 & Figure 94 Section 5.7, p.115.

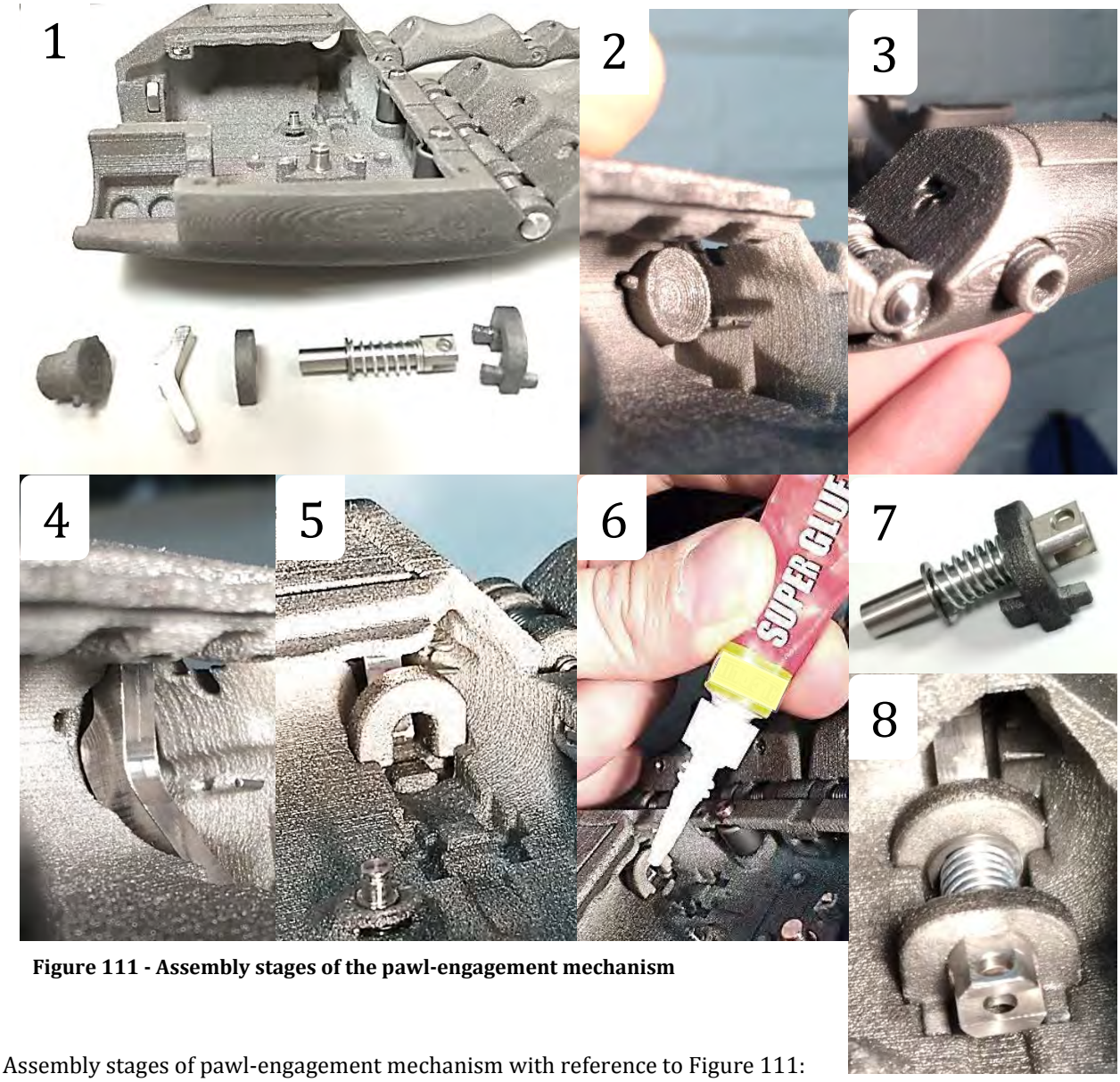

Figure 111 - Assembly stages of the pawl-engagement mechanism

Assembly stages of pawl-engagement mechanism with reference to Figure 111:

1 *– Unassembled pawl-engagement mechanism.*

2 *– Medial insertion of bayonet locking button.*

3 *–Exterior view of inserted button from lateral side.*

4 *– Medial insertion of pivoting-lever.*

5 *– Insertion of posterior arch-insert.*

6 *– Glue posterior arch-insert in place.*

7 *– Slide anterior arch-insert onto pawl-shaft with spring contacting its lateral surface.*

8 *– Insert pawl-shaft with anterior arch-insert. Glue in place as with* ***6****.*

Now that the assembly of the locking mechanism has been discussed, Figure 112 will describe the pawl assembly.

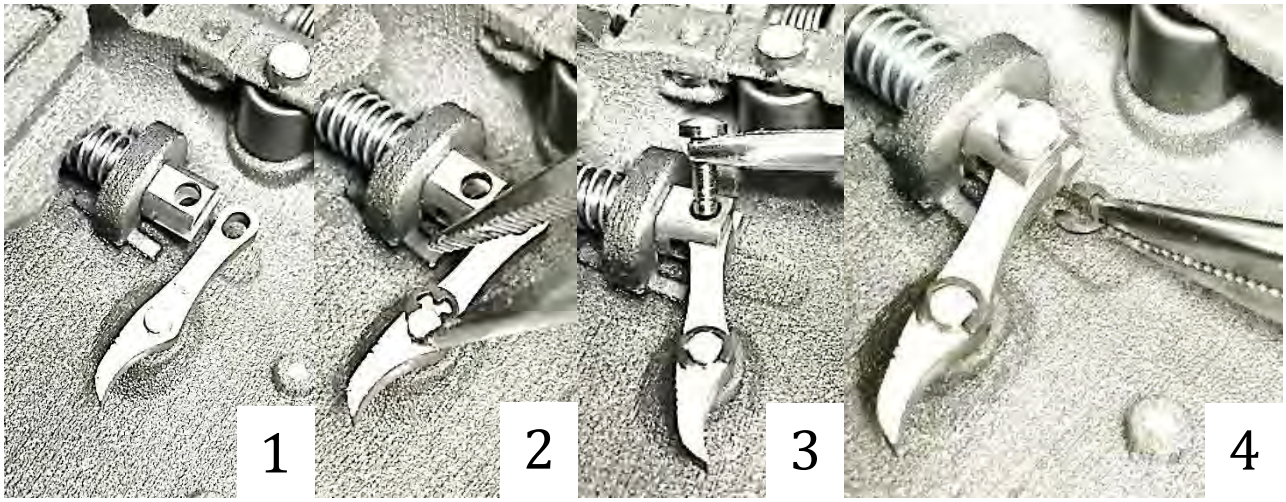

Figure 112 - Insertion and attachment of pawl.

Assembly stages of pawl with reference to Figure 112:

1 *– Insert pawl onto the pawl-swivel pin from above.*

2 *– Insert e-clip to locate pawl .*

3 *– Insert pawl locking-pin to attach pawl to the pawl-shaft.*

4 *– Insert e-clip to lock pawl locking-pin in place.*

6.2.5. Assembly of pulley-ratchet slider mechanism

For individual part descriptions, refer to Figure 90 & Figure 91 in Section 5.6, p. 114.

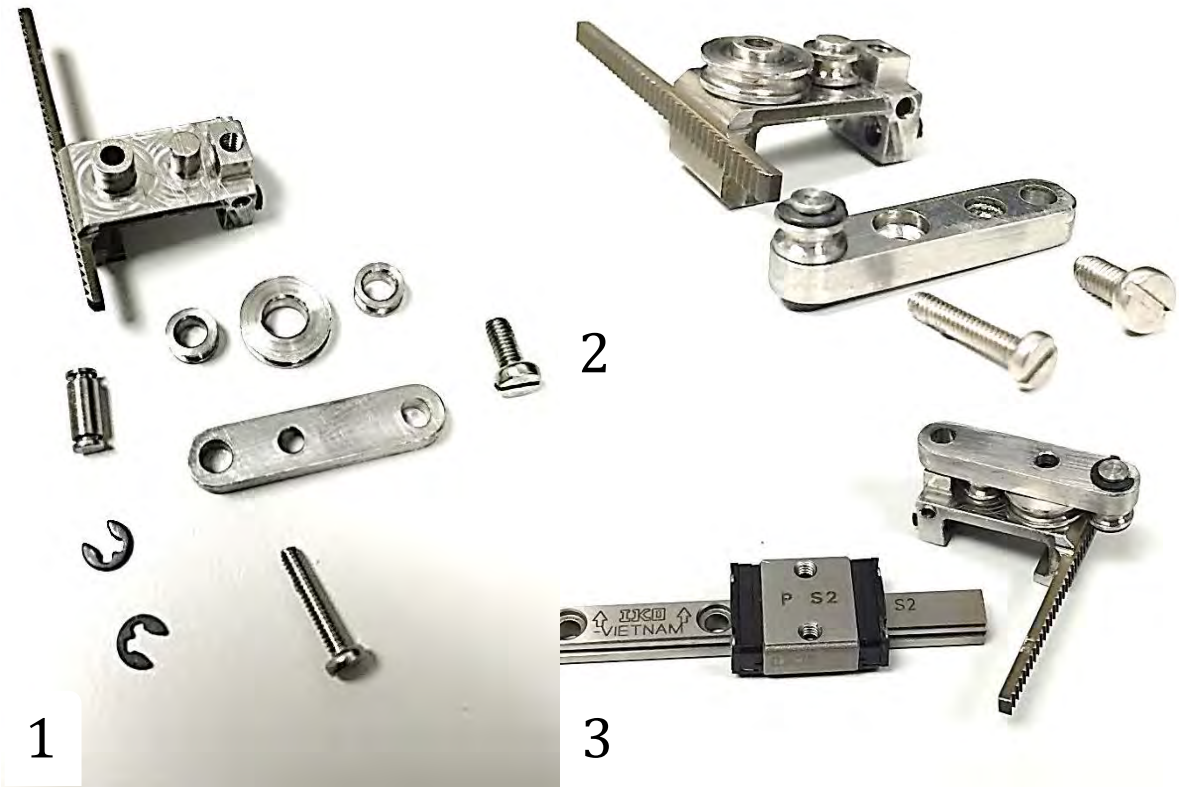

Figure 113 - Assembly stages of the pulley-ratchet slider (Part 1)

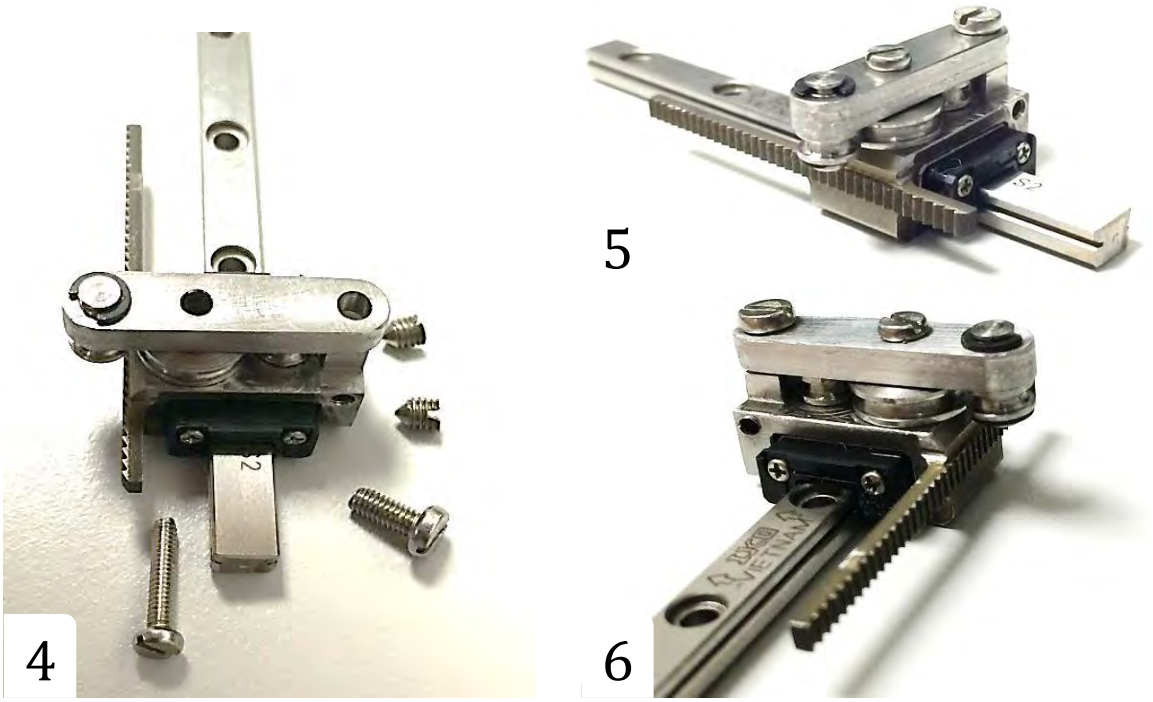

Figure 114 - Assembly stages of the pulley-ratchet slider (Part 2)

Assembly stages with reference to Figure 113 and Figure 114:

1 *– Unassembled view of pulley-ratchet components.*

2 *– Assembly of pulleys onto their respective shafts.*

3 *– Mount pulley clamping-plate onto the ratchet-carriage.*

4*–Proximal view of the ratchet-carriage mounted on the linear-bearing rail.*

5 *– Insertion of the pan-head and grub screws. Proximal view.*

6 *– Fully-assembled distal view of the pulley-ratchet slider mechanism.*

6.2.6. Assembly of differential seesaw mechanism

For individual part descriptions, refer to Figure 87 & Figure 88 in Section 5.5, p. 112.

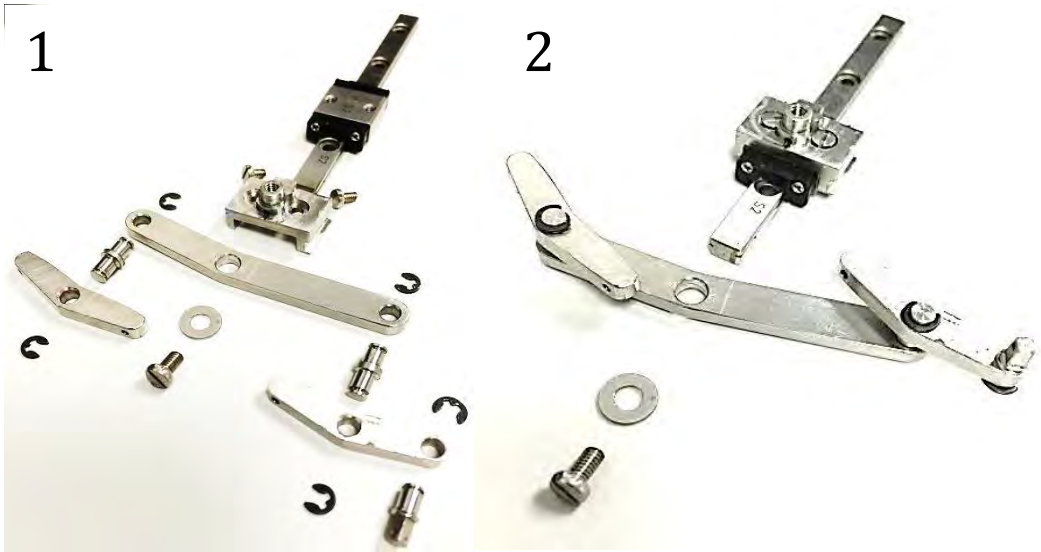

Figure 115 - Assembly stages of the differential seesaw mechanism (Part 1)

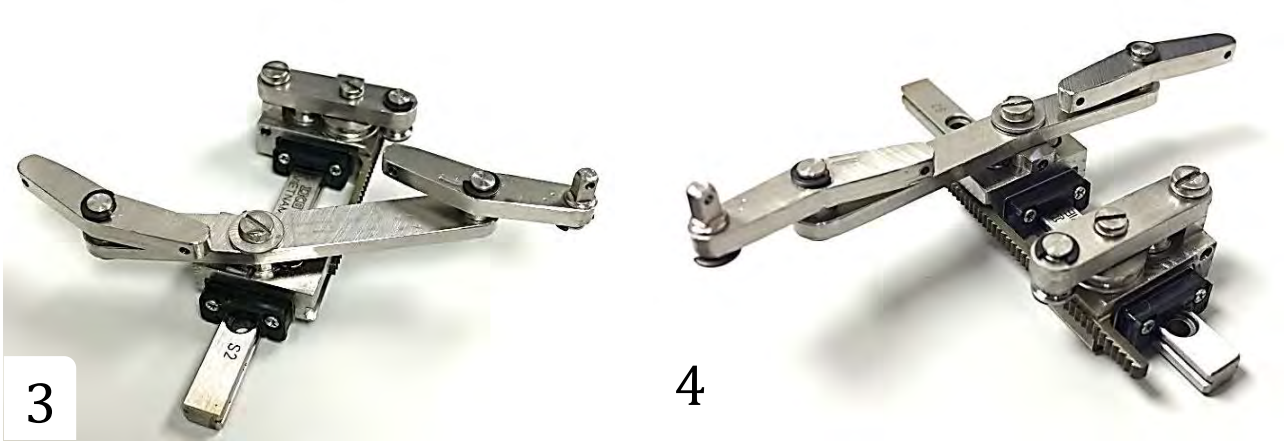

Figure 116 - Assembly stages of the differential seesaw mechanism (Part 2)

Assembly stages with reference to Figure 115 and Figure 116:

1 *– Unassembled view of differential seesaw components.*

2 *– Assembly of secondary seesaws onto primary seesaw, with swivel pins, elevating*

3*–Distal view of the fully-assembled differential seesaw slider with pulley-ratchet slider on linear-bearing rail.*

4 *– Proximal view of the fully-assembled differential seesaw slider with pulley-ratchet slider on linear-bearing rail.*

6.2.7. Wrist-stem and linear-bearing rail assembly

The assembly of the wrist-stem is shown in Figure 117, and its assembly with that of the linear-bearing rail and the differential slider-unit can be seen in Figure 118. It should be noted that the rail is affixed to the palmar structure using four self-tapping screws as shown in Figure 100, p. 119. For individual part descriptions refer to Figure 99, Figure 100 & Figure 101 in Section 5.9, p. 119.

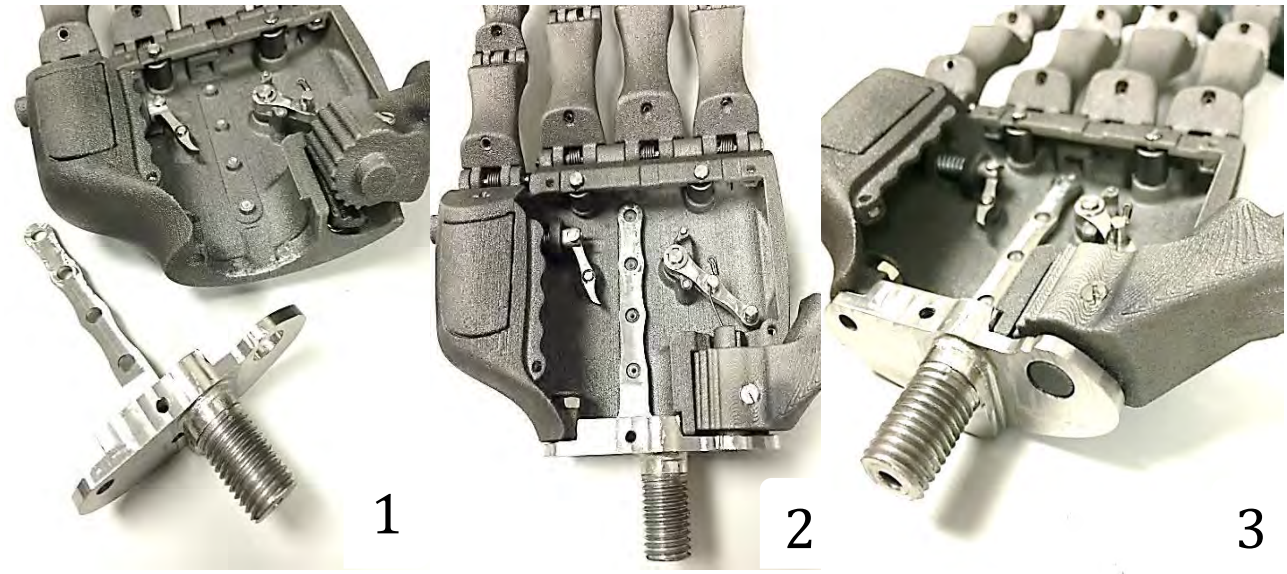

Figure 117 - Wrist-stem and linear-bearing rail assembly stages (Part 1).

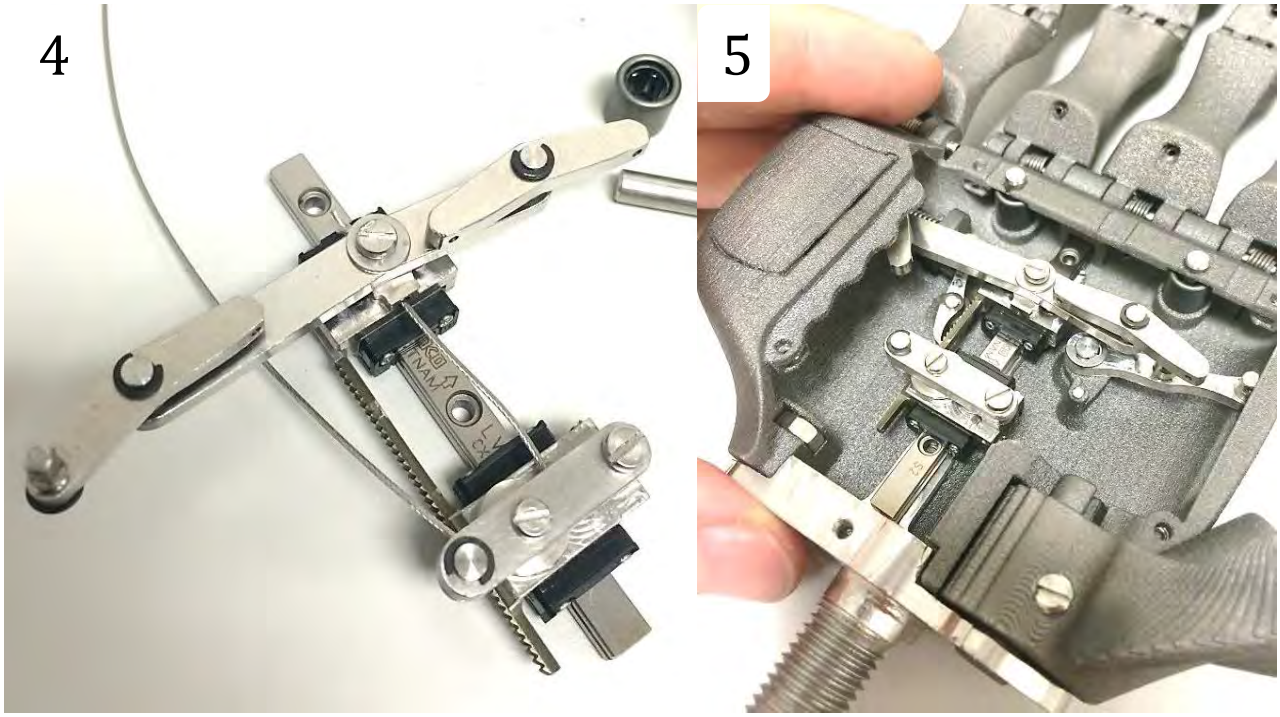

Figure 118 - Wrist-stem and linear-bearing rail assembly stages (Part 2).

Assembly stages with reference to Figure 117 and Figure 118:

1 *– Unassembled view of the wrist-stem.*

2 *– Assembled superior view of the wrist-stem.*

3 *– Proximal perspective view of the wrist-stem and location of the thumb-swivel pin into its locating hole.*

4*–Superior view of the assembled differential slider-unit, ready to be inserted into the palm, with the routing wire attached.*

5 *– Inserted differential slider-unit ready to be securely attached to the palmar structure with self-tapping screws.*

6.2.8. Routing bearing assembly

For individual part descriptions, refer to Figure 96, Figure 97 & Figure 98 in Section 5.8, p. 117.

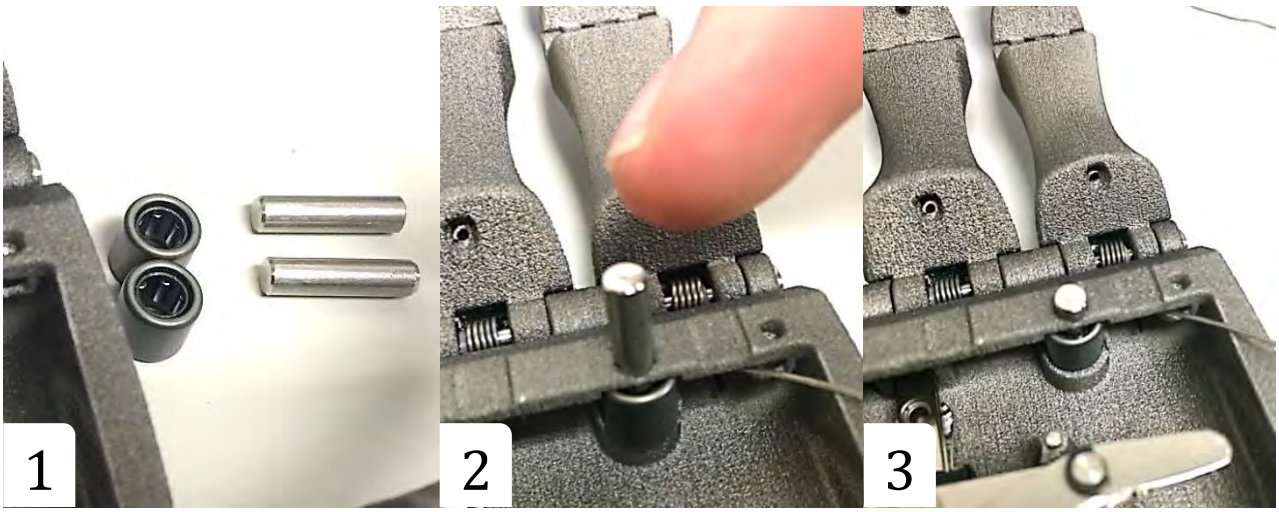

Figure 119 - Routing bearing assembly stages (Part 1).

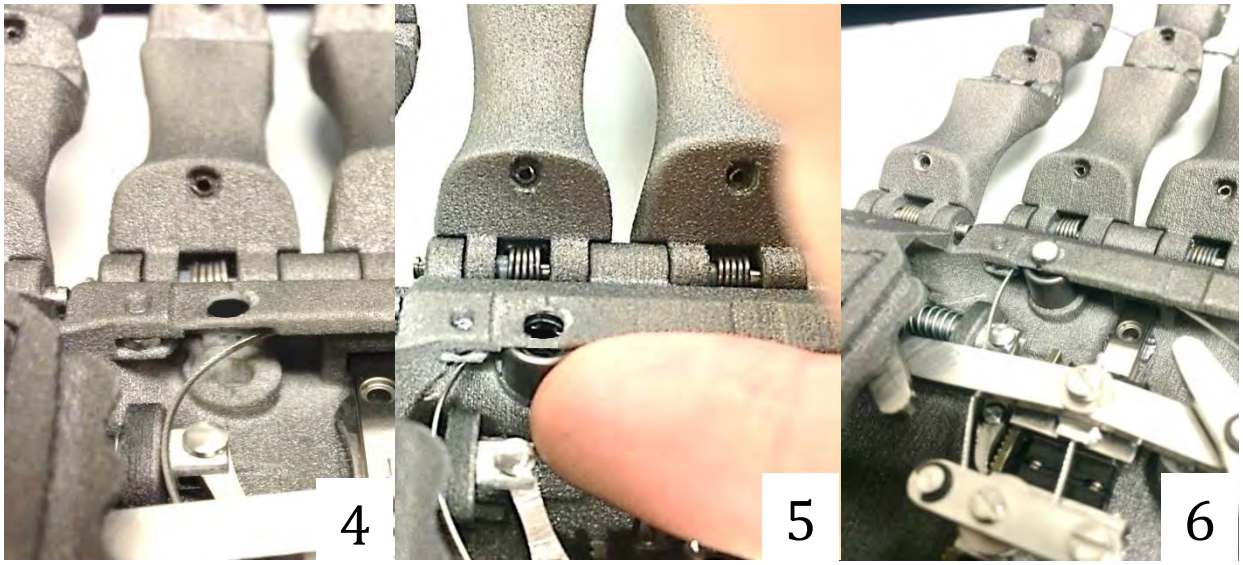

Figure 120 - Routing bearing assembly stages (Part 2).

Routing bearing assembly stages with reference to Figure 119 and Figure 120:

1 *– Unassembled view of the routing bearings and pins.*

2 *– Insertion of the right lateral routing bearing and pin, with routing cable distal to it.*

3 *– Assembled view of the right lateral routing bearing.*

4*–Left lateral routing bearing cylindrical support, awaiting insertion of routing bearing.*

5 *– Insertion of the left lateral routing bearing and pin, with routing cable distal to it.*

6*– Assembled view of the left lateral routing bearing with routing cable.*

6.2.9. Attachment of the actuating wires

The attachment locations of the actuating wires are shown in Figure 73 (p. 104), Figure 88 (p. 112) and Figure 96, (p. 117) in Chapter 5. Numerous methods were investigated for the terminal attachment of the actuating wires as shown in Section 6.2.9.1. Final selection and assembly methods are shown in Section 6.2.9.2.

6.2.9.1. Investigation/trial of attachment methods

These included various types of knots and welded beads as seen in Figure 121, as well as a selection of crimping methods using ferrules and hypodermic needles as shown in Figure 122.

Figure 121 - Terminal attachment methods of actuating wires (Part 1).

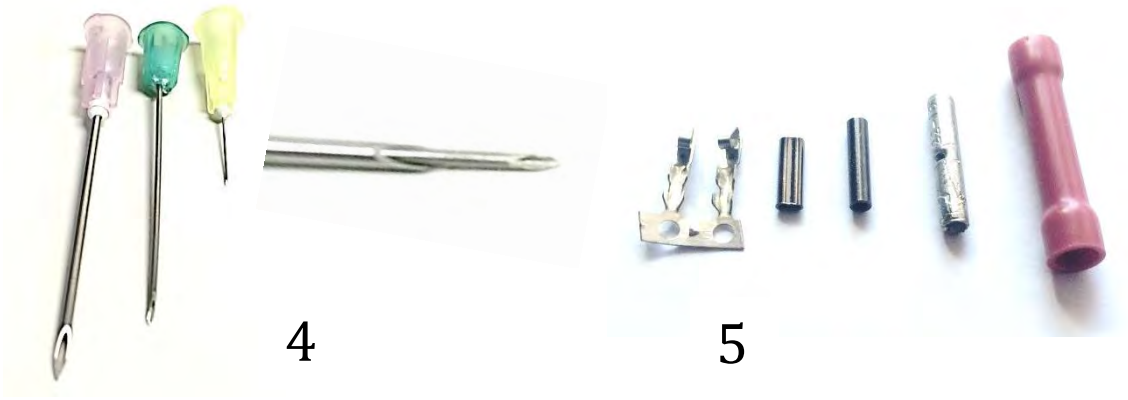

Figure 122 - Terminal attachment methods of actuating wires (Part 2).

Actuating wire attachment methods with reference to Figure 121 and Figure 122:

1 *– Overhand knot.*

2 *– Figure-of-eight knot.*

3 *– Welded bead.*

4*–Hypodermic needles placed within one another and crimped.*

5 *– Various type of ferrules for crimping.*

6.2.9.2. Final method of attachment

After testing of the numerous methods, the figure-of-eight knots were adapted for attachment of the finger actuating wires to the seesaws and distal phalanges as shown in Figure 123 and Figure 124. Furthermore, the thumb transfer-lever routing and thumb actuating cable used a figure-of-eight knot and crimped ferrule respectively. The routing cable inserting onto the seesaw-carriage was located with a figure-of-eight knot too, as its clamping screw (Number 72 in Figure 88, p. 112) caused it to fracture prematurely (Figure 124) by inducing a stress raiser. Moreover, the primary input cable was attached using a crimped ferrule instead of clamping screw for the same reason.

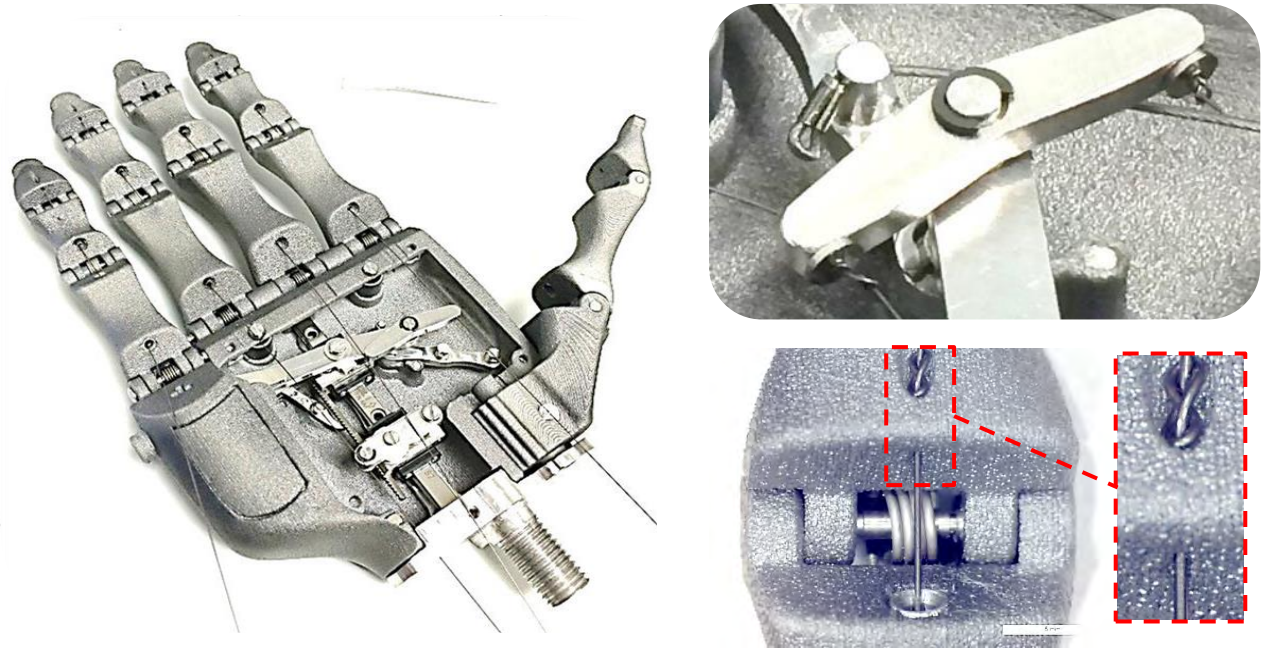

Figure 123 - Attachment of actuating and routing wires/cables (Part 1).

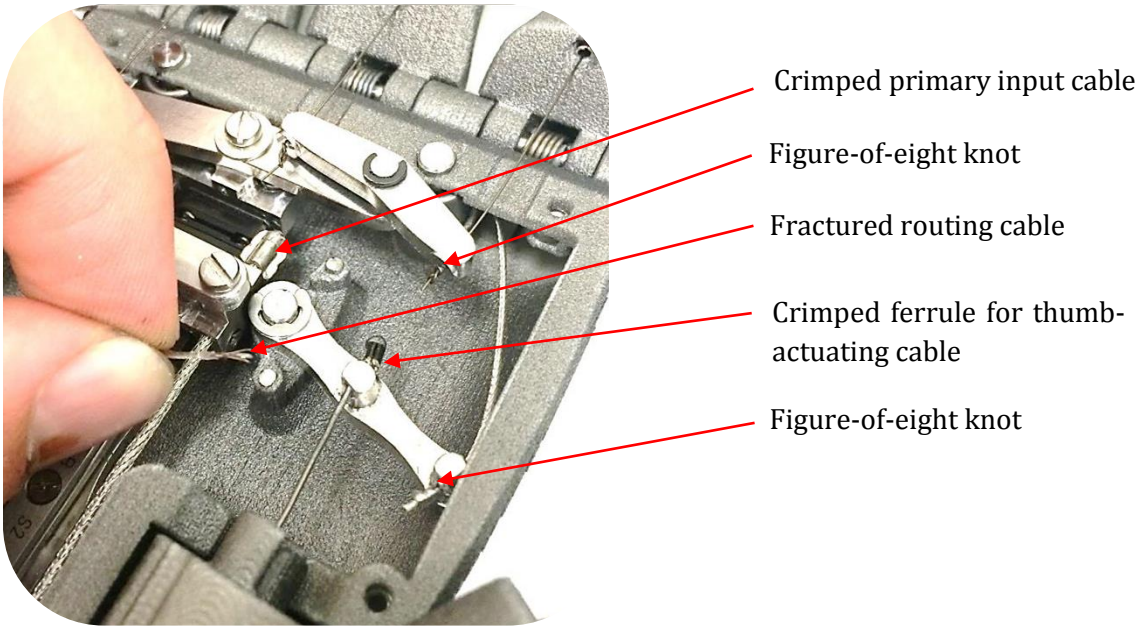

Figure 124 - Attachment of actuating and routing wires/cables (Part 2).

6.2.10. Assembly of the palmar cover

The palmar cover is attached to the palmar structure from above, as shown Figure 100 & Figure 103 in Section 5.10, p. 119, using a total of six clamping screws. Figure 125 and Figure 126 show the assembly stages of the palmar cover with its clamping screws and hexagonal clamping nuts.

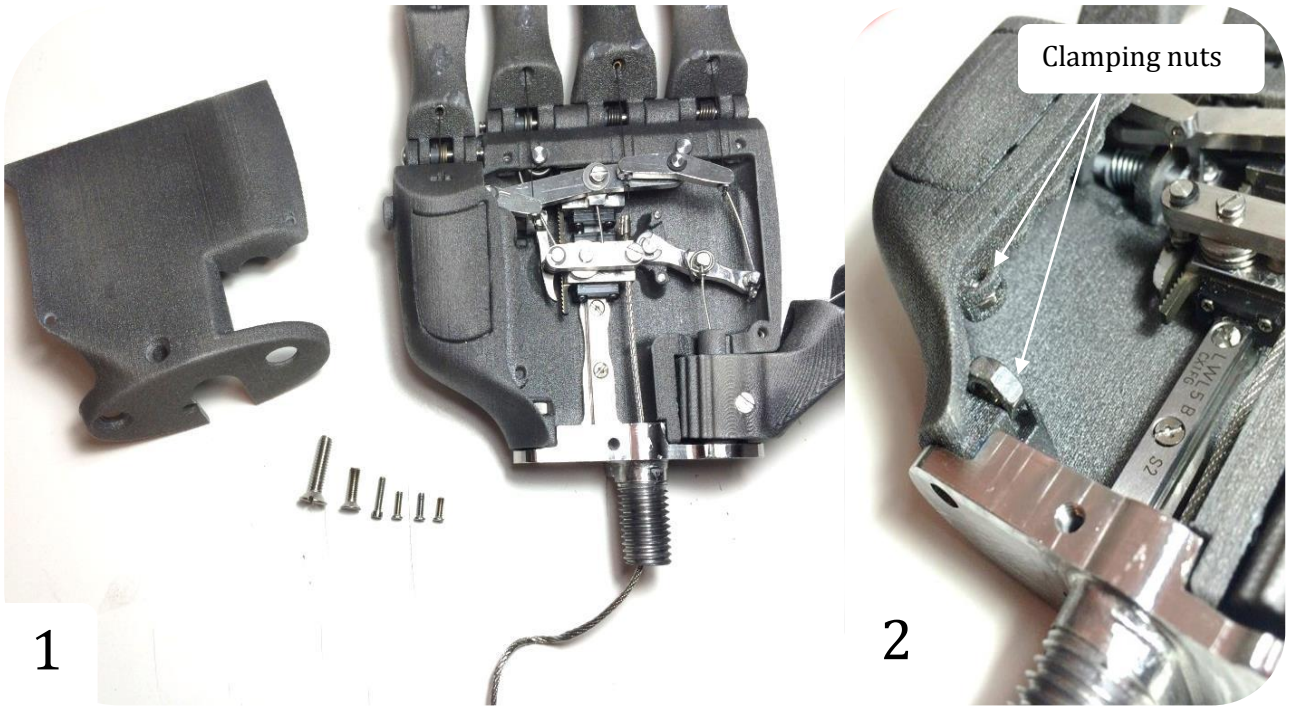

Figure 125 - Assembly of palmar cover (Part 1)

Figure 126 - Assembly of palmar cover (Part 2)

Palmar cover assembly with reference to Figure 125 and Figure 126:

1 *– Unassembled view of the palmar cover and its clamping screws.*

2 *– Insertion of the clamping nuts into hexagonal slots.*

3 *– Clamping screws pointing to their respective insertion locations.*

4*–Fastening of clamping screw.*

5 *– Assembled superior view of palmar cover.*

6 *– Assembled view of palmar cover with screwdrivers*

6.2.11. Prosthesis covering material

This section is divided into two parts. The first deals with the various rubber and silicon covering materials investigated to increase the gripping ability of the prosthesis, as described in Section 2.9.4, p. 40, whereas the second describes the selected solution for preliminary testing.

6.2.11.1. Investigation into suitable materials

Eight covering materials (shown in Figure 127) were investigated to provide a suitable covering for the prosthesis; having not only a good coefficient of friction but also a Shore hardness which provides suitable compressibility.

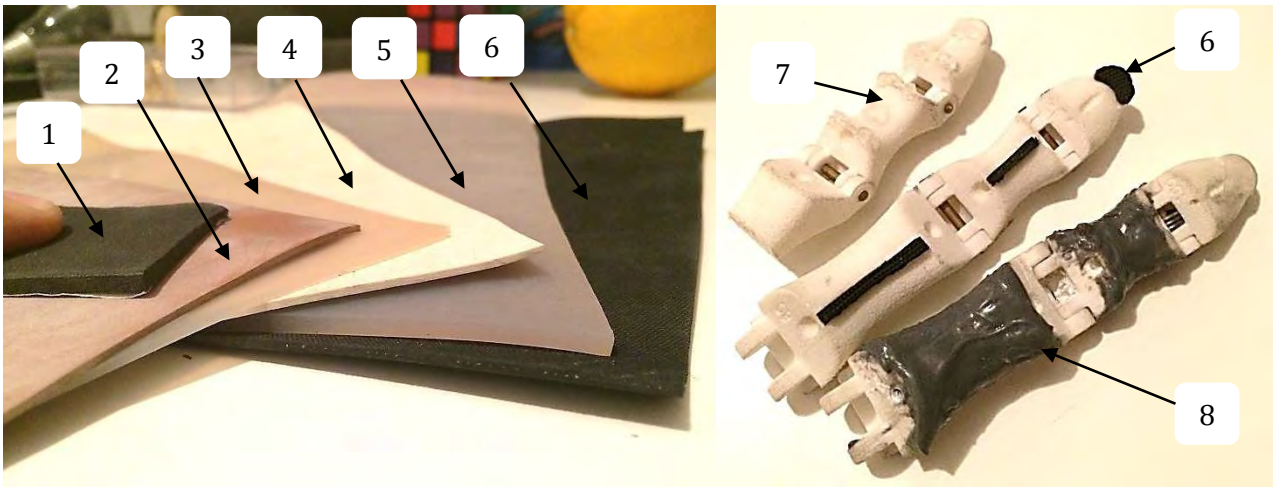

Figure 127 - Rubber and silicon prosthesis covering materials.

Referring to Figure 127, brief descriptions of the investigated materials are given below:

1. Rubber foam material
2. Natural rubber sheet (2 mm thickness)
3. Silicon-rubber sheet (2.5 mm thickness)
4. Textured white rubber sheet (2 mm thickness)
5. Silicon-rubber sheet (4 mm thickness)
6. Textured black rubber sheet (3 mm thickness)
7. Clear silicon adhesive applied with syringe.
8. Two-part silicon-rubber with 20 Shore A hardness.

The rubber foam (**1**) had good compressibility but its coefficient of friction (COF) was too low, especially when wet. The textured rubber mats (**2**, **4** & **6**) had good COF, yet their Shore hardness was too high to provide sufficient compression allowing conformity of grasps. The silicon-rubber sheets (**3** & **5**) provided sufficient COF and good compressibility, yet their adhesion to the nylon surface of the prosthesis was lacking. Furthermore, when using the two-part silicon-rubber (**8**) that could be brushed on, it too lacked sufficient adhesion; even when roughening the nylon surface with a Dremel®. The clear silicon adhesive (**7**), applied drop-wise using a syringe, provided good compressibility, acceptable adhesion to the nylon, low cost and good conformability to the structure.

Its primary drawback relating to poorer aesthetics when compared to the materials of uniform thickness.

6.2.11.2. Preliminary selection of prosthesis covering material.

Limitations relating to time meant that the clear silicon adhesive (**7**), who's practical advantages and good functionality outweighed its lacking aesthetics, was selected as the prosthesis covering material for preliminary grasp testing. Its distribution is shown in Figure 128.

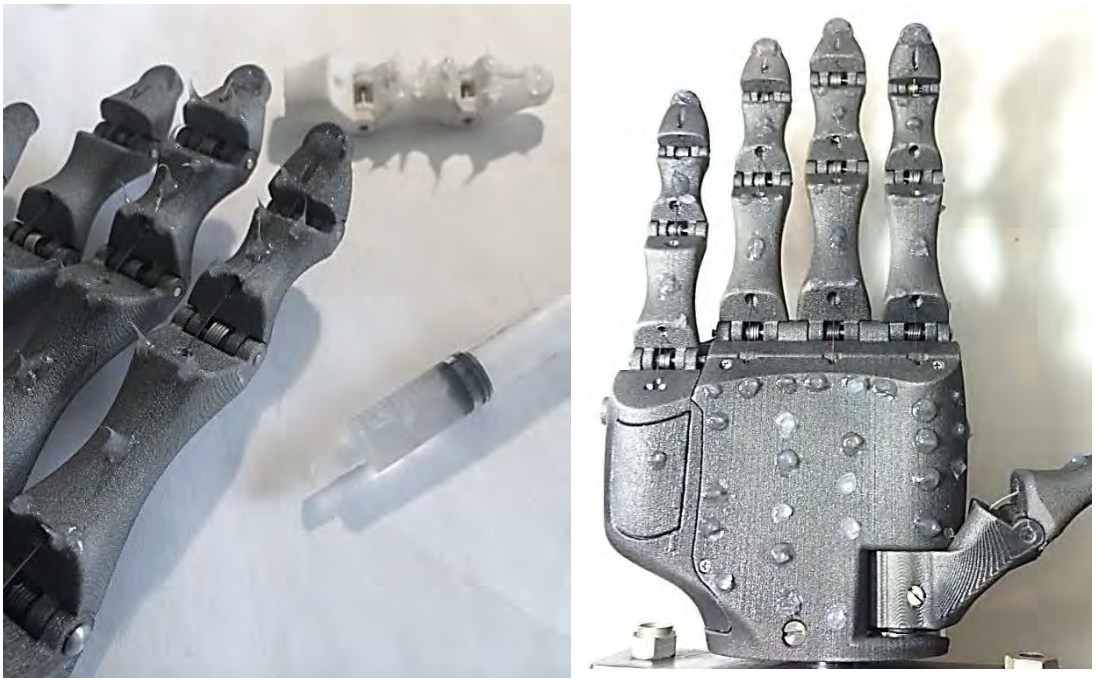

Figure 128 - Clear silicon prosthesis covering material for preliminary testing.

7

CHAPTER 7: EXPERIMENTAL PROCEDURES & PRELIMINARY PATIENT TESTING

This section deals with the qualitative and quantitative analysis of the performance of the hand and its mechanisms through numerous experimental procedures. These procedures are listed below:

7.1. Experiment 1 - Grasping capabilities of the hand prosthesis
7.2. Experiment 2 - Mechanical strength of the phalanges under hyper-extensive & lateral loads
7.3. Experiment 3 - Tensile strength of actuating wires with figure-of-eight knots
7.4. Experiment 4 - Fatigue testing of the phalangeal channel mechanism
7.5. Experiment 5 - The patient experience

"I didn't think; I experimented" – Wilhelm Röntgen

7.1. Experiment 1 – Grasping Capabilities of the Hand Prosthesis

7.1.1. Background

Patients to use their hands to grasp, manipulate and support objects of various shapes, sizes and geometries. To perform these tasks well, numerous grasp configurations need to be adapted by the hand. With reference to Section 2.9.1 (p. 29), evaluation of the types of achievable grasps mentioned is essential to the performance of the hand; especially those mentioned in Table 4, p. 31. The primary focus of which is the ease of use it gives patients during their activities of daily living, the taxonomy of each of the grasps can be referred to in Figure 31, p. 29.

7.1.2. Aim

To assess the ability of the hand to adapt various grasp configurations and whether the locking mechanism can securely maintain the grasp once the tension in the input cable is released.

7.1.3. Methodology

Determine the types of grasps the hand can perform and assess the ease with which each can be performed; focussing on the minimum grasping requirements which include the following grasps:

- Medium wrap, power sphere, lateral pinch, index finger extension, tripod, thumb-3 finger (tip grasp) and precision sphere.

Engage the ratchet locking-mechanism during each grasp, to determine whether the object is securely grasped, and disengage to determine the effort needed to release.

7.1.4. Experimental Results

Figure 129 and Figure 130 show the various grasp types achieved during the grasping experiment.

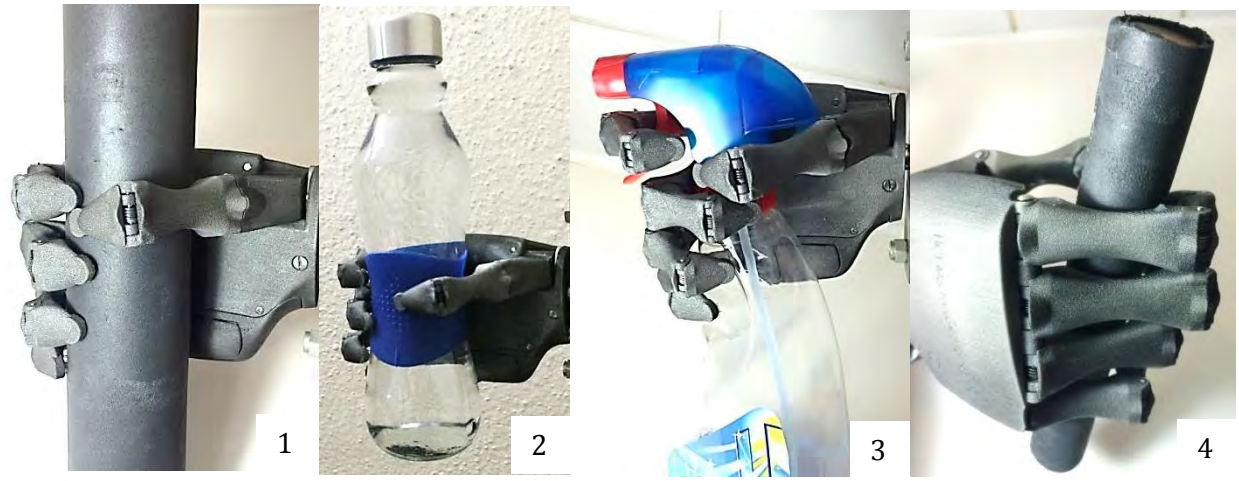

Figure 129 - Power grasping configurations of the hand prosthesis.

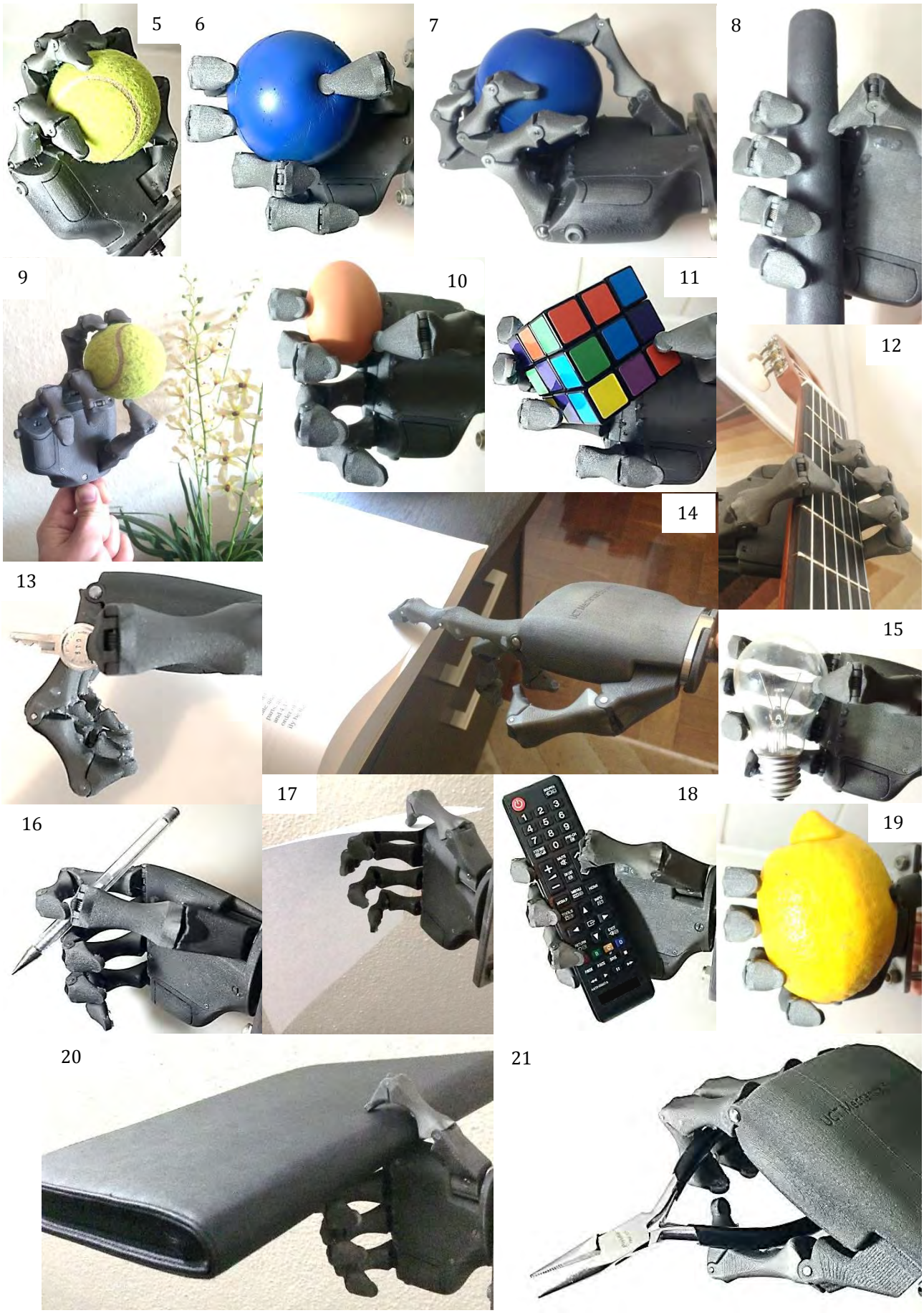

Figure 130 - Power and precision grasping configurations of the hand prosthesis.

Grasp configurations with reference to Figure 129 & Figure 130:

1 *– Medium wrap of large cylinder (Ø50mm).*

2 *– Medium wrap of non-uniform filled 500ml glass bottle*

3 *–Medium wrap of trigger spray bottle*

4 *– Medium wrap of thin cylinder (Ø25mm)*

5 *– Power sphere of tennis ball (Ø60mm)*

6 & 7 *– Power sphere of deformable ball (Ø65mm)*

8 *– Thumb-3 finger(tip grasp) of Ø25mm cylinder*

9 *– Precision sphere grasp of tennis ball*

10 *– Tripod grasp of an egg*

11 *– Thumb-3 finger(tip grasp)of Rubiks cube*

12 *– Medium wrap of guitar.*

13 *–Lateral precision grasp of key.*

14 *– Index finger extension.*

15 *– Thumb-4 finger grasp of light bulb.*

16 *– Index finger pinch of pen.*

17 *– Lateral pinch of a sheet of paper.*

18 *– Thumb-4 finger grasp of tv remote.*

19 *– Heavy wrap of large lemon.*

20 *– Lateral grasp of a folder.*

21 *– Power grasp of long-nose pliers*

7.1.5. Discussion of Results

Referring to the experimental results, the grasping experiment has shown that a large variety of power and precision grasps are achievable using the prosthetic hand. These are achieved at various locations within the thumb's range of motion (i.e. the thumb being fully adducted, fully abducted, or somewhere in-between these positions). Overall, the power grasps were all easily achievable and the prosthesis conformed extremely well to objects of non-uniform geometry, providing sufficient grasping force to maintain a secure hold. Furthermore, the ratchet mechanism in combination with the palmar cushion allowed these objects to be held securely once the tensioning force on the input-cable was released. Minimal effort was required to perform these grasps as well as release the ratchet mechanism once locked.

While the precision grasps were also achievable, they required more effort and attempts to grasp the objects securely; in particular the pen (index finger pinch) and the egg (tripod grasp). The trajectory of the thumb (being biased to close first) made it difficult to grasp these objects during the first attempt, as it would often interfere with the grasp or close prematurely. The shape of the thumb's distal phalanx made it challenging to grasp small objects of varying sizes during precision grasps, as the closing trajectory remained relatively constant, contacting the objects at different points along its trajectory depending on the object size. While some grasps required more effort than others, the prosthesis exceeded the minimum requirement for achievable grasps outlined in Table 4, p. 31; maintaining a secure grasp once input-cable tension was released.

7.2. Experiment 2 – Mechanical Strength of the Phalanges under Hyper-extensive & Lateral loads

7.2.1. Background

The necessity for this round of experiments is essential as it allows the designer to determine the limits of mechanical strength of the phalanges under hyper-extensive loading and lateral loading. The first loading condition occurs when the hand is fully extended and the user exerts palmar forces onto the phalanges; creating hyper-extensive loads. The latter occurs when the user leans on the phalanges laterally (i.e. in the radial or ulnar directions as shown in Figure 3, p. 5).

7.2.2. Aim

To determine the behaviour and strength limits of the digits, while subjected to hyper-extensive and lateral loading conditions.

7.2.3. Apparatus

These tests made use of an Instron® 3365 tensile & compressive testing machine with a 1 kN calibrated Instron® load cell (Figure 131) in combination with the clamping assembly shown in Figure 132. Reference can be made to Appendix A2 (p. A-7) for a detailed description of the clamping design. Four finger assemblies will be used, namely two 3rd digit and two 5th digit assemblies.

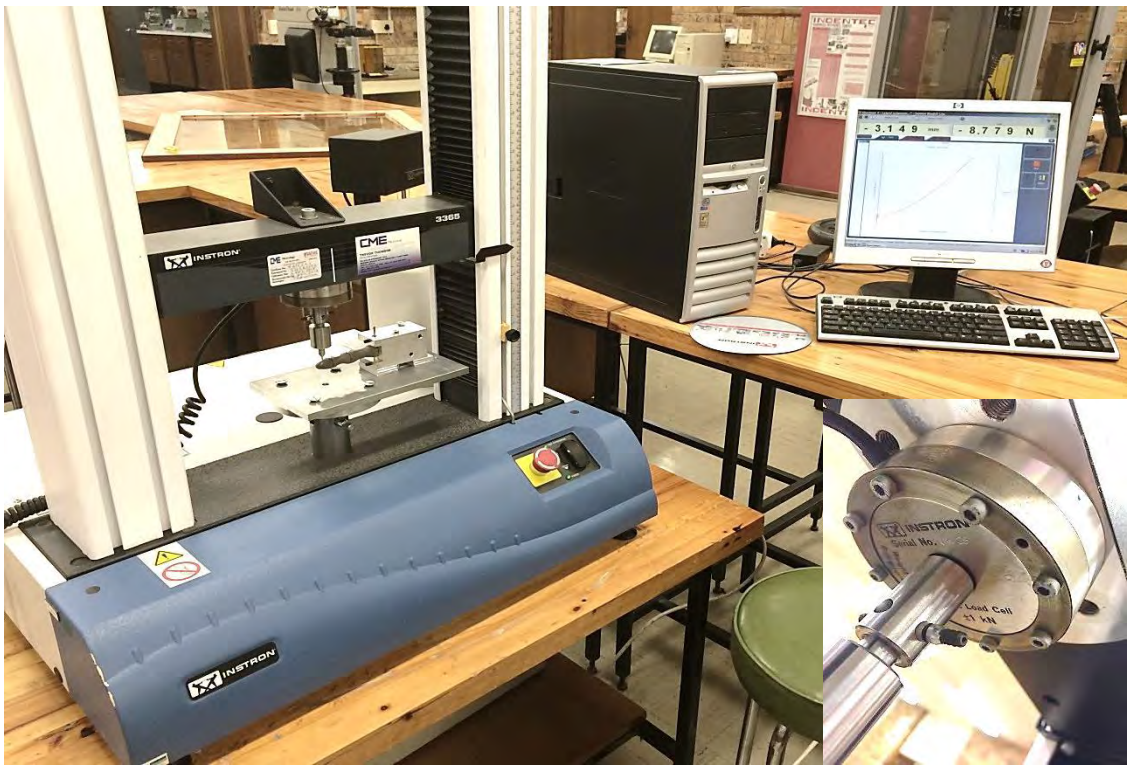

Figure 131 - Instron® 3365 strength testing setup using calibrated 1 kN load-cell (bottom right).

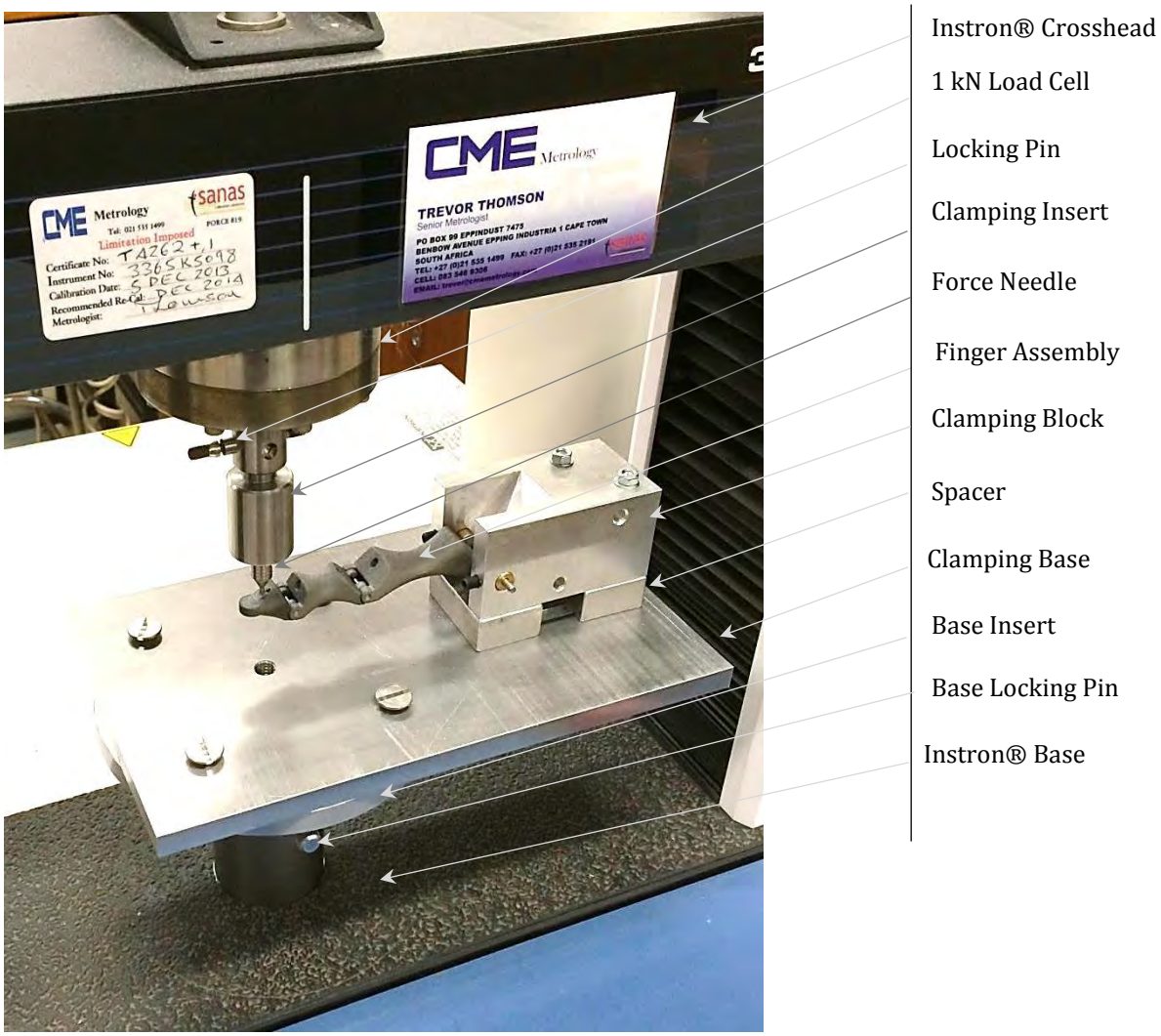

Figure 132 - Assembly of the Instron® 3365 strength test setup.

7.2.4. Methodology

- Perform a risk assessment of the experimental procedure. (See Appendix E1)
- Setup apparatus as specified in the aforementioned section and ensure all components are securely fastened.
- Initiate Instron® Bluehill software package, inputting compressive loading and displacement conditions with their respective limits. Also, input strain rate of 1% gauge length/min according to ISO 178 (2010) and ASTM D790 (2003).
- Four test configurations will be loaded and the specimens will be tested until failure; one hyperextensive loading case and one lateral loading case for each of the 3rd digit and 5th digit assemblies.
- For the two 3rd digit assemblies the gauge length is 95 mm[12]; hence a strain rate of 0.95 mm/min is inputted. The 5th digit assemblies have a gauge length of 75 mm; hence require a 0.75 mm/min strain rate according to the standards above.

[12] The gauge length is measured from the centre of the MCP pin to the load-application point.

7.2.5. Experimental Results

7.2.5.1. Specimen 1: Hyper-extensive loading of the 3rd digit

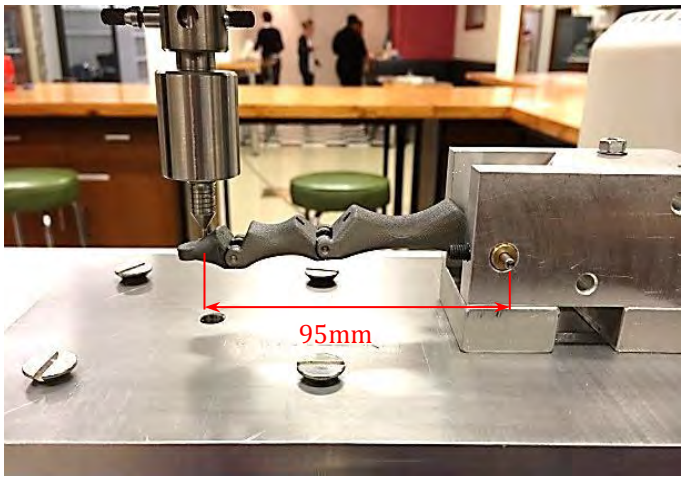

Figure 133 - Initial position of hyperextended 3rd digit specimen with 95 mm gauge length.

The specimen was loaded at a strain rate of 0.95 mm/min at a distance of 95 mm for the MCP pin, as seen in Figure 133. Referring to the load-extension curve in Figure 134, the gradual slope between 0 mm and 5 mm extension is indicative of slack in the system being absorbed as the structure is loaded. Furthermore, between 5 mm and 33 mm the structure's PA2200 nylon material is being flexed whilst still within its linear region (Figure 135, left), until the specimen bottoms out on the base plate at the maximum deflection (34.33 mm) and load (52.7 N), where a load spike is observed due to this contact (Figure 135, right). After the load is released from the specimen, the finger is at a new hyperextended rest position 12mm below its original zero datum position. This displacement can be attributed to a release of slack in the finger assembly in combination with possible structural deformation, not visible to the naked eye. Furthermore, there was no visible deformation to the posterior knuckle protrusions of the phalanges.

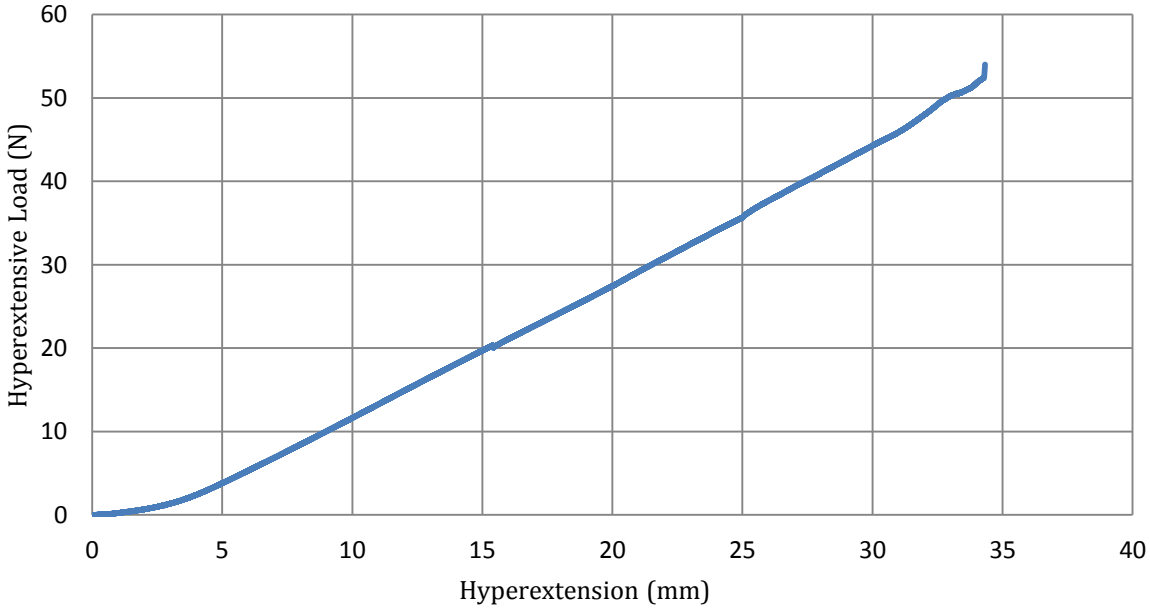

Figure 134 - Load-extension curve for hyperextensive loading of the 3rd digit

Figure 135 - Hyperextension of the finger at 22 mm displacement (left) and at 34.33 mm maximum hyperextension (right).

7.2.5.2. Specimen 2: Lateral loading of the 3rd digit

Unlike the hyperextended 3rd digit specimen, the laterally loaded specimen was loaded to destruction/fracture. From its rest position (Figure 136, left), the finger was loaded with a strain rate of 0.95 mm/min to a maximum load of 94.5 N at a lateral deflection of 27.75 mm. Figure 136 (right), shows the specimen deflected to 28.7 mm at a load of 92.2 N just prior to failure. Referring to Figure

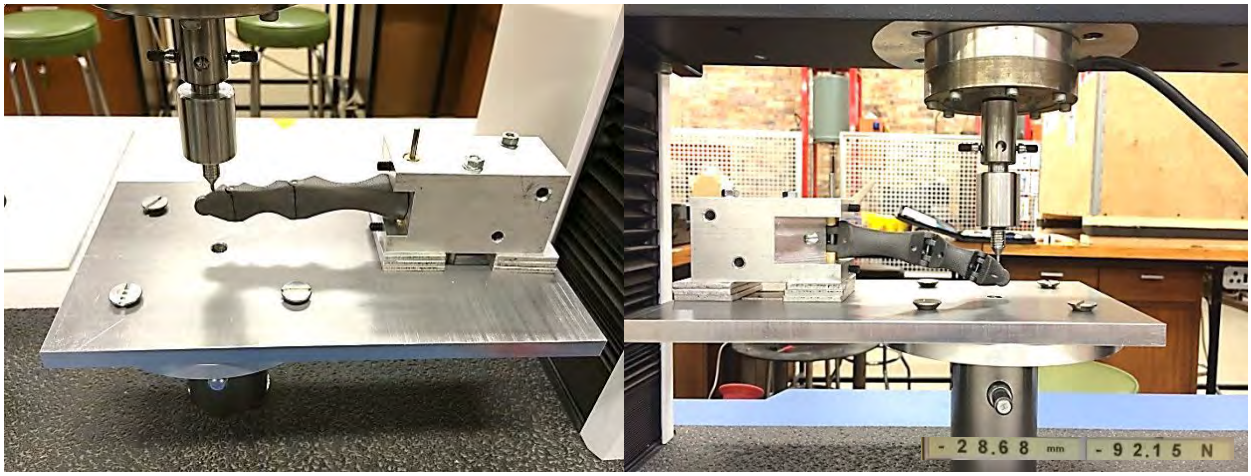

Figure 136 - Laterally loaded 3rd digit in its rest position (left) and loaded condition (right) prior to failure.

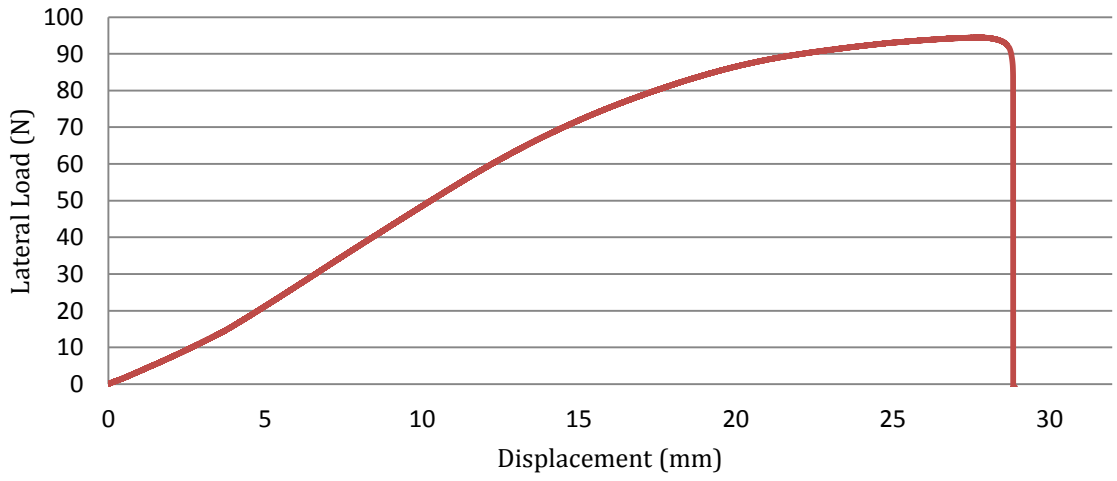

Figure 137 - Load-displacement curve of the laterally-loaded 3rd digit.

137, a gradual initial slope extends from 0 mm to 3.3 mm (unlike the 5 mm it required in the previous case), indicative of less slack and a more rigid orientation. From 3.3 mm to 12.7 mm, the behaviour of the structure appears linear elastic, after which the gradient of the slope gradually tapers off; indicative of material plasticity. According to the data, the maximum elastic load is reached at a force of 62 N; above which plastic deformation is encountered. Final fracture of the specimen occurred at 28.84 mm at the proximal interphalangeal joint of the digit. The mechanism of failure was tensile fracture of the hinges at the proximal end of the middle phalanx as seen in Figure 138.

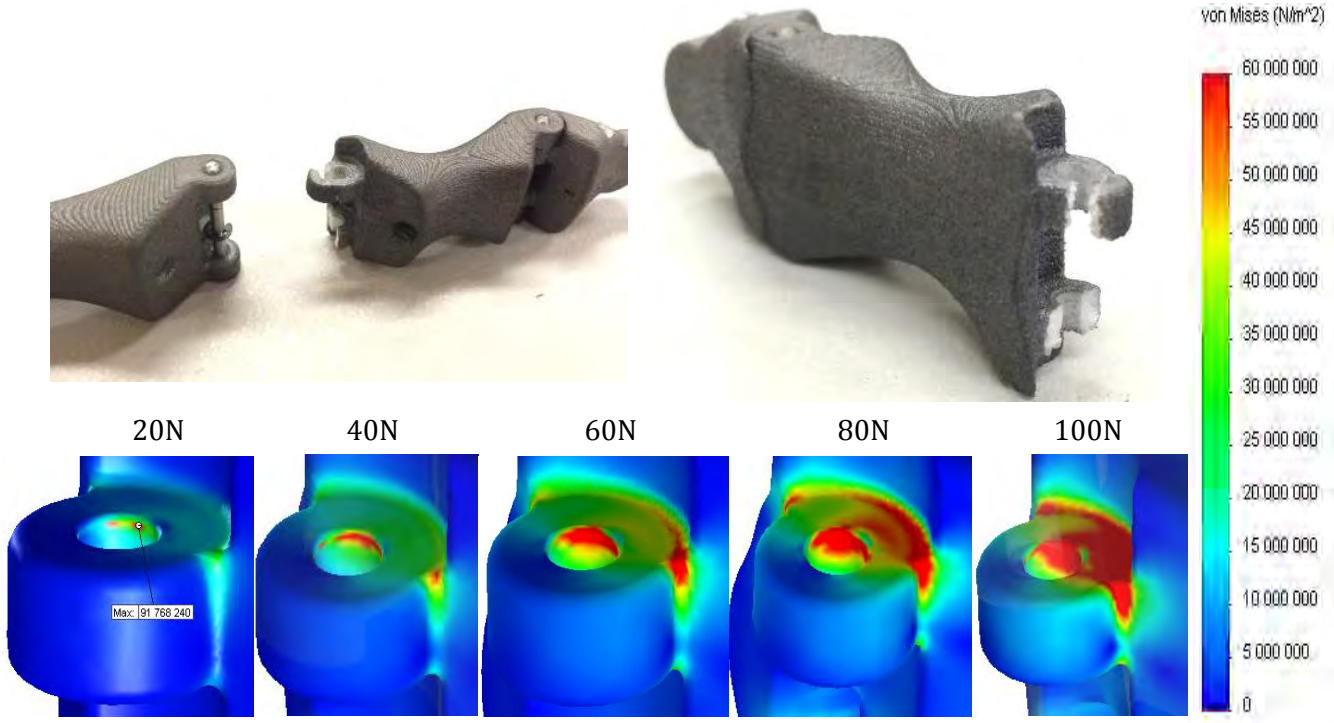

Figure 138 - Inferior perspective view (top left) and superior perspective view (top right) of the fractured hinges at the proximal end of the middle phalanx of the 3rd digit after lateral loading; with comparison to the FEA results (bottom)

Referring to Figure 138, the experimental fracture location correlates well with that of the FEA model. The location of highest stress can be seen clearly in the 20 N and 40 N loaded structures at the superior, interior border of the pin hole. As the load increases further, the high stress regions amalgamate; leading to catastrophic failure.

7.2.5.3. Specimen 3: Hyper-extensive loading of the 5th digit

The 75 mm gauge length of the 5th digit is measured in the same manner as for the 3rd digit, differing only in dimension due to the reduced size of the digit. Loaded at a strain rate of 0.75 mm/min, the specimen was hyperextended from its rest position (Figure 139, left) to its maximum displacement condition (Figure 139, right).

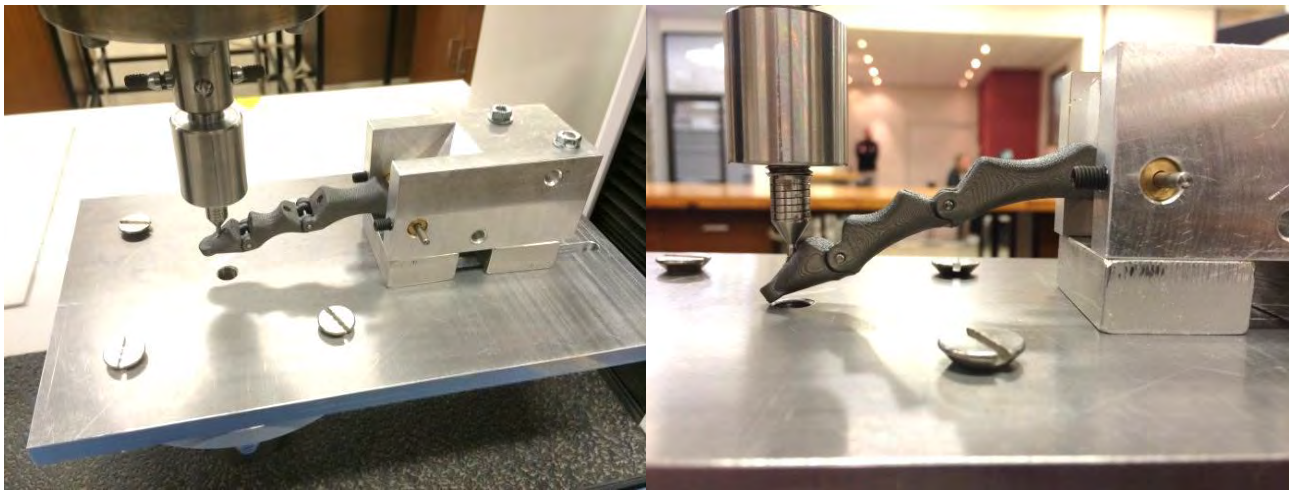

Figure 139 – Hyperextensively loaded 5th digit in its rest position (left) and final displacement condition (right).

Similar to the behaviour experienced by the 3rd digit under hyperextension, there was a gradual increase in gradient of the load-extension curve between 0.0 mm & 6.3 mm, as seen in Figure 140; which can be attributed to the slack in the system, including minor clearances between the pins and their respective phalangeal holes at each hinge-joint.

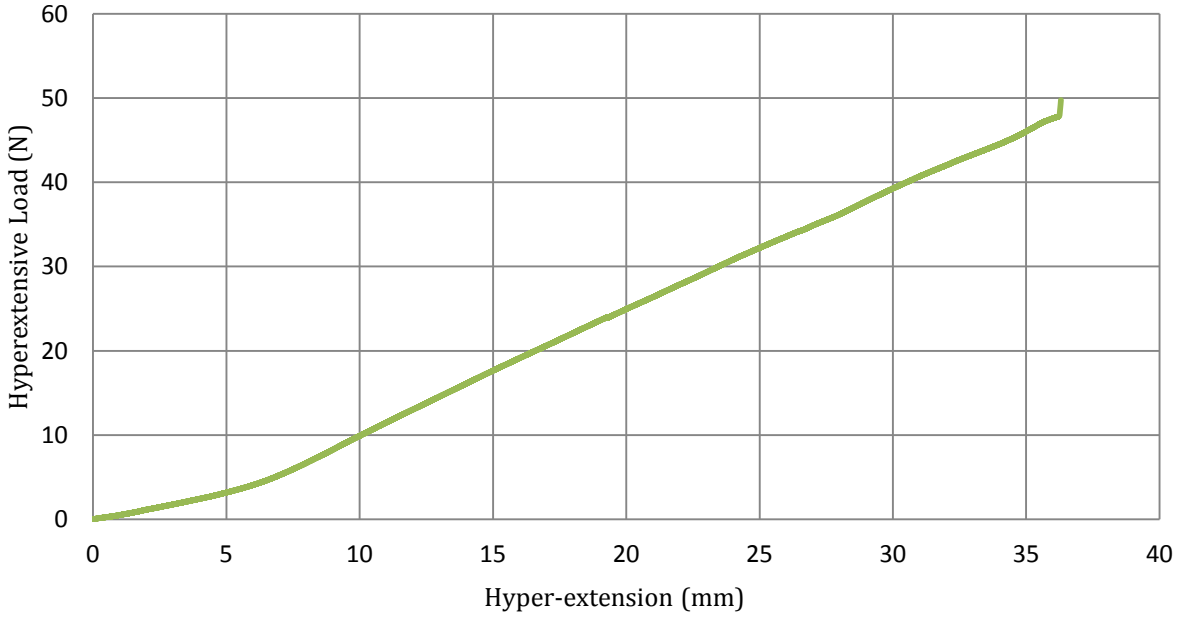

Figure 140 - Load-extension curve for hyperextensive loading of the 5th digit.

Furthermore, between 6.3 mm and 35.7 mm the behaviour of the specimen is relatively linear-elastic, indicative that is had not yet reached plasticity under 47.3 N hyperextensive loads. Moreover, the load-spike at 35.7 mm can again be attributed to the specimen making contact with the base plate (Figure 139, right).

7.2.5.4. Specimen 4: Lateral loading of the 5th digit

The 5th digit was loaded laterally from its rest position (Figure 141, left) until final fracture; at a strain rate of 0.75 mm/min. Shortly before fracture, the formation of cavities can be seen at the interphalangeal joints, especially the PIP joint (Figure 141, right). A further increase in the lateral load

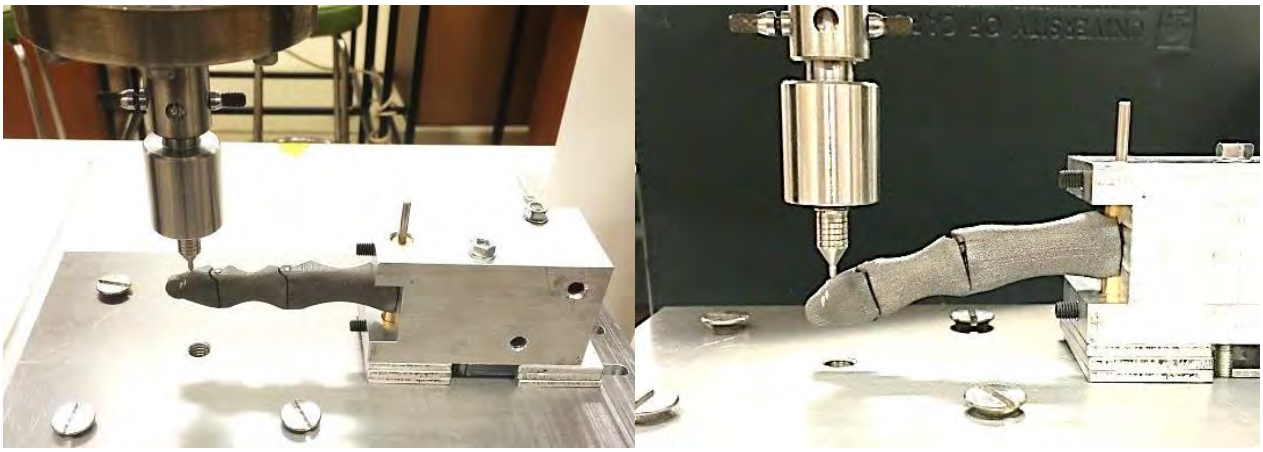

Figure 141 - Laterally loaded 5th digit in its rest position (left) and loaded condition (right) prior to failure.

surpassed the materials fracture strength and caused the specimen to fail at this joint. The fracture of the joint can be observed in Figure 142. Unlike the fracture of the 3rd digit, this specimen fractured at only one hinge; and not both simultaneously. This may be due to numerous factors including reduced material stress due to reduced leverage and applied load, as well as the influence of the decreased strain rate.

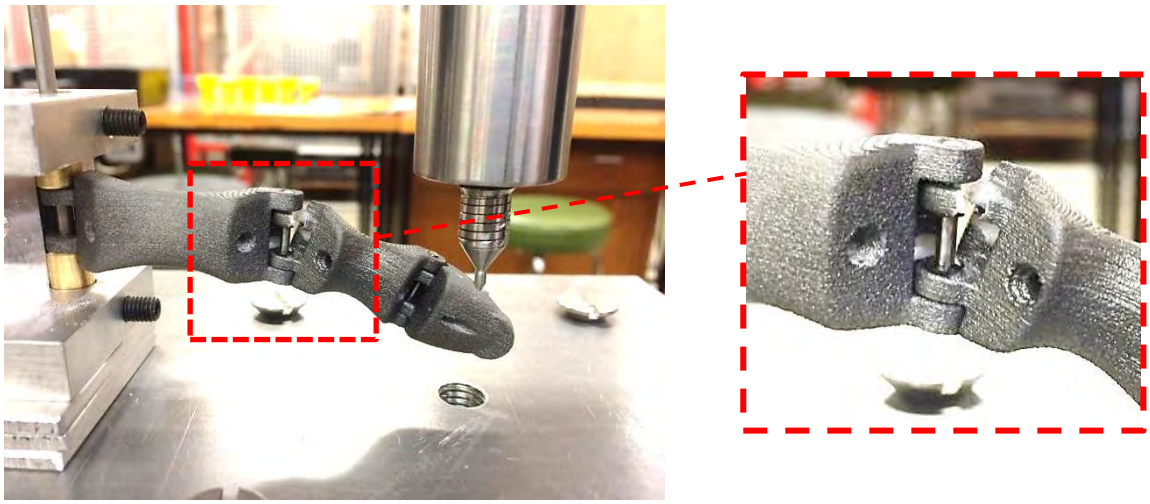

Figure 142 - Fracture of laterally-loaded 5th digit at proximal interphalangeal hinge-joint, with close-up.

Moreover, when compared to the results of the FEA investigation, the fracture location of the digit coincided with the maximum tensile stress states of the 5th digit; which were highest at the upper lateral edges of the specimen's hinges of the PIP joint as seen in Figure 143.

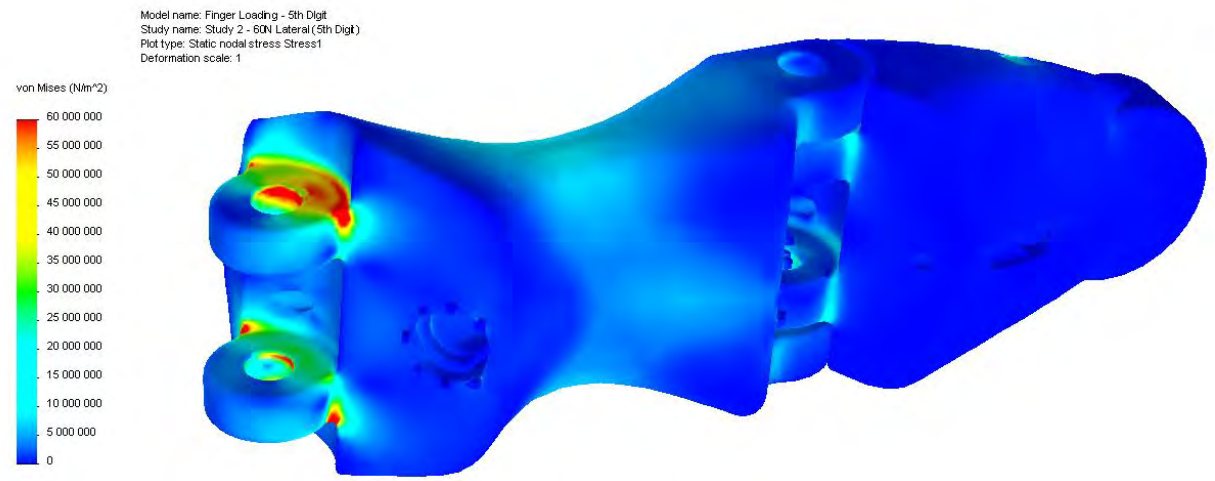

Figure 143 – Stress state of the 5th digit under 55.8 N of lateral loading from FEA investigation.

Referring to Figure 144, the initial gradient of the load-displacement curve increases non-linearly between 0 mm and 2 mm; similarly to previous specimens. Thereafter, it behaves linearly between 2mm and 10.3 mm, reaching its maximum elastic loading condition of 41.2 N. Non-linearity of the curve ensues this segment up until necking at 22.1 mm; reaching a maximum load of 64.6 N before fracturing at 23.0 mm.

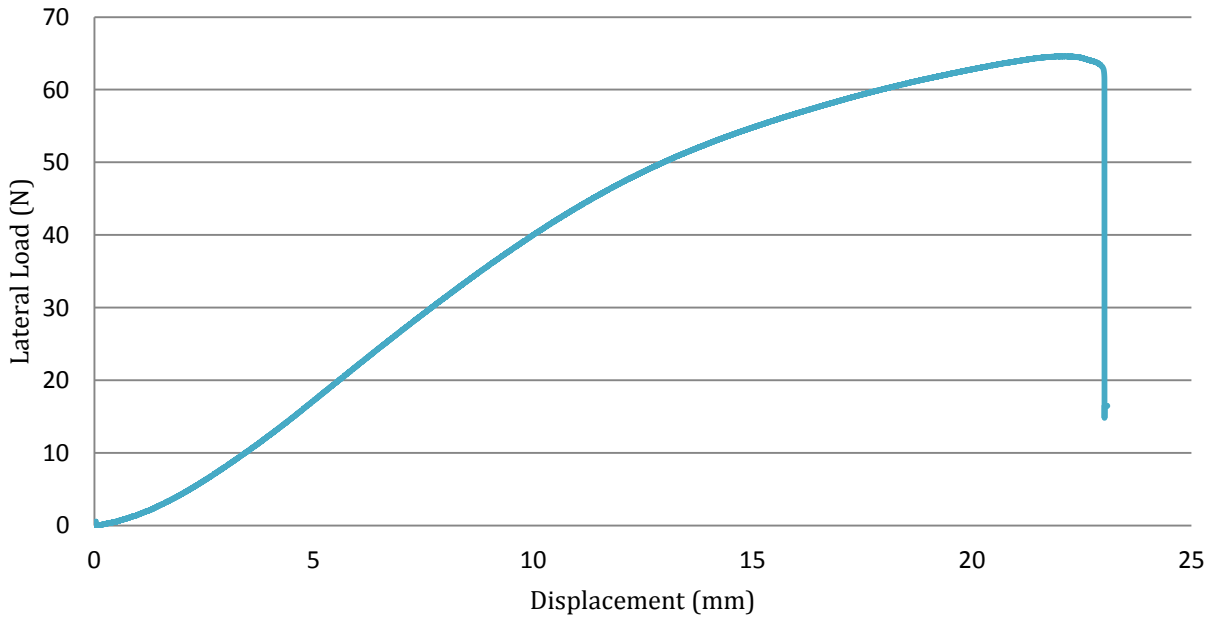

Figure 144 - Load-displacement curve of the laterally-loaded 5th digit.

7.2.6. Discussion of Results

Under hyperextensive loads, the 3rd and 5th digits exhibited similar displacement behaviour as presented in Figure 145. Both digits increased in stiffness between 0 N and 5 N as the slack in the system was absorbed, after which the slopes remained linear until the specimens bottomed-out at approximately 35 mm. The 3rd digit (blue) exhibited slightly stiffer behaviour as indicated by its

steeper slope. Both specimens had not reached their tensile stress limit when subjected to ±50 N of hyperextensive loading at the tip of the distal phalanx.

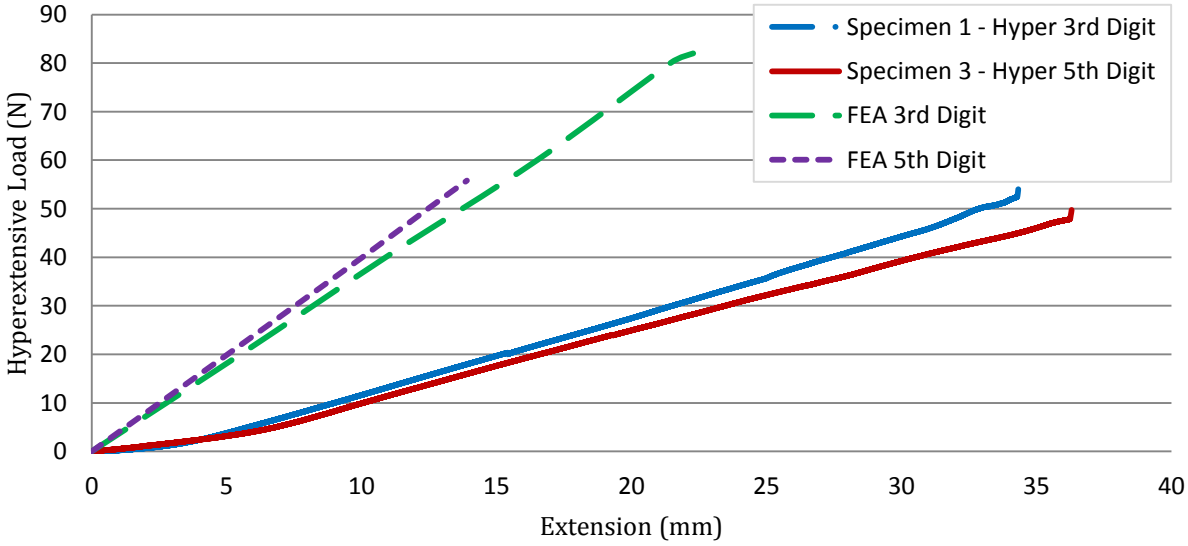

Figure 145 - Comparison of the hyperextensive load-displacement curves of the 3rd and 5th digits.

Under lateral loading conditions, the 3rd and 5th digits exhibited similar initial load-displacement behaviour as seen in Figure 146. Unlike the hyperextensive test cases, both laterally-loaded specimens fractured catastrophically; this behaviour is represented by the sharp drop-off in the load-displacement curves at 28.84 mm and 22.1 mm respectively. The 3rd digit failed at a maximum lateral force of 92.15 N, whereas the 5th digit fractured at 64.6 N.

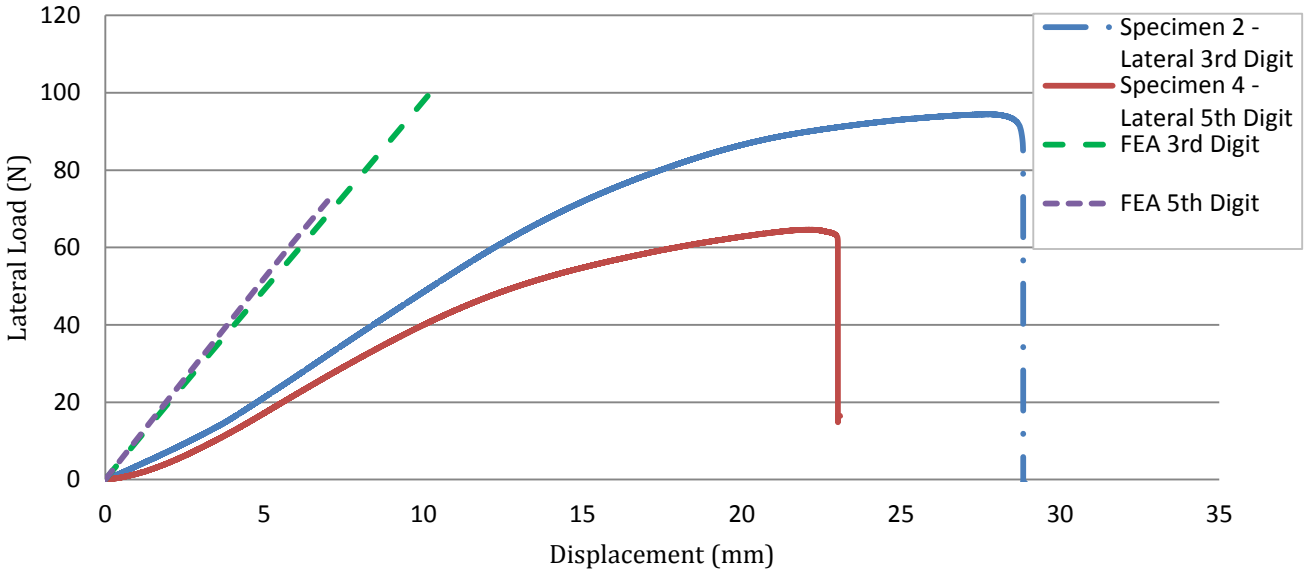

Figure 146 - Comparison of the lateral load-displacement curves of the 3rd and 5th digits.

When compared to the force-displacement behaviour of the FEA investigation in Figure 145 & Figure 146, the experimental specimens (blue & red curves) behaved less rigidly than their numerical

counterparts (green & purple curves). This behaviour is likely attributed to the presence of system slack, material non-linearities, plasticity and thermal effects which affect the displacement response. In addition to these factors are errors associated with FEA, which include modelling with simplifying assumptions, discretisation errors, truncation errors and numerical solution errors due to continuous interpolation between and extrapolation from Gauss points.

Expressing the results more simply; these experiments have shown that patients are able to carry objects (e.g. shopping bag) with a mass exceeding 5 kg on their distal phalanges in hyperextension, and laterally up to ±9 kg and ±6 kg on the 3rd and 5th distal phalanges respectively. In reality, users tend to use their middle or proximal phalanges to carry objects (Rossouw, 2013), and since these are located closer to the palm, reducing the leverage, the load-carrying ability is significantly increased beyond these masses. To verify the results and increase statistical significance, larger sample sizes should be used in future experiments.

7.3. Experiment 3 – Tensile Strength of Actuating Wires with figure-of-eight knots

7.3.1. Aim

To determine the tensile strength and mechanism of failure of various actuating wires/cables with their figure-of-eight knots.

7.3.2. Apparatus

- 1 x Instron® 3365 with 1 kN load-cell setup
- 1 x Clamping Insert with threaded loop/hook insert
- 1 x Clamping Base Assembly (Refer to Appendix A2, p. A-7 for the detailed clamping design)
- 9 x Figure-of-eight knotted US Nitinol wire (3 x Ø0.3 mm, 3 x Ø0.4 mm, 3 x Ø0.5 mm)
- 7 x Figure-of-eight knotted German Nitinol wire (3 x Ø0.31 mm, 1 x Ø0.44 mm, 3 x Ø0.5 mm)
- 3 x Figure-of-eight knotted Carbon-coated Stainless Steel braided wire (Ø0.6 mm)

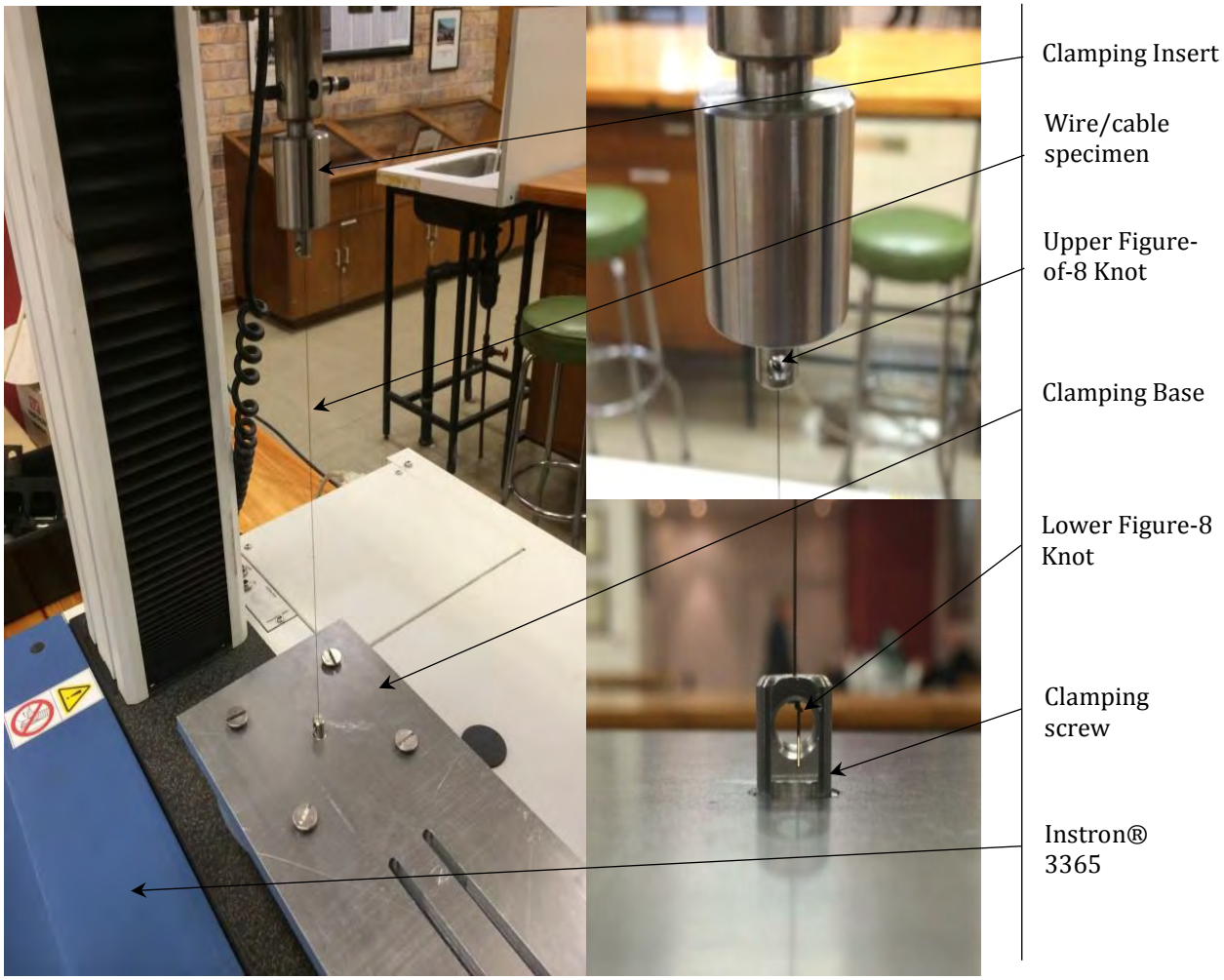

Figure 147 - Assembly of the Instron® tensile testing setup for determination of figure-of-8 knot and actuating wire/cable strength.

7.3.3. Methodology

A risk assessment of the experimental procedure was performed prior to any testing on the Instron® device (See Appendix E1). A total of 19 tensile tests were performed on wires with 7 different specifications. Six of these seven wire types had 3 tensile tests each, whereas the Ø0.44 mm German nitinol only had one test specimen due to limited material quantity. Tensile tests were performed according to ASTM D6320 (2002) in which a strain rate of 10 mm/min for knots and 25 mm/min for tensile tests on wires is specified. What is more, all specimens were within the specified gauge length of 250 mm ± 0.5%.

In order to see the dynamic as well as quasi-static response of the wires, the first two specimens of each wire specification were tested at a strain rate of 10 mm/min, whereas the third specimen was tested at 250 mm/min, instead of 25 mm/min, to investigate a worst-case dynamic-loading scenario. A pre-tension of 0.5 N was applied to each specimen prior to loading; below the specified 1 N pre-tension limit outlined in ASTM D6320 (2002). Results were recorded for each specimen and will be discussed in the ensuing section.

7.3.4. Experimental Results

Mechanical properties published by the manufacturers of the wires are listed in Table 46 below[13]. The properties represented here will be compared to the tensile testing results of this experiment, listed in Table 47, and summarised in Table 48. Furthermore, they will also be used to determine the rated (theoretical) loads of the actuating wires and thereby the degree of strength lost due to the end-knot, as shown in Table 49. For detailed stress-strain behaviour and load-displacement curves for each of the tested specimens, refer to Appendix B1, p. B-1.

Table 46 - Mechanical properties of the wires from manufacturer's datasheets.

Manufacturer	Material	Modulus of Elasticity (GPa)	Yield Strength (MPa)	Ultimate Tensile Strength (MPa)	Elongation at Break (%)	Tensile Force at Yield (N)**
Fort Wayne Metals†	NiTi 1	-	> 483	1240	> 10	> 61
Euroflex††	Nitinol SE	41.75	> 380	> 1100	> 10	> 47.8

† – Mechanical properties from manufacturer's material datasheets converted to SI units **(Fort Wayne Metals, 2014)**.
†† – Data for mechanical properties from manufacturer's datasheets **(Euroflex GmbH, 2014)**.
** - Calculated for a Ø0.4mm wire cross-section.

[13] Carbon-coated Stainless Steel Braid from Kingfisher has no available mechanical property data yet has 7 wire strands in its composite structure and is rated at 40 lbs (177.9 N).

Table 47 – Summarised tensile testing results of nitinol and carbon-coated stainless steel actuating wires.

		Specimen Number	Strain Rate (mm/min)	Force at Yield (N)	Yield Stress (MPa)	Ultimate Tensile Strength (MPa)	Elongation at Break (%)	Breaking Force (N)	Fracture Location
Monofilament Nitinol Wire	#1 Ø0.3mm (US)	1	10	36.5	520	646	15.8	47.15	Bottom Knot
		2	10	33	516	584	15.5	42.64	Bottom Knot
		3	250	37	559	610	13.9	44.57	Top Knot
		Mean	***-***	***35.5***	***531.7***	***613.3***	***15.1***	***44.79***	**-**
	#2 Ø0.31mm (German)	1	10	35.9	529	733	16.1	55.36	Top Knot
		2	10	32.6	484	934	17.3	70.50	Bottom Knot
		3	250	40.2	525	950	18.5	71.75	Top Knot
		Mean	***-***	***36.2***	***512.7***	***872.3***	***17.3***	***65.87***	**-**
	#3 Ø 0.4mm (US)	1	10	65	502	503.9	6.8	65.36	Bottom Knot
		2	10	70.2	569	619.3	16.8	80.34	Top Knot
		3	250	68.4	592	592.4	9.6	76.85	Top Knot
		Mean	***-***	***67.9***	***554.3***	***571.9***	***11.1***	***74.18***	**-**
	#4 Ø 0.44mm (German)	***1***	***10***	***70.4***	***495.3***	***576.8***	***16.9***	***87.71***	Top Knot
	#5 Ø 0.5mm (US)	1	10	97.1	518	605.3	16.6	122.69	Bottom Knot
		2	10	101.2	516	597.4	16.6	121.08	Bottom Knot
		3	250	108.8	536.8	536.8	9.2	108.80	Bottom Knot
		Mean	***-***	***102.4***	***523.6***	***579.8***	***14.1***	***117.52***	**-**
	#6 Ø 0.50mm (German)	1	10	72.5	413	991.3	20.6	194.63	Top Knot
		2	10	92.9	467	950.2	18.6	186.57	Top Knot
		3	250	86.7	443	825.6	16.3	162.10	Top Knot
		Mean	***-***	***84.0***	***441.0***	***922.4***	***18.5***	***181.10***	**-**
Multifilament St. Steel	#7 Ø 0.6mm Carbon-coated braid	1	10	38.5	214	720.2	8.7	121.27	Bottom Knot
		2	10	26.2	163	639	8.1	107.59	Top Knot
		3	250	31.3	172	546.7	8.8	92.05	Top Knot
		Mean	***-***	***32.0***	***183***	***635.3***	***8.5***	***106.97***	**-**

Table 48 – Mean mechanical properties of the test specimens as a function of manufacturer.

Manufacturer	Material	Yield strength (MPa)	Ultimate tensile strength (MPa)	Elongation at break (%)	Tensile force at yield (N)	Breaking force (N)
Fort Wayne Metals†	**NiTi 1**	**> 483**	**1240**	**> 10**	**> 94.8****	**243****
Ø0.3mm	"	531.7	613.3	15.1	35.5	44.8
Ø0.4mm	"	554.3	571.9	11.1	67.9	74.2
Ø0.5mm	"	523.6	579.8	14.1	102.4	117.5
Euroflex††	**Nitinol SE**	**> 380**	**> 1100**	**> 10**	**> 74.6****	**> 216****
Ø0.31mm	"	512.7	872.3	17.3	36.2	65.9
Ø0.44mm	"	495.3	576.8	16.9	70.4	87.7
Ø0.5mm	"	441.0	922.4	18.5	84.0	181.1

† – Mechanical properties from manufacturer's material datasheets converted to SI units **(Fort Wayne Metals, 2014)**.
†† – Data for mechanical properties from manufacturer's datasheets **(Euroflex GmbH, 2014)**.
** - Calculated using a Ø0.5 mm wire cross-section.

Table 49 - Deviation from the rated breaking and yielding forces of the actuating wires due to the figure-of-8 knots.

Wire diameter (mm)	Manufacturer and material	Rated breaking force (N)	Actual breaking force (N)	% Decrease in breaking strength (%)	Rated force at yield (N)	Actual force at yield (N)	% Deviation in yielding force (%)
Ø0.3	Fort Wayne Metals†: NiTi 1	90.5	44.8	50.5	35.2	35.5	+0.7
Ø0.4		160.8	74.2	53.9	62.7	67.9	+8.4
Ø0.5		251.3	117.5	53.2	97.9	102.4	+4.6
Ø0.31	Euroflex††: Nitinol SE	80.3	65.9	17.9	28.7	36.2	+26.2
Ø0.44		142.7	87.7	38.5	57.8	70.4	+21.8
Ø0.5		223.0	181.1	18.8	74.6	84.0	+12.6
Ø0.6	Kingfisher: Carbon-coated Stainless Steel	177.9	107	39.9	-	-	-

† – Mechanical properties from manufacturer's material datasheets converted to SI units **(Fort Wayne Metals, 2014)**.
†† – Data for mechanical properties from manufacturer's datasheets **(Euroflex GmbH, 2014)**.
** - Calculated using a Ø0.5 mm wire cross-section.
Note: Rated (theoretical) breaking and yielding force are calculated using the minimum UTS and Yield strength values from manufacturer's data in Table 46.

7.3.5. Discussion of Results

Experimental tensile testing of Figure-of-8 end-knots on seven different actuating wire specimens was completed in this experiment, in accordance with ASTM D6320 (2002). According to this standard, specimens may not break within 5 mm of the gripping points; else the results should be discarded. However, the focus of this standard is on the testing of overhand knot and wire strength at the

sample's mid span, and not at its extremities. Furthermore, the breaking strength of the figure-of-eight end-knots employed in these tests are of particular interest; therefore, all specimens are considered, regardless of their fracture location.

Referring to Table 47, it can be seen that all specimens failed at their end-knots; interfacing with either the top or bottom clamping-screws. Although the German nitinol failed more regularly at the top clamp whereas the US nitinol failed more regularly at the bottom, there was no clear link between fracture location and wire specification. Consequently, a random distribution is assumed. Additionally, an increased strain-rate corresponded to a decrease in breaking force for all specimens except specimen 1. Contrarily, this behaviour inversed when considering the force at yield, because it increased as a function of strain rate for all samples except for a single case in each of the test specimens 3, 6 & 7. Further experimentation is needed to confirm this phenomenon, as it is likely that the response time of the load cell could not accurately reflect the actual load due to the increased strain rate; causing it to overshoot.

When comparing the experimental data to the manufacturers' data in Table 46 and Table 48, all properties correlate well, except for those relating to the Ultimate Tensile Strength (UTS) of the wire; which were significantly lower. Residual stresses generated due to the tightening of the end-knots mean that specimens are expected to fracture under lower loads. Since the superelastic nature of the nitinol means that its tensile limit is reached only once necking of the specimen begins, the reduced loading condition at fracture results in the true tensile limit not being reached.

The yield strength of the US nitinol exceeds that of the German manufacture, allowing greater loading in the elastic region of the material. However, this is at the expense of ductility, which is 1.8% to 7.4% higher for the German wires; as reflected by their elongation at break. Whilst remaining in the elastic region is favourable, the increased ductility allows the wire to deform to a much greater extent, absorbing significantly higher loads (35% more for the Ø0.5 mm wire) before failing catastrophically. These are behavioural characteristics that are critical to medical devices that directly affect patients.

When considering the decrease in breaking strength due to the figure-of-eight knots, as shown in Table 49, the German nitinol wire deviated the least from its rated load (17.9% – 38.5%), followed by the carbon-coated wire (39.9%) and finally the US nitinol (50.5% - 53.9%). Also, its actual resilience to fracture was better, due to its increased ductility. All specimens exceeded the rated loads (0.7% – 26.2%), when considering the percentage deviation in yielding force. Referring to the load-displacement and stress-strain curves in Appendix B1 (p. B-1), the majority exhibited jagged behaviour within the first 2% strain, with the exception of specimen 2 in Table B8 (p. B-5) which had a large drop at 3.2% strain. These unstable loading characteristics represent the slack in the system being absorbed. The figure-of-eight end-knots also self-tighten as they are loaded, hence the slope of

the elastic region of the specimens is more gradual initially, until the slack is absorbed, and then increases at a constant linear slope under further loading.

7.3.6. Conclusions

Based on the experimental outcomes, the following conclusions have been drawn. The breaking strength of all specimens was reduced between 17.9% and 53.9% when compared to the rated theoretical load of the wires, and should be taken into consideration when focussing on the design limit of the actuating wires used in the prosthetic hand. Conversely, the yield load exceeded the rated amount for all specimens between 0.7% and 26.2%; favourably reflecting a higher elastic limit. Moreover, increased strain-rates reduced the breaking force, and increased the yielding force for the majority of the specimens. To minimise random error in results related to material anisotropy, thermal effects and non-linearities resulting from knot-tightening, increased sample numbers should be used. Also, systematic or experimental error associated with measure gauge length can be used by inferring an electronic datum on the Instron® setup; improving accuracy of strain measurements.

The mechanism of failure for all specimens was tensile fracture of the actuating wire at their end-knots; breaking at either the top or bottom clamping-screw at random. Furthermore, the experimental data obtained concurred well with that of the manufacturers, exceeding the conservative estimates in all properties except the UTS; which was significantly lower. The superelastic nature of the nitinol used meant that it only reached UTS at necking (i.e. at failure); therefore a reduction in breaking strength directly affected the UTS value. When comparing the German nitinol specimens to those of the US nitinol, it was found that increased ductility lead to an increased force to fracture; a favourable trait to prolong catastrophic failure.

7.3.7. Recommendations and Future Work

Based on the conclusions, the following recommendations are made. The number of test specimens and sample size should be increased to reduce random error and increasing statistical accuracy. Further investigation should be made into other types of terminal end-knots and locking mechanisms to reduce the loss of strength, and minimise the resulting induced stresses on the wire. Additionally, the use of alternative wires and materials should be considered, testing not only their tensile properties but also their flexural (bending) capabilities; especially when designing to minimise fatigue.

7.4. Experiment 4 – Endurance Testing of the Phalangeal Channel Mechanism

7.4.1. Background

Activities of Daily Living require patients to use their hands in almost all interactive tasks. These tasks require the hand to close hundreds of times each day, creating cyclic loads which eventually lead to the fatigue failure of various components. More specifically, the wear due to the relative motion of the tendons sliding in the finger channels is of interest; as it decreases the design life of the hand. Consequently, an experimental procedure to determine the number of cycles to failure is required. The typical number of loading cycles experienced by the hand can be found in Section 2.9.3.4, p. 39, and the detailed design of the testing apparatus can be referred to in Appendix A1, p. A-1.

7.4.2. Aim

To determine the number of cycles the tendon mechanism can withstand until failure, or test until 1,200,000 cycles.

7.4.3. Apparatus

- Sartorius Research 10 µg Scale (Figure 148)
- Pneumatic setup using Festo© products (Figure 149) (See Appendix A1 for detailed design).

Figure 148 – Sartorius research 10 µg resolution scale (left) weighing specimen (right).

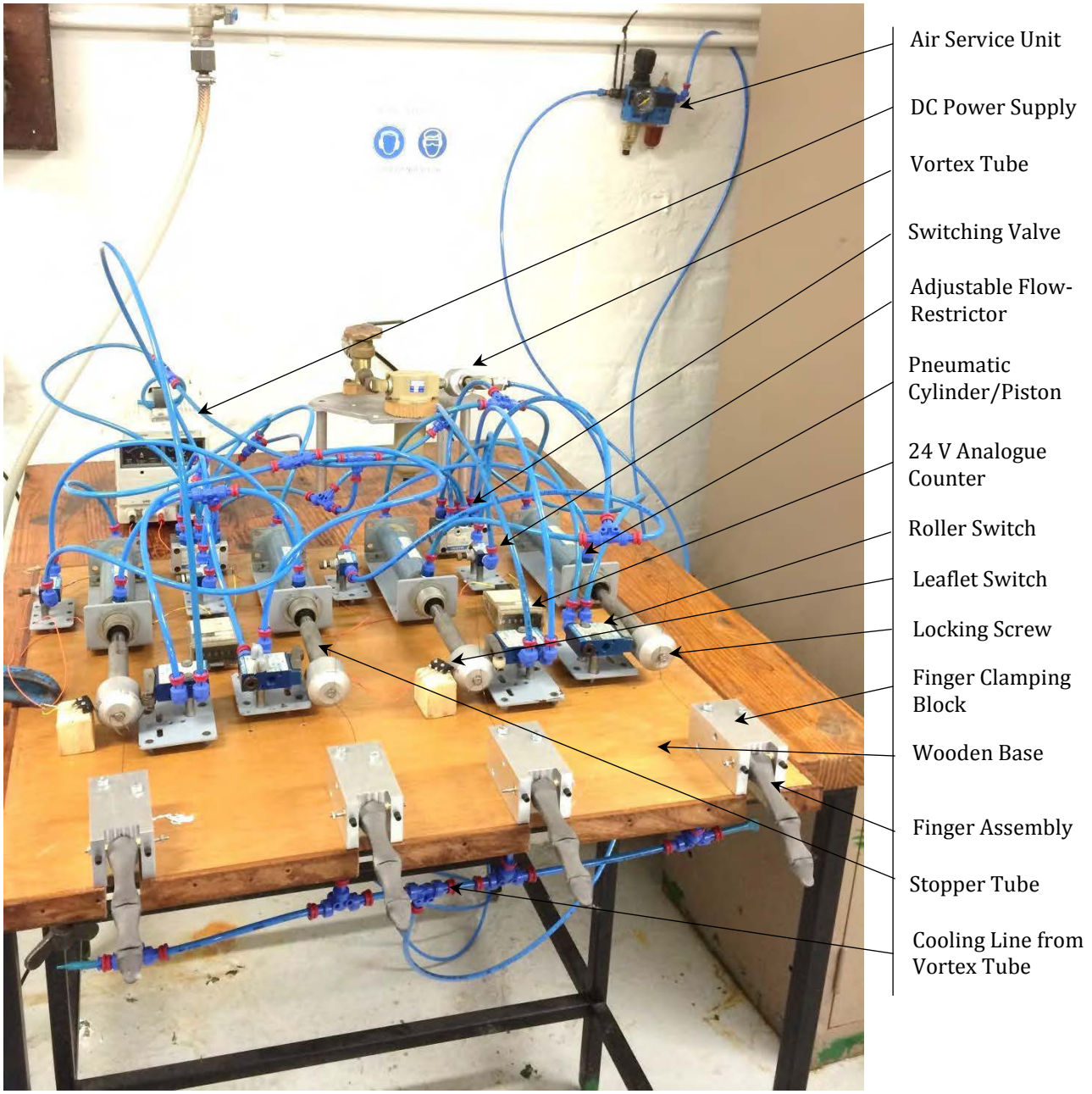

Figure 149 - Pneumatic endurance test assembly.

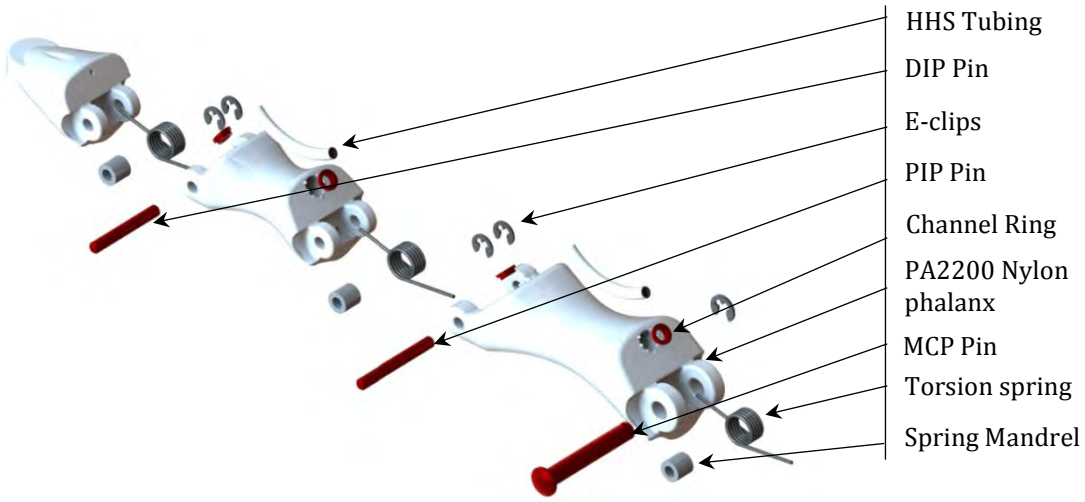

Figure 150 - Endurance testing finger assembly.

Generic Components:

Each of the four finger specimens has the following generic components:

- 1 x 3rd Digit phalangeal assembly (Graphite-coated PA-2200 Nylon)
- 1 x Ø0.6 mm, 5 turn, straight-wound torsion Springs (DIP joint)
- 1 x Ø0.6 mm, 4 turn, straight-wound torsion Springs (PIP joint)
- 1 x Ø0.7 mm, 5 turn, straight-wound torsion Springs (MCP joint)
- 3 x Polymeric spring-mandrels
- 2 x Interphalangeal (PIP & DIP) locking pins
- 1 x Metacarpophalangeal (MCP) locking pin
- 5 x E-clips and 4 x Channel rings

Unique Components:

- Actuating Cable:
  - Ø0.4 mm Nickel-Titanium (Nitinol) monofilament wire sourced directly from US manufacturer.
  - Ø0.6 mm Carbon-coated stainless steel braided-wire sourced from local retailer.
- Lining:
  - Single-layer Helical Hollow-Strand (HHS) tubing
  - Dual-layer Helical Hollow-Strand (HHS) tubing

Table 50 - Specimen configuration for endurance testing.

		Specimen 1	Specimen 2	Specimen 3	Specimen 4
Lining Type	None	✓	✗	✗	✓
	Single Layer HHS tubing	✗	✓	✗	✗
	Dual-Layer HHS tubing	✗	✗	✓	✗
Actuating Wire Type	Ø0.4mm Nickel-Titanium Monofilament	✓	✓	✓	✗
	Ø0.6mm Carbon-coated Stainless Steel braided-wire	✗	✗	✗	✓
Channel Rings		✓	✓	✓	✓

7.4.4. Methodology

1. Perform risk assessment of the experimental procedure.
2. Setup the experimental apparatus according to the displacement-control method outlined in ISO 14243-1 (2009) and test functionality.
3. Weigh each phalangeal specimen three times, according to ASTM F2025 (2000), and rotate their orientation on the calibrated 10 µg Sartorius Research scale to minimise random error. The mean of the three readings will be used to determine the wear.
4. Attach the control specimen and manually test 5 complete cycles to ensure there are no obstructions in the closing path.[14]
5. Attach the actuating cable to the cyclic unit and complete a further 5 cycles.

[14] A cycle is considered complete when a 30 mm linear displacement of the actuation cable is made to both close (flex) and re-open (extend) the three-phalanx configuration.

6. Apply a 2 Hz ± 0.2 Hz cyclic load, at displacement amplitudes of 30 mm; equivalent to the maximum flexion condition experienced by the hand during operation.
7. Test until 1,200,000 cycles, else until failure is reached.
8. Three failure criteria are considered:
   a. The fracture of the actuating cable/wire
   b. The wear of the wire through the palmar aspect of the phalanx
   c. The loosening of the internal channel components (applicable to Tests 2 & 3)
9. Document and report all significant findings.

7.4.5. Experimental Results

7.4.5.1. Results for Endurance Testing: Round 1

The specimen configurations used in the first round of endurance testing are outlined in Table 50, with a summary of the results for the first round of endurance testing shown in Table 51. Figure 52 displays the mass of the specimens prior to testing, whereas Table 53 shows the mass after testing; highlighting the difference in mass. A detailed description of the failure of each specimen is described thereafter.

Table 51 – Final results for the endurance test specimens: Round 1.

	Specimen Number and Description			
	1 Control	**2 Single Layer**	**3 Dual Layer**	**4 Carbon**
Number of cycles to failure	4077	2302[15]	2580	20 176
Failure location	*Prox. Channel Ring – Prox. Phalanx*	*Prox. Channel Ring – Prox. Phalanx*	*Prox. Channel Ring – Prox. Phalanx*	*Mid Length – Prox. Phalanx*

Table 52 - Gravimetric measurements of finger specimens for Round 1 *before* testing. †

Mass Reading (g)	Specimen Number and Description			
	1 Control	**2 Single Layer**	**3 Dual Layer**	**4 Carbon**
1	15.8734	16.37888	16.47370	16.21820
2	15.8737	16.37888	16.47380	16.21826
3	15.8737	16.37890	16.47378	16.21821
Mean	***15.87359***	***16.37889***	***16.47376***	***16.21822***

After the first round of testing, gravimetric results shown in Table 53 indicate that the mass of all specimens decreased. Specimen 3 lost the greatest amount of mass (0.14100 g), followed by specimen 2, specimen 4 and specimen 1. Furthermore, when considering mass loss per cycle, the specimen order

[15] - Wire broke at 2800 cycles at the attachment to piston and was replaced ∴ channel underwent 5102 cycles at failure
† - These measurements include the mass of the actuating wire/cable and are made according to ASTM F2025 (2000)

remained the same except for specimen 1 which had a low mass loss per cycle (0. 43 µg/cycle) due to metal on plastic contact, and specimen 4 which was even lower (0.94 µg/cycle) due to the higher number of cycles it was subjected to. Both results indicate that the dual-layer HHS tubing wore at a greater rate than the single-layer HHS tubing.

Table 53 - Gravimetric measurements of finger specimens for Round 1 *after* testing. ††

Mass Reading (g)	Specimen Number and Description			
	1 Control	2 Single Layer	3 Dual Layer	4 Carbon
1	15.86974	16.31484	16.33279	16.20935
2	15.86981	16.31491	16.33270	16.20934
3	15.86978	16.31500	16.33277	16.20970
Mean	***15.86978***	***16.31492***	***16.33276***	***16.20946***
Change in mass (g)	***-0.00381***	***-0.06397***	***-0.14100***	***-0.00876***
Total load cycles	*4077*	*5102*	*2580*	*20 176*
Mass loss per cycle (µg)	*0.94*	*12.54*	*54.65*	*0.43*

†† - These measurements include the mass of the actuating wire/cable and are made according to ASTM F2025 **(2000)**

Specimen 1: Control

The actuating wire of the control specimen failed at 4077 loading cycles. Upon closer inspection, the distal phalanx (Figure 151, left) showed no visible signs of wear in the nylon seating groove where the knot locates itself. Furthermore, both the DIP and PIP joints showed minimal signs of wear on the channel rings (Figure 151, right).

Figure 151 - Specimen 1 distal phalanx (left, centre left), DIP joint (centre right) and PIP joint (right) after first round of endurance tests.

On the contrary, the proximal stainless steel channel-ring of the MCP joint showed signs of wear caused by the nitinol actuating wire, as seen in Figure 152. Moreover, this joint is also coincides with the point of fracture of the actuating wire.

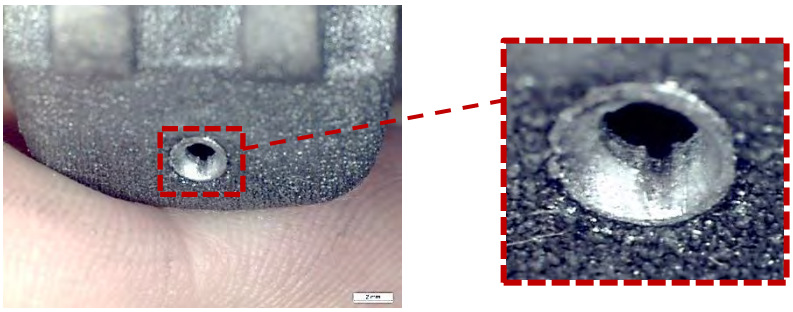

Figure 152 - Specimen 1: Wear of the MCP channel ring due to actuating wire.

Referring to Figure 153, the surface wear on the cable due to the channel ring contact can be seen (left). Also, the proximal (centre) and distal (right) fracture surfaces both display crack initiation points in their top left quadrants with a relatively smooth surface below it; indicative of a brittle fracture.

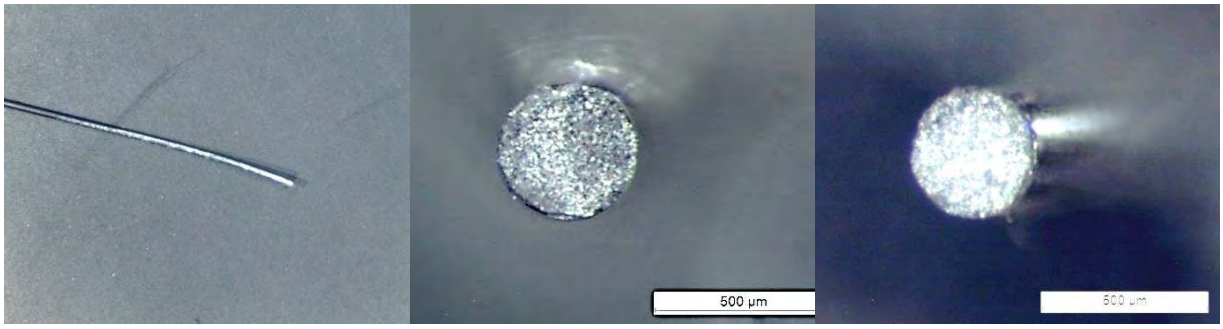

Figure 153 - Specimen 1: Surface wear of the nitinol actuating wire (left) with the proximal (centre) and distal (right) fracture surfaces of the wire.

Specimen 2: Single-layer HHS tubing

The actuating wire of this specimen failed at 2302 loading cycles. The nylon and channel rings on the distal phalanx, DIP joint and PIP joint showed no visible signs of wear or fatigue (Figure 154, top left & centre). Conversely, the MCP joint displayed clear signs of abrasive wear caused by the actuating wire, on both the HHS tubing and on the channel rings (Figure 154, top right & bottom left)

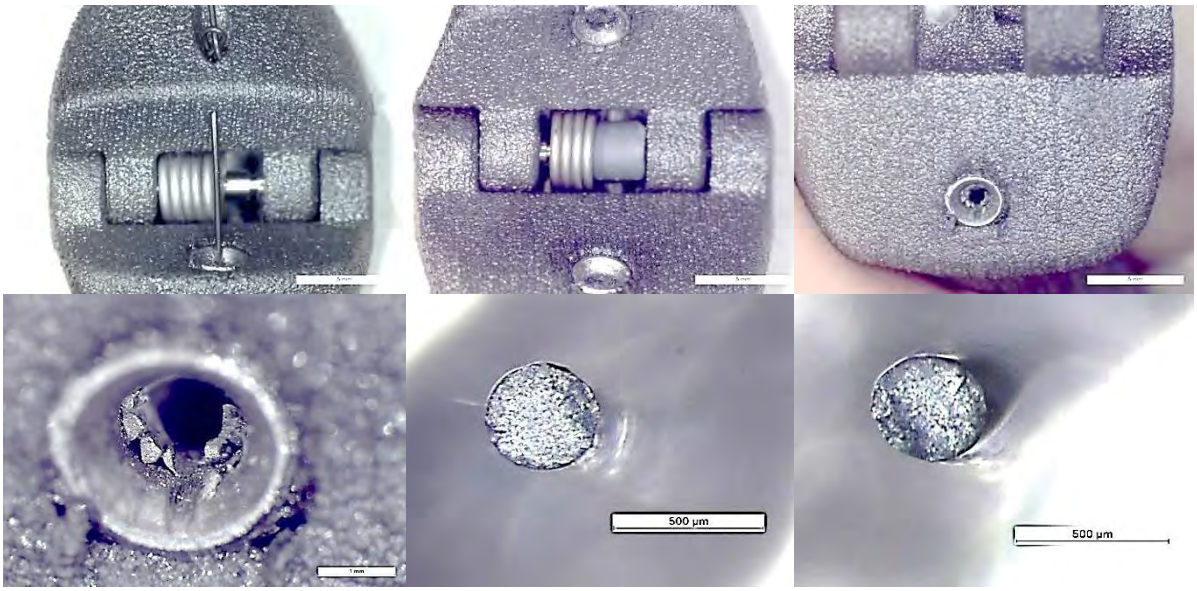

Figure 154 - Specimen 2: DIP joint (top left), PIP joint (top centre), MCP joint (top right) with close-up of MCP prox. channel ring (bottom left) and fracture surfaces of the nitinol actuating wire both prox. (bottom centre) and distal (bottom right).

While the proximal stainless steel channel ring and tubing showed clear signs of abrasive wear, the nitinol wire did not; which can be attributed to its superior surface hardness. However, the poorer flexural ability of the nitinol means that fast/brittle fracture occurs once a stress-raiser has been introduced onto its surface. This brittle behaviour is exhibited on both smooth fracture surfaces of the broken wire, who's coinciding crack initiation points are visible on the top right and bottom left for the proximal and distal fracture surfaces respectively (Figure 154, bottom centre & right).

Specimen 3: Dual-layer HHS tubing

The actuating wire of the dual-layer HHS specimen failed at 2580 loading cycles at the proximal channel ring of the proximal phalanx. Similar to the previous two specimens, the nylon superstructure showed no signs of wear at the interface with the knot. Furthermore, the channel rings of the middle phalanx showed minor signs of surface wear (Figure 155, left and centre), whereas the channel rings of the proximal phalanx as well as its HHS tubing showed visible signs of degradation (Figure 155, right).

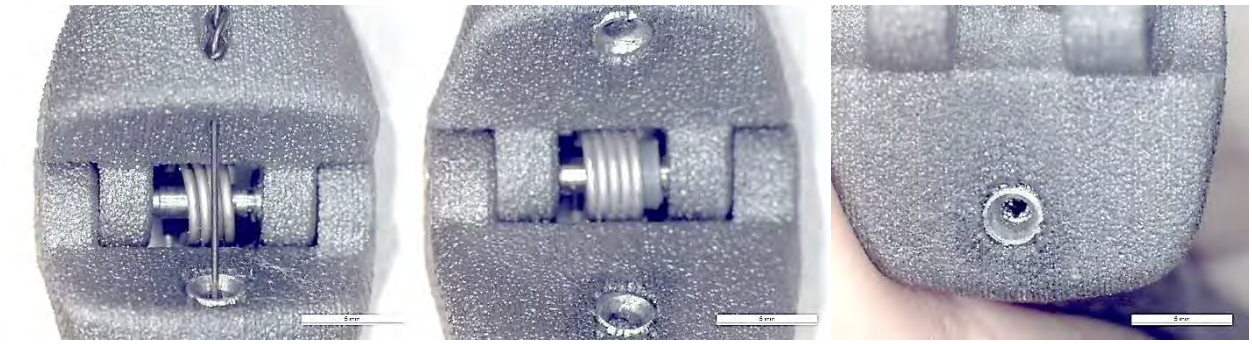

Figure 155 - Specimen 3: DIP joint (left), PIP joint (middle) and MCP joint (right).

Referring to Figure 156, from left to right, the fracture location of the nitinol actuating wire can be seen at the MCP joint. Moreover, the degradation/wear on the HHS tubing has abraded through the first layer of the tubing in the 2580 loading cycles. Additionally, the proximal and distal mating surfaces of the fractured nitinol wire exhibit similarly smooth surfaces much like the fracture surfaces of the previous nitinol specimens.

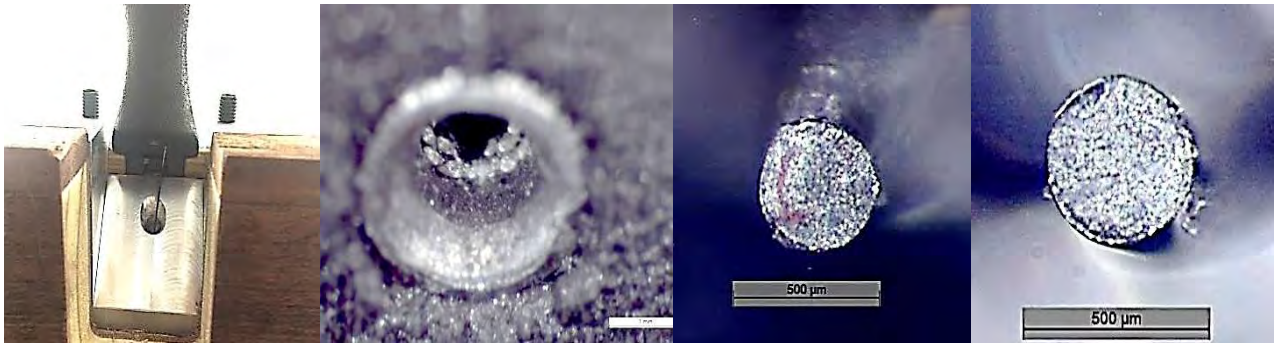

Figure 156 - Specimen 3: Actuating wire failure at MCP joint (left), wear of HHS tubing prox. phalanx (centre left), and prox. (centre right) and distal (right) fracture surfaces of the actuating wire.

Specimen 4: Carbon Coated Stainless Steel Braided-Wire

The actuating wire of this specimen failed at 20,176 loading cycles; much higher than that of the nitinol wire. The fracture of the wire occurred at the centre of the proximal phalanx (Figure 157), dissimilar to the location of fracture of the previous three specimens. Furthermore, the distal and proximal interphalangeal joints (Figure 158, left & centre left respectively) showed no signs of surface wear, while the metacarpophalangeal joint showed only minor signs of wear due to the relative motion of the carbon cable on the nylon and stainless steel channel rings (Figure 158, right). This behaviour is expected as the carbon coating has a lower surface hardness when compared to the channel ring.

Figure 157 - Specimen 4: Lateral perspective view (left) and infero-lateral view (right) of the digit with fractured actuating cable.

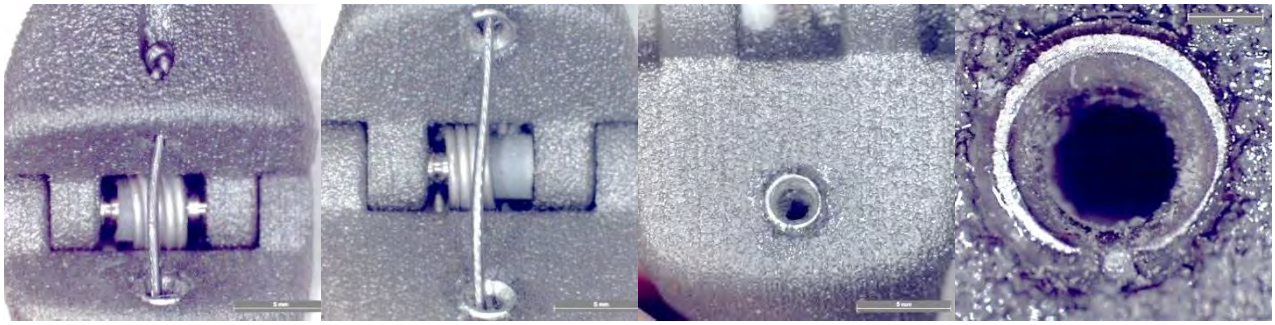

Figure 158 - Specimen 4: DIP joint (left), PIP joint (centre left), MCP channel ring (centre right) with close-up (right) showing minor signs of wear.

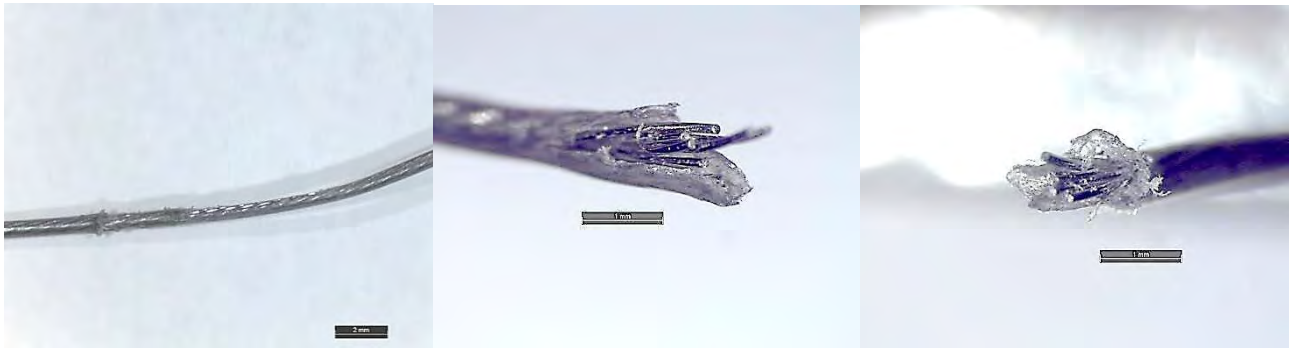

Figure 159 - Specimen 4: Lateral view of the surface wear on the actuating cable at the interface with the distal interphalangeal channel ring (left), with perspective views of the proximal and distal fracture surfaces of the failed cable (centre & right resp.).

Moreover, once the carbon layer is worn away, the stainless steel braid is exposed to the channel rings; leading to a rapid breakdown and eventually fracture of the actuating cable. The breakdown of the carbon coating experienced at the DIP joint is shown in Figure 159 (left), with the proximal and distal fracture surfaces shown in Figure 159 (centre & right).

7.4.5.2. Results for Endurance Testing: Round 2

The configurations for the second round of testing are the same as those outlined in Table 50, except that the stainless steel channel rings are removed and new actuating cables are inserted in place of the old ones. The investigation into the effects of removing the channel rings was deemed necessary due to their apparent influence on the degradation of the actuating wire. Once removed, the mass of each of the specimens was measured prior to testing (see Table 56) and recorded again after testing (see Table 57). A summary of these results (Part A of the second round of endurance testing) is shown in Table 54 below.

Table 54 - Final results for the endurance test specimens: Round 2 (Part A).

	Specimen Number and Description			
	1 Control	**2 Single Layer**	**3 Dual Layer**	**4 Carbon**
Number of cycles	7816	1224	2619	1 200 005 †
Pass/fail	Fail	Fail	Fail	Pass
Failure location	*Mid Length – Prox. Phalanx*	*Mid Length – Prox. Phalanx*	*Mid Length – Prox. Phalanx*	*No Failure*
† - The MCP spring failed at 110,334 & 133,893 cycles, and was replaced both times.				

Referring to Table 54, there is a clear indication that the nitinol wire is failing prematurely, regardless of the channel lining; reaching a maximum of 7816 cycles for the control specimen, 1224 cycles for the single layer specimen and 2619 cycles for the dual layer specimen. Unlike the nitinol, the carbon-coated cable specimen passed the requirements and reached 1,200,005 cycles. In order to see whether there was fault in the manufacture or quality of the nitinol wire, similar medical grade nitinol wire was sourced from a German manufacturer. Two different thicknesses, namely Ø0.31 mm and Ø0.44 mm, were tested to failure on the control sample; these results (Part B of the second round of endurance testing) are shown in Table 55.

Table 55 - Final results for the endurance test specimens: Round 2 (Part B).

	1 – Control Specimen	
Nitinol wire diameter (mm)	Ø 0.31	Ø 0.44
Number of cycles to failure	6480	6989
Pass/fail	Fail	Fail
Failure location	*Mid Length – Prox. Phalanx*	*Mid Length – Prox. Phalanx*

Similar to the previous results, the nitinol did not manage to surpass 8000 loading cycles. Table 56 shows the mass of the specimens prior to testing, whereas Table 57 shows the mass after testing and the difference in mass.

Table 56 - Gravimetric measurements of finger specimens for Round 2 *before* testing. †

Mass Reading (g)	Specimen Number and Description			
	1 Control	2 Single Layer	3 Dual Layer	4 Carbon
1	15.35530	15.94663	15.80399	15.54382
2	15.35531	15.94670	15.80384	15.54365
3	15.35537	15.94666	15.80385	15.54359
Mean	***15.35533***	***15.94666***	***15.80390***	***15.54369***

† - These measurements exclude the mass of the actuating wire & the channel rings, and are made in accordance with ASTM F2025 (2000).

Table 57 - Gravimetric measurements of finger specimens for Round 2 *after* testing. ††

Mass Reading (g)	Specimen Number and Description			
	1 Control	2 Single Layer	3 Dual Layer	4 Carbon
1	15.35237	15.94502	15.80296	15.54168
2	15.35240	15.94520	15.80305	15.54179
3	15.35230	15.94509	15.80300	15.54171
Mean	***15.35236***	***15.94510***	***15.80301***	***15.54173***
Change in mass (g)	***-0.00297***	***-0.00156***	***-0.00089***	***-0.00196***
Total load cycles	*21 285*	*1 224*	*2 619*	*1 200 005*
Mass loss per cycle (µg)	*0.14*	*1.27*	*0.34*	*$1.63x10^{-3}$*

†† - These measurements exclude the mass of the actuating wire & the channel rings, and are made in accordance with ASTM F2025 (2000).

Referring to Table 57, it can be seen that all the specimens decreased in mass. It should be noted that the total load cycles for each specimen, represents the number of loading cycles the specimen underwent during the second round of testing. More particularly, Specimen 1 experienced loading for both Part A and Part B of the second round of testing (i.e. all loading cycles). When referring to the mass loss per cycle, Specimen 2 experienced the highest rate of wear (1.27 µg/cycle), followed in descending order by Specimen 3 (0.34 µg/cycle), Specimen 1 (0.14 µg/cycle) and Specimen 4 ($1.63x10^{-3}$ µg/cycle) respectively. These results indicate that the single-layer HHS tubing wears at a greater rate than the dual-layer HHS tubing, when contacting nitinol wire. Moreover, the nitinol wire wears the nylon superstructure away at a greater rate than the carbon-coated stainless steel braid. Also, the carbon-on-nylon wore at a rate two orders of magnitude lower than any of the other samples, and can likely be attributed to a carbon layer depositing itself on the contact area with the nylon;

generating an artificial low-friction barrier. This behaviour is ideal for the tendon-channel mechanism and further investigation is recommended.

A description of the wear patterns and failure etiology of each of the specimens will now be described. After testing, the phalanges were split, slightly off-centre, for each specimen and their respective images were taken under a digital microscope at the locations A to H respectively, as seen in Figure 160.

Figure 160 - Inferior view of the split phalanges and image capture locations, A to H, for each of the specimens after Round 2 of endurance testing.

The letters (A to H) in Figure 160, represent a specific view of the phalangeal channel or surface. These views are identified as follows:

A. Distal view of the distal channel surface of the middle phalanx.
B. Proximal view of the distal mid-section of the middle phalanx.
C. Distal view of the proximal mid-section of the middle phalanx.
D. Proximal view of the proximal channel surface of the middle phalanx.
E. Distal view of the distal channel surface of the proximal phalanx.
F. Proximal view of the distal mid-section of the proximal phalanx.
G. Distal view of the proximal mid-section of the proximal phalanx.
H. Proximal view of the proximal channel surface of the proximal phalanx.

Specimen 1: Control

The 0.4 mm nitinol wire of the control specimen failed after 7816 cycles in Part A, at the mid-span of the proximal phalanx. In Part B, the Ø0.31 mm and Ø0.44 mm specimens failed at 6480 and 6989 cycles respectively. Cumulatively, the specimen lost material mass at a rate of 0.14 µg/cycle; the second lowest rate. Referring to Figure 161, the inferior surface of the phalangeal channel in **A** has a slight indentation. Furthermore, this indentation in the nylon can also be seen in the inferior right corner of **D** and **E**. There are no major signs of wear at the mid-sections of the phalanges as seen in **B**, **C**, **F** and **G**. **H** has two deeper grooves at the inferior border of the proximal end of the channel at the MCP joint which was likely formed by one or more of the three different wire samples tested on this specimen. The deep grooves are an indication that the contact forces at this location are at their

highest. Moreover, they coincide with the breaking point of the nitinol wire, which contact the proximal end of these grooves when the digit is at full flexion.

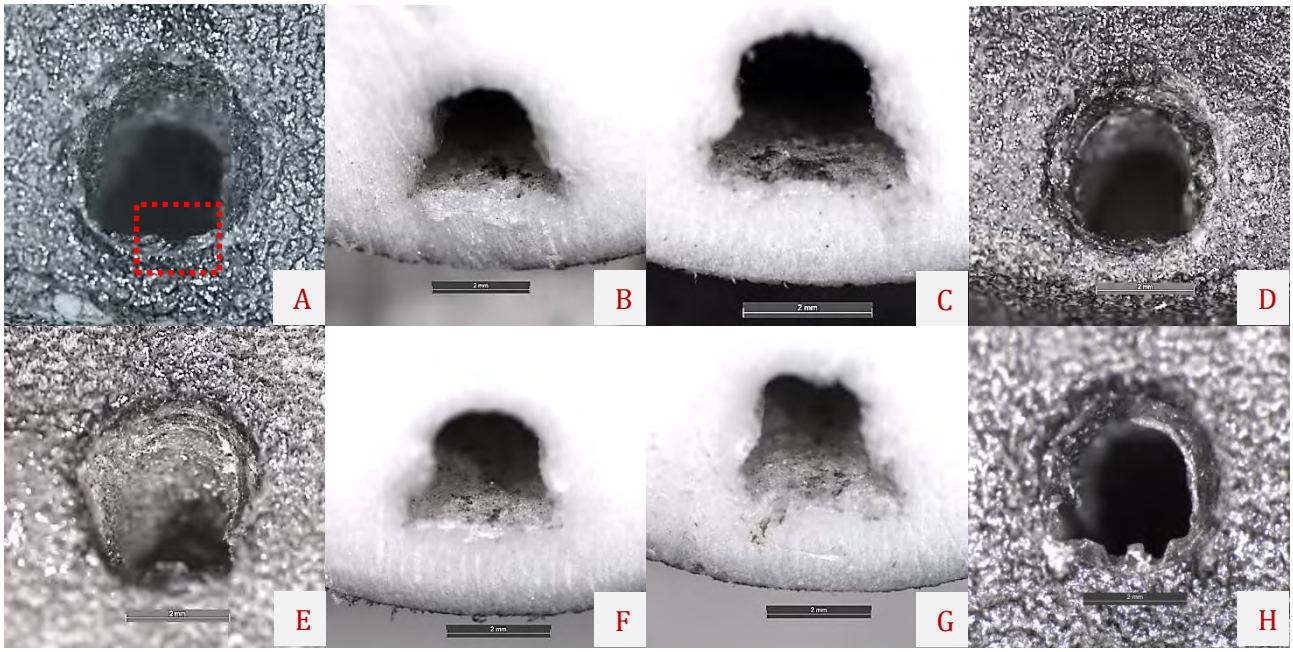

Figure 161 - Close-up views of the phalangeal channels of Specimen 1 after Round 2 of endurance testing.

Specimen 2: Single-layer HHS tubing

The Ø0.4 mm nitinol wire failed after 1224 cycles at the mid-length of the proximal phalanx. There was no significant damage to the nylon structure (**A**, **C**, **D**, **F** & **G**), except for a slight rounded indentation at

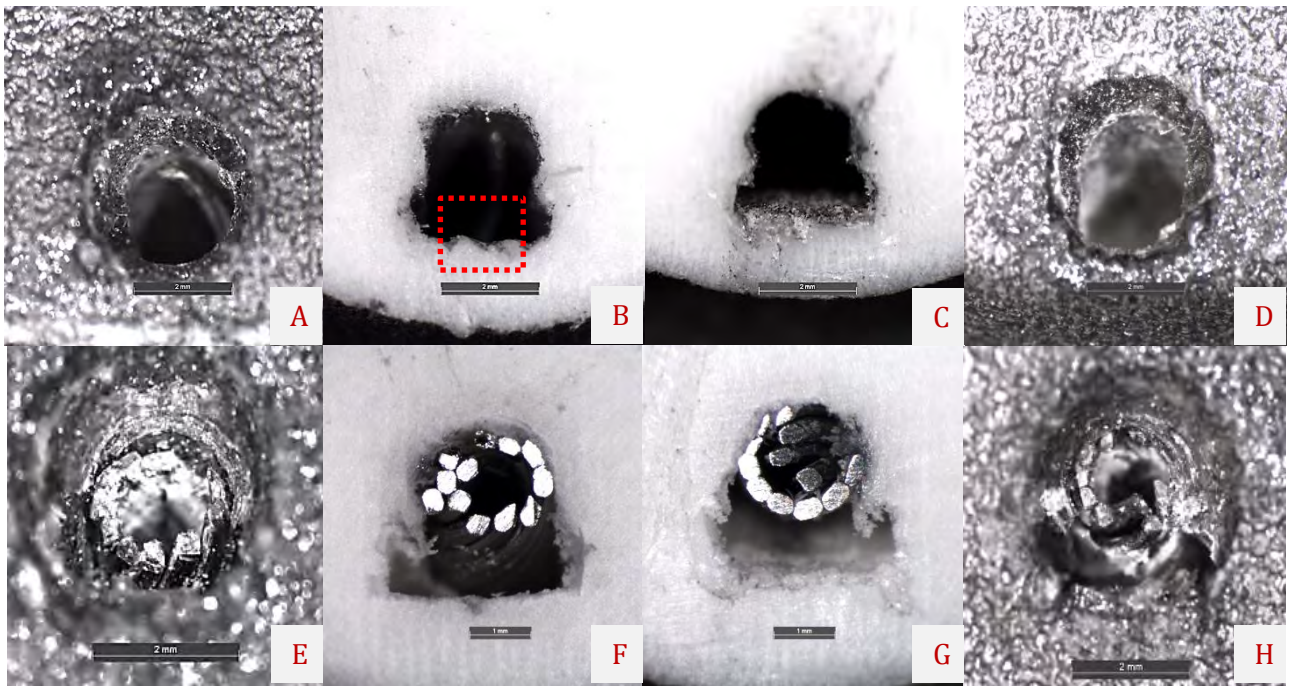

Figure 162 - Close-up view of the phalangeal channels of Specimen 2 after Round 2 of endurance testing.

the mid-section of the middle phalanx as seen in Figure 162 **B**; its shape matching the round outer surface of the tubing. Furthermore, the single-layer HHS tubing did not evoke signs of wear damage as seen in **E**, **F** and **G**. Referring to the inferior right corner of the HHS tubing in **H**, a sharp V-like crevasse created by the HHS can be seen, and is likely the cause of the failure of the nitinol wire. Again, its location at the proximal MCP joint makes it an ideal stress-raiser which coincides with the breaking point of the nitinol wire while the digit is at full-flexion.

Specimen 3: Dual-layer HHS tubing

The dual-layer HHS tubing specimen lasted a mere 2619 cycles. Failure of the nitinol wire occurred at the mid-span of the proximal phalanx, similar to specimens 2 and 3. The strands of the HHS tubing did not remain well-aligned as seen in **B**, **E**, **F** and **G** (Figure 163). Wear was minimal at **A** and **D,** whereas **C** displayed minor signs of wear at its inferior surface, coinciding with the mid-span of the middle phalanx. Major wear was exhibited at **H** as highlighted in Figure 164. This groove was the probable cause of the fracture of the nitinol wire which brushed against it during flexion of the digit.

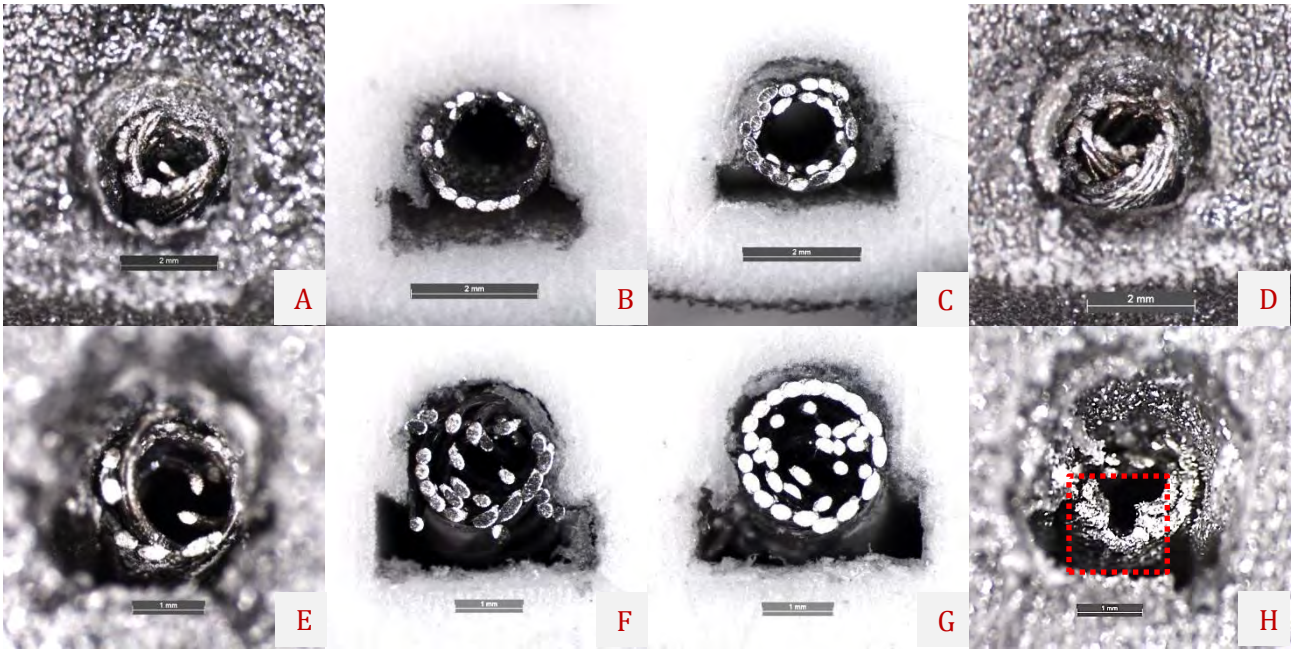

Figure 163 - Close-up view of the phalangeal channels of Specimen 3 after Round 2 of endurance testing.

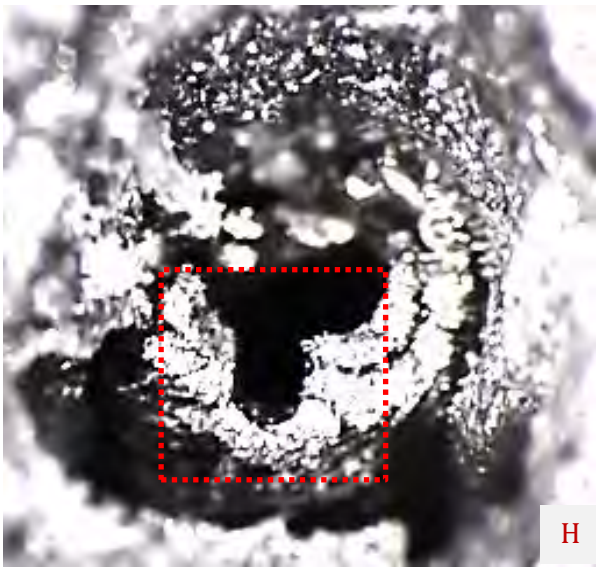

Figure 164 - Enlarged view of the wear of the dual-layer HHS tubing at the proximal end of the proximal phalangeal channel.

Specimen 4: Carbon Coated Stainless Steel Braided-Wire

Specimen 4 surpassed the requirements, reaching 1,200,005 cycles before it was stopped. Furthermore, it experienced the lowest rate of material loss at 1.63×10^{-3} µg/cycle and displayed minimal amounts of plastic flow in the nylon superstructure. Referring to the phalangeal channels of Figure 165, **A** showed no signs of wear inferiorly yet did on its superior border. Furthermore, **B** and **F** exhibited an indented groove on their inferior right lateral surface (also shown in Figure 166, centre and right respectively), whereas **C** and **G**, the proximal sides of the mid-sections, did not. This is indicative that contact pressures between the wire and nylon are greatest on the distal portion of the

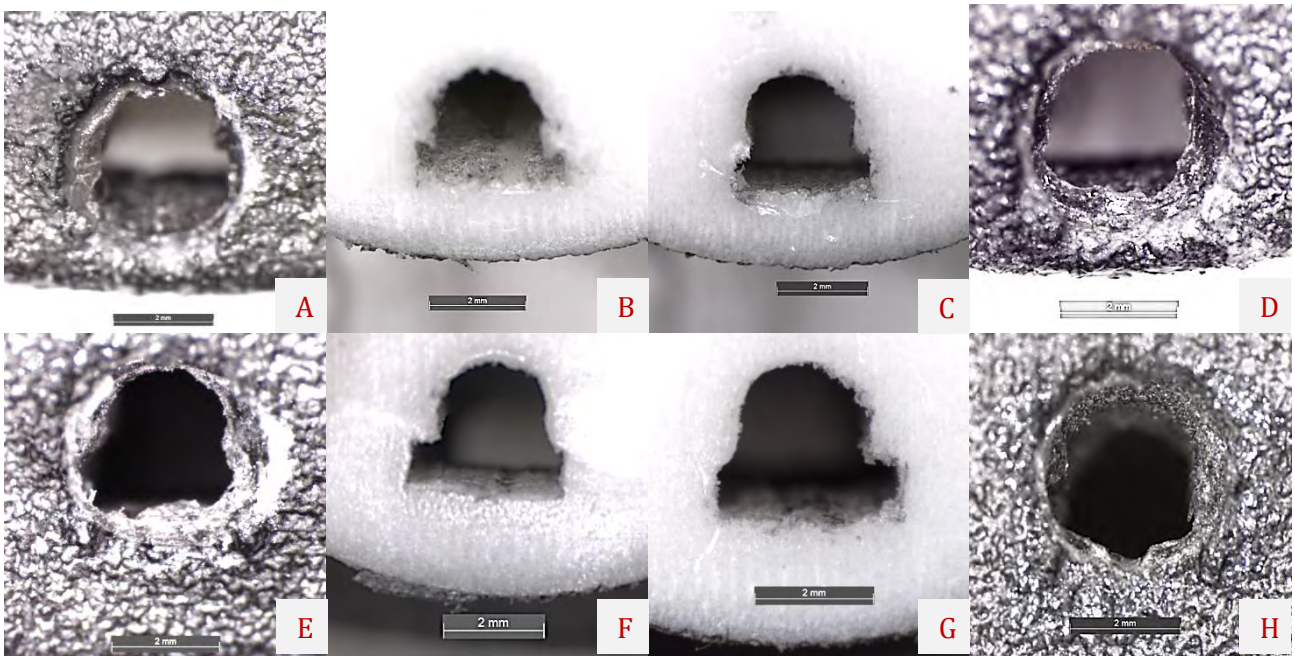

Figure 165 - Close-up view of the phalangeal channels of Specimen 4 after Round 2 of endurance testing.

internal channel, during loading of the digit (flexion). **D**, **E** and **H** all showed signs of deformation at their inferior borders, the most prominent of which was at the MCP joint of **H.** The distal seating surface of the distal phalanx (Figure 166, left) showed no signs of wear from the knot of the actuating cable. Moreover, the knot itself behaved similarly showing no signs of abrasion as shown in Figure 167 (top left). The actuating cable showed no signs of wear at the DIP joint, yet did at the PIP joint (Figure 167, centre) and at the cable coinciding with the mid-proximal phalanx (Figure 167, right). An unworn

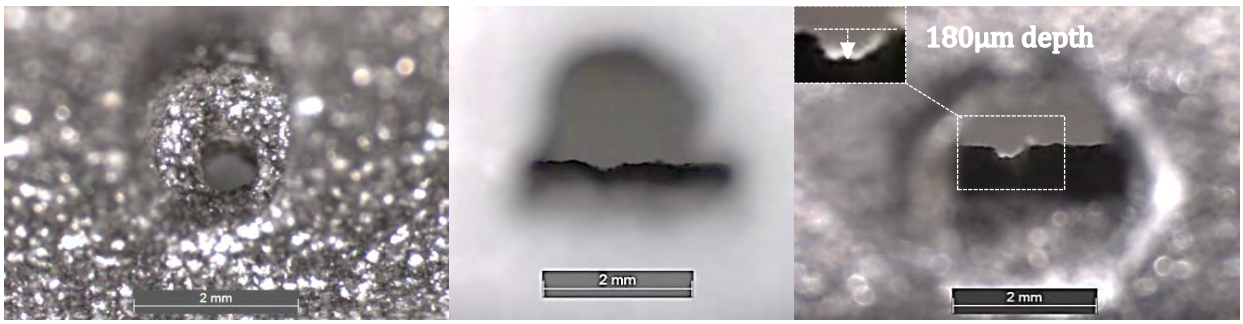

Figure 166 - Close-up view of distal phalanx seat for the wire knot (left), indentation at the centre arch of the middle phalanx (centre) and the 180µm wear-indentation at centre arch of the proximal phalanx (right).

piece of the actuating cable is shown, at a similar resolution to the other figures, for comparison (Figure 167, bottom left). Minor signs of surface wear at the interface with the MCP pin were observed (Figure 168).

Figure 167 - End knot of actuating cable (top left), an unstressed cable section for comparison (bottom left), kinked wire at PIP joint (top centre) with close-up (bottom centre), and worn coating at mid-prox. phalanx (top right) with close-up (bottom right).

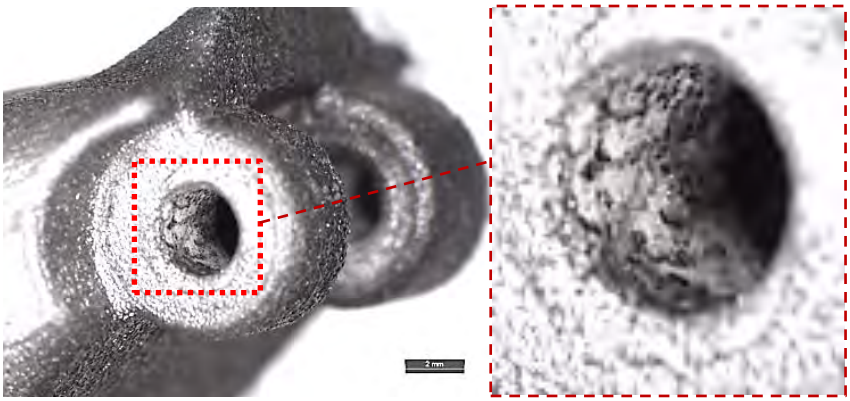

Figure 168 - Minor surface wear at MCP pin interface (centre) with close-up.

When considering the distance of relative travel of the carbon-braid on the nylon surface, the rate of abrasion wear can be inferred and compared to data obtained through standard test methods in the EOS PA2200 nylon material datasheet as seen in Figure 169. In specimen 4's particular test case, the actuating cable travelled 30 mm during flexion and 30 mm during extension, generating 60 mm of relative motion with the nylon material of the phalanx during each cycle. Consequently, 60 mm x 1,200,000 cycles = 72 km of relative motion/sliding distance.

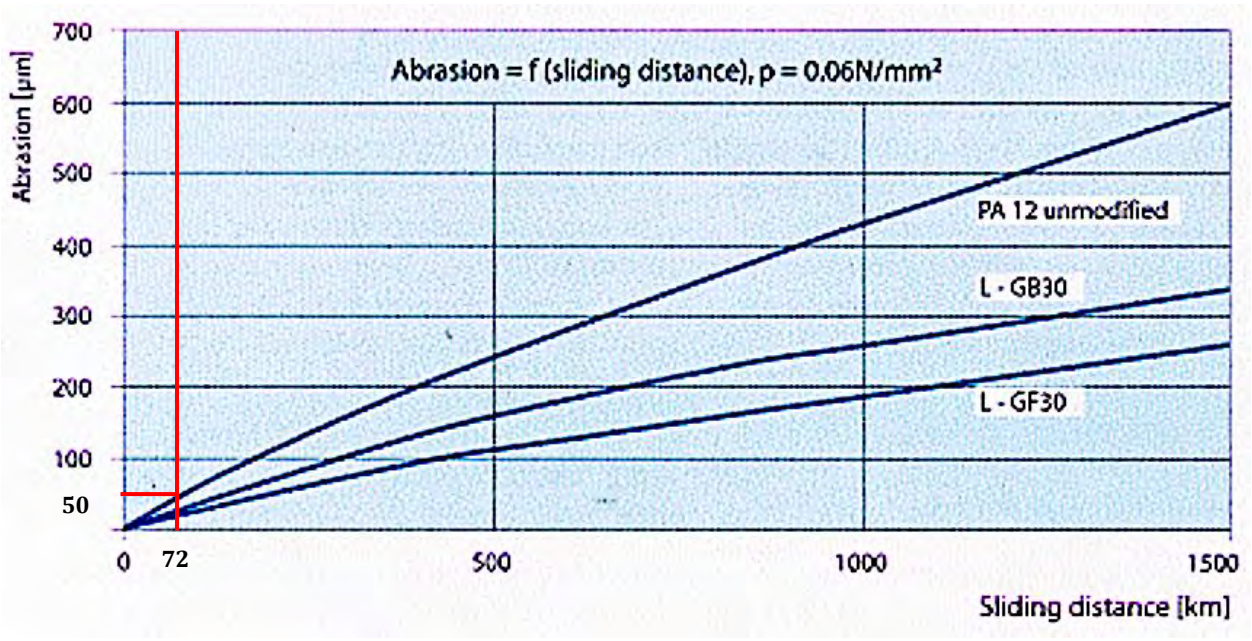

Figure 169 - Abrasion on bearing as function of the sliding distance and PA12-modification (L-GB30/glass spheres; L-GF30-glass fibres) from PA2200 Datasheet (EOS, 2004).

According to Figure 169, at a standard contact pressure of 0.06 MPa, the cable should have worn to a depth of approximately 50 µm. However, the maximum measured depth of wear at the proximal end of the proximal phalangeal channel was 180 µm (Figure 166); exceeding the amount specified. This increased wear is likely attributed to increased thermal effects or contact pressure between the cable and the nylon (i.e. greater than 60 kPa).

The mechanical response of the design has been analysed and surpassed the requirements. Consequently, the assembled prototype of the hand prosthesis was used in Experiment 5 to obtain feedback from patients and their prosthetist.

7.5. Experiment 5 – The Patient Experience

7.5.1. Background

While qualitative and quantitative analysis of the mechanical design of the hand is important in determining whether the performance outcomes of the hand were met, the final test in determining whether the prosthesis has met its goals is decided by the user. Patient feedback is therefore necessary as it will aid in the generation of a successful prosthesis.

7.5.2. Aim

To determine user satisfaction and obtain critical feedback from patients and the prosthetist with regard to the hand prosthesis.

7.5.3. Apparatus

The apparatus used in this experiment is a fully-assembled hand prosthesis and a shoulder harness for actuation. All patient interactions were performed by a qualified prosthetist.

7.5.4. Methodology

Prior to any investigation, local ethics committee approval of the study was obtained and can be referred to in Appendix E2, p. E-5. Two participants were informed of the experimental protocol and were provided with a Prosthetic Hand Evaluation Questionnaire (PHEQ); which can be referred to in Appendix F, p. F-2. They were also asked to provide their written consent to participate voluntarily. The apparatus was given to a qualified prosthetist who ensured that the device was fitted correctly and would see to the needs of the patients during the trial period. He also provided the link between the patients and the researcher. Whilst initial plans were to provide each patient with the prosthesis for a one week trial after which they were to complete the PHEQ, time and cost limitations as well as unforeseen patient difficulties led to a reduced study; the details and feedback gathered from the prosthetist is explained in the ensuing section.

7.5.5. Experimental findings

7.5.5.1. Patient experience and difficulties

During the four week allotment to patient studies, numerous difficulties were experienced. Two consenting patients were contacted by the prosthetist during the trial period. The first was a middle-aged male who had concerns regarding the colour of the prosthesis, and did not want to participate.

The second patient was a younger male, and although he was a left-handed amputee, he was still willing to try the right-handed prosthesis and give some valuable feedback. The patient was able to easily grasp uniform and non-uniform objects in various power grasps, yet had difficulty grasping smaller objects which required more precise control. It was mentioned that given more time, his ability would improve once getting a feel for the hand. Furthermore, the patient enjoyed the low force needed to actuate the prosthesis, as it required minimal effort on his part. He also mentioned that he would be willing to test it for a longer duration had it been left-handed.

Due to the time restrictions, a third patient who was a right-handed transradial amputee could not be contacted in time. Consequently, feedback from the prosthetist will be used to recommend preliminary alterations to the design, after which patient testing will resume at a later stage.

7.5.5.2. Comments by the Prosthetist

After consulting with the prosthetist during the preliminary design stages and again prior to manufacture with the final CAD design, some comments were made (prior to and after patient testing) with regard to the manufactured prototype of the prosthesis. The summarised feedback is divided into comments regarding the aesthetics and those relating to functionality, and are listed in Table 58 and Table 59 respectively as follows:

Table 58 - Prosthetist feedback regarding aesthetics.

Positive feedback	Recommended alterations
The proportions, lines and shape of the palmar structure are acceptable and look good.	Shorten the length of the proximal digits. Although they are anthropometric, patients psychologically perceive the non-natural hand to be larger than it actually is.
The central exit location of the actuating cable through the wrist stem of the prosthesis (which is usually exits dorsally in other prostheses), allows the cable to travel through the patient's socket, instead of on-top of it, exiting higher up the arm. This allows the user to hide the cable and give a better look to the hand.	Adjust the initial rest position of the digits to mimic the resting position of the natural hand.
The customisation to each patient such as size, proportion, embossing and engraving through additive manufacturing is beneficial.	Add a convex surface onto the dorsal surface of the proximal phalanges for "flow".
	Investigate different colours for the hand, or perhaps a glove.

Table 59 - Prosthetist feedback regarding functionality.

Positive feedback	Recommended alterations
The hand is lightweight and requires very low actuation force compared to other hands.	The closing trajectory of the first three digits should be adjusted to allow repeatable pinch grasps.
The release button of the ratchet mechanism provides good resistance and is easy to engage and disengage.	A PTFE or low-friction lining should be inserted into hole in the wrist stem, where the primary input-cable enters the prosthesis to prevent wear.
The conformability of the hand's digits to regular and irregularly shaped objects is very good.	Reduce the rotation positions of the thumb swivel to three instead of five. Namely, lateral grasp, index-finger pinch, and tripod grasp. This was suggested to reduce the choices a patient has and thus the cognitive effort.
The stem easily fits onto standard wrist units, and requires only a single attachment for the hand and the actuating cable in the distal portion of the patient's socket, due to their coinciding central location.	Alter the shape of the thumb's distal phalanx to be more convex to allow normal contact interaction with the grasped objects at various points throughout the closing trajectory.
	As expected, the prosthesis does not provide sufficient extensive force to extend the hand and the shoulder harness due to the harnesses own inherent internal friction. An external spring mechanism to overcome harness friction should be included by the prosthetist (i.e. a self-sufficient harness should be made or designed).
	Future myoelectric versions could use a low-cost linear-potentiometer in tandem with a harness, instead of costly surface electrodes to trigger a motor's flex-extend command.

7.5.6. Discussion of findings

Due to the limited time and number of patients, a PHEQ could not be completed in time and will not be included in this investigation. Feedback from the two patients, although limited, indicated that the older patient was less willing to try a hand that does not fulfil his aesthetic needs; choosing form over functionality. The younger patient, although willing, was unable to complete the trial due to his incompatibility to the prototype. However, his feedback showed that the required actuation force was perceived to be very low for him, and the conformability of the grasps was good. Limitations in precision grasps show that refinement may be necessary. Consequently, it is recommended that the feedback received from the patients and the prosthetist be used to refine the design, prior to further patient testing procedures.

8

CHAPTER 8: DISCUSSIONS

Using information obtained through the literature review in Chapter 2, p. 3, the conceptualisation, analysis, design, manufacture, and formulation of experimental procedures for the hand prosthesis was performed. Twenty-two concept solutions for the mechanisms of the prosthesis were conceptualised, of which seven final designs solutions were selected based on their advantages and disadvantages, as well as through a quantitative assessment measure using DSM's. These solutions were discussed in Chapter 3, p. 50, and summarised in the Morphological Chart shown in Table 33, p. 68.

Based on the concepts, design calculations for the kinematics and kinetics of the hand were evaluated through the use of an analytical model. Utilising the geometrical properties of the hand, spring deflections, actuating cable input forces, internal reaction forces and system friction, in combination with grasping forces, the model was iteratively built up and analysed as discussed in Section 4.1, p. 69. The key findings and the response of the system moments can be referred to in Section 4.1.3, p. 81. When compared to the performance of other VC devices, the hand matched the efficiency of the TRS hook; the most efficient of the VC devices. While its theoretically behaviour responded soundly, experimental testing procedures on the hand prosthesis are advisable to verify and validate the response of this model.

Spring calculations in Section 4.2, p. 96, indicate that the springs used in the thumb-swivel locking mechanism exert a total clamping force of 8.44 N and have a design factor exceeding 2. Furthermore, the shear strength of the thumb locking-plate far outweighs the stresses it experiences. The spring used in the pawl-engagement mechanism is designed to allow disengagement of the ratchet mechanism at a push force of 10 N; requiring a maximum of 20 N when the bayonet button is fully depressed. The magnitude of the initial force is specified as such to prevent involuntary disengagement of the mechanism and unforeseen opening the hand. Lastly, calculations for the respective interphalangeal torsion springs are disclosed in Table B1 and Table B2 on pages B-7 & B-8

respectively. These moments were calculated to not only to provide adequate extensive strength, but also to withstand repeatable loading until infinite life.

Once satisfied that the mechanisms of the hand responded as theoretically necessitated, the final mechanical design of the hand was completed, as shown in Chapter 5, p. 102. For reasons relating to patentability and the intellectual property, manufacturer's drawings for the manufactured parts will not be disclosed. Key specifications of the design, manufacturing techniques and the assembly of the prototype are revealed in Chapter 6, p. 123. The mass of the fully-assembled prototype was 237 g; lighter than other comparable devices which weighed between 248 g and 423 g.

With reference to Appendix D (p. D-1), the cost of the "one-off" prosthesis was R 11,628.37. This price is comparable to that of other mechanical VC hands (as mentioned in Section 2.4, p.12), includes the cost of assembly and a single maintenance service (to be performed annually or biannually depending on usage), and is below the cost limit of R18,000 specified by Rossouw (2013). The total cost may however be reduced when commercialising, through the use of larger production runs, lean manufacturing techniques and process optimisation.

Experimental procedures outlined in Section 7.1, p. 140, showed that the prosthesis achieved numerous grasps including medium wrap, power sphere, lateral pinch, index finger extension, tripod, thumb-3 finger (tip grasp) and precision sphere. Limitations experienced by the current configuration included a lack of control of the closing trajectory making precision pinch grasps challenging; especially the tripod grasp or index-finger pinch. Pros were good grasp conformability, low actuation forces and secure grip using the locking mechanism.

With reference to Appendix C, FEA revealed that the 3rd and 5th digit are able to withstand lateral loads on their distal phalanges of up to 100 N (@ δ = 10.2 mm) and 72 N (@ δ = 6.98 mm) respectively, before failing at their PIP joint. Similarly, in hyperextension they reached loads of 82 N (@ δ = 22.3 mm) and 55.8 N (@ δ = 13.9 mm), with regions of highest stress located at the inner pin-holes of the PIP joint and posterior protrusion of the MCP joint respectively. Experimental procedures outlined in Section 7.2 (p. 143) in accordance with ISO 178 (2010) & ASTM D790 (2003), indicated lateral failure of these digits at 92.2 N (@ δ = 28.7 mm) and 64.6 N (@ δ = 23 mm), both failing catastrophically at their PIP joints. In hyperextension the 3rd and 5th digits underwent 52.7 N (@ δ = 34.3 mm) and 47.3 N (@ δ = 35.7 mm) respectively, before bottoming out on the base of the test rig.

The FEA model behaved stiffer than the experimental model; reasons for the deviation included the presence of system slack in the experimental system as well as material non-linearities, plasticity and thermal effects. Possible FEA errors include modelling with simplifying assumptions, discretisation errors, truncation errors and numerical solution errors due to continuous interpolation between, and

extrapolation from, Gauss points. Overall, the experiments showed that a patient can carry objects with mass exceeding 5 kg on their distal phalanges in hyperextension, and laterally up to ±9 kg and ±6 kg on the 3rd and 5th distal phalanges respectively. Furthermore, it was stated that in reality these loads can be exceeded as patients will generally carry objects on the middle or proximal phalanx; reducing the leverage and thus decreasing the resultant bending stresses.

Tensile testing of the actuating wires and their terminal figure-of-eight knots, as presented in Section 7.3 (p. 153) according to ASTM D6320 (2002), showed that the breaking strength of all specimens reduced between 17.9% and 53.9% from their theoretical tensile strength due to the figure-of-eight knot. Conversely, the yielding strength exceeded the rated loads by 0.7% to 26.2%. Furthermore, as expected, all specimens broke within 5mm of the gripping points outlined in ASTM D6320 (2002) due to the induced stress-raiser of the terminal knot. The correspondence between manufacturer's data and experimental data correlated well, except for the nitinol's UTS values which were significantly lower. This can be attributed to the superelastic nature of nitinol, which only reaches its UTS at necking (i.e. directly proportional to breaking strength).

The endurance/fatigue testing of the phalangeal channels described in Section 7.4 (p. 159) yielded interesting results. On completion of both rounds, only one of the eight specimens surpassed the requirements for infinite life; reaching 1,200,005 cycles without failing. Through the use of visual inspection, gravimetric tests in accordance with ASTM F2025 (2000) and displacement-control guidelines from ISO 14243 (2009), the tests have shown that the HHS tubing and channel rings do not meet the requirements as their structures degrade too rapidly; the effect of which is detrimental to both the nitinol and carbon-coated actuating wires. When comparing the loss of mass of the structures, the overall loss experienced in Round 1 far outweighs that of Round 2; a large contribution of this mass-loss can be accredited to the wear of the channel rings as seen in Figure 164, p. 171. The wear of the nylon channel due to the carbon-coated braid, reached a depth of 180 μm, exceeded the theoretical wear depth of 50 μm. This is indicative that the material is either softer than specified in the manufacturer's material sheet, or the contact pressures were greater than anticipated. Overall the nitinol wire performed poorly in comparison to the carbon-coated stainless steel braid, a factor attributed to its poor flexural fatigue strength. Consequently, the braided wire running directly on the nylon channel is selected as the actuating tendon mechanism of choice.

The patient feedback from Section 7.5 (p. 175) combined with that of the prosthetist showed that refinement can be made to further improve the design. This feedback should be used sagaciously to lessen the gap between the technology and the patient, as well as to increase the confidence prosthetists will have in fitting the device to their patients.

9

CHAPTER 9: CONCLUSIONS

This dissertation has outlined the conceptualisation, design, manufacture, assembly and testing of an affordable anthropomorphic hand prosthesis. The selection of the best-suited concept solutions for the various mechanisms of the hand enabled a functioning design on which the calculations for the prototype were made. Analytical force analysis showed that the required force to close the unloaded hand was 25 N and that the input force of the cable was linearly proportional to the hands grasping forces. Furthermore, the required actuation forces matched those of the TRS hook; the most efficient VC device tested in a recent study. Moreover, it surpassed the performance of all other VC hands in that study; able to transmit a 15 N grasp force with an estimated cable input of 33.4 N; making this efficient force transfer beneficial for future external myoelectric expansion.

The 237 g fully-assembled prototype weighed less than other comparable devices, and was able to perform numerous power and precision grasping configurations used in Activities of Daily Living; with the thumb opposing the fingers within its adjustable adductive or abductive range. The palmar cushion in combination with the ratchet locking mechanism provided sufficient grasping force to maintain all grasps once the tension in the actuating cable was released; requiring a 10 N push force to release it. Furthermore, tensile and compressive testing techniques according ISO 178 (2010) and ASTM D790 (2003) in combination with an FEA investigation, showed that the 3rd and 5th digits could withstand approximately 5 kg of hyperextensive loading on their distal phalanges, and lateral loading of 9 kg and 6 kg on their distal phalanges respectively. In addition to this, the experimental results corresponded well to the predicated fracture locations and breaking forces of the FEA investigation, in spite of the FEA response being more rigid.

Tensile testing according to ASTM D6320 (2002) showed that terminal end-knots reduced the breaking strength of actuating wires between 17.9% and 53.9%. Endurance testing of the phalangeal channels yielded one successful specimen (carbon-coated stainless steel braid running on nylon) which surpassed 1,200,000 loading cycles; indicating infinite life. Patient and prosthetist feedback was obtained and should be used to make improvements to future iterations of the design.

The prototype is a true reflection of the anthropomorphic, anatomical human hand. Furthermore, it is also an accurate representation of the final commercial product. While it is not yet ascertained whether the commercial hand will be injection moulded or produced using additive manufacturing, the latter will allow customisation of colours, textures, patient proportions and individual preferences. Moreover, the internal mechanisms were produced using a combination of standard manufacturing techniques and readily available components.

The final cost of the prototype (one-off unit) was R11,628.37 incl. VAT, giving a good indication that the commercially available prosthetic hand would reach the patient at an affordable price.

10

CHAPTER 10: RECOMMENDATIONS

- Perform experimental procedures to verify and validate the response of the analytical model of the hand specified in Section 4.1, especially with regard to measuring grasping forces versus cable input forces, using a dynamometer or spring scales.
- Increase the statistical significance of the endurance testing of the digits by testing a larger sample the carbon-coated stainless steel braided wire on the nylon channel.
- Investigate alternative channel lining combinations (e.g. UHMWPE tubing with actuating wires such as Dyneema rope, Bowden cables, braided spectra cables and other thicknesses of the carbon-coated stainless steel braid).
- Test the lateral and hyperextensive loading for more specimens to increase statistical significance. Raise the hyperextensive clamping setup to enable the loading of the hyperextensive specimens to failure.
- Increase the sample numbers of the actuating wire specimens for tensile testing. Investigate alternative actuating wires, with high tensile as well as flexural strength. Investigate alternative terminal joining methods for the tendons, to improve strength of joint and ease of assembly. Perhaps laser-welding.
- Investigate a prosthetic glove, silicone-rubber coating or grip pad combinations for the prosthesis.
- Investigate a method to securely attach the springs beneath the palmar cushion.
- Attach the primary actuating cable centrally to the linear bearing, to reduce bending moments on it and increase the design life of the bearing.

- Recommendations by prosthetist and patient:
  - Increase the initial flexion of the digits of the hand to conform to the anatomical rest position.
  - Insert a polyethylene or low friction lining into the wrist stem exit-hole, through which the primary actuating cable travels.
  - Reduce the length of the digits by shortening the proximal phalanges, as patients psychologically perceive the hand prosthesis as being larger than it actually is.
  - Reduce the number of thumb-locking mechanism increments to three positions; namely, lateral grasp, index finger pinch, and tripod pinch.
  - Round the tips of the index finger and thumb, to allow more pinch positions.
  - Investigate the trajectory and the range of motion of the thumb and index finger to increase the precision of pinch grasps.
  - Investigate patient colour preferences and identify manufacturing methods to match these colours with suitable materials.
  - Adjust the camber of the dorsal surfaces of the proximal phalanges, to aesthetically improve the “flow” of the design.

11

CHAPTER 11: REFERENCES

Albright Technologies Inc., 2014. *Types and Properties of Moldable Silicone Rubber.* [Online]
Available at: http://albright1.com/types-and-properties/
[Accessed 23 August 2014].

Alexis, 2012. [Online]
Available at: http://alexisphoenix.org/ballista.php
[Accessed 11 March 2014].

Angerburg, 2010. *Gotz von Berlichingen.* [Online]
Available at: http://angerburg.blogspot.com/2010_07_25_archive.html
[Accessed 12 April 2013].

ASSH, 2013. *American Society for Surgery of the Hand Normal Range of Motion Reference Values.* [Online]
Available at: http://www.assh.org/Public/HandAnatomy/Anatomy/Pages/Normal-Range-Motion.aspx
[Accessed 18 May 2013].

ASTM D6320, 2002. *Standard Test Methods for Single Filament Hose Reinforcing Wire Made from Steel.* West Conshohocken, United States: ASTM International.

ASTM D638, 2003. *ASTM D638-03: Standard Test Method for Tensile Properties of Plastics.* West Conshohocken, PA: ASTM International.

ASTM D790, 2003. *Standard Test Methods for Flexural Properties of Unreinforced and Reinforced Plastics and Electrical Insulating Materials.* West Conshohocken, United States: ASTM International.

ASTM F2025, 2000. *Standard Test Method for Wear Testing of Polymeric Materials Used in Total Joint Prostheses.* West Conshohocken, United States: ASTM International.

ASTM F732, 2000. *Standard Test Method for Wear Testing of Polymeric Materials Used in Total Joint Prostheses.* West Conshohocken, United States: ASTM International.

ASTM G99, 2004. *Standard Test Method for Wear Testing with a Pin-on-Disk Apparatus.* West Conshohocken, United States: ASTM International.

AW Direct, 2013. *Torsion Spring.* [Online]
Available at: http://www.awdirect.com/torsion-spring-2017-2017/gojaks-and-carrier-load-acc/
[Accessed 11 September 2013].

Bacon, T. & McNaught, A., 2011. *Cable Driven Underactuated Prosthetic Hand,* Cape Town: UCT.

Bain, G., Polites, N., Higgs, B. & Heptinstall, R., 1997. *The Functional Range of Motion of the Finger Joints,* Adelaide: Dept. of Orthopaedic Surgery & Trauma, University of Adelaide.

Bao, S., 2000. *Grip Strength and Hand Force Estimation - Technical Report No: 65-1-2000,* Olympia, WA: US Department of Labour and Industries.

Becker Mechanical Hand Co., 2013. *The Imperial Hand.* [Online]
Available at: http://beckermechanicalhand.com/Products.html
[Accessed 18 April 2013].

Belter, J. T., Segil, J., Dollar, A. M. & Weir, R. F., 2011. The Mechanical Design and Performance Specifications of Anthropomorphic Prosthetic Hands. *Journal for Rehabilitation and Research Development,* TBC(TBC), pp. 1-39 TBC.

Belter, J. T., Segil, J., Dollar, A. M. & Weir, R. F., 2013. The Mechanical Design and Performance Specifications of Anthropomorphic Prosthetic Hands: A review. *Journal for Rehabilitation Research & Development (JRRD),* 50(5), pp. 599-618.

Berg, 2013. *Precision Parts.* [Online]
Available at:
http://precisionparts.wmberg.com/images/productCategories/Ratchet%20and%20Pawl.jpg
[Accessed 11 March 2014].

Biddiss, E. & Chau, T., 2007. Upper limb prosthesis use and abandonment: A survey of the last 25 years. *Prosthetics and Orthotics International,* 31(3), pp. 236-257.

Birglen, L., 2006. *AN INTRODUCTION TO THE ANALYSIS OF LINKAGE-DRIVEN COMPLIANT UNDERACTUATED FINGERS.* Philadelphia, ASME IDETC/CIE.

Birglen, L., Laliberté, T. & Gosselin, C., 2008. *Underactuated Robotic Hands.* 1st ed. Berlin: Springer.

Bobjer, O., Johansson, S. E. & Piguet, S., 1993. Friction between hand and handle: Effects of oil and lard on textured and non-textured surfaces; perception of discomfort. *Applied Ergonomics,* 24(3), pp. 190-202.

Boone, D. C. & Azen, S. P., 1979. Normal Range of Motion of Joints in Male Subjects. *Journal of Bone and Joint Surgery,* 61 A(5), pp. 756-759.

Budynas, R. G. & Nisbett, K. J., 2008. Shigley's Mechanical Enginering Design. In: 8th ed. New York: McGraw-Hill.

Budynas, R. G. & Nisbett, K. J., 2008. Shigley's Mechanical Enginering Design. In: 8th ed. New York: McGraw-Hill, pp. 400 - 408.

Burger, H. et al., 2008. Validation of the Orthotics and Prosthetics User Survey Upper Extremity Functional Status Module in People with Unilateral Upper Limb Amputation. *Journal of Rehabilation Medicine,* Volume 40, pp. 393-399.

Carrozza, M. C. et al., 2005. *A Cosmetic Prosthetic Hand with Tendon Driven Under-Actuated Mechanism and Compliant Joints: Ongoing Research and Preliminary Results.* Barcelona, Spain, IEEE, pp. 2661-2666.

Chandra, A., Chandna, P. & Deswal, S., 2011. Analysis of Hand Anthropometric Dimensions of Male Industrial Workers of Haryana State. *International Journal of Engineering (IJE),* 5(3), pp. 242-256.

Coert, J. H., Hoek van Dijke, G. A. H. S. E. R., Snijders, C. J. & Meek, M. F., 2003. Quantifying Thumb Rotation During Circumduction Utilizing a Video Technique. *Journal of Orthopaedic Research,* Volume 21, pp. 1151-1155.

Corin, J. D., Holley, T. M., Hasler, R. A. & Ashman, R. B., 1987. Mechanical Comparison of Terminal Devices. *Clinical Prosthetics and Orthotics,* 11(4), pp. 235-244.

Cutkosky, M., 1989. On Grasp Choice, Grasp Models, and the Design of Hands for Manufacturing Tasks. *Journal of Robotics and Automation,* 5(3), pp. 269-279.

Dalley, S. A., Wiste, T. E., Withrow, T. J. & Goldfarb, M., 2009. Design of a Multifunctional Anthropomorphic. *IEEE/ASME TRANSACTIONS ON MECHATRONICS,* pp. 1 - 8.

Davies, E. J., Friz, B. R. & Clippinger, F. W., 1970. Amputees and their Prostheses. *Artificial Limbs,* 14(2), pp. 19-48.

Dechev, N., Cleghorn, W. L. & Naumann, S., 2001. Multiple finger, passive adaptive grasp prosthetic hand. *Mechanism and Machine Theory,* Volume 36, pp. 1157-1173.

Dempster, W., 1955. *Space requirements of the seated operator,* Ohio: WADC Wright-Patterson Air Force Base.

Deng, K. & Ko, W. H., 1992. A study of static friction between silicon and silicon compounds. *Journal of Micromechanics and Microengineering,* 2(1), p. 14.

DIN 50324, 2007. *Tribology; Testing of friction and wear model test for sliding friction of solids (ball-on-disc system).* Berlin, Germany: DIN Deutsches Institut für Normung e. V..

Drillis, R. & Contini, R., 1966. *Body Segment Parameters (Report 1163-03),* New York: Department of Health, Education and Welfare.

Edgren, C. S., Radwin, R. G. & Irwin, C. B., 2004. Grip force vectors for varying handle diameters and hand sizes. *Human Factors,* 46(2), pp. 244-251.

El-Sherbiny, Y. M., Hasouna, A. T. & Ali, W. Y., 2012. Friction coefficient of rubber sliding against flooring materials. *ARPN Journal of Engineering and Applied Sciences,* 7(1), pp. 121-126.

Engineering Toolbox, 2014. *Friction and Coefficients of Friction.* [Online]
Available at: http://www.engineeringtoolbox.com/friction-coefficients-d_778.html
[Accessed 23 August 2014].

Engineer's Handbook, 2006. *Friction Coefficients.* [Online]
Available at: http://www.engineershandbook.com/Tables/frictioncoefficients.htm
[Accessed 23 August 2014].

Engstrom, B. & Van de Ven, C., 1999. *Therapy for Amputees (ISBN 0443059756).* 3rd ed. London: Churchill Livingstone.

EOS, 2004. *Product Information: Feinpolyamide PA 2200 for EOSINT P,* Munich: EOS GmbH.

EOS, 2014. *Datasheet Comparison: Alumide, PEEK HP3 and PA2200.* [Online]
Available at: http://eos.materialdatacenter.com/eo/material/pdf/datasheet
[Accessed 7 July 2014].

Ertas, A. & Jones, J. C., 1993. Decision Making: Decision Matrices. In: T. VenGraitis, ed. *The Engineering Design Process.* Toronto: John Wiley & Sons, Inc, pp. 73-75.

Euroflex GmbH, 2014. *Material Datasheets - Nitinol Wire Superelastic.* [Online]
Available at:
http://www.euroflex.de/fileadmin/content/PDF/Datenbl%C3%A4tter_NEU_engl/Imagebrosch%C3%

BCre_engl_web.pdf
[Accessed 26 June 2014].

Fort Wayne Metals, 2014. *Nitinol Wire: Super-Elastic Alloys – Mechanical Properties.* [Online]
Available at: http://www.fwmetals.com/nitinol-wire.php
[Accessed 26 June 2014].

Gajdos, L. B., 1967. *Resilient prosthetic foot made from elastic polymers of different hardness.* United States, Patent No. US 3335428 A.

Gee, M. G. et al., 2005. A new friction coefficient measurement system for the frictional component of touch. *Wear,* Volume 259, pp. 1437-1442.

Gill, H., 2011. *Prosthesis Covering.* United States, Patent No. US 2011/0054636 A1.

Gilroy, A., MacPherson, B. & Ross, L., 2008. *Atlas of Anatomy.* 1st ed. USA: Thieme.

Gitter, A. & Bosker, G., 2005. *Upper and Lower Extremity Prosthetics.* 4th ed. Philadelphia: Lippincott-Raven.

Gooderson, C., Knowles, D. & Gooderson, P., 1982. *The Hand Anthrometry of Male and Female Military Personnel.,* Farnborough: APRE Memorandum 82M510.

Gosselin, C., Pelletier, F. & Laliberte, T., 2008. *An Anthropomorphic Underactuated Robotic Hand with 15 Dofs and a Single Actuator.* Pasadena, IEEE.

Harris, B. et al., 2011. Inequities in access to health care in South Africa. *Journal of Public Health Policy,* Volume 32, pp. 102-123.

Heckathorne, C. W., 1992. Upper-limb prosthetics: Components for adult externally powered systems. In: J. H. Bowker, ed. *Atlas of limb prosthetics: Surgical, prosthetic, and rehabilitation principles.* St. Louis: Mosby Year Book.

Higuchi, T. & Harada, M., 2005. *Moveable Finger for Prostheses.* United States, Patent No. 6 896 704 B1.

Hosmer, 2012. *Hook Type Prosthetics.* [Online]
Available at: http://hosmer.com/products/hooks/index.html
[Accessed 16 April 2013].

Hosmer, 2012. *Mechanical Prosthetic Hands.* [Online]
Available at: http://hosmer.com/products/hands/
[Accessed 18 April 2013].

Hume, M. C., Gellman, H., McKellop, H. & Brumfield, R. H., 1990. Functional range of motion of the joints of the hand. *The Journal of Hand Surgery,* 15(2), pp. 240-243.

ICBL, 2012. *ICBL Landmine and Cluster Munition Monitor,* Stockholm: Landmine and Cluster Munition Monitor UNICEF.

IFToMM, 1991. International Federation for the Promotion of Mechanism and Machine Science - Terminology for the Theory of Machines and Mechanisms. *Mechanism and Machine Theory,* 26(5), pp. 435-539.

IKO, 2009. *IKO Needle Roller Bearing Series (CAT 5508),* Japan: Nippon Thompson Co., Ltd..

ISO 13405-1, 1996. *Prosthetics and orthotics - Classification and description of prosthetic components - Part 1: Classification of prosthetic components.* Geneva, Switzerland: International Organisation for Standardisation.

ISO 13405-2, 1996. *Prosthetics and orthotics -- Classification and description of prosthetic components -- Part 2: Description of lower-limb prosthetic components.* Geneva, Switzerland: International Organisation for Standardisation.

ISO 13405-3, 1996. *Prosthetics and orthotics - Classification and description of prosthetic components - Part 3: Description of upper-limb prosthetic components.* Geneva, Switzerland: International Organisation for Standardisation.

ISO 14242, 2012. *Implants for surgery -- Wear of total hip-joint prostheses.* Geneva, Switzerland: International Organisation for Standardisation.

ISO 14243, 2009. *Implants for surgery - Wear of total knee-joint prosthesis.* Geneva, Switzerland: International Organisation for Standardisation.

ISO 178, 2010. *Plastics -- Determination of flexural properties.* Geneva, Switzerland: International Organisation for Standardisation.

ISO 17853, 2011. *Wear of implant materials -- Polymer and metal wear particles -- Isolation and characterization.* Geneva, Switzerland: International Organisation for Standardisation.

ISO 22523, 2006. *External limb prostheses and external orthoses — Requirements and test methods.* Geneva, Switzerland: International Organisation for Standardisation.

ISO 8548-1, 1989. *Prosthetics and orthotics - Limb deficiencies - Part 1: Method of describing limb deficiencies present at birth.* Geneva, Switzerland: International Organisation for Standardisation.

ISO 8548-2, 1993. *Prosthetics and orthotics - Limb deficiencies - Part 2: Method of describing lower limb amputation stumps.* Geneva, Switzerland: International Organisation for Standardisation.

ISO 8548-3, 1993. *Prosthetics and orthotics - Limb deficiencies - Part 3: Method of describing upper limb amputation stumps.* Geneva, Switzerland: International Organisation for Standardisation.

ISO 8548-4, 1998. *Prosthetics and orthotics - Limb deficiencies - Part 4: Description of causal conditions leading to amputation.* Geneva, Switzerland: International Organisation for Standardisation.

ISO 8548-5, 2003. *Prosthetics and orthotics - Limb deficiencies - Part 5: Description of the clinical condition of the person who has had an amputation.* Geneva, Switzerland: International Organisation for Standardisation.

ISO 8549, 1989. *Prosthetics and Orthotics - Vocabulary (ISO/TC168).* Geneva, Switzerland: International Organisation for Standardisation.

ISO, 2014. *ISO/TC 168 - Prosthetics and Orthotics Standards Catalogue.* [Online]
Available at:
http://www.iso.org/iso/home/store/catalogue_tc/catalogue_tc_browse.htm?commid=53630
[Accessed 31 May 2014].

Jang, G., Lee, C., Lee, H. & Choi, Y., 2013. Robotic index finger prosthesis using stackable double 4-BAR mechanisms. *Mechatronics,* 23(3), pp. 318-325.

Kalácska, G., 2013. An engineering approach to dry friction behaviour of numerous engineering plastics with respect to the mechanical properties. *eXPRESS Polymer Letters,* 7(2), pp. 199-210.

Kameda, H., Koyama, J., Morimoto, N. & Masakatsu Sasahara, N., 2006. *Palm Mechanism for Robotic Hand.* United States, Patent No. 7059645 B2.

Kamikawa, Y. & Maeno, T., 2008. *Underactuated Five-Finger Prosthetic Hand Inspired by Grasping Force Distribution of Humans.* Nice, France, IEEE/RSJ.

Kargov, A., Werner, T., Pylatiuk, C. & Schlz, S., 2008. Development of a miniaturised hydraulic actuation system for artificial hands. *Sensors and Actuators,* A(141), pp. 548 - 557.

Kember, P., Ainsworth, L. & Brightman, P., 1981. *A Hand Anthropometric Survey of British Workers,* Cranfield: Ergonomics Laboratory, Cranfield Institute of Technology.

Klaassen, E. L., 2007. *Improving the Surface Friction of Silicone Elastomer Parts.* [Online]
Available at: http://www.emdt.co.uk/article/improving-surface-friction-silicone-elastomer-parts
[Accessed 23 August 2014].

Koganezawa, K. & Ishizuka, Y., 2008. *Novel Mechanism of Artificial Finger using Double Planetary Gear System.* Nice, France, IEEE/RSJ International Conference on Intelligent Robots and Systems.

Kulley, M., 2003. *Brown University History on Hand Prosthetics.* [Online]
Available at:
http://biomed.brown.edu/Courses/BI108/BI108_2003_Groups/Hand_Prosthetics/history.html
[Accessed 12 April 2013].

Kuppuswamy, R. & Redelinghuys, C., 2012. *MEC4055Z Course Notes.* Cape Town: University of Cape Town.

Kurichi, J. E., Bates, B. E. & Stineman, M. G., 2010. Amputation. In: J. Stone & M. Blouin, eds. *International Encyclopedia of Rehabilitation.* New York: Centre for Rehabilitation Research Information and Exchange.

Kyberd, P. et al., 2007. Survey of Upper-Extremity Prosthesis Users in Sweden. *JPO Journal of Prosthetics and Orthotics,* 19(2), pp. 55 - 62.

Lafayette, 1986. *Adult Data for Lafayette Model 78010 Dynamometer,* Indiana, USA: Lafayette.

Laliberté, T. & Gosselin, C., 2003. *Actuation System for Highly Underactuated Gripping Mechanism.* US, Patent No. 6 505 870.

Lapsley, F. M., 2013. *Interest in Bilateral Amputee Patient Needs* [Interview] (8 March 2013).

Lee, S.-J., Kong, Y.-K., Lowe, B. D. & Song, S., 2009. Handle grip span for optimising finger-specific force capability as a function of hand size. *Ergonomics,* 52(5), pp. 601-608.

Legro, M. W. et al., 1998. Prosthesis evaluation questionnaire for persons with lower limb amputations: assessing prosthesis-related quality of life. *Archives of Physical Medicine and Rehabilitation,* 79(8), pp. 931-938.

Light, C., Chappell, P. & Kyberd, P., 2002. Establishing a Standardized Clinical Assessment Tool of Pathologic and Prosthetic Hand Function: Normative Data, Reliability, and Validity. *Archives of Physical Medicine and Rehabilitation,* 83(6), pp. 776-783.

Lowe, W., 2006. *Orthopaedic Assessment in Massage Therapy.* 1st ed. Salem: Daviau Scott.

Luo, M., Mei, T., Wang, X. & Yu, Y., 2004. *Grasp characteristics of an underactuated robot hand.* New Orleans, LA, USA, IEEE International Conference on Robotics and Automation, pp. 2236-2241.

Martin, E., Desbiens, A. L., Laliberte, T. & Gosselin, C., 2001. *SARAH Hand Used for Space Operations on STVF Robot.* Genoa, Italy, Intelligent Manipulation and Grasping.

Matweb, 2014. *Material Property Data.* [Online]
Available at:
http://www.matweb.com/search/DataSheet.aspx?MatGUID=a2d0107bf958442e9f8db6dc9933fe31
[Accessed 7 July 2014].

McNaught, A. M., 2009. *Market Research into Upper Limb Prosthetics in South Africa,* Cape Town: UCT.

Meanley, S., 1995. Different Approaches and Cultural Considerations in Third World prosthetics.. *Prosthetics and Orthotics International,* Volume 19, pp. 176-180.

Monestier, J., 1987. *Total Hand Prostheses.* United States, Patent No. 4685929.

Monod, H., 1985. Contractility of muscle during prolonged static and repetitive dynamic activity. *Ergonomics,* 28(1), pp. 81-89.

Napier, J., 1956. The Prehensile Movements of the Human Hand. *The Journal of Bone and Joint Surgery,* 38 B(4), pp. 902-913.

Nel, O., 2013. *Interview at Western Cape Prosthetics Centre, Pinelands.* [Interview] (8 March 2013).

NLLIC, 2008. *Amputation Statistics by Cause - Limb Loss in the United States 1988 - 1996,* Knoxville: Amputee Coalition.

Otto Bock®, 2013. *Arm Prosthetics Otto Bock HealthCare GmbH.* [Online]
Available at: http://www.ottobock.com/cps/rde/xchg/ob_com_en/hs.xsl/3170.html
[Accessed 01 April 2013].

Otto Bock®, 2013. *German Design Award.* [Online]
Available at: http://www.ottobock.com/cps/rde/xchg/ob_com_en/hs.xsl/49809.html
[Accessed 3 May 2013].

Paik, J., Shin, B., Bang, Y. & Shim, Y., 2012. Development of an Anthropomorphic Robotic Arm and Hand for Interactive Humanoids. *Bionic Engineering,* 9(2), pp. 133-142.

Peebles, L. & Norris, B., 1998. *ADULTDATA. The Handbook of Adult Anthropometric and Strength Measurements: Data for Design Safety..* 1st ed. London: Department of Trade and Industry.

Pheasant, S. & Haslegrave, C., 2006. *Bodyspace - Anthropometry, Ergonomics and the Design of Work.* 3rd ed. Boca Raton: Taylor & Francis.

Pinson, G., 1981. *Digitally-Controlled Artificial Hand.* United States, Patent No. 4 246 661.

PolyOne, 2014. *PolyOne GLS Thermoplastic Elastomers - Understanding Hardness.* [Online]
Available at: http://www.glstpes.com/resources_technical_hardness.php
[Accessed 27 August 2014].

Prosthetic Research Study, 2006. *Prostethic Evaluation Questionnaire (PEQ).* [Online]
Available at: http://www.prs-research.org/htmPages/PEQ.html
[Accessed 7 July 2014].

Prosthetics Research Study, 1998. *Prosthesis Evaluation Questionnaire (PEQ).* [Online]
Available at: http://www.prs-research.org/Texts/PEQ_A4.pdf
[Accessed 2 April 2014].

Pylatiuk, C., Schultz, S. & Doderlein, L., 2007. Results of an Internet survey of myoelectric prothetic hand users. *Prosthetics and Orthotics International,* 31(4), pp. 362-370.

Pylatiuk, C., Schulz, S. & Kargov, A. a. B. G., 2004. Two Multiarticulated Hydraulic Hand Prostheses. *Artificial Organs,* 28(11), pp. 980-986.

RealLifeSkin , 2012. *Hand, Arm, & Finger Prosthetics.* [Online]
Available at: http://www.reallifeskin.com/hands-a-arms.html
[Accessed 03 April 2013].

Rice, M. S., Leonard, C. & Carter, M., 1998. Grip strengths and required forces in accessing everyday containers in a normal population. *The American Journal of Occupational Therapy ,* 52(8), pp. 621-626.

Richards, J., 2008. *Biomechanics in Clinic and Research.* 1st ed. Philadelphia: Churchill-Livingston Elsevier.

RoMeLa, 2010. *RAPHaEL: Robotic Air Powered Hand with Elastic Ligaments.* [Online]
Available at:
http://www.romela.org/main/RAPHaEL:_Robotic_Air_Powered_Hand_with_Elastic_Ligaments
[Accessed 18 April 2013].

Rossouw, E., 2013. *Melkbosstrand Prosthetist - Viability of Prosthetic Hand and Patient Needs in South Africa* [Interview] (15 March 2013).

Rothenhofer, G., 2009. *Linkages.* [Online]
Available at: www.web.mit.edu/2.75/resources/random/Linkages.ppt
[Accessed 7 May 2013].

RSL Steeper, 2012. *Mechanical / Spring Operated Hands.* [Online]
Available at:
http://rslsteeper.com/products/prosthetics/products/upper_limb/mechanical/hands_select_mechanical_spring_operated
[Accessed 18 April 2013].

RSL Steeper, 2013. *Bebionic 3.* [Online]
Available at: http://bebionic.com/the_hand
[Accessed 3 May 2013].

Smit, G., Bongers, R. M., Van der Sluis, C. K. & Plettenburg, D. H., 2012. Efficiency of voluntary opening hand and hook prosthetic devices: 24 years of development?. *Journal of Rehabilitation Research and Development,* 49(4), pp. 523-534.

Smit, G. & Plettenburg, D. H., 2010. Efficiency of Voluntary Closing Hand and Hook Prostheses. *Prosthetics and Orthotics International,* 34(4), pp. 411-427.

Smithsonian, 2012. *Inventing Ourselves.* [Online]
Available at: http://invention.smithsonian.org/centerpieces/inventingourselves/pop-ups/01-03.htm
[Accessed 20 April 2013].

Sollerman, C. & Ejeskar, A., 1995. Sollerman hand function test. A standardised method and its use in tetraplegic patients. *Scand J Plast Reconstr Surg Hand Surg,* Volume 29, pp. 167-176.

Statistics SA, 2010. *General Household Survey (pp. 19).* [Online]
Available at: http://indicators.hst.org.za/indicators/StatsSA/GHS_P0318June2010_revised.pdf
[Accessed 13 April 2013].

Statistics South Africa, 2001. *Prevalence of Disability in South Africa Report No. 03-02-44 (Census 2001),* Pretoria: Stats SA.

Strait, E., 2006. *Prosthetics in Developing Countries.* [Online]
Available at: http://www.oandp.org/publications/resident/pdf/DevelopingCountries.pdf
[Accessed 23 April 2013].

Strandring, S., 2008. *Gray's Anatomy - Anatomical Basis of Clinical Understanding.* 40th ed. London: Churchill Livingstone Elsevier.

Stratasys, 2013. *ABS-M30i - Medical Grade.* [Online]
Available at: http://www.stratasys.com/~/media/Main/Secure/Material%20Specs%20MS/Fortus-Material-Specs/Fortus-MS-M30i-01-13-web.pdf
[Accessed 7 July 2014].

Taylor, C. L., 1954. The biomechanics of the normal and of the amputated upper extremity. In: P. E. Klopsteg & P. D. Wilson, eds. *Human limbs and their substitutes.* New York: McGraw-Hill, pp. 169-221.

Tomlinson, S. E., Lewis, R. & Carre, M. J., 2007. *Review of the frictional properties of finger–object contact when gripping.* Sheffield, IMechE.

Touch Bionics, 2013. *i-limb ultra.* [Online]
Available at: http://www.touchbionics.com/products/active-prostheses/i-limb-ultra/
[Accessed 3 May 2013].

Tribology, 2014. *Coefficient of friction, rolling resistance and aerodynamics.* [Online]
Available at: http://www.tribology-abc.com/abc/cof.htm
[Accessed 23 August 2014].

UKLLIC, 2013. *The UK Limb Loss Information Centre 2003/2004 Referrals.* [Online]
Available at: http://limblossinformationcentre.com/rehabilitation/amputation/20032004-referrals/
[Accessed 14 April 2013].

Uygur, M., de Freitas, P. & Jaric, S., 2010. Frictional properties of different hand skin areas and grasping techniques. *Ergonomics,* 53(6), pp. 812-817.

Van Lunteren, T. & Van Lunteren-Gerritsen, E., 1997. In search of design specifications for arm prostheses. In: H. G. Stassen, T. B. Sheridan & T. Van Lunteren, eds. *Perspectives on the human controller: Essays in honor of Henk G. Stassen.* Boca Raton (FL): CRC Press.

Veatch, B., 2011. *Prosthetic Split Hook Terminal Device with adjustable pinch force, functional grasping contours and illumination.* United States, Patent No. 8 052 761.

Veijgen, N. K., 2013. *Skin friction: A novel approach to measuring in vivo human skin,* Enschede: University of Twente.

Vicatos, G., 2013. *Discussion of human anatomy and physiology* [Interview] (25 June 2013).

Vinet, R., Lozac'h, Y., Beaudry, N. & Drouin, G., 1995. Design methodology for a multifunctional hand prosthesis. *Journal of Rehabilitation Research and Development,* 32(4), pp. 316-324.

Weir, R. F., 2004. Design of Artificial Arms and Hands for Prosthetic Applications. In: M. Kutz, ed. *Standard Handbook of Biomedical Engineering and Design.* New York: McGraw-Hill, pp. 32.1-32.59.

Zhang, W. et al., 2009. Super under-actuated multi-fingered mechanical hand with modular self-adaptive gear-rack mechanism. *Industrial Robot: An International Journal,* 36(3), pp. 255-262.

Zheng, J., De La Rosa, S. & Dollar, A., 2011. *An Investigation of Grasp Type and Frequency in Daily Household and Machine Shop Tasks.* Shanghai, IEEE International.

Ziegler-Graham, K. et al., 2008. Estimating the Prevalence of Limb Loss in the United States: 2005 to 2050. *Arch Phys Med Rehabil,* Volume 89, pp. 422-429.

APPENDIX A - DESIGN OF EXPERIMENTS

A1 – Design of Pneumatic Fatigue Setup

A1.1. Aim

To design a setup capable of repeatedly loading the digits to 1,200,000 cycles; through linear actuation of the actuating cable/tendon.

A1.2. Conceptualisation and requirement of design solution

Three concepts solutions were thought of before continuing on to a final design solution. The solutions must be able to generate repeated linear displacement cycles with 30 mm amplitude, at a cyclic frequency of 2 Hz ± 0.2 Hz. Furthermore, a system to count the number of cycles and cool the specimens is required.

CONCEPT 1 – Rotating disc with linear spring slot actuator

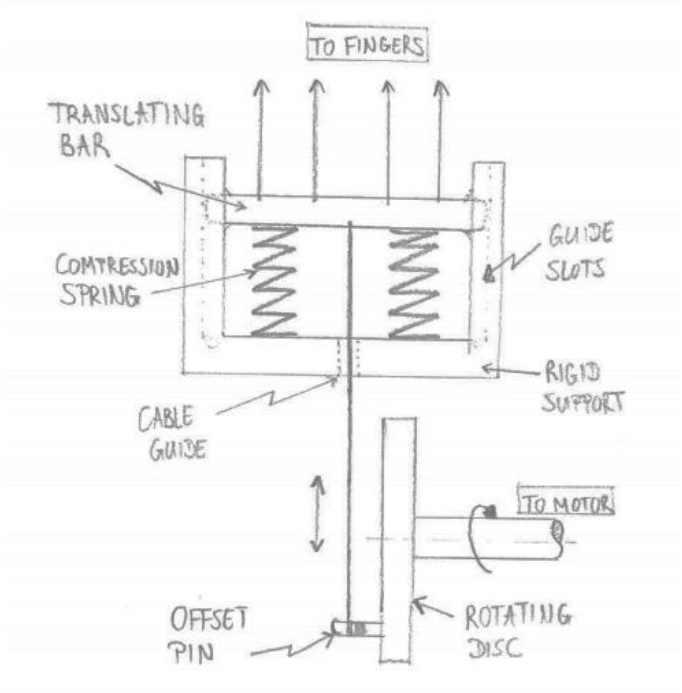

Figure A1 - Concept 1: Rotating disc endurance tester

The working of this mechanism (Figure A1) is relatively simple. The rotating disc is powered by the motor, with a gearing system to step down the rotational speed. Attached to the disc, is a swivelling pin which is free to rotate about its own axis, and has the primary actuating cable attached to it.

The cable attaches centrally to a linearly moving bar which locates into guide-slots on either end. The bar has the four finger tendon attachments and two compression springs to return it to its rest position (i.e. when the fingers are fully extended)

Advantages include simplicity of mechanisms, a set displacement stroke and uniform actuation between digits. Disadvantages include high cost of motor and gearbox, translating bar may misalign and lock in position, and vertical force component due to rotation of disc generates a non-uniform force distribution on bar.

CONCEPT 2 – Pneumatic actuation of digits

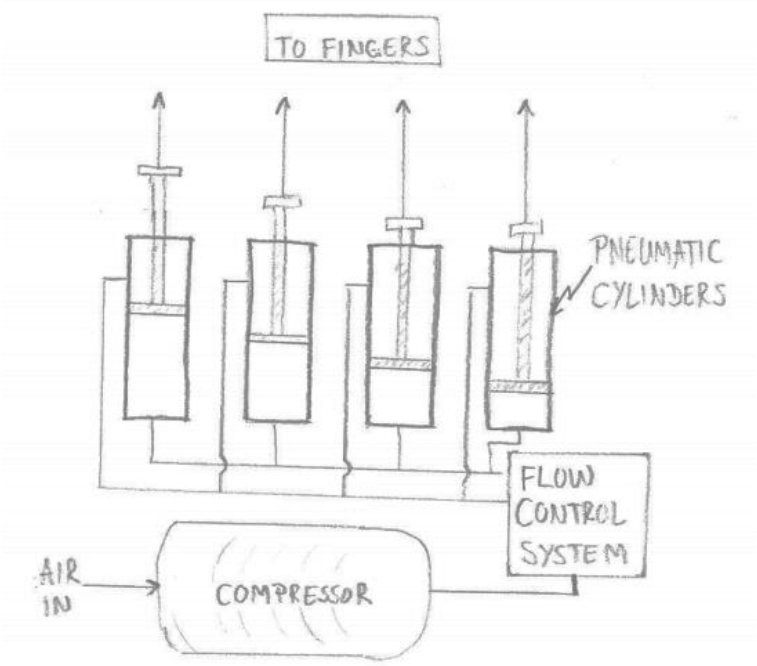

Figure A2 - Concept 2: Pneumatic endurance tester

The second concept (Figure A2) involves the use of four pneumatic actuators to linearly actuate the fingers (one for each specimen/test-case). The cylinders will use a control system to regulate their displacement with a mechanical back-up or stopper to prevent over-shooting.

The control system will also regulate the amount of air distributed to each cylinder, adjusting the frequency of oscillation. Furthermore, it would be beneficial if it could be connected in such way that individual control is possible.

Advantages of this design include direct linear actuation with relatively easy control and adjustment of displacement and cyclic frequency. Additionally, the system is relatively low cost and can be made using mostly standard components.

Disadvantages include a lack of force control, small variance in frequency due to pressure changes from main line and operating noise.

CONCEPT 3 – Rotating crank with radial ball bearings

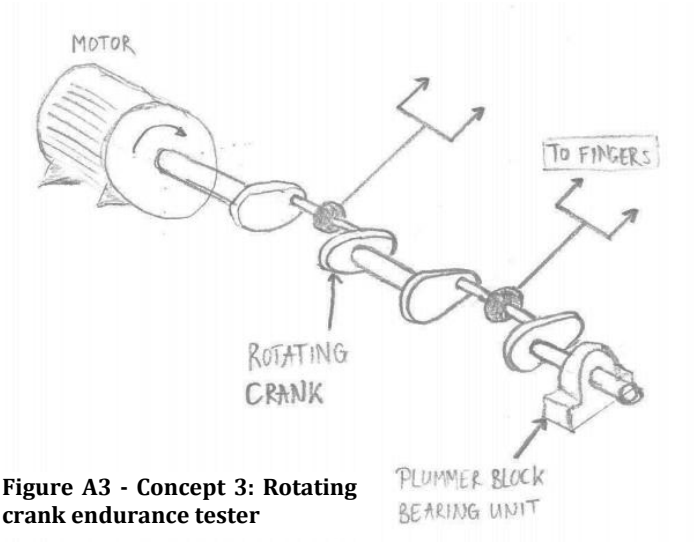

Figure A3 - Concept 3: Rotating crank endurance tester

This concept design (Figure A3) makes use of a rotating shaft with offset cranks to linearly actuate the fingers. Each crank has attached to it a ball bearing, to which the actuating cable is coupled. The inner race of the bearing will have an interference fit with the shaft, leaving the outer-race free to rotate so as not to entangle the actuating cable.

Advantages include precise displacement control and frequential accuracy. Disadvantages include high cost of the motor and machining, difficulty in securely coupling actuating cable to bearing without damaging or inhibiting its motion, and no means to individually control digits.

A1.3. Concept selection & design solution

Of the three concepts, it was decided that the pneumatic setup would best fit the requirements for the testing procedure. Availability of standard Festo® components and sensing equipment, together with the ability to individually adjust the displacement and frequency settings for each component, made it a logical choice. The schematic for the pneumatic design is outlined in Figure A4.

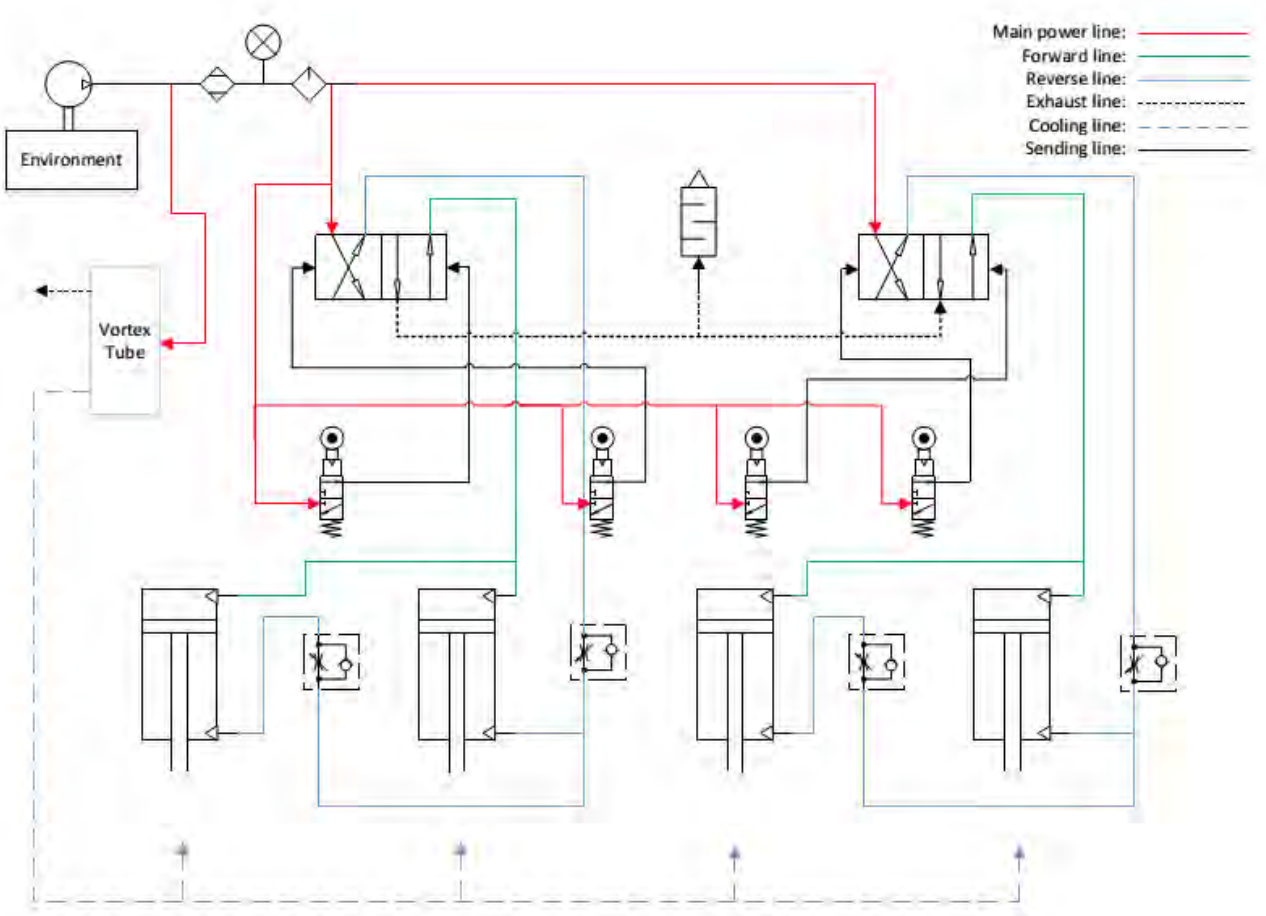

Figure A4 - Schematic diagram of the pneumatic endurance test setup

Referring to Figure A4, air from the compressor is channelled to the vortex tube (cooling line) and to the pneumatic actuating setup. Air to the actuated setup travels through a water trap and a lubricator which have a built-in pressure gauge. The power line then feeds directly into each of the four roller switches and into both switching valves. The setup is divided into two mirrored circuits, namely the left and right hand circuits, which each have two cylinders, two roller switches, two adjustable flow restrictors and a switching valve.

Each roller switch is positioned at the limit of the forward and the reverse stroke, 30 mm apart. When the switch on the reverse stroke is triggered, it actuates forward line; moving the piston forward and extending the finger. Similarly the switch on the forward stroke actuates the reverse line when triggered; moving the piston backwards and flexing the finger. The flow restrictors are incorporated

into the reverse lines of the circuit to adjust the rate of the reverse stroke, control cyclic frequency and allow balancing between the two pistons. Balancing is needed as no two pistons are identical and are likely to behave slightly differently when subjected to the same pressure. Additionally, a silencer was incorporated to reduce the noise generated by the setup.

Due to the use of pneumatics, it was a logical decision to incorporate air as the cooling mechanism. The need for cooling was deemed necessary as the frequency of the accelerated testing would increase the thermal exposure of the specimens; especially the repeated surface contact between the nylon and the actuating cable/wire. To minimise the pressure drop caused by increased flow rates, it was decided to sub-cool the air using a vortex tube, which allowed for lower volume flow rates to be used by the cooling system. The tube separates air into a hot stream (which is discarded) and cold stream, used for cooling. Mechanical stopper tubes were placed over the pistons to prevent the cylinders from overshooting and damaging the specimens.

A1.4. DC electrical counter circuit

In order to accurately count the number of cycles the specimens undergo, an electrical counting system was incorporated. This system made use of a 24 V DC power supply, two normally open spring-leaflet switches and two 24 V analogue counters. A schematic of the diagram can be seen in Figure A5 below.

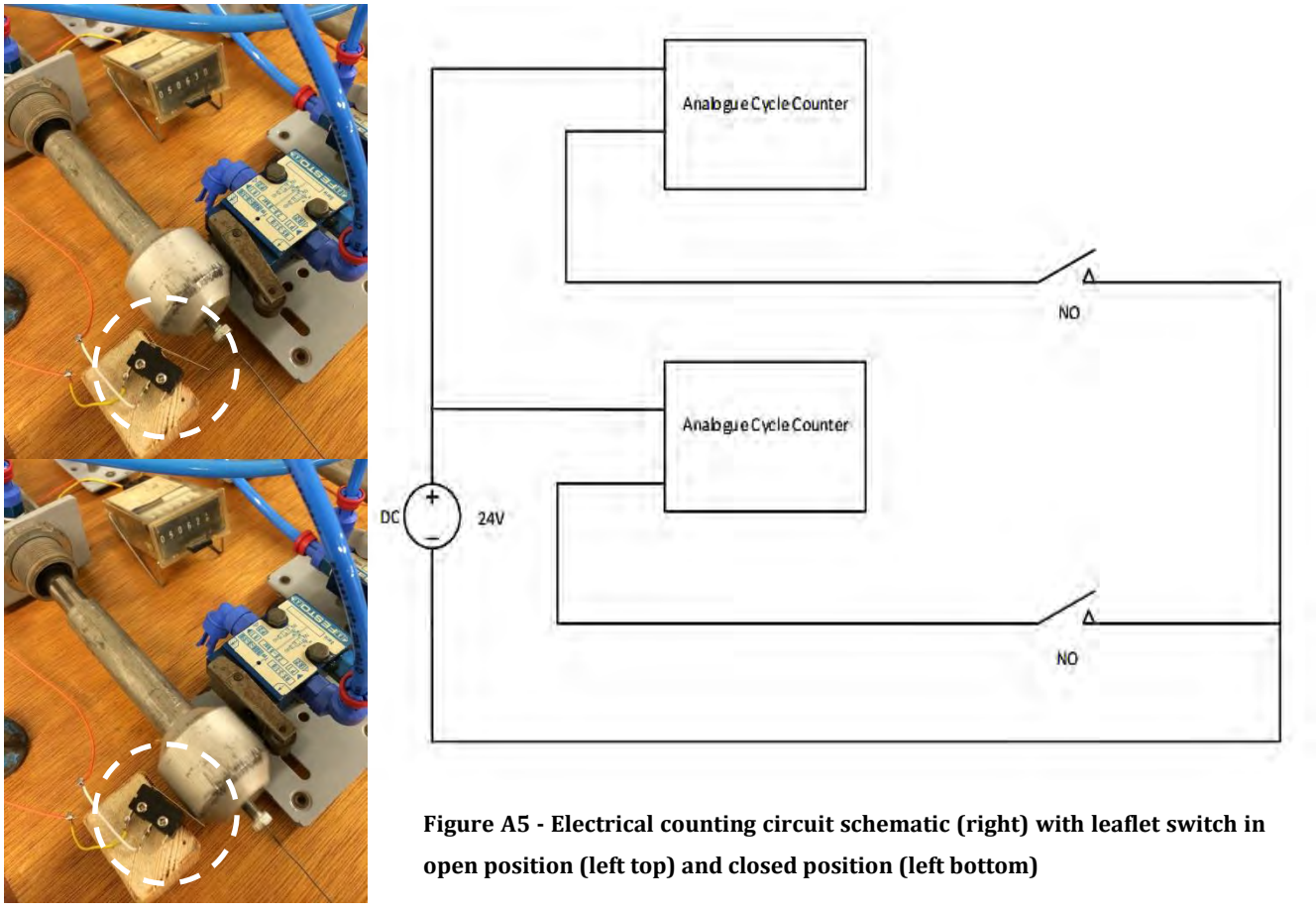

Figure A5 - Electrical counting circuit schematic (right) with leaflet switch in open position (left top) and closed position (left bottom)

A1.5. Manufacture and assembly of the setup

CNC machining of the base of the pneumatic setups was required to accurately locate each of the components; especially the roller switches with respect to each other and relative to the pistons, as this would govern the displacement of the actuation stroke.

Figure A6 - CNC Milling of wooden base

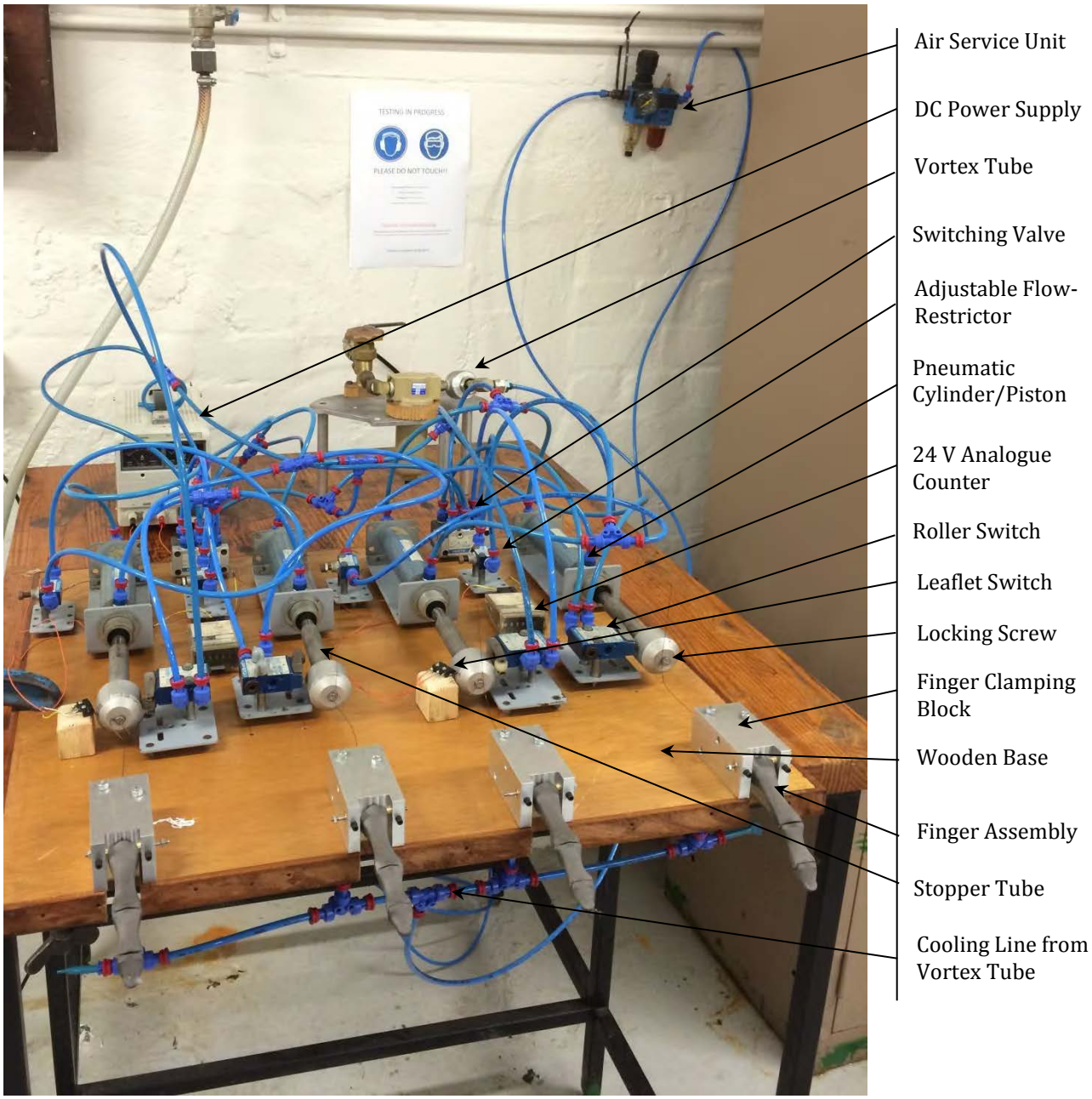

Figure A7 - Assembly of the pneumatic endurance test setup

A1.6. Commissioning of setup

After assembly, the system was started up and calibrated to an oscillating frequency of 2 Hz ± 0.2 Hz by adjusting the flow rate to each of the cylinders and taking temporal measurements. Thereafter, the actuating cables of the fingers were attached to the pneumatic cylinders using the transversely-holed screws as seen in Figure A8. However, due to the asymmetric nature of the transverse attachments, they soon failed as seen in the top centre image. Consequently, the attachment mechanism was altered to the axially-holed screws.

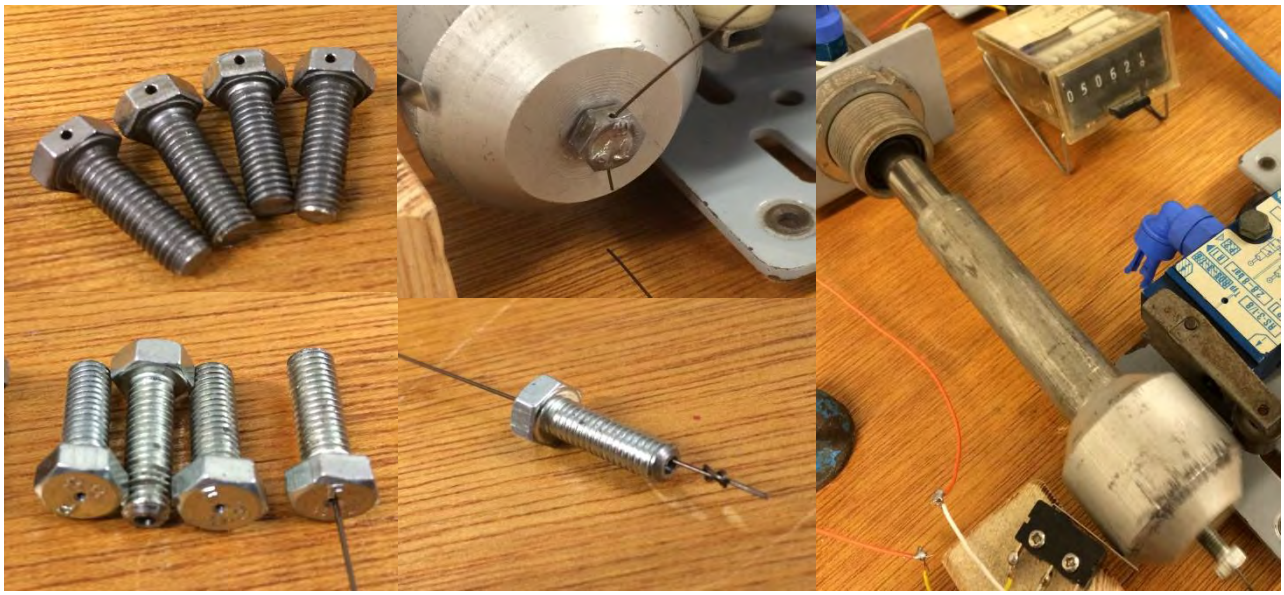

Figure A8 - Actuating cable attachment screws with transverse holes (top left & centre) and axial holes (bottom left & centre) with mechanical stopper tube (right)

The axially-holed screws had a Ø0.8 mm hole drilled into the hex end and a Ø2 mm hole from the screw end into which the stopper knot of the actuating cable locates. This mechanism prevented any further fractures at this joint. A mechanical stopper tube was inserted onto the pneumatic cylinder's shaft, allowing the piston to move a maximum of 32 mm; preventing hyper-flexion of the finger and thus averting over-loading of the actuating cable.

For experimental results and details, refer to Chapter 7.4, p. 159.

A2 – Design of Strength Testing Setups

A2.1. Aim

To design a setup capable of loading the finger specimen hyper-extensively and laterally until failure is reached. Furthermore, the load-displacement behaviour of the structure should be recorded, and the design must be easily modified to test the tensile strength of the actuating cables and their knots. All testing must be capable of adhering to criteria outlined in ISO 178 (2010), ASTM D790 (2003) and ASTM D6320 (2002).

A2.2. Specification of design solution

In order to conform to the controlled conditions specified in the aforementioned standards, the tests were performed on an Instron® 3365 tensile & compressive tester with a 1 kN calibrated load cell attached to its crosshead. A support setup to enable testing on this device was designed and manufactured, and will be outlined in this section. Moreover, the interface to the Instron® crosshead and base are shown in Figure A9 below.

Figure A9 - Instron® 3365 tensile and compressive testing machine (left) with crosshead- (top right) and base (bottom right) attachments

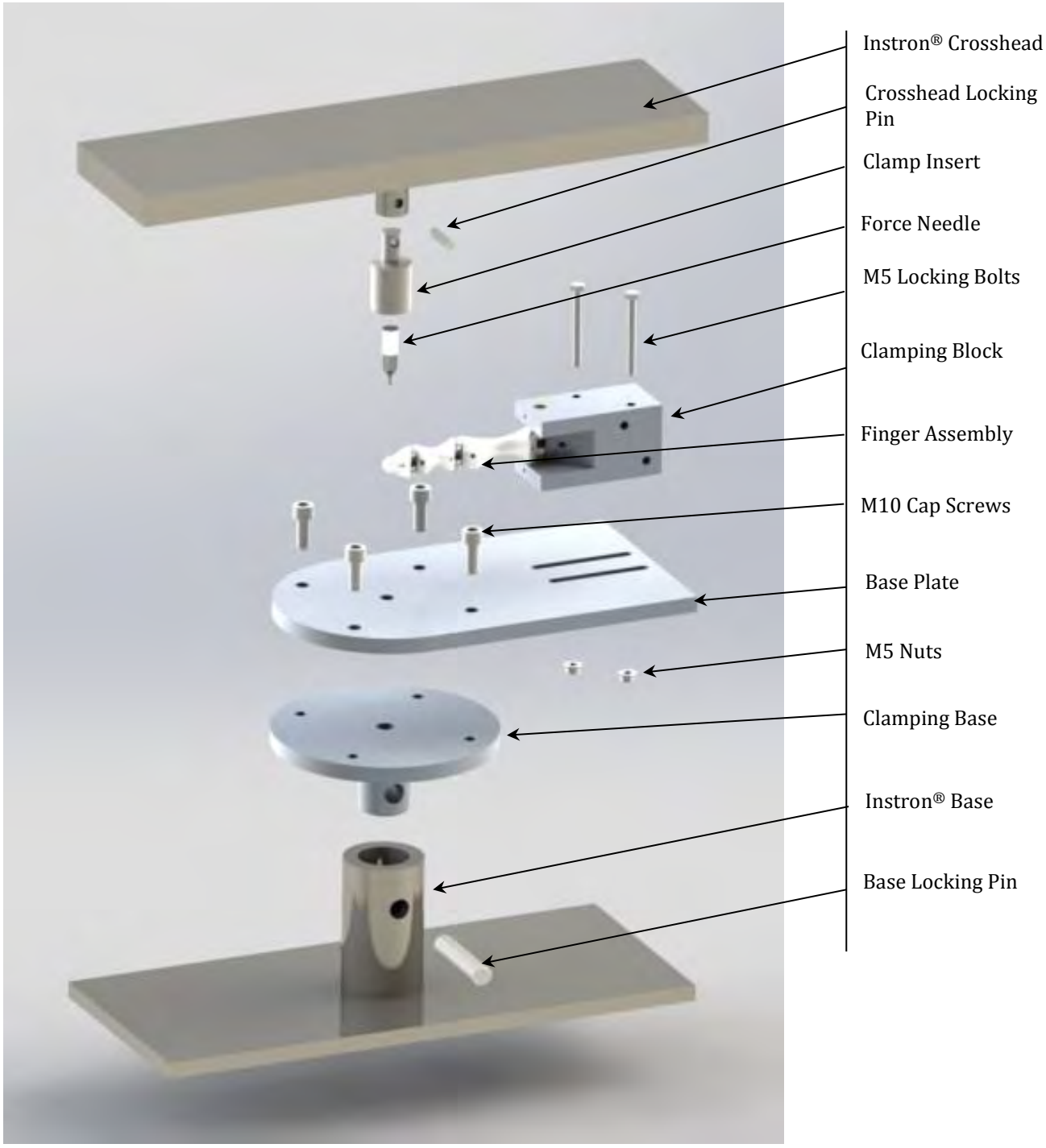

Figure A10 - Exploded assembly for lateral loading of finger specimen

Referring to Figure A10, working from the top downwards, the clamp insert slides into the crosshead and is locked in place by the crosshead locking pin. The threaded force needle screws into the clamp insert and is used to apply a compressive load to the finger, generating shear and bending stresses. Additionally, the clamping block is affixed to the base plate by two bolts and nuts, into slots which allow the leverage of the load on the finger to be altered; especially when testing fingers of differing length. The base plate is secured to the clamping base by four M10 cap screws. Furthermore, the clamping base inserts into the Instron® base, and is locked in place by the base locking pin.

The testing setup also has the ability to conform to the three testing configurations needed. The lateral and hyper-extensive setups are shown in Figure A11, and the tensile testing setup of the wire and knots using a screw insert through which the wire threads and is locked in place by its figure-8 knot, as shown in Figure A12 below.

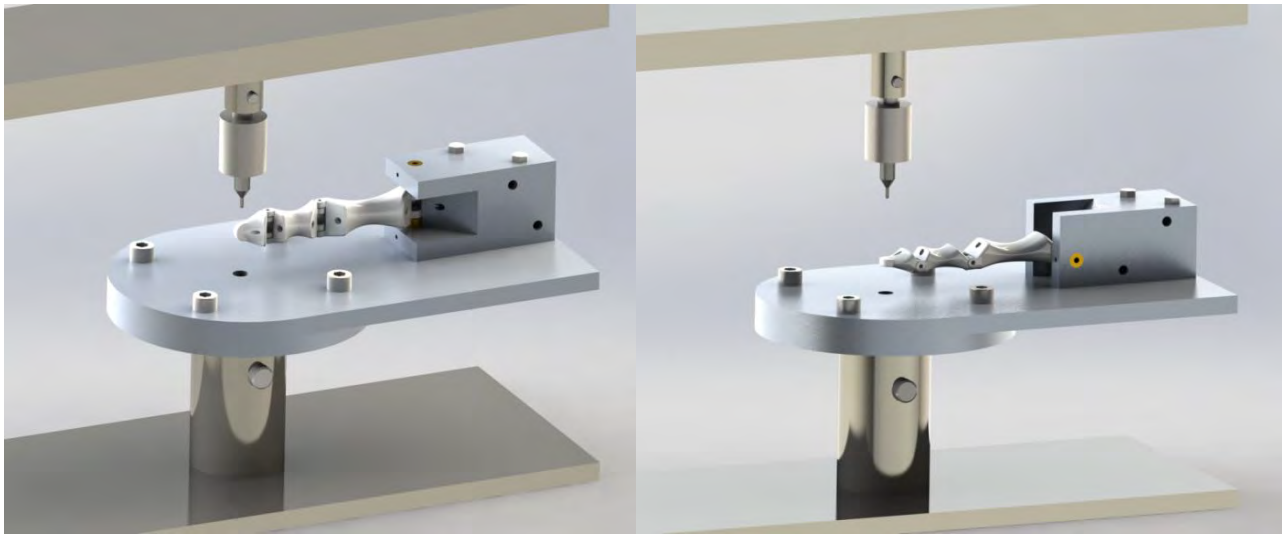

Figure A11 - Lateral (left) and hyper-extensive (right) strength testing setups for Instron® 3365

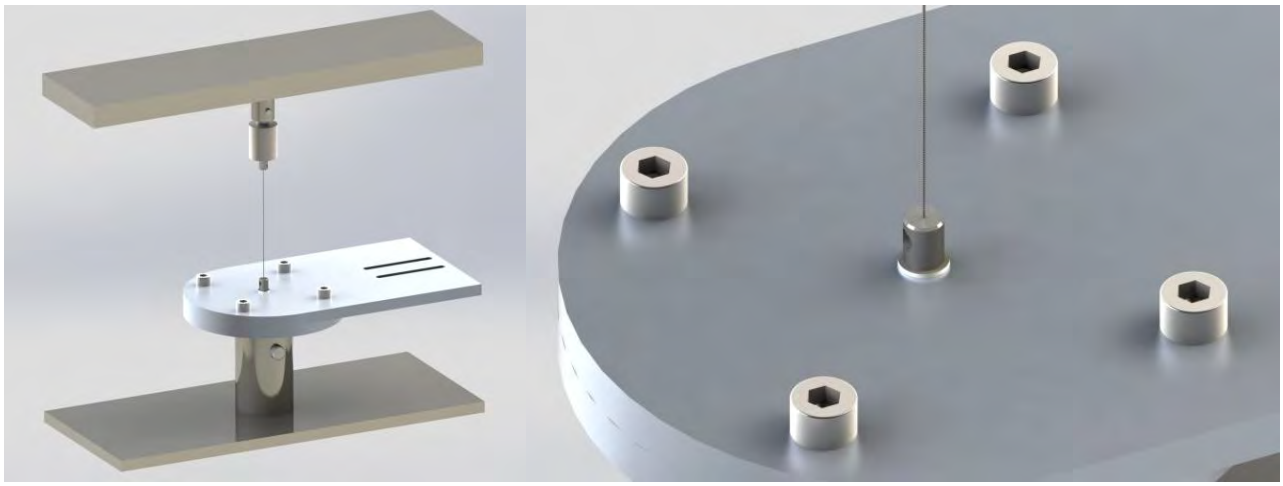

Figure A12 - Wire and knot strength testing setup for Instron® 3365

The load-displacement data will be recorded by the Instron® setup for each test case and, where applicable, be converted into stress-strain plots. For experimental test results refer back to Chapter 7.2, p. 143, and Chapter 7.3, p. 153.

APPENDIX B - TESTING DATA AND RESULTS

B1 – Experimental results of Tensile Tests

B1.1 - Ø0.3 mm US nitinol wire

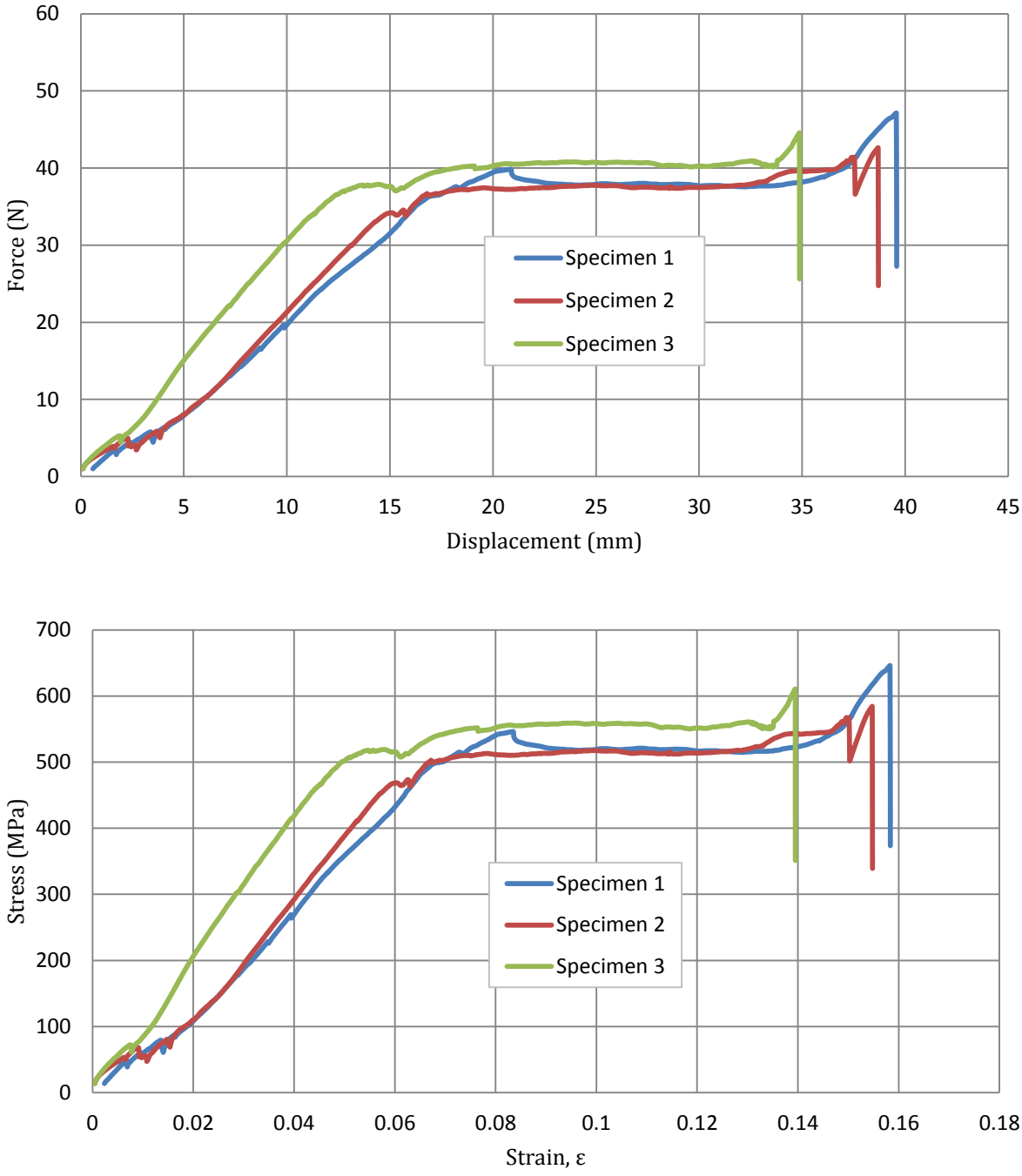

Figure B1 – Force vs. displacement (top) and stress vs. strain (bottom) graph of Ø0.3 mm US nitinol wire.

B1.2 - Ø0.31 mm German nitinol wire

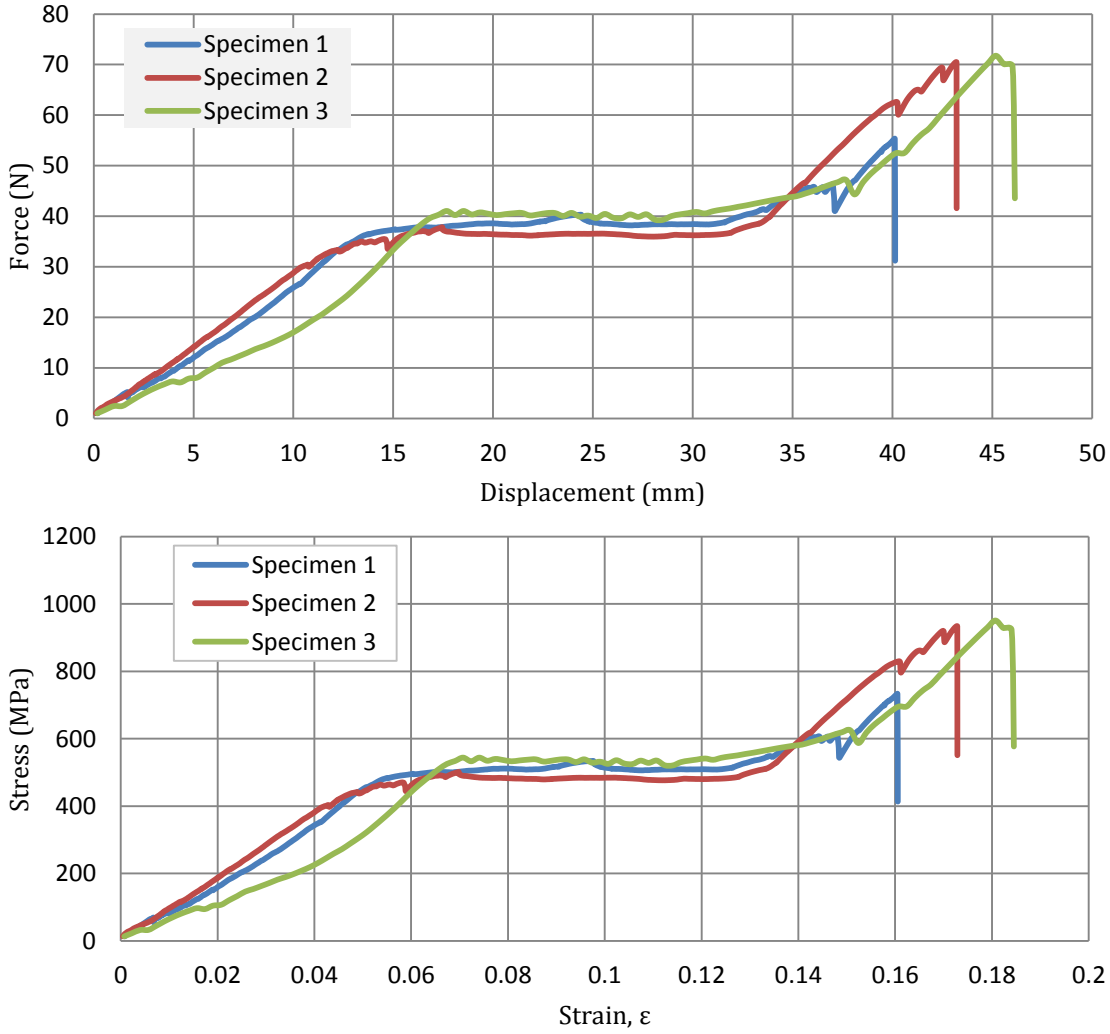

Figure B2 – Force vs. displacement (top) and stress vs. strain (bottom) graph of Ø0.31 mm German nitinol wire.

B1.3 - Ø0.4 mm US nitinol wire

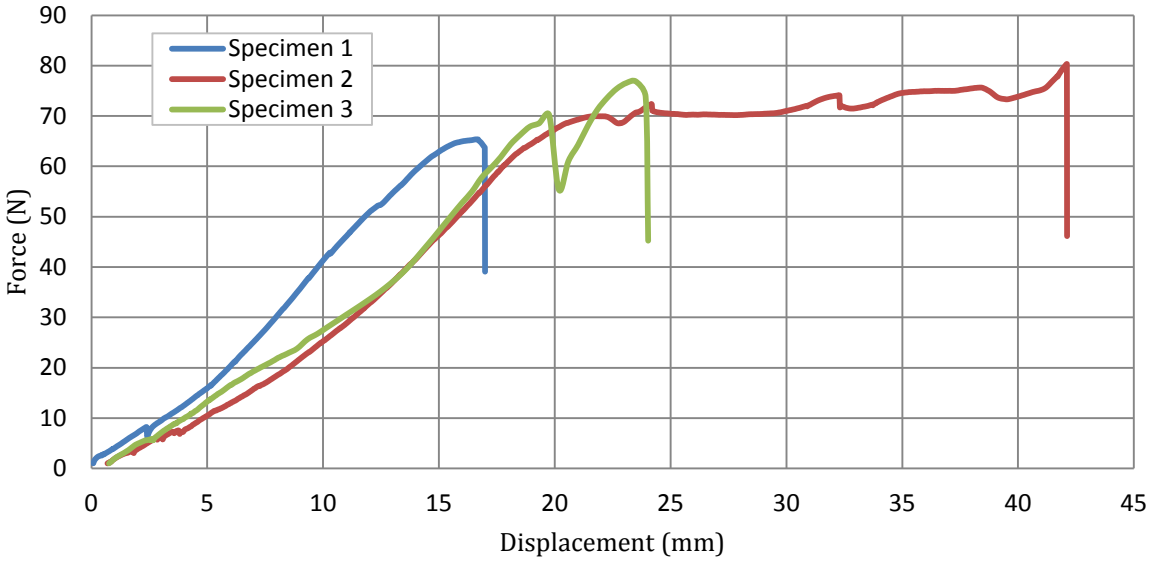

Figure B3 – Force vs. displacement graph of Ø0.4 mm US nitinol wire.

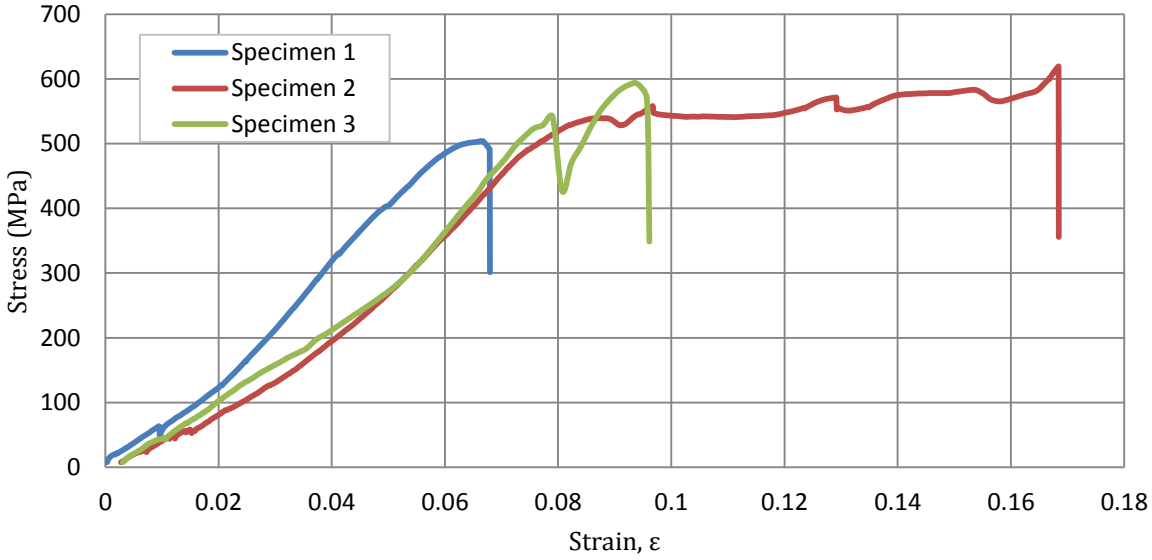

Figure B4 – Stress vs. strain graph of Ø0.4 mm US nitinol wire.

B1.4 - Ø0.44 mm German nitinol wire

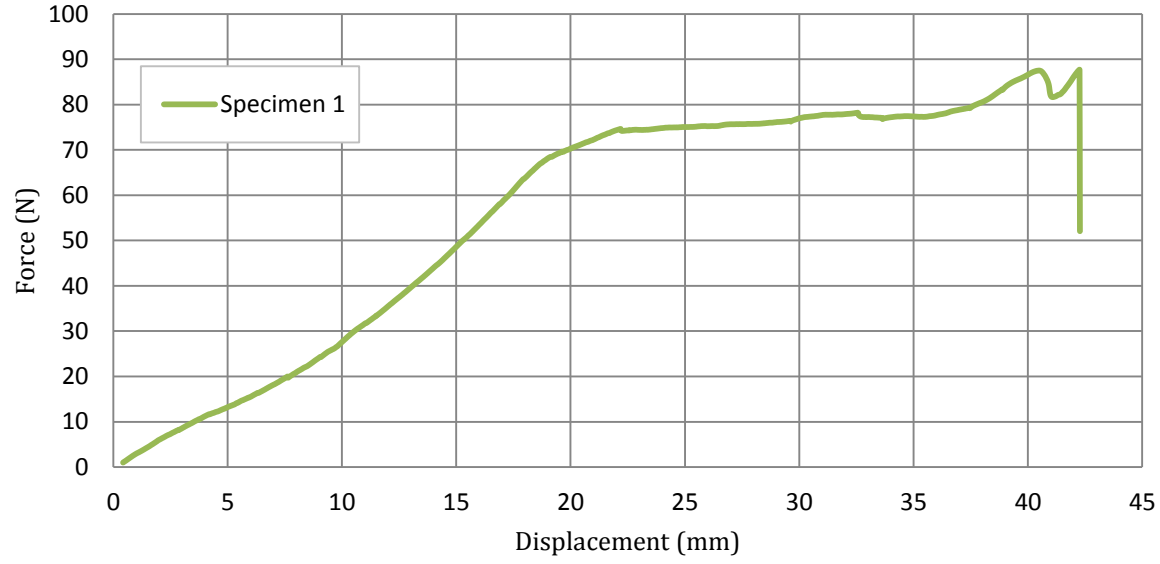

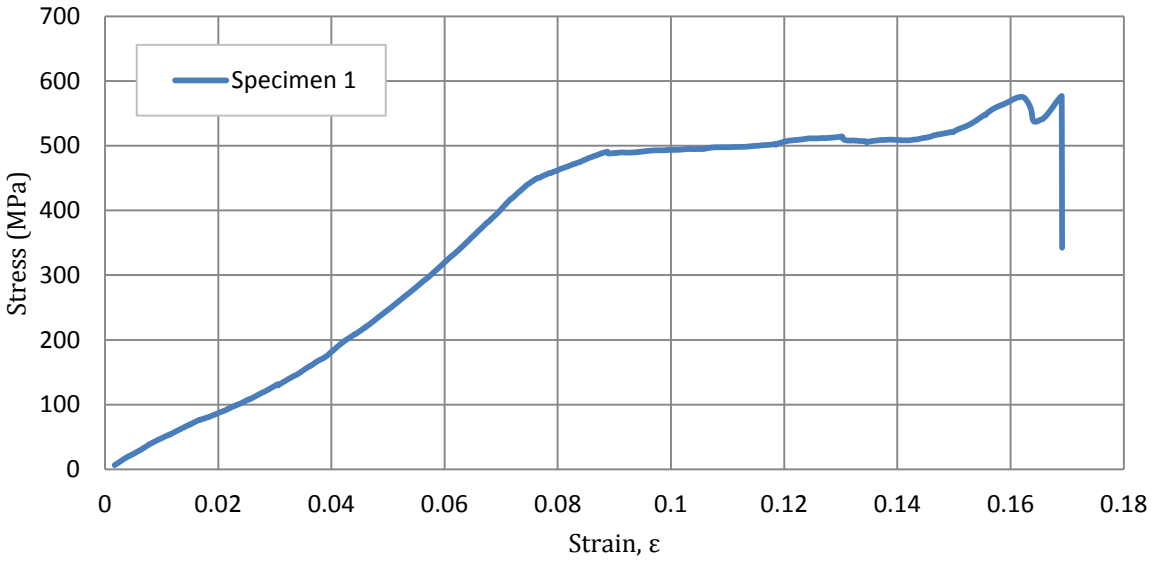

Figure B5 – Force vs. displacement (top) and stress vs. strain (bottom) graph of Ø0.44 mm German nitinol wire.

B1.5 - Ø0.5 mm US nitinol wire

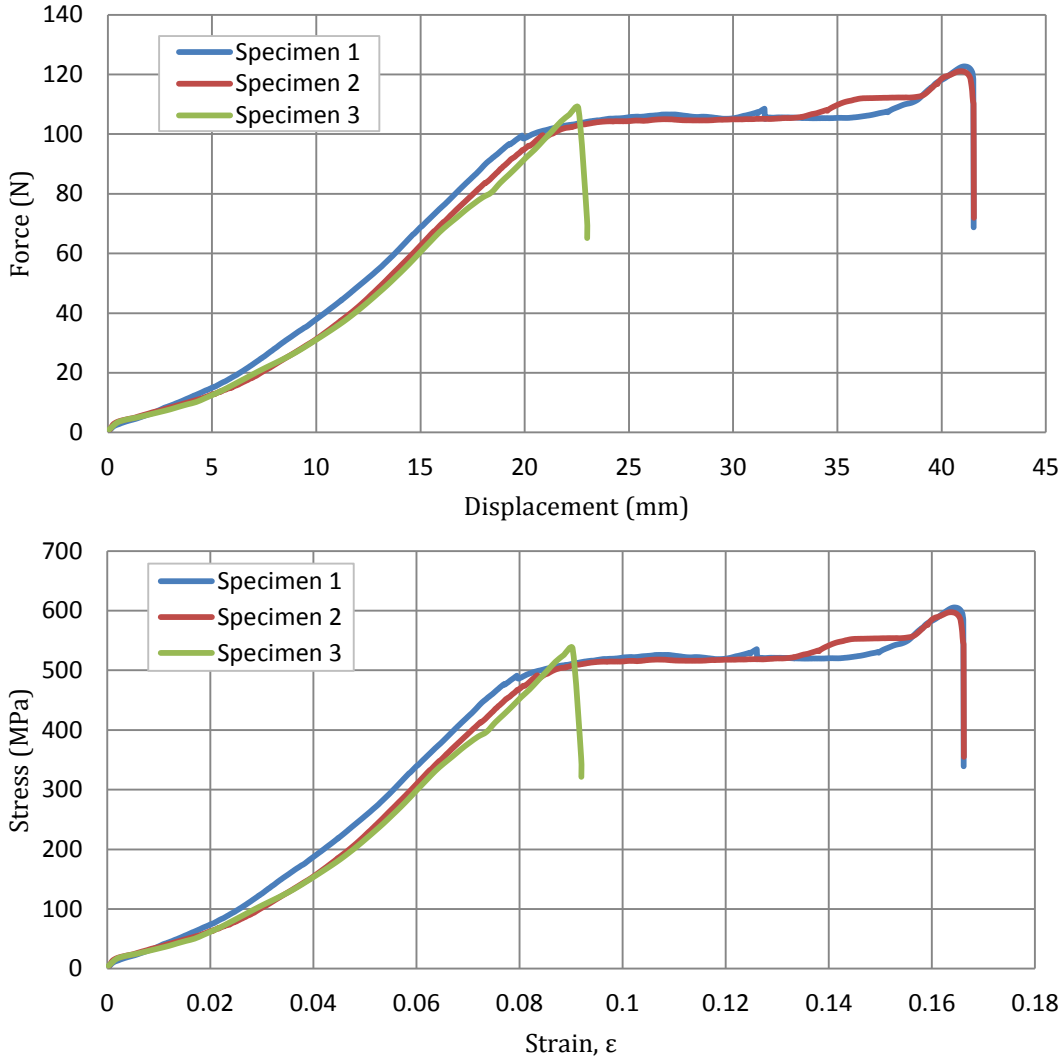

Figure B6 – Force vs. displacement (top) and stress vs. strain (bottom) graph of Ø0.5 mm US nitinol wire.

B1.5 - Ø0.50 mm German nitinol wire

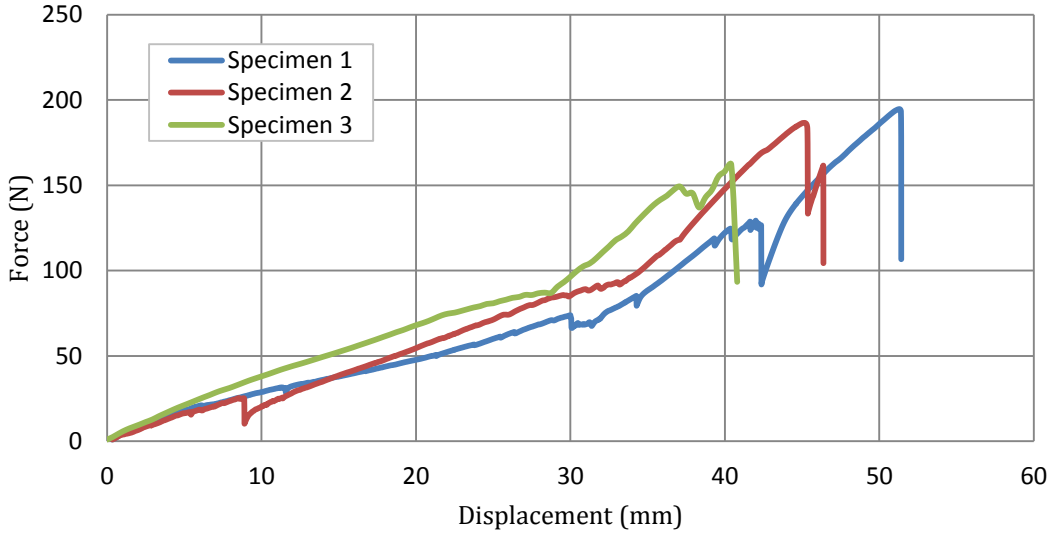

Figure B7 – Force vs. displacement graph of Ø0.50 mm German nitinol wire.

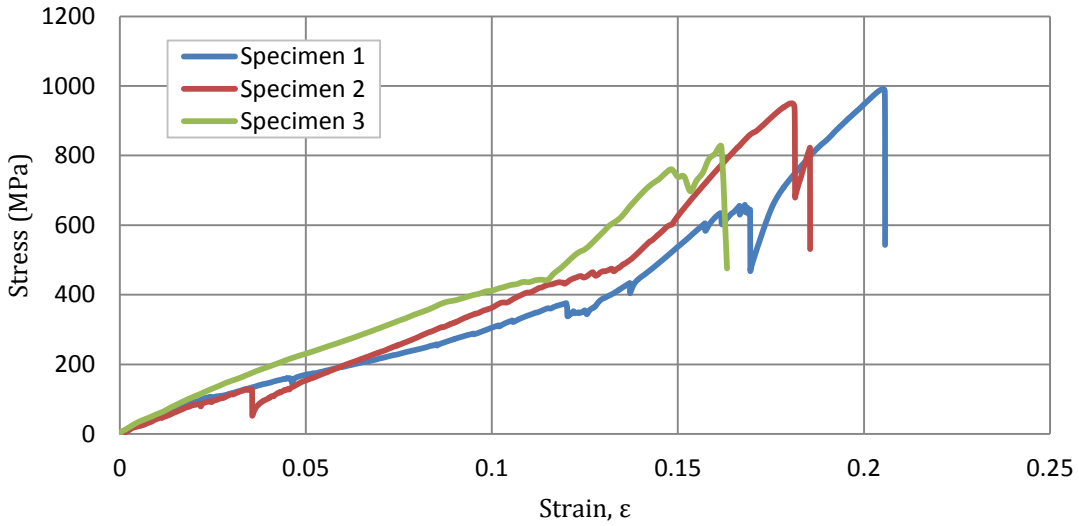

Figure B8 – Stress vs. strain graph of Ø0.50 mm German nitinol wire.

B1.6 - Ø0.6 mm Carbon-coated stainless steel braided wire

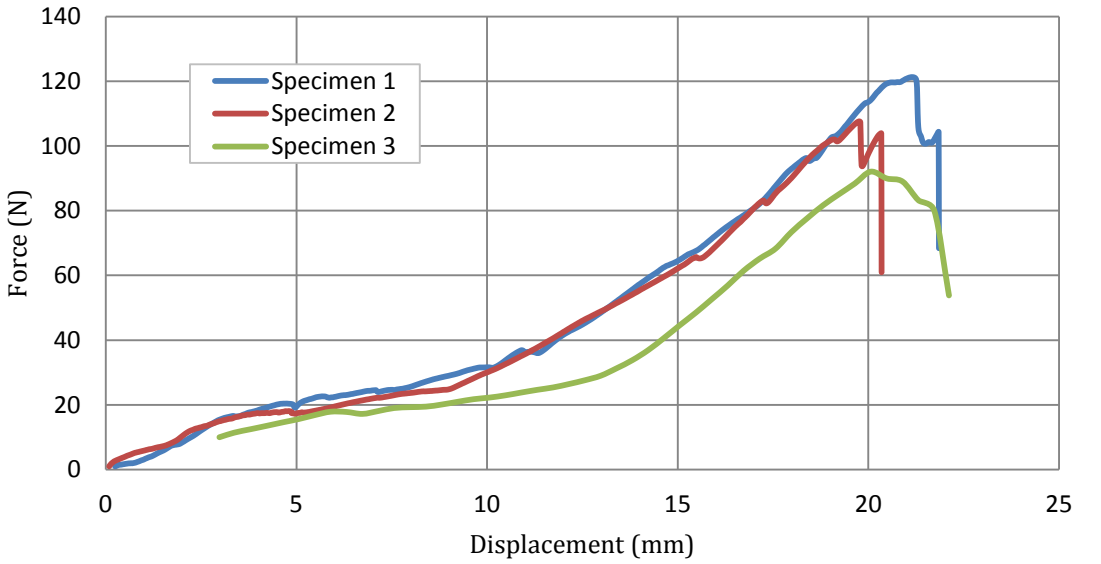

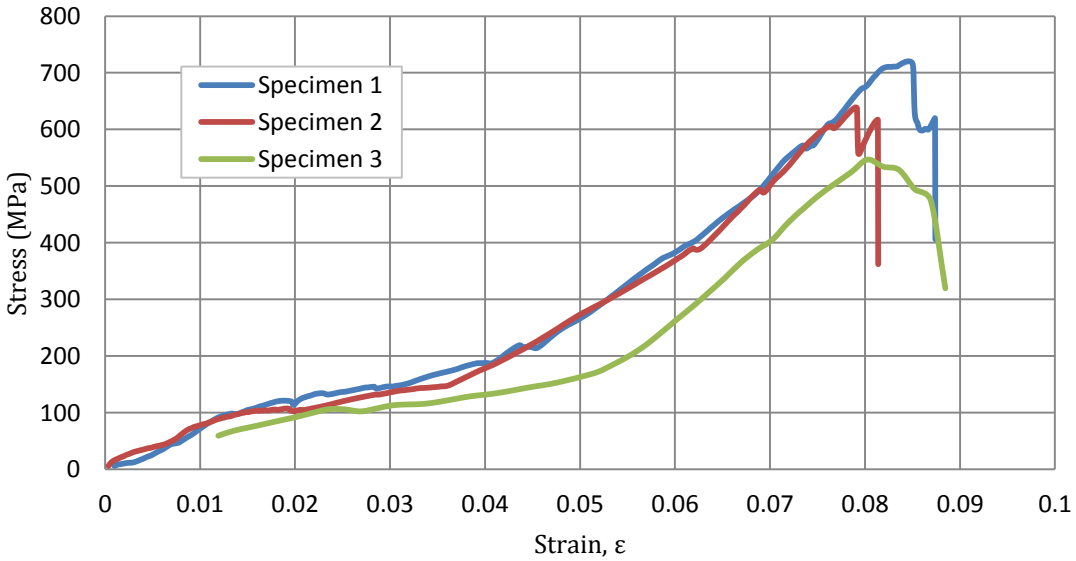

Figure B9 – Force vs. displacement (top) and stress vs. strain (bottom) graph of Ø0.6 mm carbon-coated stainless steel braided wire.

B2 – Torsion Spring Calculation Spreadsheets

This section of Appendix B, deals with the calculations for the torsion springs used in the interphalangeal and metacarpophalangeal joints of the fingers of the hand prosthesis. The following assumptions are made with respect to the calculations:

- Spring material is linear-elastic and isotropic.
- Thermal effects can be neglected
- Hysteresis caused by friction between successive coils is neglected.

Table B1 and Table B2 show calculated properties[16] of the various torsion springs with wire diameters (d) ranging between 0.5 mm and 0.9 mm respectively, and number of turns (N) between 3 and 7. Springs of interest are shown in the right hand columns of the adjusted torsion spring distribution specified in Section 4.1.3.2, Table 37, p. 83.

Referring to Table B1 and Table B2, the maximum torque limit for each of the springs was calculated and is shown in red text. The spring moments shown in the centre matrix of each table may not exceed this value. Consequently, the cells of moments below the maximum torque limit are highlighted in green, whereas the cells of moments which exceed these values are highlighted in red. Of particular interest are the initial spring moments (at 20°), maximum moments of the DIP (and thumb MCP) springs at 80° (60° +20° initial deflection), thumb IP at 100° (80° + 20° initial deflection) and the PIP & MCP springs at 110° (90° + 20° initial deflection).

Furthermore the safety factor on infinite life (n_f) should exceed 1 for the selected springs. These are calculated at deflections of 60° and 90° for the DIP joints and MCP joints respectively; as seen in the bottom two rows of Table B1 and Table B2. Those exceeding 1 (implying infinite life of 10^6 cycles) have cells highlighted in green, whereas those that do not have their cells highlighted in red, and are not expected to attain infinite loading cycles.

The springs selected using the adjusted distribution all surpass their infinite life criteria and are expected not to fail whilst operating within their design limits.

[16] Calculated using material properties equations from Shigley's 8th Edition (Budynas & Nisbett, 2008, pp. 499-538). Specified equations and tables form this text are referred to in the right hand columns of Table B1 and Table B2.

Table B1 - Tabularised torsion spring mechanical and fatigue characteristics using ASTM A228 Music wire with 5 mm mean diameter.

Mechanical Properties			
E	203.4	GPa	Shigley's pp.507 Table 10-5
A (MPa.mm^m) Music Wire ASTM A228	2211	MPa.mm^m	Shigley's pp.507 Table 10-4
Exponent, m	0.145	-	
Factor of Safety	2		

System Constants		
D mean	5	mm
r	12	mm

Wire Diameter, d (mm)		0.5				0.6				0.7				0.8				0.9				
Di (mm)		4.5				4.4				4.3				4.2				4.1				
Spring Index, C (D/d)		10				8.33				7.14				6.25				5.56				Eqn.10-2 pp.501
Stress Concentration Factor, Ki		1.081				1.098				1.116				1.135				1.155				Eqn.10-43 pp.534
UTS		2444.8				2381.0				2328.4				2283.7				2245.0				Eqn.10-14 pp.505
Sy (0.78*UTS)		1906.9				1857.2				1816.1				1781.3				1751.1				Eqn.10-57 pp.536
Max Torque Limit (N.mm)		21.7				35.9				54.8				83.2				108.5				Eqn. 10-44 pp.534
Number of turns, N		4	5	6	7	3	4	5	6	3	4	5	6	2	3	4	5	2	3	4	5	
Active Turns, Na		4.51	5.51	6.51	7.51	3.51	4.51	5.51	6.51	3.51	4.51	5.51	6.51	2.51	3.51	4.51	5.51	2.51	3.51	4.51	5.51	Eqn.10-48 pp.535
Rotations at Limiting Torque		0.368	0.460	0.552	0.644	0.220	0.294	0.367	0.441	0.182	0.242	0.303	0.363	0.108	0.162	0.216	0.270	0.088	0.132	0.176	0.220	Eqn. 10-54 pp.536
Width of Spring (mm)		2.5	3	3.5	4	2.4	3	3.6	4.2	2.8	3.5	4.2	4.9	2.4	3.2	4	4.8	2.7	3.6	4.5	5.4	
Theta (degrees)	Theta (rad)	SPRING MOMENT (N.mm)																				Eqn. 10-47 pp.535
0	0.000	0.0	0.0	0.0	0.0	0.0	0.0	0.0	0.0	0.0	0.0	0.0	0.0	0.0	0.0	0.0	0.0	0.0	0.0	0.0	0.0	
5	0.087	0.8	0.6	0.5	0.5	2.0	1.6	1.3	1.1	3.8	3.0	2.4	2.0	9.1	6.5	5.0	4.1	14.5	10.4	8.1	6.6	
10	0.175	1.5	1.3	1.1	0.9	4.1	3.2	2.6	2.2	7.6	5.9	4.8	4.1	18.1	12.9	10.1	8.2	29.0	20.7	16.1	13.2	
15	0.262	2.3	1.9	1.6	1.4	6.1	4.8	3.9	3.3	11.4	8.9	7.3	6.1	27.2	19.4	15.1	12.4	43.5	31.1	24.2	19.8	
20	0.349	3.1	2.5	2.1	1.8	8.2	6.4	5.2	4.4	15.2	11.8	9.7	8.2	36.2	25.9	20.2	16.5	58.0	41.5	32.3	26.4	
25	0.436	3.8	3.1	2.7	2.3	10.2	8.0	6.5	5.5	19.0	14.8	12.1	10.2	45.3	32.4	25.2	20.6	72.5	51.9	40.4	33.0	
30	0.524	4.6	3.8	3.2	2.8	12.3	9.6	7.8	6.6	22.8	17.7	14.5	12.3	54.3	38.8	30.2	24.7	87.0	62.2	48.4	39.6	
35	0.611	5.4	4.4	3.7	3.2	14.3	11.2	9.1	7.7	26.6	20.7	16.9	14.3	63.4	45.3	35.3	28.9	101.5	72.6	56.5	46.2	
40	0.698	6.2	5.0	4.3	3.7	16.4	12.8	10.4	8.8	30.4	23.6	19.3	16.4	72.4	51.8	40.3	33.0	116.0	83.0	64.6	52.8	
45	0.785	6.9	5.7	4.8	4.2	18.4	14.3	11.7	9.9	34.2	26.6	21.8	18.4	81.5	58.3	45.3	37.1	130.5	93.3	72.6	59.5	
50	0.873	7.7	6.3	5.3	4.6	20.5	15.9	13.0	11.0	38.0	29.5	24.2	20.5	90.5	64.7	50.4	41.2	145.0	103.7	80.7	66.1	
55	0.960	8.5	6.9	5.9	5.1	22.5	17.5	14.4	12.1	41.7	32.5	26.6	22.5	99.6	71.2	55.4	45.4	159.5	114.1	88.8	72.7	
60	1.047	9.2	7.6	6.4	5.5	24.6	19.1	15.7	13.3	45.5	35.4	29.0	24.6	108.7	77.7	58.6	49.5	174.0	124.4	96.8	79.3	
65	1.134	10.0	8.2	6.9	6.0	26.6	20.7	17.0	14.4	49.3	38.4	31.4	26.6	117.7	84.2	61.8	53.6	188.5	134.8	104.9	85.9	
70	1.222	10.8	8.8	7.5	6.5	28.7	22.3	18.3	15.5	53.1	41.3	33.8	28.6	126.8	90.6	65.0	57.7	203.0	145.2	113.0	92.5	
75	1.309	11.5	9.4	8.0	6.9	30.7	23.9	19.6	16.6	56.9	44.3	36.3	30.7	135.8	97.1	68.2	61.9	217.5	155.6	121.1	99.1	
80	1.396	12.3	10.1	8.5	7.4	32.8	25.5	20.9	17.7	60.7	47.3	38.7	32.7	144.9	103.6	71.4	64.5	232.1	165.9	129.1	105.7	
85	1.484	13.1	10.7	9.1	7.8	34.8	27.1	22.2	18.8	64.5	50.2	41.1	34.8	153.9	110.1	74.6	67.1	246.6	176.3	137.2	112.3	
90	1.571	13.8	11.3	9.6	8.3	36.9	28.7	23.5	19.9	68.3	53.2	43.5	36.8	163.0	116.5	77.8	69.7	261.1	186.7	145.3	118.9	
95	1.658	14.6	12.0	10.1	8.8	38.9	30.3	24.8	21.0	72.1	56.1	45.9	38.9	172.0	123.0	81.0	72.3	275.6	197.0	153.3	125.5	
100	1.745	15.4	12.6	10.7	9.2	41.0	31.9	26.1	22.1	75.9	59.1	48.3	40.9	181.1	129.5	84.2	74.9	290.1	207.4	161.4	132.1	
105	1.833	16.1	13.2	11.2	9.7	43.0	33.5	27.4	23.2	79.7	62.0	50.8	43.0	190.1	136.0	87.4	77.5	304.6	217.8	169.5	138.7	
110	1.920	16.9	13.8	11.7	10.2	45.1	35.1	28.7	24.3	83.5	65.0	53.2	45.0	199.2	142.4	90.6	80.1	319.1	228.2	177.6	145.3	
FATIGUE ANALYSIS																						
Alternating Moment, Ma (N.mm)		6.9	5.7	4.8	4.2	18.4	14.3	11.7	9.9	34.2	26.6	21.8	18.4	81.5	58.3	35.2	31.8	130.5	93.3	72.6	59.5	p. 539
Alternating Moment, Ma @ 60° (N.mm)		4.6	3.8	3.2	2.8	12.3	9.6	7.8	6.6	22.8	17.7	14.5	12.3	54.3	38.8	25.6	24.0	87.0	62.2	48.4	39.6	p. 539
Mean Moment, Mm (N.mm)		10.0	8.2	6.9	6.0	26.6	20.7	17.0	14.4	49.3	38.4	31.4	26.6	117.7	84.2	55.4	48.3	188.5	134.8	104.9	85.9	p. 539
r (Ma/Mm)		0.7				0.7				0.7				0.7				0.7				
Alternating Stress, σa (MPa)		609.3	498.7	422.1	365.9	954.8	743.0	608.2	514.7	1132.4	881.2	721.3	610.5	1840.4	1316.0	795.8	717.8	2106.1	1505.9	1172.0	959.2	p. 539
Alternating Stress, σa @ 60° (MPa)		406.2	332.4	281.4	243.9	636.5	495.4	405.4	343.2	754.9	587.5	480.9	407.0	1226.9	877.3	579.0	541.6	1404.0	1004.0	781.3	639.5	
Mean Stress, σa (MPa)		880.0	720.3	609.6	528.5	1379.1	1073.3	878.5	743.5	1635.6	1272.9	1041.9	881.8	2658.4	1900.9	1149.4	1036.8	3042.1	2175.2	1692.8	1385.6	p. 539
Sr (= 0.50Sut) (MPa)		1222.4				1190.5				1164.2				1141.9				1122.5				Table 10-10
Endurance Limit, Se (MPa)		651.9				634.9				620.9				609.0				598.7				Eqn. 10-58 p. 536
Endurance Strength, Sa (MPa)		576.3				561.3				548.9				538.4				529.3				Eqn. 10-59 p. 536
nf @ 60°		1.42	1.73	2.05	2.36	1.02	1.13	1.38	1.64	0.73	1.02	1.14	1.35	0.56	0.84	1.02	1.18	0.38	0.53	0.72	0.96	Eqn. 10-60 p. 537
nf @ 90°		0.95	1.16	1.37	1.58	0.86	1.00	1.11	1.23	0.48	0.62	0.84	1.07	0.29	0.58	0.72	1.07	0.24	0.39	0.52	0.73	Eqn. 10-60 p. 537

Table B2 - Tabularised torsion spring mechanical and fatigue characteristics using ASTM A228 Music wire with 7 mm mean diameter.

Mechanical Properties			
E	203.4	GPa	Shigley's pp.507 Table 10-5
A (MPa.mm^m) Music Wire ASTM A228	2211	MPa.mm^m	Shigley's pp.507 Table 10-4
Exponent, m	0.145	-	
Sactor of Safety	2	-	

System Constants		
D mean	7	mm
r	12	mm

Wire Diameter, d (mm)		0.5				0.6				0.7				0.8				0.9					
Di (mm)		6.5				6.4				6.3				6.2				6.1					
Spring Index, C (D/d)		14				11.67				10.00				8.75				7.78				Eqn.10-2	pp.501
Stress Concentration Factor, Ki		1.056				1.068				1.081				1.093				1.106				Eqn.10-43	pp.534
UTS		2444.8				2381.0				2328.4				2283.7				2245.0				Eqn.10-14	pp.505
Sy (0.78*UTS)		1906.9				1857.2				1816.1				1781.3				1751.1				Eqn.10-57	pp.536
Max Torque Limit (N.mm)		22.2				36.9				56.6				85.4				113.3				Eqn. 10-44	pp.534
Number of turns, N		4	5	6	7	3	4	5	6	3	4	5	6	2	3	4	5	2	3	4	5		
Active Turns, Na		4.36	5.36	6.36	7.36	3.36	4.36	5.36	6.36	3.36	4.36	5.36	6.36	2.36	3.36	4.36	5.36	2.36	3.36	4.36	5.36	Eqn.10-48	pp.535
Rotations at Limiting Torque		0.527	0.659	0.790	0.922	0.317	0.423	0.529	0.634	0.263	0.350	0.438	0.526	0.155	0.232	0.310	0.387	0.128	0.193	0.257	0.321	Eqn. 10-54	pp.536
Width of Spring (mm)		2.5	3	3.5	4	2.4	3	3.6	4.2	2.8	3.5	4.2	4.9	2.4	3.2	4	4.8	2.7	3.6	4.5	5.4		
Theta (degrees)	Theta (rad)	SPRING MOMENT (N.mm)																				Eqn. 10-47	pp.535
0	0.000	0.0	0.0	0.0	0.0	0.0	0.0	0.0	0.0	0.0	0.0	0.0	0.0	0.0	0.0	0.0	0.0	0.0	0.0	0.0	0.0		
5	0.087	0.6	0.5	0.4	0.3	1.5	1.2	1.0	0.8	2.8	2.2	1.8	1.5	6.9	4.8	3.7	3.0	11.0	7.7	6.0	4.8		
10	0.175	1.1	0.9	0.8	0.7	3.1	2.4	1.9	1.6	5.7	4.4	3.5	3.0	13.7	9.6	7.4	6.1	22.0	15.5	11.9	9.7		
15	0.262	1.7	1.4	1.2	1.0	4.6	3.5	2.9	2.4	8.5	6.5	5.3	4.5	20.6	14.5	11.2	9.1	33.0	23.2	17.9	14.5		
20	0.349	2.3	1.8	1.6	1.3	6.1	4.7	3.8	3.2	11.3	8.7	7.1	6.0	27.5	19.3	14.9	12.1	44.0	30.9	23.8	19.4		
25	0.436	2.8	2.3	1.9	1.7	7.6	5.9	4.8	4.0	14.1	10.9	8.9	7.5	34.3	24.1	18.6	15.1	55.0	38.6	29.8	24.2		
30	0.524	3.4	2.8	2.3	2.0	9.2	7.1	5.7	4.8	17.0	13.1	10.6	9.0	41.2	28.9	22.3	18.2	66.0	46.4	35.7	29.1		
35	0.611	4.0	3.2	2.7	2.4	10.7	8.2	6.7	5.6	19.8	15.3	12.4	10.5	48.1	33.8	26.0	21.2	77.0	54.1	41.7	33.9		
40	0.698	4.5	3.7	3.1	2.7	12.2	9.4	7.7	6.5	22.6	17.4	14.2	12.0	54.9	38.6	29.8	24.2	88.0	61.8	47.7	38.8		
45	0.785	5.1	4.2	3.5	3.0	13.7	10.6	8.6	7.3	25.5	19.6	16.0	13.5	61.8	43.4	33.5	27.2	99.0	69.6	53.6	43.6		
50	0.873	5.7	4.6	3.9	3.4	15.3	11.8	9.6	8.1	28.3	21.8	17.7	14.9	68.7	48.2	37.2	30.3	110.0	77.3	59.6	48.5		
55	0.960	6.2	5.1	4.3	3.7	16.8	12.9	10.5	8.9	31.1	24.0	19.5	16.4	75.5	53.1	40.9	33.3	121.0	85.0	65.5	53.3		
60	1.047	6.8	5.5	4.7	4.0	18.3	14.1	11.5	9.7	33.9	26.2	21.3	17.9	82.4	57.9	44.6	36.3	132.0	92.7	71.5	58.2		
65	1.134	7.4	6.0	5.1	4.4	19.8	15.3	12.4	10.5	36.8	28.3	23.1	19.4	89.3	62.7	48.3	39.3	143.0	100.5	77.4	63.0		
70	1.222	7.9	6.5	5.4	4.7	21.4	16.5	13.4	11.3	39.6	30.5	24.8	20.9	96.1	67.5	52.1	42.4	154.0	108.2	83.4	67.8		
75	1.309	8.5	6.9	5.8	5.0	22.9	17.7	14.4	12.1	42.4	32.7	26.6	22.4	103.0	72.4	55.8	45.4	165.0	115.9	89.4	72.7		
80	1.396	9.1	7.4	6.2	5.4	24.4	18.8	15.3	12.9	45.2	34.9	28.4	23.9	109.8	77.2	59.5	48.4	176.0	123.6	95.3	77.5		
85	1.484	9.6	7.8	6.6	5.7	26.0	20.0	16.3	13.7	48.1	37.1	30.2	25.4	116.7	82.0	63.2	51.4	187.0	131.4	101.3	82.4		
90	1.571	10.2	8.3	7.0	6.1	27.5	21.2	17.2	14.5	50.9	39.2	31.9	26.9	123.6	86.8	66.9	54.5	197.9	139.1	107.2	87.2		
95	1.658	10.8	8.8	7.4	6.4	29.0	22.4	18.2	15.3	53.7	41.4	33.7	28.4	130.4	91.7	70.7	57.5	208.9	146.8	113.2	92.1		
100	1.745	11.3	9.2	7.8	6.7	30.5	23.5	19.1	16.1	56.6	43.6	35.5	29.9	137.3	96.5	74.4	60.5	219.9	154.6	119.1	96.9		
105	1.833	11.9	9.7	8.2	7.1	32.1	24.7	20.1	16.9	59.4	45.8	37.2	31.4	144.2	101.3	78.1	63.5	230.9	162.3	125.1	101.8		
110	1.920	12.5	10.2	8.6	7.4	33.6	25.9	21.1	17.8	62.2	48.0	39.0	32.9	151.0	106.1	81.8	66.6	241.9	170.0	131.1	106.6		
FATIGUE ANALYSIS																							
Alternating Moment, Ma (N.mm)		5.1	4.2	3.5	3.0	13.7	10.6	8.6	7.3	25.5	19.6	16.0	13.5	61.8	43.4	33.5	27.2	99.0	69.6	53.6	43.6	p. 539	
Alternating Moment, Ma @ 60° (N.mm)		3.4	2.8	2.3	2.0	9.2	7.1	5.7	4.8	17.0	13.1	10.6	9.0	41.2	28.9	22.3	18.2	66.0	46.4	35.7	29.1	p. 539	
Mean Moment, Mm (N.mm)		7.4	6.0	5.1	4.4	19.8	15.3	12.4	10.5	36.8	28.3	23.1	19.4	89.3	62.7	48.3	39.3	143.0	100.5	77.4	63.0	p. 539	
r (Ma/Mm)		0.7				0.7				0.7				0.7				0.7					
Alternating Stress, σa (MPa)		439.6	357.6	301.4	260.5	692.1	533.5	434.0	365.8	816.7	629.6	512.2	431.7	1343.7	944.2	727.9	592.2	1529.4	1074.7	828.4	674.0	p. 539	
Alternating Stress, σa @ 60° (MPa)		293.1	238.4	201.0	173.7	461.4	355.7	289.4	243.9	544.5	419.7	341.5	287.8	895.8	629.5	485.2	394.8	1019.6	716.5	552.3	449.3		
Mean Stress, σa (MPa)		635.0	516.6	435.4	376.3	999.7	770.6	627.0	528.4	1179.7	909.4	739.8	623.6	1940.9	1363.9	1051.3	855.3	2209.1	1552.4	1196.6	973.5	p. 539	
Sr (= 0.50Sut) (MPa)		1222.4				1190.5				1164.2				1141.9				1122.5				Table 10-10	
Endurance Limit, Se (MPa)		651.9				634.9				620.9				609.0				598.7				Eqn. 10-58	p. 536
Endurance Strength, Sa (MPa)		576.3				561.3				548.9				538.4				529.3				Eqn. 10-59	p. 536
nf @ 60°		1.97	2.42	2.87	3.32	1.22	1.58	1.94	2.30	1.01	1.31	1.61	1.91	0.60	0.86	1.11	1.36	0.52	0.74	1.04	1.18	Eqn. 10-60	p. 537
nf @ 90°		1.31	1.61	1.91	2.21	0.81	1.05	1.29	1.53	0.67	0.87	1.07	1.27	0.40	0.57	0.74	1.12	0.35	0.49	0.69	1.05	Eqn. 10-60	p. 537

APPENDIX C - FINITE ELEMENT ANALYSIS

C.1. Introduction

Before building the initial prototype, it is useful to run numerical simulations to approximate the material response of various components. The Finite Element Method enables the simulation of numerous loading cases and conditions to identify areas of concern in the structure, as well as to determine the stress-distribution. Solidworks Simulation® will be used to solve the FEA, the results of which will be compared to future experimental strength tests covered in Chapter 7.

C.2. Scope of Work

The simulations will include the study of four test cases, namely the hyper-extension and lateral loading of the 3rd and 5th digits of the hand. The scope of work is to solve the structural stress state using the supplied CAD geometry, material conditions, constraints, boundary conditions and loading cases. The following numerical analysis options are excluded from the study:

- The buckling response of the structure is not considered and is outside the analysis scope.
- Material fatigue is not considered and is outside the analysis scope.
- The dynamic and or vibration/eigenmode response of the structure is not considered and is outside the analysis scope.

Furthermore, the following assumptions are also made:

- The material is homogenous and linear isotropic.
- Material plasticity is not considered due to its complex non-linear response.
- Temperature dependent material properties are not considered.
- Geometrical imperfections are ignored.
- Residual stresses in the material are not considered.
- Thermal material expansion/contraction is not considered.

C.3. CAD Geometry

The finger assemblies are shown in Figure C1, together with a rigid clamping block onto which they clamp. The clamping block performs the same support function that the palmar structure would, yet provides a rigid support structure for the phalangeal assemblies during testing. Moreover, it is easily clamped and can be interchangeably used for both the fatigue and the strength experiments discussed in subsequent chapters. Stainless steel locking pins are inserted into each interphalangeal joint about

which the phalanges pivot. These pins are omitted from the study, but their effect is modelled through pin coupling interactions. The effects of the torsional spring elements are omitted from the study to enable a worst-case scenario, as the torsion springs would increase the rigidity of the structure when deformed under both lateral and hyper-extensive loading; effectively reducing the load experienced by each of the phalanges.

The channel tubing and channel rings are also omitted as deflections of the structure are small and their presence will not strengthen the overall structure significantly. Hollow brass mandrels are inserted into each side of the clamping block to laterally support the proximal end of the proximal phalanx and locate the locking pin.

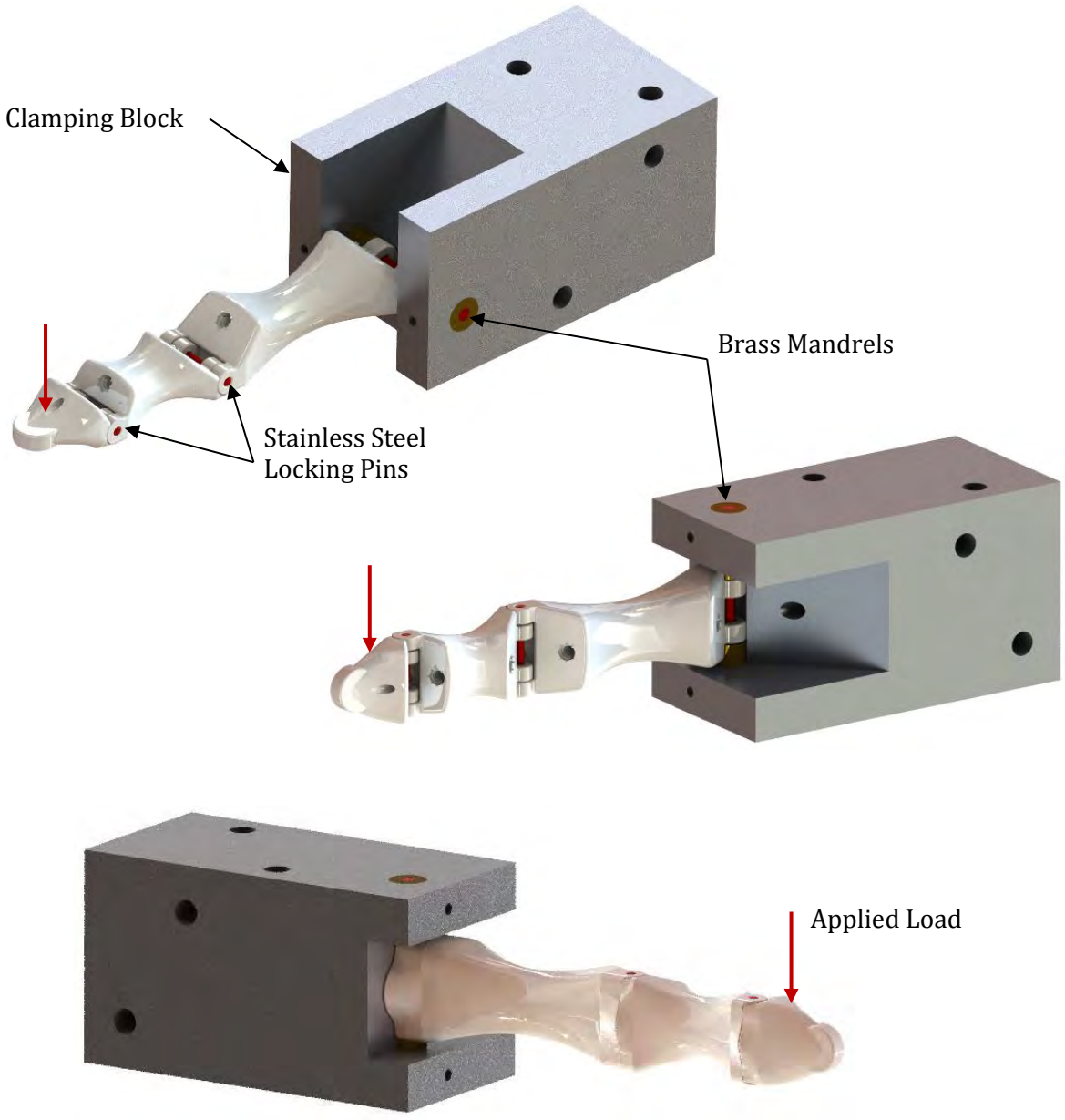

Figure C1 - FEA test specimen assembly for hyper-extensive (top) and lateral loading conditions (centre & bottom).

C.4. Mesh Details and Refinement

The deformable components of the assembly, namely the EOS PA2200 nylon phalanges, are modelled using second order continuum-based 3D parabolic tetrahedral solid elements, as shown in Figure C2. The stainless steel interphalangeal locking pins are modelled using built-in pin interactions, and therefore remain unmeshed. The additional assembly components are modelled as being rigid, namely the clamping block and brass mandrels. In addition to the meshing of the solid elements, mesh refinement is performed at areas of concern (high stress areas) as shown in Figure C3 and Figure C4, for hyperextensive loading conditions whereas the lateral refinement scheme incorporates these together with additional nodes at the inner borders of the hinges as seen in Figure C5.

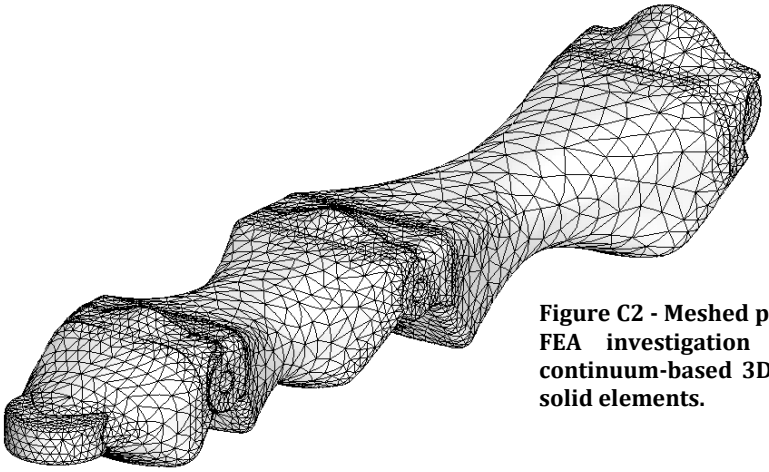

Figure C2 - Meshed phalangeal assembly for FEA investigation using second order continuum-based 3D parabolic tetrahedral solid elements.

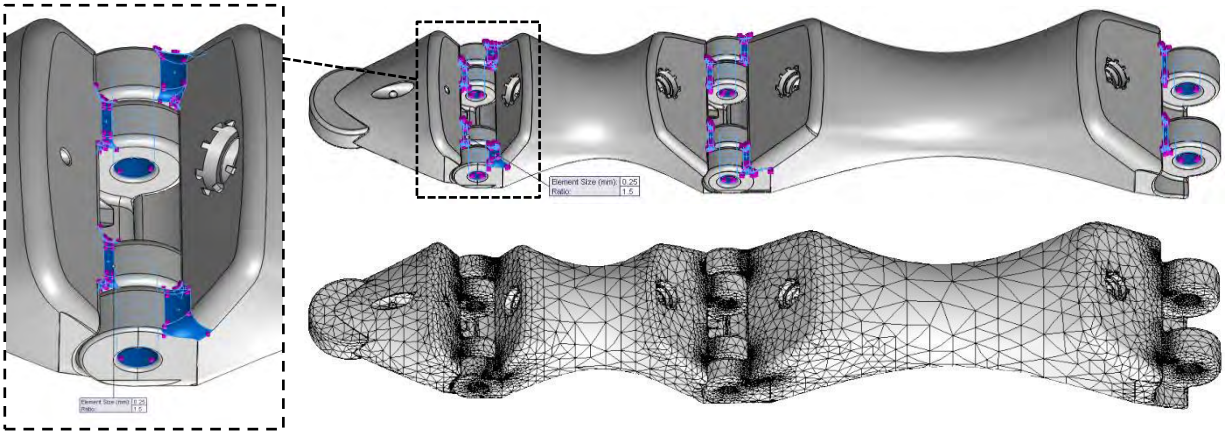

Figure C3 - Mesh refinement at high-stress areas (top right) with close-up (left) and final refined-mesh 3rd digit component for hyperextensively loaded FEA analysis.

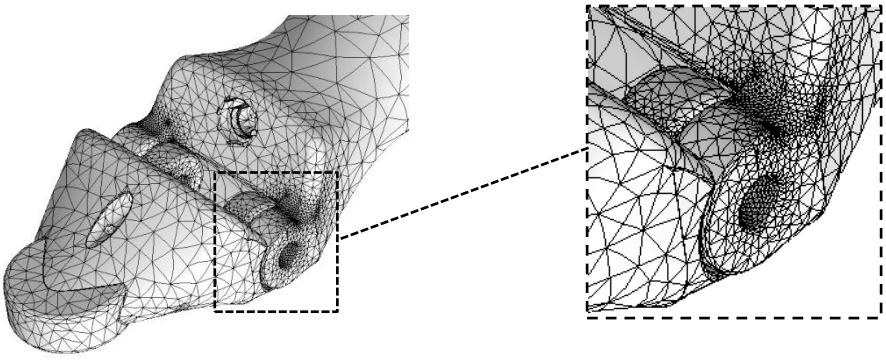

Figure C4 - Mesh refinement at Distal Interphalangeal (DIP) joint (left) with close-up (right).

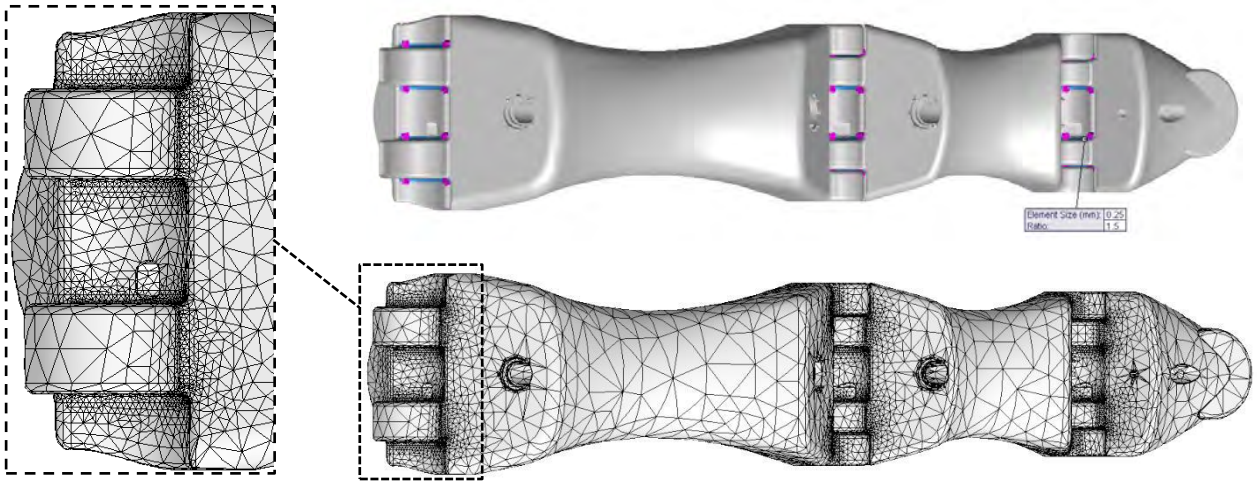

Figure C5 - Mesh refinement at high-stress areas (top right) and final refined-mesh 3rd digit component, with close-up of proximal end (left) for laterally loaded FEA analysis.

A summary of the mesh characteristics is given in Table C1.

Table C1 - Mesh Characteristics for FEA Investigation of 3rd and 5th Digits

	Hyperextensive Specimens		Lateral Specimens	
	3rd Digit	5th Digit	3rd Digit	5th Digit
Element Type	Second order continuum-based 3D parabolic tetrahedral solid elements			
Mesh Type	Mixed Mesh			
Mesher Used	Curvature based mesh			
Jacobian Points	4 points			
Mesh Quality	High			
Total Nodes	162 626	107 875	190 853	118 825
Total Elements	119 539	81 074	146 945	93 294
Total Degrees of freedom	516 444	338 460	602 835	370 806
Maximum Element Size	12.92mm	11.13mm	10.997mm	11.46mm
Minimum Element Size	0.25mm	0.25mm	0.30mm	0.30mm

C.5. Material Classification

1. The phalanges are manufactured from EOS PA2200 Nylon and are modelled using its mechanical properties.
2. Due to the polymeric nature of the phalanges, post-yielding tensile behaviour is complex and therefore a simple linear elastic model was adopted. The isotropic linear-elastic model is defined by Young's Modulus of 1.7 GPa and a Poisson Ratio equal to 0.394. Yield strength of this material is 40 MPa with UTS of 45 MPa.
3. The stainless steel locking pins are also modelled as linear-elastic, with a Young's modulus of 200 Gpa respectively and a Poisson Ratio equal to 0.28.

4. The aluminium clamping block and brass mandrels are modelled as linear-elastic structures with Young's modulus of 70 GPa and 100 GPa respectively, and a Poisson Ratio equal to 0.33. However, these components are assumed rigid in relation to the Nylon and will hence be modelled as such to reduce computational effort.
5. The effects due to weld-induced material stresses and residual stresses are not considered.

C.6. Constraints and Contact Interactions

1. Each phalanx is located in place by a locking pin, which acts has as a hinged joint interaction for rotational motion. This is modelled using a pin connector interaction (Figure C6), allowing rotation about the hinge, but no axial translation of the pin. A total of three pin connector interactions are modelled at the DIP, PIP and MCP joints respectively; for both hyperextensive and lateral testing.

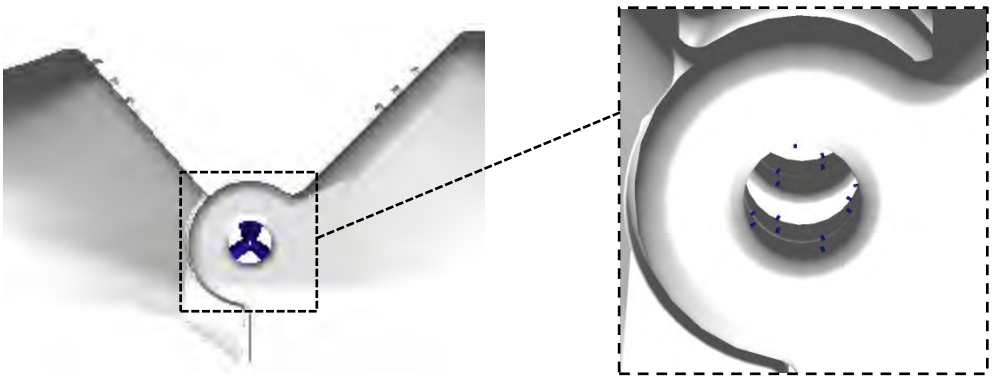

Figure C6 - Pin interaction constraints in the FEA model to simulate the locking pins of the interphalangeal hinge-joints.

2. Hyperextensive interaction between the planar surfaces of the mating posterior protrusions of the phalanges at their PIP and DIP joints are modelled as non-penetrating contact interactions, for both test cases. Conversely, the MCP protrusion is modelled as a non-penetrating contact for the lateral loading cases only.

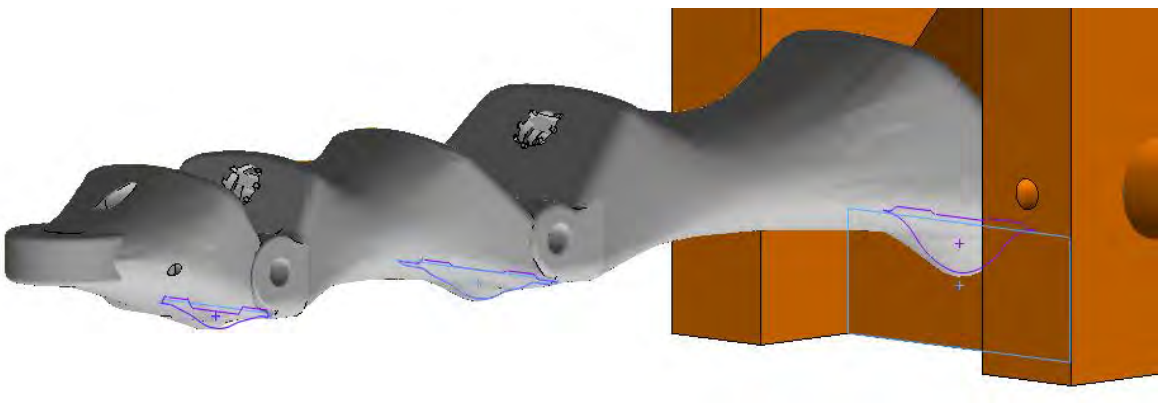

Figure C7 - Non-penetrating contact surfaces for hyperextensively and laterally loaded FEA cases.

3. For the lateral loading cases, the planar mating surfaces of the interphalangeal hinges of the DIP, PIP, and MCP joints (Figure C8) as well as the cylindrical mating surfaces (Figure C8) are given non-penetrating contact interactions, which transfer the contact forces between the phalanges.

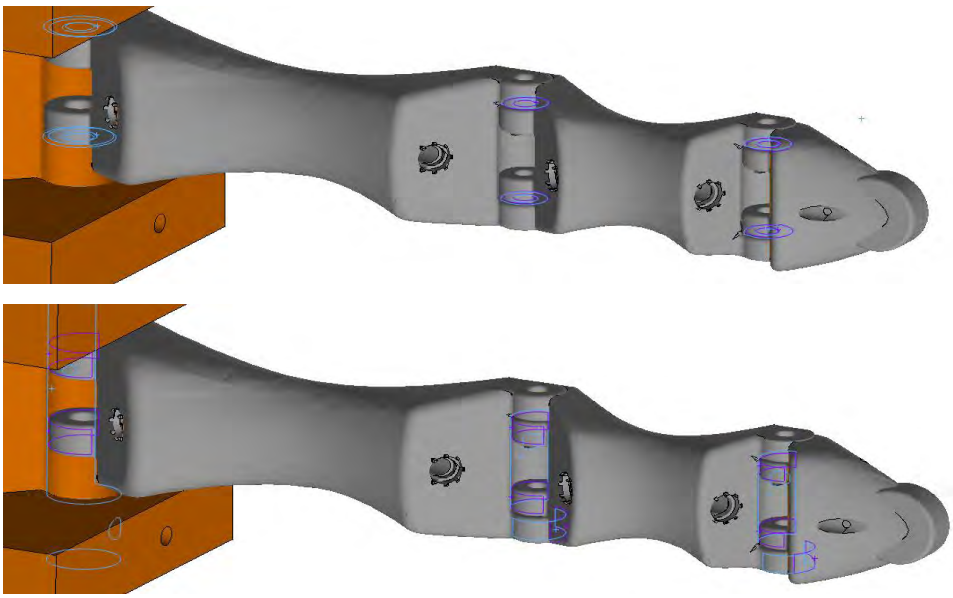

Figure C8 - Planar and cylindrical non-penetrating contact surfaces (top and bottom respectively) for laterally loaded FEA cases.

C.7. Boundary Conditions

1. The rigid clamping block and both brass mandrels are fixed for all test cases, as seen in Figure C9 (top right and left respectively), preventing translation and rotation in all directions.

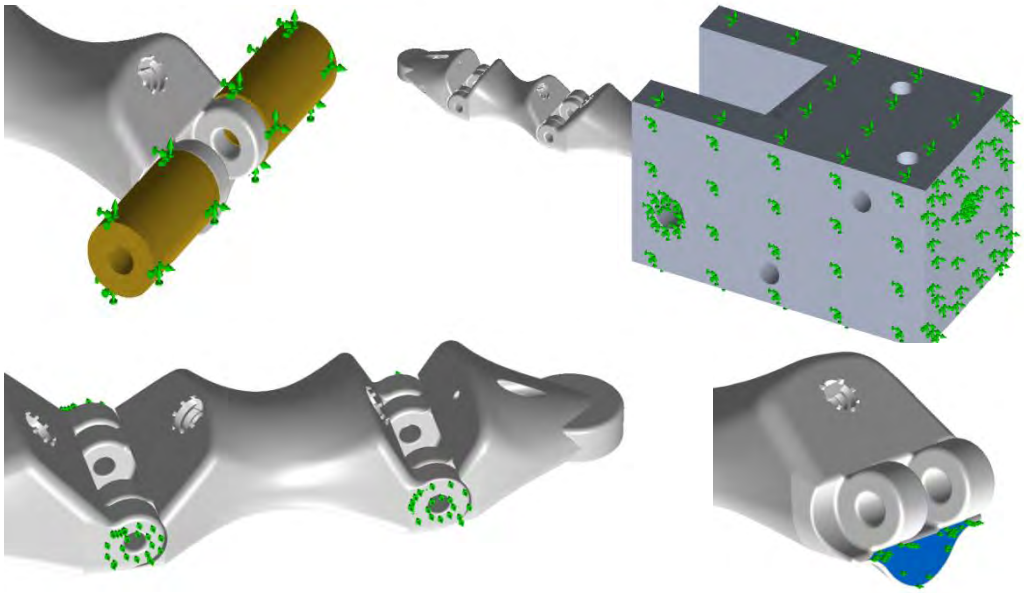

Figure C9 - Boundary conditions of the FEA models; fixed pins (top left), fixed clamping block (top right), laterally constrained PIP and DIP joint (bottom left) & proximally-constrained proximal phalanx (bottom right).

2. Two-dimensional roller/sliding contacts interact with the lateral surfaces of the proximal and middle phalanges at the PIP and DIP joints (Figure C9, bottom left); preventing motion in the x-direction (laterally), limiting translation to the YZ-plane. Hyperextensive loading cases only.
3. A two-dimensional roller/sliding contact interacts with the proximal planar surface of the posterior protrusion (knuckle) of the proximal phalanx; preventing motion in the y-direction (proximally), limiting translation to the XY-plane as shown in Figure C9 (bottom right). Hyperextensive loading cases only.
4. For the lateral loading cases, two-dimensional rollers/sliders constrain the lateral faces of the distal phalanx to motion in the XZ-plane as shown in Figure C10.

Figure C10 - Two-dimensional roller/slider boundary constraint on distal phalanx for lateral loading cases in FEA.

C.8. Load Cases and Structural Loading

Two loads are applied to each specimen (Figure C11). Firstly, a concentrated load is applied to the 3rd and 5th phalanges at gauge lengths of 95 mm and 75 mm from the axis of the MCP joint respectively. This load is varied between 20 N and 100 N for the various test cases. Secondly, a global gravitational force to the model; aligning parallel to the applied hyperextensive or lateral loads in each of the test cases.

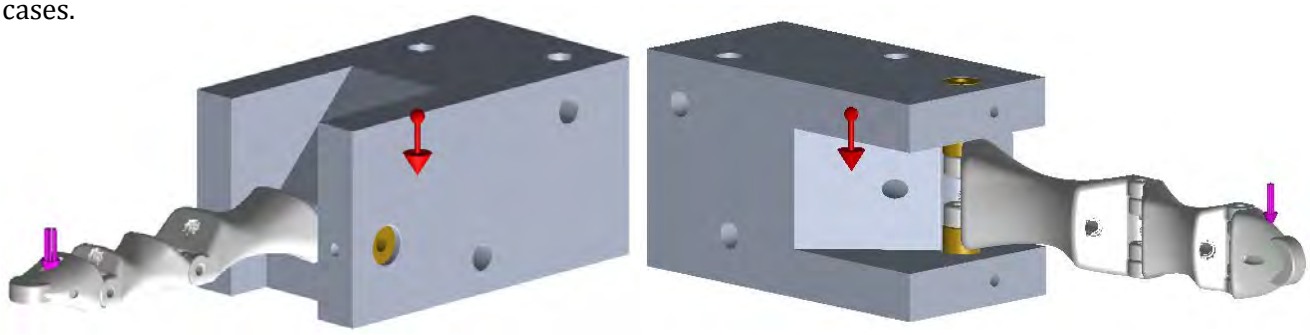

Figure C11 - Applied hyperextensive (left) and lateral (right) concentrated loads (purple arrows) with the inclusion of gravitational acceleration (red arrows).

C.9. Acceptance Criteria

Ideally, the performance of the EOS PA2200 Nylon material should remain within the elastic region, not exceeding the yield limit and tensile limits of 40 MPa and 45 MPa respectively. Minor localised plastic deformation of the structure is acceptable, provided it does not seriously affect the operation/functionality of the digit.

C.10. Summarised Results of Investigation

On completion of the FEA simulations, the following results were obtained:

C10.1. Regions of Highest Stress Concentration for Hyperextensive Loading

This portion of the study reveals areas of highest stress concentrations in the structure under hyperextensive loads. These are identified by the red areas in the opaque images (Figure C12), and the dark blue areas in the translucent images below (Figure C13).

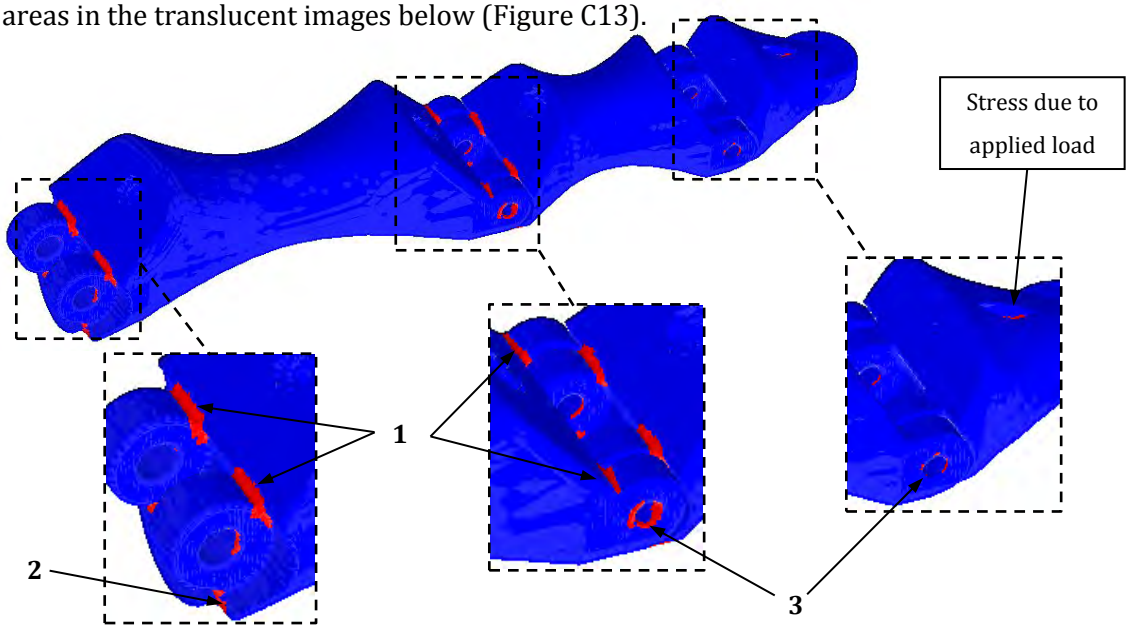

Figure C12 – Regions of highest stress concentration (red) for hyperextensive loading conditions.

As expected, the areas containing the highest concentrations of stress are located at the radii of the hinge points (1), at the lateral edges of the posterior protrusions (2), and the lateral edges of the inner pin hole (3) where the phalanges interface with each other; with the highest tensile stresses located at the PIP joint. On the distal phalanx above, the stress due to the applied load is shown.

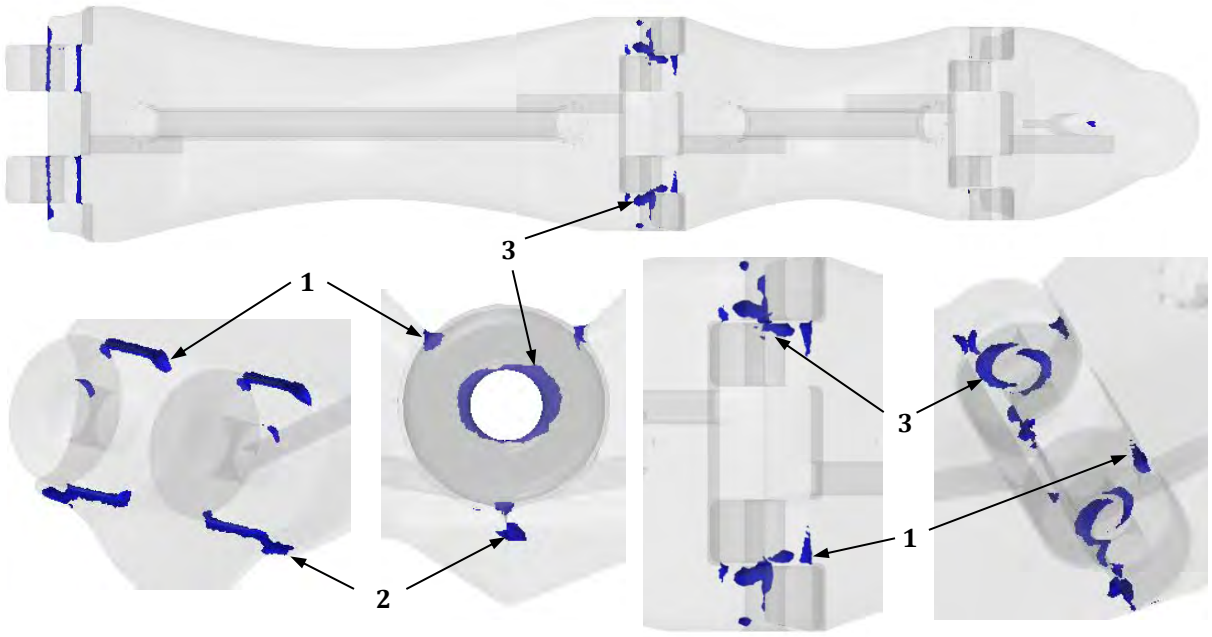

Figure C13 – Regions of highest stress concentration (blue) for hyperextensive loading conditions.

C10.2. Regions of Highest Stress Concentration for Lateral Loading

For lateral loading on the other hand, the most stressed regions are on the lateral edges (4) of the hinge interfaces as seen in (Figure C14). Similarly to the hyperextensive loading, the lateral edges of the pin hole (5) are stressed too; especially at the PIP joint as shown in (Figure C15) below.

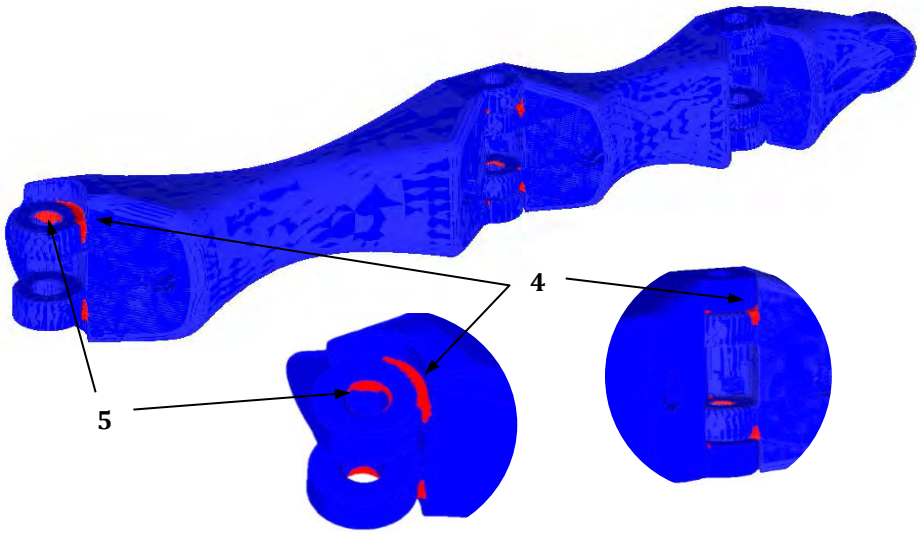

Figure C14 – Regions of highest stress concentration (red) for lateral loading conditions, with close-ups.

Referring to (Figure C15) below, the region of highest stress and thus of concern is the confluence (6) of the lateral pin hole stress and the radial-lateral stress of the hinge on the middle phalanx at the PIP joint. The combination of these tensile stresses is likely to impair the structural strength of the assembly under lateral loading.

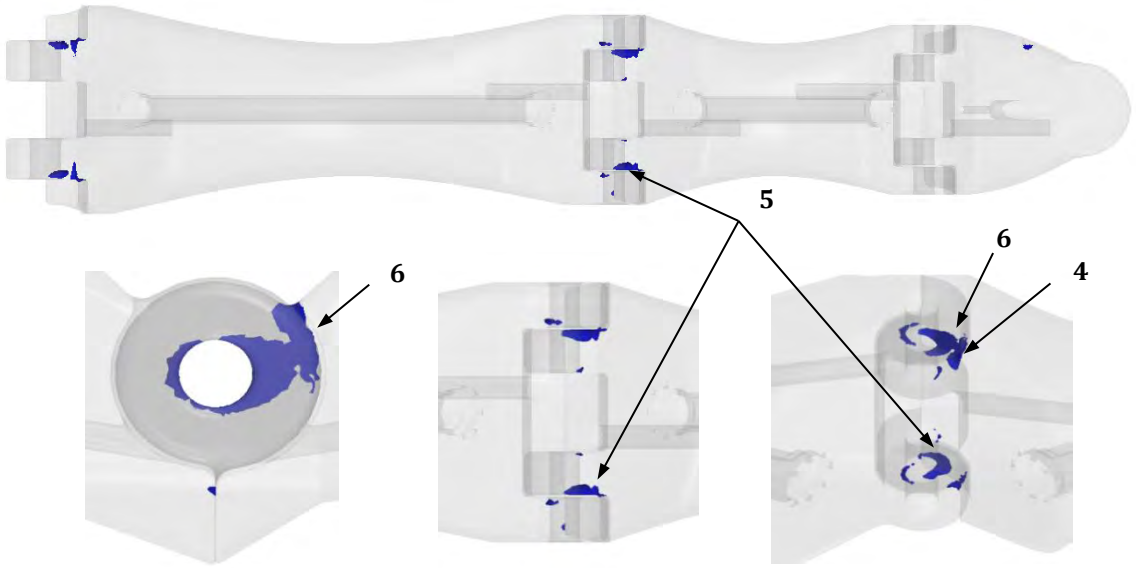

Figure C15 – Regions of highest stress concentration (blue) for lateral loading conditions (top), with close-up views of PIP joint (bottom).

Increasing the radius of the radii and cross-sectional contact area of the protrusions in future iterations of the design would lead to decreased stress concentrations. Additionally, an optimisation investigation into the relationship between pin-strength, hinge thickness and pin-hole diameter can be made to maximise the strength of the joint.

C10.3. Hyperextensive Loading of 3rd Digit

This digit was loaded at 20 N, 40 N, 60 N, 80 N and 82 N, after which the displacement behaviour is analysed and the stress state evaluated.

C10.3.1. Displacement Results

Max. Disp. @ 20 N
= 5.515 mm

Max. Disp. @ 40 N
= 10.896 mm

Max. Disp. @ 60 N
= 16.503 mm

Max. Disp. @ 80 N
= 21.438 mm

Max. Disp. @ 82 N
= 22.284 mm

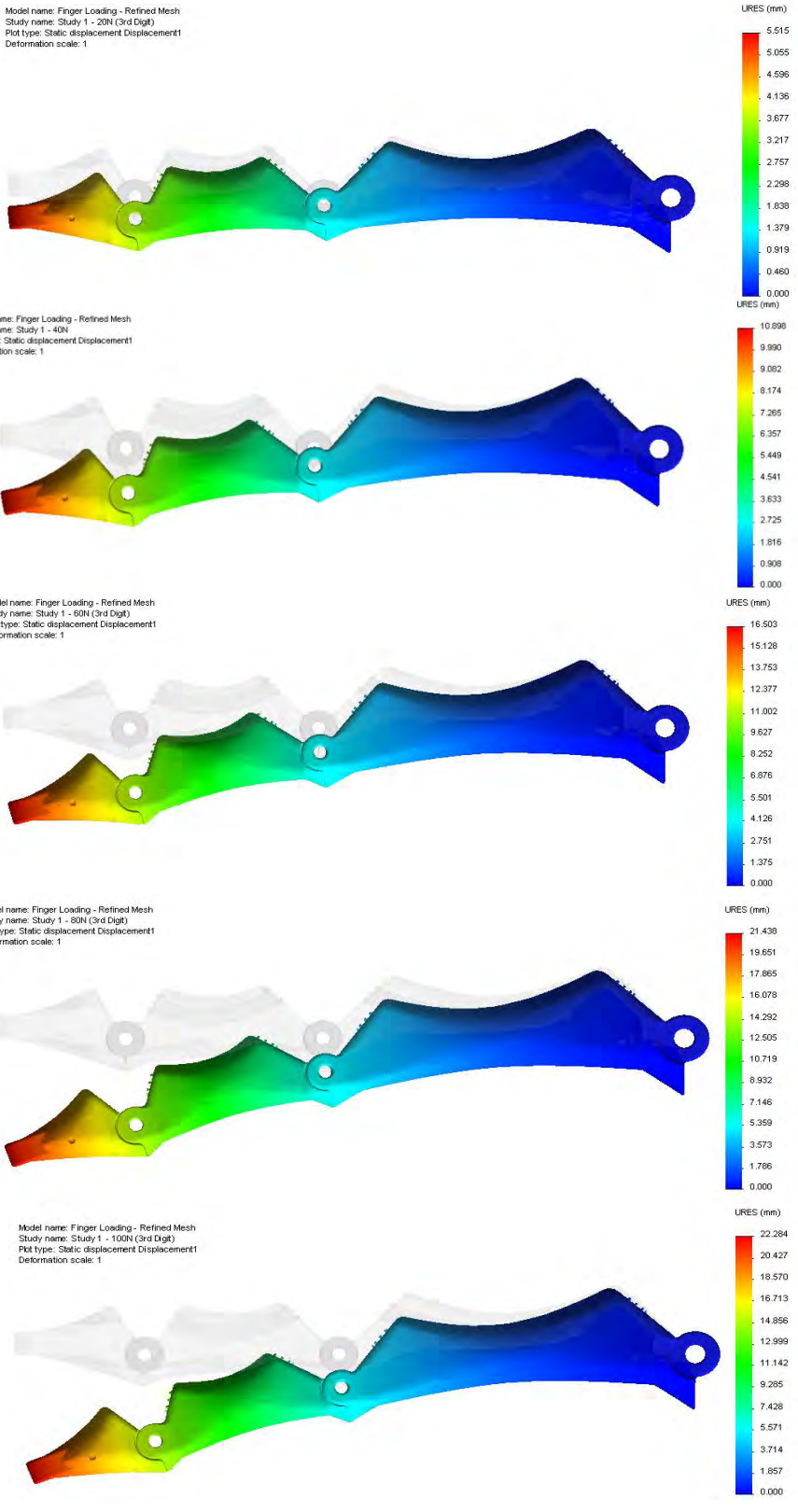

Figure C16 – Maximum displacement of 3rd digit due to hyperextensive loads.

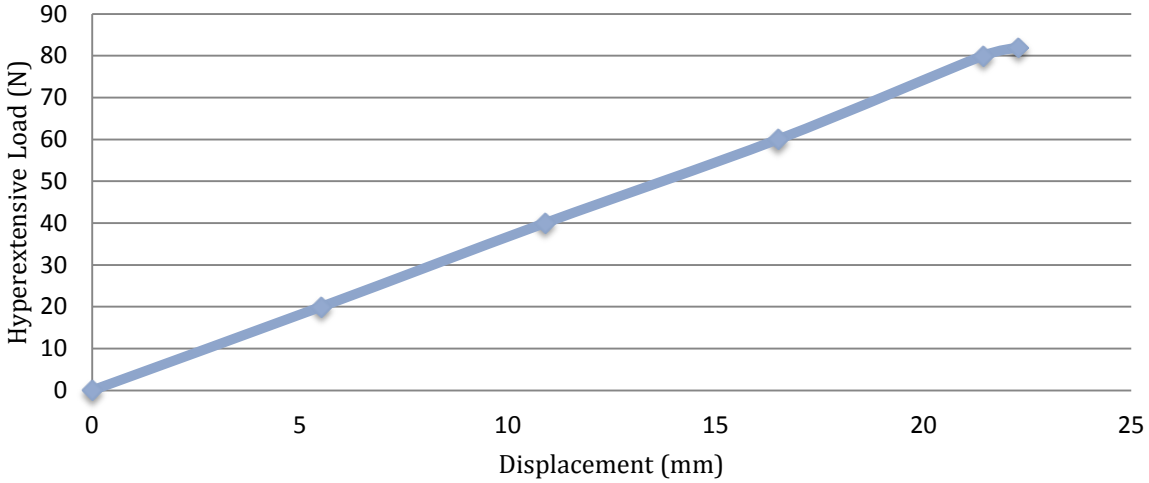

Figure C17 – Load vs. displacement behaviour of 3rd digit due to hyperextensive loading.

C10.3.2. Stress State @ 80 N

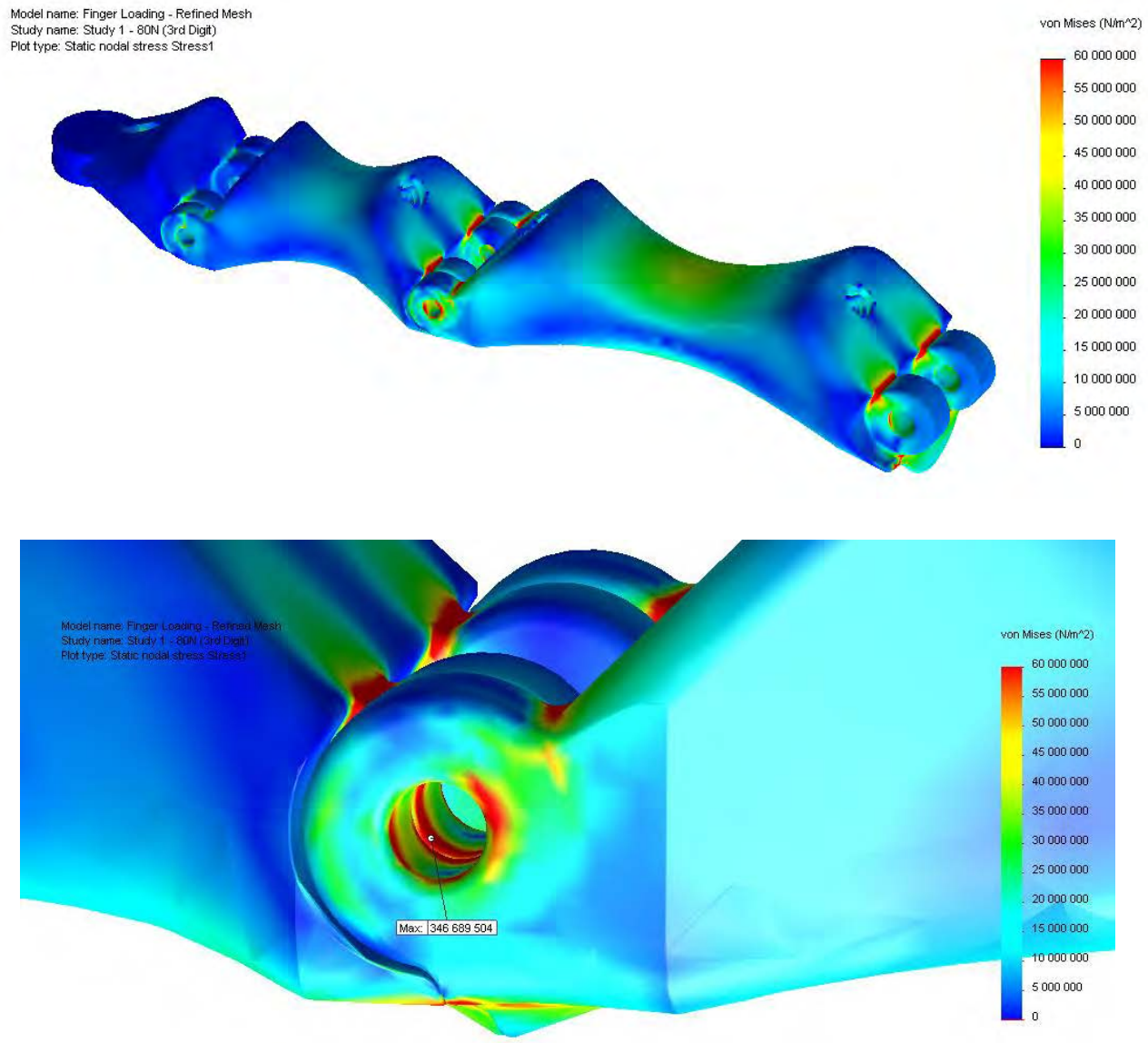

Figure C18 – von Mises Stress state of 3rd digit @ 80 N, with isometric view (top) and lateral view of the maximum stress state in the pin hole (bottom).

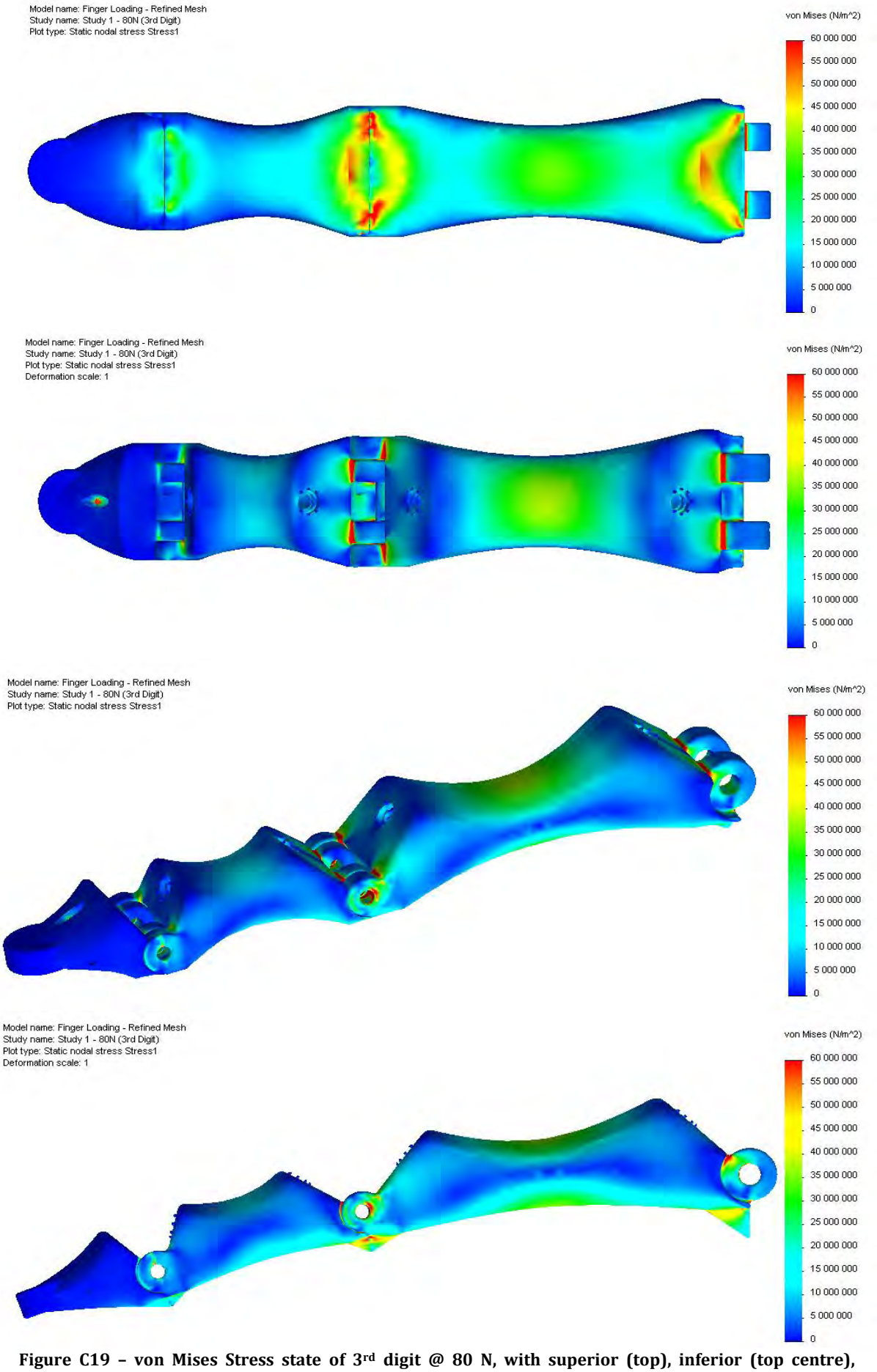

Figure C19 – von Mises Stress state of 3rd digit @ 80 N, with superior (top), inferior (top centre), isometric (bottom centre) and lateral views of the stress state.

C10.4. Hyperextensive Loading of 5th Digit

This digit was loaded at 20 N, 30 N, 40 N, 50 N and 55.8 N, after which the displacement behaviour is analysed and the stress state evaluated.

C10.4.1. Displacement Results

Max. Disp. @ 20 N
= 5.035 mm

Max. Disp. @ 30 N
= 7.535 mm

Max. Disp. @ 40 N
= 10.029 mm

Max. Disp. @ 50 N
= 12.460 mm

Max. Disp. @ 55.8 N
= 13.902 mm

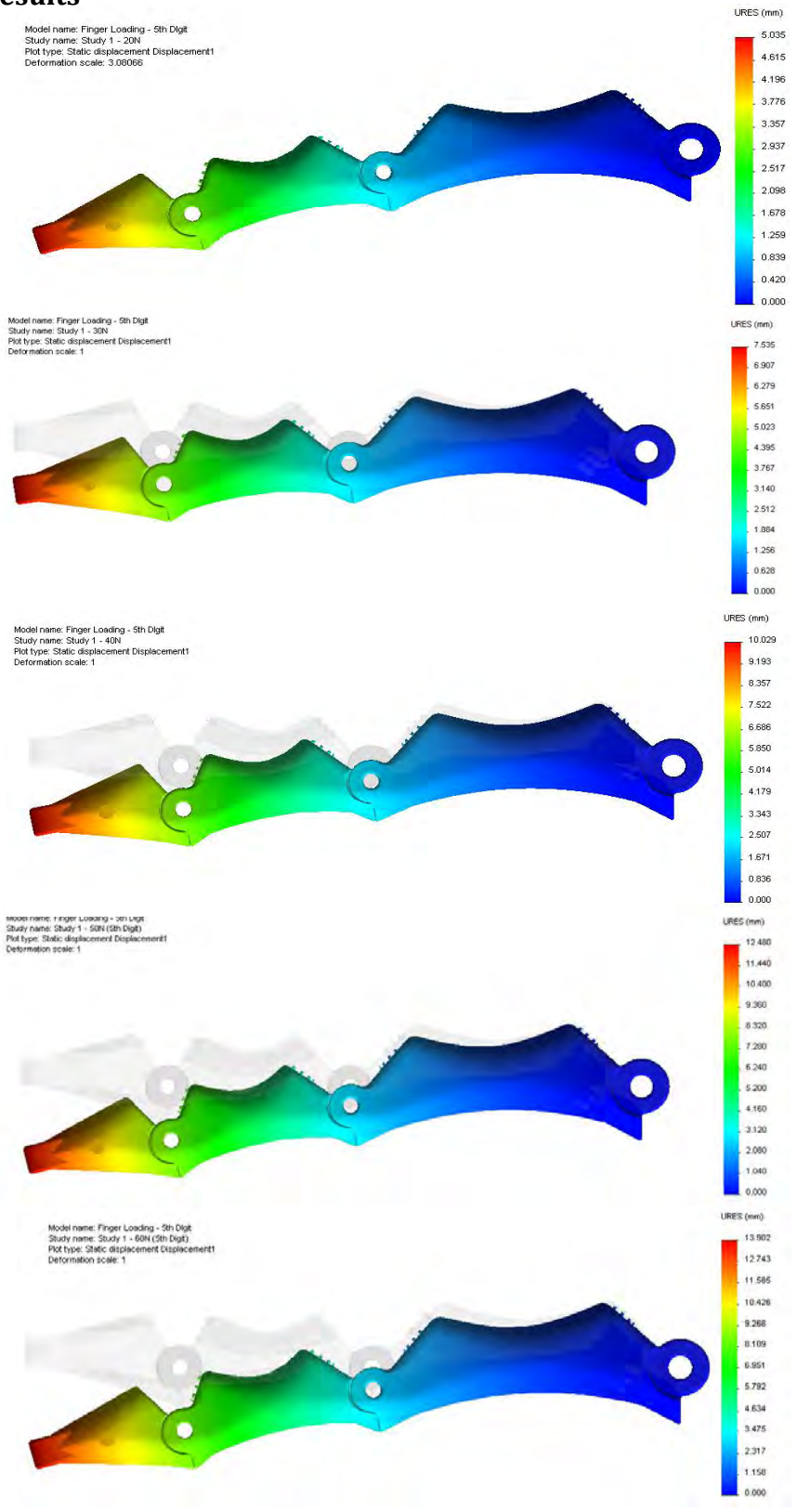

Figure C20 – Maximum displacement of 5th digit due to hyperextensive loads.

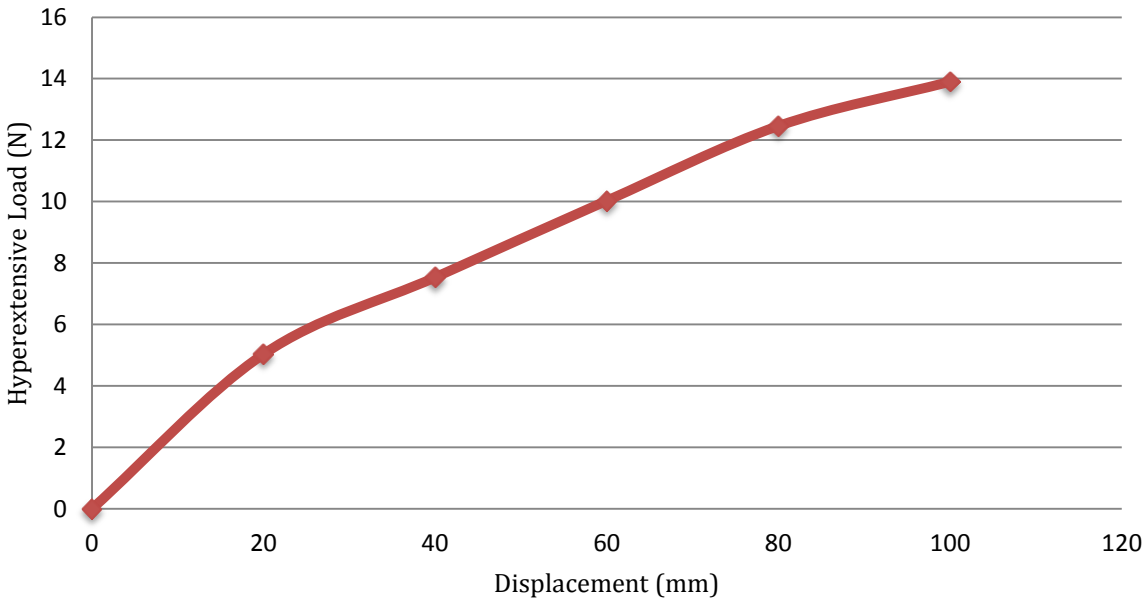

Figure C21 – Load vs. displacement behaviour of 5th digit due to hyperextensive loading.

C10.4.2. Stress State @ 55.8 N

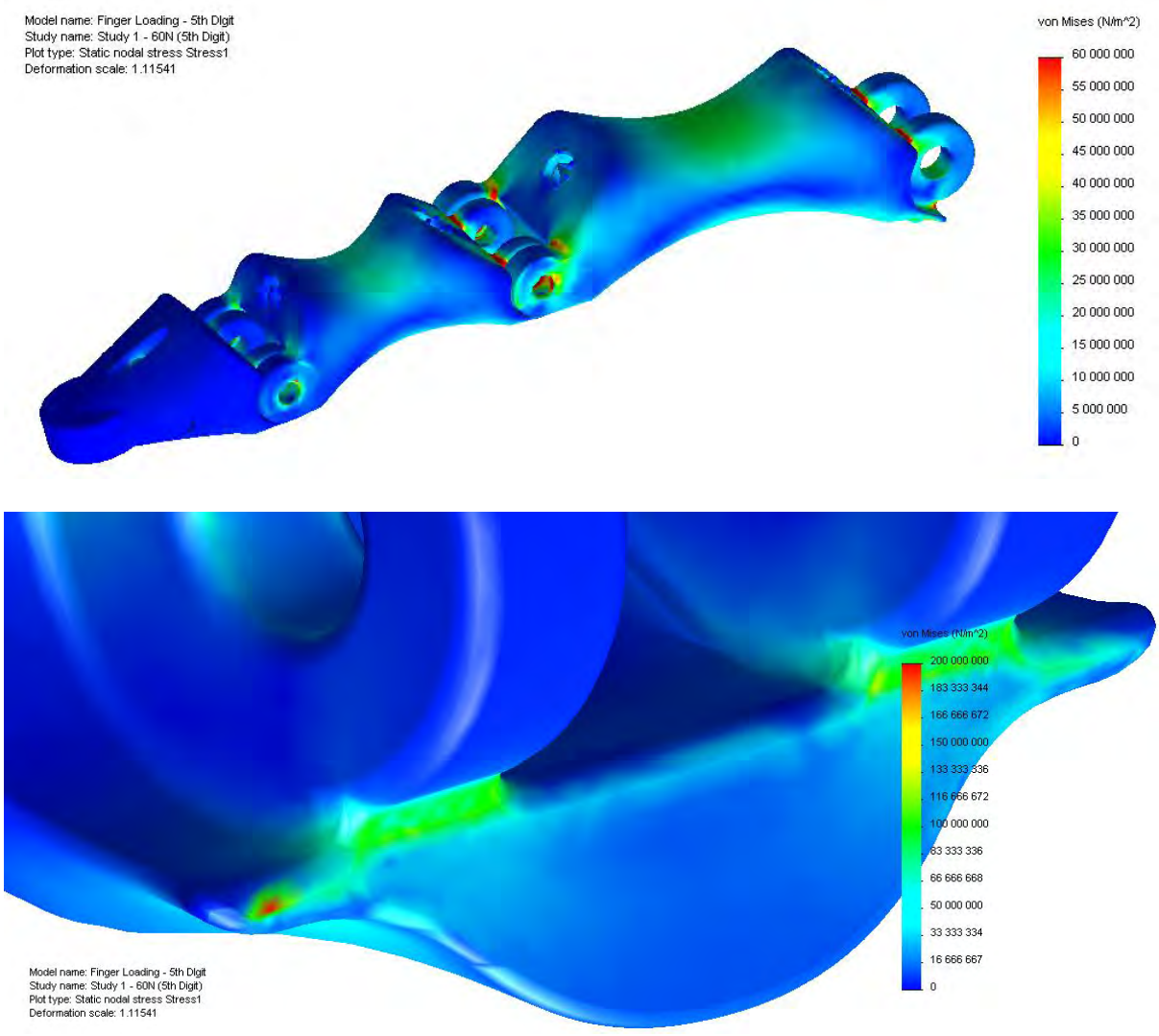

Figure C22 – von Mises Stress state of 5th digit @ 55.8 N, with isometric view (top) and proximal view of the maximum stress state at the lateral edge of the posterior protrusion (bottom).

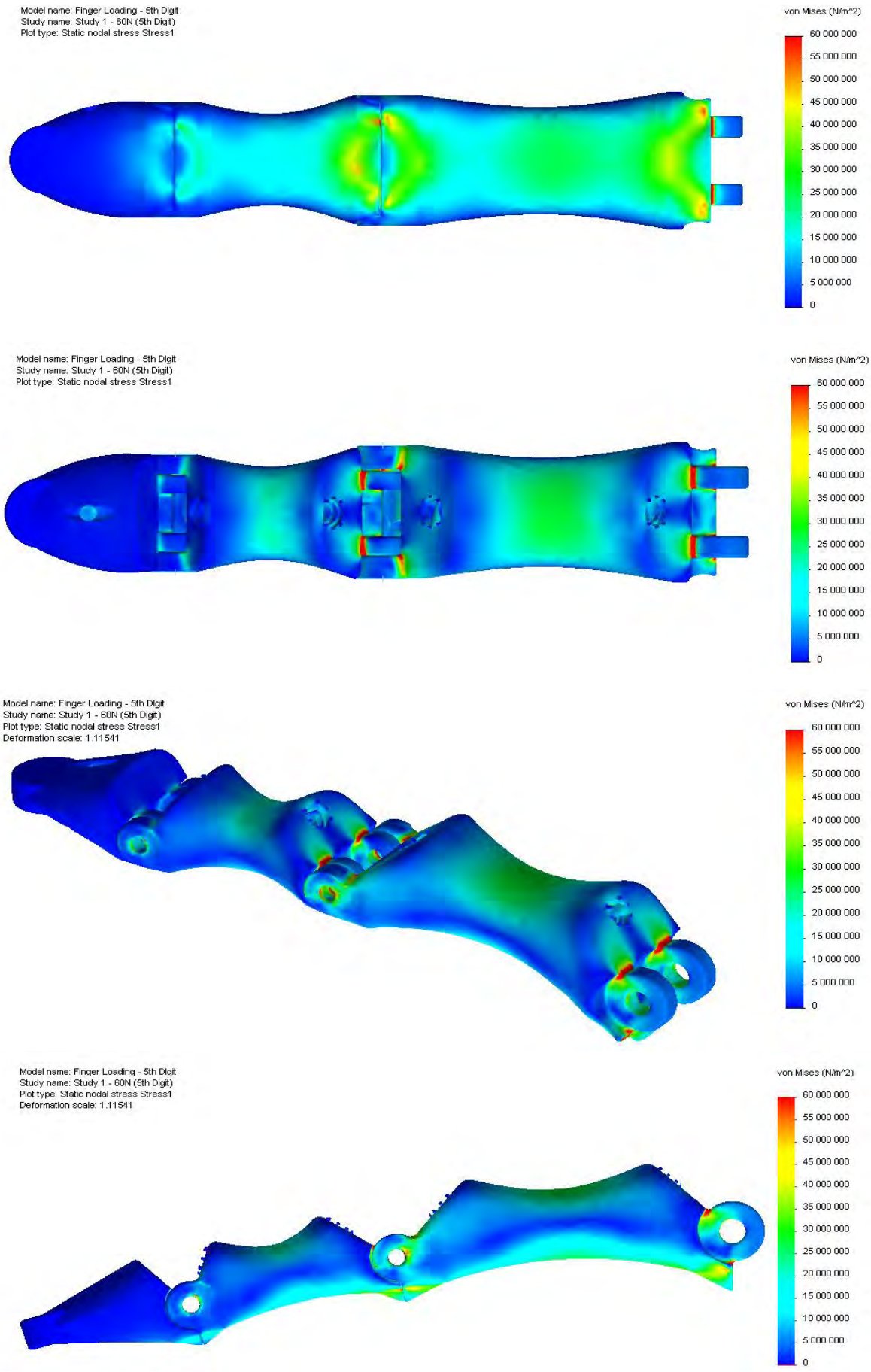

Figure C23 – von Mises Stress state of 5th digit @ 55.8 N, with superior (top), inferior (top centre), isometric (bottom centre) and lateral views of the stress state.

C10.5. Lateral Loading of 3rd Digit

This digit was loaded at 20 N, 40 N, 60 N, 80 N and 100 N, after which the displacement behaviour is analysed and the stress state evaluated.

C10.5.1. Displacement Results

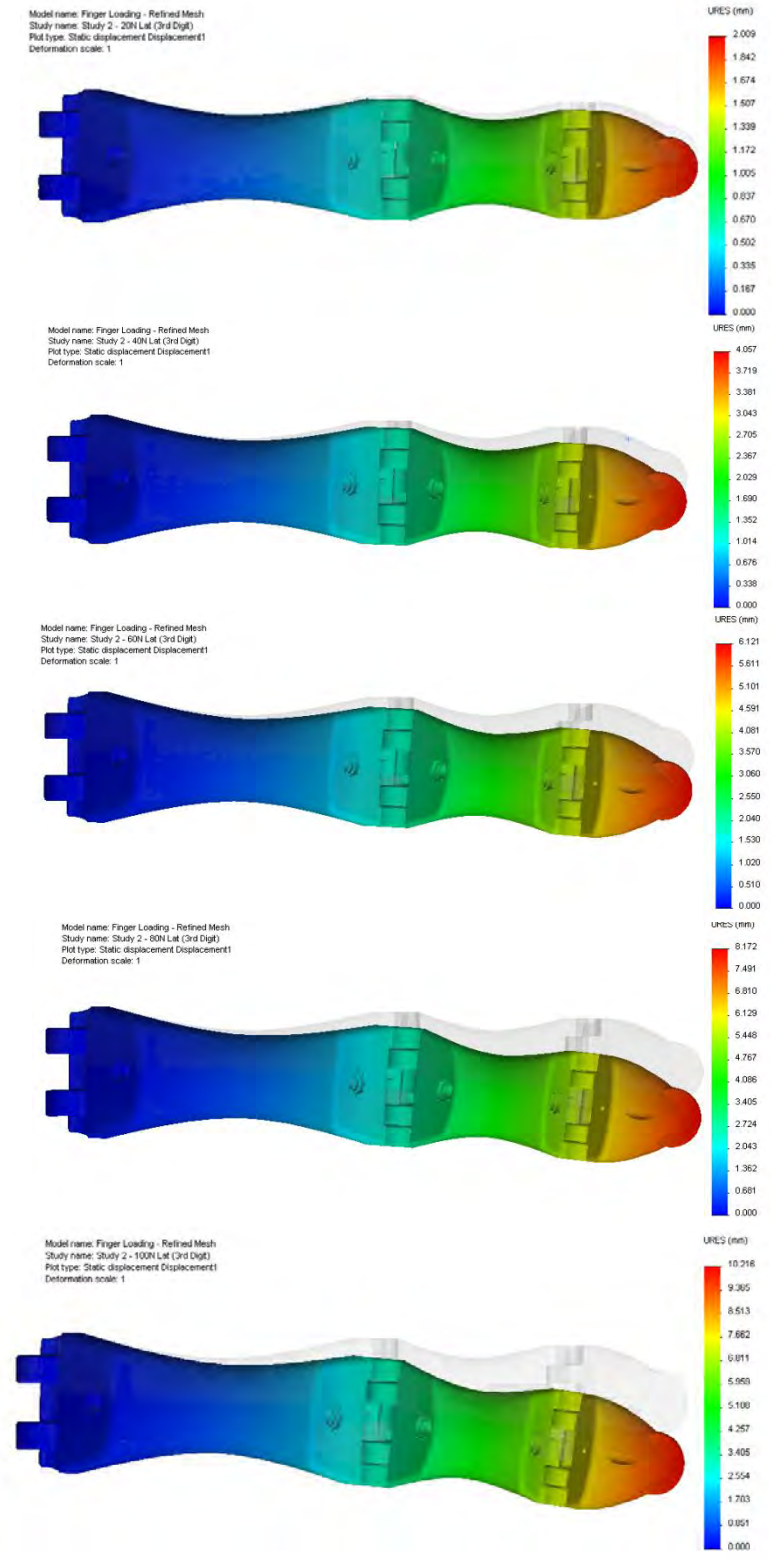

Max. Disp. @ 20 N
= 2.009 mm

Max. Disp. @ 40 N
= 4.057 mm

Max. Disp. @ 60 N
= 6.121 mm

Max. Disp. @ 80 N
= 8.172 mm

Max. Disp. @ 100 N
= 10.216 mm

Figure C24 – Maximum displacement of 3rd digit due to lateral loads.

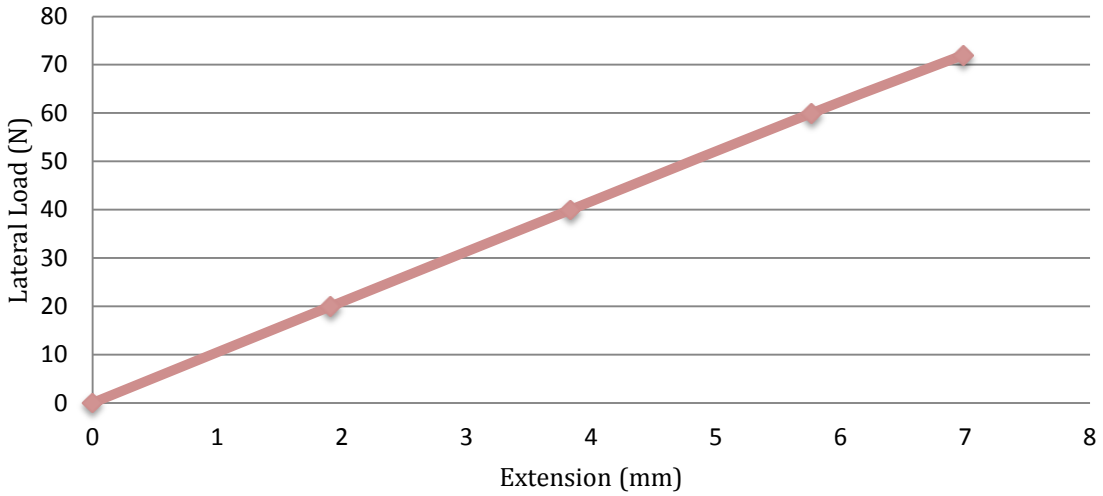

Figure C25 – Load vs. displacement behaviour of 3rd digit due to lateral loading.

C10.5.2. Stress State @ 100 N

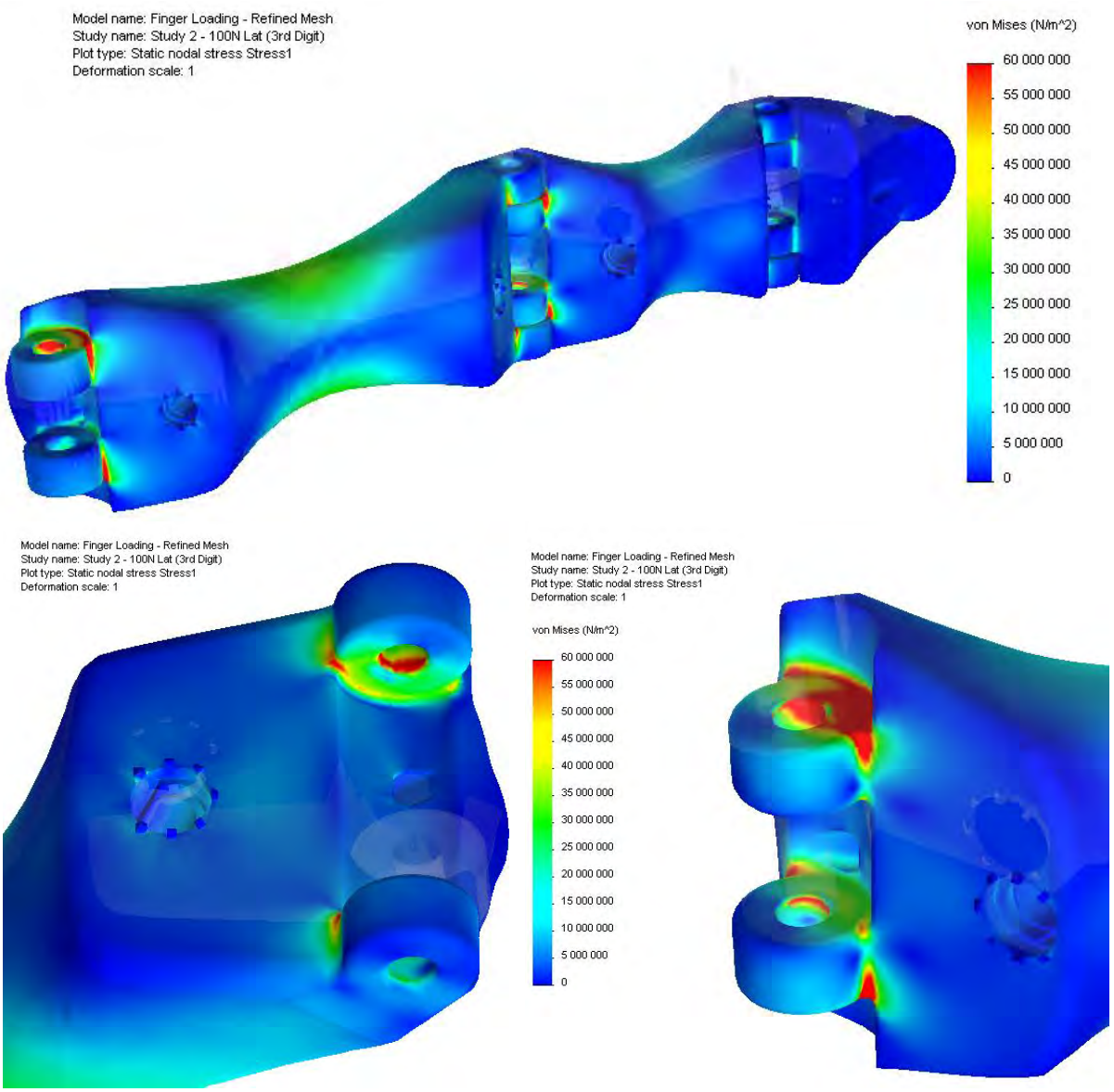

Figure C26 – von Mises Stress state of 3rd digit @ 100 N, with isometric view (top) and perspective view of the maximum stress state at the distal end of the prox. phalanx (left), and proximal end of the middle phalanx (right).

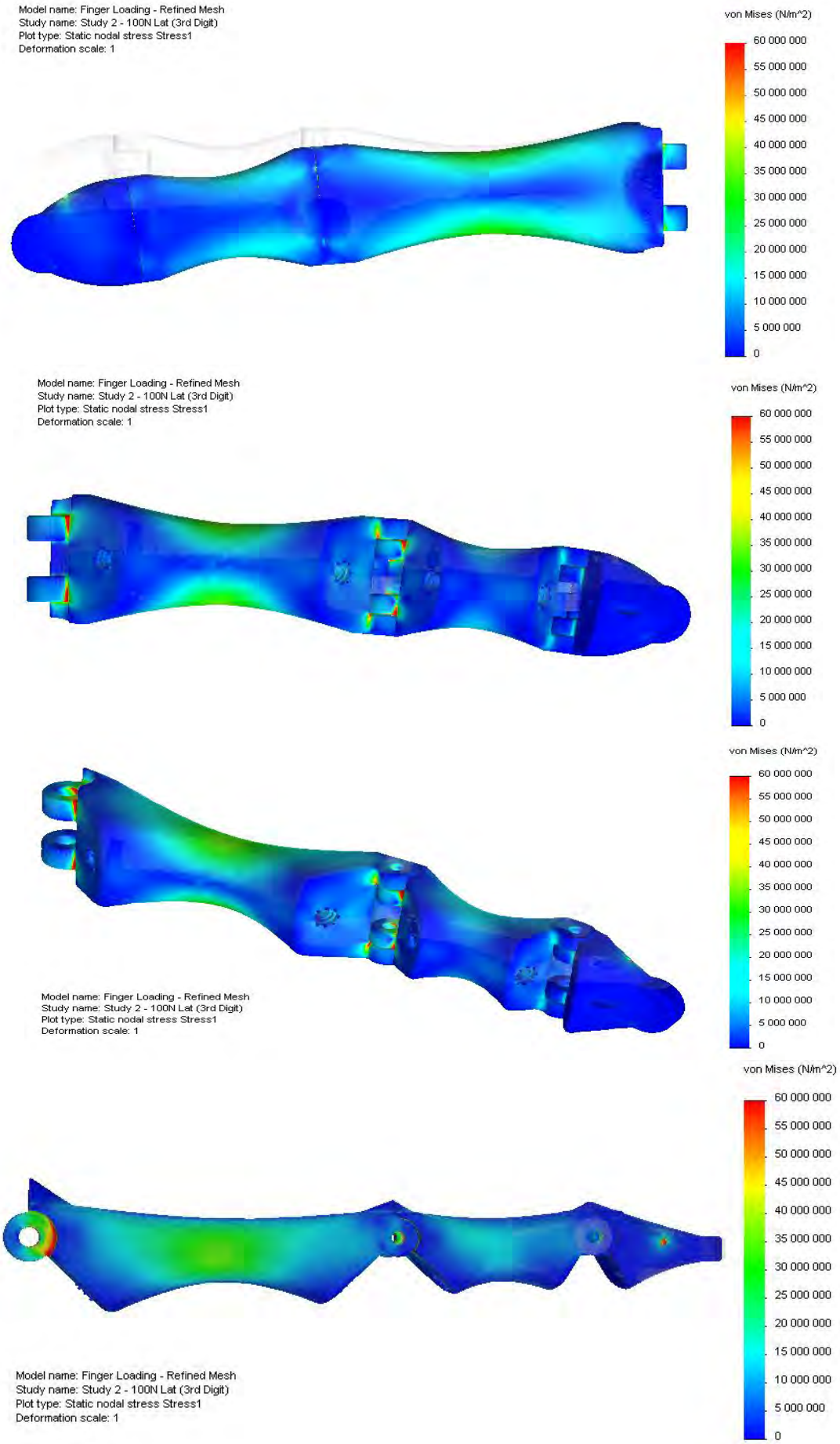

Figure C27 – von Mises Stress state of 3rd digit @ 100 N, with superior (top), inferior (top centre), isometric (bottom centre) and lateral views of the stress state.

C10.6. Lateral Loading of 5th Digit

This digit was loaded at 20 N, 40 N, 60 N, 72 N, after which the displacement behaviour is analysed and the stress state evaluated.

C10.6.1. Displacement Results

Max. Disp. @ 20 N
= 1.911 mm

Max. Disp. @ 60 N
= 3.836 mm

Max. Disp. @ 72 N
= 5.769 mm

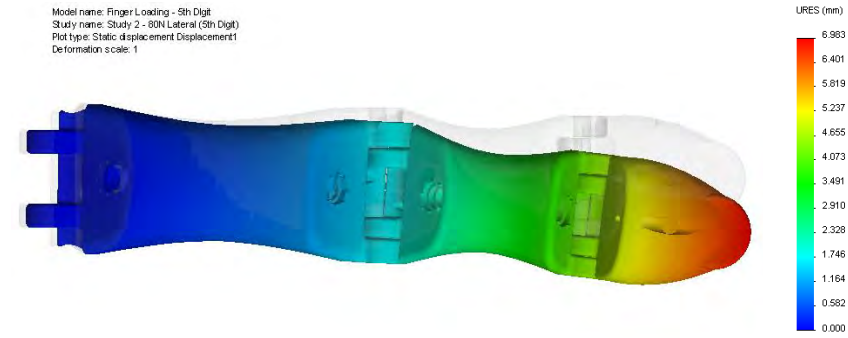

Max. Disp. @ 72 N
= 6.983 mm

Figure C28 – Maximum displacement of 5th digit due to lateral loads.

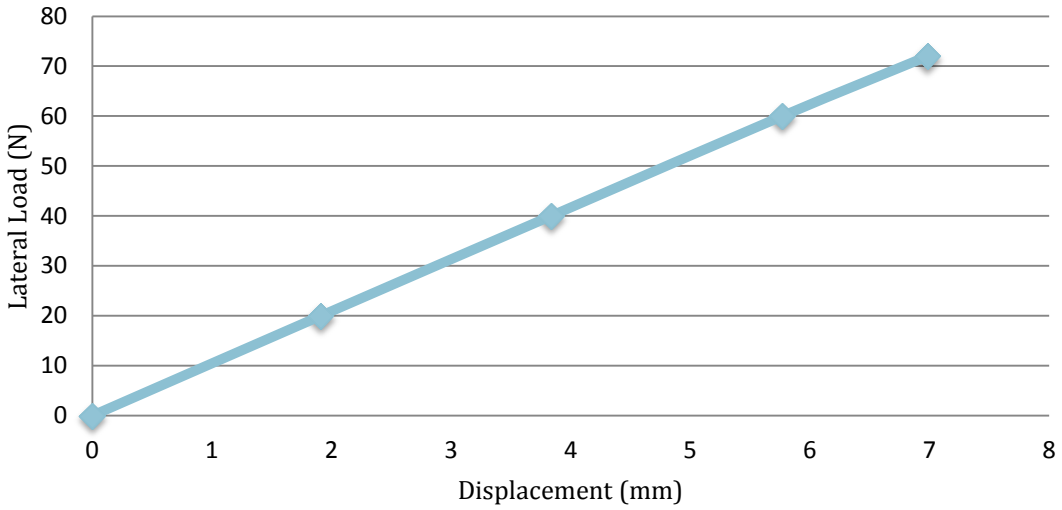

Figure C29 – Load vs. displacement behaviour of 5th digit due to lateral loading.

C10.6.2. Stress State @ 72 N

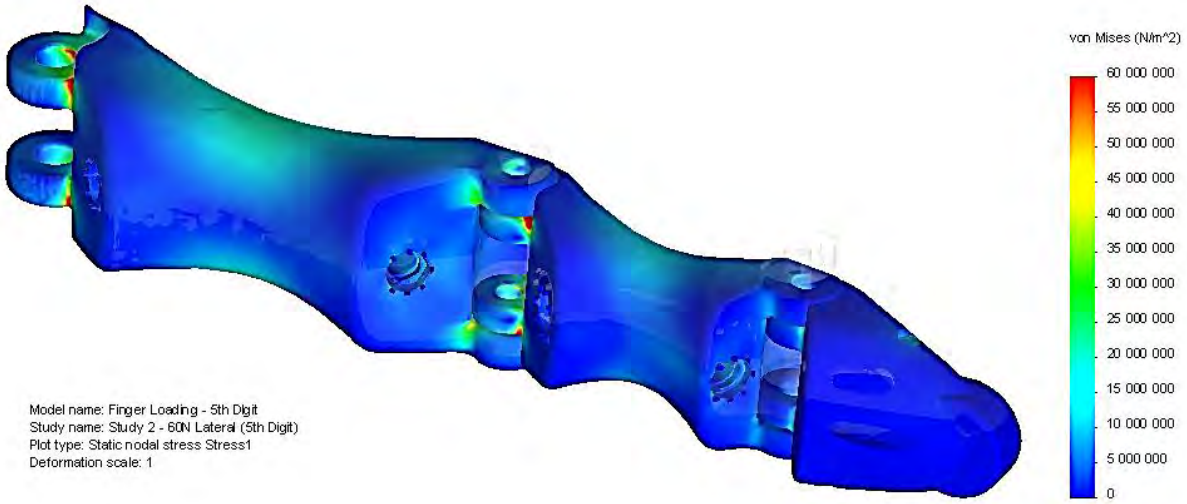

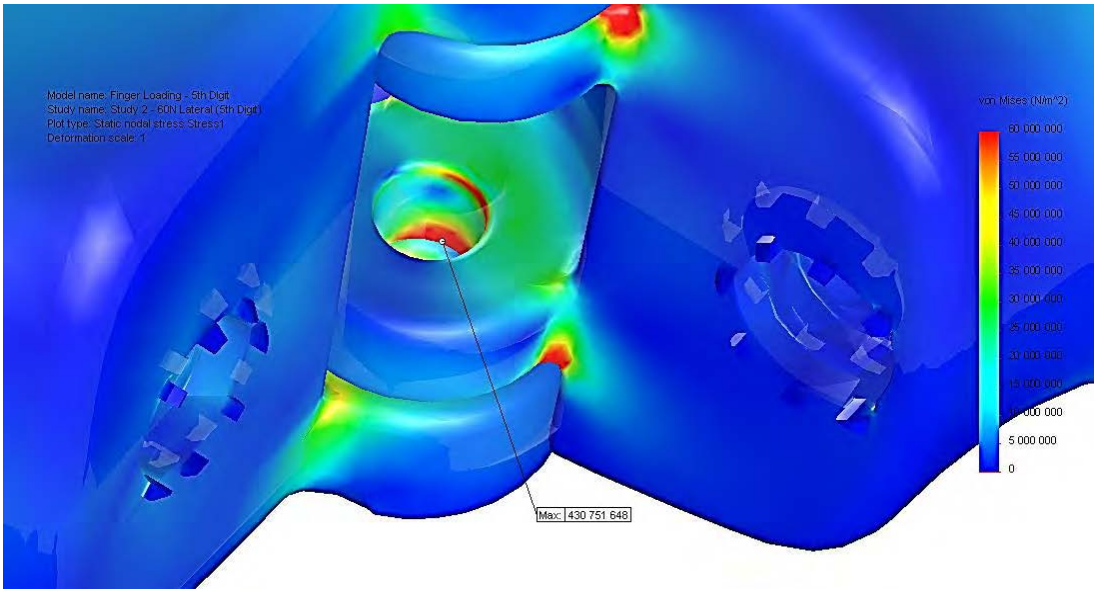

Figure C30 – von Mises Stress state of 5th digit @ 72 N, with isometric view (top) and perspective view of the maximum stress state at the lateral edge of the pin hole of the PIP joint (bottom).

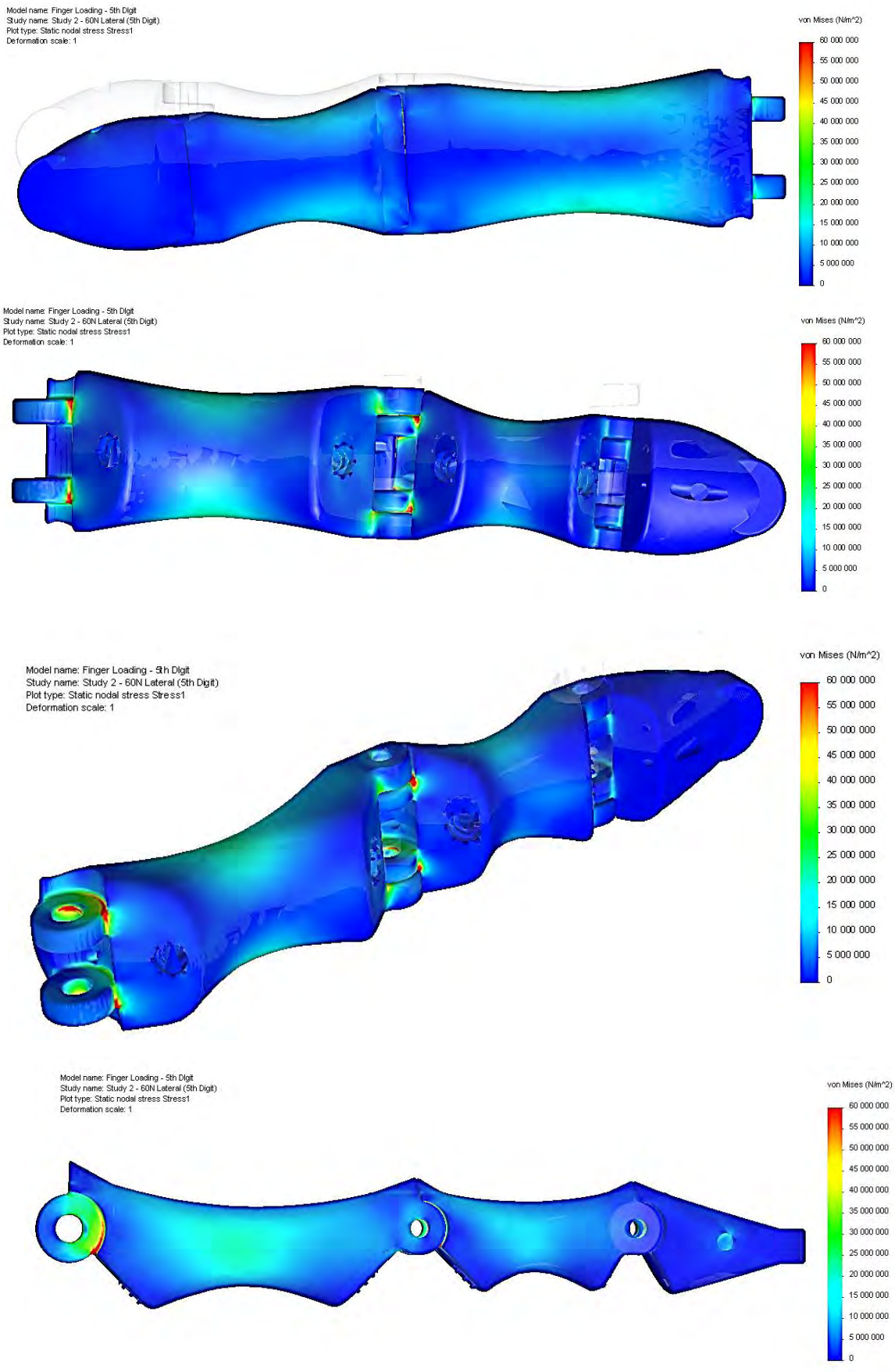

Figure C31 – von Mises Stress state of 5th digit @ 72 N, with superior (top), inferior (top centre), isometric (bottom centre) and lateral views of the stress state.

C11. Discussion of Results

For the 3rd Digit, evaluation of a 100 N hyperextensive load was not possible due to stability issues and incremental strain of the solver exceeding 25%; hence, only results up to 82 N were stored in this study. The same behaviour occurred for the 5th digit when exceeding hyperextensive and lateral loads of 55.8 N and 72 N respectively. Further non-linear analysis needs to be made to better approximate the true material and structural response. Incorporating material non-linearities and the effects of plasticity are expected to decrease the stiffness of the structure as loading increases, increasing the overall displacement thereof. Table C2 below shows the summarised linear-elastic displacement response of the digit assemblies as a function of their applied loads.

Table C2 – Summarised FEA displacement results of the hyperextensively and laterally loaded specimens.

Hyperextensive Loading				Lateral Loading			
3rd Digit		5th Digit		3rd Digit		5th Digit	
Load (N)	Displacement (mm)	Load (N)	Displacement (mm)	Load (N)	Displacement (mm)	Load (N)	Displacement (mm)
0	0	0	0	0	0	0	0
20	5.515	20	5.035	20	2.009	20	1.911
40	10.896	30	7.535	40	4.057	40	3.836
60	16.503	40	10.029	60	6.121	60	5.769
80	21.438	50	12.460	80	8.172	72	6.983
82	22.284	55.8	13.902	100	10.216		

Referring to Table C2, it can be seen that the 5th digit assembly extended less than the 3rd digit assembly when subjected to the same hyperextensive and lateral loads. This behaviour represented in Figure C32 and Figure C33 by the 5th digit's steeper slope (blue lines).

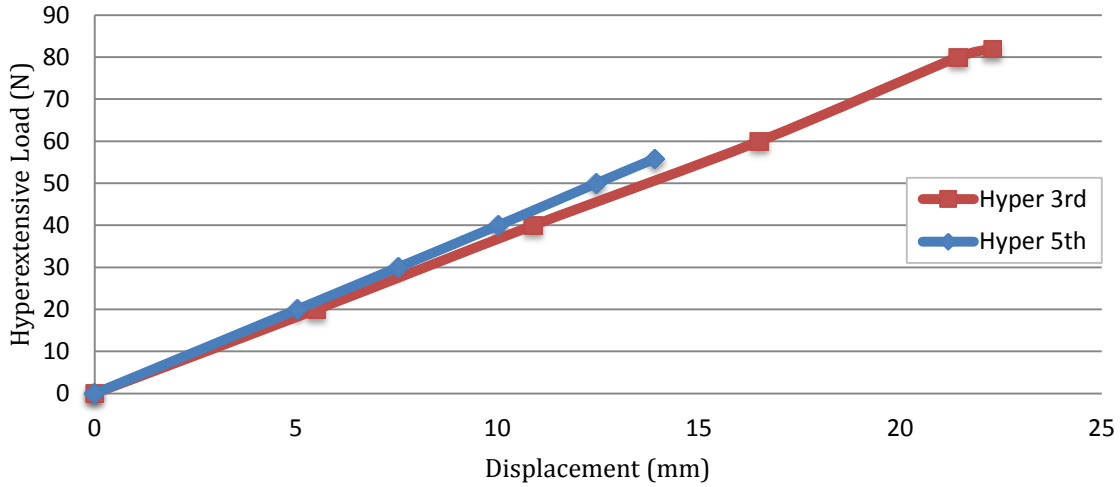

Figure C32 – Load vs. displacement comparison between 3rd and 5th digits under hyperextensive loading.

Furthermore, the 3rd digit was able to absorb 47% higher hyperextensive and 38.9% higher lateral loading than the 5th digit. Consequently, displacing 60.3% and 46.3% farther than the 5th digit, under the aforementioned loads respectively.

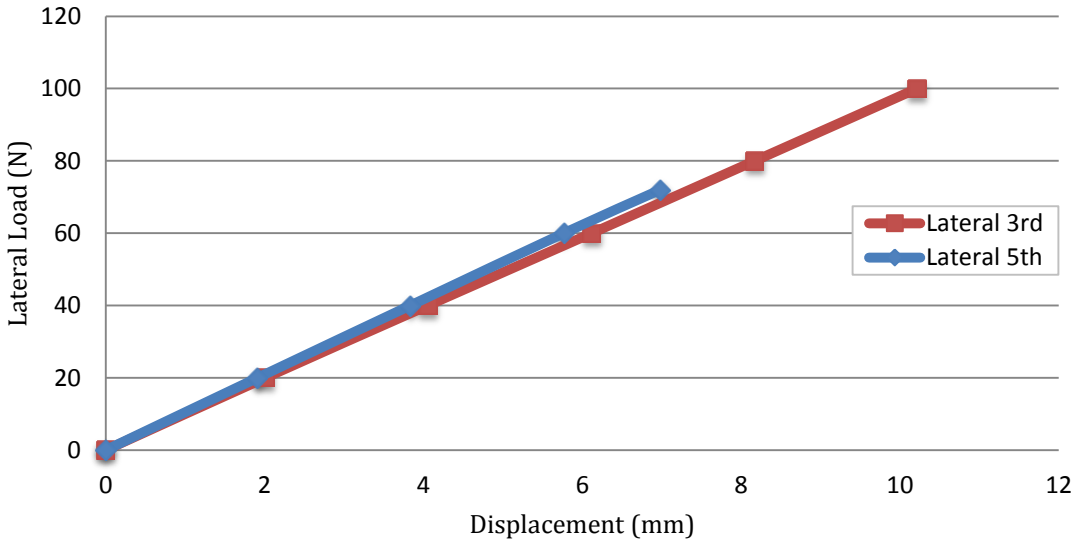

Figure C33 – Load vs. displacement comparison between 3rd and 5th digits under lateral loading.

The regions of highest stress concentration in the hyperextensive loading cases were situated at the radii of the hinges, and at the lateral edges of the posterior protrusions and pinholes. The 3rd and 5th digits had their peak stresses located at the lateral edges of the inner pin-holes at the PIP joint of the middle phalanx, and at the lateral edges of the posterior protrusion at the MCP joint of the proximal phalanx respectively. While these loads exceeded the yield point of the material under their maximum loading conditions, they remained localised and did not appear to affect the overall structural integrity as their surrounding areas did not surpass the yield point. More concerning however, was that the surface of the radii at the hinges of the MCP and PIP joints exceeded the yield at loads greater than 40N for the 3rd digit and 30 N for the 5th digit.

Under lateral loading, the areas of highest stress concentration were located at the lateral borders of the hinges and at the lateral edges of the pin holes. The peak stresses of the 3rd and 5th digits were both located at the PIP joint; at the supero-lateral edge of the hinge and the lateral edge of the superior pin hole respectively. While they both exceeded yield the lateral pin-holes of the 5th digit had localised yielding that had no major impact on structural strength. Conversely, while the stresses are initially localised at loads below ±60 N as seen in Figure C34, the confluence of the pinhole stresses and supero-lateral hinge stresses of the 3rd digit at approximately 80 N, presents concerns regarding the structure's resistance to fracture at loads exceeding this value.

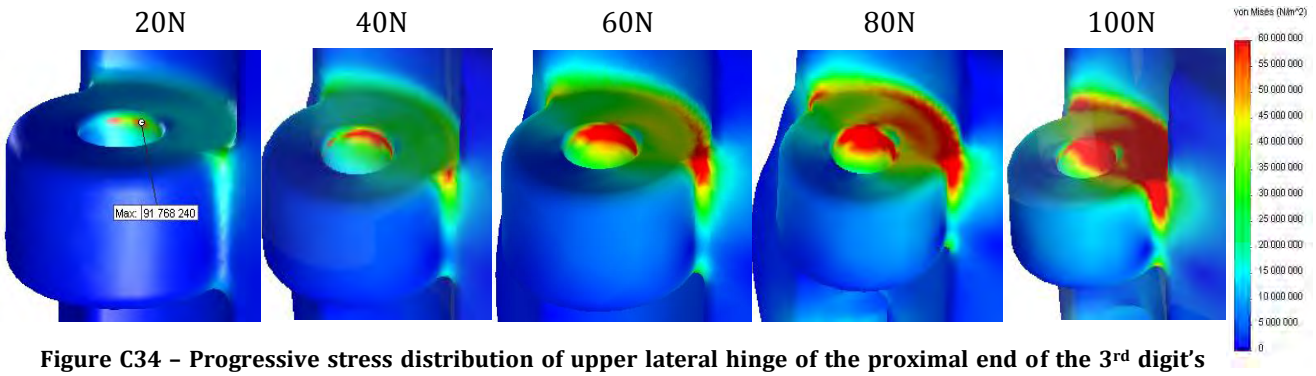

Figure C34 – Progressive stress distribution of upper lateral hinge of the proximal end of the 3rd digit's middle phalanx as lateral loads increase from left to right.

APPENDIX D - DISSERTATION BUDGET

Commercial viability of the device is of utmost importance, as this is the ultimate determining factor on whether or not manufacturing and distribution of the hand is possible. Consequently, a cost breakdown is given for the prosthetic hand and its components, both standard and manufactured, after which estimated costs of assembly and maintenance are included.

The following costing assumptions are made:

- All prices are exclusive of 14% Value Added Tax (VAT) unless otherwise stated and valid as of July 2014.
- Machining cost is R 350/hour excl. VAT as quoted by UCT Workshop Manager.
- Cost of 316 Stainless Steel is R87.15/kg excl. VAT as quoted by local supplier.
- Material costs of components are inferred from the mass of the original block or rod, before machining.
- Labour cost is calculated under the following assumptions:
    - Skilled labourer earning R8,000 per month performs the assembly
    - 22 working days per month and 6 productive hours each day
- Prices are also according to a one-off production run. Costs may be decreased significantly through larger production runs and process optimisation. Costs do not include development or research costs.
- Maintenance to be performed annually or bi-annually depending on usage, replacement components are listed in the costing form. It is preferable to include a spares kit with the hand to prevent unnecessary consultation with the prosthetist for minor repairs.

The costing model of the hand, its assembly and maintenance comprises of five primary sections. The first three related to the costing of the hand and manufacture of its components. The last two are associated with the assembly and the maintenance of the hand and its components.

PROSTHETIC HAND COSTING FORM

TOTAL COST BREAKDOWN

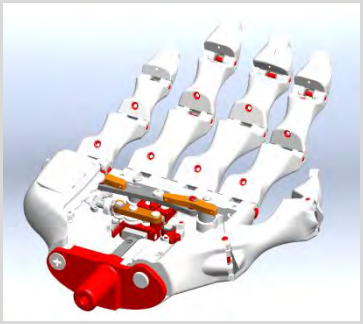

D1 – COST OF PURCHASED AND MANUFACTURED COMPONENTS ***R 9 547.91***

D1.1 - Cost of Standard Fasteners ***R 47.28***

Part No.	Item	Supplier	Quantity	Unit Cost	Total
F1	E-Clip 1.5mm (DIN 6799)	BMG	*21*	*R 0.08*	*R 1.68*
F2	E-Clip 1.9mm (DIN 6799)	BMG	*11*	*R 0.10*	*R 1.10*
F3	E-Clip 2.3mm (DIN 6799)	S&C	*1*	*R 0.13*	*R 0.13*
F4	E-Clip 3.2mm (DIN 6799)	S&C	*1*	*R 0.26*	*R 0.26*
F5	M2 St. Steel Nut - Narrow (ISO 4035)	Topfast	*4*	*R 1.04*	*R 4.15*
F6	M4 St. Steel Nut - Narrow (ISO 4035)	Topfast	*1*	*R 1.06*	*R 1.06*
F7	M2 x 8 Self-Tapping Screw (St. Steel)	Topfast	*4*	*R 1.10*	*R 4.40*
F8	M2 x 10 Pan Head Screw (ISO7045)	Topfast	*2*	*R 2.49*	*R 4.97*
F9	M2 x 4 Pan Head Screw (ISO7045)	Topfast	*2*	*R 2.38*	*R 4.77*
F10	M2.5 x 5 Pan Head Screw (ISO7045)	Topfast	*1*	*R 1.52*	*R 1.52*
F11	M3 x 3 Grub Screw - Cone Point (ISO4027)	Topfast	*2*	*R 3.88*	*R 7.75*
F12	M2.5 x 16 Countersunk Screw (ISO7046)	Topfast	*1*	*R 3.07*	*R 3.07*
F13	M4 x 16 Countersunk Screw (ISO7046)	Topfast	*1*	*R 1.20*	*R 1.20*
F14	M3 x 12 Screw St. Steel	Topfast	*1*	*R 0.87*	*R 0.87*
F15	M2 x 3 Screw St. Steel	Topfast	*1*	*R 2.71*	*R 2.71*
F16	M2 x 6 Screw St. Steel	Topfast	*2*	*R 2.28*	*R 4.56*
F17	M2 x 8 Screw St. Steel	Topfast	*1*	*R 3.09*	*R 3.09*

D1.2 - Cost of Bearings and other Standard Components ***R 1 809.48***

Part No.	Item	Supplier	Quantity	Unit Cost	Total
S1	Linear Bearing LWLC5C2R150BH	IKO	*1*	*R 1 638.00*	*R 1 638.00*
S2	694ZZ Ball Bearing (Ø9 OD, Ø6 ID, w4)	BTC	*1*	*R 8.77*	*R 8.77*
S3	TLA48Z Needle Roller Bearing	IKO	*2*	*R 30.05*	*R 60.10*
S4	Nitinol Wire (Ø0.4mm x 1m)	Fort Wayne	*1*	*R 35.09*	*R 35.09*
S5	Carbon Coated Stainless Steel Braided Wire	Kingfisher	*1*	*R 10.63*	*R 10.63*
S6	Rubber Padding and Glue	Cape Rubber	*1*	*R 56.89*	*R 56.89*

D1.3 - Cost of Manufactured Components							***R 7 691.15***
Part No.	Part	Manufacturer	Material Cost	Machining Cost @R350/hr	Quantity	Unit Cost	Total
M1	Palmar Structure Nylon PA2200	CRPM CUT	*N/A*	*N/A*	*1*	*R 4 385.96*	*R 4 385.96*
M2	Wrist Flange Stem	UCT Mech Eng	*R 132.56*	*R 350.00*	*1*	*R 482.56*	*R 482.56*
M3	Ratchet Rack	PWS Leon & UCT Mech Eng	*R 6.53*	*R 175.00*	*1*	*R 681.53*	*R 681.53*
M4	Pawl	PWS Leon	*R 0.17*	*N/A*	*1*	*R 150.17*	*R 150.17*
M5	Slider Carriage	UCT Mech Eng	*R 1.63*	*R 350.00*	*1*	*R 351.63*	*R 351.63*
M6	Primary Seesaw	UCT Mech Eng	*R 1.22*	*R 105.00*	*1*	*R 106.22*	*R 106.22*
M7	Secondary Seesaw 23	UCT Mech Eng	*R 0.49*	*R 105.00*	*1*	*R 105.49*	*R 105.49*
M8	Secondary Seesaw 45	UCT Mech Eng	*R 0.49*	*R 105.00*	*1*	*R 105.49*	*R 105.49*
M9	Seesaw Pin 23	UCT Mech Eng	*R 0.16*	*R 35.00*	*1*	*R 35.16*	*R 35.16*
M10	Seesaw Pin 45	UCT Mech Eng	*R 0.16*	*R 35.00*	*1*	*R 35.16*	*R 35.16*
M11	Seesaw Pin 5	UCT Mech Eng	*R 0.05*	*R 50.00*	*1*	*R 50.05*	*R 50.05*
M12	Thumb Transfer Lever	UCT Mech Eng	*R 2.72*	*R 140.00*	*1*	*R 142.72*	*R 142.72*
M13	Thumb Lever Pin	UCT Mech Eng	*R 0.29*	*R 58.33*	*1*	*R 58.62*	*R 58.62*
M14	Thumb Swivel Support Pins	UCT Mech Eng	*R 0.06*	*R 5.83*	*2*	*R 5.89*	*R 11.78*
M15	Thumb Bearing Washer	UCT Mech Eng	*R 0.48*	*R 28.00*	*2*	*R 28.48*	*R 56.96*
M16	Thumb Bearing Pin	UCT Mech Eng	*R 0.29*	*R 42.00*	*1*	*R 42.29*	*R 42.29*
M17	Pulley Cap	UCT Mech Eng	*R 1.02*	*R 70.00*	*1*	*R 71.02*	*R 71.02*
M18	Large Pulley	UCT Mech Eng	*R 0.27*	*R 70.00*	*1*	*R 70.27*	*R 70.27*
M19	Small Pulley	UCT Mech Eng	*R 0.10*	*R 56.00*	*2*	*R 56.10*	*R 112.20*
M20	Pulley Overhang Pin	UCT Mech Eng	*R 0.21*	*R 50.00*	*1*	*R 50.21*	*R 50.21*
M21	Routing Bearing Pin	UCT Mech Eng	*R 0.24*	*R 28.00*	*2*	*R 28.24*	*R 56.48*
M22	Pawl Release Lever	UCT Mech Eng	*R 0.85*	*R 46.67*	*1*	*R 47.52*	*R 47.52*
M23	Pawl Shaft	UCT Mech Eng	*R 1.03*	*R 87.50*	*1*	*R 88.53*	*R 88.53*
M24	Pawl Locking Pin	UCT Mech Eng	*R 0.17*	*R 58.33*	*1*	*R 58.50*	*R 58.50*
M25	Pawl Swivel Pin	UCT Mech Eng	*R 0.12*	*R 58.33*	*1*	*R 58.45*	*R 58.45*
M26	5th DIP Pin	UCT Mech Eng	*R 0.09*	*R 11.67*	*1*	*R 11.76*	*R 11.76*
M27	2nd & 4th DIP Pin	UCT Mech Eng	*R 0.10*	*R 11.67*	*2*	*R 11.77*	*R 23.54*
M28	2nd & 4th PIP and 3rd DIP Pin	UCT Mech Eng	*R 0.11*	*R 11.67*	*3*	*R 11.78*	*R 35.34*
M29	5th PIP Pin	UCT Mech Eng	*R 0.10*	*R 11.67*	*1*	*R 11.77*	*R 11.77*
M30	1st IP & 3rd PIP Pin	UCT Mech Eng	*R 0.11*	*R 11.67*	*2*	*R 11.78*	*R 23.56*
M31	1st MCP Pin	UCT Mech Eng	*R 0.21*	*R 11.67*	*1*	*R 11.88*	*R 11.88*
M32	MCP Pin 1	UCT Mech Eng	*R 1.44*	*R 11.67*	*1*	*R 13.11*	*R 13.11*
M33	MCP Pin 2	UCT Mech Eng	*R 0.48*	*R 11.67*	*1*	*R 12.15*	*R 12.15*
M34	Ø5x3 Spring Mandrels	UCT Mech Eng	*R 0.02*	*R 2.92*	*14*	*R 2.94*	*R 41.16*
M35	Ø5x9xd0.5mm Compression spring	Gellini Springs	*N/A*	*N/A*	*2*	*R 2.31*	*R 4.62*
M36	Ø6x18xd0.5mm Compression spring	Gellini Springs	*N/A*	*N/A*	*1*	*R 2.86*	*R 2.86*
M37	Ø6mm Helical torsion springs (3 < N < 6)	Gellini Springs	*N/A*	*N/A*	*14*	*R 4.65*	*R 65.10*
M38	Leaflet torsion Springs	Gellini Springs	*N/A*	*N/A*	*2*	*R 3.59*	*R 7.18*

D2 - ASSEMBLY COSTS				***R 259.07***
Item	Activity Description	Duration (min)	Labour Cost (R/min)	Total
A1	Removal of powder from phalangeal channels	*4.5*	*R 1.01*	*R 4.55*
A2	Reaming of all pin holes	*10*	*R 1.01*	*R 10.10*
A3	Assembly of finger locking mechanism & pawl	*15*	*R 1.01*	*R 15.15*
A4	Assembly of the transfer lever mount	*5*	*R 1.01*	*R 5.05*
A5	Insertion of routing bearings	*2*	*R 1.01*	*R 2.02*
A6	Assembly of proximal ratchet carriage with pulleys	*5*	*R 1.01*	*R 5.05*
A7	Assembly of distal carriage with seesaws	*10*	*R 1.01*	*R 10.10*
A8	Mounting of wrist stem and linear bearing	*10*	*R 1.01*	*R 10.10*
A9	Thumb Assembly with locking mechanism	*15*	*R 1.01*	*R 15.15*
A10	Phalangeal assembly of springs, mandrels, pins and actuating wires	*30*	*R 1.01*	*R 30.30*
A11	Attachment of actuating wires to seesaws and levers, with routing cable assembly	*30*	*R 1.01*	*R 30.30*
A12	Assembly of palmar cover and grip pads	*60*	*R 1.01*	*R 60.60*
A13	Miscellaneous time expenditure allowance	*60*	*R 1.01*	*R 60.60*

D3 - MAINTENANCE COSTS					***R 393.35***
D3.1 - Cost of Replacement Parts					***R 226.70***
Part No.	Item	Supplier	Quantity	Unit Cost	Total
F1	E-Clip 1.5mm (DIN 6799)	BMG	*21*	*R 0.08*	*R 1.68*
F2	E-Clip 1.9mm (DIN 6799)	BMG	*11*	*R 0.10*	*R 1.10*
F3	E-Clip 2.3mm (DIN 6799)	S&C	*1*	*R 0.13*	*R 0.13*
F4	E-Clip 3.2mm (DIN 6799)	S&C	*1*	*R 0.26*	*R 0.26*
S4	Nitinol Wire (Ø0.4mm x 1m)	Fort Wayne	*1*	*R 35.09*	*R 35.09*
S5	Carbon Coated Stainless Steel Braided Wire	Kingfisher	*1*	*R 10.63*	*R 10.63*
S6	Rubber Padding and Glue	Cape Rubber	*1*	*R 56.89*	*R 56.89*
M34	Ø5x3 Spring Mandrels	UCT Mech Eng	*14*	*R 2.94*	*R 41.16*
M35	Ø5x9xd0.5mm Compression spring	Gellini Springs	*2*	*R 2.31*	*R 4.62*
M36	Ø6x18xd0.5mm Compression spring	Gellini Springs	*1*	*R 2.86*	*R 2.86*
M37	Ø6mm Helical torsion springs (3 < N < 6)	Gellini Springs	*14*	*R 4.65*	*R 65.10*
M38	Leaflet torsion Springs	Gellini Springs	*2*	*R 3.59*	*R 7.18*

D3.2 - Cost of Assembly for Maintenance				***R 166.65***
Item	Activity Description	Duration (min)	Labour Cost (R/min)	Total
A14	Thumb disassembly and re-assembly with locking mechanism	*25*	*R 1.01*	*R 25.25*
A15	Phalangeal disassembly & re-assembly of springs, mandrels, pins and actuating wires	*40*	*R 1.01*	*R 40.40*
A16	Attachment of actuating wires to seesaws and levers, with routing cable assembly	*30*	*R 1.01*	*R 30.30*
A17	Disassembly & re-assembly of palmar cover and selected grip pads	*40*	*R 1.01*	*R 40.40*
A18	Miscellaneous time expenditure allowance	*30*	*R 1.01*	*R 30.30*

TOTAL COST OF THE PROSTHETIC HAND	**Totals**
D1 - COST OF PURCHASED AND MANUFACTURED COMPONENTS	***R 9 547.91***
D1.1 - Cost of Standard Fasteners	R 47.28
D1.2 - Cost of Bearings and other Standard Components	R 1 809.48
D1.3 - Cost of Manufactured Components	R 7 691.15
D2 - ASSEMBLY COSTS	***R 259.07***
D3 - MAINTENANCE COSTS	***R 393.35***
D3.1 - Cost of Replacement Parts	R 226.70
D3.2 - Cost of Assembly for Maintenance	R 166.65

Subtotal	***R 10 200.32***
+14% VAT	***R 1 428.04***
TOTAL	***R 11 628.37***

In conclusion, a **conservative cost estimate** of the manufacture, assembly and maintenance of the hand is expected to be approximately **R15 000**. Variations in price of manufacture, purchased items, labour cost and on-going development may cause this to vary. It should be noted that this is the cost estimate for a "one-off" hand, and costs could decrease significantly through larger production runs, lean manufacturing techniques and process optimisation.

APPENDIX E - RISK ASSESSMENT, ETHICS & IMPACT OF TECHNOLOGY ON SOCIETY

The sections in this appendix include the following documents:

E1 – Risk Assessment Forms

The following risk assessment forms are included:

Department of Mechanical Engineering
University of Cape Town
Risk Assessment Form – 2014

- **Risk Assessments are not required for simple workshop activities covered by the Safety Declaration. However permission must be obtained from Mr Glen Newins before commencing any activity in the Workshop.**
- **Activities performed in Mechanical Engineering laboratories only need your Supervisor's signature and do not need a Safety Officer's signature. The responsible person for the laboratory space must however be informed of your planned activity before commencing the activity.**
- **You are required to include this document (signed) in your bound project submission and mount a copy next to any rig / apparatus you are using.**

Your Name	Severin Tenim
Your Supervisor	Dr G Vicatos
Project title and number	Design of an Affordable Anthropomorphic Mechanical Prosthetic Hand
Area Safety Officer	Mr Glen Newins
Lab Responsible Person	Dr George Vicatos

This Section to be completed by the student (Must be typed and the declaration signed)			
Location (where the activity will take place):	Thermodynamics and Fluids Laboratory		
Describe the activity:	Phalangeal Fatigue Testing of Finger Channels using Pneumatic Setup		
Names of persons involved in this activity:	Dr G Vicatos Mr Severin Tenim		
Describe in detail the risks you (and others) will face during this activity and the potential consequences of your activities:	Pneumatic actuation of the rig makes use of compreessed air at a pressure of 6 bar. All pressurised equipment used is designed and manufactured by Festo. The primary risks associated with the setup are rupture or leaking of the equipment, which may cause noise and/or damage to the eyes with a pipe flinging about. Another risk is a finger getting caught between the piston and another component.		
Does your project involve the use of any materials (chemicals, gasses, etc.) which may be hazardous to health, or the environment?	No ☒	Yes ☐	
Does this activity involve any equipment / device designed or built by you which is to be plugged into mains electricity?	No ☐	Yes ☒	There is a minor DC electrical circuit which is uses a power supply outputting 24V DC current at low ampage to power two switches and two analogue counters. This circuit is used to count the number of cycles the phalanges undergo.
Does your project involve any new equipment / devices designed which contain air or gas at pressure?	No ☒	Yes ☐	
What precautions are required to protect against the risks detailed above:	To minimise the risk of injury or damage, wear safety glasses, closed shoes and always stand well away from the testing apparatus during testing. For noise, a silencer is connected to the exhaust and ear-muffs should be worn. Include safety stoppers to limit the stroke of the machine so as not to damage the test piece. Always ensure the main valve is easily accessible, include a sign above the test rig with emergency shutdown procedures, safety information and contact details. Keep fingers clear of moving parts.		
Describe the personal protective equipment (PPE) required during this activity – specify in detail:	Closed shoes, safety glasses and hearing protection to be worn at all times in the vicinity of the testing apparatus.		
Describe the shutdown procedure in detail:	Emergency shut down to be performed by closing the ball-valve of the main air-line on the wall behind the test setup.		
Describe any relevant emergency procedures, e.g. spillage response etc.	Notify area safety officer of any incidents. Alternatively, the closest safety officer if the primary officer is not present. Contact the nearest first aider should it be required. Call emergency services if it is serious.		

I declare that I am aware of the risks associated with this activity and will take all necessary steps to mitigate these risks.	**Signature**	**Date**
	Signed by candidate	30 May 2014

This section to be completed by the Project Supervisor		*Tick relevant box below.*
Level of supervision required (Please tick relevant block)	A = work may not take place without supervisor present.	
	B = work may not take place without a 2nd party present.	
	C = no specific extra supervision requirements.	
I am satisfied that my student is aware of the risks associated with this activity and grant approval for it to proceed.	**Signature**	**Date**

This section to be completed by the Area Safety Officer for work at SAFL or BISRU or CME.		
A satisfactory Risk Assessment has been performed and I grant approval for this activity to proceed.	**Signature**	**Date**

Department of Mechanical Engineering
University of Cape Town
Risk Assessment Form – 2014

- **Risk Assessments are not required for simple workshop activities covered by the Safety Declaration. However permission must be obtained from Mr Glen Newins before commencing any activity in the Workshop.**
- **Activities performed in Mechanical Engineering laboratories only need your Supervisor's signature and do not need a Safety Officer's signature. The responsible person for the laboratory space must however be informed of your planned activity before commencing the activity.**
- **You are required to include this document (signed) in your bound project submission and mount a copy next to any rig / apparatus you are using.**

Your Name	Severin Tenim
Your Supervisor	Dr G Vicatos
Project title and number	Design of an Affordable Anthropomorphic Mechanical Prosthetic Hand
Area Safety Officer	Prof R Knutsen
Lab Responsible Person	Ms P Park-Ross

This Section to be completed by the student (Must be typed and the declaration signed)			
Location (where the activity will take place):	Centre for Materials Engineering (CME)		
Describe the activity:	Tensile and Compressive Testing of the Phalanges and Actuating Wires/Cables		
Names of persons involved in this activity:	Mr Severin Tenim		
	Ms P Park-Ross		
Describe in detail the risks you (and others) will face during this activity and the potential consequences of your activities:	A hydraulic tensile tester is used in the experimental procedure. Risks involve getting a hand or limb caught between the crosshead and the workpiece, rapid fracture of a specimen may cause a piece of nylon or wire to be projected, and bottoming out of the mechanism may damage the load-cell or uncalibrate it.		
Does your project involve the use of any materials (chemicals, gasses, etc.) which may be hazardous to health, or the environment?	No	Yes	
	☒	☐	
Does this activity involve any equipment / device designed or built by you which is to be plugged into mains electricity?	No	Yes	
	☒	☐	
Does your project involve any new equipment / devices designed which contain air or gas at pressure?	No	Yes	
	☒	☐	
What precautions are required to protect against the risks detailed above:	Hands are to be kept away from the work area at all times during testing. Eye protection and closed shoes are to be worn at all times. Limits on the stroke of the crosshead and the maximum force are to be set to prevent damage to equipment. Keep surrounding area clear and maintain the emergency shutdown switch within reach at all times during testing. Post signage on the apparatus with safety information, contact details and emergency shutdown procedures.		
Describe the personal protective equipment (PPE) required during this activity – specify in detail:	Closed shoes and safety glasses to be worn at all times in the vicinity of the testing apparatus.		
Describe the shutdown procedure in detail:	Push the RED EMERGENCY STOP BUTTON in case of an emergency. Alternatively, the program can be stopped by clicking the END TEST icon on the computer.		
Describe any relevant emergency procedures, e.g. spillage response etc.	Notify area safety officer of any incidents. Alternatively, the closest safety officer if the primary officer is not present. Contact the nearest first aider should it be required. Call emergency services if it is serious.		

I declare that I am aware of the risks associated with this activity and will take all necessary steps to mitigate these risks.	**Signature**	**Date**
	Signed by candidate	04 June 2014

This section to be completed by the Project Supervisor		*Tick relevant box below.*
Level of supervision required (Please tick relevant block)	A = work may not take place without supervisor present.	
	B = work may not take place without a 2nd party present.	
	C = no specific extra supervision requirements.	
I am satisfied that my student is aware of the risks associated with this activity and grant approval for it to proceed.	**Signature**	**Date**

This section to be completed by the Area Safety Officer for work at SAFL or BISRU or CME.		
A satisfactory Risk Assessment has been performed and I grant approval for this activity to proceed.	**Signature**	**Date**

E2 –Assessment of Ethics in a Research Project

EBE Faculty: Assessment of Ethics in Research Projects (Rev2)

Any person planning to undertake research in the Faculty of Engineering and the Built Environment at the University of Cape Town is required to complete this form before collecting or analysing data. When completed it should be submitted to the supervisor (where applicable) and from there to the Head of Department. If any of the questions below have been answered YES, and the applicant is NOT a fourth year student, the Head should forward this form for approval by the Faculty EIR committee: submit to Ms Zulpha Geyer (Zulpha.Geyer@uct.ac.za; Chem Eng Building, Ph 021 650 4791).
NB: A copy of this signed form must be included with the thesis/dissertation/report when it is submitted for examination

This form must only be completed once the most recent revision EBE EiR Handbook has been read.

Name of Principal Researcher/Student: **Severin Tenim** Department: **Mechanical Engineering**

Preferred email address of the applicant: **sevtenim@gmail.com**

If a Student: Degree: **MSc** Supervisor: **Dr George Vicatos**

If a Research Contract indicate source of funding/sponsorship: **N/A**

Research Project Title: **Design of a Low-cost Mechanical Prosthetic Hand**

Overview of ethics issues in your research project:

Question 1: Is there a possibility that your research could cause harm to a third party (i.e. a person not involved in your project)?	YES	X NO
Question 2: Is your research making use of human subjects as sources of data? If your answer is YES, please complete Addendum 2.	X YES	NO
Question 3: Does your research involve the participation of or provision of services to communities? If your answer is YES, please complete Addendum 3.	YES	X NO
Question 4: If your research is sponsored, is there any potential for conflicts of interest? If your answer is YES, please complete Addendum 4.	YES	X NO

If you have answered YES to any of the above questions, please append a copy of your research proposal, as well as any interview schedules or questionnaires (Addendum 1) and please complete further addenda as appropriate. Ensure that you refer to the EiR Handbook to assist you in completing the documentation requirements for this form.

I hereby undertake to carry out my research in such a way that

- there is no apparent legal objection to the nature or the method of research; and
- the research will not compromise staff or students or the other responsibilities of the University;
- the stated objective will be achieved, and the findings will have a high degree of validity;
- limitations and alternative interpretations will be considered;
- the findings could be subject to peer review and publicly available; and
- I will comply with the conventions of copyright and avoid any practice that would constitute plagiarism.

Signed by:

	Full name and signature	Date
Principal Researcher/Student:	Severin Tenim	02.04.2014

This application is approved by:

Supervisor (if applicable):		
HOD (or delegated nominee): *Final authority for all assessments with NO to all questions and for all undergraduate research.*		
Chair : Faculty EIR Committee For applicants other than undergraduate students who have answered YES to any of the above questions.		2/4/2014

ADDENDUM 1:
Please append a copy of the research proposal here, as well as any interview schedules or questionnaires:

Research Proposal

The aim of the MSc dissertation is to design, manufacture, test, optimise and implement a low-cost mechanical prosthetic hand. Once the initial prototype has been built, experimentally lab-tested and optimised, it is intended to be used by voluntary patients in order to get their valuable feedback. While theoretical models and analytical analysis is important to quantitatively analyse the performance of the hand, it is critical to get direct feedback from the people whose lives it is intending to benefit on a daily basis; only they will be able to truly assess the hand's performance.

The study will be conducted in close collaboration with the patient's existing prosthetist(s), Mr Eugene Rossouw (Rossouw-Kritzinger Orthotists & Prosthetists) and/or Ms Olwen Nel (Pinelands Prosthetics Centre), who will fit the device and ensure the patient's needs are taken care of through every step. They will personally oversee the entire process from start to finish, creating a link between Severin Tenim (MSc researcher) and the patient. Patient confidentiality is of utmost importance therefore no personal details will be recorded. Should the patients choose to remain anonymous, they will only deal with their prosthetist, who will give feedback in a separate session to the researcher. Written consent forms will also be signed by the patients prior to any activities (Please see this form on page 1 of the attached questionnaire).

The intended duration of the study will span 1-2 weeks per patient. After/during which they will complete a questionnaire on various factors including comfort, performance and ease of use (Please see attached questionnaire). Furthermore, recommendations for improvement will be included in the questionnaire, as well as any preferences/features which patients would like to see in the present or future iterations of the design. Moreover, since it is a prosthetic device, the method is non-invasive and includes no subcutaneous or percutaneous procedures. Patients will simply screw off their existing prosthetic and attach the new one to the sleeve designed by their prosthetist. The device is also purely mechanical; hence no electrical inputs/systems are present.

ADDENDUM 2: To be completed if you answered YES to Question 2:

It is assumed that you have read the UCT Code for Research involving Human Subjects (available at http://web.uct.ac.za/depts/educate/download/uctcodeforresearchinvolvinghumansubjects.pdf) in order to be able to answer the questions in this addendum.

2.1 Does the research discriminate against participation by individuals, or differentiate between participants, on the grounds of gender, race or ethnic group, age range, religion, income, handicap, illness or any similar classification?	YES	NO X
2.2 Does the research require the participation of socially or physically vulnerable people (children, aged, disabled, etc) or legally restricted groups?	YES	NO X
2.3 Will you not be able to secure the informed consent of all participants in the research? (In the case of children, will you not be able to obtain the consent of their guardians or parents?)	YES	NO X
2.4 Will any confidential data be collected or will identifiable records of individuals be kept?	YES	NO X
2.5 In reporting on this research is there any possibility that you will not be able to keep the identities of the individuals involved anonymous?	YES	NO X
2.6 Are there any foreseeable risks of physical, psychological or social harm to participants that might occur in the course of the research?	YES	NO X
2.7 Does the research include making payments or giving gifts to any participants?	YES	NO X

If you have answered YES to any of these questions, please describe below how you plan to address these issues:

Due to the device being a prosthetic, patients who have had an amputation will be consulted. Patients who participate will be more experienced and of legal age to give their own consent. They will have all used prosthetic devices for numerous years, and will participate voluntarily. There will be no discrimination in choosing patients, nor will the study require the participation of socially or physically vulnerable people. The aim of the prosthetic hand (and hence the study) is to improve their standard of living, making it of paramount importance to get direct feedback from patients who will be using the device on a daily basis. The number one priority is the patient, their confidentiality and their comfort.

E3 – Impact of Technology on Society

Department of Mechanical Engineering

University of Cape Town

Impact of technology on society

Name	Mr Severin Tenim
Supervisor	Dr George Vicatos
Project Title	Design of an Affordable Anthropomorphic Mechanical Prosthetic Hand

In the space provided below, please write up to 250 words on how the technology in your project impacts on society. You can consider "society" in three spheres: 1) your fellow students and other staff members, 2) the institution more generally, and 3) the broader society. You may need to consider the "downstream" impact of the technology in your project if you are undertaking a focused research-based project.

The impact of this technology on fellow students and staff members may expand their knowledge on the workings of a mechanical prosthetic hand as well as numerous manufacturing capabilities through the use of additive manufacturing techniques; more commonly known as 3D-printing. It will not only expose them to the possibilities in the Biomedical and Biomechanical Engineering field, but also to the state of technology today.

The University of Cape Town will benefit from this technology as it is first and foremost their intellectual property. The research improves the state of technology of the department's biomedical division, headed by Dr George Vicatos. The improvement of the technology is expected to enhance the University's reputation in the field and possibly attract more candidates, with the ultimate goal being to produce world-class research and outputs. The institution may also benefit in a financial capacity as patenting of this device, through UCT's RCIPS, enables commercial benefits.

The broader society will benefit the most from this technology. Those involved with the design, manufacturing, distribution and fitment of this device will benefit both financially and experientially. More significantly, the quality of life of patients and their families is expected to be greatly improved; especially those whom have suffered the traumatic experience of losing an upper limb. The technology is expected to increase the accessibility of this device as an affordable, functional and aesthetically pleasing prosthesis, which many patients, even those with medical insurance, cannot currently access. Our hands are utilised thousands of times each day, often unbeknown to us. Consequently, patients will experience a direct stream of positive feedback in their everyday lives. While the true functionality of the anatomical hand is exceedingly complex and bordering on impossible to mimic, it is the purpose of this device to provide a suitable substitute, which enables patients to perform most of their activities of daily living.

The improvement in lifestyle is priceless and one of utmost importance in society today. If the quality of life of just one person has been improved through use of this device, then the endeavour has been a successful one.

Signed	Date
	03 April 2014

APPENDIX F - PROSTHETIC HAND EVALUATION QUESTIONNAIRE (PHEQ)

Prosthetic Hand Evaluation Questionnaire (PHEQ)

June 2014

Compiled by S. Tenim

Excerpts taken from Prosthetic Evaluation Questionnaire (PEQ) by Legro, et al. (1998), available through Prosthetics Research Study (1998), and the evaluation of Orthotic and Prosthetic User Survey (OPUS) for Upper Extremity Functional Status (UEFS) by Burger, et al. (2008).Please note minor modifications were made to the original content.

CONSENT FORM

Hello, my name is Severin and I am a researcher at the University of Cape Town (UCT) from the Department of Mechanical Engineering. My Masters dissertation involves the design of a low-cost mechanical prosthetic hand and I am conducting this survey to get your direct feedback on how the device performed.

- The purpose of this study is to determine your experiences with the hand, both positive and negative, so that I can see what has been done correctly and where I can improve the design to better suit your needs.
- I am not going to ask you for any personal information and your identity will remain completely confidential.
- Your valuable input will benefit not only yourself, but all patients using the device. Your participation will require answering the questionnaire.
- I do not expect there to be any risks involved with the process, but as is common with most prostheses, there may be slight experiences of discomfort with the sleeve and shoulder harness (Rossouw, 2014). To minimise any discomfort, your prosthetist Eugene will make sure your socket fits as comfortably as you want it, and adjust the harness to your liking. You may contact him at any time should you feel any discomfort.
- Please do not use the hand for any harmful activities such as holding a hot cup of coffee or kettle, or placing a hot pot on a stove. Also, please do not use the hand in activities that may harm other people or property should it malfunction.
- Please be as truthful as possible when answering the questions.

PATIENT CONSENT

- I hereby give my consent to participate in this study.
- I understand that I am taking part voluntarily without being coerced into doing so and am doing so at my own risk.
- I am aware that my identity will remain confidential.
- I understand that I can withdraw from the study at any time without any consequences.

_____ _____

Signature of Participant Date

Modified version of Prosthesis Evaluation Questionnaire (PEQ) by Legro, et al. (1998)
adapted from Prosthetics Research Study, Seattle, WA, USA (1998)

Introduction

The Prosthetic Hand has been developed since its conceptualisation in the beginning of 2013, and is finally assembled and ready for its first round of trials. Thank you for electing to take part in this voluntary survey, your direct feedback is extremely important to the progress and improvement of the hand. Both positive and negative feedback will be much appreciated as it allows us to determine what we have done correctly, and also identifies areas in which we can improve the current and future designs for you.

Instructions

As you read each question, remember there is no right or wrong answer. Just think of YOUR OWN OPINION on the topic and make a mark THROUGH the line anywhere along the line from one end to the other to show us your opinion.

Example:

How important is it to you to have tea in the morning?

NOT AT ALL EXTREMELY IMPORTANT

Over the past week, rate your morning tea.

TERRIBLE EXCELLENT

OR check __ I haven't drunk tea in the morning in the past week.

This example shows that the person who answered these questions feels that having tea in the morning is important. He/she also thinks the tea lately has not been very good.

If he/she hadn't drunk any tea in the last week, he/she would have put a check by that statement instead of putting a mark on the line between TERRIBLE and EXCELLENT.

Please answer ALL the questions.

As in the previous example, make a mark across the line rather than using an X or an O.

Modified version of Prosthesis Evaluation Questionnaire (PEQ) by Legro, et al. (1998)
adapted from Prosthetics Research Study, Seattle, WA, USA (1998)

GROUP 1

These first questions are about YOUR PROSTHESIS.

A. Over the past week, rate how happy you have been with your current prosthesis.

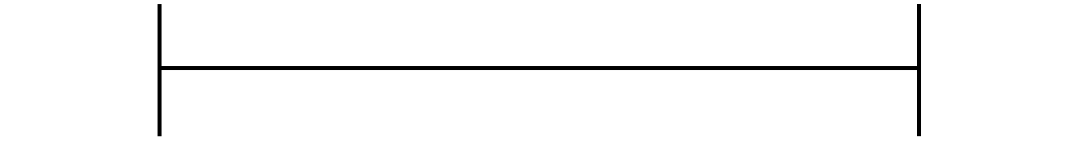

EXTREMELY UNHAPPY EXTREMELY HAPPY

B. Over the past week, rate the fit of your prosthesis.

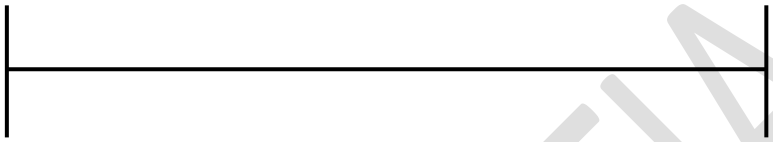

TERRIBLE EXCELLENT

C. Over the past week, rate the weight of your prosthesis.

TERRIBLE EXCELLENT

D. Over the past week, rate your comfort when using your prosthesis.

TERRIBLE EXCELLENT

E. Over the past week, rate how much energy it took to use your prosthesis for as long as you needed it.

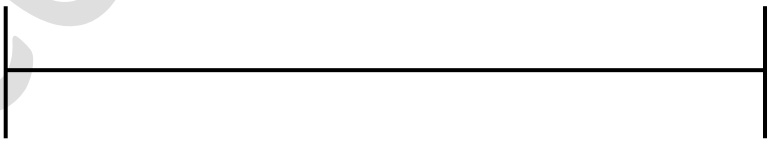

EXHAUSTING NONE AT ALL

F. Over the past week, rate the ease of putting on (donning) your prosthesis.

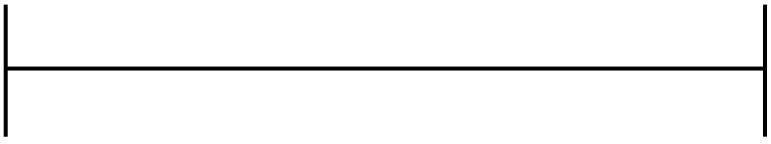

DIFFICULT VERY EASY

Modified version of Prosthesis Evaluation Questionnaire (PEQ) by Legro, et al. (1998)
adapted from Prosthetics Research Study, Seattle, WA, USA (1998)

G. Over the past week, rate how your prosthesis has looked.

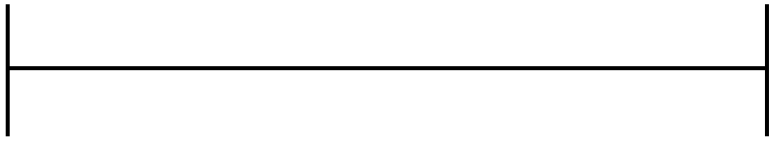

TERRIBLE EXCELLENT

H. Over the past week, rate how often your prosthesis made squeaking, clicking, or belching sounds.

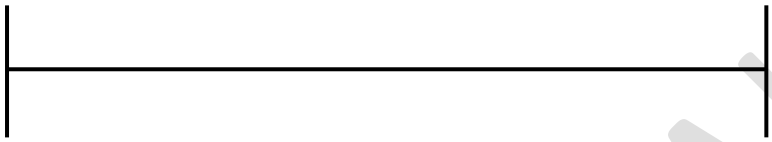

ALWAYS NEVER

I. If it made any sounds in the past week, rate how bothersome these sounds were to you.

EXTREMELY BOTHERSOME NOT AT ALL

OR check ___ it made no sounds.

J. Over the past week, rate the damage done to your clothing by your prosthesis.

EXTENISVE DAMAGE NONE

K. Over the past week, rate the damage done to your prosthesis cover.

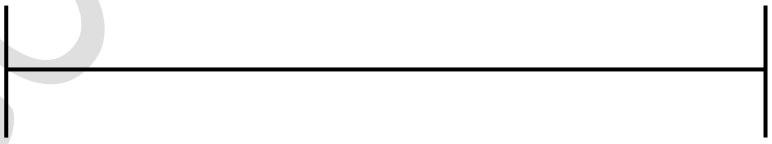

EXTENISVE DAMAGE NONE

OR check ___ there is no cover on my prosthesis**.**

L. Over the past week, rate how limited your choice of clothing was because of your prosthesis.

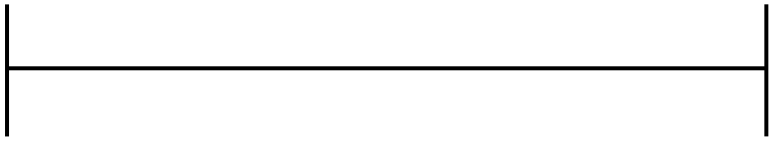

VERY LIMITED NOT AT ALL

Modified version of Prosthesis Evaluation Questionnaire (PEQ) by Legro, et al. (1998)
adapted from Prosthetics Research Study, Seattle, WA, USA (1998)

M. Over the past week, rate how much of the time your residual limb was swollen to the point of changing the fit of your prosthesis.

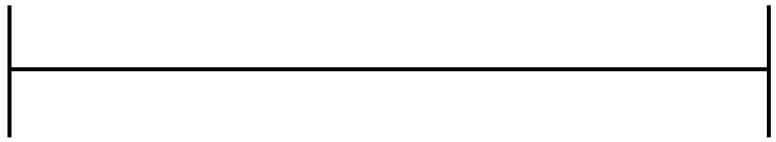

ALL THE TIME NEVER

N. Over the past week, rate any rash(es) that you got on your residual limb.

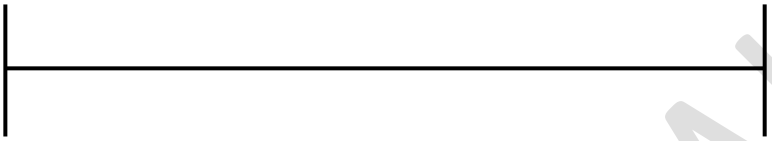

EXTREMELY BOTHERSOME NONE AT ALL

OR check __ I had no rashes on my residual limb in the last week.

O. Over the past week, rate any blisters or sores that you got on your residual limb.

EXTREMELY BOTHERSOME NONE AT ALL

OR check __ I had no blisters or sores on my residual limb in the last week.

GROUP 2

The next section covers very SPECIFIC BODILY SENSATIONS. Here are our definitions:

1. SENSATIONS are feelings like "pressure", "tickle" or a sense of position or location, such as the toes being curled. Amputees have described sensations in their missing (phantom) limb such as "the feeling that my (missing) foot is wrapped in cotton."

2. PAIN is a more extreme sensation described by terms such as "shooting", "searing", "stabbing", "sharp", or "ache".

3. PHANTOM LIMB refers to the part that is missing. People have reported feeling sensations and/or pain in the part of the limb that has been amputated — that is, in their phantom limb.

4. RESIDUAL LIMB (STUMP) refers to the portion of your amputated limb that is still physically present.

REGARDING SENSATIONS IN YOUR PHANTOM LIMB

A. Over the past week, rate how often you have been aware of non-painful sensations in your phantom limb.

a. ___ never
b. ___ only once or twice
c. ___ fairly often (2-3 times)

Modified version of Prosthesis Evaluation Questionnaire (PEQ) by Legro, et al. (1998)
adapted from Prosthetics Research Study, Seattle, WA, USA (1998)

d. ___ very often (4-6 times)
e. ___ several times every day
f. ___ all the time or almost all the time

B. If you had non-painful sensations in your phantom limb during the past week, rate how intense they were on average.

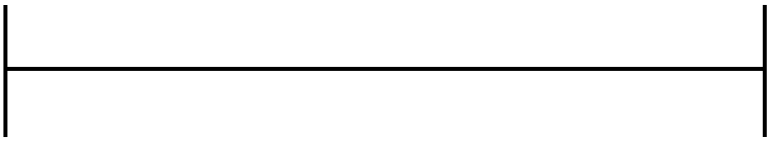

EXTREMELY INTENSE EXTREMELY MILD

OR check ___ I did not have non-painful sensations in my phantom limb.

C. Over the past week, how bothersome were these sensations in your phantom limb?

EXTREMELY INTENSE NOT VERY INTENSE

OR check ___ I did not have non-painful sensations in my phantom limb.

D. Over the past week, rate how often you had pain in your phantom limb.
a. ___ never
b. ___ only once or twice
c. ___ fairly often (2-3 times)
d. ___ very often (4-6 times)
e. ___ several times every day
f. ___ all the time or almost all the time

E. How long does your phantom limb pain usually last?
a. ___ I have none
b. ___ a few seconds
c. ___ a few minutes
d. ___ several minutes to an hour
e. ___ several hours
f. ____ a day or two
g. ____more than two days

F. If you had any pain in your phantom limb this past month, rate how intense it was on average.

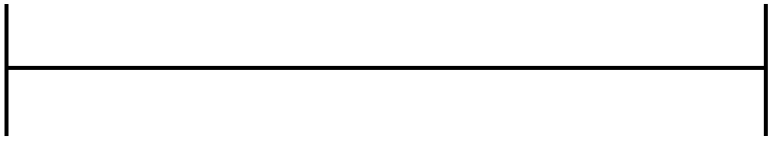

EXTREMELY BOTHERSOME NOT AT ALL

OR check ___ I did not have any pain in my phantom limb.

Modified version of Prosthesis Evaluation Questionnaire (PEQ) by Legro, et al. (1998)
adapted from Prosthetics Research Study, Seattle, WA, USA (1998)

G. In the past week how bothersome was the pain in your phantom limb?

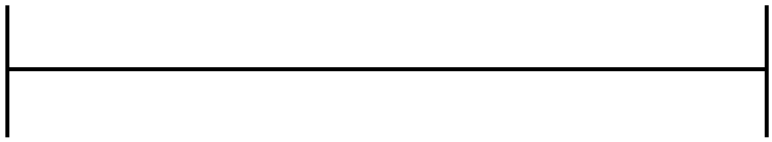

EXTREMELY INTENSE EXTREMELY MILD

OR check _____ I did not have any pain in my phantom limb.

H. Over the past week, rate how often you had pain in your residual limb.

a. ___ never
b. ___ only once or twice
c. ___ fairly often (2-3 times)
d. ___ very often (4-6 times)
e. ___ several times every day
f. ___ all the time or almost all the time

I. If you had any pain in your residual limb over the past week, rate how intense it was on average.

EXTREMELY BOTHERSOME NOT AT ALL

OR check ___ I did not have any pain in my residual limb.

J. OVER THE past week how bothersome was the pain in your residual limb?

EXTREMELY BOTHERSOME EXTREMELY MILD

OR check ___ I did not have any pain in my residual limb.

K. Over the past week, rate how often you experienced back pain.

a. ___ never
b. ___ only once or twice
c. ___ fairly often (2-3 times)
d. ___ very often (4-6 times)
e. ___ several times every day
f. ___ all the time or almost all the time

L. If you had any back pain over the past week, rate how intense it was on average.

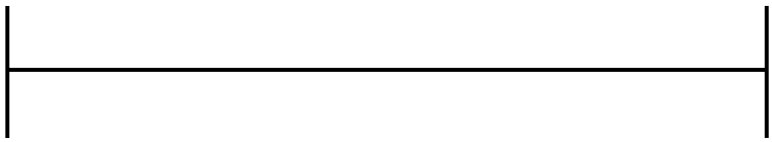

EXTREMELY INTENSE EXTREMELY MILD

OR check ___ I had no back pain.

Modified version of Prosthesis Evaluation Questionnaire (PEQ) by Legro, et al. (1998)
adapted from Prosthetics Research Study, Seattle, WA, USA (1998)

M. OVER THE past week how bothersome was the back pain?

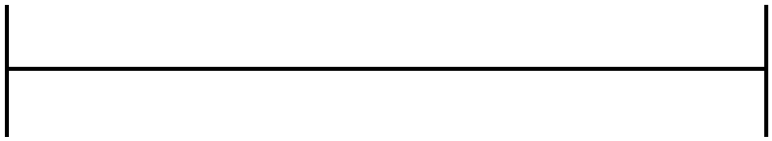

ALL THE TIME NEVER

OR check ___ I had no back pain.

Group 3

This section is about some of the SOCIAL AND EMOTIONAL ASPECTS OF USING A PROSTHESIS.

A. Over the past week, rate how often the desire to avoid strangers' reactions to your prosthesis made you avoid doing something you otherwise would have done.

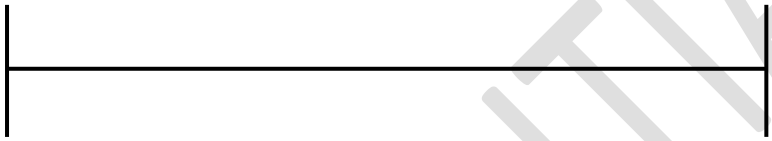

ALL THE TIME NEVER

B. Over the past week, rate how frequently you were frustrated with your prosthesis.

EXTREMELY FRUSTRATED NOT AT ALL

C. If you were frustrated with your prosthesis at any time over the past month, think of the most frustrating event and rate how you felt at that time.

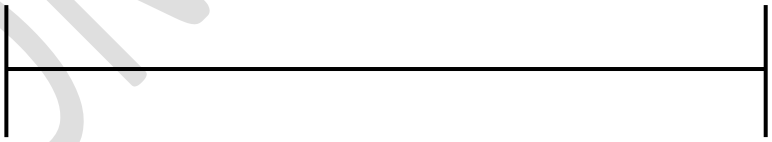

EXTREMELY BOTHERSOME NOT AT ALL

OR check ___ I have not been frustrated with my prosthesis

Modified version of Prosthesis Evaluation Questionnaire (PEQ) by Legro, et al. (1998)
adapted from Prosthetics Research Study, Seattle, WA, USA (1998)

Group 4

The following section asks about YOUR SATISFACTION WITH PARTICULAR SITUATIONS given that you have an amputation.

A. Over the past week, rate how satisfied you have been with your prosthesis.

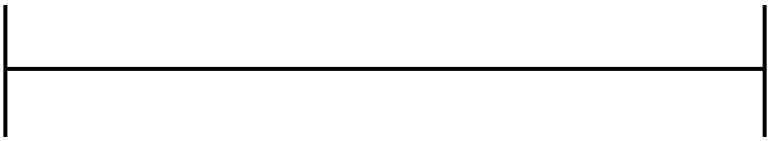

EXTREMELY DISSATISFIED EXTREMELY SATISFIED

B. Over the past week, how would you rate your quality of life?

WORST POSSIBLE BEST POSSIBLE

C. How satisfied are you with the person who fit your current prosthesis?

EXTREMELY DISSATISFIED EXTREMELY SATISFIED

D. How satisfied are you with the training you have received on using your current prosthesis?

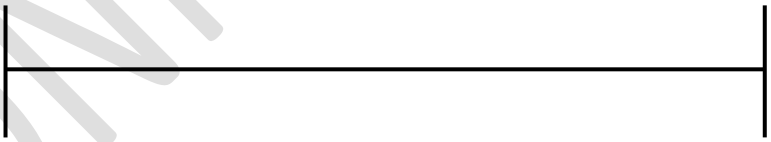

EXTREMELY DISSATISFIED EXTREMELY SATISFIED

OR check ____ I have not had any training with my current prosthesis.

E. Overall, how satisfied are you with the prosthetic training you have received since your amputation?

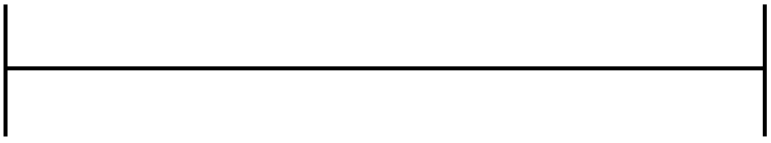

EXTREMELY DISSATISFIED EXTREMELY SATISFIED

OR check ____ I have not had any training since my amputation.

Modified version of Prosthesis Evaluation Questionnaire (PEQ) by Legro, et al. (1998)
adapted from Prosthetics Research Study, Seattle, WA, USA (1998)

Group 5

This next section asks you to rate your ability TO DO YOUR DAILY ACTIVITIES when you are having problems with your prosthesis.

A. When the fit of my prosthesis is poor, I will get...

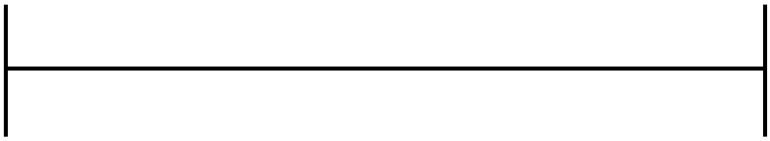

NOTHING DONE EVERYTHING DONE

B. When the comfort of my prosthesis is poor, I will get...

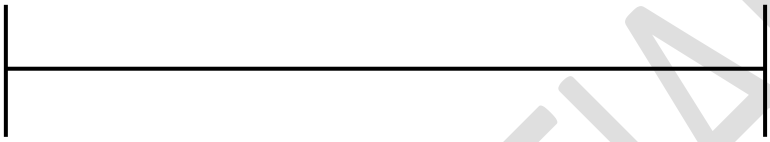

NOTHING DONE EVERYTHING DONE

C. Without my prosthesis, I will get...

NOTHING DONE EVERYTHING DONE

Group 6

This last section asks you to rate HOW IMPORTANT different aspects (or qualities) of your prosthesis are to you.

A. How important is it that the weight of your prosthesis feels right?

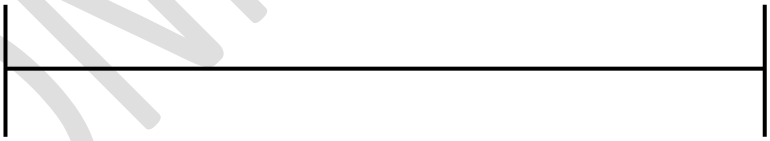

NOT AT ALL EXTREMELY IMPORTANT

B. How important is the ease of putting on (donning) your prosthesis?

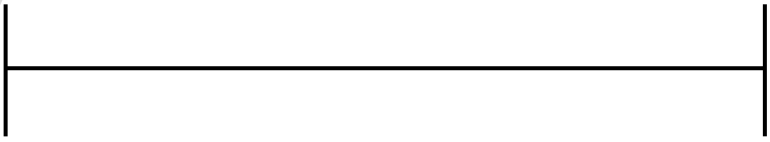

NOT AT ALL EXTREMELY IMPORTANT

C. How important is the appearance of your prosthesis (how it looks)?

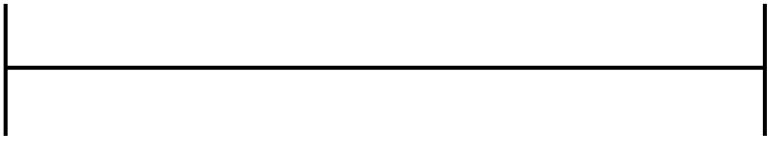

NOT AT ALL EXTREMELY IMPORTANT

Modified version of Prosthesis Evaluation Questionnaire (PEQ) by Legro, et al. (1998)
adapted from Prosthetics Research Study, Seattle, WA, USA (1998)

D. How important is it that your prosthesis' covering is durable (cannot be torn, dented, easily scratched, or discoloured)?

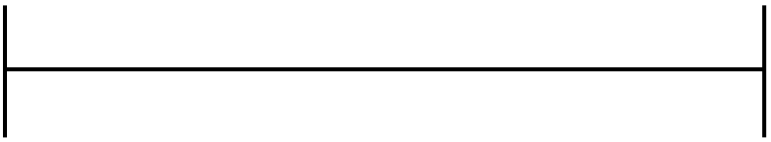

NOT AT ALL EXTREMELY IMPORTANT

OR check __ there is no covering on my prosthesis.

E. How bothersome is it when you sweat a lot inside your prosthesis (in the sock, liner or socket)?

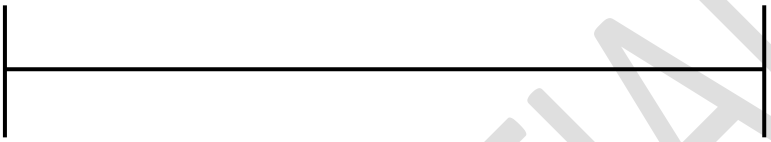

EXTREMELY BOTHERSOME NOT AT ALL

F. How bothersome to you is swelling in your residual limb (stump)?

EXTREMELY BOTHERSOME NOT AT ALL

G. How bothersome is it to see people looking at you and your prosthesis?

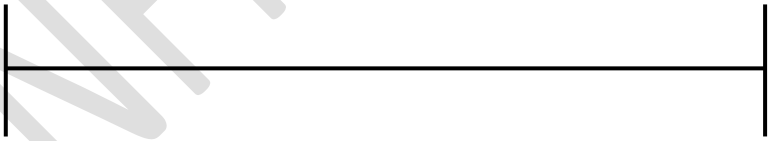

EXTREMELY BOTHERSOME NOT AT ALL

Final Notes[1]

A. If any of the following have happened in the past week, please check off and give a brief description:

___ a serious medical problem (yours)
___ a noticeable change in pain
___ a serious personal problem (yours)
___ a serious problem in the family
___ some other big change has occurred in your life

If you checked any of the five previous items, please give a brief description.
OR check ____ I have not had any of the above happen in the past week.

[1] End of the section pertaining to the Prosthetic Evaluation Questionnaire (PEQ) as available from Prosthetics Research Study (PRS) (1998)

Please indicate how easily you perform the following activities. Kindly tick only **one** box per task.[2]

	Task	Not Able To	Difficult	Easy	Very Easy
1	*Wash Face*				
2	*Put toothpaste on brush and brush teeth*				
3	*Brush/comb hair*				
4	*Put on and remove T-shirt*				
5	*Button shirt with front buttons*				
6	*Attach end zipper and zip jacket*				
7	*Put on socks*				
8	*Tie shoe laces*				
9	*Use fork or spoon*				
10	*Pour from 340ml can*				
11	*Write name legibly*				
12	*Use scissors*				
13	*Open door with knob*				
14	*Carry laundry basket*				
15	*Dial a touch-tone phone*				
16	*Fold a bath towel*				
17	*Open an envelope*				
18	*Stir a bowl*				
19	**Put on and take off prosthesis**				

B. Please share with us anything else about you or your prosthesis that you think would be helpful for us to know. Suggestions for improvements are most welcome. (You may use the other side of this page if there is not enough space).

[2] Orthotics and Prosthetics User Survey (OPUS) as evaluated and modified by Burger, et al. (2008) to determine the Upper Extremity Functional Status (UEFS).

THANK YOU VERY MUCH!

Bibliography

Burger, H. et al., 2008. Validation of the Orthotics and Prosthetics User Survey Upper Extremity Functional Status Module in People with Unilateral Upper Limb Amputation. *Journal of Rehabilation Medicine,* Volume 40, pp. 393-399.

Legro, M. W. et al., 1998. Prosthesis evaluation questionnaire for persons with lower limb amputations: assessing prosthesis-related quality of life. *Archives of Physical Medicine and Rehabilitation,* 79(8), pp. 931-938.

Prosthetics Research Study, 1998. *Prosthesis Evaluation Questionnaire (PEQ).* [Online] Available at: http://www.prs-research.org/Texts/PEQ_A4.pdf
[Accessed 2 April 2014].

Rossouw, E., 2014. *Experiences and expected risks while using a prosthesis* [Interview] (22 January 2014).

APPENDIX G - EOS MATERIAL DATA

This data is applicable to the EOS PA2200 Nylon material used in the additive manufacturing of the palmar structure of the hand prosthesis. Calculations made in Section 4.2.1.1 (p. 97) as well as the material properties used in the FEA investigation in Appendix C ,are based on this material data.

Fine Polyamide PA 2200 for EOSINT P

Application:

PA 2200 is suitable for use in all EOSINT P systems with fine polyamide option.
The recommended layer thickness is 0.15 mm. Unexposed powder can be reused. Depending on building time it has to be mixed with fresh powder by a ratio of 2:1 to 1:1 (old : new) in order to guarantee constant process parameters and persisting part quality.

Typical applications of the material are fully functional prototypes with high end finish right from the process. They easily withstand high mechanical and thermal load.

Material Properties:

Average grain size	Laser diffraction	60	µm
Bulk density	DIN 53466	0,435 - 0,445	g/cm³
Density of laser-sintered part	EOS-Method	0,9 - 0,95	g/cm³

Mechanical Properties:*

Tensile Modulus	DIN EN ISO 527	1700 ± 150	N/mm²
Tensile strength	DIN EN ISO 527	45 ± 3	N/mm²
Elongation at break	DIN EN ISO 527	20 ± 5	%
Flexural Modulus	DIN EN ISO 178	1240 ± 130	N/mm²
Charpy - Impact strength	DIN EN ISO 179	53 ± 3,8	kJ/m²
Charpy - Notched impact strength	DIN EN ISO 179	4,8 ± 0,3	kJ/m²
Izod – Impact Strength	DIN EN ISO 180	32,8 ± 3,4	kJ/m²
Izod – Notched Impact Strength	DIN EN ISO 180	4,4 ± 0,4	kJ/m²
Ball indentation hardness	DIN EN ISO 2039	77,6 ± 2	
Shore D - hardness	DIN 53505	75 ± 2	

EOS GmbH – Electro Optical Systems
Robert-Stirling-Ring 1
D-82152 Krailling / München
Telephone: +49 (0)89 / 893 36-0
Telefax: +49 (0)89 / 893 36-285
Internet: www.eos.info

Thermal Properties:

Melting point	DIN 53736	172 - 180	°C
Vicat softening temperature B/50	DIN EN ISO 306	163	°C
Vicat softening temperature A/50	DIN EN ISO 306	181	°C

* The mechanical properties depend on the x-, y-, z-position and on the exposure parameters used.

The data are based on our latest knowledge and are subject to changes without notice. They do not guarantee properties for a particular part and in a particular application.

EOS GmbH – Electro Optical Systems

Robert-Stirling-Ring 1
D-82152 Krailling / München

Telephone: +49 (0)89 / 893 36-0
Telefax: +49 (0)89 / 893 36-285
Internet: www.eos.info

Zertifikat , Biokompatibilität PA 2200

BIOSERVICE

BIOCOMPATIBILITY
CERTIFICATE

Testmaterial: **PA 2200**

Supplier: EOS GmbH
Pasinger Strasse 2, D-82152 Planegg

Studies performed: The following studies were performed in order to determine the biocompatiblity of the product PA 2200 according to ISO 10993-1:

CYTOTOXICITY
SENSITISATION, polar extract
SENSITISATION, non-polar extract
INTRACUTANEOUS REACTIVITY

Results: **The product did not show any adverse effects in the studies performed. Therefore, the biocompatiblity of the test material was proved.**

BSL BIOSERVICE Scientific Laboratories GmbH Munich
Behringstraße 6
D-82152 Planegg

Dr. Achim Albrecht
Biological Safety Testing
Date: April 10, 2001

BIOSERVICE Scientific Laboratories GmbH
GLP
EN 45001